Development and Application of Quantitative and Qualitative Mass Spectrometry Techniques to Probe Crustacean Neuropeptides and Beyond

By

Amanda Rae Buchberger Jones

A dissertation submitted in partial fulfillment of

the requirements for the degree of

Doctor of Philosophy

(Chemistry)

at the

University of Wisconsin-Madison

2018

Date of Final Oral Examination: June 14th, 2018

This dissertation is approved by the following members of the Final Oral Exam Committee:

Lingjun Li, Professor, Pharmacy and Chemistry

John Wright, Professor, Chemistry

Sandro Mecozzi, Professor, Pharmacy and Chemistry

Lloyd Smith, Professor, Chemistry

Acknowledgements

First of all, I want to thank my PhD advisor, Dr. Lingjun Li. She has had faith in me throughout my entire graduate career, and I am eternally thankful for the opportunities she has provided me. Without her, I would have never discovered my passion for bioanalytical chemistry, and I can only hope to be as successful as a researcher and mentor in my future career endeavors.

I would also like to thank all of my committee members, Dr. John Wright, Dr. Sandro Mecozzi, and Dr. Lloyd Smith for providing feedback on not only my thesis but also my thesis background oral and original research proposal. They have supported me during my time at University of Wisconsin-Madison, and I will be forever grateful for their patience and quality time they have taken to help me develop into a better scientist and future educator.

It should be noted that I would have never come to graduate school without the support of my undergraduate research mentor, Dr. Jim Phillips. Even throughout graduate school, I have reached out to him for advice, as I know that he will give me the hard-to-hear truth. I feel very fortunate to have been a part of his research, as it gave me the passion for scientific research along with skills that have set me apart in graduate school. Also, thank you to Dr. Amy Lovett-Racke, my faculty supervisor at the Ohio State University during my summer research experience, for providing me an atmosphere that sparked my interest into biologically-relevant research.

I have had the honor to work alongside several student colleagues in the Lingjun Li Lab. In particular, I would like to acknowledge Dr. Erin Gemperline, who was my original graduate student mentor in research and in life. In particular, she connected me with the right people to learn the skills I need, including mass spectrometry imaging, liquid chromatography, or others. I

also feel more competent in instrumental troubleshooting and general method development due to her guidance. Dr. Tyler Greer and Dr. Dustin Frost taught me everything I know about quantitative proteomics and tag synthesis that we do in the lab, which has provided me with publishing and patent opportunities. Dr. Chuanzi Ouyang provided me with the tools I need to be successful in crustacean neuropeptide research. Also, thank you to Dr. Zhidan Liang and Dr. Bingming Chen for teaching and trusting me in laboratory when it came time for them to graduate. I want to send a special thanks to Jill Johnson for teaching me cell culture and being an inspiration to me in laboratory work and life attitude. I also want to thank all the people that trusted me to mentor them, including Sheila Liu, Kellen DeLaney, Chris Sauer, and Nhu Vu. In particular, thank you to Kylie Helfenbein, an undergraduate researcher in our lab, for being a pleasure to mentor. Finally, to all of those that have made my graduate career even a little less stressful (if not already mentioned), including Dr. Chris Lietz, Dr. Qing Yu, Dr. Ling Hao, Tony Chen, Xueqin Pang, Qinjingwen Cao, Caitlin Keller, Xiaofang Zhong, Pingli Wei, Qinying Yu, Jerry Li, and Meng Xu, thank you!

I have been supported financially by many different institutions, which have provided me with opportunities beyond my wildest dreams. In particular, I want to highlight the National Institute of Health for my fellowship (F31GM119365); the Chemistry Department Graduate Student-Faculty Liaison Committee (GSFLC) travel grant and UW-Madison's Graduate School conference presentation funds for chances to travel to research conferences; and finally the Oak Ridge Associate Universities (ORAU) and the Lindau Foundation for allowing me the one-in-a-lifetime chance to travel to Lindau, Germany and talk with young scientists and Nobel Laureates about the field of chemistry. I cannot express my gratitude enough.

Beyond the lab, the School of Pharmacy has been great in providing support. This includes Dr. Cameron Scarlett and Molly Pellitteri-Hahn from the Analytical Instrumentation Center in the School of Pharmacy, who were beyond helpful in with their instrument expertise. I would also like to thank Josh Cutler, for always being helpful in making sure our building is running efficiently, Joan Palmer, and Jordan Allen, both for aiding in my fellowship application and funding coordination.

Finally, I would like to thank all of my family and friends who have supported me through thick and thin during the last 5 years of graduate school. In particular, I want to thank my parents; Susanne Buchberger, Julia Bonnstetter, and Dave and Linda Jones; my siblings, Crystal Buchberger and Luke Jones; and all my extended family, in particular my grandma Rosie Buchberger and late grandma Donna Jones, for listening to me talk about my research (even if you didn't understand it) and bragging about it to all your friends. I hope you are all proud of me and continue to be throughout the next few years. I want to also thank my near and far friends who keep me in touch with the real world and how far life has come. Most importantly, I want to thank my husband, Cody Jones, who has been with me for 10 years of support through undergraduate and graduate school stress. He constantly believed in me and reminded me it "would all work out," even when everything seemed to be falling apart. I am so glad to have you never let me give up on my dreams.

For all those I have mentioned: again, thank you.

Table of Contents

Development and Application of Quantitative and Qualitative Mass Spectrometry Techniques to Probe Crustacean Neuropeptides and Beyond

Amanda Rae Buchberger Jones
Under the Supervision of Professor Lingjun Li
University of Wisconsin-Madison

Abstract

Biomolecules, especially neuropeptides, are highly involved in the stress response. Due to their biological and chemical complexity, studying neuropeptides in mammals is challenging. To address this challenge, this thesis employs both model organisms and mass spectrometry (MS) to better characterize neuropeptides and their role in stress. For example, crustaceans provide a simple, well-characterized network for method development while also being ecological relevant to stressors of interest (*e.g.*, hypoxia and salinity). With MS, we can probe perturbations at a global level both quantitatively and qualitatively. Quantitatively, several tagging agents have been explored to improve multiplexing and extend to novel applications. For example, MS imaging, a powerful technique capable of determining the localization of hundreds of biomolecules without prior knowledge of their structure, is inherently qualitative. While useful for relative comparisons between conditions, the application of quantitative tagging reagents to MS imaging explored in this work could advance quantitative MS imaging techniques. Overall, this work improves methodology for probing biomolecules, such as neuropeptides, while expanding biological information about neuropeptides and their roles in stress.

Chapter 1

Introduction and Research Summary

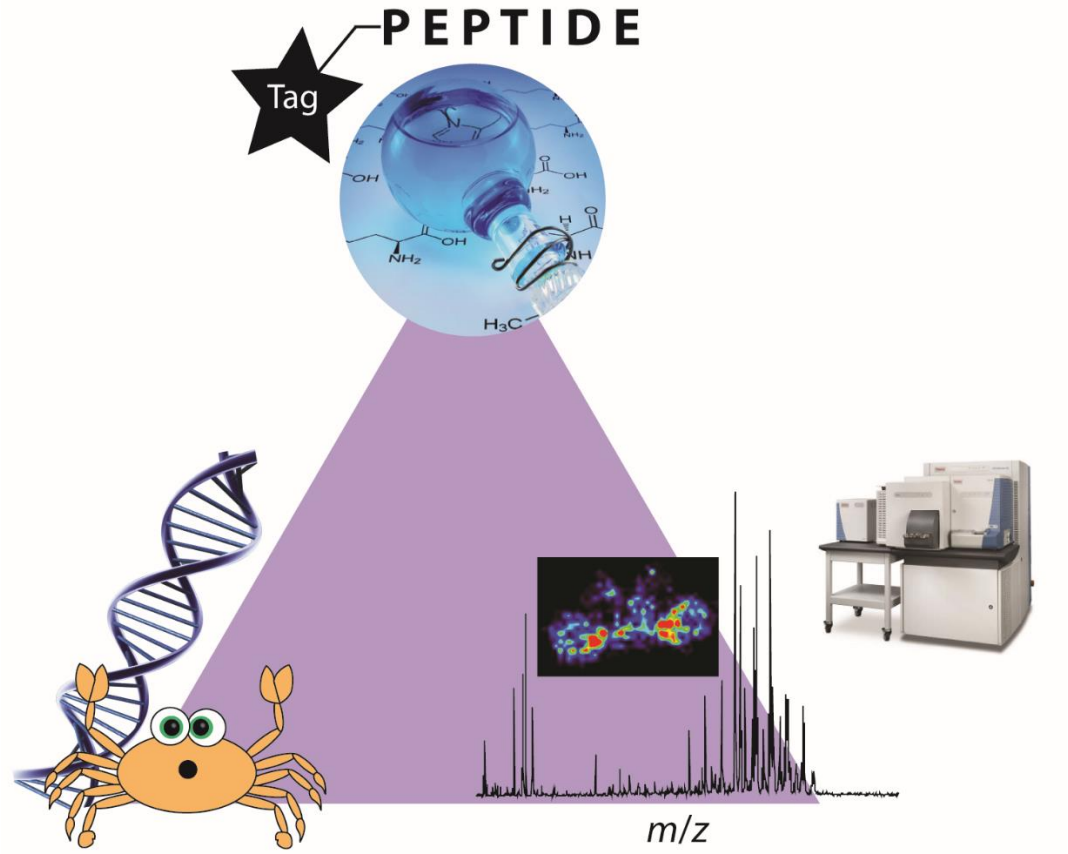

Introduction

Mass spectrometry (MS) has proven to be a powerful, multi-dimensional analytical technique to potentially identify, quantify, and localize biological molecules simultaneously.[1-4] This work focuses on developing and applying methodology to further improve MS for analyzing crustacean neuropeptides and beyond. Both matrix-assisted laser desorption/ionization (MALDI) and liquid chromatography (LC) electrospray ionization (ESI) are utilized to demonstrate the complementary nature of these two ionization strategies for crustacean neuropeptides. To study distribution differences, MS imaging techniques were also evaluated for several different complex biological systems. This dissertation shows the power and potential of MS and MS imaging to answer questions ranging from basic scientific endeavors to current health concerns.

Research Summary

Chapter 1 provides a general summary of this work along with the major findings in each study. Brief background information for the combination of MS and neuropeptide analysis is found in *Chapter 2*.[1] If more background is needed in MS imaging or general neuropeptide analysis techniques, references are available in *Appendices VI* and *VII*, respectively.[4, 5] Updates on all methodologies related to the analysis of crustacean-based models, including potentially relevant quantitative tags, are included in *Appendix II*.[6] *Appendix VIII* provides more information on quantitative tagging strategies, particularly for proteomics (*publication pending*).

Environmental stressors are consistently testing organisms to the game "survival of the fittest." Many have developed mechanisms to avoid fatal consequences. We believe that neuropeptides, complex signaling molecules of the nervous system, are key regulators in how

individuals handle stress.[7-9] Due to the natural diversity of neuropeptides, vertebrates provide a challenging biological matrix to study neuropeptides, especially on a global scale. On the other hand, the use of invertebrate model organisms, such as crustaceans, provide a simplified, well-characterized network to probe the neuropeptidomic changes.[7-10] Since there is no complete genomic information for crustacean species, we have worked on creating a comprehensive database for our analysis.[11-16] In general, we utilize high-resolution mass spectrometry instrumentation to characterize the changes in neuropeptide content due to environmental stressors, some of which will be discussed below (*Chapters 3, 4, 5, and 6*).

Hypoxia stress, or lack of oxygen (O_2), is well recognized in estuaries where many crustacean species reside.[17] *Chapters 3* and *4* provide two different facets of this stress: a severity and a time-based understanding, respectively in the blue crab, *Callinectes sapidus*. In *Chapter 3*, 50%, 20%, and 10% O_2 exposure for 1 hour were all compared for their neuropeptidomic content using MALDI-MS to a control in three major crustacean neuroendocrine tissues. In this study, duplex dimethyl labeling, also known as reductive dimehtylation, was utilized, showing many significant changes in neuropeptides among different exposure conditions. In *Chapter 4*, 4-plex dimethyl labeling was developed to characterize the neuropeptidomic differences among 0 hours (control), 1 hour, 4 hours, and 8 hours of 10% O_2 exposure. In comparison to the previous study, MALDI-MS and LC-ESI-MS were both used to provide a more comprehensive picture of the significant neuropeptidomic changes in five different neuropeptide-rich tissues. These results have the potential to be translated to higher order organisms, including mice, rats, or humans.

Human hypoxia is often coupled to having high carbon dioxide (CO_2) in the respiratory system, also known as hypercapnia.[18] In order to characterize the differences between hypoxia and hypercapnia, a MS imaging-based approach was taken as described in *Chapter 5*. A wash

method to increase neuropeptide signals and matrix application method were optimized and applied to this study. Using advanced statistical software, several neuropeptide distributions were shown to be significantly different between the several conditions investigated, including control (100% O_2, pH 8.3), severe hypoxia (10% O_2, pH 8.3), mild hypoxia (50% O_2, pH 8.3), and hypercapnia (50% O_2, pH 7.6-7.8), in the *C. sapidus*.

Chapter 6 details studies on quantitation and localization changes in another environmental stressor, salinity stress.[9] In this case, two different color morphs for the green crab, *Carcinus maenas*, were exposed to both high (60 parts per thousand (ppt)) and low (0 ppt) salinity compared to a control (30 ppt) using duplex dimethyl labeling. Interestingly, the two color morphs showed distinct changes due to the same stress, concluding that one was more tolerant to salinity stress. A time course study was also investigated for high salinity stress. Finally, a MALDI-MS imaging study was performed to understand localization differences in stressed animals between the two color morphs.

Most of the studies above utilize dimethyl labeling for relative, quantitative comparison of crustacean neuropeptides.[8, 9] Quantitation is done prior to any fragmentation (*i.e.*, at the MS1 level), which allows for theoretically all the neuropeptides to be relatively quantified. Several different MS1 quantitation strategies exist besides dimethyl labeling, one of which is isotopic *N, N*-dimethyl leucine (iDiLeu).[19, 20] Both dimethyl labeling and iDiLeu boast 5-plex labeling, which allows for both relative and absolute quantitation. iDiLeu has already shown the potential for absolute quantitation by labeling one channel with the sample of interest and the other four channels with a calibration curve, specifically for neuropeptides in LC-ESI-MS.[20]

In comparison to LC-ESI-MS, quantitative MALDI-MS imaging is less implemented in the research community, in part due to several technical challenges.[4] *Chapter 7* focuses on

developing an absolute quantitation method for MALDI-MS imaging using 5-plex iDiLeu and dimethyl labeling.[20, 21] This included transferring the solution-based methodology to be compatible with an imaging platform and optimizing application parameters. This chapter provides a summary of all the techniques utilized with future goals and considerations.

Quantitation at the MS1 level can be difficult due to the increased spectral complexity, especially for tags that have several Dalton (Da) spacings, such as iDiLeu and dimethyl labeling.[20, 21] *Chapter 8* discusses the development of a new mass difference tag, dimethyl pyrimidinyl ornithine (DiPyrO), which utilizes mass defect to create small mDa spacings that reduce spectral complexity while also allowing for MS1-based quantitation.[22] This tag boasts up to 8-plex labeling with the most advanced, high-resolution instrumentation, easy synthesis, and applicability to any sample type in comparison to other, MS1 mass defect-based quantitation strategies.[23]

In collaboration with the Wisconsin Institute for Scientific Literacy, *Chapter 9* describes this work for a more general audience. Finally, *Chapter 10* concludes the thesis with discussion of future directions for all the projects above, especially in terms of quantitative strategies for crustacean neuropeptides and MALDI-MS imaging. Other interesting projects, including crustacean cell culture, rat uterus imaging, and a male-female comparison of crustacean neuropeptides, are presented in *Appendix III*, *IV*, and *V*, respectively. All my accomplishments resulting from this work and beyond, including grants, publications, patents, and presentations, are summarized in *Appendix I*.

References

1. Buchberger, A.; Yu, Q.; Li, L., *Annu Rev Anal Chem (Palo Alto Calif)* **2015,** *8* (1), 485-509.

2. Li, L. J.; Sweedler, J. V., Peptides in the Brain: Mass Spectrometry-Based Measurement Approaches and Challenges. In *Annual Review of Analytical Chemistry*, Annual Reviews: Palo Alto, 2008; Vol. 1, pp 451-483.

3. Dreisewerd, K., *Analytical and Bioanalytical Chemistry* **2014,** *406* (9-10), 2261-2278.

4. Buchberger, A. R.; DeLaney, K.; Johnson, J.; Li, L. J., *Analytical Chemistry* **2018,** *90* (1), 240-265.

5. DeLaney, K.; Buchberger, A. R.; Atkinson, L.; Grunder, S.; Mousley, A.; Li, L. J., *Journal of Experimental Biology* **2018,** *221* (3).

6. DeLaney, K.; Buchberger, A.; Li, L., *Methods Mol Biol* **2018,** *1719*, 247-269.

7. Wang, J. H.; Zhang, Y. Z.; Xiang, F.; Zhang, Z. C.; Li, L. J., *Journal of Chromatography A* **2010,** *1217* (26), 4463-4470.

8. Chen, R. B.; Xiao, M. M.; Buchberger, A.; Li, L. J., *Journal of Proteome Research* **2014,** *13* (12), 5767-5776.

9. Zhang, Y.; Buchberger, A.; Muthuvel, G.; Li, L., *Proteomics* **2015**.

10. Christie, A. E.; Stemmler, E. A.; Dickinson, P. S., *Cell Mol Life Sci* **2010,** *67* (24), 4135-69.

11. Chen, R. B.; Jiang, X. Y.; Conaway, M. C. P.; Mohtashemi, I.; Hui, L. M.; Viner, R.; Li, L. J., *Journal of Proteome Research* **2010,** *9* (2), 818-832.

12. Cape, S. S.; Rehm, K. J.; Ma, M.; Marder, E.; Li, L. J., *Journal of Neurochemistry* **2008,** *105* (3), 690-702.

13. Ma, M. M.; Bors, E. K.; Dickinson, E. S.; Kwiatkowski, M. A.; Sousa, G. L.; Henry, R. P.; Smith, C. M.; Towle, D. W.; Christie, A. E.; Li, L. J., *General and Comparative Endocrinology* **2009,** *161* (3), 320-334.

14. Ma, M. M.; Wang, J. H.; Chen, R. B.; Li, L. J., *Journal of Proteome Research* **2009,** *8* (5), 2426-2437.

15. Hui, L. M.; Xiang, F.; Zhang, Y. Z.; Li, L. J., *Peptides* **2012,** *36* (2), 230-239.

16. Hui, L. M.; D'Andrea, B. T.; Jia, C. X.; Liang, Z. D.; Christie, A. E.; Li, L. J., *General and Comparative Endocrinology* **2013,** *184*, 22-34.

17. Diaz, R. J.; Rosenberg, R., *Oceanography and Marine Biology - an Annual Review, Vol 33* **1995,** *33*, 245-303.

18. Kelsen, S. G.; Fleegler, B.; Altose, M. D., *American Review of Respiratory Disease* **1979,** *120* (3), 517-527.

19. Greer, T.; Li, L. J., Isotopic N,N-Dimethyl Leucine (iDiLeu) for Absolute Quantification of Peptides Using a Standard Curve Approach. In *Quantitative Proteomics by Mass Spectrometry, 2nd Edition*, Sechi, S., Ed. Humana Press Inc: Totowa, 2016; Vol. 1410, pp 195-206.

20. Greer, T.; Lietz, C. B.; Xiang, F.; Li, L. J., *Journal of the American Society for Mass Spectrometry* **2015,** *26* (1), 107-119.

21. Wu, Y.; Wang, F. J.; Liu, Z. Y.; Qin, H. Q.; Song, C. X.; Huang, J. F.; Bian, Y. Y.; Wei, X. L.; Dong, J.; Zou, H. F., *Chemical Communications* **2014,** *50* (14), 1708-1710.

22. Frost, D. C.; Buchberger, A. R.; Li, L., *Anal Chem* **2017**.

23. Hebert, A. S.; Merrill, A. E.; Stefely, J. A.; Bailey, D. J.; Wenger, C. D.; Westphall, M. S.; Pagliarini, D. J.; Coon, J. J., *Molecular & Cellular Proteomics* **2013,** *12* (11), 3360-3369.

Chapter 2

Advances in Mass Spectrometric Tools for Probing Neuropeptides

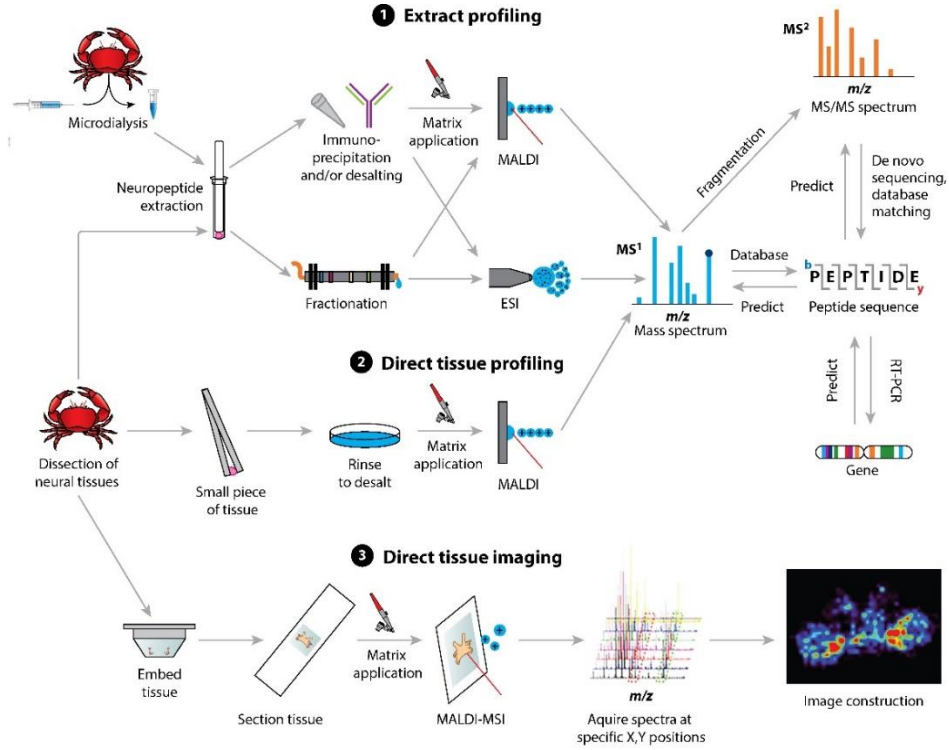

Modified from:

Amanda R. Buchberger, Qing Yu, Lingjun Li. "Advances in Mass Spectrometric Tools for Probing Neuropeptides." Invited Contribution. *Annual Review of Analytical Chemistry*, 2015, 8: 485-509.

Keywords Mass Spectrometry, Neuropeptidomics, Microdialysis, Quantitation, Mass Spectrometric Imaging, Sample Preparation

Abstract

Neuropeptides are important mediators in the functionality of the brain and other neurological organs. Because neuropeptides exist in a wide range of concentrations, appropriate characterization methods are needed to provide dynamic, chemical, and spatial information. Mass spectrometry and compatible tools have been a popular choice in analyzing neuropeptides. There has been several advances and challenges, both of which are the focus of this review. Discussions range from sample collection to bioinformatic tools, although avenues such as quantitation and imaging are included. Further development of the presented methods for neuropeptidomic mass spectrometric analysis is inevitable, which will lead to a further understanding of the complex interplay of neuropeptides and other signaling molecules in the nervous system.

Introduction

Neuromodulation via signaling peptides can initiate a wide variety of responses for numerous conditions including food intake, pain, and other environmental challenges.[1-3] One class of increasingly studied signaling peptides is neuropeptides, for which their structural and functional diversity requires the development of sophisticated analytical tools. Neuropeptides are typically short amino acid chains, although they have an unprecedented variety of sizes ranging from 3 to more than 70 residues.[1] Their physiological function includes the ability to signal between neurons or neurons and other targets, but even structurally similar neuropeptides can produce very different responses while also possessing conserved functions with other family members.[4] This diversity has made the global discovery and characterization of neuropeptides challenging.

Anabolism of neuropeptides begins in the neurons, where they are synthesized from RNA chains as a prepropeptide.[1] After multiple processing steps, including cleavages and modifications (*e.g.,* C-terminal amidation), the resultant propeptide, which can contain several neuropeptides, is packaged into vesicles along with the processing enzymes to produce final biologically active peptides. Upon stimulation, such as high-frequency firing, the secretory vesicles fuse with the plasma membrane and release the fully processed neuropeptides from the neuron, allowing them to bind to a receiving target.[5] Targets can lie nearby within a specific tissue or in a more distant location where the neuropeptide has to travel through the circulating fluid. Once at their target, neuropeptides bind with high affinity, and the signal subsides only after peptidases break down the neuropeptides. However, the anabolism and catabolism of an neuropeptide can vary dramatically between the location of the neuron, and intracellular processes may be extracellular in different regions of the body.[6]

Even with complete genetic coverage, given the production's natural complexity, it is difficult to predict the structure and function of a single neuropeptide produced. Compared with mammals, the networks of invertebrates are simplified and have been utilized to allow for neuropeptide characterization. Neuropeptide homologs also exist between invertebrates, such as crustaceans, and vertebrates, suggesting a conservation of signaling molecules, pathways, and other complex behaviors across species.[7-10] By studying these simplified networks, we can gain a better understanding of a more complex nervous system, such as that of humans.

Measuring neuropeptides requires approaches and platforms that provide sensitive and specific chemical, dynamic, and spatial information. Classical techniques, such as immunoassays (*e.g.,* radioimmunoassay), are nonspecific, require lots of sample material, and/or need prior

structural knowledge.[1] Antibody-based immunochemical methods also have difficulty differentiating between isoforms of a neuropeptide, although this was recently achieved.[1, 11]

To compare, mass spectrometry (MS) provides selectivity through accurate mass measurement and tandem MS (MS/MS) sequence confirmation without consuming large amounts of sample. As a result, various facets of MS have been used as powerful tools for neuropeptide analysis. The small differences between isoforms' mass-to-charge ratios (*m*/*z*) measured using high-resolution, accurate-mass MS instrumentation can easily distinguish one isoform from the other.[12, 13] In addition to accurate precursor mass measurement, product ion fragmentation mass spectra (MS/MS) enable the discovery of novel neuropeptides from several families through de novo sequencing and BLAST strategies, thereby expanding the neuropeptidome of the corresponding organism.[14-17] Furthermore, quantification of neuropeptides, both relative and absolute, has evolved from label-free methods to isotopic labeling strategies, providing a more dynamic view of the neuropeptide changes in comparative studies.[18] To acquire accurate data, proper handling and separation of the samples are key, especially in specialized MS techniques such as in vivo methods and MS imaging.

The general workflow and major approaches for neuropeptide analysis can be readily transferred and utilized across species, although the specific materials used will vary. **Figure 1** outlines these strategies using crustacean as a model organism. Throughout this review, these general methodologies are discussed, highlighting the major advances in each area as well as the major discoveries and challenges that still exist.

Sample Collection and Preparation

The first major step is collection and proper sample handling of the neuropeptide-containing tissues. These samples are well-known for being complex, owing to proteases, lipids, salts, *etc.*, which can create problems with intra/interscan dynamic range and ion suppression during MS analysis.[1] Therefore, it is critical to reduce chemical complexity of an neuropeptide sample before analysis. As shown in **Figure 1**, several workflow pathways exist depending on the type of information sought from the neuronal sample.

Extract Versus Direct Profiling

In neuropeptide experiments utilizing mechanical/chemical extraction, pooling of several tissues, organs, and cells into one sample is often desirable. This creates a neuropeptide-rich sample that can be used either to discover or to monitor neuropeptides. Depending on the model system used, various schemes for neuropeptide extraction have been developed. To break down cellular walls, homogenization using a glass manual homogenizer or a probe sonicator is employed. Released neuropeptides are immediately vulnerable to chemical degradation, and protease activity must be reduced during extraction. Postmortem degradation, which is even more intensified in mammalian tissue, can produce protein fragments that interfere with neuropeptide identification.[13, 19-21] Commonly, samples are just snap frozen, although this is ineffective and reduces the number of peptides identified compared with other stabilization methods.[22, 23] Denaturation and precipitation of proteases can be achieved with acidified organic solvents, such as acidified methanol, acetone, or ethanol, though these extraction solvents may need to be coupled with other methods or each other to increase peptide identification.[5] Through combination of these solvent systems, for example, the four-step "mixing on column" extraction method, neuropeptide identification rates have been increased by fivefold (*i.e.,* from 100 to more than 500 neuropeptides identified by mixing on column).[24] Microwave irradiation, boiling in

extraction buffers, or heat stabilization are also effective in minimizing postmortem degradation.[22-24] By use of the Stabilizer T1 denator, a commercial heat stabilization system, Sturm *et al.* observed a reduction in interference due to degradation products in crustacean tissues.[23] This method boiling when directly compared with similar tissues acquired from the same blue crab.

Although technological advance have made MS analysis of single tissue homogenates more accessible, unlike homogenization and extraction, direct tissue analysis is a much simpler sample preparation technique that enables comparison between individual samples or animals. Once dissected out and rinsed with water to desalt, the tissue can be directly placed onto a glass slide or sample plate for analysis. In contrast to pooling tissues for extraction, in situ direct analysis simplifies the workflow; it minimizes artifacts, contamination, and sample loss. Even with smaller sample sizes, high sensitivity can be obtained, as demonstrated by the studies above. Finally, the spatial information gained from direct tissue analysis is often lost when homogenates are pooled.

Single Cell Analysis

The use of single cell analysis has allowed for the profiling of rare, low-concentration neuropeptides within a heterogeneous population. Individual cells usually contain each form of a bioactive molecule, meaning these analyses can provide mechanistic signaling information.[11, 25-29] In single-cell MS, researchers must carefully consider special strategies and instrumentation, such as the appropriate microscope and capillary for cell transfer. Several sample preparation and technological advances have been made regarding microanalysis of single cells (for a recent review, see [30]). Notably, immunohistochemical methods are useful for localizing and identifying clusters, but antibodies can be unspecific, require prior knowledge, and can hinder MS analysis

because fixation of the analytes is normal practice. Recently, by using a heating step, investigators reversed these crosslinks and determined that neuron samples produce signals similar to those of freshly dissected cells while causing minimal Schiff base formation.[27] Although many neuropeptide functions remain elusive, the demonstration of single-cell MS in many organisms is the stepping stone to combining functional studies with neuropeptidomic profiling.

Liquid Collection Methods: in vivo Monitoring

Alternatively, liquid-based collection methods can be used to sample neuropeptides from media such as blood or other biofluids. These procedures provide the distinct advantage of determining whether a peptide is secreted while delivering an extract that is less complex than tissue homogenates. Biofluid sample collection is most often done by using a needle attached to a syringe to withdraw a specified volume of liquid that supposedly contains neuropeptides. Although simple, needle sampling can be stressful to the organism, thus producing artificial circulating neuropeptides that can skew results. Biofluids, such as crustacean hemolymph, are also protein abundant, and degradation products lead to the suppression of trace-level neuropeptides.[7]

These limitations have led to the development of new sample collection strategies to measure in vivo changes that can further our understanding of important biological questions.[31] These techniques target the extracellular space, which enables researchers to monitor secretion and dynamic changes due to a stimulus or normal rhythm. Such work provides valuable insights into an neuropeptide's possible functional role. The two most common in vivo sampling methods are push-pull perfusion and microdialysis (MD), although MD has acquired the most attention for method development owing to its minimal disturbance to the animal.[5, 32-34] Both approaches

require the insertion of a sampling probe into a specific region of the brain or circulation system. Many recent reviews include ample discussion on the technical considerations involved in MD.[7, 8, 33] When coupled to MD techniques, MS offers an attractive tool that can provide sensitivity, aid in identification, and allow for confident quantitation.

Challenges still exist with MD in vivo measurements, specifically whether they provide a balance between both sensitivity and temporal dynamics. Temporal resolution, defined as the shortest time duration over which a dynamic change event can be observed, is required to understand the possible functionality of neuropeptide targets. Short time points intrinsically lead to small volumes and low neuropeptide concentrations, and the limited sensitivity provided by MS may often hinder the detection of these low-level signaling molecules. Increasing the collection volume will alleviate this issue but at the cost of temporal resolution. Another strategy is to add a rapid preconcentration step prior to analysis, which Zhou *et al.* demonstrated using Sprague-Dawley rats with an optimized system.[35]

One way to increase the amount of neuropeptides in small sample volumes is by improving their recovery rate, which, according to in vitro studies, is approximately 20—30% for neuropeptides.[8] One option is to use affinity agents within the probe, such as C18 magnetic micro- or nanoparticles.[8] Recovery is enhanced, allowing for the increased sensitivity required for confident MS detection. For example, compared with other affinity agents, antibody-coated nanoparticles provide significantly improved recovery for six neuropeptides in the Jonah crab, *Cancer borealis* (see **Figure 2**).[8]

Qualitative Analysis of the Neuropeptidome

Normally in MS, a top-down approach, or the analysis of intact molecular species, is used for neuropeptide detection. By contrast, in a bottom-up approach, samples are subjected to proteolytic digestion prior to analysis. Once prepared, MS investigation requires the ionization of the analytes. Two common ionization methods utilized for neuropeptide studies are matrix-assisted laser desorption/ionization (MALDI) and electrospray ionization (ESI). Although MALDI-based methods provide high sensitivity, simple sample preparation, and are tolerant to contaminants, this technique preferentially produces singly charged ions. This simplifies the spectra for quantitative analysis, but it can be a problem when the mass range achievable is limited on a high-resolution instrument such as the Orbitrap. Fragmentation of singly charged ions is also inefficient, making MALDI-MS alone insufficient for large-scale neuropeptidomic analyses. By contrast, ESI-MS offers greater coverage of the peptidome owing to its ability to produce multiply charged ions and to promote efficient fragmentation for sequence derivation. However, via recent advances in MALDI instruments using laserspray ionization and similar techniques, researchers have produced multiply charged ions under various pressure (*e.g.,* atmospheric) conditions.[36-41]

Separations

Owing to its natural complexity, crude extracts must be simplified prior to MS analysis. Initially, samples can be simplified with a reversed-phase (C18) or strong cation exchange desalting system, such as ZipTip or SepPak, depending on the type and amount of neuropeptide material available. When the purpose of the experiment is to investigate a specific neuropeptide or family, immunocapture techniques can be utilized to enrich the sample.[42] Even with these methods, tissue extracts require chromatographic separation prior to MS analysis to allow for characterization of the wide dynamic range of neuropeptides in a sample.[13, 43-46]

Liquid chromatography (LC) is the most common separation method coupled to MS in neuropeptidomic studies. When a sample is injected, it is loaded onto a trap column, which concentrates and desalts the neuropeptide sample prior to nano-LC separation and subsequent MS analysis. To improve neuropeptidome coverage, two orthogonal separation methods can be coupled to provide a multidimensional separation.[13, 43, 44] In the past, online reversed-phase liquid chromatography (RPLC) was coupled to an SDS-PAGE (sodium dodecylsulfate polyacrylamide gel electrophoresis) gel to achieve an orthogonal separation. Unfortunately, manual manipulation (*e.g.*, cutting bands) was required before the samples could be coupled to a mass spectrometer. Today, it is commonplace to couple two different LC stationary phases together, offline or online, to provide enhanced resolution, increased sensitivity, and reduce sample complexity. The first dimension of separation is often strong cation exchange or high-pH reverse phase.[13, 43] Recently, an online RPLC/RPLC system, the first dimension containing a C18 column and the second with a polar-RP column, allowed for the accurate and sensitive quantitation of endogenous oxytocin in rat brain and plasma.[44]

When the available sample volume is low and sample consumption is a concern, capillary electrophoresis (CE) can provide high-resolution separation for MS analysis. Online coupling is common with ESI sources, whereas MALDI instruments, which require the introduction of matrix, are frequently utilized offline. Several CE-MS interfaces exist; these are nicely reviewed elsewhere.[47] One notable highlight is a novel SPE preconcentration method coupled to online CE-ESI-MS, which produced a 5,000-fold improvement in the limit of detection of neuropeptides.[48] Although CE-ESI-MS has some limitations, such as nonindependent optimization, intolerance to salts, and MS sampling rate, offline CE-MALDI-MS provides the opposite characteristics. Discrete fractions are usually acquired during separation, which

decreases column resolution featured in CE analysis. Collection and detection of a continuous CE trace circumvent this issue. Using MS imaging, which is discussed below in more detail, to image the entire CE trace, our group successfully separated individual neuropeptides and accurately acquired their relative quantity via dimethyl labeling.[45]

An MS-separation technology based on the mobility of biomolecules in the gaseous phase, known as ion mobility mass spectrometry (IM-MS), has recently been used in the study of neuropeptides.[49-52] Traditional IM-MS separates molecules on the basis of their mass, charge, and different gas-phase conformations, which causes ions to travel at different velocities through a drift gas in the presence of an electrical field.[53] Other ion mobility separation modes exist. For example, differential, or field-asymmetrical, ion mobility spectrometry separates ions by measuring their mobility in time-varying electric fields.[51, 54] The creation of dimers or molecular complexes also causes mobility differences. For example, IM-MS showed that neuropeptides interact with amyloid-beta peptides in Alzheimer's disease, leading to the understanding of the disease process and the possible choice of biomarkers.[49] Ion mobility detects even minute structural differences within a peptide, such as epimeric differences or post-translational modifications (PTMs), demonstrating the selectivity of this technique.[51, 52] Recently, Jia *et al.* used traveling-wave IM-MS to discern between L- and D-amino-acid-containing peptide fragments.[52]

Characterization

Once neuropeptides are introduced as gas-phase ions into the mass spectrometer, a precursor scan is performed, from which putative identifications can be made on the basis of the exact mass compared with those in a database. However, many organisms lack genomic information, and de novo sequencing is required to identify peptides. Initially, product ion scans

are acquired for each peptide-like precursor for preliminary sequence information. A precursor is then chosen for fragmentation into characteristic pieces to aid in peptide identification. There are several product ion fragmentation methods, such as collision-induced dissociation (CID), high-energy collisional dissociation (HCD), and electron-transfer dissociation (ETD), each of which provides complementary information for structural elucidation. Although CID has been the predominant technique, it may be biased and promote incorrect sequences via sequence scrambling and PTM removal.[50] HCD and ETD may serve as alternative methods to combat these disadvantages. Although mechanistically similar (*i.e.*, bombardment with neutral ions to produce b and y ions), HCD lacks biases in structural size, amino acid content, and low-molecular-weight cutoff that plague CID. Conversely, ETD utilizes electrons to cause random fragmentation to a target ion to produce orthogonal c and z ions. In combination, the complementary fragmentation methods CID and ETD have provided more complete neuropeptide coverage.[55]

To facilitate better fragmentation and sequencing, many chemical derivatization schemes have been utilized. By introducing a mass shift at either the C or N terminus, easier differentiation between the b and y ions is readily achieved for de novo peptide sequencing. Owing to the specificity of a label for a particular side group, chemical labeling also determines which amino acids are present in a peptide. Choice of derivatization is important, as some additions may lead to a decrease in ionization and fragmentation frequencies. Successfully developed methods include acetylation, methyl esterification, and dimethyl labeling.[9, 56-59] In particular, dimethylation, which introduces a mass shift of 28 Daltons (Da) to primary amines (*i.e.*, N terminus and lysine residues), has been utilized to determine amino acid content for mid-sized peptides, such as crustacean hyperglycemic hormone precursor--related peptides.[59]

Bioinformatic Tools

LC-MS/MS is a high-throughput method that produces large data files that require robust bioinformatic tools to parse the MS data to confidently identify and quantify neuropeptides. As stated previously, neuropeptides undergo many processing steps prior to becoming biologically active.[1, 5] This limits the amount of information a genetic sequence can provide, but many bioinformatics tools have been created to facilitate prediction of the final peptide forms from the prohormones produced.[60-66] One such tool allows for the prediction of prohormones (NeuroPID) and is effective in metazoan proteomes.[60] By using several logistic regression models depending on the species of interest, the NeuroPred application suite predicts likely cleavage sites of a prohormone, thus allowing for the discovery of novel neuropeptides and prediction of expected neuropeptides.[61] Southey *et al.* used NeuroPred to locate the prohormone genes and predict cleavage sites to produce a cattle database, which can be useful for comparable species whose complete genome sequences are not available.[67]

Once MS data have been acquired, manual matching or an automated search with a database such as SwePep or Neuropedia is the simplest way to identify neuropeptides.[62, 63] However, there is a trade-off in prohormone and sequence coverage when working with small samples, such as single cells or direct profiling, as opposed to tissue-extract analysis. Individual cells are likely to contain each form of the prohormone that produces biologically active peptides. Yet, peptide sequence coverage is best when neuropeptide-rich extracts are used. Although neuropeptides can be identified with mass matching, the use of MS/MS spectral data increases the confidence of assignments and can be critical for novel neuropeptide discovery or PTM mapping.[68] When a genome is available, standard proteomic-based searches such as Mascot can be utilized. Otherwise, de novo sequencing is required. Manual de novo sequencing

is time consuming, but several software packages such as PEAKS facilitate de novo sequencing.[64] Although de novo sequencing is a powerful tool, it does not always produce accurate results. Several programs such as SPIDER, BLAST, and MEME can be employed for homology searches. These platforms compare putative peptide sequences against a database of closely related species. This strategy may not provide complete sequence information for the peptide in question; however, they can provide key evolutionary and functional roles of the peptide.[65] Several workflows have been developed to use the many available tools, such as BLAST, Uniprot database, and PepNovo, that facilitate peptide identification from complex data sets.[66] It is expected that new bioinformatics tools will emerge, providing more confident assignments while increasing the high-throughput nature of MS.

Neuropeptide Quantitation

Another aspect in determining neuropeptide functions is to assess their quantitative regulation in response to a physiological change or manipulation. However, the heterogeneity of ionization efficiency, unpredictable bias, and suppression effects of complex mixtures may complicate quantitative MS analysis. The necessity for accurate quantitation information has sparked the development of several strategies to address these problems. Currently, lack of standardization exists for a neuropeptide-level quantitation strategy. This has led to a growing interest in creating robust MS-based approaches to quantify neuropeptides in targeted and nontargeted workflows.

Absolute Quantitation

There are two main types of MS quantitation strategies: absolute and relative quantitation. Owing to the inherent defects mentioned above, an analyte's intensity or peak area

in a spectrum is alone not a reliable indicator of the amount of the analyte in the sample. To determine the absolute amount of a neuropeptide in a sample, internal standards, either a homologue or a stable isotope-labeled target peptide, must be included. The abundance of the target peptide is compared with that of the internal standard and back calculated to the initial concentration of the standard using a predetermined standard curve. Initial homologous internal standards suffered from different hydrophobicity, LC elution profiles, and ionization efficiency, resulting in inaccurate quantitation.[1, 69, 70] Subsequent stable isotope-labeled internal standards were introduced for target peptide quantification to improve measurement accuracy and precision. For example, Desiderio & Kai used an O^{18} stable isotope-labeled internal standard of methionine enkephalin and leucine enkephalin to quantify targetpeptides in canine thalamus extract.[71] In this study, both the stable isotope-labeled internal standards and endogenous neuropeptides have indistinguishable physicochemical.[71] Thus, the neuropeptides coeluted and were analyzed simultaneously by MS, thereby avoiding inaccuracy caused by different hydrophobicity effects. Subsequent studies used a selected-reaction monitoring approach to evaluate the amount of methionine-enkephalin and of a larger neuropeptide, β-endorphin, in human pituitaries down to picomolar levels.[72-74] With this approach as the foundation, Gerber *et al.* later developed the absolute quantification of proteins.[75] In recent years, this method has been modified and applied to measure concentrations of multiple neuropeptides in different chemical environments. Kheterpal *et al.* employed stable isotopes ^{13}C and ^{15}N on the leucine residue to generate a standard curve for MIF-1 (Pro-Leu-Gly-NH_2), which has potent therapeutic effects in depression and Parkinson's disease, thereby facilitating measurement of its actual concentration in the mouse brain.[76]

Relative Quantitation

In contrast to absolute quantitation, relative quantitation experiments do not provide information about the actual amount of a specific neuropeptide within a sample. Rather, relative quantitation experiments aim to compare the fold change of neuropeptides between multiple samples/treatments and then yield a ratio or relative change. This approach can be broken down into two main categories based on whether the underlying methodology uses a chemical label to modify neuropeptides within a sample: label-free and labeling approaches.

Label-Free Quantitation

Label-free quantitative approaches rely on the comparison of different features between independent LC-MS and LC-MS/MS measurements. As such, reproducible chromatograms are key to providing accurate results. These approaches have drawn more attention during the past few years because label-based approaches always cost more and require additional sample preparation steps. Two widely used label-free quantitative methods are spectral counting and peptide peak-intensity/area measurement.

Spectral counting has its roots in bottom-up proteomic experiments and is based on the observation that more abundant proteins have a greater chance or higher frequency to be sampled in tandem MS scans than do low-abundance proteins (**Figure 3a**).[77] In neuropeptide applications, relative quantitation by spectral counting compares the number of identifications of the same peptide between different samples. Using spectral counting, Southey *et al.* investigated the roles of proprotein convertase subtilisin/kexin type 1 inhibitor peptides and other peptides associated with feeding behavior in the suprachiasmatic nucleus.[18] However, in spectral counting, if peptides are to be identified and thus quantified, they must trigger MS/MS acquisition. Thus, while spectral counting works better for highly abundant neuropeptide samples where MS/MS events are readily triggered, this method is less reliable when peptides are present in trace

amounts.[78] Estimated ratios can be significantly suppressed, and low-abundance neuropeptides may be left unquantified. Spectral counting is also less sensitive toward small-fold changes (<2 orders of magnitude).[79] Finally, each neuropeptide elutes at a single time point for MS/MS fragmentation, reducing the sampling depth. As a result, spectral counting is less than ideal for neuropeptide quantitation.

An alternative label-free approach to spectral counting is peak-intensity/area measurement, which is illustrated in **Figure 3b**. This technique measures and compares the chromatographic peak areas of peptide precursor ions from different runs. The theory behind this strategy is that the peak intensity/area of ions after detection correlates with ion concentrations within a sample. Lee *et al.* used such an approach to study the circadian rhythms system of rat suprachiasmatic nucleus and found ten endogenous peptides that showed differences between day and night.[80]

Although peak-intensity measurement seems conceptually straightforward, its use requires caution during data processing to ensure reproducible and accurate detection and quantitation between individual sample runs. Concerns may arise when coeluting peptides in a complex mixture having similar *m*/*z* values that are overlapped with peptides of interest, especially when using low-resolution MS instruments.[81, 82] In such cases, complication of the extracted ion chromatogram and, therefore, quantitation accuracy occurs. Variation in peak intensities, retention times, and *m*/*z* values of the same peptide between technical replicates should also be appropriately normalized. Therefore, this label-free technique necessitates computational processing to take into account all these factors. Myriad software solutions for label-free experiments, most of which are designed for proteomic studies, are currently available on the market.[83-86] Total ion current normalization as well as normalization to internal standards

(*e.g.*, bovine serum albumin (BSA) peptides) are two widely accepted and simple approaches.[3, 87-89] Several statistical, mathematical methods have been evaluated on endogenous peptide samples.[90, 91] Kultima *et al* concluded that their novel method, linear regression followed by analysis order normalization (RegrRun), was superior to all the other nine methods compared.[91] Compared to the raw data collected from three different species, RegrRun decreased the median standard deviation by 42–43% between replicates on average, whereas other methods only reduced the median standard deviation by 15–28%. Later on, this approach was employed to investigate the effect of cyanobacterial toxin β-N-methylamino-l-alanine on neurodegenerative disease and several proteins and peptides were revealed to have does-dependent responses.[92]

Labeling Quantitation

Stable isotopic labeling strategies allow simultaneous comparison of multiple samples by introducing a mass difference tag to the peptide. The technique usually makes use of stable heavy isotopes of ^{13}C, ^{15}N, ^{18}O, and ^{2}H. Labeling reagents with heavy or light isotopes introduce a mass shift into different samples, and by comparing intensities of mass-shifted peaks within the same spectrum, relative peptide ratios can be visualized. Mass defect, which exploits the differences between nominal mass and exact mass of peptides, is continually used in quantitative proteomic applications, although neuropeptide-compatible approaches are currently in development.[93] Overall, the combination of these effects is a powerful way to increase the analytical throughput of quantitation via multiplexing. Experimentally, stable isotope labels can be introduced metabolically or chemically.

Metabolic Labeling

Metabolic labeling incorporates isotopes into peptides during cell growth and duplication by feeding organisms with a special isotope-enriched medium.[94, 95] Ong *et al.* improved the

metabolic labeling approach by inventing stable isotope labeling by amino acids in cell culture (SILAC).[96] SILAC takes advantage of the fact that organisms have to incorporate essential amino acids from the environment for protein synthesis. By providing heavy- or light-labeled essential amino acids in the growth media, usually arginine or lysine, SILAC introduces mass difference tags into target organisms, ideally with a 100% incorporation efficiency after a few generations. Subsequent pooling of differently labeled samples will help avoid errors from sample preparations. Enzymatic digestion using trypsin produces peptides that contain at least one arginine or lysine residue at a peptide's C terminus, allowing the peptides to be quantified. Multiple proteomic studies have employed SILAC,[97-99] whereas hardly any neuropeptide work has been reported. Although metabolic labeling of whole animals is a powerful tool, it is both expensive and limited to animals that can be raised in the lab. In addition, the global incorporation of isotopic elements into an animal may lead to different phenotypes. Many groups have already utilized SILAC for global protein quantification in both plants and animals, and this powerful tool could be useful for future neuropeptidomic investigations.[100-102]

Chemical Labeling

Relative quantitation via chemical labeling relies on chemical reactions between a labeling reagent and a peptide target to produce a certain mass shift into different biological samples. This can be seen in either the precursor spectrum (mass-difference approaches, *e.g.*, dimethyl labeling) or the product ion fragmentation spectrum [isobaric reagents, *e.g.*, isobaric tags for relative and absolute quantification (iTRAQ), tandem mass tag (TMT), N, N-dimethyl leucine (DiLeu)].

Several chemical labeling strategies have been successfully applied to MS1 neuropeptide quantitation in recent years. Common labeling approaches include succinic anhydride, 4-

trimethylammoniumbutyryl (TMAB), and dimethyl labeling, in which primary amines of N termini and ε amino groups of lysine residues are chemically derivatized. Duplex succinic anhydride tags with a 4-Da mass difference facilitated the quantification of approximately 50% of known bee brain neuropeptides in the context of foraging. Eight neuropeptides show robust and dynamic regulation during foraging procedure or with different foraging preferences.[103]

Developed by Regnier's group, TMAB labels contain a quaternary amine labeled with methyl groups that impart a permanent positive charge on the peptide.[104] Originally, only two forms were synthesized (*e.g.*, a heavy form containing nine ^{2}H and a light form without ^{2}H). However, two additional forms containing three and six ^{2}H were later synthesized and tested.[105] This scheme features several advantages (low cost, simple synthesis, and labels that differ by 3 Da or more) and eliminates the major limitation of other isotopic labeling reagents (*e.g.*, labeled peptides do not coelute on high-performance LC). This labeling technique has been utilized in a large variety of neuropeptide studies that required more than duplex tags to label all samples.[15, 106, 107] A drawback of this labeling scheme is that the quaternary amine causes the label to be unstable in many different MS applications.[105]

Isotopic formaldehyde labeling is one of the first chemical labeling approaches used for neuropeptide quantitation. This labeling scheme adds two methyl groups to any primary amine in the peptide (*e.g.*, N terminus or lysine ε amino group). By labeling neuropeptides with light or heavy formaldehyde (CH_2O or CD_2O), a 28-Da or 32-Da mass shift, respectively, will be generated. The 4-Da mass difference between light- and heavy-labeled peptides allows for direct comparison of the same peptide from different samples.[108-110] Later, Boersema *et al.* modified this protocol and successfully introduced triplex formaldehyde reagents (CH_2O, CD_2O, and

$^{13}CD_2O$), although this increase in multiplexing comes at the cost of increased spectral complexity at the MS1 level.[111]

Researchers can also generate chemical labeling reagents that allow for highly multiplexed quantification to be performed in product ion MS/MS scans. Tandem MS-level techniques enable simultaneous quantitation and peptide sequencing from a single MS/MS spectrum and allow increased multiplexing without increased mass spectral complexity. Isobaric mass tags, such as TMT, iTRAQ, and DiLeu, allow for multiplexed comparison of samples in parallel (**Figure 4**).[112-116] These MS/MS isobaric tags are composed of an amine-reactive group, a mass balance group, and a reporter group. The mass balance group counterbalances the mass difference possessed by the reporter group, which ensures that peptides labeled with different reporter ion channels are detected as a single precursors in the parent scan. Upon MS/MS fragmentation, distinct reporter ions unique to each labeled sample are observed in the low *m*/*z* region. By comparing reporter ion intensities within the same MS/MS spectra, peptides from different samples can be compared within a single LC run. iTRAQ reagents have been used for peptidomic analysis of the effect of prolyl oligopeptidase inhibition in the rat brain.[117] With reduced cost per experiment, DiLeu reagents developed by our group display comparable, if not better, performance compared with that of iTRAQ.[115] Recently, DiLeu was used in a study of the neuropeptidomic expression changes in a major neuronal ganglion at multiple developmental stages of the lobster *Homarus americanus*.[118]

Distribution Analysis by MS Imaging

Although focus has been placed on the chemical identity of neuropeptides, spatial localization can provide important information for understanding functionality, delivering a

powerful tool for scientists. Many methods, such as staining or isolation of a neuroendocrine structure, exist, but they can be cumbersome and require antibodies or selective probes. First introduced by Caprioli *et al.*, MS imaging has been applied to several different tissue types and various molecular sizes over the past several years.[119, 120] These data presentations vary from peptide profiling to several clinical applications.[89, 121] In a MS imaging experiment, mass spectra are collected via a predefined grid along an x-y coordinate system on the tissue. Once ions are collected from each position, their intensities can be assigned according to the grid created, and a heat-map display can be generated for every compound detected, producing hundreds of two-dimensional images displaying the spatial localization of any detected ions of interest. Because MS imaging is not highly quantitative, applications and bioinformatics tools, such as Quantinetix and other novel in-house software, are in development to offer quantitative analysis of the MS imaging data.[122]

Special Consideration for MS Imaging

Several MS imaging methods have been established, although their usage depends on the type of analyte and resolution required. Secondary-ion mass spectrometry provides cellular-level resolution of submicrons but is typically limited to the ionization of small-molecule compounds such as lipids and other metabolites.[123] Nanostructure-initiator mass spectrometry, a matrix-free method that performs well when working with low mass-to-charge (*m*/*z*) species such as lipids, is not optimal in imaging neuropeptides.[124] Our group and others showed that MALDI has enabled the study of large biological peptides and proteins, making it a popular choice for neuropeptides.[120, 123, 125-127]

Special sample preparation steps must be taken to preserve the tissue and prevent degradation prior to analysis (for a recent summary, see [123]). These strategies have allowed for

the characterization of a range of peptides and have been successfully applied to studies requiring single-cell resolution.[128, 129] Three-dimensional tissue imaging has also been achieved by analyzing consecutive slices of a two-dimensional tissue and in silico combining the images to show the distribution along a three-dimensional z-axis (**Figure 5**).[130]

Mass and Space

Three areas of MS imaging have undergone major development: mass resolution, mass range, and spatial resolution. With the development of MALDI-FTMS (Fourier-transform mass spectrometer) instrumentation, such as the MALDI-FTICR (Fourier-transform ion cyclotron resonance) and Orbitrap technologies, high-resolution accurate mass measurements are achievable. For the American cockroach, the hybrid MALDI-LTQ-Orbitrap XL mass spectrometer provides both high mass accuracy and high mass resolving power of neuropeptides directly from tissue slices.[131] Unfortunately, the cost of high-resolution "ion-trap-based" technologies limits the upper mass range to approximately *m*/*z* 4,000. Thus, methods to increase the mass range of these instruments have been an important area of development.[36-41, 132] High *m*/*z* tissue imaging is challenging even for time-of-flight (TOF) instruments, which have a theoretically infinite mass range. Several groups have developed specialized sample preparation techniques, equipment, and matrices to increase the mass range of detectable ions in TOF instruments.[133-135] Mainini *et al.* successfully detected proteins up to 135 kDa using ferulic acid as a MALDI matrix.[135]

As stated previously, MALDI is well-known for primarily producing only singly charged ions. However, several recent studies reported on the production of multiply charged ions on commercially available MALDI instruments by laserspray ionization, matrix-assisted inlet ionization, or matrix-assisted ionization vacuum.[36, 38-40] By creating multiply charged ions, more

efficient tandem MS fragmentation can be achieved when using ETD or CID. Using an intermediate pressure MALDI source with laserspray ionization, the Trimpin group showed the measurement of +12 ubiquitin ions (8.5 kDa).[36] Although MS imaging is used primarily as a top-down approach, in situ digestion on tissue slices has emerged as another strategy to bring larger neuropeptides into the appropriate mass range of a mass analyzer.[136] Instead of directly imaging intact neuropeptides, a bottom-up approach is taken, and the enzymatically digested peptide fragments are visualized and colocalized on the tissue slice. With the appropriate bioinformatics tools (*e.g.*, PEAKS; for more examples, see above), the corresponding large neuropeptides may then be identified. Many factors including the choice of the enzyme, matrix, and instrumentation need to be considered when optimizing in situ digestion (for quality reviews, see [136, 137]). Notably, researchers have developed a novel graphene-immobilized trypsin platform for on-tissue digestion that provides more complete sequence coverage compared with on-plate digestion of BSA (77% versus 30%).[138] With the development of high-resolution and accurate mass measurements, MS/MS and/or orthogonal ESI-MS experiments have successfully imaged and identified larger neuropeptides and neuroproteins.[139, 140]

MS imaging data relevance depends on the pixel size acquired, which is directly related to the spatial resolution achievable by the experimental setup.[125, 141] Spatial resolution is chosen by the step size the plate takes to raster the laser across the tissue, which is primarily defined by the diameter of the laser beam. To increase spatial resolution, investigators have developed several approaches, such as traditional "microprobe" mode, "microscope" mode, oversampling, and parafilm stretching, all of which are summarized elsewhere.[129, 142] Recently, the Spengler lab developed a home-built MALDI source paired to the LTQ-Orbitrap that allows for step sizes down to 5 μm.[143] These developments allowed for high-resolution imaging of neuropeptides

such as oxytocin and vasopressin in the mouse pituitary gland.[143] As spatial resolution continues to improve, single-cell imaging will become more accessible for researchers. Both cell cultures and dissected cells have been used, although special consideration must be made to create the images.[128, 129, 144] For example, cells in culture have been stretched prior to placing them on slides and analyzed by MALDI-TOF/TOF, which allowed for the spatial mapping of several ions.[129] These methods will become more refined, and efforts will be extended toward subcellular analysis.

Specialized Applications: Coupling Separations to Mass Spectrometry Imaging

Neuropeptide MS imaging has also been used in applications outside of tissue slices, specifically CE fractionation or LC separation.[45, 46, 145] Normally, distinct fractions are deposited on MALDI plates as individual spots and analyzed by MS.[146, 147] This approach can cause a decrease in separation resolution. To preserve temporal resolution, the separated mixture may be continuously deposited across the MALDI plate surface. Although time-consuming, manual profiling of this continuous trace can be performed. However, MS imaging enables simplified analysis of the column eluent. MS imaging has been coupled to both CE-MALDI and LC-MALDI workflows, thus allowing for high-temporal resolution separation of neuropeptides.[45, 46, 145] CE-MS imaging has led to a four- to sixfold increase in peptide coverage.[45] By separating isotopic formaldehyde labeled neuropeptides from a complex mixture of crustacean pericardial organ extract, quantitative information can also be obtained with CE-MS imaging (**Figure 6**).[45] With the development of new columns or separation strategies, these successful analysis strategies will be applied to other neuropeptide-rich media, such as microdialysates.

Concluding Remarks

As technologies and methodologies are further developed, additional neuropeptides will be discovered and interrogated using a variety of workflows. Although generally well-developed, MS-based neuropeptide studies still have many areas that need elaboration, especially for low-volume samples. Both qualitative and quantitative characterization strategies have been developed, allowing important biological questions to be answered. The amount of data acquired from a single MS run has only increased, and the bioinformatics tools available will continue to mature to meet these needs. As future technologies enhance the information acquired, we expect to see an expansion of the use of MS for neuropeptidomic analysis.

Summary Points

1. With its ability to provide maximum information from very small sample volumes, MS has become a powerful tool for the characterization of the neuropeptidome. As instrumentation advances along with innovative sampling strategies, MS-based tools will continue to find widespread utilities in different animal systems.
2. It is clear that not one platform can provide simultaneous chemical, spatial, and temporal information. Thus, the development of tools for better in vivo measurements, MS imaging, and peptide sequencing should be coupled with new separation or sample preparation steps within new multifaceted approaches.
3. Owing to its high-throughput nature, MS has led to the growth of new characterization techniques and bioinformatics tools. Commercially available instrumentation and downloadable bioinformatics tools make data processing more efficient and much simpler. Yet, new methods will be created.

4. High-resolution instrumentation has provided new depth toneuropeptide characterization. Further improvements are surely in development, and new tools (*e.g.*, isobaric quantitative tags that are constructed using subtle mass defects) will be established to utilize their power.

Future Issues

1. Although several resources have been established for the quantitation of neuropeptides, the number and availability of such are stunted in comparison to proteomic studies. Nevertheless, further development of cost-effective, multiplexed reagents will be key to allow cross comparisons in high throughput. With the ability to multiplex, absolute quantification using same-run calibration curves will facilitate targeted neuropeptide investigations.
2. Although MS imaging has become a popular tool exploring the spatial distribution of neuropeptides, it still requires further method advancement to better measure neuropeptides. In situ digestion and multiply charged ion production methods are still in their infancy, and focus should be on maturing their use for larger neuropeptides. Furthermore, increasing spatial resolution to visualize subcellular peptide distributions will require innovation in instrumentation and sampling strategies.
3. Although there are hopes of applying MS to more complex systems (*i.e.*, humans), work with MS as a whole is limited to well-characterized model organisms. The global progression of all MS preparatory steps must continue to answer any new and interesting questions related to neuropeptide research in these more complex situations.

Acknowledgements

Preparation of this article is supported in part by the National Science Foundation (CHE-1413596) and National Institutes of Health through grant 1R01DK071801. L.L. acknowledges an H.I. Romnes Faculty Fellowship. The authors thank Dustin Frost in the Li Research Group for assistance in manuscript editing and figure creation.

Disclosure Statement

The authors are not aware of any affiliations, memberships, funding, or financial holdings that might be perceived as affecting the objectivity of this review.

References

1. Li, L. J.; Sweedler, J. V., Peptides in the Brain: Mass Spectrometry-Based Measurement Approaches and Challenges. In *Annual Review of Analytical Chemistry*, Annual Reviews: Palo Alto, 2008; Vol. 1, pp 451-483.

2. Hokfelt, T.; Broberger, C.; Xu, Z. Q. D.; Sergeyev, V.; Ubink, R.; Diez, M., *Neuropharmacology* **2000,** *39* (8), 1337-1356.

3. Frese, C. K.; Boender, A. J.; Mohammed, S.; Heck, A. J. R.; Adan, R. A. H.; Altelaar, A. F. M., *Analytical Chemistry* **2013,** *85* (9), 4594-4604.

4. Morimoto, R.; Satoh, F.; Murakami, O.; Totsune, K.; Saruta, M.; Suzuki, T.; Sasano, H.; Ito, S.; Takahashi, K., *Nutrition* **2008,** *24* (9), 878-884.

5. Van Eeckhaut, A.; Maes, K.; Aourz, N.; Smolders, I.; Michotte, Y., *Bioanalysis* **2011,** *3* (11), 1271-1285.

6. von Bohlen und Halbach, O., *Current Protein & Peptide Science* **2005,** *6* (4), 355-371.

7. Yu, Q.; OuYang, C.; Liang, Z.; Li, L., *EuPA Open Proteomics* **2014,** *3* (0), 152-170.

8. Schmerberg, C. M.; Li, L. J., *Analytical Chemistry* **2013,** *85* (2), 915-922.

9. Yew, J. Y.; Kutz, K. K.; Dikler, S.; Messinger, L.; Li, L. J.; Stretton, A. O., *Journal of Comparative Neurology* **2005,** *488* (4), 396-413.

10. Bruzzone, F.; Lectez, B.; Tollemer, H.; Leprince, J.; Dujardin, C.; Rachidi, W.; Chatenet, D.; Baroncini, M.; Beauvillain, J. C.; Vallarino, M.; Vaudry, H.; Chartrel, N., *Journal of Neurochemistry* **2006,** *99* (2), 616-627.

11. Jarecki, J. L.; Viola, I. R.; Andersen, K. M.; Miller, A. H.; Ramaker, M. A.; Vestling, M. M.; Stretton, A. O., *Acs Chemical Neuroscience* **2013,** *4* (3), 418-434.

12. Hui, L. M.; Xiang, F.; Zhang, Y. Z.; Li, L. J., *Peptides* **2012,** *36* (2), 230-239.

13. Dowell, J. A.; Vander Heyden, W.; Li, L., *Journal of Proteome Research* **2006,** *5* (12), 3368-3375.

14. Hui, L. M.; D'Andrea, B. T.; Jia, C. X.; Liang, Z. D.; Christie, A. E.; Li, L. J., *General and Comparative Endocrinology* **2013,** *184*, 22-34.

15. Castro, L. M.; Cavalcanti, D. M.; Araujo, C. B.; Rioli, V.; Icimoto, M. Y.; Gozzo, F. C.; Juliano, M.; Juliano, L.; Oliveira, V.; Ferro, E. S., *J Proteomics* **2014**.

16. Predel, R.; Neupert, S.; Garczynski, S. F.; Crim, J. W.; Brown, M. R.; Russell, W. K.; Kahnt, J.; Russell, D. H.; Nachman, R. J., *Journal of Proteome Research* **2010,** *9* (4), 2006-2015.

17. Xie, F.; Romanova, E. V.; Sweedler, J. V., Neuropeptidomics of the Mammalian Brain. In *Neuroproteomics*, Li, K. W., Ed. Humana Press Inc: Totowa, 2011; Vol. 57, pp 229-242.

18. Southey, B. R.; Lee, J. E.; Zamdborg, L.; Atkins, N., Jr.; Mitchell, J. W.; Li, M.; Gillette, M. U.; Kelleher, N. L.; Sweedler, J. V., *Anal Chem* **2014,** *86* (1), 443-52.

19. Che, F. Y.; Biswas, R.; Fricker, L. D., *Journal of Mass Spectrometry* **2005,** *40* (2), 227-237.

20. Parkin, M. C.; Wei, H.; O'Callaghan, J. P.; Kennedy, R. T., *Analytical Chemistry* **2005,** *77* (19), 6331-6338.

21. Colgrave, M. L.; Xi, L.; Lehnert, S. A.; Flatscher-Bader, T.; Wadensten, H.; Nilsson, A.; Andren, P. E.; Wijffels, G., *Proteomics* **2011,** *11* (7), 1264-1276.

22. Stingl, C.; Soderquist, M.; Karlsson, O.; Boren, M.; Luider, T. M., *Journal of Proteome Research* **2014,** *13* (6), 2807-2817.

23. Sturm, R. M.; Greer, T.; Woodards, N.; Gemperline, E.; Li, L. J., *Journal of Proteome Research* **2013,** *12* (2), 743-752.

24. Zhang, X. Z.; Petruzziello, F.; Zani, F.; Fouillen, L.; Andren, P. E.; Solinas, G.; Rainer, G., *Journal of Proteome Research* **2012,** *11* (5), 2819-2827.

25. Bai, L.; Romanova, E. V.; Sweedler, J. V., *Analytical Chemistry* **2011,** *83* (7), 2794-2800.

26. Neupert, S.; Predel, R., Peptidomic Analysis of Single Identified Neurons. In *Peptidomics: Methods and Protocols*, Soloviev, M., Ed. Humana Press Inc: Totowa, 2010; Vol. 615, pp 137-144.

27. Neupert, S.; Rubakhin, S. S.; Sweedler, J. V., *Chemistry & Biology* **2012,** *19* (8), 1010-1019.

28. Neupert, S.; Fusca, D.; Schachtner, J.; Kloppenburg, P.; Predel, R., *Journal of Comparative Neurology* **2012,** *520* (4), 694-716.

29. Rubakhin, S. S.; Sweedler, J. V., *Analytical Chemistry* **2008,** *80* (18), 7128-7136.

30. Romanova, E. V.; Aerts, J. T.; Croushore, C. A.; Sweedler, J. V., *Neuropsychopharmacology* **2014,** *39* (1), 50-64.

31. Torregrossa, M. M.; Kalivas, P. W., *Pharmacology Biochemistry and Behavior* **2008,** *90* (2), 261-272.

32. Mabrouk, O. S.; Kennedy, R. T., *Journal of Neuroscience Methods* **2012,** *209* (1), 127-133.

33. Li, Q.; Zubieta, J. K.; Kennedy, R. T., *Analytical Chemistry* **2009,** *81* (6), 2242-2250.

34. Behrens, H. L.; Li, L. J., Monitoring Neuropeptides In Vivo via Microdialysis and Mass Spectrometry. In *Peptidomics: Methods and Protocols*, Soloviev, M., Ed. Humana Press Inc: Totowa, 2010; Vol. 615, pp 57-73.

35. Zhou, Y.; Mabrouk, O. S.; Kennedy, R. T., *Journal of the American Society for Mass Spectrometry* **2013,** *24* (11), 1700-1709.

36. Inutan, E. D.; Wang, B. X.; Trimpin, S., *Analytical Chemistry* **2011,** *83* (3), 678-684.

37. McEwen, C. N.; Larsen, B. S.; Trimpin, S., *Analytical Chemistry* **2010,** *82* (12), 4998-5001.

38. Trimpin, S.; Inutan, E. D.; Herath, T. N.; McEwen, C. N., *Molecular & Cellular Proteomics* **2010,** *9* (2), 362-367.

39. Li, J.; Inutan, E. D.; Wang, B. X.; Lietz, C. B.; Green, D. R.; Manly, C. D.; Richards, A. L.; Marshall, D. D.; Lingenfelter, S.; Ren, Y.; Trimpin, S., *Journal of the American Society for Mass Spectrometry* **2012,** *23* (10), 1625-1643.

40. Trimpin, S.; Inutan, E. D., *Journal of the American Society for Mass Spectrometry* **2013,** *24* (5), 722-732.

41. Trimpin, S.; Inutan, E. D.; Herath, T. N.; McEwen, C. N., *Analytical Chemistry* **2010,** *82* (1), 11-15.

42. Ma, M. M.; Sturm, R. M.; Kutz-Naber, K. K.; Fu, Q.; Li, L. J., *Biochemical and Biophysical Research Communications* **2009,** *390* (2), 325-330.

43. Dowell, J. A.; Frost, D. C.; Zhang, J.; Li, L. J., *Analytical Chemistry* **2008,** *80* (17), 6715-6723.

44. Zhang, G. D.; Zhang, Y. Z.; Fast, D. M.; Lin, Z. S.; Steenwyk, R., *Analytical Biochemistry* **2011,** *416* (1), 45-52.

45. Zhang, Z. C.; Ye, H.; Wang, J. H.; Hui, L. M.; Li, L. J., *Analytical Chemistry* **2012,** *84* (18), 7684-7691.

46. Wang, J. H.; Ye, H.; Zhang, Z. C.; Xiang, F.; Girdaukas, G.; Li, L. J., *Analytical Chemistry* **2011,** *83* (9), 3462-3469.

47. Zhong, X. F.; Zhang, Z. C.; Jiang, S.; Li, L. J., *Electrophoresis* **2014,** *35* (9), 1214-1225.

48. Medina-Casanellas, S.; Dominguez-Vega, E.; Benavente, F.; Sanz-Nebot, V.; Somsen, G. W.; de Jong, G. J., *Journal of Chromatography A* **2014,** *1328*, 1-6.

49. Soper, M. T.; DeToma, A. S.; Hyung, S. J.; Lim, M. H.; Ruotolo, B. T., *Physical Chemistry Chemical Physics* **2013,** *15* (23), 8952-8961.

50. Jia, C. X.; Wu, Z.; Lietz, C. B.; Liang, Z. D.; Cui, Q.; Li, L. J., *Analytical Chemistry* **2014,** *86* (6), 2917-2924.

51. Shvartsburg, A. A.; Creese, A. J.; Smith, R. D.; Cooper, H. J., *Analytical Chemistry* **2010,** *82* (19), 8327-8334.

52. Jia, C. X.; Lietz, C. B.; Yu, Q.; Li, L. J., *Analytical Chemistry* **2014,** *86* (6), 2972-2981.

53. Kanu, A. B.; Dwivedi, P.; Tam, M.; Matz, L.; Hill, H. H., *Journal of Mass Spectrometry* **2008,** *43* (1), 1-22.

54. A Shvartsburg, A.; A Anderson, G.; D Smith, R., *Mass spectrometry (Tokyo, Japan)* **2013,** *2* (Spec Iss), S0011.

55. Hayakawa, E.; Menschaert, G.; De Bock, P. J.; Luyten, W.; Gevaert, K.; Baggerman, G.; Schoofs, L., *Journal of Proteome Research* **2013,** *12* (12), 5410-5421.

56. Yew, J. Y.; Dikler, S.; Stretton, A. O., *Rapid Communications in Mass Spectrometry* **2003,** *17* (24), 2693-2698.

57. Ma, M. M.; Kutz-Naber, K. K.; Li, L. J., *Analytical Chemistry* **2007,** *79* (2), 673-681.

58. Fu, Q.; Li, L. J., *Analytical Chemistry* **2005,** *77* (23), 7783-7795.

59. Jia, C. X.; Lietz, C. B.; Ye, H.; Hui, L. M.; Yu, Q.; Yoo, S.; Li, L. J., *Journal of Proteomics* **2013,** *91*, 1-12.

60. Ofer, D.; Linial, M., *Bioinformatics* **2014,** *30* (7), 931-940.

61. Southey, B. R.; Amare, A.; Zimmerman, T. A.; Rodriguez-Zas, S. L.; Sweedler, J. V., *Nucleic Acids Research* **2006,** *34*, W267-W272.

62. Falth, M.; Skold, K.; Norrman, M.; Svensson, M.; Fenyo, D.; Andren, P. E., *Molecular & Cellular Proteomics* **2006,** *5* (6), 998-1005.

63. Kim, Y.; Bark, S.; Hook, V.; Bandeira, N., *Bioinformatics* **2011,** *27* (19), 2772-2773.

64. Ma, B.; Zhang, K. Z.; Hendrie, C.; Liang, C. Z.; Li, M.; Doherty-Kirby, A.; Lajoie, G., *Rapid Communications in Mass Spectrometry* **2003,** *17* (20), 2337-2342.

65. Baggerman, G.; Liu, F.; Wets, G.; Schoofs, L., *Trends in Comparative Endocrinology and Neurobiology* **2005,** *1040*, 59-65.

66. Clynen, E.; Liu, F.; Husson, S. J.; Landuyt, B.; Hayakawa, E.; Baggerman, G.; Wets, G.; Schoofs, L., Bioinformatic Approaches to the Identification of Novel Neuropeptide Precursors. In *Peptidomics: Methods and Protocols*, Soloviev, M., Ed. Humana Press Inc: Totowa, 2010; Vol. 615, pp 357-374.

67. Southey, B. R.; Rodriguez-Zas, S. L.; Sweedler, J. V., *Bmc Genomics* **2009,** *10*, 11.

68. Falth, M.; Svensson, M.; Nilsson, A.; Skold, K.; Fenyo, D.; Andren, P. E., *Journal of Proteome Research* **2008,** *7* (7), 3049-3053.

69. Desiderio, D. M.; Yamada, S.; Tanzer, F. S.; Horton, J.; Trimble, J., *J Chromatogr* **1981,** *217*, 437-52.

70. Kosanam, H.; Ramagiri, S.; Dass, C., *Anal Biochem* **2009,** *392* (1), 83-9.

71. Desiderio, D. M.; Kai, M., *Biomed Mass Spectrom* **1983,** *10* (8), 471-9.

72. Kusmierz, J. J.; Sumrada, R.; Desiderio, D. M., *Anal Chem* **1990,** *62* (21), 2395-400.

73. Dass, C.; Kusmierz, J. J.; Desiderio, D. M., *Biol Mass Spectrom* **1991,** *20* (3), 130-8.

74. Desiderio, D. M.; Zhu, X., *J Chromatogr A* **1998,** *794* (1-2), 85-96.

75. Gerber, S. A.; Rush, J.; Stemman, O.; Kirschner, M. W.; Gygi, S. P., *Proceedings of the National Academy of Sciences of the United States of America* **2003,** *100* (12), 6940-6945.

76. Kheterpal, I.; Kastin, A. J.; Mollah, S.; Yu, C.; Hsuchou, H.; Pan, W., *Peptides* **2009,** *30* (7), 1276-81.

77. Liu, H. B.; Sadygov, R. G.; Yates, J. R., *Analytical Chemistry* **2004,** *76* (14), 4193-4201.

78. Wasinger, V. C.; Zeng, M.; Yau, Y., *Int J Proteomics* **2013,** *2013*, 180605.

79. Old, W. M.; Meyer-Arendt, K.; Aveline-Wolf, L.; Pierce, K. G.; Mendoza, A.; Sevinsky, J. R.; Resing, K. A.; Ahn, N. G., *Mol Cell Proteomics* **2005,** *4* (10), 1487-502.

80. Lee, J. E.; Zamdborg, L.; Southey, B. R.; Atkins, N., Jr.; Mitchell, J. W.; Li, M.; Gillette, M. U.; Kelleher, N. L.; Sweedler, J. V., *J Proteome Res* **2013,** *12* (2), 585-93.

81. Neilson, K. A.; Ali, N. A.; Muralidharan, S.; Mirzaei, M.; Mariani, M.; Assadourian, G.; Lee, A.; van Sluyter, S. C.; Haynes, P. A., *Proteomics* **2011,** *11* (4), 535-553.

82. Nahnsen, S.; Bielow, C.; Reinert, K.; Kohlbacher, O., *Molecular & Cellular Proteomics* **2013,** *12* (3), 549-556.

83. Rudnick, P. A.; Wang, X.; Yan, X.; Sedransk, N.; Stein, S. E., *Mol Cell Proteomics* **2014,** *13* (5), 1341-51.

84. Weisser, H.; Nahnsen, S.; Grossmann, J.; Nilse, L.; Quandt, A.; Brauer, H.; Sturm, M.; Kenar, E.; Kohlbacher, O.; Aebersold, R.; Malmstrom, L., *J Proteome Res* **2013,** *12* (4), 1628-44.

85. Wong, J. W.; Cagney, G., *Methods Mol Biol* **2010,** *604*, 273-83.

86. Listgarten, J.; Emili, A., *Molecular & Cellular Proteomics* **2005,** *4* (4), 419-434.

87. Fouillen, L.; Petruzziello, F.; Veit, J.; Bhattacharyya, A.; Kretz, R.; Rainer, G.; Zhang, X., *J Proteomics* **2013,** *80*, 311-9.

88. Salisbury, J. P.; Boggio, K. J.; Hsu, Y. W.; Quijada, J.; Sivachenko, A.; Gloeckner, G.; Kowalski, P. J.; Easterling, M. L.; Rosbash, M.; Agar, J. N., *Mol Brain* **2013,** *6*, 60.

89. Shariatgorji, M.; Svenningsson, P.; Andren, P. E., *Neuropsychopharmacology* **2014,** *39* (1), 34-49.

90. Callister, S. J.; Barry, R. C.; Adkins, J. N.; Johnson, E. T.; Qian, W. J.; Webb-Robertson, B. J.; Smith, R. D.; Lipton, M. S., *J Proteome Res* **2006,** *5* (2), 277-86.

91. Kultima, K.; Nilsson, A.; Scholz, B.; Rossbach, U. L.; Falth, M.; Andren, P. E., *Molecular & Cellular Proteomics* **2009,** *8* (10), 2285-2295.

92. Karlsson, O.; Kultima, K.; Wadensten, H.; Nilsson, A.; Roman, E.; Andren, P. E.; Brittebo, E. B., *J Proteome Res* **2013,** *12* (4), 1678-90.

93. Sleno, L., *Journal of Mass Spectrometry* **2012,** *47* (2), 226-236.

94. Oda, Y.; Huang, K.; Cross, F. R.; Cowburn, D.; Chait, B. T., *Proceedings of the National Academy of Sciences of the United States of America* **1999,** *96* (12), 6591-6596.

95. Krijgsveld, J.; Ketting, R. F.; Mahmoudi, T.; Johansen, J.; Artal-Sanz, M.; Verrijzer, C. P.; Plasterk, R. H.; Heck, A. J., *Nat Biotechnol* **2003,** *21* (8), 927-31.

96. Ong, S. E.; Blagoev, B.; Kratchmarova, I.; Kristensen, D. B.; Steen, H.; Pandey, A.; Mann, M., *Molecular & Cellular Proteomics* **2002,** *1* (5), 376-386.

97. Ong, S. E., *Anal Bioanal Chem* **2012,** *404* (4), 967-76.

98. Jin, L.; Huo, Y.; Zheng, Z.; Jiang, X.; Deng, H.; Chen, Y.; Lian, Q.; Ge, R.; Deng, H., *Mol Cell Proteomics* **2014**.

99. Alqahtani, A.; Heesom, K.; Bramson, J.; Curiel, D.; Ugai, H.; Matthews, D., *J Gen Virol* **2014**.

100. Lewandowska, D.; ten Have, S.; Hodge, K.; Tillemans, V.; Lamond, A. I.; Brown, J. W. S., *Plos One* **2013,** *8* (8), 8.

101. Zanivan, S.; Krueger, M.; Mann, M., In Vivo Quantitative Proteomics: The SILAC Mouse. In *Integrin and Cell Adhesion Molecules: Methods and Protocols*, Shimaoka, M., Ed. Humana Press Inc: Totowa, 2011; Vol. 757, pp 435-450.

102. Kruger, M.; Moser, M.; Ussar, S.; Thievessen, I.; Luber, C. A.; Forner, F.; Schmidt, S.; Zanivan, S.; Fassler, R.; Mann, M., *Cell* **2008,** *134* (2), 353-364.

103. Brockmann, A.; Annangudi, S. P.; Richmond, T. A.; Ament, S. A.; Xie, F.; Southey, B. R.; Rodriguez-Zas, S. R.; Robinson, G. E.; Sweedler, J. V., *Proc Natl Acad Sci U S A* **2009,** *106* (7), 2383-8.

104. Zhang, R.; Sioma, C. S.; Thompson, R. A.; Xiong, L.; Regnier, F. E., *Anal Chem* **2002,** *74* (15), 3662-9.

105. Morano, C.; Zhang, X.; Fricker, L. D., *Anal Chem* **2008,** *80* (23), 9298-309.

106. Gelman, J. S.; Sironi, J.; Castro, L. M.; Ferro, E. S.; Fricker, L. D., *Journal of Neurochemistry* **2010,** *113* (4), 871-880.

107. Che, F. Y.; Fricker, L. D., *Journal of Mass Spectrometry* **2005,** *40* (2), 238-249.

108. Hsu, J. L.; Huang, S. Y.; Chow, N. H.; Chen, S. H., *Anal Chem* **2003,** *75* (24), 6843-52.

109. Hui, L.; Zhang, Y.; Wang, J.; Cook, A.; Ye, H.; Nusbaum, M. P.; Li, L., *ACS Chem Neurosci* **2011,** *2* (12), 711-722.

110. Jia, C.; Yu, Q.; Wang, J.; Li, L., *Proteomics* **2014**.

111. Boersema, P. J.; Aye, T. T.; van Veen, T. A. B.; Heck, A. J. R.; Mohammed, S., *Proteomics* **2008,** *8* (22), 4624-4632.

112. Thompson, A.; Schafer, J.; Kuhn, K.; Kienle, S.; Schwarz, J.; Schmidt, G.; Neumann, T.; Johnstone, R.; Mohammed, A. K.; Hamon, C., *Anal Chem* **2003,** *75* (8), 1895-904.

113. Dayon, L.; Hainard, A.; Licker, V.; Turck, N.; Kuhn, K.; Hochstrasser, D. F.; Burkhard, P. R.; Sanchez, J. C., *Anal Chem* **2008,** *80* (8), 2921-31.

114. Ross, P. L.; Huang, Y. L. N.; Marchese, J. N.; Williamson, B.; Parker, K.; Hattan, S.; Khainovski, N.; Pillai, S.; Dey, S.; Daniels, S.; Purkayastha, S.; Juhasz, P.; Martin, S.; Bartlet-Jones, M.; He, F.; Jacobson, A.; Pappin, D. J., *Molecular & Cellular Proteomics* **2004,** *3* (12), 1154-1169.

115. Xiang, F.; Ye, H.; Chen, R. B.; Fu, Q.; Li, L. J., *Analytical Chemistry* **2010,** *82* (7), 2817-2825.

116. Frost, D. C.; Greer, T.; Li, L., *Analytical chemistry* **2015,** *87* (3), 1646-54.

117. Tenorio-Laranga, J.; Valero, M. L.; Mannisto, P. T.; Sanchez del Pino, M.; Garcia-Horsman, J. A., *Anal Biochem* **2009,** *393* (1), 80-7.

118. Jiang, X. Y.; Chen, R. B.; Wang, J. H.; Metzler, A.; Tlusty, M.; Li, L. J., *Acs Chemical Neuroscience* **2012,** *3* (6), 439-450.

119. Caprioli, R. M.; Farmer, T. B.; Gile, J., *Analytical Chemistry* **1997,** *69* (23), 4751-4760.

120. Chatterji, B.; Pich, A., *Expert Review of Proteomics* **2013,** *10* (4), 381-388.

121. Minerva, L.; Boonen, K.; Menschaert, G.; Landuyt, B.; Baggerman, G.; Arckens, L., *Analytical Chemistry* **2011,** *83* (20), 7682-7691.

122. Kallback, P.; Shariatgorji, M.; Nilsson, A.; Andren, P. E., *Journal of Proteomics* **2012,** *75* (16), 4941-4951.

123. Gemperline, E.; Chen, B. M.; Li, L. J., *Bioanalysis* **2014,** *6* (4), 525-540.

124. Sturm, R. M.; Greer, T.; Chen, R. B.; Hensen, B.; Li, L. J., *Analytical Methods* **2013,** *5* (6), 1623-1628.

125. Mark, L.; Maasz, G.; Pirger, Z., *Acta Biologica Hungarica* **2012,** *63*, 113-122.

126. Hanrieder, J.; Ljungdahl, A.; Andersson, M., *Journal of visualized experiments : JoVE* **2012,** (60).

127. Ye, H.; Hui, L. M.; Kellersberger, K.; Li, L. J., *Journal of the American Society for Mass Spectrometry* **2013,** *24* (1), 134-147.

128. Berman, E. S. F.; Fortson, S. L.; Kulp, K. S., Preparation of Single Cells for Imaging Mass Spectrometry. In *Mass Spectrometry Imaging: Principles and Protocols*, Rubakhin, S. S.; Sweedler, J. V., Eds. Humana Press Inc: Totowa, 2010; Vol. 656, pp 253-265.

129. Zimmerman, T. A.; Rubakhin, S. S.; Sweedler, J. V., *Journal of the American Society for Mass Spectrometry* **2011,** *22* (5), 828-836.

130. Chen, R. B.; Hui, L. M.; Sturm, R. M.; Li, L. J., *Journal of the American Society for Mass Spectrometry* **2009,** *20* (6), 1068-1077.

131. Verhaert, P.; Pinkse, M. W. H.; Strupat, K.; Conaway, M. C. P., Imaging of Similar Mass Neuropeptides in Neuronal Tissue by Enhanced Resolution MALDI MS with an Ion Trap - Orbitrap (TM) Hybrid Instrument. In *Mass Spectrometry Imaging: Principles and Protocols*, Rubakhin, S. S.; Sweedler, J. V., Eds. Humana Press Inc: Totowa, 2010; Vol. 656, pp 433-449.

132. Trimpin, S.; Ren, Y.; Wang, B. X.; Lietz, C. B.; Richards, A. L.; Marshall, D. D.; Inutan, E. D., *Analytical Chemistry* **2011,** *83* (14), 5469-5475.

133. Leinweber, B. D.; Tsaprailis, G.; Monks, T. J.; Lau, S. S., *Journal of the American Society for Mass Spectrometry* **2009,** *20* (1), 89-95.

134. van Remoortere, A.; van Zeijl, R. J. M.; van den Oever, N.; Franck, J.; Longuespee, R.; Wisztorski, M.; Salzet, M.; Deelder, A. M.; Fournier, I.; McDonnell, L. A., *Journal of the American Society for Mass Spectrometry* **2010,** *21* (11), 1922-1929.

135. Mainini, V.; Bovo, G.; Chinello, C.; Gianazza, E.; Grasso, M.; Cattoretti, G.; Magni, F., *Molecular Biosystems* **2013,** *9* (6), 1101-1107.

136. Cillero-Pastor, B.; Heeren, R. M. A., *Journal of Proteome Research* **2014,** *13* (2), 325-335.

137. Franck, J.; Arafah, K.; Barnes, A.; Wisztorski, M.; Salzet, M.; Fournier, I., *Analytical Chemistry* **2009,** *81* (19), 8193-8202.

138. Jiao, J.; Miao, A. Z.; Zhang, X. Y.; Cai, Y.; Lu, Y.; Zhang, Y.; Lu, H. J., *Analyst* **2013,** *138* (6), 1645-1648.

139. Groseclose, M. R.; Andersson, M.; Hardesty, W. M.; Caprioli, R. M., *Journal of Mass Spectrometry* **2007,** *42* (2), 254-262.

140. Schober, Y.; Schramm, T.; Spengler, B.; Rompp, A., *Rapid Communications in Mass Spectrometry* **2011,** *25* (17), 2475-2483.

141. Rompp, A.; Spengler, B., *Histochemistry and Cell Biology* **2013,** *139* (6), 759-783.

142. Ye, H.; Greer, T.; Li, L. J., *Journal of Proteomics* **2012,** *75* (16), 5014-5026.

143. Guenther, S.; Rompp, A.; Kummer, W.; Spengler, B., *International Journal of Mass Spectrometry* **2011,** *305* (2-3), 228-237.

144. Li, H. H.; Hummon, A. B., *Analytical Chemistry* **2011,** *83* (22), 8794-8801.

145. Zhang, Z. C.; Jiang, S.; Li, L. J., *Journal of Chromatography A* **2013,** *1293*, 44-50.

146. Wang, J. H.; Zhang, Y. Z.; Xiang, F.; Zhang, Z. C.; Li, L. J., *Journal of Chromatography A* **2010,** *1217* (26), 4463-4470.

147. Fan, Y.; Rubakhin, S. S.; Sweedler, J. V., *Analytical Chemistry* **2011,** *83* (24), 9557-9563.

Figures

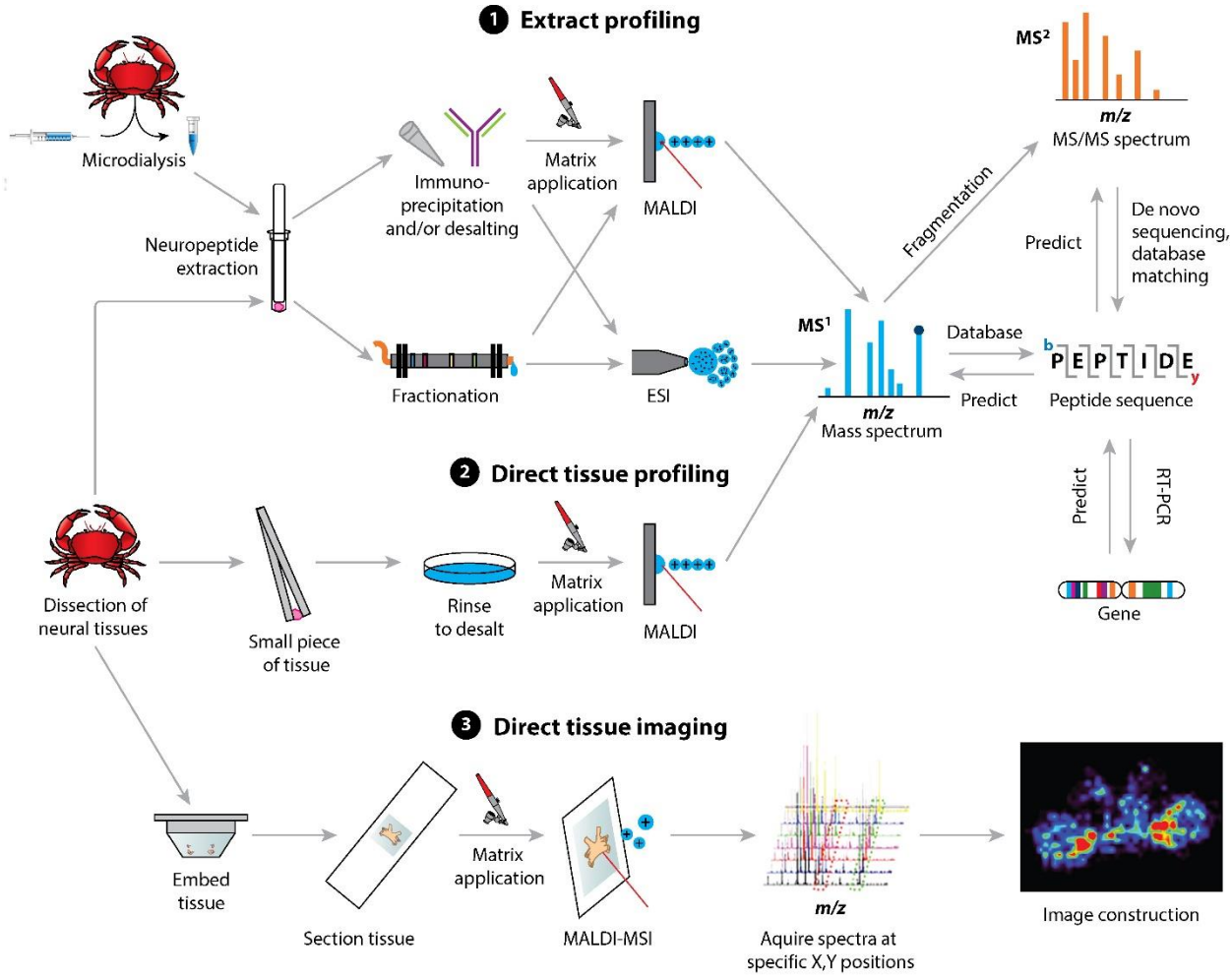

Figure 1. General overview of sample preparation and data analysis strategies for neuropeptide analysis by MS. Three major sample preparation pathways exist: (1) extract profiling, (2) direct tissue profiling, and (3) direct tissue imaging. Once spectra have been collected, peptides can be identified via database searches, de novo sequencing, and/or prediction algorithms.

Abbreviations: ESI, electrospray ionization; MALDI, matrix-assisted laser desorption/ionization; MS, mass spectrometry; MSI, MS imaging; RT-PCR, reverse-transcription polymerase chain reaction.

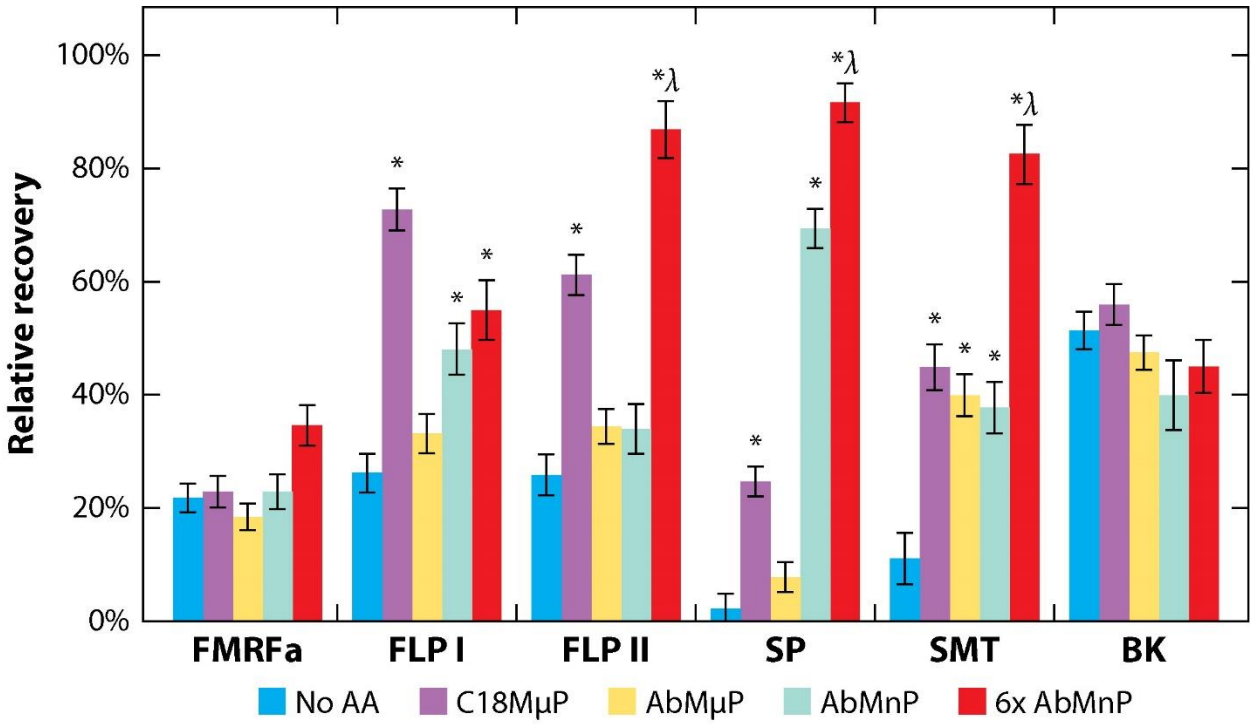

Figure 2. Recovery rates for several crustacean neuropeptides for different AAs using microdialysis. Conditions with $p < 0.05$ and compared with No AA are indicated with one asterisk. Significant differences ($p < 0.05$) for the AbMnP condition are indicated with a lambda. Adapted with permission.[8] Abbreviations: AbMnP, antibody-coated magnetic nanoparticle; AA, affinity agent; BK, bradykinin; FLP, *Homarus americanus* FMRFamide like peptide; FMRFa, FMRFamide (Phe-Met-Arg-Phe); SMT, Somatostatin-14; SP, Substance P.

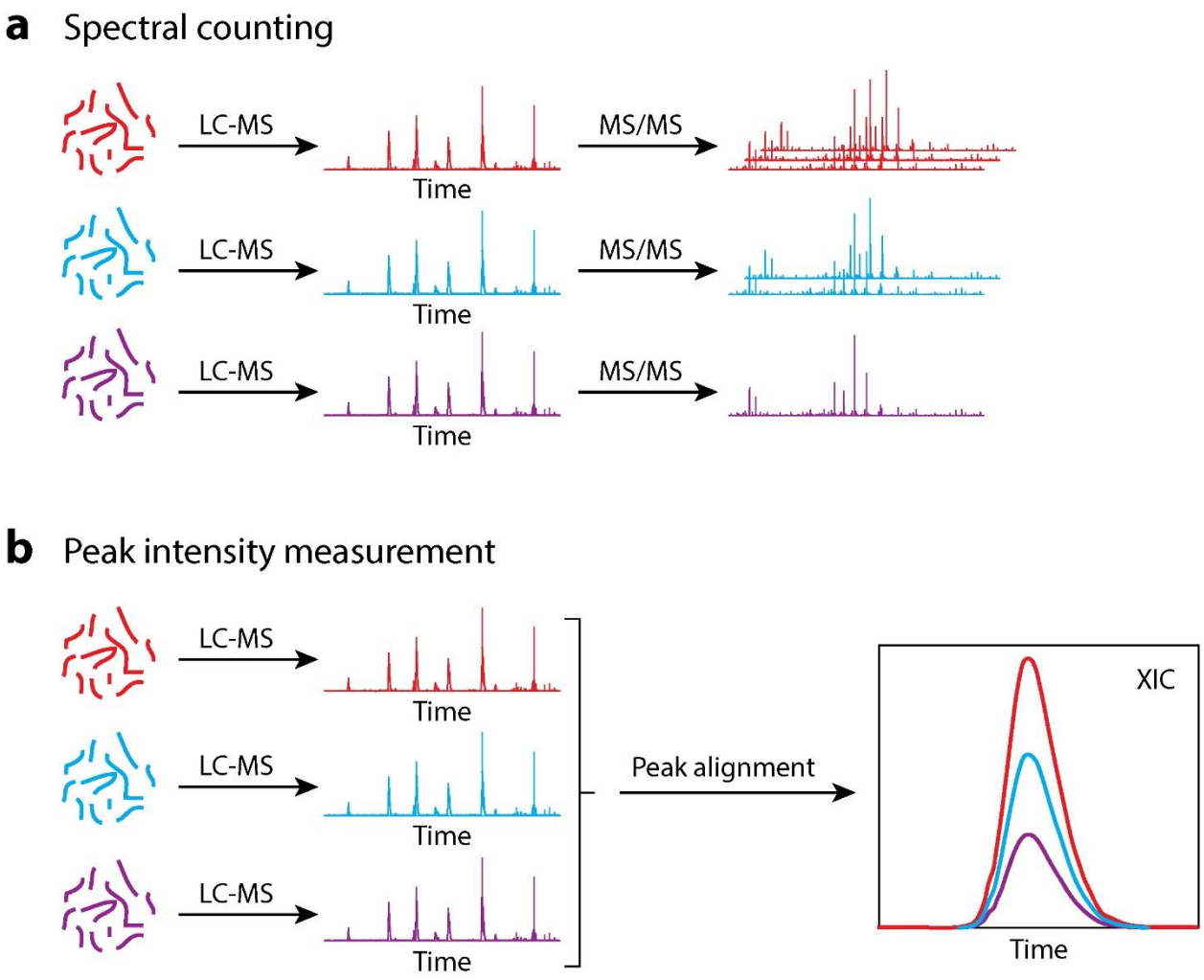

Figure 3. Representation of two label-free relative quantitation strategies. (*a*) Spectral counting uses the fact that more abundant peptides enable acquisition of more tandem MS scans. (*b*) Peak-area measurements utilize the chromatogram to provide quantitative information. Abbreviations: LC, liquid chromatography; MS, mass spectrometry; XIC, extracted ion chromatogram.

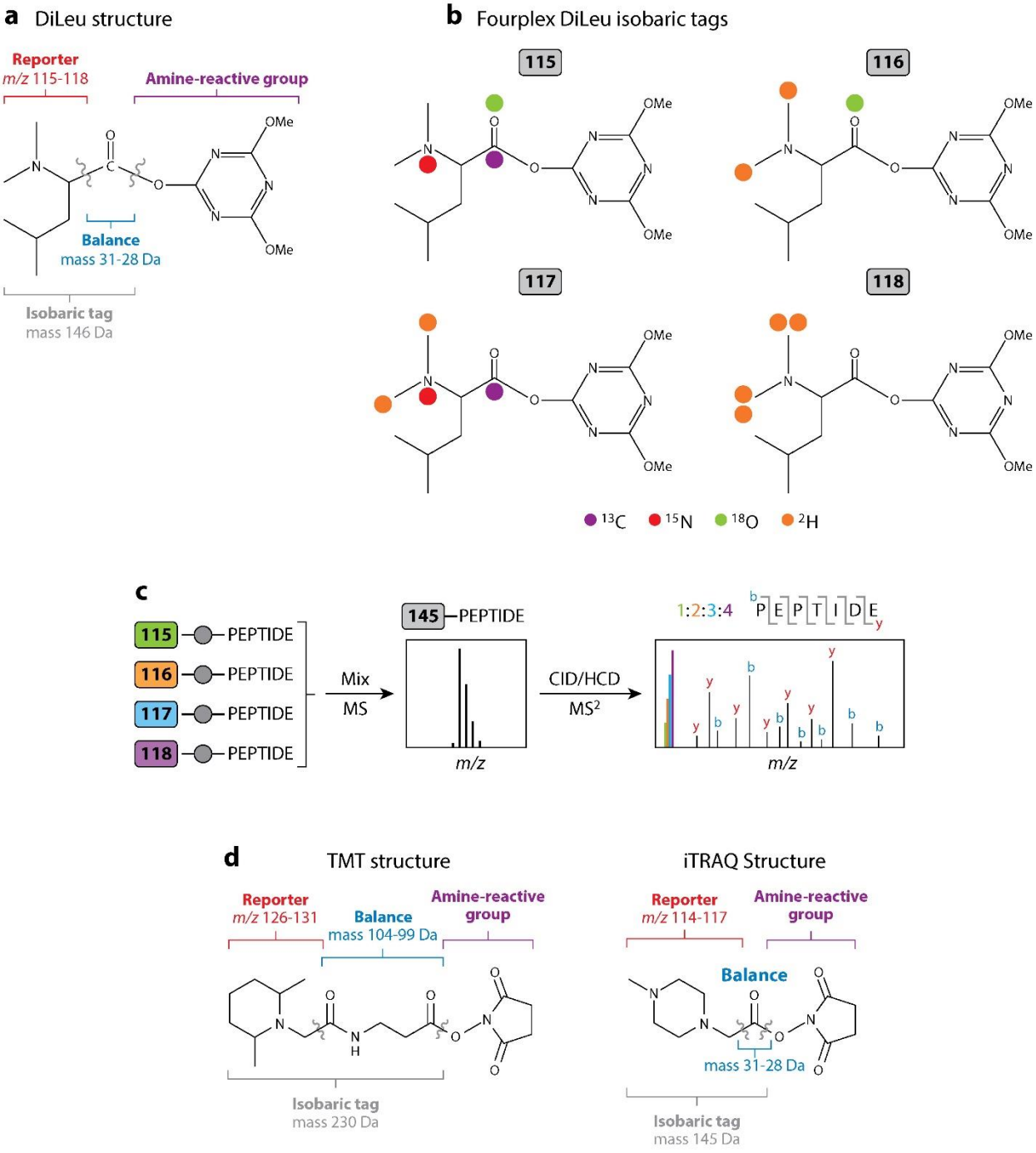

Figure 4. Isobaric chemical labels used for MS/MS quantitation. (a) Structure of DiLeu reagent showing reporter group, balance group, and amine-reactive group. Fragmentation of labeled peptides by CID/HCD generates reporter ions at *m/z* 115.1, 116.1, 117.1, and 118.1, and the carbonyl balance group is lost as a neutral species. (b) Fourplex DiLeu reporter ion

structures. Each colored dot represents a location where a stable isotope has been incorporated, allowing for the mass of each reporter to differ by 1 Da. (c) General workflow for quantitation employing fourplex DiLeu isobaric tags. Initially, four samples containing a peptide of interest are differentially labeled and mixed. During MS analysis, differentially labeled peptides are measured at the same *m*/*z* in the parent scan; upon precursor isolation and fragmentation by CID/HCD in the MS/MS scan, unique reporter ions are generated in the low mass region along with b- and y-type peptide backbone fragment ions, allowing quantitation and sequence identification of the peptide of interest. (d) Structures of TMT and iTRAQ isobaric tags. Labeling workflows for each are similar to the scheme illustrated in panel *c*. Abbreviations: CID, collisional-induced dissociation; DiLeu, N-dimethyl leucine; HCD, high-energy collisional dissociation; iTRAQ, isobaric tags for relative and absolute quantification; MS, mass spectrometry; TMT, tandem mass tag.

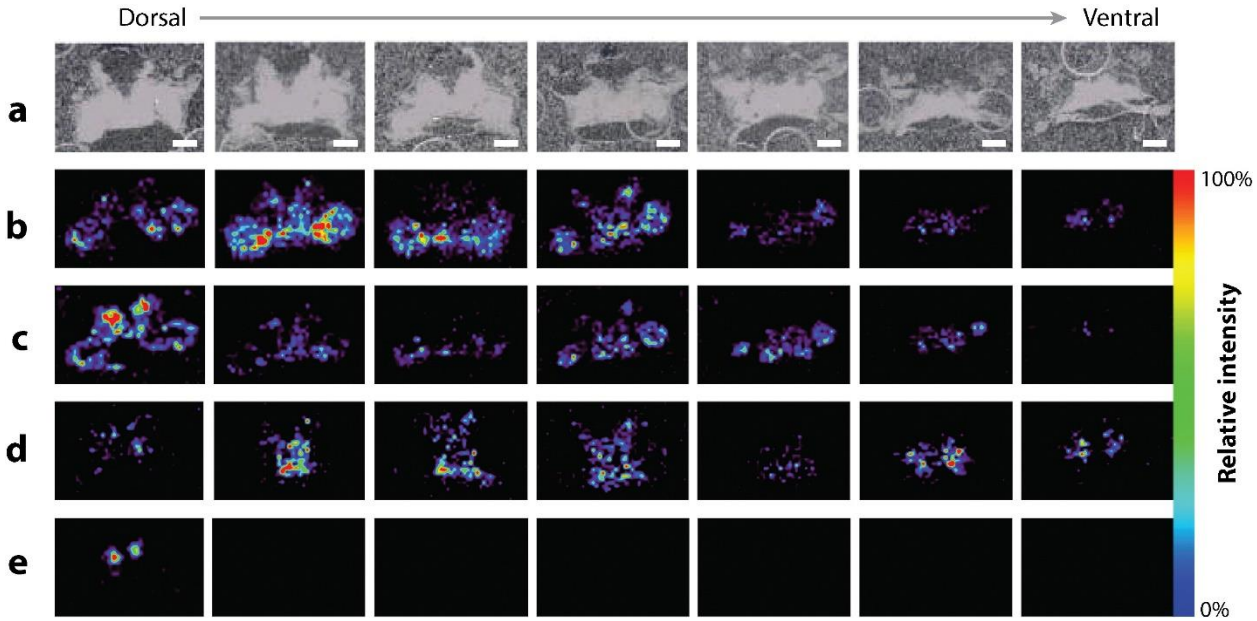

Figure 5. Three-dimensional analysis of the crustacean brain to show high spatial information of several neuropeptides of interest. Consecutive sections were analyzed to show the distribution in the z-plane of the tissue. Mass spectrometry (MS) images use an intensity scheme ranging from red, which is considered high (100%), to black/blue, which is considered low (0%). (a) Optical images of each consecutive section from the dorsal to ventral regions of the brain. Several neuropeptides were imaged showing a wide variety of distributions: (b) CabTRP la APSGFLGMRamide (*m*/*z* 934.5), (c) Orcokinin NFDEIDRSGFGFA (*m*/*z* 1474.1), (d) Orcokinin NFDEIDRTGFGFH (*m*/*z* 1554.7), and (e) RFamide SMPSLRLRFa (*m*/*z* 1105.6).

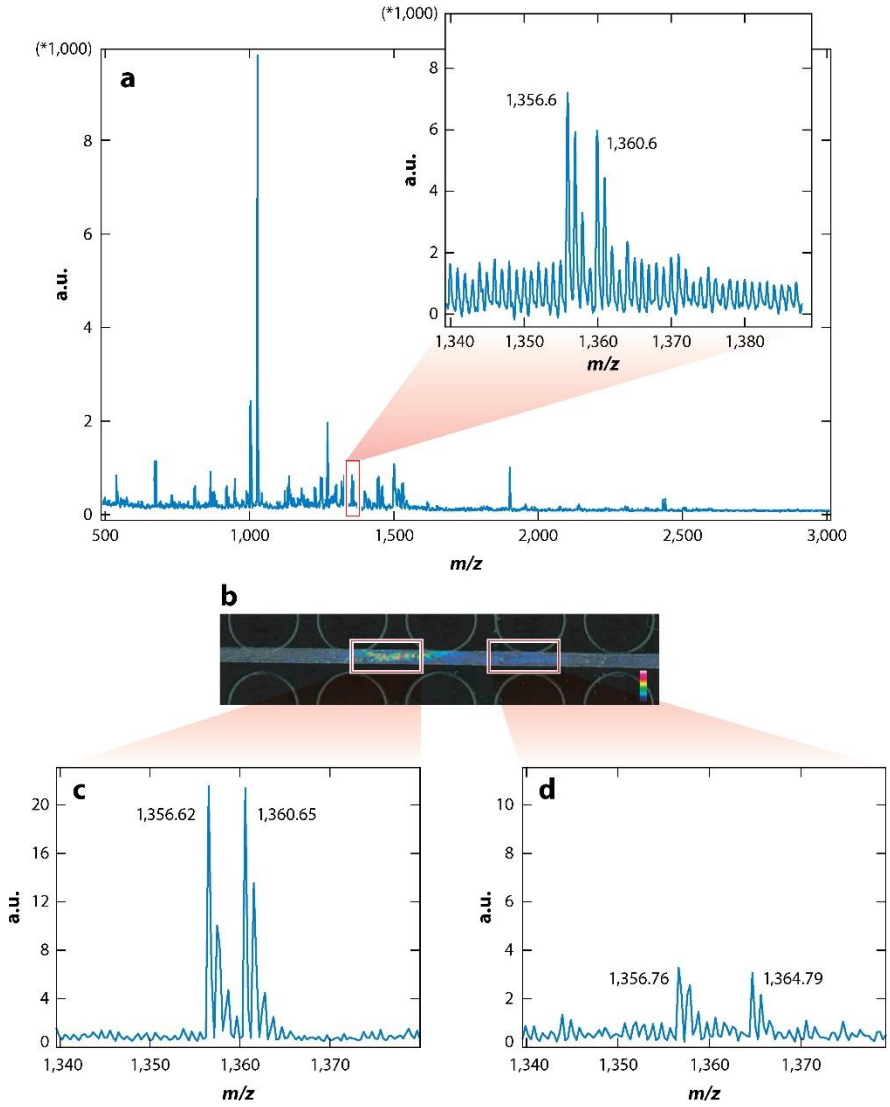

Figure 6. PACE-MS imaging for quantitative analysis of formaldehyde-labeled neuropeptide peak pairs. (a) Representative spectrum of neuropeptide extract from crustacean pericardial organ by MALDI-MS highlighting two peak pairs. (b) MS image of the CE trace. (c, d) Mass spectra corresponding to the highlighted regions in the CE trace. Two distinct peak pairs are separated into two color regions for accurate quantitation. Adapted with permission.[45]

Abbreviations: PACE, pressure-assisted capillary electrophoresis; CE, capillary electrophoresis; MALDI, matrix-assisted laser desorption/ionization; MS, mass spectrometry.

Chapter 3

Mass Spectrometric Profiling of Neuropeptides in *Callinectes sapidus* during Hypoxia Stress

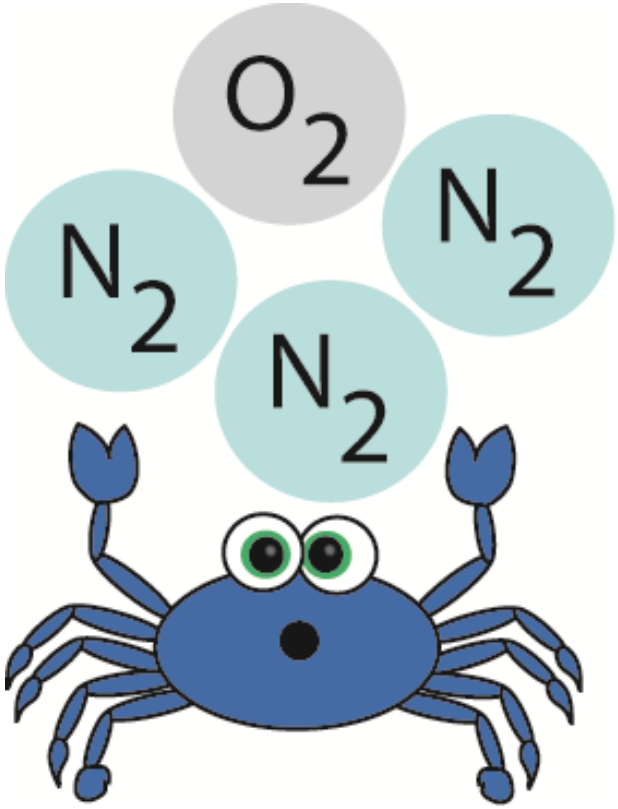

Modified from:

Amanda R. Buchberger, Kellen DeLaney, Yang Liu, Kylie Helfenbein, Nhu Q. Vu, Lingjun Li. "Mass Spectrometric Profiling of Neuropeptides in *Callinectes sapidus* during Hypoxia Stress." In Preparation, 2018.

Keywords: *Callinectes sapidus*, Mass Spectrometry, Neuropeptide, Hypoxia Stress, Reductive Dimethylation

Abstract

Oxygen (O_2) is a critical component of life, as without proper O_2 levels, cells are unable to respire, meaning glucose cannot be utilized. Thus, hypoxia (low O_2 levels) is a well-documented stressor, in particular in aquatic environments. Neuropeptides are a major class of regulators for stress-induced responses; however, their global expression changes during stress are not well characterized due to the natural complexity of the nervous system. Beyond being a neurological model organism, crustaceans are regularly exposed to hypoxia, making them a relevant system for this study. Several neuropeptide families, including orcokinins, RFamides, and allatostatin A-types, show dynamic dysregulation due to hypoxia stress. In particular, the brain showed the most dynamic changes with a survival mechanism "switching" (*i.e.,* significant increase to decrease) of neuropeptide content between moderate and severe hypoxia (*e.g.,* NFDEDRSGFA, FDAFTTGFGHS, NRNFLRFamide, and APSGFLGMRamide). Globally, neuropeptides in different tissues appeared to react uniquely at the various severities of hypoxia, including LSSSNSPSSTPL and NFDEIDRSSFGF. In complement to the tissue-specific neuropeptide expression level changes in response to hypoxia stress revealed in the current study, future studies will focus on neuropeptide levels in hemolymph to fully characterize the dynamic neuropeptidomic changes due to hypoxia stress.

Introduction

Hypoxia, or low oxygen (O_2) levels, poses a physiological challenge for many organisms, especially aquatic invertebrates. Estuarine ecosystems, for example, are well known to have seasonal hypoxic/anoxic zones (*e.g.,* dead zones) from stratification of the water due to eutrophication (*i.e.,* enrichment of the environment with nutrients).[1-3] The presence of these

zones decreases the quality of the habitat leading to mortality of organisms unable to escape. Several studies have been done to understand the physical and biochemical changes that occur due to these conditions.[4-13] Flounder growth rates were seen to drop by ~90% at low O_2 levels when coupled to temperature elevation.[4] Feeding rates also decreased at all temperatures when the flounder was exposed to hypoxia. Furthermore, in the estuarine fish *Fundulus grandis*, reproduction rates were reduced considerably after hypoxia exposure.[5] It is clear that hypoxia stress can have a major effect on the population of an organism, and the evolutionarily developed mechanisms to survive need to be studied.

Crustaceans are well known for residing and surviving where hypoxia is rampant. The blue crab, *Callinectes sapidus*, for example, is a well-studied organism in hypoxia research, as it mainly resides in coastal estuaries, such as the Chesapeake Bay.[6-13] While the survival of blue crabs in low dissolved oxygen levels does decline with increasing exposure time, crabs still have a surprisingly high survival rate, with over 80% surviving at <20% oxygen saturation for 30 hours.[10] Molecularly, another study showed that hypoxia has a dramatic impact on phenoloxidase enzyme activity in *C. sapidus*, which can have a direct effect on the organisms ability to fight deadly infections.[6] Other players, such as hemocyanin, the protein that assists in oxygen transfer in the body, has been shown to be different for hypoxia-tolerant and hypoxia-sensitive crustaceans.[7, 9, 10] Ultimately, there is a lack of knowledge on the precise molecular mechanisms that allow crustaceans to survive during such stressful conditions.

Neuropeptides, one of the most diverse and complex class of signaling molecules, are thought to be major regulators of stress response. Several stress-based studies on neuropeptides have been done with crustaceans, primarily focusing on temperature or salinity stress.[14, 15] With their simple, well-characterized nervous system, crustaceans, especially the blue crab, provide

not only a model organism for neuropeptide studies but also a relevant system for understanding environmental hypoxia stress. Currently, the only neuropeptide studies involving hypoxia and crustaceans have been crustacean hyperglycemic hormone (CHH) and crustacean cardioactive peptide (CCAP).[12, 16-19] Other invertebrates, such as *C. elegans*, have been used for hypoxia studies, such as the investigation of how hypoxia-inducible transcription factor-1 upregulated serotonin and the following neurological alterations.[20] Overall, all studies have focused on a single neuropeptide or signaling pathway, leaving a high demand for a global neuromodulation study of hypoxia-induced stress.

Here, we utilized matrix-assisted laser desorption/ionization (MALDI) mass spectrometry (MS) technology to profile the global neuropeptidomic changes with high mass resolution in the blue crab *Callinectes sapidus*.[21] Three tissues, including the sinus gland (SG), brain, and the pericardial organ (PO), were collected to understand the dynamic changes due to three different severities of hypoxia stress. Not only were distinct trends seen across each tissue type, especially the brain, but neuropeptides found in all three tissues also showed variable expression changes depending on the hypoxic severity (*e.g.,* allatostatin A-type NPYSFGLamide, mass-to-charge ratio (*m/z*) 796.399). Studies exploring hemolymph are required in the future to understand the secretion of these neuropeptides over the course of different exposure time due to long-term effects of hypoxia.

Materials and Methods

Methanol (MeOH), glacial acetic acid (GAA), ammonium bicarbonate, and all crab saline components (see below) were purchased from Fisher Scientific (Pittsburgh, PA). H_2-formaldehyde, $^2H_2$-formaldehyde, and borane pyridine were acquired from Sigma-Aldrich (St.

Louis, MO). 2, 5-dihydroxybenzoic acid (DHB) was obtained from Acros Organics (Morris, New Jersey), while formic acid (FA) was purchased through Fluka (Mexico City, Mexico). All water used in this study was doubly distilled on a Millipore filtration system (Burlington, MA) or Fisher HPLC grade (Pittsburgh, PA), and C18 Ziptips were purchased from Millipore (Burlington, MA).

Animals and Stress Experiment

Female blue crabs, *Callinectes sapidus*, were either purchased from Midway Asian Market (Madison, WI) or LA Crawfish Company (Natchitoches, LA). After transport, crabs were allowed to recover in artificial seawater made to be 35 parts per thousand (ppt), 17-18 °C, and 8-10 parts per million (ppm) dissolved O_2 (~80-100% O_2 water saturation) for several days prior to being exposed to hypoxia. For stress experiments, the tank was sparged with nitrogen (N_2) gas for 30-40 minutes prior to placing a crab in the tank in order to bring the dissolved O_2 down to the desired level as measured by a Pinpoint II Oxygen Monitor, which was calibrated prior to each experiment. The levels of interest included severe hypoxia (1 ppm, ~10% O_2 water saturation, n=7), moderate hypoxia (2 ppm, ~20% O_2 water saturation, n=5), and mild hypoxia (5 ppm, ~50% O_2 water saturation, n=5). A plastic tarp was placed on top of the water's surface to minimize water-air oxygen exchange during the course of the experiment. A crab was then placed in the tank to allow hypoxia exposure for 1 hour. The crab was then anesthetized on ice for 20 minutes, sacrificed, and tissues of interest were collected as previously described.[22] All dissections were performed in chilled (approximately 10 ºC) physiological saline (composition: 440 mM NaCl; 11 mM KCl; 13 mM $CaCl_2$; 26 mM $MgCl_2$; 10 mM Trizma acid; pH 7.4 (adjusted with NaOH)).

Sample Preparation

For each sample, tissues from 3 crabs were pooled together and extracted with a manual homogenizer with chilled acidified MeOH (90:9:1 MeOH:H_2O:GAA; volume (v):v:v). The sample was centrifuged at 13,200 rpm for 10 minutes, and the supernatant was collected. The resulting pellet was re-extracted twice, with the supernatant collected each time. The combined supernatant fractions were dried down in a Savant SCV100 Speedvac concentrator. All crude extracts were purified using C18 ZipTips following the manufacturer's protocol. All samples were centrifuged at 13,200 rpm prior to purification to pellet any particulates. Control and hypoxia-exposed samples were then differentially labeled using duplex reductive methylation using a previously published protocol.[14, 15, 23] All control samples were labeled with H_2-formaldehyde (+28.0313 Daltons (Da)), while all hypoxia-exposed (stress) samples were labeled with $^2H_2$-formaldehyde (+32.0564 Da). Borane pyridine was used as the reducing agent, and ammonium bicarbonate was used to quench the reaction. After labeling, control and experimental samples were mixed at a 1:1 ratio and dried down prior to analysis.

MS Data Collection and Analysis

Samples were redissolved at one tissue set (exposed/control) per 5 µL (*i.e.,* 15 µL for 3 pooled tissue), spotted 1:1 with 150 mg/mL DHB (in 50:50 MeOH:H_2O with 0.1% FA) in triplicate and analyzed in the *m/z* 500-2000 range at a resolution of 60,000 on the Thermo Scientific MALDI-LTQ-Orbitrap XL. The peak list was exported from Thermo Xcalibur software, and a program written in Java was used to find neuropeptides in the peak list by accurate mass matching within a ±5 ppm error to a custom, in-house crustacean neuropeptide database, with an intensity threshold cutoff of 100. If both light and heavy-labeled peaks were found, a peak ratio was calculated by dividing the intensity of the heavy peak by that of the light peak. A peak ratio of "1.0" means no change in abundance between the stressed sample and a

control. A student's two-tailed t-test was used to determine statistical significance of the results. Only those neuropeptides found in at least 2 out of 3 technical replicates and in at least 3 biological replicates were analyzed for statistical differences. A p-value<0.05 was said to be significant.

Results and Discussion

Dynamic Changes Due to Variable Hypoxia Stress

Hypoxia is a well-documented phenomenon in the environment that has a high impact on marine species, in particular crustaceans that live on the ocean floor. These invertebrates have developed mechanisms to survive harsh conditions, especially when escape is not possible. In order to compare the neuropeptidomic changes due to different severities of hypoxia of interest (severe (1 ppm O_2, 10% O_2 water saturation), moderate (2 ppm O_2, 20% O_2 water saturation), and mild (5 ppm O_2, 50% O_2 water saturation)) to control conditions (8-10 ppm O_2, 80-100% O_2 water saturation), a duplex dimethyl labeling strategy was utilized to increase throughput and quantitative accuracy. An example spectrum is shown in **Figure 1**, where the light labels (closed hexagon) and heavy labels (open hexagon) reflect neuropeptide levels in the control and hypoxia-affected crustacean, respectively. In this example, it can be visually inferred that the highlighted neuropeptides from the orcokinin family decrease due to hypoxia stress. These intensity levels can be visualized in bar graphs to infer trends across different severities of hypoxia in various tissue types, including the SG, brain, and PO (**Figures S1, 2,** and **3,** respectively).

Located in the eyestalks of the crab, the SG is a neuroendocrine organ close to the brain (*i.e.,* the central nervous system) and is known to secrete peptide hormones or neuropeptides

involved in blood glucose levels and hydro-mineral balance.[24, 25] Compared to the other tissues in this study, the SG's changes appear muted, as shown in **Figure S1**. Most of the neuropeptides identified show no differences compared to a control, except for in the most extreme case of hypoxia (1 ppm O_2), including orcokinins NFDEIDRGFG (*m/z* 1256.554) and NFDEIDRSGFGFA (*m/z* 1474.660). In fact, many neuropeptides show no change at all in all three severities, including proctolin RYLPT (*m/z* 649.367), RFamide GHRNFLRFamide (*m/z* 1045.580), and tachykinin YPSGFLGMRamide (*m/z* 1026.519) (**Table S1**). The only outlier to this trend was CHH precursor-related peptide (CPRP) RSAEGLGRMamide (*m/z* 975.515), which showed significant changes for the severe (1ppm O_2 and mild (5 ppm O_2) hypoxia, but not the moderate (2 ppm O_2). From the above results, it is clear that the mild (5 ppm O_2) and moderate (2 ppm O_2) hypoxia does not majorly affect the SG within an hour of exposure. Even if a neuropeptide's levels were affected by the severe hypoxia (1 ppm O_2) (**Table S1**), the dynamic range of the changes was relatively minimal compared to changes we see in the brain (**Table S2**) and PO (**Table S3**). Interestingly, HL/IGSL/IYRamide (*m/z* 844.479) only shows significant changes in the SG at severe hypoxia, thus it likely plays a distinct role in how the SG handles hypoxia stress compared to the brain and PO, suggesting tissue-specific response of this peptide.

Likely due to its central regulatory role in the nervous system, the brain has the most dynamic changes when increasing the hypoxic severity (**Figure 2**, **Table S2**).[25] Very few neuropeptides, one example being CPRP LSSSNSPSSTPLG (*m/z* 1233.596), showed a trend towards increased expression due to hypoxia, no matter the severity. But, the most distinct and interesting trend was the following: no change at 5 ppm O_2, a significant increase at 2 ppm O_2, and either no change or significant decrease at 1 ppm O_2. This was seen across several neuropeptide families, such as allatostatin A-type PRNYAFGLamide (*m/z* 936.505), RFamide

NRNFLRFamide (*m/z* 965.543), and tachykinin YPSGFLGMRamide (*m/z* 1026.519). It appears that between 2 ppm and 5 ppm O_2 there may be a survival mechanism "switching" point. This was consistent with what was observed during the actual stress exposure, as a physical difference was seen between the behaviors of the crustaceans of the 1 ppm O_2 and the 5 ppm/2 ppm exposed crabs, where the latter groups were more active. Beyond the significant changes, it was interesting to see that two families, tachykinins and RFamides, show little change compared to a control in any hypoxia severity (**Table S2**). Both of these families have human neuropeptide homologs (substance P and neuropeptide Y, respectively) that have been previously implicated in mammalian hypoxia stress.[26-32] The lack of detection of statistically significant differences in these molecules in response to hypoxia stress could be due to (a) biological variability and/or (b) instrumental sensitivity. Further experiments to target these neuropeptidomic families will be a priority.

In contrast to the SG and brain, the PO comes in direct contact with the heart, meaning all secretions can have a direct impact on the animal's reaction to stress by modulating the frequency or amplitude of heart contractions.[25, 33] In general, similar trends occur in this tissue as what was previously discussed, as demonstrated in **Figure 3** and **Table S3**. We still see the survival mechanism "switching" as seen in the brain (**Figure 2**), where the 2 ppm O_2 severity had the most significant changes in neuropeptidome content. Some neuropeptides showed constant downregulation (allatotropin GFKNVEMMTARGFamide (*m/z* 1486.729)) or upregulation (CPRP LSSSNSPSSTPLG (*m/z* 1233.596)) due to all cases of hypoxic severity. This neuropeptide content change occurs independent of the hypoxic severity, which could be a part of a "flight or fight" response. Another homologous trend includes only the severe hypoxia (1 ppm O_2) case creating significant changes (CPRP GFLSQDVHS (*m/z* 989.469)). While it may

not be as affected as the brain, the PO plays a distinct role in how the blue crab handles hypoxia stress.

Whole System Trends

Across the three tissues studied, several neuropeptides were unique to one tissue but there were also many that overlap, as shown in **Figure 4**. The brain contained the fewest unique neuropeptides compared to the SG and PO (*i.e.,* neuroendocrine organs). The most interesting nine neuropeptides lie in the center, as they were identified in all three tissues in at least two biological replicates. Since we considered only those neuropeptides found in three biological replicates for statistical analysis, it should be noted that only two neuropeptides (Proctolin RYLPT (*m/z* 649.397) and Others HL/IGSL/IYRamide (*m/z* 844.479)) were found in all three tissues for all three conditions and three biological replicates, and their changes were minimal. Trends for three select neuropeptides found in multiple tissues are illustrated in **Figure 5**.

In **Figure 5a**, allatostatin A-type NPYSFGLamide (*m/z* 796.399) showed no change compared to a control for any tissue at 5 ppm O_2. In the brain, as the severity was decreased, NPYSFGLamide showed distinct increase (*ratio* = 0.047 to 3.742) and then dramatic decrease (*ratio* = 3.742 to 1.025) for 2 ppm O_2 and 5 ppm O_2, respectively. Although we cannot comment these trends statistical significance, this was similar trend that we see in the brain for other neuropeptides (*e.g.,* allatostatin B-type). The trend in the brain has no consistency with the PO, which showed an increase in neuropeptide amount that leveled off (*ratio* = ~2.5) as severity decreased, and the SG, which showed no change even as the O_2 saturation was lowered. Allatostatin A-type neuropeptides are known to be localized throughout the nervous system of the crustacean including neuroendocrine organs and synapses, suggesting that they work both locally and as long-distance hormones.[34] Their function is also well-defined as inhibitory

neuro/myo-modulators, in particular targeting the cardiac neuromuscular system and stomatogastric nervous systems (STNS).[34] While we have not studied tissue within either of these systems, NPYSFGLamide could be indirectly affecting them by targeting the PO, which is in direct contact with the heart, and the brain, which is connected to the STNS.

Similarly, orcokinins are located throughout the crustacean nervous system and can act locally and long distance.[34] While they are involved in modulating the STNS, they also have known roles in increasing frequency and amplitude of spontaneous hindgut contraction.[34] In **Figure 5b**, orcokinin NFDEIDRSSFA (*m/z* 1433.633) seems to show consistently across all tissue types besides the PO, although we are unable to comment on the statistical changes for this neuropeptides in the PO. Several other orcokinins were found in all three tissues, including NFDEIDRSSFGF (*m/z* 1300.580), NFDEIDRSSFGFA (*m/z* 1504.670), and NFDEIDRSSFGFN (*m/z* 1547.676), all of which have variable responses to hypoxia stress. In fact, NFDEIDRSSFGFN shows no changes due to hypoxia stress in any tissue. This is an example of the diverse roles that neuropeptides from the same family have within the crustacean nervous system.

Finally, when looking at CPRP LSSSNSPSSTPLG (*m/z* 1233.596) (**Figure 5c**), the brain once again exhibited interesting trends, where the neuropeptide level increased at lower severity (5 ppm O_2) (*ratio* = 12.745) and decreased as severity was increased (*ratio* = 4.684 and 2.431 for 2ppm and 1 ppm O_2, respectively). In general, this trend was consistent with the SG, although we cannot comment on statistically significant changes, but the PO shows no difference in response regardless of hypoxic severity (*ratio* = ~4.5). CPRPs are co-released with CHH, an important neuropeptide for the crustacean's regulating glucose use.[34] In the literature, CHH was the only neuropeptide that has been implicated in how blue crabs handle hypoxia stress, where CHH

levels in the hemolymph increased in response to hypoxia stress.[12] This could also imply an increase in CPRPs. In our studies, CPRP levels decreased in all tissues as the hypoxic severity was increased. The decrease could indicate the release into the hemolymph, matching well with previous literature, although all of the CPRP levels were still higher than those in a control crab. Thus, we may be seeing a buildup phase prior to the release of the CHH/CPRPs. One thing to note is that different variants of CHH are known to be produced in the PO and the SG, so it is interesting that we see the most variable response in the brain.[34, 35] It could indicate that the brain was a target of these CPRPs that were being produced elsewhere or that was already circulating. This aligns well with the fact that we see the most dynamic neuropeptidomic changes overall in the brain (**Table S2**) compared to the SG (**Table S1**) and PO (**Table S3**). To understand these results, (a) a time course study to quantify neuropeptide levels in the hemolymph as well as (b) a top-down MS approach to characterize changes in CHH are of interest in the future.

Conclusions and Future Directions

It is clear that neuropeptides play a dynamic role in how crustaceans, specifically *C. sapidus*, survive hypoxia stress, and even neuropeptides from different tissues appear to have distinct functions in the animal's ability to handle this stress. It is suggested that between 2 ppm and 1 ppm O_2, there is a "switch" that occurs where the published defensive behaviors are observed, which was supported in our studies. The brain (*i.e.,* the central nervous system) provides the strongest evidence of this assumption, although it will require more severity-specific resolution in our studies to quantitatively determine the exact level of hypoxia at which this occurs. Studies involving how the duration of exposure affects crustacean neuropeptides are underway along with incorporating electrospray ionization MS to improve peptidomic coverage

and identification.

Acknowledgements

This work was supported by a National Science Foundation grant (CHE- 1710140) and the National Institutes of Health (NIH) through grant 1R01DK071801. A.R.B. would like to thank NIH for a General Medical Sciences NRSA Fellowship 1F31GM119365. K.D. acknowledges a predoctoral fellowship supported by the NIH, under Ruth L. Kirschstein National Research Service Award T32HL007936 from the National Heart Lung and Blood Institute to the University of Wisconsin-Madison Cardiovascular Research Center. N.Q.V. would like to thank a Biotechnology Training Program predoctoral traineeship sponsored by the National Institute of General Medical Sciences of the National Institutes of Health under Award Number T32GM008349.

References

1. Diaz, R. J.; Rosenberg, R., *Oceanography and Marine Biology - an Annual Review, Vol 33* **1995,** *33*, 245-303.

2. Gray, J. S.; Wu, R. S. S.; Or, Y. Y., *Marine Ecology Progress Series* **2002,** *238*, 249-279.

3. Santana, R.; Lessa, G. C.; Haskins, J.; Wasson, K., *Estuaries and Coasts* **2018,** *41* (1), 99-113.

4. Neilan, R. M.; Rose, K., *Journal of Theoretical Biology* **2014,** *343*, 54-68.

5. Landry, C. A.; Steele, S. L.; Manning, S.; Cheek, A. O., *Comparative Biochemistry and Physiology a-Molecular & Integrative Physiology* **2007,** *148* (2), 317-323.

6. Tanner, C. A.; Burnett, L. E.; Burnett, K. G., *Comparative Biochemistry and Physiology a-Molecular & Integrative Physiology* **2006,** *144* (2), 218-223.

7. Stover, K. K.; Burnett, K. G.; McElroy, E. J.; Burnett, L. E., *Biological Bulletin* **2013,**

224 (2), 68-78.

8. Brouwer, M.; Larkin, P.; Brown-Peterson, N.; King, C.; Manning, S.; Denslow, N., *Mar Environ Res* **2004,** *58* (2-5), 787-92.

9. Bell, G. W.; Eggleston, D. B.; Noga, E. J., *Biological Bulletin* **2009,** *217* (2), 161-172.

10. Bell, G. W.; Eggleston, D. B.; Noga, E. J., *Oecologia* **2010,** *163* (1), 57-68.

11. Hardy, K. M.; Follett, C. R.; Burnett, L. E.; Lema, S. C., *Comparative Biochemistry and Physiology a-Molecular & Integrative Physiology* **2012,** *163* (1), 137-146.

12. Chung, J. S.; Zmora, N., *Febs Journal* **2008,** *275* (4), 693-704.

13. Webster, S. G., *Journal of Experimental Biology* **1996,** *199* (7), 1579-1585.

14. Chen, R. B.; Xiao, M. M.; Buchberger, A.; Li, L. J., *Journal of Proteome Research* **2014,** *13* (12), 5767-5776.

15. Zhang, Y.; Buchberger, A.; Muthuvel, G.; Li, L., *Proteomics* **2015**.

16. Shan, D. Y.; Fu, H. T.; Qiao, H.; Sun, S. M.; Zhang, W. Y.; Jin, S. B.; Jiang, S. F.; Gong, Y. S.; Xiong, Y. W.; Wu, Y., *Journal of the World Aquaculture Society* **2018,** *49* (2), 356-365.

17. Hui, M.; Song, C. W.; Liu, Y.; Li, C. L.; Cui, Z. X., *Plos One* **2017,** *12* (5), 17.

18. Mosco, A.; Pegoraro, S.; Giulianini, P. G.; Edomi, P., *Journal of Crustacean Biology* **2013,** *33* (1), 56-61.

19. Chung, J. S.; Webster, S. G., *Endocrinology* **2005,** *146* (12), 5545-5551.

20. Chang, A. J.; Bargmann, C. I., *Proceedings of the National Academy of Sciences of the United States of America* **2008,** *105* (20), 7321-7326.

21. Buchberger, A.; Yu, Q.; Li, L., *Annu Rev Anal Chem (Palo Alto Calif)* **2015,** *8* (1), 485-509.

22. Gutierrez, G. J.; Grashow, R. G., *J Vis Exp* **2009,** (25).

23. DeLaney, K.; Buchberger, A.; Li, L., *Methods Mol Biol* **2018,** *1719*, 247-269.

24. Fu, Q.; Goy, M. F.; Li, L. J., *Biochemical and Biophysical Research Communications* **2005,** *337* (3), 765-778.

25. Hopkins, P. M., *General and Comparative Endocrinology* **2012,** *175* (3), 357-366.

26. Poncet, L.; Denoroy, L.; Dalmaz, Y.; Pequignot, J. M.; Jouvet, M., *Brain Research* **1996,** *733* (1), 64-72.

27. Wang, Z. Z.; Dinger, B.; Fidone, S. J.; Stensaas, L. J., *Neuroscience* **1998,** *83* (4), 1273-1281.

28. Lee, E. W.; Michalkiewicz, M.; Kitlinska, J.; Kalezic, I.; Switalska, H.; Yoo, P.; Sangkharat, A.; Ji, H.; Li, L. J.; Michalkiewicz, T.; Ljubisavljevic, M.; Johansson, H.; Grant, D. S.; Zukowska, Z., *Journal of Clinical Investigation* **2003,** *111* (12), 1853-1862.

29. Moss, I. R.; Laferriere, A., *Respiratory Physiology & Neurobiology* **2002,** *131* (1-2), 15-27.

30. Husson, S. J.; Mertens, I.; Janssen, T.; Lindemans, M.; Schoofs, L., *Prog Neurobiol* **2007,** *82* (1), 33-55.

31. Dockray, G. J., *Exp Physiol* **2004,** *89* (3), 229-35.

32. Coast, G. M.; Schooley, D. A., *Peptides* **2011,** *32* (3), 620-31.

33. Stangier, J.; Hilbich, C.; Beyreuther, K.; Keller, R., *Proceedings of the National Academy of Sciences of the United States of America* **1987,** *84* (2), 575-579.

34. Christie, A. E.; Stemmler, E. A.; Dickinson, P. S., *Cell Mol Life Sci* **2010,** *67* (24), 4135-69.

35. Webster, S. G.; Keller, R.; Dircksen, H., *General and Comparative Endocrinology* **2012,** *175* (2), 217-233.

Figures

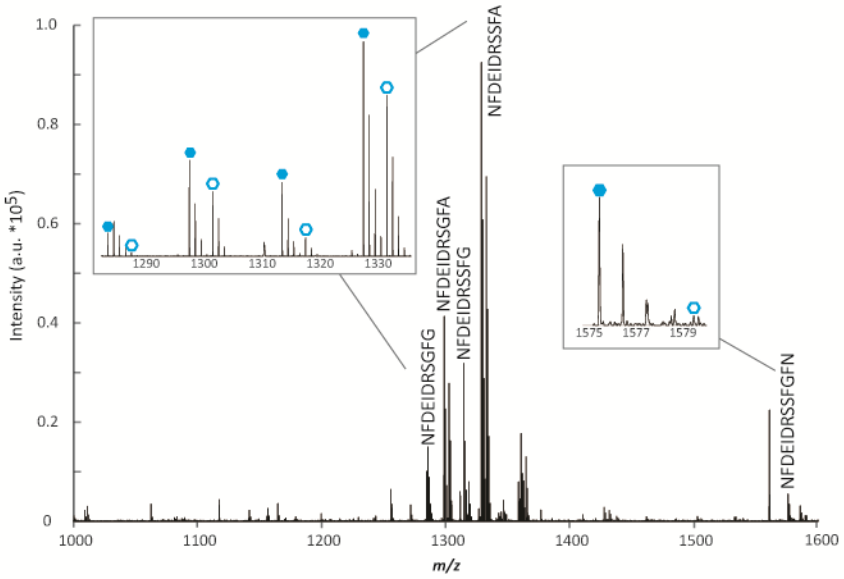

Figure 1. A representative MALDI-MS spectrum where duplex dimethyl labeling was utilized to compare neuropeptide levels between a control (light labeled, closed hexagons) and hypoxia (10% O_2 water saturation, 1 hour) stressed (heavy labeled, open hexagons) blue crabs. Several orcokinin neuropeptides are highlighted.

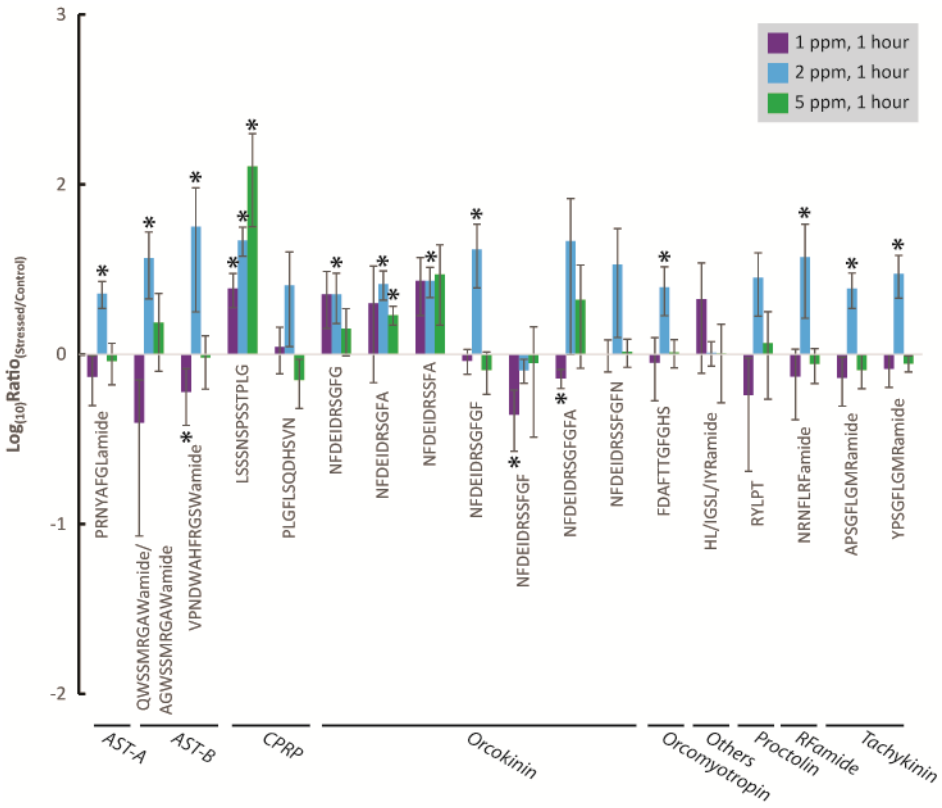

Figure 2. Bar graphs that represent the dynamic neuropeptide changes due to severe (purple), moderate (blue), and mild (green) hypoxia for the brain. The x-axis shows the neuropeptides' sequences, while the y-axis represents the log-base 10 of the ratio of hypoxia-stressed divided by control. A log-base 10 ratio close to 0 indicates no change in neuropeptides for that hypoxia condition compared to the control. Neuropeptides that were deemed significant ($p<0.05$) in their change are indicated with an asterisk (*). The error bars represent standard error of the mean (SEM). AST-A: Allatostatin A-type; AST-B: Allatostatin B-type; CPRP: CHH Precursor Related Peptide.

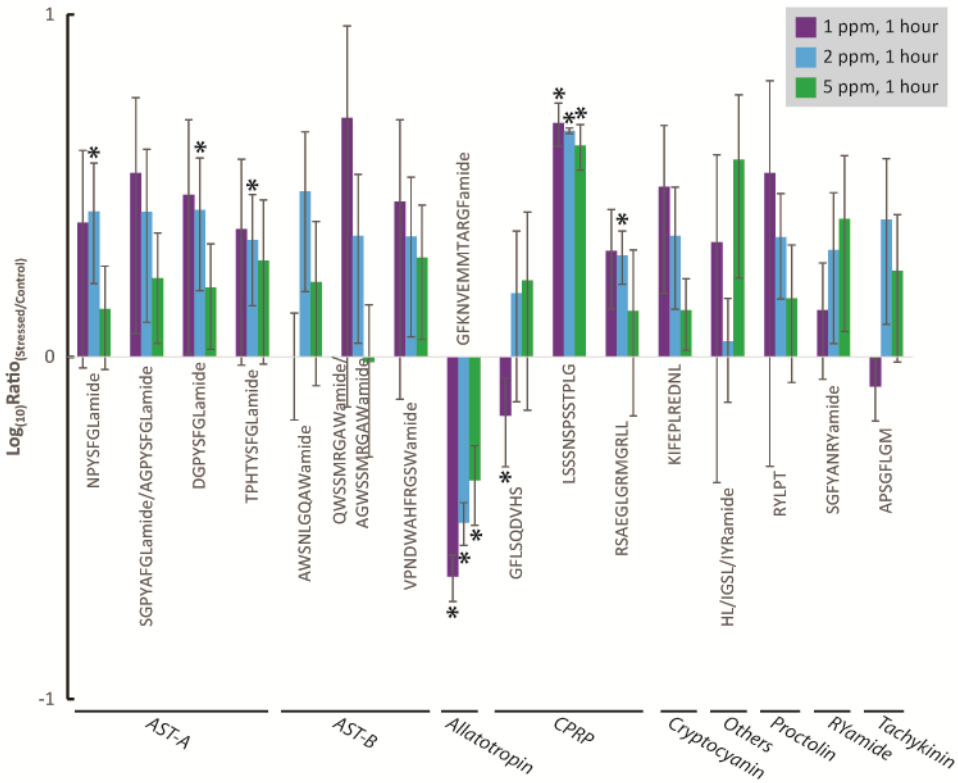

Figure 3. Bar graphs that represent the dynamic neuropeptide changes due to severe (purple), moderate (blue), and mild (green) hypoxia for the PO. The x-axis shows the neuropeptides' sequences, while the y-axis represents the log-base 10 of the ratio of hypoxia-stressed divided by control. A log-base 10 ratio close to 0 indicates no change in neuropeptides for that hypoxia condition compared to the control. Neuropeptides that were deemed significant ($p<0.05$) in their change are indicated with an asterisk (*). The error bars represent standard error of the mean (SEM). AST-A: Allatostatin A-type; AST-B: Allatostatin B-type; CPRP: CHH Precursor Related Peptide.

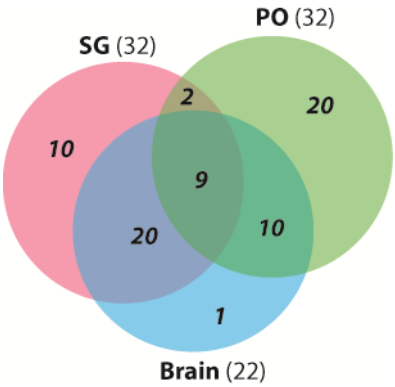

Figure 4. A Venn diagram depicting the neuropeptide overlap (regardless of expression changes) of the three tissues studied. Only neuropeptides that were found in all 3 conditions (severe, moderate, and mild hypoxia) and in at least 2 bioreplicates in a tissue were included.

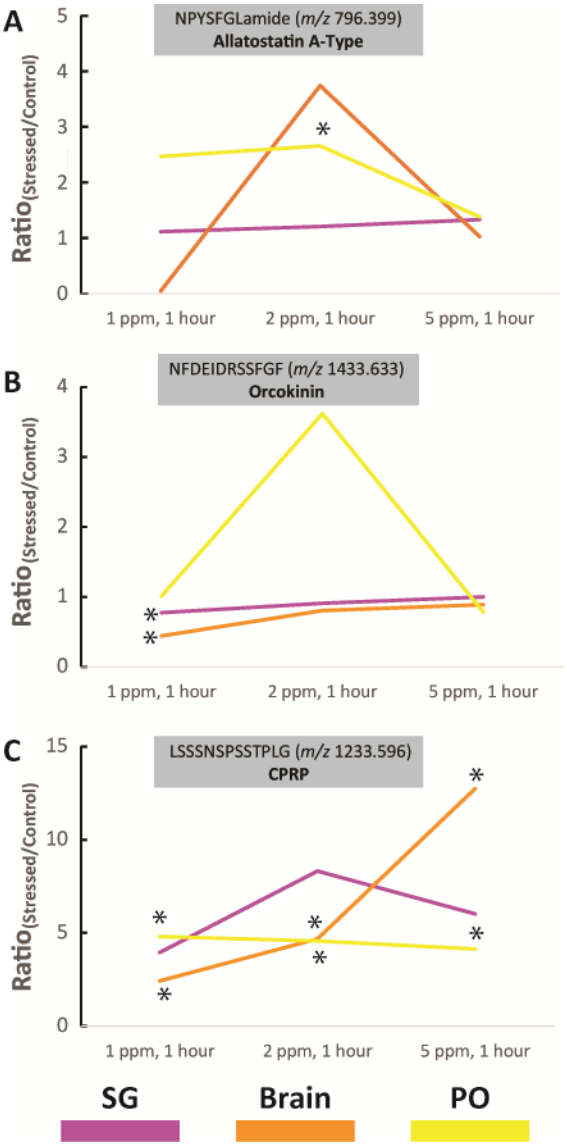

Figure 5. Line graphs showing the variable changes between the same neuropeptide in the SG (pink), brain (orange) and PO (yellow). (a) Allatostatin A-type NPYSFGLamide (*m/z* 796.399). (d) Orcokinin NFDEIDRSSFGF (*m/z* 1300.580). (c) CPRP LSSSNSPSSTPLG (*m/z* 1233.596). Neuropeptides that were deemed significant ($p<0.05$) in their change are indicated with an asterisk (*). Due to lack of appearances in biological replicates, significant changes cannot be determined for the brain for (a), the PO for (b), and SG for (c).

Supplemental Information

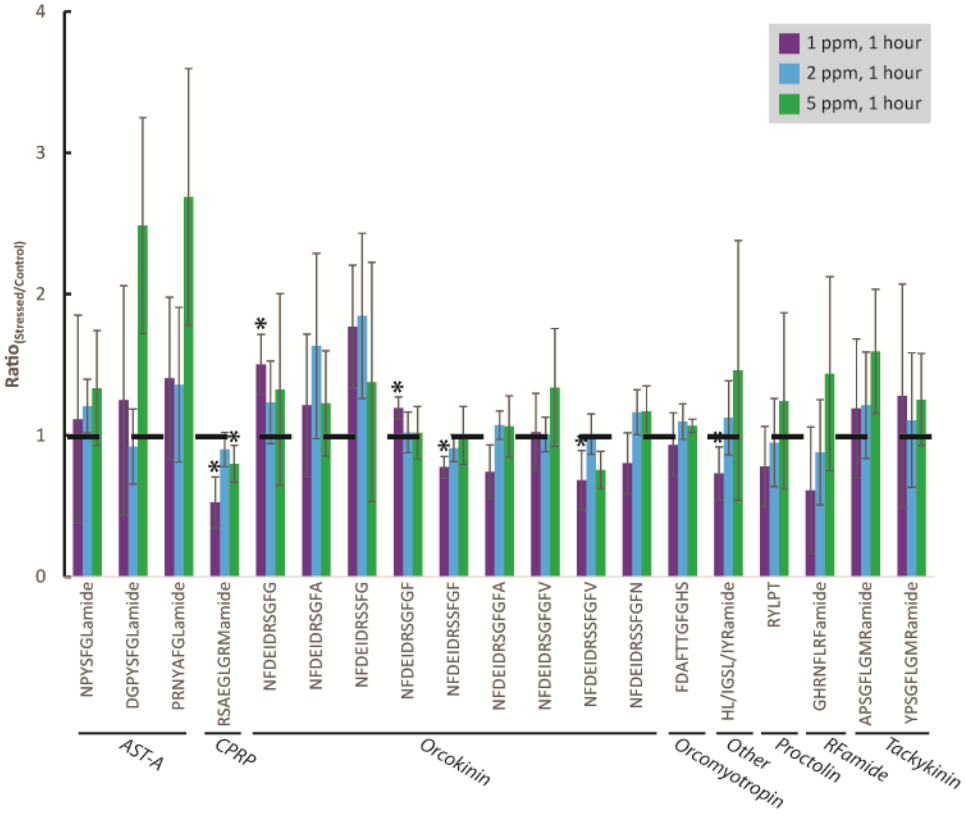

Figure S1. Bar graphs that represent the dynamic neuropeptide changes due to severe (purple), moderate (blue), and mild (green) hypoxia for the SG. The x-axis shows the neuropeptides' sequences, while the y-axis represents the ratio of hypoxia-stressed divided by control. The dotted line marks a ratio of 1, which indicates no difference between the stressed and control samples. Neuropeptides that were deemed significant ($p<0.05$) in their change are indicated with an asterisk (*). The error bars represent standard error of the mean (SEM). AST-A: Allatostatin A-type; CPRP: CHH Precursor Related Peptide.

Table S1. Ratios (stressed/control) of neuropeptides in the SG that were detected in all three conditions. The highlighted cells are those were significant changes ($p<0.05$) were calculated. SEM: standard error of the mean.

			1 ppm, 1 hour			2 ppm, 1 hour			5 ppm, 1 hour		
Family	Sequence	*m/z*	Ratio	SEM	p-Value	Ratio	SEM	p-Value	Ratio	SEM	p-Value
Allatostatin A-type	NPYSFGLamide	796.399	1.115	0.735	0.2797	1.207	0.190	0.3110	1.334	0.407	0.9571
	DGPYSFGLamide	854.404	1.249	0.810	0.3757	0.921	0.266	0.3723	2.486	0.765	0.0449
	PRNYAFGLamide	936.505	1.404	0.574	0.5525	1.358	0.548	0.9670	2.687	0.909	0.1975
CPRP	RSAEGLGRMamide	975.515	0.526	0.179	**0.0158**	0.900	0.122	0.1664	0.798	0.133	**0.0466**
Orcokinin	NFDEIDRSGFG	1256.554	1.502	0.213	**0.0187**	1.234	0.292	0.6543	1.324	0.678	0.5415
	NFDEIDRSGFA	1270.570	1.212	0.504	0.6795	1.632	0.656	0.3841	1.225	0.374	0.7836
	NFDEIDRSSFG	1286.565	1.769	0.437	0.0519	1.846	0.585	0.1609	1.378	0.847	0.5447
	NFDEIDRSGFGF	1403.623	1.193	0.080	**0.0256**	1.021	0.145	0.8567	1.019	0.186	0.8179
	NFDEIDRSSFGF	1433.633	0.775	0.076	**0.0043**	0.910	0.095	0.1219	0.999	0.205	0.5847
	NFDEIDRSGFGFA	1474.660	0.741	0.190	0.0576	1.072	0.101	0.4150	1.063	0.218	0.8460
	NFDEIDRSGFGFV	1502.691	1.023	0.274	0.7898	1.006	0.121	0.7963	1.339	0.418	0.5581
	NFDEIDRSSFGFV	1532.702	0.682	0.211	**0.0398**	1.009	0.143	0.7573	0.755	0.130	0.0535
	NFDEIDRSSFGFN	1547.676	0.803	0.215	0.0957	1.163	0.160	0.2416	1.170	0.180	0.3366
Orcomyotropin	FDAFTTGFGHS	1186.516	0.932	0.227	0.2926	1.097	0.125	0.4252	1.067	0.048	0.0813
Others	HL/IGSL/IYRamide	844.479	0.731	0.187	**0.0331**	1.124	0.262	0.9747	1.461	0.919	0.4497
Proctolin	RYLPT	649.367	0.778	0.285	0.0641	0.949	0.312	0.2974	1.242	0.625	0.3417
RFamide	GHRNFLRFamide	1045.580	0.610	0.449	0.1429	0.880	0.373	0.3875	1.436	0.687	0.8943
Tachykinin	APSGFLGMRamide	934.493	1.191	0.491	0.6374	1.213	0.376	0.8958	1.594	0.440	0.1921
	YPSGFLGMRamide	1026.519	1.281	0.790	0.6790	1.108	0.476	0.6146	1.253	0.326	0.6553

Table S2. Ratios (stressed/control) of neuropeptides in the brain that were detected in all three conditions. The highlighted cells are those were significant changes ($p<0.05$) were calculated. SEM: standard error of the mean.

			1 ppm, 1 hour			2 ppm, 1 hour			5 ppm, 1 hour		
Family	**Sequence**	***m/z***	**Ratio**	**SEM**	**p-Value**	**Ratio**	**SEM**	**p-Value**	**Ratio**	**SEM**	**p-Value**
Allatostatin A-type	PRNYAFGLamide	936.505	0.738	0.239	0.1739	2.268	0.408	**0.0002**	0.911	0.250	0.2743
Allatostatin B-type	QWSSMRGAWamide/ AGWSSMRGAWamide	1107.515	0.395	0.310	0.0502	3.682	1.561	**0.0008**	1.538	0.744	0.5890
	VPNDWAHFRGSWamide	1470.703	0.602	0.220	**0.0235**	5.646	3.871	**0.0134**	0.955	0.332	0.3053
CPRP	LSSSNSPSSTPLG	1233.596	2.431	0.549	**0.0056**	4.684	0.907	**0.0000**	12.745	7.101	**0.0013**
	PLGFLSQDHSVN	1313.648	1.104	0.339	0.8538	2.551	1.443	0.2183	0.706	0.227	0.0577
Orcokinin	NFDEIDRSGFG	1256.554	2.246	0.829	0.5504	2.256	0.739	**0.0344**	1.416	0.437	0.5511
	NFDEIDRSGFA	1270.570	1.989	1.308	0.9559	2.588	0.501	**0.0001**	1.700	0.218	**0.0025**
	NFDEIDRSSFA	1300.580	2.704	1.012	0.2313	2.699	0.543	**0.0001**	2.946	1.460	0.4877
	NFDEIDRSGFGF	1403.623	0.914	0.152	0.2502	4.137	1.687	**0.0040**	0.806	0.225	0.1188
	NFDEIDRSSFGF	1433.633	0.442	0.173	**0.0349**	0.804	0.130	0.1191	0.889	0.564	0.1548
	NFDEIDRSGFGFA	1474.660	0.722	0.094	**0.0045**	4.629	3.636	0.9772	2.089	1.262	0.6294
	NFDEIDRSSFGFN	1547.676	1.002	0.214	0.5640	3.375	2.122	0.3988	1.032	0.194	0.8617
Orcomyotropin	FDAFTTGFGHS	1186.516	0.892	0.359	0.2897	2.478	0.792	**0.0184**	1.024	0.193	0.8198
Others	HL/IGSL/IYRamide	844.479	2.112	1.339	0.8492	1.018	0.167	0.8367	1.009	0.491	0.5364
Proctolin	RYLPT	649.367	0.575	0.371	0.1365	2.817	1.141	0.0904	1.162	0.618	0.4445
RFamide	NRNFLRFamide	965.543	0.740	0.329	0.2573	3.732	2.104	**0.0326**	0.876	0.204	0.2187
Tachykinin	APSGFLGMRamide	934.493	0.728	0.233	0.1487	2.433	0.575	**0.0010**	0.810	0.184	0.1223
	YPSGFLGMRamide	1026.519	0.820	0.180	0.2009	2.977	0.843	**0.0011**	0.882	0.095	0.0965

Table S3. Ratios (stressed/control) of neuropeptides in the PO that were detected in all three conditions. The highlighted cells are those were significant changes ($p<0.05$) were calculated. SEM: standard error of the mean.

			1 ppm, 1 hour			2 ppm, 1 hour			5 ppm, 1 hour		
Family	Sequence	*m/z*	Ratio	SEM	p-Value	Ratio	SEM	p-Value	Ratio	SEM	p-Value
Allatostatin A-type	NPYSFGLamide	796.399	2.469	1.541	0.6458	2.658	1.023	**0.0143**	1.380	0.462	0.9748
	SGPYAFGLamide/ AGPYSFGLamide	810.415	3.443	2.274	0.4519	2.651	1.388	0.0969	1.697	0.603	0.7982
	DGPYSFGLamide	854.404	2.973	1.952	0.5971	2.689	1.126	**0.0172**	1.595	0.541	0.8435
	TPHTYSFGLamide	1021.510	2.361	1.416	0.6629	2.195	0.783	**0.0157**	1.912	0.959	0.9844
Allatostatin B-type	AWSNLGQAWamide	1031.506	0.998	0.344	0.6452	3.046	1.494	0.0833	1.655	0.832	0.9199
	QWSSMRGAWamide/ AGWSSMRGAWamide	1107.515	4.991	4.276	0.7209	2.258	1.161	0.1857	0.965	0.455	0.3280
	VPNDWAHFRGSWamide	1470.703	2.840	2.088	0.9117	2.246	1.100	0.2374	1.950	0.827	0.8470
Allatotropin	GFKNVEMMTARGFamide	1486.729	0.228	0.035	**0.0000**	0.328	0.047	**0.0000**	0.436	0.114	**0.0055**
CPRP	GFLSQDVHS	989.469	0.673	0.196	**0.0429**	1.535	0.796	0.6123	1.673	0.975	0.9674
	LSSSNSPSSTPLG	1233.596	4.813	0.692	**0.0000**	4.573	0.087	**0.0000**	4.141	0.632	**0.0000**
	RSAEGLGRMGRLL	1415.790	2.038	0.659	0.0509	1.980	0.350	**0.0024**	1.362	0.690	0.6050
Cryptocyanin	KIFEPLREDNL	1373.742	3.137	1.606	0.2465	2.255	0.878	0.0783	1.367	0.322	0.3457
Others	HL/IGSL/IYRamide	844.479	2.162	1.733	0.3420	1.109	0.373	0.5722	3.766	2.067	0.8395
Proctolin	RYLPT	649.367	3.443	2.965	0.5034	2.237	0.761	0.1007	1.482	0.641	0.7748
RYamide	SGFYANRYamide	976.464	1.370	0.510	0.9805	2.055	0.962	0.5318	2.529	1.342	0.2959
Tachykinin	APSGFLGM	779.376	0.819	0.169	0.1144	2.519	1.276	0.1382	1.784	0.818	0.9612

Chapter 4

A Temporal Study of the Perturbation of Crustacean Neuropeptides Due to Severe Hypoxia Stress Using 4-Plex Reductive Dimethylation

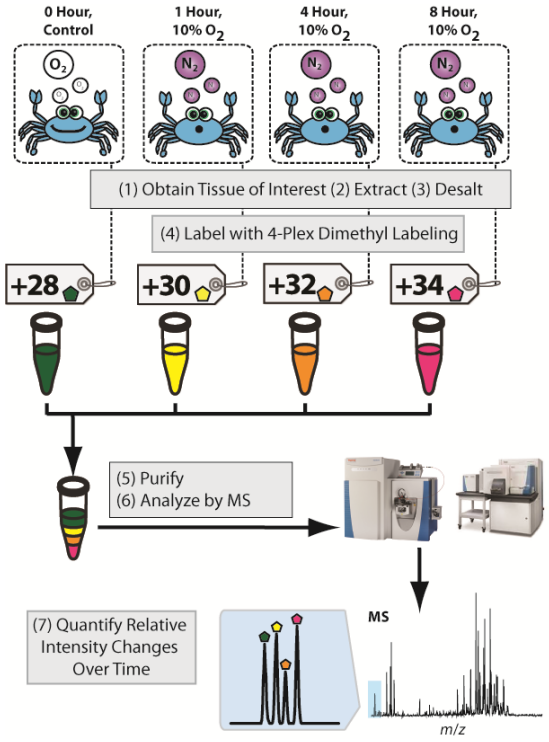

Modified from:

Amanda R. Buchberger[¥], Chris Sauer[¥], Nhu Q. Vu, Kellen DeLaney, Lingjun Li. "A Temporal Study of the Perturbation of Crustacean Neuropeptides Due to Severe Hypoxia Stress Using 4-Plex Reductive Dimethylation." In Preparation, 2018. [¥]Co-First Authors

Keywords: *Callinectes sapidus*, Mass Spectrometry, Neuropeptide, Hypoxia, Reductive Dimethylation

Abstract

Hypoxia (*i.e.,* low oxygen (O_2) levels) is a common environmental challenge for several aquatic species, including fish and invertebrates. In order to survive or escape these conditions, these animals have developed novel biological mechanisms, mainly regulated by neuropeptides. By utilizing mass spectrometry, this study aims to provide a global perspective of neuropeptides in the blue crab, *Callinectes sapidus*, and their changes over time (0, 1, 4, and 8 hours) due to severe (~10% O_2 water saturation) hypoxia stress using a 4-plex dimethyl labeling strategy to increase throughput. Using electrospray ionization and matrix-assisted laser desorption/ionization provided complementary coverage, 48 neuropeptides were identified with only four overlapping between the two ionization techniques. Interesting trends include (1) changes only after 4+ hours exposure (*e.g.,* RFamide AYPSLRLRFamide), (2) a return to basal levels after 8 hours' exposure following an initial response (*e.g.,* allatostatin A-type DPYAFGLRHTSFVLTAFGLamide), and (3) an oscillating pattern (*e.g.,* CHH precursor related peptide (CPRP) RSAEGLGRMamide), although many neuropeptides showed no significant changes. Overall, challenges still exist for the large-scale quantitation using 4-plex dimethyl labeling of neuropeptides, likely due to spectral complexity, and further applications towards optimizing instrumental parameters are a priority.

Introduction

Estuaries and coastal ecosystems are increasingly threatened by climate change, poorly managed wastewater, and agricultural and industrial runoff.[1] These factors often lead to eutrophication of coastal waters, causing large algal blooms and subsequent hypoxic (*i.e.,* low oxygen (O_2)) episodes that can last for hours to days.[2] Aquatic hypoxia also occurs naturally from

a multitude of hydrodynamic and meteorological effects.[3] During hypoxic episodes, the dissolved O_2 (DO) in the water greatly decreases, causing massive dead zones and a reduction in biodiversity as organisms are deprived of oxygen. Environmental hypoxia occurs most frequently in the spring and summer and can last for months.[3] As commercially-fished species rapidly perish during these times, the repercussions of hypoxia become economic as well as environmental.[4]

Although many aquatic organisms are affected by hypoxia, the blue crab, *Callinectes sapidus*, is of particular interest. The blue crab possesses both environmental and economic relevance as it is frequently fished from estuaries plagued by eutrophication and hypoxia.[2] In the literature, hypoxia has been shown to cause decreased rates of reproduction, growth, and feeding, and increased mortality rates in aquatic species.[5] Due to the adverse effects of hypoxia, the blue crab has developed interesting ways of surviving the low levels of DO. Prior studies have observed hypoxia-initiated defensive behaviors, including inactivity, self-burying, and migration towards shallower, more O_2-rich, waters.[5] Additionally, the composition of hemocyanin (*i.e.*, O_2 transport protein analogous to hemoglobin) has been shown to change in response to hypoxia, demonstrating physiological defensive mechanisms as well.[6, 7]

The variable behavioral and physiological changes in *C. sapidus* suggest the presence of complex signaling pathways involved in survival. Neuropeptides are short amino acid chains that act as signaling molecules within the nervous and neuroendocrine system. Previously, neuropeptides have been implicated in a range of environmental stress responses, including temperature and salinity fluctuations.[8, 9] They can have highly diverse effects within the body while also maintaining low *in vivo* concentrations.[10] Prior research has shown that the crustacean hyperglycemic hormone (CHH) is a neuropeptide involved in regulating the response to hypoxia in the blue crab,[11] but no work has thoroughly characterized other neuropeptidomic changes. By

examining the neuropeptide expression changes in the blue crab, their role in survival can be better understood.

Unfortunately, the high chemical diversity, low *in vivo* concentrations, and rapid degradation of neuropeptides makes their study challenging. Mass spectrometry (MS)—both matrix-assisted laser desorption/ionization (MALDI) and electrospray ionization (ESI)—has proven to be an effective method of analyzing neuropeptides as it has high sensitivity, high specificity, and can provide both quantitative and sequence information. Additionally, because it requires no prior knowledge of the analyte, MS is ideal for discovering novel neuropeptides involved in response to hypoxia. Relative quantitation of neuropeptides by MS is typically achieved by employing either MS1-based labeling strategies (*e.g.*, dimethyl labeling, iDiLeu, and mTRAQ),[12-14] or tandem MS (MS/MS) labels (*e.g.,* iTRAQ, TMT, and DiLeu) .[15-17] MS/MS reporters require the neuropeptide be selected for fragmentation to be quantified. The low abundance of many neuropeptides, however, makes their selection for MS/MS less likely. For this reason, MS1-based labeling strategies are often selected for neuropeptide quantitative analyses.

Previously, experiments have utilized duplex dimethyl labeling to analyze neuropeptidomic changes in crustaceans.[8, 9] Stable isotopes, supplied by isotopic formaldehyde, are added to the N-termini and lysine side chains of peptides by reductive dimethylation, adding two methyl groups, which add either 28.03130 or 32.05641 Daltons (Da) to each primary amine, depending on the stable isotopes incorporated. The heavy- and light-labeled samples are analyzed simultaneously to provide relative quantitation information between experimental and control conditions. Though effective, duplex labeling requires an individual control sample for each experimental sample. Expanding the multiplexing capabilities of dimethyl labeling strategies greatly reduces the number of samples needed as multiple samples can be compared to a single

control. Simultaneous analysis of the differentially labeled samples also reduces the instrument time required and the run-to-run variability. A 4-plex dimethyl labeling method is achieved by selecting formaldehyde with different combinations of $^{12}C/^{13}C$ and $^{1}H/^{2}H$, providing four distinct mass additions (+28.03130, +30.03801, +32.05641, and +34.06312 Da) that can be incorporated at the N-termini and lysine residues via reductive dimethylation.[18-20] This is a cost-effective approach to increase both throughput and quantitative abilities.

In this study, 4-plex dimethyl labeling was used to quantify the relative changes in expression of neuropeptides in *Callinectes sapidus* after 1, 4, and 8 hours of hypoxia exposure. These exposure durations are reflective of hypoxia exposure before blue crabs manage to escape hypoxic episodes and have been studied previously.[5] The multiplexed samples were analyzed by both MALDI- and ESI-MS to provide enhanced, complementary coverage of the crustacean neuropeptidome.[21] In fact, only four of the 48 identified neuropeptides were found in both ESI- and MALDI-MS analyses. Several trends were revealed in this time course study, the most interesting being a oscillating expression pattern seen in neuropeptides such as orcokinin NFDEIDRSSFA, CHH precursor related peptide (CPRP) RSAEGLGRMamide, and other neuropeptide hormone, such as HL/IGSL/IYRamide.

Materials and Methods

Methanol (MeOH), acetonitrile (ACN), glacial acetic acid (GAA), ammonium bicarbonate, and all crab saline components (see below) were purchased from Fisher Scientific (Pittsburgh, PA). Formaldehyde (CH_2O), ^{13}C-formaldehyde ($^{13}CH_2O$), $^{2}H_2$-formaldehyde ($C^{2}H_2O$), $^{13}C,^{2}H_2$-formaldehyde ($^{13}C^{2}H_2O$), and borane pyridine complex (~8M BH_3) were acquired from Sigma-Aldrich (St. Louis, MO). 2,5-dihydroxybenzoic acid (DHB) was obtained

from Acros Organics (Morris, New Jersey), and formic acid (FA) was purchased from Fluka (Mexico City, Mexico). All water (H_2O) used in this study was either HPLC grade or doubly distilled on a Millipore filtration system (Burlington, MA), and C18 Ziptips were purchased from Millipore (Burlington, MA). All LC solvents were Fisher Optima Grade.

Animals and Stress Experiment

All female blue crabs, *Callinectes sapidus*, were either purchased from LA Crawfish Company (Natchitoches, LA). After transport, crabs were allowed to recover in artificial seawater made to be 35 parts per thousand (ppt), 17-18 °C, and 8-10 parts per million (ppm) (~80-100%) O_2 for several days prior to being exposed. To mimic severe hypoxia (1 ppm, ~10% O_2), a tank was sparged with N_2 gas for 30-40 minutes to bring the DO down to the desired level as measured by a Pinpoint II Oxygen Monitor prior to adding a crab. A plastic tarp was placed on top of the water's surface to minimize water-air oxygen exchange during sparging. A crab was then placed in the tank for the desired amount of time (*i.e.,* 1 hour, 4 hours, or 8 hours), anesthetized on ice for 20 minutes, and sacrificed for its organs of interest as previously described.[22] All dissections were performed in chilled (approximately 10 ºC) physiological saline (composition: 440 mM NaCl; 11 mM KCl; 13 mM $CaCl_2$; 26 mM $MgCl_2$; 10 mM Trizma acid; pH 7.4 (adjusted with NaOH)).

Sample Preparation

For each bioreplicate, one set of tissues was extracted with a Fisherbrand Model 120 probe sonicator/sonic dismembrator with chilled acidified MeOH (90:9:1 MeOH:H_2O:GAA; volume (v):v:v). Each sample was sonicated three times for 8 seconds at 50% amplitude with a 15 second break in between each sonication. After centrifugation at 20,000 rpm for 20 minutes at 4 °C, the supernatant was collected and dried down in a Savant SCV100 Speedvac. All crude

extracts were purified using C18 ZipTips following the manufacturer's protocol. All samples were centrifuged at high speed (>10,000 rpm) briefly prior to purification. Control and hypoxia-exposed samples were differentially labeled using reductive dimethylation using a previously published protocol with slight modifications,[18-20] Borane pyridine was the reducing agent. The samples were all differentially labeled as follows: (a) control (*i.e,* 0 hours) with formaldehyde (CH_2O, +28.03130 Da), (b) 1 hr exposure with ^{13}C-formaldehyde ($^{13}CH_2O$, +30.04391 Da), (c) 4 hr exposure with $^{2}H_2$-formaldehyde ($C^{2}H_2O$, +32.05641 Da), and (d) 8 hr exposure with ^{13}C, d_2-formaldehyde ($^{13}C^{2}H_2O$, +34.06902 Da). All samples were mixed 1:1:1:1 after being quenched with ammonium bicarbonate. The multiplexed samples were then processed two different ways: (a) spotted with 150 mg/mL DHB (in 50:50 MeOH:H_2O with 0.1% FA) on a stainless-steel plate to be analyzed by a Thermo MALDI-LTQ-Orbitrap XL or (b) purified again with C18 ZipTips and analyzed by a Thermo Q Exactive (QE) coupled to a Waters nanoAquity system.

MS Data Collection

MALDI samples were spotted in triplicate and analyzed in the mass-to-charge ratio (*m/z*) 500-2000 range at a resolution of 60,000 on the MALDI-LTQ-Orbitrap XL. ESI samples were injected in triplicate onto a homemade C18 column (14-16 cm), from which the analytes were eluted using a 90-minute gradient (10% B to 35% B) with H_2O (0.1% FA) (A) and ACN (0.1% FA) (B) and analyzed by the QE in a mass range of *m/z* 200-2000 with a top 15 data-dependent acquisition method with high-energy collision dissociation. MS1 and MS/MS spectra were collected at a 70,000 and 17,500 mass resolution, respectively.

Data Analysis

Data collected by MALDI-MS was analyzed by exporting all the *m/z* values from Xcalibur and processed using a custom program written in Java by accurate mass matching (±5 ppm) with

an intensity threshold of 100. Neuropeptides were identified by matching their masses to an in-house database, accounting for the addition of +28.03130, +30.03801, +32.05641, and +34.06312 Da on the N-terminus from isotopic reductive dimethylation. ESI-MS raw data were imported into PEAKS 8.5 software for *de novo* sequencing and database matching. Quantitation was performed manually from the exported PEAKS database search results and the corresponding peak areas for the tandem MS-identified neuropeptides. All fragments of a neuropeptides were equally weighted in calculating ratios. No isotopic correction was considered for our datasets. For both MALDI and ESI analyses, all channels were normalized by taking individual intensity or peak areas divided by the total intensity or peak area. Ratios were then calculated by taking dividing the normalized intensity of either the +30.03801, +32.05641, or +34.06312 channel by the +28.03130 channel's normalized intensity. Statistical significance between experimental and control samples was determined by a Dunnett's test, which is utilized for comparing multiple experimental conditions to a single control.[23, 24]

Results and Discussion

Hypoxia is rampant in coastal estuaries, and profiling the molecules (*e.g.,* neuropeptides) that are implicated in the stress, especially in crustaceans who tend to reside in these areas, response is a priority.[4, 25] In particular, a temporal component is important to consider more than just the immediate response to a stress. Short term changes could be due to the hyperarousal, and long-term exposure could reveal an alternative, possibly novel mechanism for surviving these stressful conditions until the hypoxic episode ends, which could be a few hours to days.[26] In order to examine four time points (*i.e.,* 0, 1, 4, and 8 hours), a multiplexing strategy was implemented using reductive dimethylation. In the literature, this technique has been utilized in a

2-plex, 3-plex, and 5-plex form, but a 4-plex version has not been investigated further.[9, 12, 18, 27-30] Because our version does not require the addition of deuterium reducing agent, we use a borane pyridine complex, which has already been proven to be successful for the 2-plex reductive dimethylation model (**Figure 1**).[8, 9, 20, 30] One concern for multiplexing beyond 2-plex is isotopic overlap, and formulas have been derived to handle this issue specifically for 5-plex reductive methylation. This is not a major concern for our studies however, due to the low molecular weight of most the neuropeptides in this study.[19]

Figure 2a shows an example spectrum of allatostatin B-type VPNDWAHRFGSWamide (*m/z* 1470.703) found in the PO from our 4-plex labeled experimental data set. As expected, we see four distinct peaks in the spectra that were separated by ~2 Da. In this spectra, we also can see a dynamic, overall increase in neuropeptide expression due to increased time exposure of hypoxia stress. To test the quantitative accuracy of this system, **Figure 2b** shows 1:1:1:1 box plots of the ratio across all 4 channels, which were all within a <15% error range. Compared to 2-plex reductive dimethylation, which traditionally has been used for crustacean neuropeptidomic studies,[8, 9, 30] one particular challenge is finding all channels due to spectral complexity, which we see in our dataset (**Tables S1** and **S2**), in our study, we were able to identify 48 neuropeptides across five different tissues (*i.e.,* sinus gland (SG), brain, pericardial organ (PO), commissarial ganglion (CoG), and thoracic ganglion (TG)).

In our analysis, both MALDI- and ESI-MS were utilized due to their complementary ionization mechanisms, but it should be noted that there are major differences in (a) instruments and (b) data analysis pathways.[21] Interestingly, out of the 48 total neuropeptides identified, only 4 were found by both MALDI- and ESI-MS (**Figure 3**). These overlapped peptides include HL/IGSL/IYRamide (*m/z* 844.479) found in the SG, orcokinin NFDEIDRSGFA (*m/z* 1198.579)

found in the SG, allatostatin B-type SGDWSSLRGAWamide (*m/z* 1220.581) found in the PO, and VPNDWAHFRGSWamide (*m/z* 1470.703) found in the PO. None of the overlapping neuropeptide channels were found to be significantly different. Interestingly, for allatostatin B-type SGDWSSLRGAWamide, only the +28.03130 and +30.03801 channels were found by ESI-MS, but the +28.03130, +32.05641, and +34.06312 channels were identified in MALDI-MS. In order to be quantified, we require at least one stress channel (*i.e.,* + 30, +32, or +34) and the control channel (*i.e.,* +28). Thus, in this case, the ESI-MS analysis provided us with the +30/+28 ratio, while the MALDI-MS analysis allowed us to calculate the +32/28 and the +34/+30 ratios. One neuropeptide (*i.e.,* VPNDWAHFRGSWamide) was identified in all 4 channels for both ESI- and MALDI-MS, though the MALDI and ESI ratios did not appear to match (0.614, 0.581, and 0.480 for ESI; 1.191, 1.195, 1.540 for MALDI). In general, it was clear that there were distinct families that were only identified in the MALDI results, such as proctolin, RFamide, RYamide, tachykinin, and cryptocyanin. On the other hand, orcomyotropin and pigment dispersing hormone (PDH) were only identified in the ESI data, although orcomyotropin has been identified in MALDI data sets in the past (see *Chapter 3*). The ESI data provides a unique opportunity to look at larger neuropeptides. Two CPRP neuropeptides (*i.e.*, RSAEGLGRMGRLLASLKSDTVTPLRGFEGETGHPLE and RSAEGLGRMGRLLASLKSDTVTPLRGFEGETGHPLE) along with the PDH neuropeptide family were outside the MALDI-LTQ-Orbitrap XL's mass range. Conversely, many of the smaller (<*m/z* 1000) neuropeptides were identified by MALDI-MS.

Neuropeptides identified in the ESI- and MALDI-MS dataset in at least three biological replicates are shown in **Tables S1** and **S2**, respectively. All neuropeptides that had a statistically significantly change at any point during the hypoxia exposure time course are highlighted in

Figure 4. From this, several trends were revealed: (1) While an initial response was observed, after 8 hours of exposure the neuropeptide levels return to those similar to a control (*i.e.,* basal levels). This could be interpreted as a hyperarousal response. Allatostatin A-type DPYAFGLRHTSFVLYAFGLamide was the only neuropeptide that illustrated this trend. In crustaceans, allatostatin A-type neuropeptides were well documented for being inhibitory neuro/myomodulators.[31] By possibly decreasing the crab's heartbeat, the nervous system may be giving the crab an initial survival mechanism for short bouts of hypoxia. (2) Neuropeptides were increased or decreased after a certain duration of hypoxia exposure, either 4 or 8 hours. Unlike trend 1, this delay aligns more with the "fight" in the "flight-or-fight" response, where the crustacean has developed a mechanism to handle the hypoxia stress after initial attempts to escape were unsuccessful. This trend was seen for allatostatin B-type STNWSSLRSAWamide (*m/z* 1293.633) in the SG, CPRP RSAEGLGRMGRLLASLKSDTVTPLRGFEGETGHPLE (*m/z* 3838.003) in the SG, RFamide AYPSLRLRFamide (*m/z* 1121.658) and tachykinin APSGFLGMRamide (*m/z* 934.493) in the brain. It is difficult to decode why these families all appear to have similar trends due to their various and/or unknown functions, although it should be noted that most of them were localized in the SG.[31] While this may be due to more neuropeptides being identified in the SG than the brain, the SG could play more of a role in the crab's ability to survive in the long-term "fight" response. (3) An oscillating pattern was observed. After 1 hour of exposure, there was a significant change in the neuropeptide content, followed by a return to normal at the 4 hour time point. Finally, after eight hours of exposure, there is a similar, significant change as seen at 1 hour. This can either be an increasing (*i.e.,* allatostatin A-type SPRLTYFGLamide (*m/z* 1052.589) in brain, CPRP RSAEGLGRMamide (*m/z* 975.516) in SG, and others HL/IGSL/IYRamide (*m/z* 844.479) in SG) or decreasing (*i.e.,*

orcokinin NFDEIDRSSFA (*m/z* 1228.559) in SG) trend. Once again, the variety of neuropeptides and families makes it difficult to make any conclusions, although the only decreased neuropeptide was an orcokinin, which is known to increase the frequency and amplitude of contractions in the hindgut.[31] In general, the crab may be going in and out of either escape or coma-like activities in order to survive the harsh, hypoxic environment.

When comparing to results reported in *Chapter 3*, seven different neuropeptides were found to overlap in our MALDI-MS analyses. Several of these were consistent with each other in that no significant changes were seen after one hour of severe hypoxia exposure (1 ppm or 10% O_2 water saturation), including tachykinin APSGFLGMRamide (*m/z* 934.493; brain), allatostatin A-type NPRSFGLamide (*m/z* 796.399; PO), allatostatin B-type VPNDWAHRFGSWamide (*m/z* 1470.703; PO), proctolin RYLPT (*m/z* 649.367; PO), and RYamide SGFYANRYamide (*m/z* 976.464; PO). In the SG, there were two neuropeptides (*i.e.,* HL/IGSL/IYRamide (*m/z* 844.479) and CPRP RSAEGLGRMamide (*m/z* 975.515)) that showed significant changes in both studies. Unfortunately, the trends we observe were opposite. In *Chapter 3*, we see a downregulation in HL/IGSL/IYRamide and RSAEGLGRMamide, while here we observe an upregulation in the same tissue. This was likely due to number of animals used, which will increase biological variability, or analytical variation. One other possibility is from where our crustacean species were obtained. In *Chapter 3*, all crabs for the 1 hour 1 ppm O_2 saturation exposure were obtained over a three-year period from the Midway Asian Market in Madison, Wisconsin, which acquires crabs from the Maryland area. For the present study, all crustaceans were collected over a one-month period from LA Crawfish Co. in Louisiana. Not only could the timeline account for the biovariability observed but also could the location. Some crustaceans, deemed hypoxia-tolerant or hypoxia-sensitive, can have different hemocyanin phenotypes when collected from two

different coastal bodies.[7] Also, different years can have different seasonal environmental factors that need to be considered, which could have affected the congruency our results.[32]

In order to quantify a neuropeptide, the neuropeptide must be identified in at least the control and one other channel. Unfortunately, this does not allow us to analyze neuropeptides that were expressed only after hypoxia exposure. The CoG provides us an excellent example, as out of the neuropeptides identified, four neuropeptides were only identified in the control, while the other eight only appeared after hypoxia exposure occurred. **Table S3** provides a representative sample of those neuropeptides that were unquantifiable in all five tissues. It should be noted that our analysis requires that the neuropeptide to be found in at least four out of five biological replicates to be "identified." Thus, neuropeptides may have been present in all four channels, but those neuropeptides may be below the detection limit of our instrument or data analysis parameters. All tissues had neuropeptides that were only measurable in the control condition, such as allatostatin A-type GPYSFGLamide (*m/z* 739.377) in both the CoG and PO. This could indicate that they were released into the hemolymph or degraded. Similar to trend 2, several examples of neuropeptides that only appear after severe hypoxia exposure. Some neuropeptides appear over the entire time course (*e.g.,* allatostatin B-type AWSNLGQAWamide (*m/z* 1031.506) in PO, crypotocyanin KIFEPLRDKN (*m/z* 1259.711) in SG, and CPRP RSVEGVSRMEKLLT (*m/z* 1604.879) in the TG, while others may only appear after or for a certain time period. For example, allatostatin A-type LKAYDFGLamide (*m/z* 925.514) in the brain, cryptocyanin YKIFEPLRES *(m/z* 1281.684) in the CoG, and allatostatin A-type AGPYAFGLamide (*m/z* 794.420) in the PO, were only expressed after 1 hour of severe hypoxia exposure and then disappeared. This was also seen for 4 hour exposure for RYamide L/IFVGGSRYamide (*m/z* 897.494) in the brain and PO, burscion (*m/z* 13257.451) in the PO, and

orcokinin DRDEIDRSSFA (*m/z* 1271.554) in the PO. Interestingly, these were all mainly found in the PO, which could indicate a distinct role for the PO after 4 hours of stress. The extended time for exposure revealed different sets of neuropeptides, eleven neuropeptides (*e.g.,* RFamide ALDRNFLRFamide (*m/z* 1150.648) in the brain and allatostatin B-type STDWSSLRSAWamide (*m/z* 1294.618) in the PO) only showed up after 8 hours of stress, although we cannot comment if their expression was maintained after this point due to the limitations of our study. Finally, in the brain, an oscillating pattern similar to previous trend 3 was observed for two neuropeptides (*i.e.,* RFamide APQGNFLRFamide (*m/z* 1048.569) and RYamide LGRVSNRYamide (*m/z* 954.516)). Overall, due to the variable neuropeptide families, their functions, and various tissues, it is difficult to formulate true roles that each of these grouping may affect the crustacean, although it is clear that they all play distinct roles in how the crustacean survives both short- and long-term hypoxia stress.[31]

Of particular interest to hypoxia stress are RFamides, RYamides, and tachykinins, because their mammalian homologs, neuropeptide Y (NPY) and substance P (SP), have been implicated in hypoxia stress.[33-39] Both RFamides and RYamides showed variable expression due to severe hypoxia stress. Both families known for their dynamic roles in the nervous system, and it is expected that they will have a diverse response due to stress.[31] In the brain, PO, and SG, several RFamide and RYamide isoforms appeared consistently only after hypoxia stress. Many of these were highlighted in the trends above, including RFamide ALDRNFLRFamide (*m/z* 1150.648) in the brain, RFamide APQGNFLRFamide (*m/z* 1048.569) in the brain, RYamide LGRVSNRYamide (*m/z* 954.516) in the brain, and RYamide L/IFVGGSRYamide (*m/z* 897.494) in the brain and PO. Interestingly, in the TG, there was only one RFamide (*i.e.,* RFamide LNRNFLRFamide (*m/z* 1078.627)) isoform that was expressed after 8 hours of severe hypoxia

stress. The other two RFamides (*i.e.,* LGRPNFLRFamide (*m/z* 1118.658) and SMPTLRLRFamide (*m/z* 1119.646)) were only identified in the control, which could mean that they were degraded or released into the hemolymph to possibly target the cardiac or stomatogastic neuromuscular systems.[31] The variety of changes between RFamides and RYamides, which are homologs to NPY, emphasizes the importance of analyzing isoforms due to their possible different functions within the body, especially in understanding stress.[37, 38] A singlular tachykinin family neuropeptide (SGFLGMRamide (*m/z* 766.403)) was identified in the PO, and our results show that it was only present after 8 hours of severe hypoxia stress. Being homologous to SP, tachykinins may be more important for long-term hypoxia stress compared to the dynamic patterns seen for the various RFamide isoforms.[40] Either way, validation studies with hemolymph are of interest to truly characterize if these neuropeptides were being released (if the neuropeptides was only in the control) or were already present in the hemolymph to target these tissues after exposure to hypoxia stress (if they appear after hypoxia stress).

Conclusions and Future Directions

Neuropeptidomic studies offer new possibilities in untangling complex signaling pathways involved in a wide range of biological process, such as environmental stress response. Characterization of neuropeptides, however, presents many challenges as these signaling molecules are highly diverse and the analysis is often sample-limited. By utilizing isotopic reductive dimethylation, we demonstrate the efficacy of using multiplex labeling to quantify neuropeptidomic changes in the blue crab, *Callinectes sapidus*, after exposure to different durations of severe hypoxia. Several statistically significant changes were observed in both the MALDI and ESI data sets. Compared to the 2-plex labeling strategies used in the past, the 4-plex

method yielded fewer neuropeptide identifications and higher quantitative variability. In the future, we will improve this by (a) collecting more biological replicates and (b) pooling more animals together like the duplex studies (see *Chapter 3*). To complement the data presented here and offer further validation, analyzing the spatial distribution of neuropeptides using MS imaging would allow us to observe changes that would otherwise be missed by analyzing only expression changes. Furthermore, analysis of the crustacean circulating fluid (*i.e.,* hemolymph) could demonstrate the secretion and transport of specific signaling molecules.

Acknowledgements

This work was supported by a National Science Foundation grant (CHE- 1710140) and the National Institutes of Health (NIH) through grant 1R01DK071801. A.R.B. would like to thank NIH for a General Medical Sciences National Ruth L. Kirschstein Research Service Award (NRSA) Fellowship 1F31GM119365. C.S. and N.Q.V. would like to thank the National Institute of General Medical Sciences of the NIH under Award Number T32GM008349 for the Biotechnology Training Program Predoctoral Traineeship support. K.D. acknowledges a predoctoral fellowship supported by the NIH under NRSA T32 HL 007936 from the National Heart Lung and Blood Institute to the University of Wisconsin-Madison Cardiovascular Research Center.

References

1. Barbier, E. B.; Hacker, S. D.; Kennedy, C.; Koch, E. W.; Stier, A. C.; Silliman, B. R., *Ecological Monographs* **2011,** *81* (2), 169-193.

2. Rabalais, N. N.; Diaz, R. J.; Levin, L. A.; Turner, R. E.; Gilbert, D.; Zhang, J., *Biogeosciences* **2010,** *7* (2), 585-619.

3. Diaz, R. J.; Rosenberg, R., *Oceanography and Marine Biology - an Annual Review, Vol 33* **1995,** *33*, 245-303.

4. Santana, R.; Lessa, G. C.; Haskins, J.; Wasson, K., *Estuaries and Coasts* **2018,** *41* (1), 99-113.

5. Stover, K. K.; Burnett, K. G.; McElroy, E. J.; Burnett, L. E., *Biological Bulletin* **2013,** *224* (2), 68-78.

6. Bell, G. W.; Eggleston, D. B.; Noga, E. J., *Biological Bulletin* **2009,** *217* (2), 161-172.

7. Bell, G. W.; Eggleston, D. B.; Noga, E. J., *Oecologia* **2010,** *163* (1), 57-68.

8. Zhang, Y.; Buchberger, A.; Muthuvel, G.; Li, L., *Proteomics* **2015**.

9. Chen, R. B.; Xiao, M. M.; Buchberger, A.; Li, L. J., *Journal of Proteome Research* **2014,** *13* (12), 5767-5776.

10. Li, L. J.; Sweedler, J. V., Peptides in the Brain: Mass Spectrometry-Based Measurement Approaches and Challenges. In *Annual Review of Analytical Chemistry*, Annual Reviews: Palo Alto, 2008; Vol. 1, pp 451-483.

11. Chung, J. S.; Zmora, N., *Febs Journal* **2008,** *275* (4), 693-704.

12. Kovanich, D.; Cappadona, S.; Raijmakers, R.; Mohammed, S.; Scholten, A.; Heck, A. J. R., *Analytical and Bioanalytical Chemistry* **2012,** *404* (4), 991-1009.

13. Greer, T.; Lietz, C. B.; Xiang, F.; Li, L. J., *Journal of the American Society for Mass Spectrometry* **2015,** *26* (1), 107-119.

14. Hwang, C. Y.; Kim, K.; Choi, J. Y.; Bahn, Y. J.; Lee, S. M.; Kim, Y. K.; Lee, C.; Kwon, K. S., *Proteomics* **2014,** *14* (1), 121-132.

15. Wiese, S.; Reidegeld, K. A.; Meyer, H. E.; Warscheid, B., *Proteomics* **2007,** *7* (3), 340-350.

16. Werner, T.; Becher, I.; Sweetman, G.; Doce, C.; Savitski, M. M.; Bantscheff, M., *Analytical Chemistry* **2012,** *84* (16), 7188-7194.

17. Xiang, F.; Ye, H.; Chen, R. B.; Fu, Q.; Li, L. J., *Analytical Chemistry* **2010,** *82* (7), 2817-2825.

18. Wu, Y.; Wang, F. J.; Liu, Z. Y.; Qin, H. Q.; Song, C. X.; Huang, J. F.; Bian, Y. Y.; Wei, X. L.; Dong, J.; Zou, H. F., *Chemical Communications* **2014,** *50* (14), 1708-1710.

19. Tashima, A. K.; Fricker, L. D., *J Am Soc Mass Spectrom* **2018,** *29* (5), 866-878.

20. DeLaney, K.; Buchberger, A.; Li, L., *Methods Mol Biol* **2018,** *1719*, 247-269.

21. Stapels, M. D.; Barofsky, D. F., *Analytical Chemistry* **2004,** *76* (18), 5423-5430.

22. Gutierrez, G. J.; Grashow, R. G., *J Vis Exp* **2009,** (25).

23. McHugh, M. L., *Biochemia Medica* **2011,** *21* (3), 203-209.

24. Jaki, T.; Hothorn, L. A., *Archives of Toxicology* **2013,** *87* (11), 1901-1910.

25. Gray, J. S.; Wu, R. S. S.; Or, Y. Y., *Marine Ecology Progress Series* **2002,** *238*, 249-279.

26. Wasson, K.; Lyon, B. E., *Behavioral Ecology* **2005,** *16* (6), 1037-1041.

27. Hsu, J. L.; Huang, S. Y.; Chen, S. H., *Electrophoresis* **2006,** *27* (18), 3652-3660.

28. Boersema, P. J.; Raijmakers, R.; Lemeer, S.; Mohammed, S.; Heck, A. J. R., *Nature Protocols* **2009,** *4* (4), 484-494.

29. Boersema, P. J.; Aye, T. T.; van Veen, T. A. B.; Heck, A. J. R.; Mohammed, S., *Proteomics* **2008,** *8* (22), 4624-4632.

30. Zhang, Y.; DeLaney, K.; Hui, L.; Wang, J.; Sturm, R. M.; Li, L., *J Am Soc Mass Spectrom* **2018**.

31. Christie, A. E.; Stemmler, E. A.; Dickinson, P. S., *Cell Mol Life Sci* **2010,** *67* (24), 4135-69.

32. Lycett, K. A.; Chung, J. S.; Pitula, J. S., *Plos One* **2018,** *13* (2), 14.

33. Poncet, L.; Denoroy, L.; Dalmaz, Y.; Pequignot, J. M.; Jouvet, M., *Brain Research* **1996,** *733* (1), 64-72.

34. Wang, Z. Z.; Dinger, B.; Fidone, S. J.; Stensaas, L. J., *Neuroscience* **1998,** *83* (4), 1273-1281.

35. Lee, E. W.; Michalkiewicz, M.; Kitlinska, J.; Kalezic, I.; Switalska, H.; Yoo, P.; Sangkharat, A.; Ji, H.; Li, L. J.; Michalkiewicz, T.; Ljubisavljevic, M.; Johansson, H.; Grant, D. S.; Zukowska, Z., *Journal of Clinical Investigation* **2003,** *111* (12), 1853-1862.

36. Moss, I. R.; Laferriere, A., *Respiratory Physiology & Neurobiology* **2002,** *131* (1-2), 15-27.

37. Husson, S. J.; Mertens, I.; Janssen, T.; Lindemans, M.; Schoofs, L., *Prog Neurobiol* **2007,** *82* (1), 33-55.

38. Dockray, G. J., *Exp Physiol* **2004,** *89* (3), 229-35.

39. Coast, G. M.; Schooley, D. A., *Peptides* **2011,** *32* (3), 620-31.

40. Satake, H.; Kawada, T.; Nomoto, K.; Minakata, H., *Zoolog Sci* **2003,** *20* (5), 533-49.

Figures

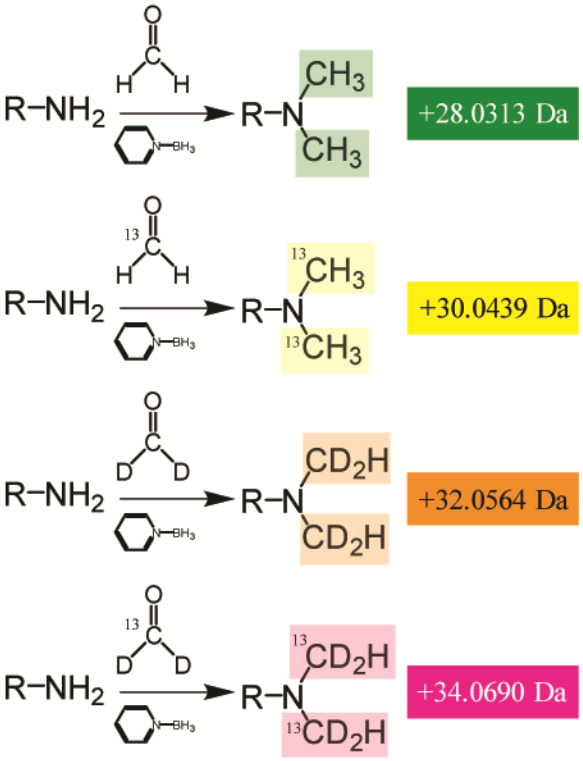

Figure 1. Reaction scheme for each version of the 4-plex reductive dimethylation utilized in this study. ^{13}C and ^{2}H (*i.e.,* D) were the only isotopes utilized.

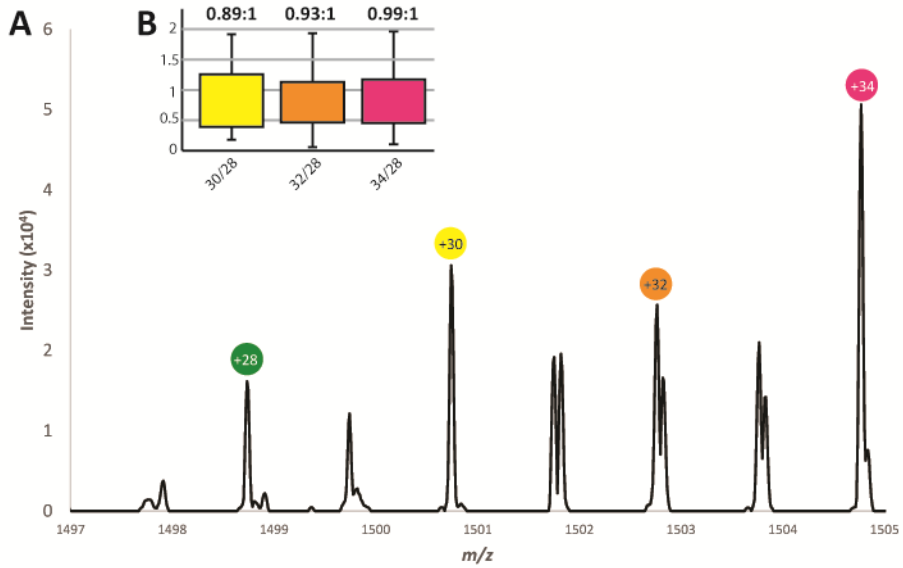

Figure 2. (a) Sample spectrum of 4-plex reductive dimethylation. Each label is spaced by ~2 Da. The representative neuropeptide is allatostatin B-type VPNDWAHRFGSWamide (*m/z* 1470.703) found in the PO. (b) A representative box plot of 1:1:1:1 labeling.

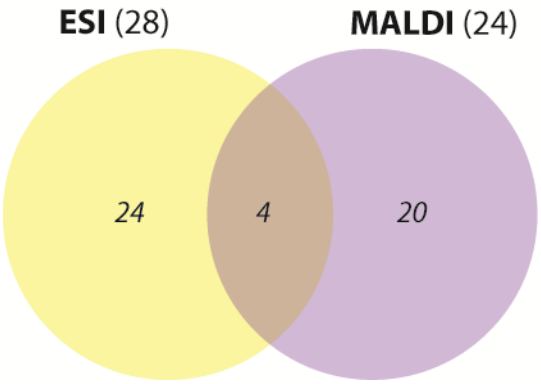

Figure 3. A Venn diagram depicting the neuropeptide overlap (regardless of expression changes) between ESI- and MALDI-MS. Only neuropeptides that were found in at least 2 bioreplicates in at least the control and one other channel in the SG, brain, PO, CoG, or TG were included. The four neuropeptides that overlapped included (1) HL/IGSL/IYRamide (*m/z* 844.479) (SG), (2) orcokinin NFDEIDRSGFA (*m/z* 1198.549) (SG), (3) allatostatin B-type SGDWSSLRGAWamide (*m/z* 1220.581) (PO), and (4) allatostatin B-type VPNDWAHFRGSWamide (*m/z* 1470.703) (PO).

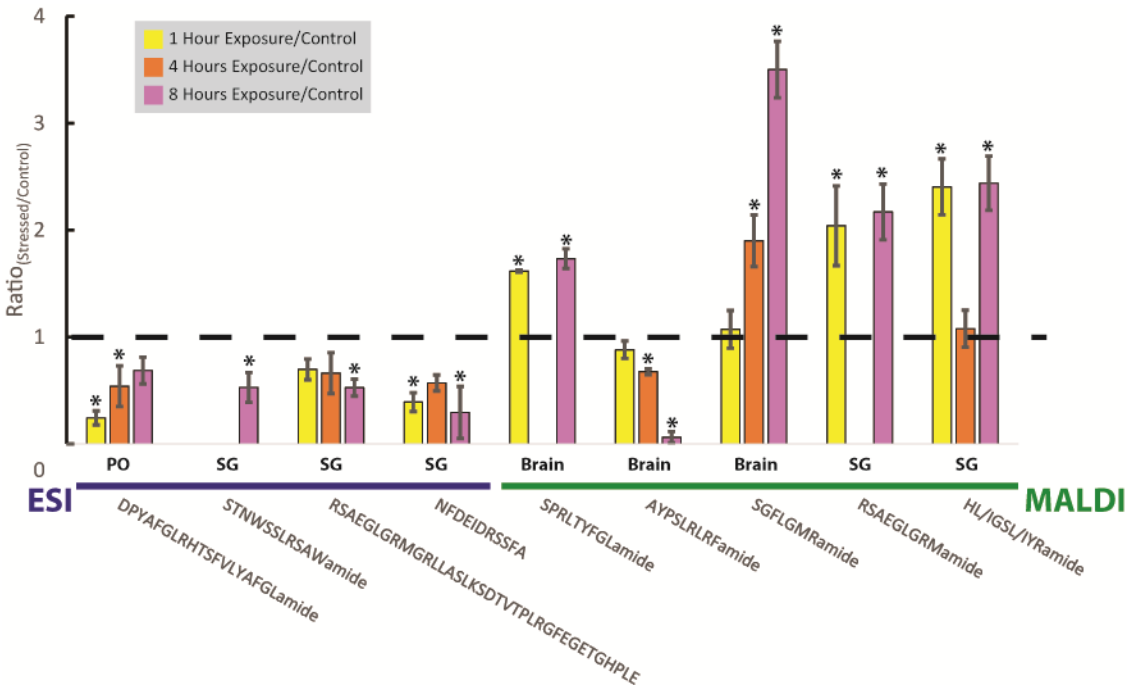

Figure 4. A bar graph of all neuropeptides found to have significant differences between a control and one of the three time points (*i.e.,* 1 hour (yellow), 4 hour (orange), and 8 hour (pink)) for severe (*i.e.,* 1 ppm O2) hypoxia exposure. The x-axis shows the neuropeptides' sequences, while the y-axis represents the ratio of hypoxia-stressed to a control. The dotted, black line represents a ratio of 1, indicating no change between the stressed condition and a control. The asterisk (*) represents statistical significance determined by a Dunnett's test. The error bars represent standard error of the mean (SEM).

Supplemental Information

Table S1. Ratios (stressed/control) of neuropeptides in the brain that were detected in at least three biological replicates in the ESI-MS results. The highlighted cells (*e.g.,* yellow, orange, or pink) are those were significant changes based upon the Dunnett's test. Blacked out cells are those that were identified in fewer than three biological replicates. Four neuropeptides (*i.e.,* HL/IGSL/IYRamide (*m/z* 844.479) and orcokinin NFDEIDRSGFA (*m/z* 1198.579) in the SG; allatostatin B-type SGDWSSLRGAWamide (*m/z* 1220.581) and VPNDWAHFRGSWamide (*m/z* 1470.703) in the PO) overlapped with the MALDI-MS data. SEM: standard error of the mean.

				1 ppm O2, 1 hour			1 ppm O2, 4 hours			1 ppm O2, 8 hours		
Tissue	Family	Sequence	m/z	Ratio	SEM	Sig?	Ratio	SEM	Sig?	Ratio	SEM	Sig?
Brain	Allatostatin B-type	TGWNKFQGSWamide	1209.580							1.739	0.143	N
	Others	HL/IGSL/IYRamide	844.479							0.846	0.113	N
PO	Allatostatin A-type	DPYAFGLRHTSFVLYAFGLamide	1209.580	0.244	0.066	Y	0.540	0.190	Y	0.687	0.125	N
	Allatostatin B-type	TSWGKFQGSWamide	1182.569				1.228	0.358	N	0.677	0.172	N
		TGWNKFQGSWamide	1209.580	0.517	0.135	N	1.074	0.257	N	0.631	0.128	N
		SGDWSSLRGAWamide	1220.581	0.994	0.340	N						
		STNWSSLRSAWamide	1293.633	1.052	0.165	N	0.757	0.287	N	0.622	0.146	N
		NNNWTKFQGSWamide	1380.644	0.975	0.258	N	0.995	0.327	N	0.520	0.190	N
		VPNDWAHFRGSWamide	1470.703	0.614	0.257	N	0.581	0.162	N	0.480	0.178	N
	CPRP	RSAEGLGRMGRLLASLKSDTVTPLRGFEGETGHPLE	3838.003	0.930	0.105	N	1.218	0.170	N	0.594	0.145	N
	Orcokinin	DFDEIDRSGFGFA	1475.644				0.509	0.196	N			
SG	Allatostatin B-type	TSWGKFQGSWamide	1182.569							0.660	0.130	N
		STNWSSLRSAWamide	1293.633							0.528	0.140	Y
	CPRP	RSAEGLGRMGRLLASLKSDTVTPLRGFEGETGHPLE	3838.003	0.696	0.097	N	0.662	0.191	N	0.527	0.080	Y
	Orcokinin	NFDEIDRSGFA	1198.549				0.770	0.085	N			
		NFDEIDRSSFA	1228.559	0.391	0.087	Y	0.570	0.075	N	0.294	0.243	Y
		NFDEIDRSSFGFN	1547.676							1.311	0.437	N
		DFDEIDRSSFGFN	1548.660				1.780	0.293	N	0.640	0.082	N
	Orcomyotropin	FDAFTTGFGHS	1186.516	0.844	0.246	N	1.067	0.081	N	1.373	0.241	N
	Others	HL/IGSL/IYRamide	844.479				0.636	0.101	N			
	PDH	QELHVPEREAVANLAARILKIVHAPHDAAGVPHKRN SELINSLLGISALMNEAamide	5712.103	0.491	0.328	N	0.807	0.306	N	0.164	0.123	N
		QEDLKYFEREVVSELAAQILRVAQGPSAFVAGPHKR NSELINSLLGIPKVMNDAamide	5947.165	0.725	0.138	N						
		QELKYQEREMVAELAQQIYRVAQAPWAAAVGPHK RNSELINSILGLPKVMNDAamide	5973.138				0.590	0.088	N			

Table S2. Ratios (stressed/control) of neuropeptides in the brain that were detected in at least three biological replicates in the MALDI-MS results. The highlighted cells (*e.g.,* yellow, orange, or pink) are those were significant changes based upon the Dunnett's test. Blacked out cells are those that were identified in fewer than three biological replicates. Four neuropeptides (*i.e.,* HL/IGSL/IYRamide (*m/z* 844.479) and orcokinin NFDEIDRSGFA (*m/z* 1198.579) in the SG; allatostatin B-type SGDWSSLRGAWamide (*m/z* 1220.581) and VPNDWAHFRGSWamide (*m/z* 1470.703) in the PO) overlapped with the ESI-MS data. SEM: standard error of the mean.

				1 ppm O2, 1 hour			1 ppm O2, 4 hours			1 ppm O2, 8 hours		
Tissue	Family	Sequence	m/z	Ratio	SEM	Sig?	Ratio	SEM	Sig?	Ratio	SEM	Sig?
Brain	Allatostatin A-type	SPRLTYFGLamide	1052.589	1.616	0.010	Y				1.733	0.093	Y
	RFamide	SMPTLRLRFamide	1119.646	0.957	0.160	N	1.117	0.108	N	1.156	0.225	N
		AYPSLRLRFamide	1121.658	0.882	0.081	N	0.676	0.028	Y	0.062	0.053	Y
	Tachykinin	APSGFLGMRamide (-NH3)	917.462	1.269	0.490	N				2.218	0.825	N
		SGFLGMRamide	934.493	1.071	0.176	N	1.901	0.241	Y	3.501	0.264	Y
PO	Allatostatin A-type	NPYSFGLamide	796.399	0.606	0.225	N	1.060	0.137	N	1.242	0.099	N
	Allatostatin B-type	SGDWSSLRGAWamide	1220.581				2.167	0.322	N	1.552	0.497	N
		VPNDWAHFRGSWamide	1470.703	1.191	0.314	N	1.195	0.173	N	1.540	0.400	N
	CPRP	RSVEGASRMEKLL	1475.800				0.776	0.256	N			
	Cryptocyanin	KIFEPLREDNL	1373.742							0.864	0.312	N
	Proctolin	RYLPT	649.367	0.988	0.338	N	1.046	0.262	N	1.834	0.493	N
	RYamide	SGFYANRYamide	976.464	1.987	0.900	N	1.994	0.727	N	0.939	0.347	N
SG	CPRP	RSAEGLGRMamide	975.515	2.041	0.372	Y				2.170	0.260	Y
	Orcokinin	NFDEIDRSGFA	1198.549	1.066	0.151	N	1.033	0.161	N	0.864	0.196	N
		NFDEIDRSGFG	1256.554	1.536	0.342	N	1.204	0.267	N			
	Others	HL/IGSL/IYRamide	844.479	2.405	0.262	Y	1.078	0.174	N	2.439	0.253	Y

Table S3. Select neuropeptides that were unquantifiable. Only neuropeptides that appeared in over four biological replicates were selected. AST-A: Allatostatin A-type; AST-B; Allatostatin B-type.

Tissue	Family	Sequence	m/z	M/E?	Control?	1 Hour?	4 Hour?	8 Hour?
Brain	AST-A	EPYAFGLamide	795.404	M			X	X
		LKAYDFGLamide	925.514	M		X		
		SKSPYSFGLamide	984.515	M			X	X
	AST-B	STNWSSLRSAWamide	1293.633	E				X
	CPRP	RSVEGVSRMEKLLT	1604.879	M		X		X
	PDH	QREPTASKCQAATELAIQILQAVKGAHTGVAAGPHKRNSELINSLLGLPKFMIDA	5792.122	E	X			
	RFamide	APQGNFLRFamide	1048.569	M		X		X
		ALDRNFLRFamide	1150.648	M				X
		AYNRSFLRFamide	1172.632	M				X
		YGSDRNFLRFamide	1273.644	M				X
	RYamide	L/IFVGGSRYamide	897.494	M			X	
		LGFVSNRYamide	954.516	M		X		X
CoG	AST-A	GPYSFGLamide	739.377	M	X			
	Cryptocyanin	YKIFEPLRES	1281.684	M		X		
PO	AST-A	GPYSFGLamide	739.377	M	X			
		AGPYAFGLamide	794.420	M		X		
		PSMYAFGLamide	884.433	M	X			
		LKAYDFGLamide	925.514	M	X			
	AST-A/RFamide	EPYEFGLamide/DPSFLEFamide	853.409	M	X			
	AST-B	AWSNLGQAWamide	1031.506	E		X	X	X
		STDWSSLRSAWamide	1294.618	M				X
	Bursicon	DECSLRPVIHILSYPGCTSKPIPSFACQGRCTSYVQVSGSKLWQTERSMCCQESGEREAAITLNCPKPRPGEPKEKKVLTRAPIDCMCRPCTDVEEGTVLAQKIANFIQDSMPDSVPFLK	13257.451	E			X	
	Orcokinin	DFDEIDRSGFA	1271.554	E			X	
		NFDEIDRSSFA	1300.580	M				X
	RYamide	L/IFVGGSRYamide	897.494	M			X	
	Tachykinin	SGFLGMRamide	766.403	M				X
SG	Cryptocyanin	KIFEPLRDKN	1259.711	M		X	X	X
	Orcokinin	NFDEIDRSGFGFA	1474.660	M				X
TG	AST-A	PDM(O)YGFGLamide	914.408	M		X		
		LVKYSFGLamide	925.551	M				X
	AST-B	AWSNLGQAWamide	1031.506	M	X			
	CPRP	RSAQGLGKMERLL	1458.821	M	X			
		NTPLGDLSGSLGHPVE	1592.792	M				X
		RSVEGVSRMEKLLT	1604.879	M		X	X	X
	TG	LNRNFLRFamide	1078.627	M				X
		LGRPNFLRFamide	1118.658	M	X			
		SMPTLRLRFamide	1119.646	M	X			

Chapter 5

Improved Sample Preparation for Comparative MALDI-MS Imaging of the Crustacean Brain under Hypoxia and Hypercapnia Stress

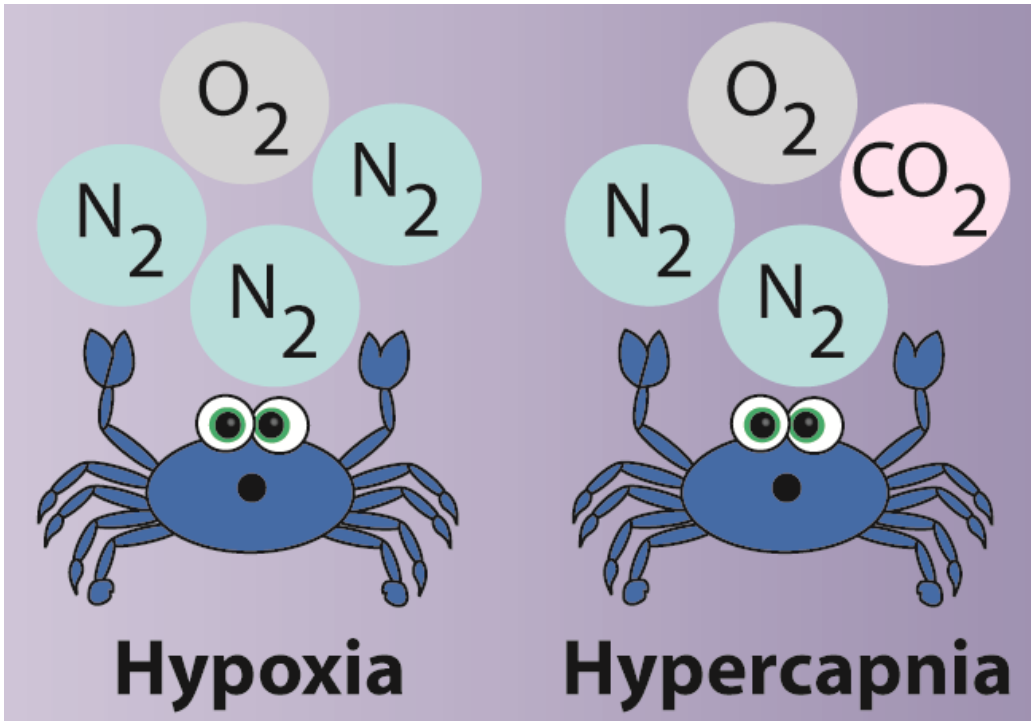

Modified from:

Amanda R. Buchberger, Nhu Q. Vu, Jillian Johnson, Lingjun Li. "Improved Sample Preparation for Comparative MALDI-MS Imaging of the Crustacean Brain under Hypoxia and Hypercapnia Stress." In Preparation, 2018.

Keywords*:* Crustaceans, Neuropeptides, Hypoxia, Hypercapnia, Mass Spectrometry Imaging

Abstract

Matrix-assisted laser desorption/ionization (MALDI)-MS imaging has been utilized to image a variety of biomolecules, including neuropeptides. Washing a tissue section is an effective way to eliminate interfering background and improve detection of low concentration target analyte molecules, however many previous methods have been incompatible with neuropeptides. Using crustaceans as a neurological model organism, we developed a new washing procedure and applied this method to characterize neuropeptide changes due to stress. Specifically, hypoxia and hypercapnia stress are environmentally a concern for crustaceans, making them a relevant model for this study. Furthermore, since crustacean neuropeptides are homologous to those found in humans, results from these studies can be applied to understand potential roles of neuropeptides involved in medical hypoxia and hypercapnia.

Introduction

Mass spectrometry (MS) imaging has found popularity because of its ability to provide relative molecular abundance and localization information simultaneously within a single tissue section. Unlike immuno-based assays, which require prior knowledge about the molecules of interest, thousands of species can be imaged in a single sample run, including unknown molecules.[1] Originally developed in 1997, matrix-assisted laser desorption/ionization (MALDI) – MS imaging has been applied to several molecular species, including metabolites, peptides, and proteins.[1, 2] In general, MS imaging has the power to map the spatial localization of a molecule, which could provide important clue to possible function of this molecule.

As with all analytical techniques, the success of MALDI-MS imaging is dependent upon proper sample preparation. For MALDI-MS imaging, the basic workflow requires an optimized

matrix application step after proper sectioning of the biological tissue. While this has been successful in the past, innovative techniques are being added to this workflow to increase molecular depth and image quality.[1] In particular, researchers are focusing on both (a) properly removing contaminants and (b) modifying molecules of interest prior to matrix application. Some examples include enzymatic digestion, chemical derivatization, and even incubation vapor chambers.[1, 3-5] Washing is one of the simplest methods to remove contaminants and enrich molecules. By immersing the tissue section in a solvent of choice for a desired amount of time, one can fix proteins (*e.g.,* Carnoy's solution) or release molecules from formalin-fixed paraffin-embedded tissue section.[1, 6, 7] The most common and effective wash solvents seen in the literature are alcohol-based.[8]

Even with the constant development of new methodology, an appropriate wash has not been found compatible for several molecular species, in particular, neuropeptides.[9] Dysregulation of neuropeptides, which are diverse signaling molecules in the brain, can have long-lasting physiological effects, suggesting they are of high interest in many social and biochemical behavioral studies.[10] Extensive washing tends to remove peptides due to their solubility in water, thus these washes need to be short and precisely timed. One group has used a 70% ethanol (EtOH) (10 seconds) followed by two 90% EtOH washes (10 seconds each) for rat neuropeptides, although this is the only example seen in the literature and is similar to washes used for protein MS imaging analysis.[11]

Compared to mammals, crustaceans have been utilized as a model system for neuropeptide-based studies due to their simple, well-characterized networks.[12] This is especially useful for comprehensive global analysis, which lends well to untargeted MS imaging-based studies.[13] Crustacean neuropeptides are also known to be homologous to many of those found in

humans, thus findings from crustacean-based studies can be applied to human studies in the future.[14-17] Specifically, crustaceans have been used to study the role of neuropeptides in the stress response, including temperature and salinity stress.[13, 18, 19] Other stressors, including hypoxia (*e.g.,* low oxygen (O_2) levels) and hypercapnia (*e.g.,* low O_2 and high carbon dioxide (CO_2) levels), are interesting due to their relevance to human respiratory distress (*e.g.,* asthma) or disease (*e.g.,* cancer).[20-24] In particular, there is a lack of understanding of the molecular changes that occur due to hypoxia and hypercapnia stress. Hypoxia and related pH stress (*i.e.,* hypercapnia) are well documented as environmental barriers for crustacean species.[25-32] Cellular respiration is a key process in the body, so it is imperative to further our knowledge of hypoxia and hypercapnia's effect on the nervous system.[20]

Here, we present a new washing method to enrich crustacean neuropeptides in brain tissue. Upon optimization of the washing procedure, neuropeptide identifications were increased by 1.15-fold, and normalized intensities were increased by 5.28-fold. This new sample preparation method was applied to characterize the localization changes of crustacean neuropeptides in four different stress conditions in the brain: (a) control (pH = 8.3, 100% O_2 water saturation), (b) severe hypoxia (pH = 8.3, 10% O_2 water saturation), (c) mild hypoxia (pH = 8.3, 50% O_2 water saturation), and (d) hypercapnia (pH = 7.6-7.8, 50% O_2 water saturation) for 2 hours. Statistically significant changes were seen for several neuropeptides, including the RFamide (*e.g.,* RQFLRFamide (mass-to-charge ratio (*m/z*) 865.516) and LPGVENFLRFamide (*m/z* 1061.626)) neuropeptide family, which is homologous to human opioids and neuropeptide Y.[15-17]

Materials and Methods

All water (H_2O) used in this study was doubly distilled on a Millipore filtration system

(Burlington, MA) or Fisher HPLC grade. Difco™ gelatin, plain glass microscope slides, all crab saline components (see below), and methanol (MeOH) were obtained from Fisher Scientific (Pittsburgh, PA). EtOH utilized in this study was from Pharmco-Aaper (Chicago, IL). Formic acid (FA) was purchased from Fluka (Mexico City, Mexico), and the 2, 5-dihydroxybenzoic acid (DHB) was obtained from Acros Organics (Morris, New Jersey).

Animals and Stress Experiments

All female blue crabs, *Callinectes sapidus*, were either purchased from Midway Asian Market (Madison, WI) or LA Crawfish Company (Natchitoches, LA). After transport, crabs were allowed to recover in seawater made to be 35 parts per thousand, 17-18 °C, 8-10 parts per million (ppm) O_2 (80-100% O_2 saturation), and pH = 8.3 for several days prior to being exposed to stressful conditions. For hypoxia experiments, a crab-less 10 gallon tank was sparged with N_2 gas for 30-40 minutes to bring the dissolved O_2 down to the desired level (*i.e.,* 1 ppm or 5 ppm O_2) (10% and 50% O_2 saturation, respectively). For hypercapnia experiments, a crab-less 10 gallon tank was sparged with CO_2 gas for 5 minutes to lower the pH to 7.6-7.8, which also lowered the dissolved O_2 levels (*i.e.,* 5 ppm O_2) (50% O_2 saturation). A plastic tarp is placed on top of the water's surface to minimize H_2O-air O_2 exchange during the course of the experiment. A crab was then placed in the tank for the desired amount of time (*i.e.,* 2 hours) before being anesthetized on ice and obtaining the brain as previously described.[33]

Sample Preparation

Freshly dissected brains were embedded in gelatin (in small plastic cups) and sectioned using a Micro HM525 cryostat (Thermo Scientific). The 12 micron thick sections were thaw mounted onto plain glass microscope slides and stored at -80 °C until use. Prior to use, samples were then dried in a vacuum chamber for 10-20 minutes. Samples were then submerged into

varying ratios of EtOH:H_2O for either 10 or 30 seconds using a slide staining system (Tissue-Tek). After drying under vacuum (*i.e.,* 15-20 minutes), matrix (*i.e.,* 40 mg/mL DHB in 50:50 MeOH:H_2O and 0.1% FA) was applied with a commercial TM-Sprayer (HTX Technologies, LLC) with the following optimized parameters: 0.1 mL/min syringe flow rate; 12 passes, 0.5 min dry time, 1250 mm/min nozzle velocity, 80 °C, and 3 mm track spacing. Samples were then analyzed immediately after matrix application. Control brains were used for all method optimization. To determine if salts are being removed after washing, the osmolarity (*i.e.,* salt content) of the wash solution after the tissue section was submerged in it and was determined by using an Advanced Instruments Model 325 Single-Sample Osmometer. To characterize the wash off, samples were spotted 1:1 with 150 mg/mL DHB (in 50:50 MeOH:H_2O and 0.1% FA).

Data Collection and Analysis

Samples were run on a MALDI-LTQ-Orbitrap XL (Thermo Fisher). A mass range of *m/z* 500-2000 was used along with the following parameters: 30,000 mass resolution and 75 micron spatial resolution. Raw data files were exported into an imZML format (using Thermo Fisher ImageQuest; Version 1.1.0 Build 54) to be imported into MSiReader (Version 1.00) or SCiLs lab software (Bremen, Germany).[34] Files were loaded into MSiReader together and normalized to the TIC to generate images. Accurate mass matching (AMM) (±10 parts per million (ppm)) to a homebuilt database was used to manually identify neuropeptides and their distributions. Lipids were identified by AMM (± 5 ppm) to the online LIPID MAPS database.[35] When distributions were compared, all images were normalized to the same intensity scale. Co-localization analysis was performed using the Coloc2 FIJI plugin on FIJI (FIJI Is Just ImageJ).[36] To determine statistically significant changes between control, hypoxia, and hypercapnia samples, samples were identified by AMM (±5 ppm) and analyzed by a student's t-test using SCiLs software

(Bruker; Bremen, Germany). In order to correct for the multi-comparison analysis, a Bonferroni correction was applied for the four comparisons, decreased the desired p-value from 0.05 to 0.0125.[37]

Results and Discussion

Wash Optimization and Characterization

In order to increase neuropeptide signals in the crustacean brain tissue, several different washes with varying amount of EtOH:H_2O were investigated: 100:0, 85:15, 70:30, 50:50, 30:70, 15:85, and 0:100 (volume (v):v). All washes were investigated for either 10 seconds or 30 seconds. A basic workflow is shown in **Figure 1**.

As one increased the amount of H_2O, the number of neuropeptide identifications increased, with 50:50 to 15:85 (EtOH:H_2O) showing the highest number of neuropeptides (Avg. ~30 neuropeptides), although 100% water showed a major decrease in neuropeptides when washed for 30 seconds compared to 10 seconds (18 versus 25 neuropeptides, respectively). The top 3 wash solutions were 50:50, 30:70, and 15:85 EtOH:H_2O, with each time duration investigated further with intensity analysis. Average normalized intensity showed an increase for all washes compared to a control by 3-5 fold, although the 50:50 wash, both 10 seconds and 30 seconds, provided the highest overall signal intensity (~5x), as shown in **Figure 2**.

In order to pick the most effective wash, co-localization analysis was performed on the 10 and 30 second 50:50 EtOH:H_2O washes. For *m/z* 865.516 (RFamide RQFLRFamide), we obtained a Pearson's correlation coefficient of 0.71 and a Mander's split coefficients 1 and 2 values of 0.896 and 0.897, respectively (**Table S1**).[36] The Pearson's correlation coefficient, which ranges from -1 to 1, relates the intensity colocalization between two images, in which

values closer to one are considered more colocalized.[36] The Mander's coefficient, which ranges from 0 to 1, determines spatial correlation between two images, where values closer to 1 are considered to be more correlated.[36] Thus, for *m/z* 865.516, it appears that the washes show identical changes to the localization of the neuropeptide. For *m/z* 1071.562 (TNYGGFLRFamide), 1119.646 (SMPTLRLRFamide), 1124.632 (GLSRNYLRFamide), and 1150.648 (ALDRNFLRFamide), high values for intensity and spatial distribution colocalization were found for both 10 second and 30 second washes (**Table S1**). Due to the lack of differences between these two wash conditions, the 10 second 50:50 EtOH:H_2O was chosen as the optimal wash for neuropeptides in this study. It should be noted that these colocalization tests here are automatically thresholded in FIJI to account for non-zero pixel overlap, however new statistical colocalization algorithms are currently in development that are not dependent upon the background to minimize the accounted effect of non-zero pixel overlap, which can artificially increase colocalization coefficient values.[36, 38]

For this wash system (50:50 EtOH:H_2O for 10 seconds), several neuropeptides were enriched. In fact, compared to a control (n=4), 34 neuropeptides showed an increase in signal after washing. It should be noted that three neuropeptides did not show any signal change, and six neuropeptides showed a signal decrease after washing. Several examples are shown in **Figure 3**. These trends were seen consistently across bioreplicates and technical replicates, an example of both shown in **Figures S1** and **S2**, respectively. While we lose some neuropeptides in this washing process, it is clear that there was an overall positive effect with enhanced detection of majority of neuropeptides due to the additional wash step.

Hydrophobicity analysis was also performed to find trends in which neuropeptides were removed while others increased in signals. Based upon the number of residues that are

characterized as hydrophobic divided by the total number of residues, each peptide's hydrophobicity was calculated and compared. Other online calculators, including Peptide 2.0, SSR Calculator, and Biosyn, were used to confirm our calculations and observations.[39] Overall, it appears that there is no clear trend, but, interestingly, most of the peptides that were more hydrophobic show a signal decrease after wash (**Table S2**). It should also be noted that most of these peptides were smaller, including *m/z* 808.435 (allatostatin A-type AAPYAFGLamide) and *m/z* 826.446 (allatostatin A-type TVAYGFGLamide), likely due to amino acids with hydrophobic side chains have a bigger effect on smaller peptides. There were obvious outliers to this trend though, including *m/z* 1019.590 (RFamide APRNFLRFamide), *m/z* 1061.574 (RFamide LPGVNFLRFamide), and *m/z* 1106.611 (RFamide LNPSNFLRFamide), which all decreased but showed low or no hydrophobic nature (**Table S2**). In general, smaller neuropeptides appeared to decrease in signal after being washed, while larger neuropeptides appeared to increase in signal, which could be related to hydrophobicity. Unfortunately, these results appear counterintuitive when thinking about how water-based washes tend to hydrophilic species, including salt. Thus, our results may be due to the unique biology of the crustacean tissue or other, special molecular characteristics of the neuropeptides.

Several different avenues were investigated to determine factors that contributed to enhanced detection of neuropeptides after washing protocol. Other biologically relevant species such as lipids and interfering background such as salts appeared to show signal increase or minor decrease, respectively, compared to control. Thus, while the washes were increasing neuropeptide signals, they were also increasing lipid signals likely due to the removal of salts. One point to note is that the salt concentration did not appear to decrease dramatically, but the measured osmolality values (*e.g.,* 1 and 4 mOsm before and after washing) were near the method

detection limit of the instrument, and its lack of sensitivity at these values could limit our analysis. When analyzing the post tissue wash solution, it did contain neuropeptides, such as *m/z* 1061.574 (orcokinin TRPDIANLYamide), that were observed to be removed from the tissue, confirming that the wash itself was removing these neuropeptides.

Hypoxia and Hypercapnia Comparison

The optimized wash system was utilized to characterize the neuropeptidomic changes between four different conditions: a) control (pH = 8.3, 100% O_2 water saturation), (b) severe hypoxia (pH = 8.3, 10% O_2 water saturation), (c) mild hypoxia (pH = 8.3, 50% O_2 water saturation), and (d) hypercapnia (pH = 7.6-7.8, 50% O_2 water saturation), all exposed for 2 hours. A representative group of neuropeptides that were calculated to have statistically significant changes are shown in **Table S3**.

Figure 4 illustrates several neuropeptides that are dysregulated due to hypoxia or hypercapnia stress. In some cases, there were clear changes in intensity and localization, such as **Figures 4d-f**, while **Figures 4b-c** require more sophisticated computational analysis to discriminate changes. Using the student's t-test for determining statistical significance (**Table S3**), many of the conditions were different from the control, including *m/z* 975.541 (cardioacceletory peptide (CAP) pELYAFPRVamide), *m/z* 1031.590 (RFamide AHKNFLRFamdie), *m/z* 1061.626 (RFamide LPGVNFLRFamide), and *m/z* 1079.611 (RFamide LDRNFLRFamide). In particular, **Figure 4d** shows that the neuropeptide (RFamide AHKNFLRFamide, *m/z* 1031.590) was absent in the control but was readily detected when the crustacean was exposed to hypoxia or related stress. This was also the case in **Figures 4f and 4g**. The opposite trend was seen in **Figure 4e**, where the neuropeptide appears to be released into the hemolymph (*i.e.,* crustacean hemolymph) or degraded due to exposure to stress since there was

only localization around the edge of the tissue. **Figure 4b and 4c** are difficult to infer what was occurring in the system, although it was clear that the neuropeptides exhibited substantial changes in relative abundance throughout the entire tissue (**Figure 4b**) or in specific ganglions (**Figure 4c**).

Besides comparing *in situ* peptide expression patterns only between the stress condition and a control, differences were also tested between both the moderate and severe hypoxia (*i.e.,* was there difference in localization and intensity due the hypoxic severity?) and moderate hypoxia and hypercapnia (*i.e.,* were the changes due to the hypoxia or also the inclusion of CO_2?). This can be aligned with statistically significant differences from the control (*m/z* 1065.595, 1119.646, and 1120.604) as well as not being significantly different from the control (*m/z* 1007.579). In the case of *m/z* 1007.579 (RFamide PKSNFLRFamide), both the two hypoxia severities were different from each other, suggesting that dysregulation of this neuropeptide was related to the hypoxic severity. More biological replicates are required to distinguish these minute differences. Another interesting trend was that several neuropeptides only exhibited significant changes due to pH stress, such as *m/z* 1024.557 (RFamide GLSRNYLRFamide), which suggested that the changes were directly related to the inclusion of CO_2, not just hypoxia.

Interestingly, most of the neuropeptides exhibiting statistically significant changes were RFamides, a crustacean neuropeptide family that is homologous to opioids and neuropeptide Y (NPY).[15-17] In crustaceans, RFamides, also known as FMRFamide-like peptides (FLPs), have various well documented functions, including modulation of the cardiac and stomatogastric neuromuscular system along with exoskeleton muscles.[40] They also work as autocrine/paracrine modulators while also circulating as hormones. Overall, it is obvious that RFamides can play various roles due to its diverse targets and functional roles. NPY has already been implicated in

hypoxia stress (*e.g.,* in rats), demonstrating that crustacean neuropeptides react similarly to those in higher order organisms.[41, 42] Another crustacean neuropeptide family (*i.e.,* tachykinin) that is homologous to human substance P, which has previously been implicated in hypoxia stress were also identified in our experiments.[14, 41] Like RFamides, tachykinin and related peptides work both locally and as long-distance circulating hormones as well as being implicated in decapod neuromuscular modulation. Unlike RFamides, all tachykinin-related neuropeptides showed no statistically significant changes were seen besides one (*m/z* 605.304; APSFGQamide). For this neuropeptide, only the two hypoxia severities (*i.e.,* 10% vs. 50% O_2) and the hypoxia and hypercapnia (*i.e.,* 50% O_2 vs. pH) conditions were significantly different, meaning none of the 3 stress conditions were significantly different from a control. This could mean that, since RFamides seem to play a more comprehensive role in how crustaceans handle hypoxia and hypercapnia stress, NPY could also be a more dominant player how humans handle respiratory distress and other hypoxia/hypercapnia prominent conditions.

Conclusions and Future Directions

Crustacean neuropeptides are important biomolecules due to their role in the stress response. Using MALDI-MS imaging, a new wash-based was developed in order to improve detection of neuropeptides and better understand their role in both hypoxia and hypercapnia stress. It would be of interest to further expand our ability to image other crustacean neuropeptides, specifically by utilizing different matrices and exploring other enrichment strategies. Comparison to quantitative tissue and hemolymph data is also needed to fully understand the dynamic changes due to stress, such as the distinction between degradation and release into the crustacean hemolymph (*i.e.,* blood). Furthermore, this wash method can be

applied to future imaging studies including mapping their localization in other crustacean tissues (*e.g.,* pericardial organ).

Acknowledgements

This work was supported by a National Science Foundation grant (CHE-1710140) and the National Institutes of Health (NIH) through grant 1R01DK071801. A.R.B. acknowledges the NIH General Medical Sciences F31 Fellowship (1F31GM119365) for funding. N.Q.V. would like to thank a UW-Madison Biotechnology Training Program Traineeship sponsored by the National Institute of General Medical Sciences of the NIH under Award Number T32GM008349. J.J. and L.L. acknowledge the University of Wisconsin Carbone Cancer Center Pancreas Cancer Task Force for the funds to complete this project. We would also like to thank the Zeeh Station in the University of Wisconsin-Madison School of Pharmacy for use of the Osmometer.

References

1. Buchberger, A. R.; DeLaney, K.; Johnson, J.; Li, L. J., *Analytical Chemistry* **2018,** *90* (1), 240-265.

2. Caprioli, R. M.; Farmer, T. B.; Gile, J., *Analytical Chemistry* **1997,** *69* (23), 4751-4760.

3. Heijs, B.; Holst, S.; Briaire-de Bruijn, I. H.; van Pelt, G. W.; de Ru, A. H.; van Veelen, P. A.; Drake, R. R.; Mehta, A. S.; Mesker, W. E.; Tollenaar, R. A.; Bovee, J.; Wuhrer, M.; McDonnell, L. A., *Analytical Chemistry* **2016,** *88* (15), 7745-7753.

4. Barre, F. P. Y.; Flinders, B.; Garcia, J. P.; Jansen, I.; Huizing, L. R. S.; Porta, T.; Creemers, L. B.; Heeren, R. M. A.; Cillero-Pastor, B., *Analytical Chemistry* **2016,** *88* (24), 12051-12059.

5. Angerer, T. B.; Magnusson, Y.; Landberg, G.; Fletcher, J. S., *Analytical Chemistry* **2016,** *88* (23), 11946-11954.

6. O'Rourke, M. B.; Raymond, B. B. A.; Djordjevic, S. P.; Padula, M. P., *Rapid*

Communications in Mass Spectrometry **2015,** *29* (7), 637-644.

7. O'Rourke, M. B.; Padula, M. P., *Biotechniques* **2016,** *60* (5), 229-+.

8. Seeley, E. H.; Oppenheimer, S. R.; Mi, D.; Chaurand, P.; Caprioli, R. M., *Journal of the American Society for Mass Spectrometry* **2008,** *19* (8), 1069-1077.

9. Buchberger, A.; Yu, Q.; Li, L., *Annu Rev Anal Chem (Palo Alto Calif)* **2015,** *8* (1), 485-509.

10. Hokfelt, T.; Broberger, C.; Xu, Z. Q. D.; Sergeyev, V.; Ubink, R.; Diez, M., *Neuropharmacology* **2000,** *39* (8), 1337-1356.

11. Hanrieder, J.; Ljungdahl, A.; Andersson, M., *Journal of visualized experiments : JoVE* **2012,** (60).

12. Hopkins, P. M., *General and Comparative Endocrinology* **2012,** *175* (3), 357-366.

13. Zhang, Y.; Buchberger, A.; Muthuvel, G.; Li, L., *Proteomics* **2015**.

14. Satake, H.; Kawada, T.; Nomoto, K.; Minakata, H., *Zoolog Sci* **2003,** *20* (5), 533-49.

15. Husson, S. J.; Mertens, I.; Janssen, T.; Lindemans, M.; Schoofs, L., *Prog Neurobiol* **2007,** *82* (1), 33-55.

16. Dockray, G. J., *Exp Physiol* **2004,** *89* (3), 229-35.

17. Coast, G. M.; Schooley, D. A., *Peptides* **2011,** *32* (3), 620-31.

18. Chen, R. B.; Xiao, M. M.; Buchberger, A.; Li, L. J., *Journal of Proteome Research* **2014,** *13* (12), 5767-5776.

19. Wang, J. H.; Zhang, Y. Z.; Xiang, F.; Zhang, Z. C.; Li, L. J., *Journal of Chromatography A* **2010,** *1217* (26), 4463-4470.

20. Rolfe, D. F. S.; Brown, G. C., *Physiological Reviews* **1997,** *77* (3), 731-758.

21. Harris, A. L., *Nature Reviews Cancer* **2002,** *2* (1), 38-47.

22. Kelsen, S. G.; Fleegler, B.; Altose, M. D., *American Review of Respiratory Disease* **1979,** *120* (3), 517-527.

23. Semenza, G. L., *Journal of Applied Physiology* **2000,** *88* (4), 1474-1480.

24. Sud, S.; Friedrich, J. O.; Taccone, P.; Polli, F.; Adhikari, N. K. J.; Latini, R.; Pesenti, A.; Guerin, C.; Mancebo, J.; Curley, M. A. Q.; Fernandez, R.; Chan, M. C.; Beuret, P.; Voggenreiter, G.; Sud, M.; Tognoni, G.; Gattinoni, L., *Intensive Care Medicine* **2010,** *36* (4), 585-599.

25. Bell, G. W.; Eggleston, D. B.; Noga, E. J., *Biological Bulletin* **2009,** *217* (2), 161-172.

26. Bell, G. W.; Eggleston, D. B.; Noga, E. J., *Oecologia* **2010,** *163* (1), 57-68.

27. Brouwer, M.; Larkin, P.; Brown-Peterson, N.; King, C.; Manning, S.; Denslow, N., *Mar Environ Res* **2004,** *58* (2-5), 787-92.

28. Stover, K. K.; Burnett, K. G.; McElroy, E. J.; Burnett, L. E., *Biological Bulletin* **2013,** *224* (2), 68-78.

29. Tanner, C. A.; Burnett, L. E.; Burnett, K. G., *Comparative Biochemistry and Physiology a-Molecular & Integrative Physiology* **2006,** *144* (2), 218-223.

30. Chung, J. S.; Zmora, N., *Febs Journal* **2008,** *275* (4), 693-704.

31. Hardy, K. M.; Burnett, K. G.; Burnett, L. E., *American Journal of Physiology-Regulatory Integrative and Comparative Physiology* **2013,** *305* (11), R1356-R1366.

32. Hardy, K. M.; Follett, C. R.; Burnett, L. E.; Lema, S. C., *Comparative Biochemistry and Physiology a-Molecular & Integrative Physiology* **2012,** *163* (1), 137-146.

33. Gutierrez, G. J.; Grashow, R. G., *J Vis Exp* **2009,** (25).

34. Bokhart, M. T.; Nazari, M.; Garrard, K. P.; Muddiman, D. C., *Journal of the American Society for Mass Spectrometry* **2018,** *29* (1), 8-16.

35. Sud, M.; Fahy, E.; Cotter, D.; Brown, A.; Dennis, E. A.; Glass, C. K.; Merrill, A. H.; Murphy, R. C.; Raetz, C. R. H.; Russell, D. W.; Subramaniam, S., *Nucleic Acids Research* **2007,** *35*, D527-D532.

36. Aaron, J. S.; Taylor, A. B.; Chew, T. L., *Journal of Cell Science* **2018,** *131* (3), 10.

37. Benjamini, Y.; Hochberg, Y., *Journal of the Royal Statistical Society Series B-Methodological* **1995,** *57* (1), 289-300.

38. Wang, S. L.; Arena, E. T.; Eliceiri, K. W.; Yuan, M., *Ieee Transactions on Image*

Processing **2018,** *27* (2), 622-636.

39. Wang, S.; Xiao, C. S.; Jiang, L. Y.; Ling, L.; Chen, X. S.; Guo, X. H., *Analytica Chimica Acta* **2018,** *999*, 114-122.

40. Christie, A. E.; Stemmler, E. A.; Dickinson, P. S., *Cell Mol Life Sci* **2010,** *67* (24), 4135-69.

41. Poncet, L.; Denoroy, L.; Dalmaz, Y.; Pequignot, J. M.; Jouvet, M., *Brain Research* **1996,** *733* (1), 64-72.

42. Lee, E. W.; Michalkiewicz, M.; Kitlinska, J.; Kalezic, I.; Switalska, H.; Yoo, P.; Sangkharat, A.; Ji, H.; Li, L. J.; Michalkiewicz, T.; Ljubisavljevic, M.; Johansson, H.; Grant, D. S.; Zukowska, Z., *Journal of Clinical Investigation* **2003,** *111* (12), 1853-1862.

43. Krokhin, O. V.; Ezzati, P.; Spicer, V., *Analytical Chemistry* **2017,** *89* (10), 5526-5533.

Figures

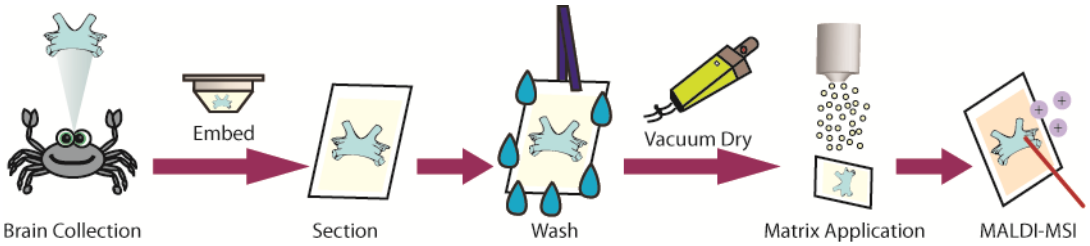

Figure 1. A pictorial schematic of the proposed wash method for crustacean neuropeptides. After collecting the brain from the control or exposed crab, the tissue is embedded in gelatin for sectioning using a cryostat. Next, sections are washed in the optimal wash solution and dried under vacuum. Matrix is then applied prior to be analyzed by MALDI-MS imaging.

Figure 2. Comparison of the top three washes with number of neuropeptides identified (blue bars) and the normalized signal intensity (purple dots). The number of neuropeptides varied slightly between these conditions and a control, but the intensity spiked for the 50:50 H_2O:EtOH washes.

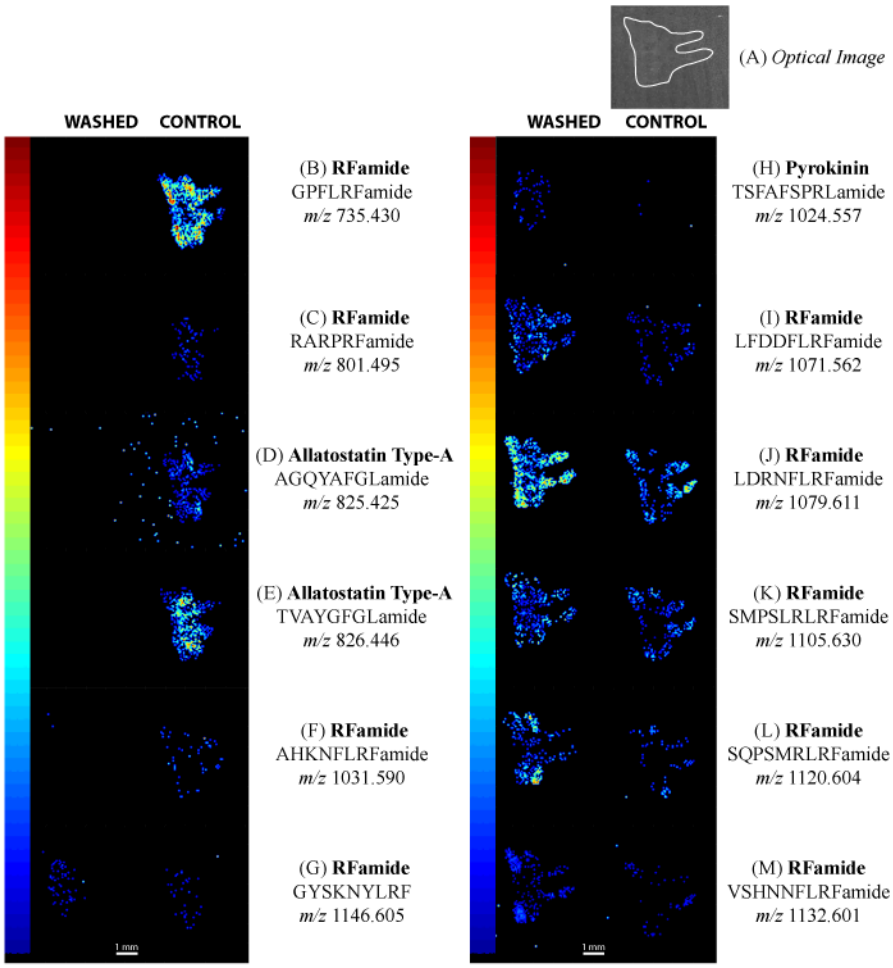

Figure 3. Examples of neuropeptide image changes due to the wash step in serial sections of a crustacean brain. (A) An optical image of the crustacean brain. The elongated tubes point towards the commissural ganglion of the crustacean nervous system. (B)-(F) Crustacean neuropeptides that were removed due to the washing step. (G) A neuropeptide image example that did not have a change in intensity or localization due to the washing step. (H)-(M) Neuropeptides that had a clear signal increase due to the washing step. All washed-control comparisons are generated at the same TIC normalized signal intensity level. The white line represented a 1 mm scale bar.

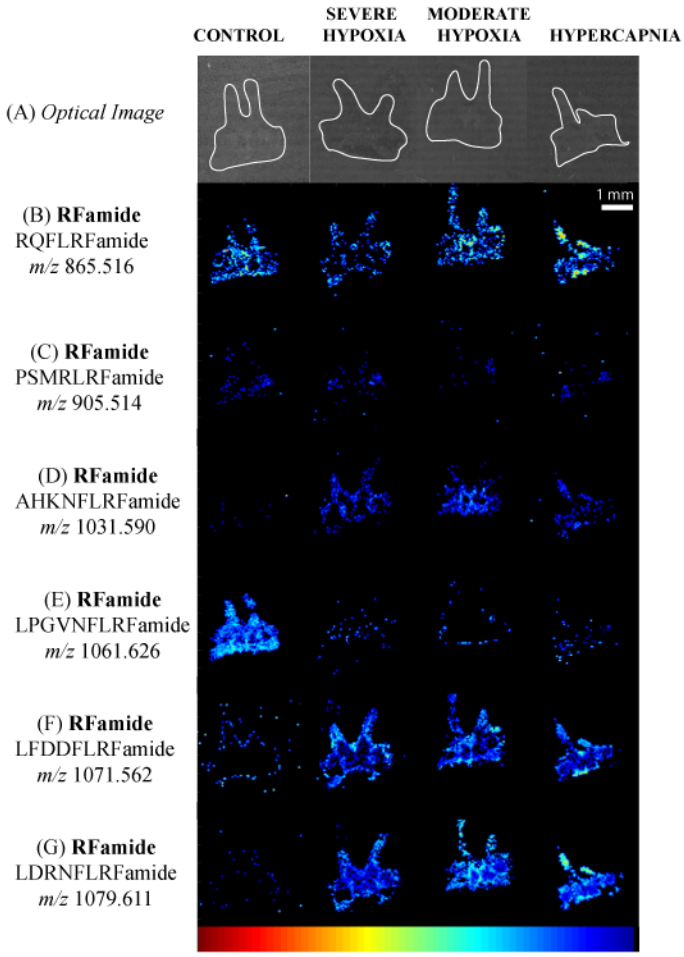

Figure 4. Examples of neuropeptides and their changes due to hypoxia and hypercapnia stress compared to a control. (a) Optical image of each washed condition. (b)-(g) Statistically significant ($p<0.0125$) neuropeptides between either severe hypoxia vs. control, moderate hypoxia vs. control, hypercapnia vs. control, severe hypoxia vs. moderate hypoxia, and moderate hypoxia vs. hypercapnia, with a table of these results provided in **Table S2**. The elongated tubes point towards the commissural ganglion of the crustacean nervous system. The white line represented a 1 mm scale bar.

Supplemental Information

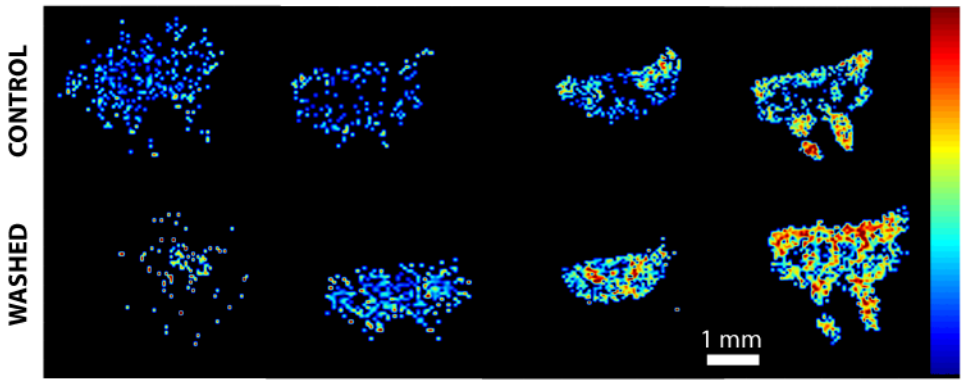

Figure S1. One technical replicate example of different bioreplicates (*m/z* 1061.626, orcokinin TPRDIANLYamide) (n=4) a control and washed brain. The top row shows the control brains, while the bottom row shows the washed (50:50 H_2O:EtOH for 10 seconds) brains. The elongated tubes point towards the commissural ganglion of the crustacean nervous system. The intensity scale is based upon the TIC normalized signal, ranging from 0 to $1x10^{-3}$. The white line represented a 1 mm scale bar. From visual inspection, the neuropeptide signal appears to increase after the wash consistently across all biological replicates.

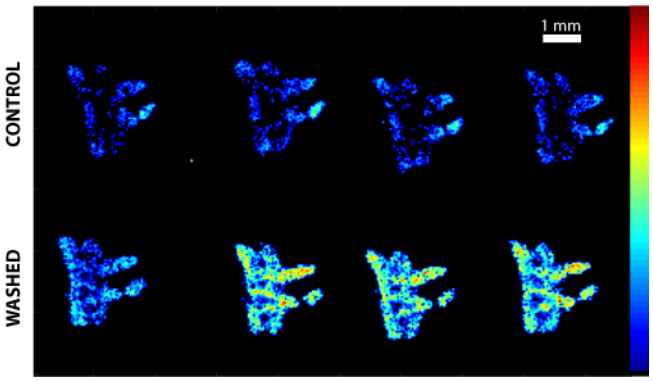

Figure S2. Example technical replicate images (*m/z* 1079.611, RFamide LDRNFLRFamide) (n=4) of one bio-replicate of a control and washed brain. All technical replicates are serial sections from the same crustacean brain. The top row shows the control brains, while the bottom row shows the washed (50:50 H_2O:EtOH for 10 seconds) brains. The elongated tubes point towards the commissural ganglion of the crustacean nervous system. The intensity scale is based upon the TIC normalized signal, ranging from 0 to $1.75x10^{-3}$. The white line represented a 1 mm scale bar. From visual inspection, the neuropeptide signal appears to increase after the wash consistently across all technical replicates.

Table S1. Colocalization analysis results for 5 representative neuropeptides between the 10 second and 30 second 50:50 EtOH:H_2O wash. The Pearson's correlation coefficient relates to intensity localization, while the Mander's split coefficient 1 and Mander's split coefficient 2 coefficients convey spatial localization. The Mander's split coefficient 1 is the projection of the 10 second wash tissue image onto the 30 second tissue wash image. The Mander's split coefficient 2 is the opposite. The Costes value (ranging from 0 to 1) confirms that our results are not from random chance by randomizing the pixels and re-performing the Pearson's and Mander's analysis.

m/z	Sequence	Pearson's	Mander's 1	Mander's 2	Costes
865.516	RQFLRFamide	0.71	0.896	0.897	1
1071.562	TNYGGFLRFamide	0.79	0.953	0.941	1
1119.646	SMPTLRLRFamide	0.83	0.945	0.958	1
1124.632	GLSRFNYLRFamide	0.83	0.971	0.981	1
1150.648	ALDRNFLRFamide	8.3	0.964	0.937	1

Table S2. Hydrophobicity analysis of select crustacean neuropeptides. Neuropeptides that were decreased (↓), increased (↑), or had no change (*) after the wash are indicated in the "Change" column. The "Manual," Biosyn," "Peptide 2.0," and "HI (Pred)" are all conditionally formatted with blue being high hydrophobicity, white being in the middle, and red being low hydrophobicity. The "Manual" calculation is done by taking the number of residues that are characterized as hydrophobic divided by the total number of residues. "Biosyn" and "Peptide 2.0" are freely available online calculators. "HI (Pred)" is a predicted hydrophobic index using a previously published method.[43]

m/z	Sequence	Change	Manual	Biosyn	Peptide 2.0	HI (Pred)	Genscript
801.495	RARPRFamide	↓	75.00	33.33	50.00	1.39	basic
808.435	AAPYAFGLamide	↓	100.00	75.00	75.00	15.74	neutral
822.451	VGPYAFGLamide	*	85.71	62.50	62.50	16.45	neutral
825.425	AGQYAFGLamide	↓	80.00	62.50	50.00	14.31	neutral
826.446	TVAYGFGLamide	↓	71.43	62.50	50.00	16.43	neutral
893.499	ARPYAFGLamide	*	83.33	62.50	62.50	12.38	basic
1061.626	LPGVNFLRFamide	↑	62.50	55.56	66.67	16.35	basic
1065.609	YKIFEPLR	↑	57.14	50.00	50.00	10.23	basic
1071.562	LFDDFLRFamide	↑	50.00	62.50	62.50	21.14	acidic
1080.570	DGGRNFLRFamide	↑	50.00	33.33	33.33	11.07	basic
1105.630	SMPSLRLRFamide	↑	66.67	44.44	55.56	13.80	basic
1123.612	GNRNFLRFamide	↑	60.00	37.50	37.50	9.45	basic
1132.601	VSHNNFLRFamide	↑	37.50	44.44	44.44	10.07	basic
1138.612	YSQVSRPRFamide	↑	42.86	33.33	33.33	7.21	basic
1181.617	SENRNFLRFamide	↑	33.33	33.33	33.33	9.77	basic

Table S3. Representative p-values for all neuropeptides that were found to be significant ($p<0.0125$) in their intensity changes in at least one of the 5 comparisons (severe hypoxia (1 ppm O_2 (10% O_2), pH 8.3) vs. control (8-10 ppm O_2 (100% O_2), pH 8.3), moderate hypoxia (5 ppm O_2 (50% O_2), pH 8.3) vs. control, hypercapnia (5 ppm O_2 (50% O_2), pH 7.6-7.8) vs. control, severe hypoxia vs. moderate hypoxia, and moderate hypoxia vs. hypercapnia). CAP: cardioacceleratory peptide.

				Control vs. 10% O_2	Control vs. 50% O_2	Control vs. pH	10% O_2 vs. 50% O_2	50% O_2 vs. pH
Family	Neuropeptide	m/z	± [Da]	p-Value	p-Value	p-Value	p-Value	p-Value
CAP	pELYAFPRVamide	975.541	0.005	9.75E-23	6.43E-17	1.74E-20	5.73E-01	3.16E-01
Pyrokinin	TSFAFSPRLamide	1024.557	0.005	6.05E-02	6.84E-01	5.69E-08	7.07E-01	1.74E-12
RFamide	RNFLRFamide	851.500	0.004	5.33E-01	6.94E-02	3.84E-01	1.49E-04	2.11E-04
	RQFLRFamide	865.516	0.004	3.08E-09	7.22E-01	7.34E-07	6.35E-07	1.41E-08
	PSMRLRFamide	905.514	0.005	2.95E-08	9.73E-23	3.74E-01	7.90E-05	2.59E-16
	GPRNFLRFamide	1005.574	0.005	7.47E-06	4.49E-01	2.10E-13	5.72E-02	1.41E-07
	PKSNFLRFamide	1007.579	0.005	9.97E-01	3.47E-02	4.98E-01	6.44E-03	3.25E-04
	AHKNFLRFamide	1031.590	0.005	7.93E-09	2.04E-07	4.15E-03	9.65E-01	1.06E-01
	APQGNFLRFamide	1048.569	0.005	1.06E-04	2.67E-02	2.27E-03	7.13E-01	8.59E-01
	LPGVNFLRFamide	1061.626	0.005	0.00E+00	0.00E+00	0.00E+00	1.00E+00	1.00E+00
	DRNFVLRFamide	1065.595	0.005	4.97E-15	1.33E-03	3.68E-11	2.57E-04	4.60E-02
	LFDDFLRFamide	1071.562	0.005	7.07E-01	2.81E-01	2.53E-41	7.13E-01	4.75E-27
	LDRNFLRFamide	1079.611	0.005	0.00E+00	3.76E-43	2.86E-37	7.13E-01	6.30E-01
	DGGRNFLRFamide	1080.570	0.005	7.75E-14	6.84E-01	0.00E+00	1.04E-10	5.64E-39
	APNKNFLRFamide	1105.627	0.002	7.03E-01	2.81E-01	3.53E-02	8.47E-01	3.02E-05
	SMPSLRLRFamide	1105.630	0.002	7.07E-01	9.09E-01	5.63E-05	3.71E-01	1.11E-06
	SMPTLRLRFamide	1119.646	0.006	1.86E-31	1.23E-04	1.46E-16	1.35E-11	2.34E-03
	SQPSMRLRFamide	1120.604	0.006	4.99E-05	4.22E-37	6.29E-18	3.76E-16	3.25E-04
	GLSRNYLRFamide	1124.632	0.006	8.02E-10	9.35E-02	1.43E-02	1.69E-18	1.04E-07
	VSHNNFLRFamide	1132.601	0.006	1.00E+00	1.03E-14	0.00E+00	2.66E-15	3.77E-26
	LGDRNFLRFamide	1136.632	0.006	4.77E-04	5.24E-01	4.28E-14	2.34E-08	1.44E-21
	GYSKNYLRFamide	1146.605	0.006	7.07E-01	2.86E-03	1.51E-01	6.85E-05	4.88E-01

Chapter 6

Expression and Distribution of Neuropeptides in the Nervous System of the Crab *Carcinus maenas* and their Roles in Environmental Stress

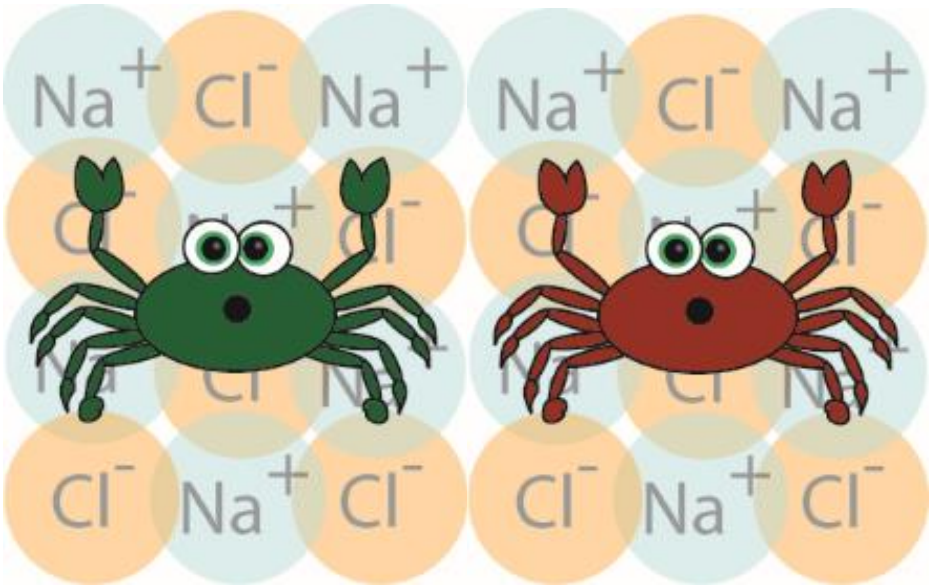

Modified from:

Yuzhuo Zhang[¥], **Amanda R. Buchberger**[¥], Gajan Muthavel, Lingjun Li. "Expression and distribution of neuropeptides in the nervous system of the crab *Carcinus maenas* and their roles in environmental stress." Invited Contribution. *PROTEOMICS*, 2015, 15 (23-24): 3969-79. [¥]Co-first authors

Keywords: Crustacean; Mass Spectrometry, Neuropeptides, Dimethyl Labeling , Salinity Stress

Abstract

Environmental fluctuations, such as salinity, impose serious challenges to marine animal survival. Neuropeptides, signaling molecules involved in the regulation process, and the dynamic changes of their full complement in the stress response have yet to be investigated. Here, a MALDI-MS-based stable isotope labeling quantitation strategy was used to investigate the relationship between neuropeptide expression and adaptability of Carcinus maenas to various salinity levels, including high (60 parts per thousand (ppt)) and low (0 ppt) salinity, in both the crustacean pericardial organ (PO) and brain. Moreover, a high salinity stress time course study was conducted. MS imaging of neuropeptide localization in Carcinus maenas PO was also performed. As a result of salinity stress, multiple neuropeptide families exhibited changes in their relative abundances, including RFamides (*e.g.*, APQGNFLRFamide), RYamides (*e.g.*, SSFRVGGSRYamide), allatostatin B-types (*e.g.*, VPNDWAHFRGSWamide), and orcokinins (*e.g.*, NFDEIDRSSFGFV). The MS imaging data revealed distribution differences in several neuropeptides (*e.g.*, SGFYANRYamide) between color morphs, but salinity stress appeared to not have a major effect on the localization of the neuropeptides.

Introduction

Significant environmental fluctuations, such as in salinity levels, pose great physiological challenges to a variety of organisms. Acclimation to different conditions is crucial to an animal's survival, however the precise mechanism of how this process occurs remains elusive. Increasing evidence suggests that neuropeptides play an important role in stress regulation.[1-6] Unfortunately, a comprehensive view of the neuropeptides involved in the stress response is lacking and required to understand their functions inside the nervous system. As one of the most important

and complex class of signaling molecules, neuropeptides are bioactive peptides that occur in the nervous system but can also be expressed in non-neuronal tissues. Due to neuropeptides' natural diversity and chemical complexity, a nervous system that is relatively simple would be beneficial to investigate a neuropeptide's modulatory effect (*i.e.,* function) at the system and circuit level. Crustaceans (*e.g.,* crabs and lobsters) provide a simple, well-characterized neurological platform for the study of behaviors, including feeding, molting, and reproduction.[7-16] The crustacean nervous system is comprised of the neuroendocrine nervous system (*e.g.,* pericardial organs (PO)), stomatogastric nervous system (STNS), and the CNS (*e.g.,* brain).[17] In addition, this model organism has previously served as an important system for the research of environmental stress related responses, providing valuable information on neuropeptides' roles in the regulation process.[3, 4, 6, 18-25]

In this study, the green crab Carcinus maenas is employed as an experimental model. Originating from Europe, green crabs are one of the most invasive marine species well known for their adaptability to a wide range of environmental conditions.[26] Therefore, *C. maenas* serves as a model organism to explore the roles of neuropeptides in acclimation to salinity changes.[21, 24, 26, 27] Largely determined by the local environment, the shell colors of green crab are variable, ranging from a dark green to a reddish brown.[28] It should be noted that crabs with red shells are stronger, more aggressive, but appear to avoid areas with undesirable environmental conditions, such as low salinity.[29] Given the negative biological and economic impact of *C. maenas*, great effort should be devoted to exploring their nervous system to develop molecular tools to prevent further ecological damage.[30] A recent study of the green crab identified 122 neuropeptides, including 49 peptides first-time described in *C. maenas* and 42 novel peptides in any crustaceans.[31] Furthermore, crustacean hyperglycemic hormones (CHHs), a neuropeptide

superfamily, were identified and found to be involved in the stress response in the green crab using a RIA.[15, 25]

MS has gained a lot of attention for neuropeptidomic analysis studies.[32] With its tolerance to salts, simple sample preparation, and fast acquisition time, MALDI-based methods have been extensively used to investigate neuropeptide changes, including several studies involving stressors.[6, 8, 21] Recently, MALDI-based MS imaging has gained increased attention as a powerful tool to obtain molecular maps of biomolecules.[32-36] This technique can provide spatial distribution of compounds of interest in a similar manner to traditional techniques such as chemical staining, immunohistochemistry, and RIAs without requiring prior knowledge of the target analytes.[37-39] Moreover, MS imaging can maintain an analyte's molecular distribution while avoiding the disadvantages of sample extraction, purification, and separation.[40, 41]

Here, isotopic dimethyl labeling coupled to MALDI-MS was utilized to investigate the quantitative changes of several neuropeptide families in the crustacean brain and PO. The results showed that green crabs with different shell colors (*i.e.*, red or green) responded differently towards stress, with red shell individuals being less tolerant. Comparing low and high salinity stress, all crabs showed a more significant response to high salinity conditions. A time course study of high salinity stress was performed to determine the dynamics of neuropeptide expression upon exposure to salinity changes in the green shell green crabs. MS imaging was also employed to illustrate the distribution changes of neuropeptides of interest in the PO due to salinity stress, enabling detailed mapping of individual isoforms of various neuropeptides.

Materials and Methods

All methods are described briefly below. Please see the supplementary information for more details.

Animals and Salinity Stress Experiments

Both red and green shell Carcinus maenas were exposed to normal (30 parts per thousand (ppt)), high (60 ppt), or low (0 ppt) salinity for a predetermined amount of time ranging from 5 hours (h) to 48h. Crabs were cold anesthetized, and the neuronal organs were dissected out.[42] All the dissection and sample processing steps were exactly the same between the two shell types.

Sample Preparation

Neuropeptides were extracted from the sample tissue by manual homogenization with acidified MeOH and desalted with C18 Ziptips. To allow for relative quantitation via dimethylation, extracts were either labeled with formaldehyde (CH_2O) (control) or deuterium formaldehyde (C^2H_2O) (stressed) and mixed in equal amounts. The resulting mixture was spotted with CHCA and analyzed by MALDI-TOF/TOF. For imaging experiments, the dissected PO was mounted onto the MALDI-TOF/TOF sample plate and coated with DHB.

MS Analysis and Imaging

A model 4800 MALDI-TOF/TOF analyzer (Applied Biosystems, Framingham, MA) equipped with a 200 Hz, 355 nm Nd:YAG laser was used for extract quantitation and tissue imaging. Image acquisition was performed with the 4800 Imaging application (Novartis, Basel, Switzerland).

Quantitative Data Analysis

The same approaches were used for both high salinity and low salinity stress experiments. Neuropeptide extracts from salinity stressed and control animals were differentially labeled and mixed with 1:1 ratio. The abundance ratio for each neuropeptide in stressed versus

control crabs was determined by dividing the heavy labeled peak intensity (stressed) with the respective light labeled peak intensity (control).

Results and Discussion

Neuropeptide Content Changes between High Salinity Stress and Control in the PO

As a major neuroendocrine organ in crustaceans, the PO can release peptide hormones to modulate the motor patterns of neuronal circuits in the STNS, which are located close to the crustacean's heart. Thus, the involvement of this neuroendocrine organ with stress regulation by releasing neuropeptides can be expected. Here, to investigate how neuropeptides in the PO are involved in the stress regulation, a duplex dimethyl labeling strategy with formaldehyde in conjunction with MALDI-MS was utilized to measure quantitative changes in neuropeptides between control and stressed animals.

Fourteen neuropeptides from 4 families were examined for both green (n=6) and red (n=6) shell individuals' POs. Significant changes were observed for members from several neuropeptide families ($p<0.05$) after high salinity stress, indicated with asterisks in **Figure 1a**. All important values are included in **Table S1**. In general, the results were variable depending on the color morph studied. For green shell individuals, only a few neuropeptides exhibited significant changes in relative content levels. For example, allatostatin B-type VPNDWAHFRGSWamide (mass-to-charge ratio (*m/z*) 1470.7) showed great increase after stress ($p<0.005$), which could be indicative of no release from the tissue due to a silent neuron or a delayed released. Other neuropeptides, such as the RYamide SSRFVGGSRYamide (*m/z* 1114.5), decreased significantly ($p<0.05$). This observation suggests that these peptides, once the crab has been exposed to high salinity stress, could have been released from the PO or degraded.

Compared to the green color morphs, red individuals after high salinity stress showed a more extreme response, as almost all quantified neuropeptide content levels changed upon exposure to the high salinity stress. Allatostatin B-type VPNDWAHFRGSWamide (*m/z* 1470.7) levels were significantly elevated ($p<0.005$), whereas the RYamide SSRFVGGSRYamide (*m/z* 1114.5) showed a decreasing trend ($p<0.005$). Both of these content changes were consistent with the green color morph crabs. However, all RFamide peptide levels in red individuals rose significantly after high salinity stress ($p<0.05$).

It was found that only 5 neuropeptides in green shell crabs showed significant content changes, whereas 10 neuropeptides in red shell crabs exhibited significant content changes. Furthermore, the neuropeptide content changes seen in the red morph were much more intense than those observed in the green morph. These findings suggest that green morph crabs show not only better tolerance to low salinity stress but also to high salinity stress.[29] From this observation, greater peptidome stability, which is a potential molecular clue for better adaptability, is implied for green individuals compared to red shell variants. It should be noted that a neuropeptide may or may not carry the same weight in terms of stabilizing the peptidome, and further studies will need to be performed to validate our conclusions. As discussed, this color morph difference is not only genetically related but also largely due to local environment factors which affect the crab molting.[28] A red shell color indicates that the crab took a longer time to molt, particularly inter molt, which helps them to gain greater size, heavier weight, thicker carapaces, and thus an advantage in mating.[43] However, a tradeoff is that the red morph crabs are physiologically less tolerant to harsh environments.[29] These observations lead us to believe there is a molecular, specifically neuropeptidomic, connection among reproductive success, morphological evolution,

and environmental adaptability. More in-depth investigations will be required to fully understand the underlying mechanism and establish the correlation.

Neuropeptide Content Changes in the Brain Tissue of Animals Subjected to High Salinity Stress and Controls

The brain is an important neural organ in the CNS, which plays a crucial role in behavior and physiological condition regulation in both mammals and crustaceans.[44-48] **Figure 1b** illustrates the neuropeptide changes in green and red morph brain tissue in response to high salinity stress, with all valuable numbers included in **Table S2**. In green individuals (n=4), all 8 neuropeptides in 5 families kept the same levels after stress, while in red individuals (n=4), all orcokinins and most RFamide peptides exhibited elevated content levels after stress ($p<0.05$). RFamides are a conserved peptide family throughout different animal nervous systems, and they have been shown to be involved in cardiovascular function, modulation of muscle contraction, control of locomotor activity, and water balance.[49-51] Orcokinin peptides are the most abundant neuropeptide family in crab brain, which have been reported to exert neuromodulatory effects on the lobster pyloric neural circuits.[52] It should be noted that, while the STNS contains many intrinsic orcokinin neurons, it is not clear how the brain can exert direct effects on the pyloric circuits. Overall, the increase of RFamide and orcokinin isoforms after high salinity exposure suggests their possible involvement in the stress response. In contrast, SIFamide, 10 tachykinin, and HIGSLYRamide (*m/z* 844.5) peptides remained unchanged in both color morphs, suggesting they have no role in the acute stress response. While not detected here, previous research has shown that other peptide families (*e.g.*, angiotensin-like peptides) would increase during chronic stress.[3]

These different neuropeptide changes in Carcinus maenas with diverse shell colors in response to high salinity stress in both the PO and the brain indicate that different growth environments may determine the tolerance to environmental stress for the crustacean, which is consistent with previous ecological research.[29] Thus, the relationship between environments and evolutionary benefits (*e.g.*, shell differences) would be an area for future investigation. Also, special considerations should be made when executing physiological studies, as the origin of animals should be always an important control factor taken into account.

Neuropeptide Content Changes in the PO and Brain of Animals Subjected to Low Salinity Stress and Control Animals

In addition to high salinity stress, neuropeptide changes in response to low salinity stress were also investigated. **Figure 2a** compares the neuropeptide content change between green (n=5) and red (n=6) shell crab POs, with all the important values included in **Table S3**. All RYamides (*e.g.*, FVGGSRYamide (*m/z* 784.4)) in red individuals experienced a significant decrease ($p<0.05$), reduced by almost 25% of the original levels. A smaller degree of decrease was observed for RFamides (*e.g.*, NRNFLRFamide (*m/z* 965.5)), exhibiting only a ~10% decrease after low salinity stress ($p<0.05$). In contrast, in the green color morphs, RFamide DGNRNFLRFamide (*m/z* 1137.6) and all allatostatin B-type family members (*e.g.*, VPNDWAHFRGSWamide (*m/z* 1470.7)) were significantly increased after low salinity stress ($p<0.05$).

Figure 2b shows the neuropeptide content changes in the brains between crabs with red 11 (n=5) and green (n=5) shell colors, and **Table S4** details all of these observations. Interestingly, red and green individuals almost showed no significant response to low salinity stress. All neuropeptide expression besides the RFamide DGNRNFLRFamide in red shell crabs

stayed at the same level, while only 4 neuropeptides showed a significant increase of less than 5% in green shell crabs.

Neuropeptide Content Differences in Response to Different Salinity Stresses

When comparing high and low salinity stress in the two shell colors, there is a distinct difference in expression of the measured peptides. In the high salinity stress study, 10 neuropeptides in the red shell crab PO showed significant changes. 9 of these neuropeptides showed significant increase, most of which were larger than 20% ($p<0.05$). In contrast, in the red shell crab PO low salinity stress study, only 7 neuropeptides showed significant decrease, and only 2 showed more than a 20% level change ($p<0.05$). For green shell crabs, four neuropeptides showed significant content level changes in high salinity stress PO experiments. Only five neuropeptides were involved in low salinity stress regulation of the green morph PO, exhibiting elevation in their content levels ($p<0.05$). We can thus conclude that high salinity stress is a more severe stress for Carcinus maenas than low salinity stress. This is inferred from not only the number and amount of neuropeptides having content changes due to the particular salinity stress but also the severity of the responses observed.

Animals have different adaptability to low or high salinity, which can be related to genetic factors. Many crustacean species were reported to have a better tolerance to low salinity stress than high salinity stress, like Moina affinis and Homarus.[53, 54] As mentioned above, our research results show that Carcinus maenas crustaceans also have a better tolerance to low salinity stress, which can be explained by green crabs living habitat. C. maenas is a non-native invasive predator that frequently migrates across oceans and experiences fresh water regions, thus it has developed a better tolerance to low salinity environment. When comparing between color morphs, we found even though the green shell crab showed a better stress tolerance to high

salinity stress, but the neuropeptide families involved and trends in the regulation were still similar between the red and green shell crabs. However, in low salinity stress, most neuropeptides in the red morph experienced a reduction, while those in green morph exhibited an increase in their content levels. This phenomenon is interesting because it raises the question whether different color morphs in the same species can have different neuropeptide regulation mechanisms under certain physiological conditions. Further investigation with electrophysiology experiments, such as extracellular recording of the STNS and PO, will need to be performed to provide robust evidence.

When comparing the neuropeptide content changes in response to acute stress in the PO and brain, it is interesting to observe that the extent of regulatory responses in the brain is smaller than that of PO regardless of the color morphs and different salinity stress conditions. This observation triggers an interest in exploring the relationship between neuroendocrine organs and the CNS. In previous research, signaling molecules in neuroendocrine organs were shown to play a role in regulating the mammalian nervous system.[55-57] Combining research on mammalian model systems and our own study, it is believed that neuroendocrine organs in the crustacean can also play a role in the regulation of CNS responses. Our data show that the PO exhibits a more intense response compared to brain in acute stress, although it is likely they work together to overcome the stress caused by salinity changes. However, a more in-depth investigation of chronic stress and adaptability will need to be performed to fully understand the underlying mechanism.

Time Course Study

In order to better understand the dynamics of neuropeptide changes in response to stress, we also conducted a time course study of the green color morph of C. maenas in response to high

salinity stress. Measurements were taken at 5h, 12h, 24h, and 48h after exposure, and all results are shown in **Figure 3**, **Table S5**, and **Table S6**. In a previous experimental study, researchers performed more acute stress studies ranging from 1h to 2h.[4, 58] We are more interested in a longer time adaptability; thus we selected 24h and 48h time periods, setting our time points according to a similar experiment design.[59] For each time point, at least 6 replicates of experiment were performed. In **Figure 3a**, a majority of neuropeptide levels stayed at the same level after 5h stress in the crustacean PO. Two exceptions were allatostatin B-type neuropeptide VPNDWAHFRGSWamide, which increased by ~20%, and orcokinin NFDEIDRSSFGFV, which decreased by ~25%. After 12h of stress, only the allatostatin B-type peptide VPNDWAHFRGSWamide showed a statistical change, increasing from the 5h increase. It should be noted that we did see two out of ten groups of experimental animals exhibit an unusual high levels of NFDEIDRSSFGN (*m/z* 1547.7), producing a clearly higher average relative ratio (~1.4). After 24h elapsed, four neuropeptide levels dropped compared to a control. Finally, only three neuropeptides, two allatostatin B-types and one orcokinin, showed a significant difference after 48h exposure.

The brain tissue results are shown in **Figure 3b**. None of the neuropeptide content levels showed significant changes after 5h of stress, as discussed before, but several neuropeptides exhibited extreme changes in their neuropeptide content over time. For example, tachykinin and NRNFLRFamide showed significant increase after 12h of high salinity stress. After 24h stress, a majority of neuropeptide content levels experienced a drop, including HIGSLYRamide, tachykinin, and SIFamide. These 10% drops were also maintained after 48h. All other neuropeptides had no major changes after 48h when compared to a control. Overall, the differential time course response of neuropeptide expressions observed in the PO and brain after

high salinity stress could be related to the release, degradation, and/or accumulation of these peptides, accentuating the diverse physiological roles played by different types of neuropeptides in the decapod crustaceans. More information on these mechanisms could be determined by the study of the crustacean hemolymph during salinity stress, including the use of microdialysis.[32]

Neuropeptide Localization in the PO

Previous studies have shown that a rich repertoire of neuropeptides exist in the crustacean PO [7, 60, 61].[7, 60, 61] To investigate correlation of neuropeptide function and localization, MALDI-MS imaging was used to map the distribution of several neuropeptides of interest in the PO. Intact POs were collected from both green (n=3) and red (n=3) shell C. maenas, and images of numerous neuropeptides were obtained.

Figure 4 shows the localization of 3 most abundant neuropeptide families of green and red shell green crab PO. allatostatin B-types (*e.g.*, STNWSSLRSAWamide (*m/z* 1293.6)) showed very similar spatial localization within the family. They were prevalent all over the PO tissue with highest concentration in the anterior bar and posterior bar region of both green and red shell crustacean POs. The RFamide family peptides (*e.g.*, DGNRNFLRFamide (*m/z* 1137.6)) were not as abundant as the allatostatin B-types in the C. maenas PO. They also existed throughout the whole tissue in both morphs, but they were more concentrated in posterior part of green shell crabs. The small difference in localization of the RFamide family between these two morphs during high and low salinity can be related to the quantitative study.

The most abundant neuropeptides in the C. maenas PO belong to the RYamide family (*e.g.*, SSRFVGGSRYamide (*m/z* 1114.6)). The localization pattern among the family members is quite similar, as all RYamide peptides were highly concentrated in dorsal trunk, anterior, and posterior region in crabs of both shell colors. They were most abundant in posterior region

especially for 15 red shell green crabs. Other peptides like proctolin RYLPT (*m/z* 649.4), CCAP PFCNAFTCamide (*m/z* 956.4), and HIGSLYRamide (*m/z* 844.5) shared similar localization patternsto the allatostatin B-type family.

Neuropeptide localization patterns between the two morphs were quite similar in RYamide and allatostatin B-type families. For RFamide, their patterns exhibited slight differences not only between morphs but also among peptide families, indicating the distinct physiological functions of each member of the respective family, which also can be related to the quantitation study. Intensity variation between two morph images could also be due to the error induced by sample preparation and matrix application. It should be noted though that all of the above localizations are consistent with previously collected immunochemistry data in both C. maenas and other crustacean species.[62-65] Our study presents the first survey of neuropeptide localization in the C. maenas PO using MALDI-MS imaging, which suggests that the peptide content changes due to stress may correlate to the peptide's distribution pattern.

Concluding Remarks

In summary, we employed isotopic dimethyl labeling and MALDI-MS based methodology to quantitatively study neuropeptide regulation of environmental stress in both the brain and the PO. Green color morphs of C. maenas demonstrated a better tolerance to salinity stress, with fewer, less intense changes in relative abundances of neuropeptides compared to the red morphs. Different neuropeptides were observed to be involved in the stress regulation between the two morphs, associating environmental factors with possible genetic involvement. Time course studies were also carried out to investigate the dynamics of neuropeptide expression changes upon exposure to environmental stress. Finally, MALDI-MS imaging was utilized to

characterize the spatial distribution of a multitude of neuropeptides within various peptide families in their respective neuronal terminals in the PO.

Acknowledgements

The authors thank the University of Wisconsin-Biotechnology Center Mass Spectrometry Facility, Dr. Amy Harms, and Dr. Mike Sussman for access to the MALDI-TOF/TOF instrument. This work was supported in part by a National Science Foundation grant (CHE-1413596) and the National Institutes of Health through grant R01DK071801. L.L. acknowledges an H. I. Romnes Faculty Fellowship.

Conflict of Interest

The authors have declared no conflict of interest.

References

1. Chen, Y. C.; Bender, R. A.; Brunson, K. L.; Pomper, J. K.; Grigoriadis, D. E.; Wurst, W.; Baram, T. Z., *Proceedings of the National Academy of Sciences of the United States of America* **2004,** *101* (44), 15782-15787.

2. Hiremagalur, B.; Kvetnansky, R.; Nankova, B.; Fleischer, J.; Geertman, R.; Fukuhara, K.; Viskupic, E.; Sabban, E. L., *Molecular Brain Research* **1994,** *27* (1), 138-144.

3. Delorenzi, A.; Dimant, B.; Frenkel, L.; Nahmod, V. E.; Nassel, D. R.; Maldonado, H., *Journal of Experimental Biology* **2000,** *203* (22), 3369-3379.

4. Chung, J. S.; Zmora, N., *Febs Journal* **2008,** *275* (4), 693-704.

5. McCormick, D. A.; Nusbaum, M. P., *Current Opinion in Neurobiology* **2014,** *29*, IV-VII.

6. Chen, R. B.; Xiao, M. M.; Buchberger, A.; Li, L. J., *Journal of Proteome Research* **2014,** *13* (12), 5767-5776.

7. Chen, R. B.; Ma, M. M.; Hui, L. M.; Zhang, J.; Li, L. J., *Journal of the American Society for Mass Spectrometry* **2009,** *20* (4), 708-718.

8. Chen, R. B.; Hui, L. M.; Cape, S. S.; Wang, J. H.; Li, L. J., *Acs Chemical Neuroscience* **2010,** *1* (3), 204-214.

9. Hui, L.; Zhang, Y.; Wang, J.; Cook, A.; Ye, H.; Nusbaum, M. P.; Li, L., *ACS Chem Neurosci* **2011,** *2* (12), 711-722.

10. Christie, A. E.; Kutz-Naber, K. K.; Stemmler, E. A.; Klein, A.; Messinger, D. I.; Goiney, C. C.; Conterato, A. J.; Bruns, E. A.; Hsu, Y. W. A.; Dickinson, P. S., *Journal of Experimental Biology* **2007,** *210* (4), 699-714.

11. Christie, A. E.; Stemmler, E. A.; Dickinson, P. S., *Cell Mol Life Sci* **2010,** *67* (24), 4135-69.

12. Fanjul-Moles, M. L., *Comparative Biochemistry and Physiology C-Toxicology & Pharmacology* **2006,** *142* (3-4), 390-400.

13. Webster, S. G., Neuropeptides inhibiting growth and reproduction in crustaceans. In *Recent advances in arthropod endocrinology.*, Coast, G. M.; Webster, S. G., Eds. Cambridge University Press: Cambridge, UK, 1998.

14. Nagaraju, G. P. C., *Journal of Experimental Biology* **2011,** *214* (1), 3-16.

15. Chung, J. S.; Webster, S. G., *Development* **2004,** *131* (19), 4751-4761.

16. Phlippen, M. K.; Webster, S. G.; Chung, J. S.; Dircksen, H., *Journal of Experimental Biology* **2000,** *203* (3), 521-536.

17. Hopkins, P. M., *General and Comparative Endocrinology* **2012,** *175* (3), 357-366.

18. Chung, J. S.; Bembe, S.; Tamone, S.; Andrews, E.; Thomas, H., *General and Comparative Endocrinology* **2009,** *162* (2), 129-133.

19. Chung, J. S.; Webster, S. G., *General and Comparative Endocrinology* **2006,** *147* (2), 206-213.

20. Chung, K. S., *Rev Biol Trop* **2001,** *49* (1), 9-13.

21. Wang, J. H.; Zhang, Y. Z.; Xiang, F.; Zhang, Z. C.; Li, L. J., *Journal of Chromatography A* **2010,** *1217* (26), 4463-4470.

22. Wilcockson, D. C.; Chung, J. S.; Webster, S. G., *Cell and Tissue Research* **2002,** *307* (1), 129-138.

23. Webster, S. G., *Journal of Experimental Biology* **1996,** *199* (7), 1579-1585.

24. Lovett, D. L.; Tanner, C. A.; Glomski, K.; Ricart, T. M.; Borst, D. W., *Comparative Biochemistry and Physiology a-Molecular & Integrative Physiology* **2006,** *143* (1), 67-77.

25. Chung, J. S.; Webster, S. G., *Endocrinology* **2005,** *146* (12), 5545-5551.

26. Cohen, A. N.; Carlton, J. T.; Fountain, M. C., *Marine Biology* **1995,** *122* (2), 225-237.

27. Chung, J. S.; Zmora, N.; Katayama, H.; Tsutsui, N., *General and Comparative Endocrinology* **2010,** *166* (3), 447-454.

28. Brian, J. V.; Fernandes, T.; Ladle, R. J.; Todd, P. A., *Journal of Experimental Marine Biology and Ecology* **2006,** *329* (1), 47-54.

29. McKnight, A.; Mathews, L. M.; Avery, R.; Lee, K. T., *Crustaceana* **2000,** *73*, 763-768.

30. Hanfling, B.; Edwards, F.; Gherardi, F., *Biocontrol* **2011,** *56* (4), 573-595.

31. Ma, M. M.; Bors, E. K.; Dickinson, E. S.; Kwiatkowski, M. A.; Sousa, G. L.; Henry, R. P.; Smith, C. M.; Towle, D. W.; Christie, A. E.; Li, L. J., *General and Comparative Endocrinology* **2009,** *161* (3), 320-334.

32. Buchberger, A.; Yu, Q.; Li, L., *Annu Rev Anal Chem (Palo Alto Calif)* **2015,** *8* (1), 485-509.

33. Jiao, J.; Miao, A. Z.; Zhang, X. Y.; Cai, Y.; Lu, Y.; Zhang, Y.; Lu, H. J., *Analyst* **2013,** *138* (6), 1645-1648.

34. Wang, J. N.; Qiu, S. L.; Chen, S. M.; Xiong, C. Q.; Liu, H. H.; Wang, J. Y.; Zhang, N.; Hou, J.; He, Q.; Nie, Z. X., *Analytical Chemistry* **2015,** *87* (1), 422-430.

35. Patterson, N. H.; Thomas, A.; Chaurand, P., *Journal of Mass Spectrometry* **2014,** *49* (7), 622-627.

36. Caprioli, R. M.; Farmer, T. B.; Gile, J., *Analytical Chemistry* **1997,** *69* (23), 4751-4760.

37. Sousa, G. L.; Lenz, P. H.; Hartline, D. K.; Christie, A. E., *General and Comparative Endocrinology* **2008,** *156* (3), 454-459.

38. Polanska, M. A.; Yasuda, A.; Harzsch, S., *Cell and Tissue Research* **2007,** *330* (2), 331-344.

39. Gallus, L.; Bottaro, M.; Ferrando, S.; Girosi, L.; Ramoino, P.; Tagliafierro, G., *Microscopy Research and Technique* **2006,** *69* (8), 636-641.

40. Cornett, D. S.; Reyzer, M. L.; Chaurand, P.; Caprioli, R. M., *Nature Methods* **2007,** *4* (10), 828-833.

41. Chaurand, P.; Norris, J. L.; Cornett, D. S.; Mobley, J. A.; Caprioli, R. M., *Journal of Proteome Research* **2006,** *5* (11), 2889-2900.

42. Kutz, K. K.; Schmidt, J. J.; Li, L. J., *Analytical Chemistry* **2004,** *76* (19), 5630-5640.

43. Reid, D. G.; Abello, P.; Kaiser, M. J.; Warman, C. G., *Estuarine Coastal and Shelf Science* **1997,** *44* (2), 203-211.

44. Spear, L. P., *Neuroscience and Biobehavioral Reviews* **2000,** *24* (4), 417-463.

45. Chrousos, G. P.; Gold, P. W., *Jama-Journal of the American Medical Association* **1992,** *267* (9), 1244-1252.

46. Huber, R.; Smith, K.; Delago, A.; Isaksson, K.; Kravitz, E. A., *Proceedings of the National Academy of Sciences of the United States of America* **1997,** *94* (11), 5939-5942.

47. Tierney, A. J.; Kim, T.; Abrams, R., *Microscopy Research and Technique* **2003,** *60* (3), 325-335.

48. Torfs, P.; Nieto, J.; Cerstiaens, A.; Boon, D.; Baggerman, G.; Poulos, C.; Waelkens, E.; Derua, R.; Calderon, J.; De Loof, A.; Schoofs, L., *European Journal of Biochemistry* **2001,** *268* (1), 149-154.

49. McGaw, I. J.; McMahon, B. R., *Biological Bulletin* **1995,** *188* (2), 186-196.

50. Bechtold, D. A.; Luckman, S. M., *Journal of Endocrinology* **2007,** *192* (1), 3-15.

51. Mercier, A. J.; Friedrich, R.; Boldt, M., *Microscopy Research and Technique* **2003,** *60* (3), 313-324.

52. Li, L. J.; Pulver, S. R.; Kelley, W. P.; Thirumalai, V.; Sweedler, J. V.; Marder, E., *Journal of Comparative Neurology* **2002,** *444* (3), 227-244.

53. Zhao, W.; Yu, B.; Wang, T.; Song, L., *Ying Yong Sheng Tai Xue Bao* **2006,** *17* (8), 1521-5.

54. Lignot, J. H.; Charmantier, G., *J Histochem Cytochem* **2001,** *49* (8), 1013-23.

55. Malagon, M.; Vaudry, H.; Vanstrien, F.; Pelletier, G.; Gracianavarro, F.; Tonon, M. C., *Neuroscience* **1993,** *57* (3), 777-786.

56. Compere, V.; Lanfray, D.; Castel, H.; Morin, F.; Leprince, J.; Dureuil, B.; Vaudry, H.; Pelletier, G.; Tonon, M. C., *Journal of Molecular Endocrinology* **2010,** *44* (5), 295-299.

57. Ozawa, H., *J Nippon Med Sch* **2005,** *72* (6), 316-25.

58. Seo, J. S.; Lee, K. W.; Rhee, J. S.; Hwang, D. S.; Lee, Y. M.; Park, H. G.; Ahn, I. Y.; Lee, J. S., *Aquat Toxicol* **2006,** *80* (3), 281-9.

59. De Martinez Gaspar Martins, C.; Bianchini, A., *Comp Biochem Physiol A Mol Integr Physiol* **2009,** *152* (3), 366-71.

60. DeKeyser, S. S.; Kutz-Naber, K. K.; Schmidt, J. J.; Barrett-Wilt, G. A.; Li, L., *J Proteome Res* **2007,** *6* (5), 1782-91.

61. Fu, Q.; Kutz, K. K.; Schmidt, J. J.; Hsu, Y. W.; Messinger, D. I.; Cain, S. D.; de la Iglesia, H. O.; Christie, A. E.; Li, L., *J Comp Neurol* **2005,** *493* (4), 607-26.

62. Stangier, J.; Dircksen, H.; Keller, R., *Peptides* **1986,** *7* (1), 67-72.

63. Dircksen, H.; Keller, R., *Cell and Tissue Research* **1988,** *254* (2), 347-360.

64. Christie, A. E.; Skiebe, P.; Marder, E., *Journal of Experimental Biology* **1995,** *198* (12), 2431-2439.

65. Skiebe, P.; Dietel, C.; Schmidt, M., *Journal of Comparative Neurology* **1999,** *414* (4), 511-532.

Figures

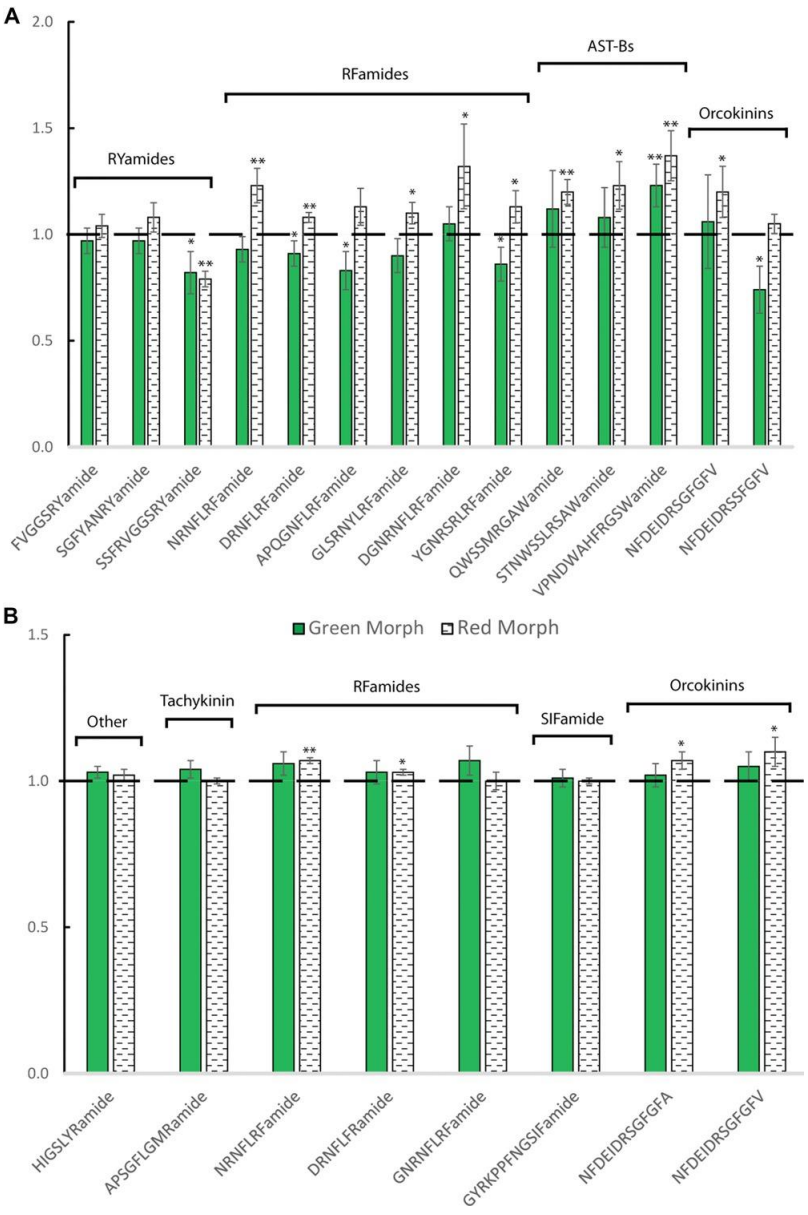

Figure 1. Content changes of neuropeptides of interest in Carcinus maenas (a) PO (n=6) and (b) brain (n=4) between a control and 5h of high salinity stress. For each pair, the bars on the left refer to changes in the green morph, while the bars on the right correspond to the red morph. Each group contained two POs or one brain. A ratio equal to one denotes no change between stress and control conditions, marked by a dotted line. The error bars depict the SEM of the measured ratio. Asterisks indicate significance levels (student's t test): *, $p<0.05$, **, $p<0.005$.

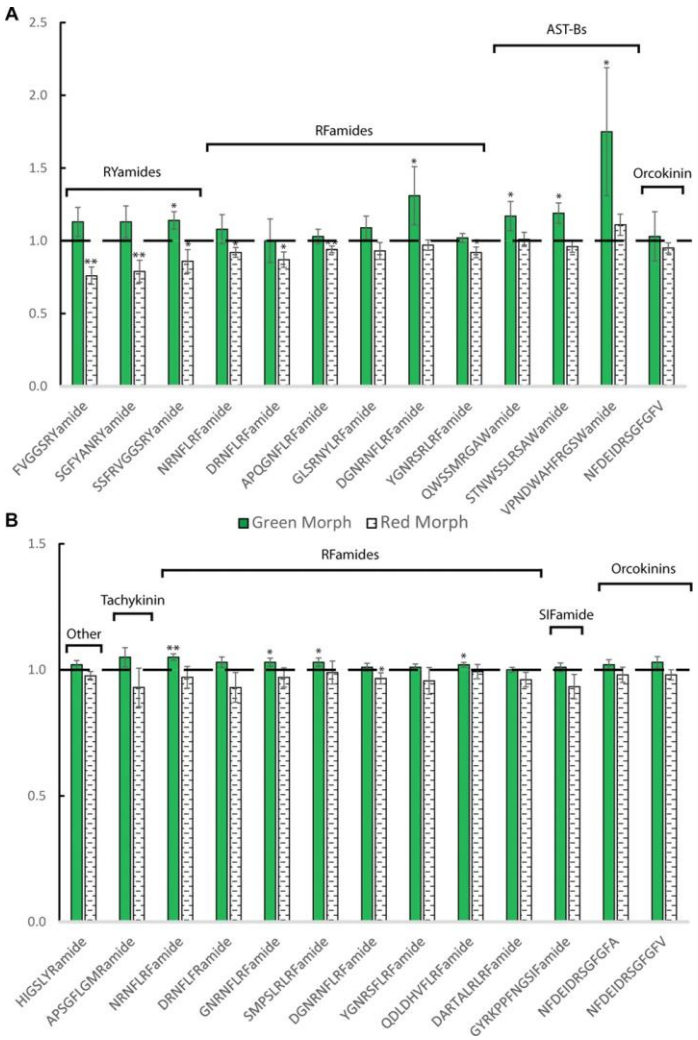

Figure 2. Content changes of neuropeptides of interest in Carcinus maenas (a) PO (n=5) and (b) brain (n=5) between a control and 5h of low salinity stress. For each pair, the bars on the left refer to changes in the green morph, while the bars on the right correspond to the red morph. Each group contained two POs or one brain. A ratio equal to one denotes no change between stress and control conditions, marked by a dotted line. The error bars depict the SEM of the measured ratio. Asterisks indicate significance levels (student's t test): *, $p<0.05$, **, $p<0.005$.

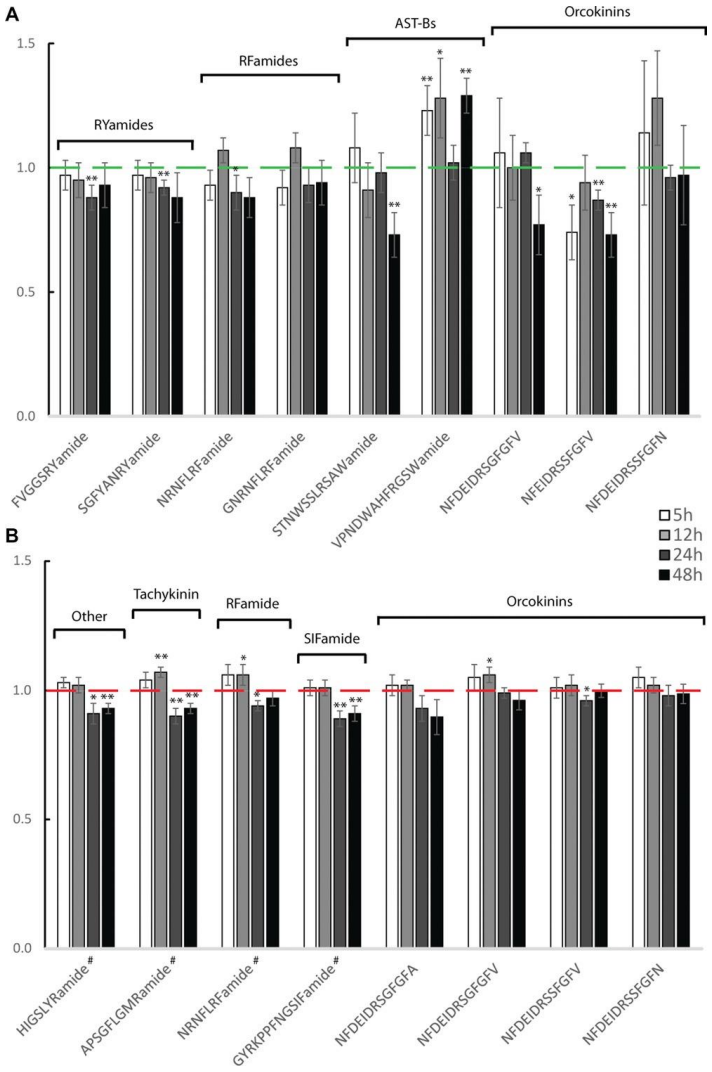

Figure 3. Time course study of Carcinus maenas neuropeptide content changes due to high salinity stress for the (a) PO and (b) brain for the green color morph. 6 groups for 5h, 10 groups for 12 h, 6 groups for 24h, 6 groups for 48h (each group has two POs or one brain). A ratio equal to one denotes no change between stress and control conditions, marked by a dotted line. The error bars depict the SEM of the measured ratio. Asterisks indicated significance levels (student's t test): *, $p<0.05$, **, $p<0.005$. ANOVA tests where the peptide changes were found to be significant are indicated by a pound sign (#) by the peptide name.

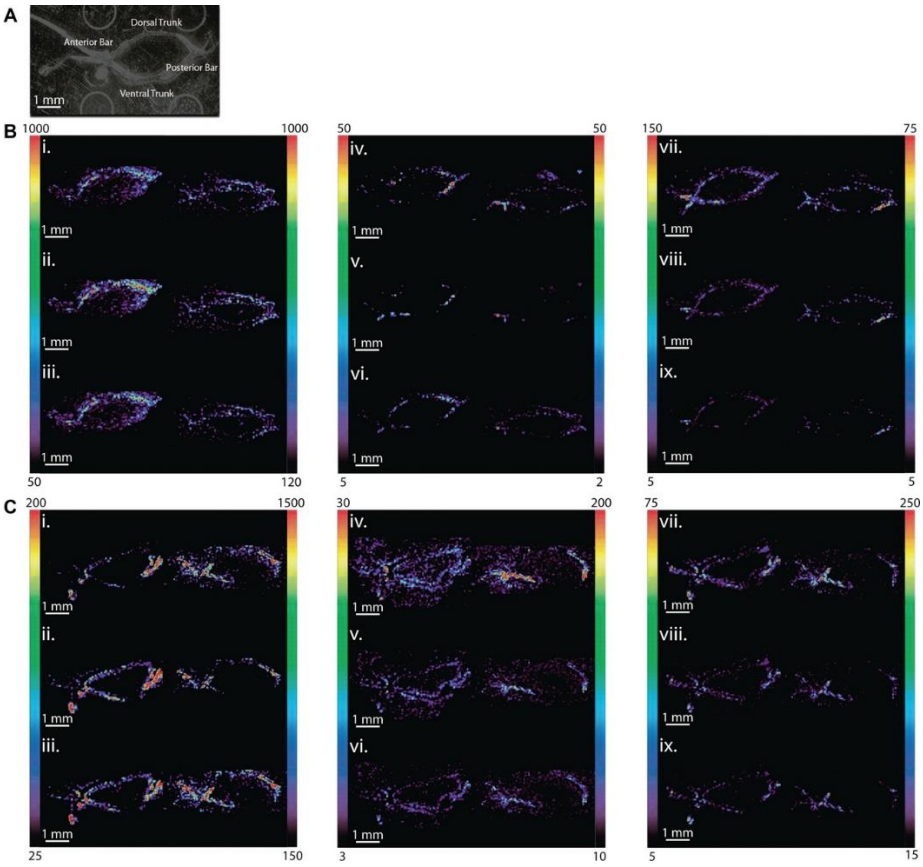

Figure 4. MALDI-MS imaging analysis of several neuropeptides in the C. maenas PO. (a) Optical image of a PO on a MALDI plate. The main body of the decapod crustacean PO consists of anterior region, posterior region, dorsal trunk, and ventral trunk. Neuropeptide localization in (b) green shell and (c) red shell C. maenas PO for both control (left) and stressed (right) animal are shown. Visualized neuropeptides pertain to three families, including RYamides ((i) FVGGSRYa (*m/z*784.5), (ii) SGFYANRYa (*m/z* 976.5), and (iii) pEGFYSQRYa (*m/z* 1030.5)), RFamides ((iv) NRNFLRFa (*m/z* 965.5), (v) GNRNFLRFa (*m/z* 1022.6), and (vi) DGNRNFLRFa (*m/z* 1137.6)), and allatostatin B-types ((vii) QWSSMRGAWa (*m/z* 1107.6), (viii) STNWSSLRSAWa (*m/z* 1293.6), and (ix) VPNDWAHFRGSWa (*m/z* 1470.7)).

Supporting Information

Table S1 Content changes of neuropeptides in the POs from *Carcinus maenas* green (n=6) and red (n=6) individuals between 5h high salinity stressed individuals and a control. Each group had two POs. Bold font indicates significant changes after stress.

			Green Morph			Red Morph		
	m/z	Sequence	Ratio	SEM	p-Value	Ratio	SEM	p-Value
RYamide	784.41	FVGGSRYamide	0.97	0.06	2.98E-01	1.04	0.05	4.40E-01
	976.46	SGFYANRYamide	0.97	0.06	3.64E-01	1.08	0.07	2.06E-01
	1114.47	SSFRVGGSRYamide	**0.82**	**0.10**	**1.05E-02**	**0.79**	**0.04**	**2.54E-05**
RFamide	965.54	NRNFLRFamide	0.93	0.06	7.05E-02	**1.23**	**0.08**	**1.05E-03**
	966.53	DRNFLRFamide	**0.91**	**0.06**	**3.38E-02**	**1.08**	**0.02**	**9.44E-04**
	1048.57	APQGNFLRFamide	**0.83**	**0.09**	**1.83E-02**	1.13	0.09	6.21E-02
	1124.63	GLSRNYLRFamide	0.90	0.08	6.65E-02	**1.10**	**0.05**	**1.86E-02**
	1137.59	DGNRNFLRFamide	1.05	0.08	5.67E-01	**1.32**	**0.20**	**3.21E-02**
	1158.62	YGNRSRLRFamide	**0.86**	**0.08**	**2.51E-02**	**1.13**	**0.08**	**3.77E-02**
AST-B	1107.58	QWSSMRGAWamide	1.12	0.18	5.37E-01	**1.20**	**0.06**	**3.82E-04**
	1293.63	STNWSSLRSAWamide	1.08	0.14	6.54E-01	**1.23**	**0.11**	**1.58E-02**
	1470.70	VPNDWAHFRGSWamide	**1.23**	**0.10**	**3.82E-03**	**1.37**	**0.12**	**5.09E-04**
Orcokinin	1502.69	NFDEIDRSGFGFV	1.06	0.22	7.87E-01	**1.20**	**0.12**	**3.88E-02**
	1532.70	NFDEIDRSSFGFV	**0.74**	**0.11**	**7.33E-03**	1.05	0.04	1.91E-01

Table S2. Comparison of neuropeptide content changes in green shell (n=6) and red shell (n=4) *C. maenas* brain after 5h high salinity stress compared to a control. Each group contained one brain. Bold font indicates significant changes after stress.

			Green Morph			Red Morph		
	m/z	Sequence	Ratio	SEM	p-Value	Ratio	SEM	p-Value
Others	844.48	HIGSLYRamide	1.03	0.02	1.36E-01	1.02	0.02	3.14E-01
Tachykinin	934.49	APSGFLGMRamide	1.04	0.03	1.15E-01	1.00	0.01	9.47E-01
RFamide	965.54	NRNFLRFamide	1.06	0.04	8.26E-02	**1.07**	**0.01**	**2.41E-05**
	966.53	DRNFLFRamide	1.03	0.04	2.65E-01	**1.03**	**0.01**	**5.87E-03**
	1022.56	GNRNFLRFamide	1.07	0.05	9.60E-02	1.00	0.03	9.57E-01
SIFamide	1381.50	GYRKPPFNGSIFamide	1.01	0.03	8.52E-01	1.00	0.01	7.11E-01
Orcokinin	1474.66	NFDEIDRSGFGFA	1.02	0.04	6.30E-01	**1.07**	**0.03**	**1.22E-02**
	1502.69	NFDEIDRSGFGFV	1.05	0.05	2.43E-01	**1.10**	**0.05**	**2.67E-02**

Table S3 Content changes of neuropeptides in the POs from *Carcinus maenas* green (n=5) and red (n=5) individuals between 5h low salinity stressed individuals and a control. Each group had two POs. Bold font indicates significant changes after stress.

			Green Morph			Red Morph		
	m/z	Sequence	Ratio	SEM	p-Value	Ratio	SEM	p-Value
RYamide	784.41	FVGGSRYamide	1.13	0.10	1.38E-01	**0.76**	**0.06**	**8.70E-04**
	976.46	SGFYANRYamide	1.13	0.11	1.22E-01	**0.79**	**0.08**	**8.52E-03**
	1114.47	SSFRVGGSRYamide	**1.14**	**0.06**	**1.45E-02**	**0.86**	**0.08**	**4.78E-02**
RFamide	965.54	NRNFLRFamide	1.08	0.10	3.88E-01	**0.92**	**0.03**	**1.34E-02**
	966.53	DRNFLRFamide	1.00	0.15	7.21E-01	**0.87**	**0.05**	**1.02E-02**
	1048.57	APQGNFLRFamide	1.03	0.05	5.18E-01	**0.94**	**0.02**	**4.90E-03**
	1124.63	GLSRNYLRFamide	1.09	0.08	1.73E-01	0.93	0.06	1.39E-01
	1137.59	DGNRNFLRFamide	**1.31**	**0.20**	**4.11E-02**	0.97	0.04	2.53E-01
	1158.62	YGNRSRLRFamide	1.02	0.03	3.69E-01	**0.92**	**0.04**	**1.63E-02**
AST-B	1107.58	QWSSMRGAWamide	**1.17**	**0.10**	**3.94E-02**	1.01	0.05	9.22E-01
	1293.63	STNWSSLRSAWamide	**1.19**	**0.07**	**5.88E-03**	0.96	0.04	2.87E-01
	1470.70	VPNDWAHFRGSWamide	**1.75**	**0.44**	**7.18E-03**	1.11	0.07	8.25E-02
Orcokinin	1502.69	NFDEIDRSGFGFV	1.03	0.17	7.67E-01	0.95	0.04	7.71E-02

Table S4. Comparison of neuropeptide content changes in green shell (n=4) and red shell (n=6) *C. maenas* brain after 5h low salinity stress compared to a control. Each group contained one brain. Bold font indicates significant changes after stress.

			Green Morph			Red Morph		
	m/z	Sequence	Ratio	SEM	p-Value	Ratio	SEM	p-Value
Others	844.48	HIGSLYRamide	1.02	0.02	8.73E-02	0.98	0.02	7.06E-02
Tachykinin	934.49	APSGFLGMRamide	1.05	0.04	9.87E-02	0.93	0.08	2.09E-01
RFamide	965.54	NRNFLRFamide	**1.05**	**0.01**	**2.22E-03**	0.97	0.04	3.22E-01
	966.53	DRNFLFRamide	1.03	0.02	1.24E-01	0.93	0.06	1.30E-01
	1022.56	GNRNFLRFamide	**1.03**	**0.02**	**3.00E-02**	0.97	0.04	2.74E-01
	1105.63	SMPSLRLRFamide	**1.03**	**0.02**	**4.00E-02**	0.99	0.05	6.90E-01
	1137.59	DGNRNFLRFamide	1.01	0.02	5.59E-01	**0.97**	**0.02**	**5.54E-02**
	1158.62	YGNRSFLRFamide	1.01	0.01	2.16E-02	0.96	0.05	2.63E-01
	1288.68	QDLDHVFLRFamide	**1.02**	**0.01**	**2.16E-02**	0.99	0.03	7.00E-01
	1314.78	DARTALRLRFamide	1.00	0.01	9.99E-01	0.96	0.03	9.37E-02
SIFamide	1381.50	GYRKPPFNGSIFamide	1.01	0.02	2.83E-01	0.93	0.05	8.47E-02
Orcokinin	1474.66	NFDEIDRSGFGFA	1.02	0.02	2.64E-01	0.98	0.03	2.83E-01
	1502.69	NFDEIDRSGFGFV	1.03	0.02	1.42E-01	0.98	0.02	2.25E-01

Table S5. Comparison of neuropeptide content changes in green shell C. *maenas* PO after 5h (n=6), 12h (n=10), 24h (n=6), and 48h (n=6) of high salinity stress compared to a control. Each group contained two POs. Bold font indicates significant changes after stress.

			5h			12h			24h			48h			ANOVA
	m/z	Sequence	Ratio	SEM	p-Value	Ratio	SEM	p-Value	Ratio	SEM	p-Value	Ratio	SEM	p-Value	p-Value
RYamide	784.41	FVGGSRYamide	0.97	0.06	3.45E-01	0.95	0.07	2.51E-01	**0.88**	**0.05**	**3.91E-03**	0.93	0.09	1.89E-01	2.79E-01
	976.46	SGFYANRYamide	0.97	0.06	3.35E-01	0.96	0.06	2.85E-01	**0.92**	**0.03**	**1.83E-03**	0.88	0.10	9.27E-02	2.70E-01
RFamide	965.54	NRNFLRFamide	0.93	0.06	6.09E-02	1.07	0.05	1.08E-01	**0.90**	**0.07**	**3.51E-02**	0.88	0.08	5.35E-02	1.88E-01
	1022.57	GNRNFLRFamide	0.92	0.07	8.62E-02	1.08	0.06	9.79E-02	0.93	0.07	6.53E-02	0.94	0.09	2.37E-01	4.75E-01
AST-B	1293.63	STNWSSLRSAWamide	1.08	0.14	7.46E-01	0.91	0.11	1.47E-01	0.98	0.08	3.88E-01	**0.73**	**0.09**	**1.68E-03**	3.65E-01
	1470.70	VPNDWAHFRGSWamide	**1.23**	**0.10**	**2.13E-03**	**1.28**	**0.16**	**2.57E-02**	1.02	0.07	9.44E-01	**1.29**	**0.07**	**7.74E-05**	8.93E-01
Orcokinin	1502.69	NFDEIDRSGFGFV	1.06	0.22	6.23E-01	1.00	0.13	6.87E-01	1.06	0.04	9.10E-02	**0.77**	**0.12**	**1.24E-02**	3.15E-01
	1532.70	NFEIDRSSFGFV	**0.74**	**0.11**	**7.15E-03**	0.94	0.11	2.47E-01	**0.87**	**0.04**	**6.47E-04**	**0.73**	**0.09**	**2.62E-03**	3.85E-01
	1547.7	NFDEIDRSSFGFN	1.14	0.29	9.45E-01	1.28	0.19	1.01E-01	0.96	0.05	3.01E-01	0.97	0.20	3.85E-01	6.47E-01

Table S6. Comparison of neuropeptide content changes in green shell C. *maenas* brain after 5h (n=6), 12h (n=10), 24h (n=6), and 48h (n=6) of high salinity stress compared to a control. Each group contained one brain. Bold font indicates significant changes after stress.

			5hr			12h			24h			48h			ANOVA
	m/z	Sequence	Ratio	SEM	p-Value	Ratio	SEM	p-Value	Ratio	SEM	p-Value	Ratio	SEM	p-Value	p-Value
Others	844.48	HIGSLYRamide	1.03	0.02	1.36E-01	1.02	0.03	3.39E-01	**0.91**	**0.04**	**7.30E-03**	**0.93**	**0.02**	**1.77E-03**	**1.41E-02**
Tachykinin	934.49	APSGFLGMRamide	1.04	0.03	1.15E-01	**1.07**	**0.02**	**8.58E-04**	**0.90**	**0.03**	**8.64E-04**	**0.93**	**0.02**	**2.69E-04**	**2.48E-04**
RFamide	965.54	NRNFLRFamide	1.06	0.04	8.26E-02	**1.06**	**0.04**	**2.77E-02**	**0.94**	**0.02**	**5.46E-03**	0.97	0.03	7.69E-02	**3.00E-04**
SIFamide	1381.50	GYRKPPFNGSIFamide	1.01	0.03	8.52E-01	1.01	0.03	7.72E-01	**0.89**	**0.03**	**3.51E-04**	**0.91**	**0.03**	**1.15E-03**	**1.71E-02**
Orcokinin	1474.66	NFDEIDRSGFGFA	1.02	0.04	6.30E-01	1.02	0.02	2.69E-01	0.93	0.05	9.61E-02	0.90	0.07	5.88E-02	2.34E-01
	1502.69	NFDEIDRSGFGFV	1.05	0.05	2.43E-01	**1.06**	**0.03**	**7.70E-03**	0.99	0.02	3.17E-01	0.96	0.04	1.49E-01	1.51E-01
	1532.72	NFDEIDRSSFGFV	1.01	0.04	8.70E-01	1.02	0.04	4.20E-01	**0.96**	**0.02**	**3.40E-02**	1.00	0.03	8.72E-01	5.26E-01
	1547.68	NFDEIDRSSFGFN	1.05	0.04	1.53E-01	1.02	0.03	4.57E-01	0.98	0.04	3.31E-01	0.99	0.04	5.38E-01	5.41E-01

Materials and Methods (Extended)

Methanol (MeOH), acetonitrile (ACN), formic acid (FA), glacial acetic acid (GAA), borane pyridine, and formaldehyde (CH_2O) were purchased from Fisher Scientific (Pittsburgh, PA). $^2H_2$-formaldehyde (C^2H_2O) was purchased from Isotech (Miamisburg, OH), and DHB was obtained from MP Biomedicals, Inc. (Solon, OH). CHCA was purchased from Sigma-Aldrich (St. Louis, MO). Acidified MeOH was prepared using 90% MeOH, 9% GAA, and 1% water (H_2O). All water used in this study was doubly distilled on a Millipore filtration system (Bedford, MA), and C18 Ziptips were purchased from Millipore (Billerica, MA).

Animals and Salinity Stress Experiments

Both red and green shell green crabs *Carcinus maenas* were purchased from The Marine Biological Lab (Woods Hole, Massachusetts, USA). Animals were maintained without food in an artificial seawater tank (30 parts per thousand (ppt) salinity at 12-13 °C) for 5 days before use. In the high salinity stress experiments, crabs were kept in 60 ppt artificial seawater for 5 hours (h), 12h, 24h, or 48h. For the low salinity stress experiments, crabs were kept in artificial seawater 0 ppt for 5h. Crabs were then cold anesthetized by packing in ice for 15 minutes. All dissections were performed in chilled (approximately 10 ^oC) physiological saline (composition: 440 mM NaCl; 11 mM KCl; 13 mM $CaCl_2$; 26 mM $MgCl_2$; 10 mM HEPES acid; pH 7.4 (adjusted with NaOH)). The details of dissection were described previously [42]. All the dissection and sample processing steps were exactly the same between the two shell types.

Sample Preparation

Neuropeptides were extracted from the tissue samples with an appropriate amount of acidified MeOH and manually homogenized. The resulting homogenate was centrifuged at

13,200 rpm for 10 minutes, and the supernatant was transferred to a clean tube and placed on ice. The homogenizer was further rinsed with acidified MeOH, and the resulting solution was used to then wash the pellet and centrifuged for 8 minutes before it was added to the supernatant tube. The rinse and wash steps were repeated three times. The final, combined supernatant was dried down using a Savant SC 110 SpeedVac concentrator (Thermo Electron Corporation, West Palm Beach, FL). The sample was then resuspended in 8 μL of Millipore water containing 0.1% FA (volume (v)/v). To remove lipids and salts before the formaldehyde labeling reaction, the crude extract was processed by a C_{18} Ziptip according to the product instruction.

To achieve duplex dimethyl labeling, a 3 μL aliquot of tissue extract from the PO or brain was labeled in solution by adding 0.7 μL borane pyridine (C_5H_8BN, 120 mM in 10% MeOH), and then mixed with formaldehyde (CH_2O, 4% in H_2O, 0.5 μL) for control samples or deuterium formaldehyde (C^2H_2O, 4% in H_2O, 0.5 μL) for stressed samples. The samples were then left in room temperature for 15 minutes to complete the labeling reaction. 4 μL of each heavy and light labeled solution were combined. The resulting mixture was spotted on a target plate and was analyzed by MALDI- TOF/TOF.

For imaging experiments, the freshly dissected PO was rinsed briefly by dipping in deionized water for two seconds to decrease salt content. It was then mounted onto a MALDI-TOF/TOF sample plate and kept in a desiccator for one hour. Before imaging acquisition, five coats of DHB (150 mg/mL in 50% MeOH, v/v) were applied on the tissue surface using an airbrush (Paasche airbrush company, Chicago, IL) with 30-second intervals between each cycle.

Mass Spectrometry and Imaging

<u>MALDI-TOF/TOF</u>

A model 4800 MALDI-TOF/TOF analyzer (Applied Biosystems, Framingham, MA) equipped with a 200 Hz, 355 nm Nd:YAG laser was used for extract quantitation and imaging. Acquisitions were performed in positive ion reflectron mode, and instrument parameters were set using the 4000 Series Explorer software (Applied Biosystems). Mass spectra were obtained by averaging 900 laser shots covering a mass range of *m/z* 500-2000. 5 mg/mL of CHCA in 50% ACN (v/v) was used as the matrix. For sample spotting, 0.4 μL of sample was spotted on MALDI plate first, allowed to dry, and then followed by 0.4 μL matrix.

MALDI Imaging

Image acquisition was performed on the model 4800 MALDI-TOF/TOF analyzer (Applied Biosystems, Framingham, MA, USA) using the 4800 Imaging application (Novartis, Basel, Switzerland) available through the MALDI-MS imaging website (www.maldi-msi.org). To generate images, spectra were collected at 100 μm intervals in both the *x* and *y* dimensions across the surface of the sample. Each mass spectrum was generated by averaging 200 laser shots over the mass range of *m*/*z* 800-2000. Individual spectra were acquired using 1.0 ns binning to yield 27812 data points per spectrum. Image files were processed, and extracted ion images were created using the TissueView software package (Applied Biosystems, Framingham, MA, USA).

Quantitative Data Analysis

The same approaches were used for both high and low salinity stress experiments. Stressed and control extractions from one salinity stress experiment were differentially labeled and mixed with 1:1 ratio. Each resulting sample was spotted on the MALDI plate twice, from which the resulting spectra were analyzed by manual mass matching from an in-house crustacean neuropeptide database. The matched 4 Dalton (Da)-spaced peak pairs' intensities were extracted

for both known and unidentified neuropeptides. The raw intensities were then natural log normalized prior to further data processing. The abundance ratio for each neuropeptide in stressed versus control crabs was determined by dividing the heavy labeled peak intensity (stressed) with the respective light labeled peak intensity (control). Average ratios were calculated from the two duplicate spectra. Student's two-sample, two-tailed t-tests were performed to evaluate the differences between stressed and control samples using Microsoft Excel (p value <0.05). Prior to the t-test, the intensity of the CH_2O or C^2H_2O labeled peak was normalized by dividing by the total, log normalized intensity of the peak pairs to eliminate differences of ionization efficiency between acquisitions. ANOVA tests as well as individual t-tests were performed on the time course data using Microsoft Excel (p value <0.05). While the t-tests discerned differences between the expression at that point and a control, the ANOVA tested for any differences between the 4 individual time points.

Chapter 7

In situ Labeling for the Absolute Quantitation of Crustacean Neuropeptides with Mass Spectrometry Imaging

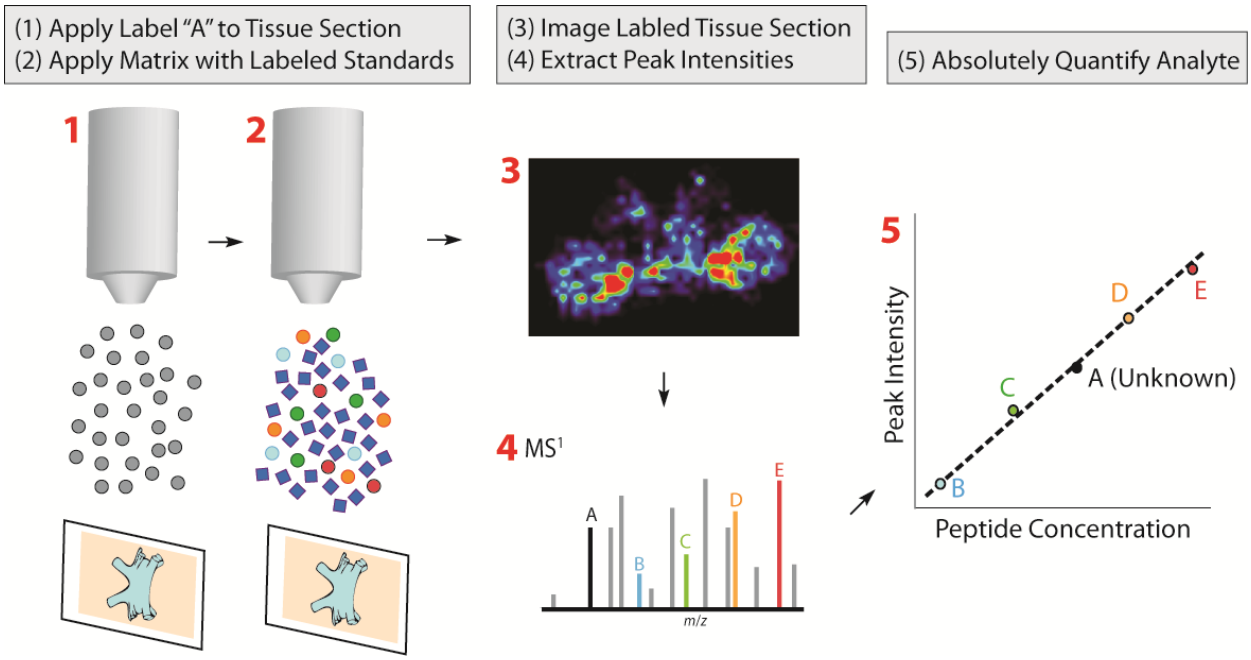

This work will be continued by Nhu Q. Vu and Meng Xu.

Keywords: MALDI-MS Imaging, *In situ* Labeling, Absolute Quantitation, Isotopic DiLeu, Dimethyl Labeling

Abstract

Quantitative mass spectrometry (MS) imaging provides an ideal workflow to extract both quantitative and localization information of an analyte of interest from a single tissue section. Unfortunately, especially in matrix-assisted laser desorption/ionization (MALDI)-MS imaging, challenges still remain, including ion suppression differences and tissue heterogeneity. By combining *in situ* derivatization and isotopic labeling strategies, we propose to build an on-tissue calibration curve to absolutely quantify neuropeptides in the crustacean brain. Both 5-plex isotopic N, N-dimethyl leucine (iDiLeu) and dimethyl labeling (DM) were applied, although optimization of in-solution and spot-based labeling was required for iDiLeu prior to application on tissue. Unfortunately, neither approach shows efficient labeling currently. One case of success was seen for DM labeling of a selected peptide (mass-to-charge ratio (*m/z*) 844.479, HL/IGSL/IYRamide), for which >95% labeling was observed, although reproducibility proves to be an issue. The wide range of application and incubation techniques proves to complicate the next steps, although employing different derivatization techniques or examining different target molecules (*e.g.*, metabolites) may offer promising solutions in the future.

Introduction

Mass spectrometry (MS) imaging has developed a reputation for its ability to localize molecules of interest in any tissue section without prior knowledge of their structure or labeling.[1-3] Matrix-assisted laser desorption/ionization (MALDI)-MS imaging in particular has been one of the most popular approaches for analyzing biological samples.[1] To prepare samples for MALDI-MS imaging, a tissue is usually thinly sectioned and thaw mounted onto glass microscope slides prior to being sprayed with a matrix. Inside the instrument, an (x, y) grid is

formed over the surface of the sample, each square being a "pixel." A mass spectrum is then collected at each pixel, and, using sophisticated computational software, individual mass-to-charge ratio's (*m/z*) intensity can be extracted from each pixel and reformed into a heat map image.[1] This means that, compared to immuno-based techniques where only one analyte can be imaged at a time, we can extract images for theoretically hundreds of molecules from a singular MS imaging run.[1-3] With all the advances in this field, MS imaging is rapidly evolving and requires continuous technological and method development to match the current demand.

The current stigma with MS imaging is its inherently "semi-quantitative" nature, especially MALDI-MS. Due to the tissue heterogeneity, sample topography, and variable ion suppression, researchers have struggled to confidently extract quantitative information.[1, 4] In the past, parallel liquid chromatography (LC) analysis of a serial tissue section was required to both fully identify and quantify a molecule of interest.[5, 6] While still applicable for confirmation of results, researchers are developing new and innovative methods for extracting quantitative information using MS imaging.[1] The easiest method for this is direct relative comparison of different tissue sections, although this tends to be more "semi-quantitative" even with proper normalization and other pre- and post-processing steps.[7-11] While other relative comparison strategies exist (*e.g.*, generation of reporter ions), absolute quantitation strategies have clearly been the most popular and accurate in the literature.[4, 11] The use of an internal standard applied all over the tissue using a commercial sprayer is employed for both absolute and relative quantitation but less frequently than building an on-tissue calibration curve.[7, 12-14] To build a calibration curve, the standards of interest are usually spotted or applied to a separate, serial "control" section or into tissue homogenates. Unfortunately, we are still plagued with inaccurate quantitation with heterogeneous tissue sections (*e.g.,* brain), continuity issues between serial

sections, and lack of access to computational workflows. However, as MALDI-MS imaging methods are becoming increasingly efficient, imaging and LC workflow results are becoming more similar.[6, 15]

In order to circumvent these disadvantages in absolute quantitation MS imaging, an isotopic labeling strategy can be developed. By incorporating different amounts or combinations of stable isotopes (*e.g.*, ^{2}H, ^{13}C, ^{15}N, ^{18}O), we can distinguish between samples inside a MS instrument in a singular run by their *m/z* value.[16] In LC-MS workflows, an unknown sample is labeled with a tag with a distinct isotopic structure. Then, standards of a molecule of interest are labeled with different isotopic combinations (two ^{2}H vs two ^{1}H) and mixed with the previously labeled, unknown sample. When analyzed on a MS, an in-solution calibration curve can be extracted and used to absolutely quantify the molecule of interest. This can be translated to a MALDI-MS imaging workflow, as shown in **Figure 1**. Initially, a tissue section is labeled with one of the tags while the other tags are used to label standards of the molecule of interest at different concentrations. The standards are then applied with the matrix prior to the section being imaged by MALDI-MS imaging. As with the in-solution technique, we construct a calibration curve to quantify the molecule of interest. This can be done for the whole tissue (*e.g.*, brain), one discrete region of the tissue (*e.g.*, brain ganglion), or on a pixel-by-pixel basis. While this is a novel approach for *in situ* MALDI MS imaging, on-tissue labeling for a variety of molecular species is well-documented in the literature, meaning the proposed technique is feasible.[6, 7, 11, 17-19]

The initial challenge is selecting the proper labeling scheme to target the molecular species of interest. For absolute quantitation, at least four calibration points are needed, thus our isotopic labeling schemes must include a minimum of five isotopic combinations.[20, 21] Another

consideration is the spacings between tags, as many MALDI instruments only allow for a maximum mass resolution of 100,000 (at *m/z* 400), meaning we are limited to spacings of a few Daltons (Da) rather than mDa. In particular, we are interested in labeling primary amines, which are available on the N-terminus of all peptides (except for N-terminally blocked peptides). Two tagging systems (*i.e.*, isotopic N,N-dimethyl leucine (iDiLeu) and dimethyl labeling (DM)) both have (a) 5 different isotope combinations along with (b) 3 and 2 Da mass spacings between the tags, respectively.[20, 21] The different isotope combinations and structures for each of these 5-plex tagging systems are shown in **Figure S1**. Both of these tags target primary amines, meaning it can easily target peptides and proteins due to having a primary amine at the N-terminus.

Here, we describe the attempt to successfully *in situ* label crustacean neurological peptides (*i.e.*, neuropeptides) in the brain tissue using both iDiLeu and DM labeling schemes. Crustaceans have been utilized as a model system to understand neuromodulation, while neuropeptides provide an excellent system for method development and biological application to understanding absolute quantitative changes due to major physiological processes (*e.g.*, stress or feeding).[22-25] Spots of neuropeptide standards were able to be successfully labeled by iDiLeu >95% labeling. Unfortunately, *in situ* labeling was not achieved for either iDiLeu or DM consistently at this point. Different, novel application conditions, incubation strategies, and even labeling schemes are being considered for future experiments.

Material and Methods

Methanol (MeOH), acetonitrile (ACN), glacial acetic acid (GAA), Difco™ gelatin, plain glass microscope slides, sodium hydroxide (NaOH), and all crab saline components (see below) were purchased from Fisher Scientific (Pittsburgh, PA). Formaldehyde (CH_2O), dry

dimethylformamide (DMF), dry dichloromethane (DCM), triethylammonium bicarbonate (TEAB), hydroxylamine (NH_2OH), sodium cyanoborohydride ($NaBH_3CN$), and 4-(4,6-Dimethoxy-1,3,5-triazin-2-yl)-4-methylmorpholinium chloride (DMTMM) were acquired from Sigma-Aldrich (St. Louis, MO). 5-dihydroxybenzoic acid (DHB) and dry ACN were obtained from Acros Organics (Morris, New Jersey), while formic acid (FA) was purchased through Fluka (Mexico City, Mexico). N-methylmorpholine (NMM) was obtained from TCI (Portland, OR). Ethanol (EtOH) utilized in this study was from Pharmco-Aaper (Chicago, IL). Yeast protein and digestion enzymes were acquired from Promega Corporation (Madison, WI). Neuropeptide standards were from American Peptide Company (Fisher Scientific). All water (H_2O) used in this study was doubly distilled on a Millipore filtration system (Burlington, MA) or HPLC grade. All LC solvents were Fisher Optima Grade.

Animals Housing and Care

All female blue crabs, *Callinectes sapidus*, were either purchased from Midway Asian Market (Madison, WI) or LA Crawfish Company (Natchitoches, LA). After transport, crabs were allowed to recover in seawater made to be 35 parts per thousand (ppt) and 12-14 °C for several days prior to experiments. A crab was anesthetized on ice for 20 minutes and sacrificed for their tissues of interest (*e.g.,* brain) as previously described.[26] All dissections were performed in chilled (approximately 10 ºC) physiological saline (composition: 440 mM NaCl; 11 mM KCl; 13 mM $CaCl_2$; 26 mM $MgCl_2$; 10 mM Trizma acid; pH 7.4 (adjusted with NaOH)).

Sample Preparation

<u>iDiLeu Workflow</u>

iDiLeu d0 (*i.e.*, non-isotopic DiLeu, DiLeu 114) was synthesized as previously published.[20, 27] **Figure S2** shows the basic workflow for labeling with DiLeu, and a step-by-step

guide to activating the tag and labeling peptides of interest is published elsewhere.[27, 28] Briefly, a 0.7x molar ratio DMTMM and NMM solution (*e.g.*, in DMF) was added to an aliquoted, inactive iDiLeu tag (*e.g.*, 1 mg) and allowed to vortex for 30-40 minutes, forming an amine-reactive triazine-ester on the iDiLeu tag. The activated iDiLeu d0 was then added to a solution of peptides of interest at a 20:1 label:peptide ratio. The final solution should be ~30% aqueous, usually by addition of TEAB buffer to maintain a pH ~8. The solution was then mixed for 30 minutes to 2 hours, depending on the molecular target and label:peptide ratio.[29-31] The resulting solution was then quenched by addition of NH_2OH to ~0.25%. Prior to running by LC-MS, the labeled sample was cleaned up sequentially by strong cation exchange (*e.g.*, PolyLC Inc. TopTips with PolySULFOETHYL A Material) and desalting (*e.g.*, Agilent C18 OMIX tips). Modifications to this method (*i.e.*, solvent composition, activation time, label:peptide ratio, labeling time, labeling temperature, and H_2O/buffer integration) are discussed below. All solvents utilized in this workflow were anhydrous.

In-Solution Optimization

Yeast (*S. cerevisiae*) protein (MS Compatible Yeast Protein Extract, Intact) was digested using a trypsin/LysC enzyme mix (Trypsin/Lys-C Mix, Mass Spec Grade) following the manufacturer's recommend procedure. Tryptic peptides were labeled in-solution following the protocol above with modifications (see *Results and Discussion*). All samples were analyzed with at least two technical replicates.

Spot-Based Analysis

Neuropeptide-rich crustacean tissues were extracted using a manual homogenizer with chilled acidified MeOH (90:9:1 MeOH:H_2O:GAA), and the supernatant was collected after the sample was centrifuged at 13,200 rpm for 10 minutes. The resulting pellet was re-extracted

twice, with the supernatant collected each time. The combined supernatant fraction was dried down in a Savant SCV100 Speedvac. All crude extracts were purified using C18 ZipTips following the manufacturer's protocol. All samples were centrifuged at high speed prior to purification to pellet any particulates. To calculate how many peptide species were in all tissues of interest, the Pierce Quantitative Colorimetric Peptide Assay was used following the manufacturer's protocol.

For the labeling procedure, neuropeptide extracts or standards were spotted onto a MALDI stainless steel plate. iDiLeu d0 was activated using an optimized protocol (*i.e.*, 45 minutes in ACN) immediately prior to labeling. Three types of experiments were performed. (1) Spots were allowed to dry prior to having activated label added on top and allowed to react. (2) Spots were allowed to dry and then rehydrated before having the activated label being added. (3) Spots had the activated label added prior to drying. After being allowed to react, the sample can be quenched by addition of 5% NH_2OH. DHB matrix was then added to the dried spot prior to MALDI-MS analysis.

Tissue Section Preparation

Freshly dissected brains were embedded in gelatin (in small plastic cups) and sectioned using a Micro HM525 cryostat (Thermo Scientific). The 12-16 μm thick sections were thaw mounted onto plain glass microscope slides (Fisher Scientific) and stored at -80 °C till use. Prior to use, sample were then dried in a desiccator box or vacuum chamber for 10-20 minutes.

The labeling system of interest was prepared immediately prior to analysis. For iDiLeu d0, the label was activated and diluted in ACN. The DM reagents were dissolved in H_2O. For reference to in-solution DM, please see previous chapters and publications.[32] All labeling systems were applied using a commercial TM-Sprayer (HTX Technologies, LLC). The volume

applied varied depending on the desired label:peptide ratio, which was based upon the peptidomic density of the tissue section (mg/mm^2). To calculate the average concentration of peptides in a single tissue section, a Pierce Quantitative Colorimetric Peptide Assay was used following the manufacturer's protocol (*i.e.*, 3.3 μg for a 16 μm section). The area of the brain was determined using ImageJ (*i.e.*, 0.095 cm^2). It should be noted that brains were embedded in ice instead of gelatin only for this experiment due to gelatin's interference with the peptide assay's colorimetric reagents. An appropriate TM sprayer method was developed considering the peptidomic density of the tissue section. Parameters, including labeling concentration, nozzle temperature, velocity, and syringe pump speed, were all varied to optimize application of the label. The equation used to calculate application density is shown in **Equation S1**. After applying the label, the tissue section was incubated for a desired amount of time (see *Results and Discussion*).

Matrix (*i.e.*, 40 mg DHB in 50:50 MeOH:H_2O and 0.1% FA) was then applied using the TM-Sprayer with the following optimized parameters: 0.1 mL/min syringe flow rate; 12 passes, 0.5 min dry time, 1250 mm/min nozzle velocity, 80 °C, and 3 mm track spacing. Samples were then run immediately after matrix application. Control brains were used for all method optimization. All experiments were run with a serial brain section to represent a control. An example method sheet is provided in the *Supplemental Materials* for both iDiLeu and DM.

MS Data Collection and Analysis

Initial re-optimization of the in-solution iDiLeu labeling was performed on a Thermo Fisher Q-Exactive (QE) mass spectrometer connected to a Waters NanoAcquity LC system. Samples were injected onto a homemade C18 column (14-16 cm) using a 90 minute gradient (10% B to 35% B) with H_2O (0.1% FA) (A) and ACN (0.1% FA) (B). MS and tandem MS

spectra (top 15 data dependent acquisition with high-energy collision dissociation) were run at a 70,000 and 17,500 mass resolution, respectively, in the *m/z* 200-2000 mass range. Spot-based optimization and MALDI-MS imaging analysis were performed on a MALDI-LTQ-Orbitrap XL (Thermo Fisher). A mass range of *m/z* 500-2000 and at least 30,000 mass resolution was used for all experiments. For imaging experiments, the spatial resolution was 75 micron.

Data Analysis

All yeast tryptic peptides were identified with Thermo Fisher Proteome Discoverer (Version 1.4). A custom modification was created for iDiLeu d0 (+114.115 Da) for both lysines and the N-terminus. Labeling efficiency was calculated by considering the difference between the number of peptides identified between (a) dynamic lysine and N-terminus labeling and (b) static lysine and N-terminus labeling. The number of proteins identified should be equal if 100% labeling is achieved.

Spectra generated from analysis of the spot-labeled neuropeptides were averaged in Xcalibur, and all peaks and their intensities were exported into Excel.+ A custom Java program was used to (a) identify neuropeptides and (b) determine their efficiency of labeling with iDiLeu d0. All neuropeptides were identified using ±5 parts per million (ppm) mass error and an intensity threshold of 100.

For imaging experiments, raw data files were exported to .imZML format (using Thermo Fisher ImageQuest; Version 1.1.0 Build 54) followed by importing into MSiReader (Version 0.9 or 1.00). Files were normalized to the TIC to generate images with a ±5 ppm error from known neuropeptides in our homebuilt crustacean database. In order to identify the neuropeptides (labeled and unlabeled), ImageQuest was used to average the signals found in the brain tissue, from which the centroid peaks and their intensities were extracted for accurate mass matching

(±10 ppm) to a homebuilt crustacean database using a custom Java program. All accurate mass matched neuropeptides were compared to the generated images for final identification. Labeling efficiency was calculated using another Java program that divides the intensity of the labeled neuropeptide *m/z* by the total intensity of both the labeled the unlabeled neuropeptide *m/z* in the same sample. All reported *m/z* values are in the [mass+H] form.

Results and Discussion

In order to develop a better method for absolute quantitation MS imaging, here, well-vetted isotopic labeling strategies are being translated from in-solution to on-tissue workflows, including iDiLeu and DM. **Figure 1** illustrates a general workflow, which is applicable to all labeling strategies, not just iDiLeu or DM.

iDiLeu

The first step in utilizing iDiLeu labels is to activate the inactive form to a triazine, amine-reactive form. The original, in-solution workflow utilizes dry DMF as the activation solvent, although it doesn't evaporate away and has to be removed through further clean up. Unfortunately, this makes DMF an unideal solvent choice for applying iDiLeu to tissue sections, so an alternative solvent was investigated. DCM, which has been used as an alternative labeling solvent, and ACN, which is commonly used in MS imaging workflows, were tested for their iDiLeu labeling efficiency of tryptic peptides using the original optimized workflow shown in **Figure S2**. While DMF produces 100% labeling, DCM and ACN provided 0.85% and 61.96% labeling, respectively. Thus, ACN was chosen as the solvent for iDiLeu activation for all future studies. The labeling efficiency for ACN was improved by optimizing the activation time, labeling ratio, and labeling time, which was found to be 45 minutes, 25:1 (label:peptide), and 90

minutes, respectively. Compared to the original workflow, the label:peptide ratio was only slightly affected, but the activation time and labeling time greatly increased. With that in mind, we were only able to get ~80% labeling of tryptic peptides at optimal conditions with ACN compared to DMF. A standard mixture of six neuropeptides (unlabeled in **Figure 2a**) showed ~70% labeling (with and without quenching) using the optimized in-solution ACN conditions.

Prior to on-tissue labeling, direct spot labeling was done for preliminary optimization. In general, for on-tissue experiments, four different characteristics need to be considered: (1) changing the label:peptide ratio, (2) integration of H_2O or a buffer, (3) labeling time, and (4) labeling temperature. All of these were also considered in spot-based analysis. Initial experiments on both fresh and dried spots showed >90% labeling (with and without quenching) of the standard neuropeptide mixture (unlabeled: **Figure 2a**; labeled: **Figure 2b**) at room temperature. Interestingly, even though the reaction was allowed to proceed for 90 minutes prior to addition of the quenching agent or DHB matrix, the spots appeared to dry after 30 minutes. One major difference between our spot labeling and the solution-based workflow was the incorporation of an aqueous component, which was adjusted to ~30% in the solution-based workflow. The triazine ester reaction with primary amines is pH dependent, and TEAB (0.5M), which buffers around pH ~8, was utilized when labeling in solution. Both TEAB (**Figure 2c**) and a H_2O (pH=8) (**Figure 2d**) solutions were used to hydrate pre-dried spots prior to the addition of iDiLeu. All produced acceptable labeling, although 60 and 30 minutes labeling time produced optimal labeling for TEAB and pH=8 H_2O, respectively (**Table S1**). Overall, a 25:1 label:peptide ratio was maintained throughout.

Even with consideration of all four parameters above, little success was seen for *in situ* labeling of neuropeptides in crustacean brain tissue (**Table S2**). It should be noted that a

label:peptide ratio of 10:1 was maintained in all experiments in order to conserve iDiLeu. This can be demonstrated further by comparing the amount of iDiLeu utilized in a LC-MS experiment (1 mg) to our imaging experiments (20-40 mg). While inexpensive to synthesize these iDiLeu reagents, the overall process of synthesis, clean up, and final allocating could be time consuming. Unfortunately, reducing the label:peptide ratio is not ideal and may lead to lower labeling, although some have used DiLeu, which uses a similar activation and labeling procedure to iDiLeu, at lower ratios with success.[30] In general, low-level of labeling was seen overall, but high efficiency labeling was seen for low intensity neuropeptides. Unfortunately, this does not translate well in the MS images. **Figure 3a** shows an ideal situation, where all the intensity in the unlabeled *m/z* in the control tissue is converted to the labeled *m/z* in the sprayed tissue with minimal diffusion. Whenever applying a chemical reagent to a tissue section, including matrix, it is important to minimize any diffusion that may occur. Beyond no labeling (**Figure 3d**, DLPKVDTALK, *m/z* 1099.636), applying iDiLeu appears to also contribute to the background noise (**Figure 3b**, DPSFLEFamide, *m/z* 853.409), which could suggest substantial ion suppression upon application of the activated iDiLeu reagent. To determine the failure point, since all the spots previously analyzed were desalted, another iteration of experiments was performed on undesalted spots, which showed low labeling consistent with what was seen in the on-tissue experiments. It can be inferred that the high salt content of crustacean tissue hinders the labeling of neuropeptides and/or primary amines in the tissue, and a better way to desalt the tissue or the tissue section is needed to allow for derivatization of these molecules. One consideration could be inclusion of a washing step, such as the one from *Chapter 5* applied to DM labeling (see below).

Dimethyl Labeling

Unlike iDiLeu, DM labeling methodology has been applied previously to spot on tissue to provide localized dimethylation to improve crustacean neuropeptidomic identification on-tissue. Before the commercialization of MALDI MS imaging, spotting onto specific brain regions provided low-resolution localization information without requiring advanced instruments or technology. The in-solution workflow that provided inspiration is shown in **Figure S3**. When comparing the DM labeling efficiency results found in **Table S3** and **Table S4** to those of iDiLeu (**Table S2**), the labeling efficiency was overall much higher. Due to the still inherantly low intensity values, Condition 12 incorporated a washing step (50:50 EtOH:H_2O for 10 seconds) prior to labeling to improve detection of neuropeptides, which was discussed separately in *Chapter 5*. The washing step did increase the overal intensity, although this was not reflected in the labeling efficiency observed. It should be noted that the labeling efficiency does not take into consideration a control section, as we calculate the labeling efficiency of the neuropeptide by dividing the intensity of the labeled peptide *m/z* by the total intensity of both the labeled and unlabeled peptide *m/z* in the sprayed section. This means that these labeling efficiency calculations for both native and DM were skewed for several neuropeptides, and the images should always be checked for true labeling.

Unfortunately, DM was still plagued with the same issues as iDiLeu with background noise (**Figure 3c**, DFSAWAamide, *m/z* 695.315) and little to no labeling (**Figure 3e**, KPKTEKK, *m/z* 858.541). Successful (>95%) labeling was achieved for *m/z* 844.479 (HL/IGSL/IYRamide) using condition #7 (**Table S3**), as shown in **Figure 3f**. This is a prime example, as no diffusion was visualized along with near 100% labeling efficiency. Unfortunately, this was not repeatable (Condition 7 vs 9; **Table S3** and **S4**, respectively). This could be due to using different brain sections, as the neuropeptide (*m/z* 844.479;

HL/IGSL/IYRamide) was not even present in the control tissue in Condition 9's experiment. More interestingly, there were several examples of neuropeptide signals that "appeared" after labeling in both unlabeled and labeled *m/z* (**Figure 4**). This difference suggested that the specific neuropeptide was not present in the control tissue, but signal became apparent after addition of the DM reagents. Some examples that are seen consistently throughout different conditions are shown in **Figure 4**. One case, RFamide pQRNFLRFamide (**Figure 4b**), should not be labeled due to its N-terminus being blocked by the pyroglutamine post-translational modification, so it is likely not this neuropeptide but an interfering molecule. Thus, these examples and others should be investigated further by on-tissue tandem MS (MS/MS) to confirm their identities.[33]

Once labeling is achieved consistently, applying peptide standards to the tissue section for absolute quantitation is the next step. Two different avenues can be taken: (1) spraying the standards separately from the matrix or (2) adding the standards to the matrix for application. This is a challenge due to determining the appropriate concentration to spray which requires the guess-and-check method. In preliminary experiments, unlabeled bradykinin (*m/z* 1060.569) was utilized. When sprayed before the matrix, there appeared to be ion supression in the brain itself, although applying with the matrix provided homogenous application of the standard without differntial ion suppression between the geletin and tissue. It should be noted that in both cases, standard *m/z* dominated each pixel's spectra. Also, these experiments should be repeated since the standard mass was also found in the control section, which had no standard applied separately or in the matrix.

Literature Analysis

Our first step is analogous to determining on-tissue derivatization strategies for MS imaging, which is rampant throughout the literature for a variety of molecular species.

Derivatization is typically used to increase ionization of typically difficult to analyze molecules. In the last few years, people have found ways to derivatize fatty acids, steroids, metabolites, N-glycans, tryptic peptides, and even elements.[6, 7, 11, 17-19, 34-41] Some LC-MS methods in the literature also have potential for application to MS imaging.[42-45]

For two of the steroid studies, Girard's reagent T (GirT) was used as the derivatization agent, although the application and incubation methodology was distinctly different. This highlights a general challenge in the MS imaging field, as inconsistency in methods comes from differences in equipment or use of non-commercial/modified instruments. Both groups utilized commercial sprayers (*i.e.*, HTX TM Sprayer and SunChrom SunCollect) and both used a humidity chamber (*i.e.*, with H_2O only or 50:50 MeOH:H_2O).[11, 18] In comparison, another steroid study employed a novel 2-fluoro-1-methylpyridinium *p*-tolunesolfonate to derivatize cannabinoids, although they focused on using a handheld airbrush, which was difficult to reproduce between people in the same lab let alone between labs.[17] The use of a different derivatization agent is likely due to structural differences in the steroids highlighted here. Both fatty acid and glycan derivatization have unique methods due to their structures, although the same challenges and differences highlighted above are still true.[6, 19]

The most comparable literature comes from the Andren Lab, where neurotransmitters were derivatized using pyrylium salts.[7, 34] This reaction scheme targets primary amines, which is analogous to the current study and provided inspiration for all method considerations. While an automated sprayer was utilized (*i.e.*, HTX TM Sprayer), the incubation technique was very unique, in that, during the 15 minute room temperature incubation, the sample was dried by nitrogen every 5 minutes.[7, 34] They also utilize a 50:50 Meth:H_2O hydration chamber. Even when

replicating this successful publication with slight modification, it was clear that DM and DiLeu require unique, novel methods to increase labeling efficiency.

Conclusions and Future Directions

In situ labeling has great promise to provide more accurate absolute quantitation on tissue for MS imaging workflows. Through our investigation, both iDiLeu and DM require more optimization to provide better data processing pipelines and consistent labeling, although DM shows the most promise. This is not only due to the potential for absolute quantitation but also the derivatization aspect that has shown DM provides better MS/MS fragmentation for neuropeptides.[46] Furthermore, derivatization has shown a lot of promise for metabolites and other molecular species, as shown in the literature analysis. Thus, focus could shift towards both iDiLeu's and DM's labeling efficiency onto amine-containing metabolites. Finally, investigation of previously successful methods may provide insight as well as new avenues since theoretically derivatization schemes can be modified to include stable isotopes to become new methods for *in situ* absolute quantitation. In general, due to the massive data sets, confounding factors (*e.g.*, signal in sprayed but not control section), or overlap in labeled and unlabeled *m/z* of interest (*i.e.*, spectral complexity or even double labeling), a better data analysis pipeline should be considered for more thourough analysis of these large data sets for more accurate understanding of the labeling quality.

Acknowledgements

This work is supported in part by the National Institutes of Health (R01 DK071801) and the National Science Foundation (CHE-1710140). A.R.B. would

like to acknowledge National Institutes of Health-General Medical Sciences NRSA Fellowship (1F31GM119365). A.R.B. would like to thank Kellen DeLaney for assistance in data processing and Java knowledge, Jillian Johnson and Caitlin Keller for discussion, and Chris Sauer for assistance with figure creation. The Thermo MALDI-LTQ-Orbitrap XL was purchased through an NIH shared instrument grant (NCRR S10RR029531).

References

1. Buchberger, A. R.; DeLaney, K.; Johnson, J.; Li, L. J., *Analytical Chemistry* **2018,** *90* (1), 240-265.

2. Caprioli, R. M., *Journal of the American Society for Mass Spectrometry* **2015,** *26* (6), 850-852.

3. Caprioli, R. M.; Farmer, T. B.; Gile, J., *Analytical Chemistry* **1997,** *69* (23), 4751-4760.

4. Hansen, H. T.; Janfelt, C., *Analytical Chemistry* **2016,** *88* (23), 11513-11520.

5. Prentice, B. M.; Chumbley, C. W.; Caprioli, R. M., *Journal of the American Society for Mass Spectrometry* **2017,** *28* (1), 136-144.

6. Wu, Q.; Comi, T. J.; Li, B.; Rubakhin, S. S.; Sweedler, J. V., *Analytical Chemistry* **2016,** *88* (11), 5988-5995.

7. Shariatgorji, M.; Nilsson, A.; Goodwin, R. J. A.; Kallback, P.; Schintu, N.; Zhang, X. Q.; Crossman, A. R.; Bezard, E.; Svenningsson, P.; Andren, P. E., *Neuron* **2014,** *84* (4), 697-707.

8. Miyamoto, S.; Hsu, C. C.; Hamm, G.; Darshi, M.; Diamond-Stanic, M.; Decleves, A. E.; Slater, L.; Pennathur, S.; Stauber, J.; Dorrestein, P. C.; Sharma, K., *Ebiomedicine* **2016,** *7*, 121-134.

9. Heijs, B.; Tolner, E. A.; Bovee, J. V. M. G.; van den Maagdenberg, A. M. J. M.; McDonnell, L. A., *Journal of Proteome Research* **2015,** *14* (12), 5348-5354.

10. Jung, J. W.; Lee, M. S.; Choi, H. J.; Jung, S.; Lee, Y. J.; Hwang, G. S.; Kwon, T. H., *American Journal of Physiology-Renal Physiology* **2016,** *310* (11), F1317-F1327.

11. Cobice, D. F.; Livingstone, D. E. W.; Mackay, C. L.; Goodwin, R. J. A.; Smith, L. B.; Walker, B. R.; Andrew, R., *Analytical Chemistry* **2016,** *88* (21), 10362-10367.

12. Bergman, H. M.; Lundin, E.; Andersson, M.; Lanekoff, I., *Analyst* **2016,** *141* (12), 3686-3695.

13. Shariatgorji, M.; Strittmatter, N.; Nilsson, A.; Kallback, P.; Alvarsson, A.; Zhang, X. Q.; Vallianatou, T.; Svenningsson, P.; Goodwin, R. J. A.; Andren, P. E., *Neuroimage* **2016,** *136*, 129-138.

14. Chumbley, C. W.; Reyzer, M. L.; Allen, J. L.; Marriner, G. A.; Via, L. E.; Barry, C. E.; Caprioli, R. M., *Analytical Chemistry* **2016,** *88* (4), 2392-2398.

15. Theron, L.; Centeno, D.; Coudy-Gandilhon, C.; Pujos-Guillot, E.; Astruc, T.; Remond, D.; Barthelemy, J. C.; Roche, F.; Feasson, L.; Hebraud, M.; Bechet, D.; Chambon, C., *Proteomes* **2016,** *4* (4), 16.

16. Kovanich, D.; Cappadona, S.; Raijmakers, R.; Mohammed, S.; Scholten, A.; Heck, A. J. R., *Analytical and Bioanalytical Chemistry* **2012,** *404* (4), 991-1009.

17. Beasley, E.; Francese, S.; Bassindale, T., *Analytical Chemistry* **2016,** *88* (20), 10328-10334.

18. Barre, F. P. Y.; Flinders, B.; Garcia, J. P.; Jansen, I.; Huizing, L. R. S.; Porta, T.; Creemers, L. B.; Heeren, R. M. A.; Cillero-Pastor, B., *Analytical Chemistry* **2016,** *88* (24), 12051-12059.

19. Holst, S.; Heijs, B.; de Haan, N.; van Zeijl, R. J. M.; Briaire-de Bruijn, I. H.; van Pelt, G. W.; Mehta, A. S.; Angel, P. M.; Mesker, W. E.; Tollenaar, R. A.; Drake, R. R.; Bovee, J.; McDonnell, L. A.; Wuhrer, M., *Analytical Chemistry* **2016,** *88* (11), 5904-5913.

20. Greer, T.; Lietz, C. B.; Xiang, F.; Li, L. J., *Journal of the American Society for Mass Spectrometry* **2015,** *26* (1), 107-119.

21. Wu, Y.; Wang, F. J.; Liu, Z. Y.; Qin, H. Q.; Song, C. X.; Huang, J. F.; Bian, Y. Y.; Wei, X. L.; Dong, J.; Zou, H. F., *Chemical Communications* **2014,** *50* (14), 1708-1710.

22. Chen, R. B.; Xiao, M. M.; Buchberger, A.; Li, L. J., *Journal of Proteome Research* **2014,** *13* (12), 5767-5776.

23. Zhang, Y.; Buchberger, A.; Muthuvel, G.; Li, L., *Proteomics* **2015**.

24. Wang, J. H.; Zhang, Y. Z.; Xiang, F.; Zhang, Z. C.; Li, L. J., *Journal of Chromatography A* **2010,** *1217* (26), 4463-4470.

25. Zhang, Y.; DeLaney, K.; Hui, L.; Wang, J.; Sturm, R. M.; Li, L., *J Am Soc Mass Spectrom* **2018**.

26. Gutierrez, G. J., *Cancer Borealis* Stomatogastric Nervous System Dissection. Grashow, R. G., Ed. JOVE, 2009.

27. Greer, T.; Li, L. J., Isotopic N,N-Dimethyl Leucine (iDiLeu) for Absolute Quantification of Peptides Using a Standard Curve Approach. In *Quantitative Proteomics by Mass Spectrometry, 2nd Edition*, Sechi, S., Ed. Humana Press Inc: Totowa, 2016; Vol. 1410, pp 195-206.

28. Frost, D. C.; Li, L. J., High-Throughput Quantitative Proteomics Enabled by Mass Defect-Based 12-Plex DiLeu Isobaric Tags. In *Quantitative Proteomics by Mass Spectrometry, 2nd Edition*, Sechi, S., Ed. Humana Press Inc: Totowa, 2016; Vol. 1410, pp 169-194.

29. Greer, T.; Hao, L.; Nechyporenko, A.; Lee, S.; Vezina, C. M.; Ricke, W. A.; Marker, P. C.; Bjorling, D. E.; Bushman, W.; Li, L. J., *Plos One* **2015,** *10* (8), 20.

30. Hao, L.; Johnson, J.; Lietz, C. B.; Buchberger, A.; Frost, D.; Kao, W. J.; Li, L. J., *Analytical Chemistry* **2017,** *89* (2), 1138-1146.

31. Hao, L.; Zhong, X. F.; Greer, T.; Ye, H.; Li, L. J., *Analyst* **2015,** *140* (2), 467-475.

32. DeLaney, K.; Buchberger, A.; Li, L., *Methods Mol Biol* **2018,** *1719*, 247-269.

33. OuYang, C.; Chen, B.; Li, L., *Journal of the American Society for Mass Spectrometry* **2015,** *26* (12), 1992-2001.

34. Shariatgorji, M.; Nilsson, A.; Kallback, P.; Karlsson, O.; Zhang, X.; Svenningsson, P.; Andren, P. E., *Journal of the American Society for Mass Spectrometry* **2015,** *26* (6), 934-939.

35. Liu, X.; Hummon, A. B., *Scientific Reports* **2016,** *6*, 10.

36. Shimma, S.; Kumada, H. O.; Taniguchi, H.; Konno, A.; Yao, I.; Furuta, K.; Matsuda, T.; Ito, S., *Analytical and Bioanalytical Chemistry* **2016,** *408* (27), 7607-7615.

37. Toue, S.; Sugiura, Y.; Kubo, A.; Ohmura, M.; Karakawa, S.; Mizukoshi, T.; Yoneda, J.; Miyano, H.; Noguchi, Y.; Kobayashi, T.; Kabe, Y.; Suematsu, M., *Proteomics* **2014,** *14* (7-8), 810-819.

38. Manier, M. L.; Spraggins, J. M.; Reyzer, M. L.; Norris, J. L.; Caprioli, R. M., *Journal of Mass Spectrometry* **2014,** *49* (8), 665-673.

39. Franck, J.; El Ayed, M.; Wisztorski, M.; Salzet, M.; Fournier, I., On Tissue Protein Identification Improvement by N-Terminal Peptide Derivatization. In *Mass Spectrometry Imaging: Principles and Protocols*, Rubakhin, S. S.; Sweedler, J. V., Eds. Humana Press Inc: Totowa, 2010; Vol. 656, pp 323-338.

40. Cobice, D. F.; Mackay, C. L.; Goodwin, R. J. A.; McBride, A.; Langridge-Smith, P. R.; Webster, S. P.; Walker, B. R.; Andrew, R., *Analytical Chemistry* **2013,** *85* (23), 11576-11584.

41. Chacon, A.; Zagol-Ikapitte, I.; Amarnath, V.; Reyzer, M. L.; Oates, J. A.; Caprioli, R. M.; Boutaud, O., *Journal of Mass Spectrometry* **2011,** *46* (8), 840-846.

42. Muller, M. J.; Bruns, H.; Volmer, D. A., *Analytical and Bioanalytical Chemistry* **2017,** *409* (10), 2705-2714.

43. Qi, B. L.; Liu, P.; Wang, Q. Y.; Cai, W. J.; Yuan, B. F.; Feng, Y. Q., *Trac-Trends in Analytical Chemistry* **2014,** *59*, 121-132.

44. Nishikaze, T.; Okumura, H.; Jinmei, H.; Amano, J., *International Journal of Mass Spectrometry* **2013,** *333*, 8-14.

45. Tanaka, M.; Hong, S. M.; Akiyama, S.; Hu, Q. Q.; Matsui, T., *Molecular Nutrition & Food Research* **2015,** *59* (8), 1541-1549.

46. Fu, Q.; Li, L. J., *Analytical Chemistry* **2005,** *77* (23), 7783-7795.

Figures

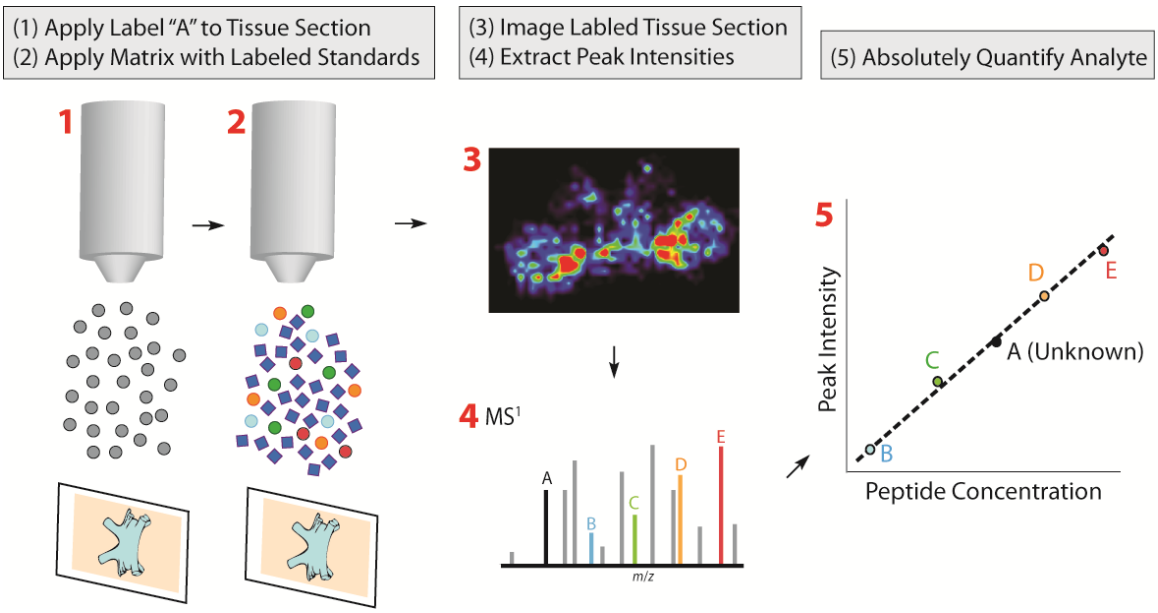

Figure 1. Generic workflow for MS imaging *in situ* labeling for absolute quantitation. After applying the tissue section with the label of interest (*e.g.*, iDiLeu d0 or DM D0),[20, 21, 27] various concentrations of a standard will be labeled with the other four isotopically different tags and mixed into the matrix solution, which will be applied at a known spatial density. The tissue section will then be imaged by a MALDI-MS instrument. The labeled on-tissue sample and standards' intensities will then be extracted from the spectra. A calibration curve will be built from the standards, and the on-tissue concentration of the neuropeptide of interest will be determined.

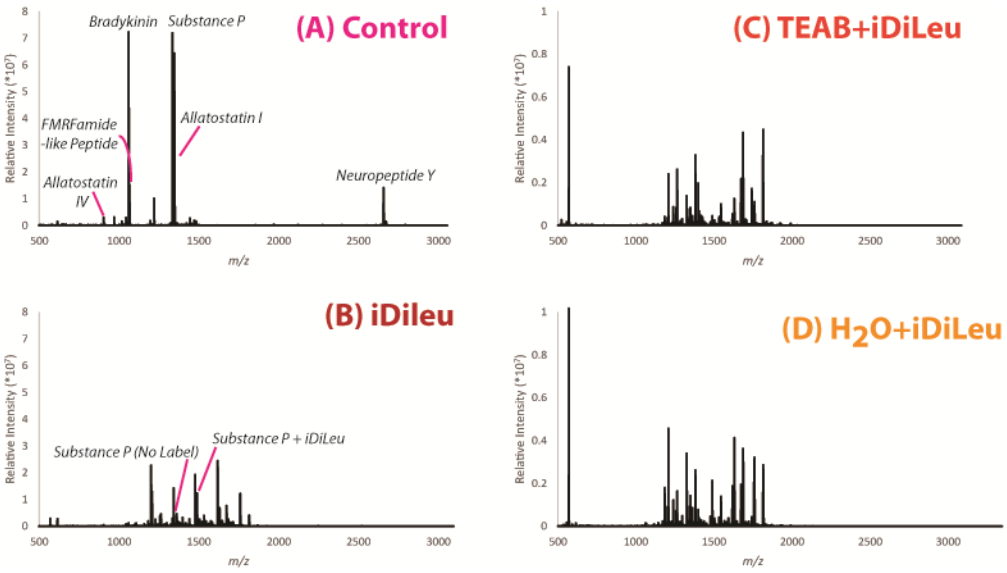

Figure 2. Mass spectra of neuropeptide standards after spot labeling with iDiLeu d0 and possible hydration agents. (a) Unlabeled, control neuropeptide standard mixture. Six different standards were added, which are indicated in the spectrum. (b) Neuropeptide standard mixture with the addition of just iDiLeu d0 after spot was allowed to dry. An example of a partially labeled peptide is highlighted. (c) Neuropeptide standard mixture after the dried spot was rehydrated with 0.05M TEAB followed by addition of iDiLeu d0. (d) Neuropeptide standard mixture after the dried spot was rehydrated with pH=8 H_2O (adjusted with NaOH) followed by addition of iDiLeu d0. In (b)-(d), the peaks range from partially labeled peptides to interfering ions that come from either the labeling reagents or hydration buffer. The labeling efficiency of conditions (c)-(d) are shown in **Table S1**.

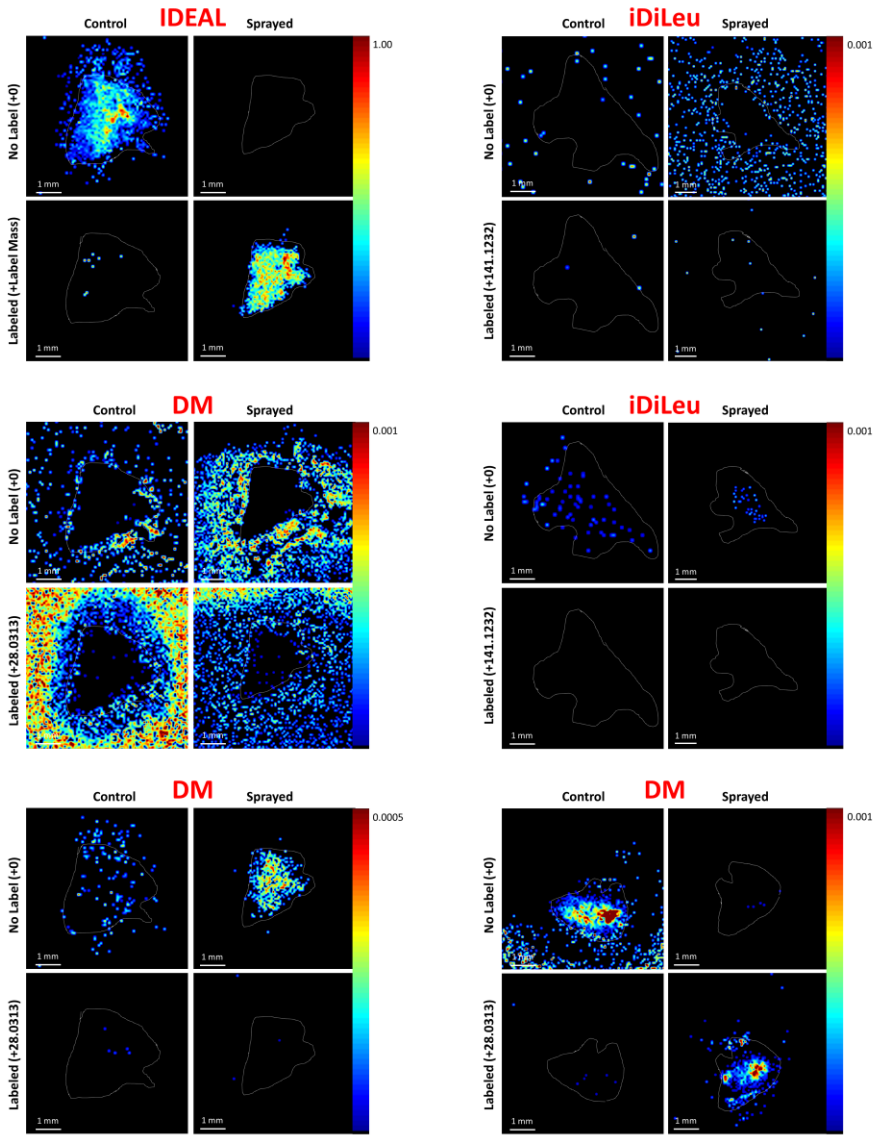

Figure 3. Example images of *in situ* on-tissue labeling neuropeptides in the crustacean brain using both iDiLeu d0 and DM D0. The control and sprayed sections are serial sections from the same crustacean brain. The white line represented a 1 mm scale bar. In each group, we see 4 panels: (1) left upper corner, the unlabeled neuropeptide *m/z* in a control brain; (2) left lower corner, the labeled neuropeptide *m/z* in a control brain; (3) right upper corner, the unlabeled neuropeptide *m/z* in a iDiLeu or DM sprayed brain; (4) right lower corner, the labeled neuropeptide *m/z* in a iDiLeu or DM sprayed brain. (a) The ideal example of 100% labeling. No

signal of the labeled m/z should be seen in the control brain, while the unlabeled neuropeptide *m/z* should be present. After being sprayed with either iDiLeu or DM labels, the neuropeptide should be labeled, meaning no signal should be see in the sprayed, unlabeled *m/z* panel while the signal should be present in the sprayed, labeled *m/z* section. No diffusion should be noticeable. (b)-(c) Examples of neuropeptides that the application of iDiLeu d0 and DM D0, respectively show an increase in background noise. (d)-(e) Examples of neuropeptides with no labeling after application of iDiLeu d0 and DM D0, respectively, was observed. (f) An example of 100% labeling of a neuropeptide after applying DM D0. Identifications: (b) Theoretical DPSFLEFamide, *m/z* 853.409. (c) Theoretical DFSAWAamide, *m/z* 695.315. (d) Theoretical DLPKVDTALK, *m/z* 1099.636. (e) Theoretical KPKTEEK, *m/z* 858.541. (f) Theoretical HL/I/GSL/IYRamide, *m/z* 844.479.

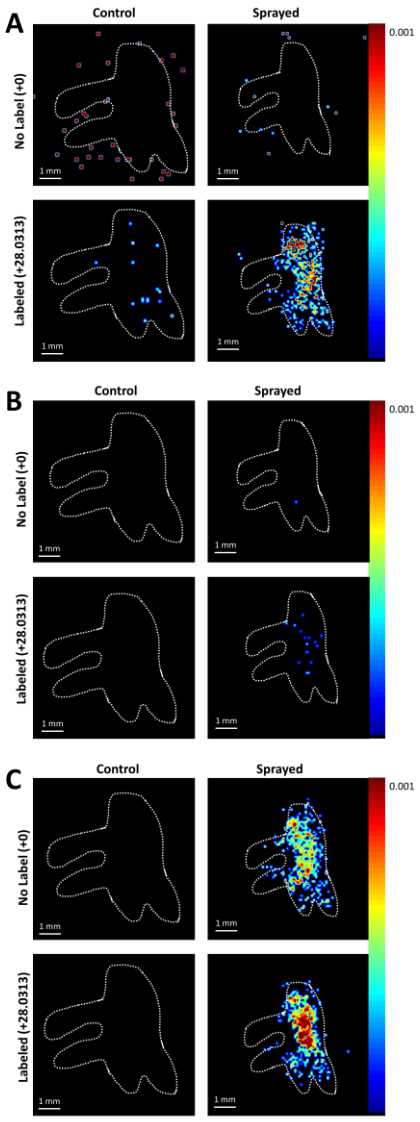

Figure 4. Example images of *in situ* on-tissue labeling of neuropeptides in the crustacean brain using DM D0. The control and sprayed sections are serial sections from the same crustacean brain. The white line represented a 1 mm scale bar. In each group, we see 4 panels: (1) left upper corner, the unlabeled neuropeptide *m/z* in a control brain; (2) left lower corner, the labeled neuropeptide *m/z* in a control brain; (3) right upper corner, the unlabeled neuropeptide *m/z* in a DM sprayed brain; (4) right lower corner, the labeled neuropeptide *m/z* in a DM sprayed brain. All of these images contain unusual cases, as the control tissue contains no signal, but the

sprayed tissue contains signal at the unlabeled *m/z* and/or labeled *m/z*. (a) Theoretical GGSLYSFGLamide, *m/z* 899.462. (b) Theoretical pQRNFLRFamide, *m/z* 960.532. (c) Theoretical GPKNFLRFamide, *m/z* 977.568.

Supplemental Information

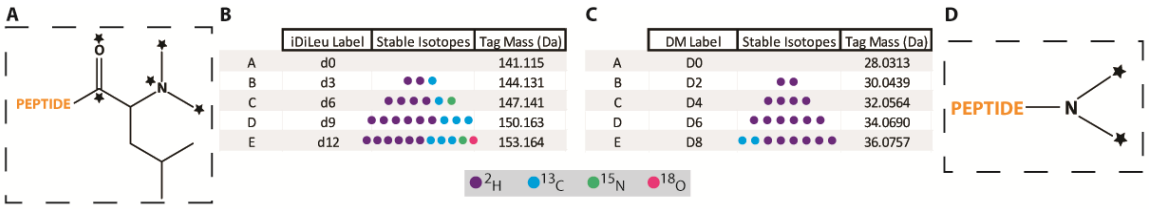

Figure S1. Isotopic combinations and structures for 5-plex iDiLeu (a-b) and the 5-plex DM (c-d). Stars indicate where isotopes are incorporated, and each circle denotes a different isotopic species that is utilized. The corresponding tag mass additions are also shown. iDiLeu has mass spacings of ~3 Da, while DM has mass spacings of ~2 Da. The labeling scheme for iDiLeu and DM are shown in **Figure S2** and **S3**, respectively. Appropriate starting reagents for each reaction can be found in the corresponding references. [21, 27]

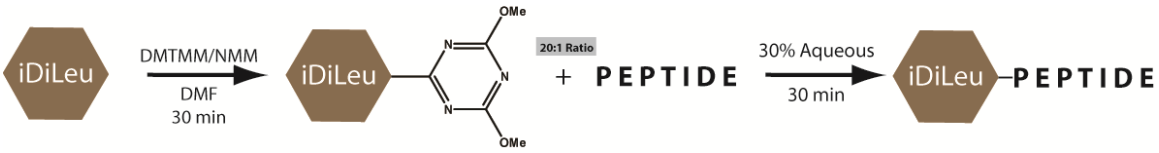

Figure S2. A schematic of the activation and labeling process of iDiLeu in solution. Since DMF is not compatible with spraying onto a tissue section, the solvent composition, activation time, label:peptide ratio, and labeling time needed to be re-optimized. After a new in-solution workflow is optimized, the label:peptide ratio, labeling time, labeling temperature, and H_2O/buffer integration must be considered at the tissue section application stage.

Figure S3. A schematic of the labeling process for DM. For on-tissue labeling, the concentration and ratio of formaldehyde and borane pyridine along with the incubation time and temperature are areas to optimize.

$$Label\ Density\ (\frac{mg}{mm^2})$$

$$= \frac{(Number\ of\ Passes)(Label\ Concentration(\frac{mg}{mL}))(Flow\ Rate\ \left(\frac{mL}{\min}\right))}{(Nozzle\ Velocity\ \left(\frac{mm}{min}\right))(Track\ Spacing\ (mm))}$$

Equation S1. TM Sprayer equation for calculating application density.

Table S1. Optimized conditions for spot-based labeling of iDiLeu d0 and the corresponding labeling efficiency.

Water/Buffer	Labeling Time (min)	Labeling Efficiency (%)
H_2O	30	**97.1**
	60	89.3
	90	84.3
	120	81.3
TEAB	30	67.7
	60	**93.5**
	90	84.2
	120	84.8

Table S2. All conditions attempted for iDiLeu on-tissue application along with the calculated labeling efficiency. The 50:50 MeOH:H_2O incubation condition was a saturated 50:50 MeOH:H_2O chamber placed in a hydration chamber (*i.e.*, 37 °C H_2O bath).

	1	2	3	4
Labeling Ratio	10:1	10:1	10:1	10:1
Application Solvent	Acetonitrile	Acetonitrile	Acetonitrile	Acetonitrile w/ TEAB
Incubation Time	2 Hours	24 Hours	1.5 Hours	1.5 Hours
Incubation Conditions	Room Temp	Room Temp	50:50 MeOH:H_2O	50:50 MeOH:H_2O
%Labeling	**16.4%**	7.4%	11.2%	8.3%

Table S3. Some conditions (1-7) attempted for DM on-tissue application along with the calculated labeling efficiency. Conditions 1 and 2 vary by their TM application method, with Condition 1 being a "wet" application and Condition 2 being a "dry" application. The hydration chamber was a H_2O bath set at 37°C. The 50:50 MeOH:H_2O incubation condition was a saturated 50:50 MeOH:H_2O chamber placed in a hydration chamber (*i.e.*, 37 °C H_2O bath).

	1	2	3	4	5	6	7
Amount Applied	1% CH_2O	1% CH_2O	4% CH_2O	1% CH_2O	1% CH_2O	1% CH_2O	1% CH_2O
Incubation Time	1 Hour	1 Hour	4 Hours	4 Hours	4 Hour	1 Hour	1 Hour
Incubation Conditions	Hydration Chamber	Hydration Chamber	Hydration Chamber	Hydration Chamber	Room Temp	Room Temp	50:50 MeOH:H_2O
%Labeling	34.5%	**46.2%**	41.3%	33.4%	36.2%	39.5%	42.1%
	**WET	**DRY					

Table S4. Some conditions (8-12) attempted for DM on-tissue application along with the calculated labeling efficiency The 50:50 MeOH:H_2O incubation condition was a saturated 50:50 MeOH:H_2O chamber placed in a hydration chamber (*i.e.*, 37 °C H_2O bath). The 50:50 MeOH:H_2O^+ incubation condition was a saturated 50:50 MeOH:H_2O chamber placed in a warmed (37 °C) chamber. V = vacuum chamber dried; DB = desiccator box dried; WASHED = washed in 50:50 EtOH:H_2O for 10 seconds prior to being labeled.

	8	9	10	11	12
Amount Applied	1% CH_2O	1% CH_2O	1% CH_2O	1% CH_2O	1% CH_2O
Incubation Time	0.5 Hour	1 Hour	1 Hour	1 Hour	1 Hour
Incubation Conditions	50:50 MeOH:H_2O	50:50 MeOH:H_2O	50:50 MeOH:H_2O^+	50:50 MeOH:H_2O^+	50:50 MeOH:H_2O^+
%Labeling	52.4%	34.0%	41.0%	43.2%	47.9%
			**V	**DB	WASHED

Sample iDiLeu Experimental Set Up

Purpose: *(Fill in depending on purpose of experiment)*

Aliquot 20 mg aliquot (dry down)

Make up DMTMM/NMM activation solution(s) in dry solvent (0.7x DMTMM/NMM to DiLeuAA-OH)

- 31 mg DMTMM BF_4 dissolved in 990 µL of dry ACN w/ 10.36 µL NMM*
- DO IN 1.5 mL tube (will transfer to larger tube later)

Triazine ester activation – to the 20 mg tube of DiLeuAA-OH

- Add 1000 µL of activation solution; sonicate if necessary%
- Vortex for 45 min at RT
- Spin down particulate (30s) if any
- Yields 14 mg (14000 µg) activated DiLeuAA-Trz label

Labeling On-Tissue with DiLeuAA-Trz

- Dilute activated DiLeu to 2.8 mg/mL (5 mL Total) (Add 1500 µL 0.05M TEAB and 2500 µL ACN)
- Wait for 2.5 min to allow sample to get through plumbing (Detached Loop)

  Apply using following TM Sprayer method:

  - 0.2 mL/min flow rate
  - 800 mm/min velocity
  - 12 passes
  - 3 mm track spacing (Final Density: 0.0028 -> Goal: 0.0026) (10:1 ratio)
- Incubate in 50:50% MeOH:H_2O Saturated Chamber for 90 min

Spray with DHB (40 mg/mL) to run on MALDI-Orbitrap

NOTE: Make sure to run a non-labeled brain as a control.

*NOTE: Can dissolve in half this volume, but one would then take half the amount added to activation solution. %NOTE: Add in 50 µL of this solution for every 1 mg tube activated.

Sample DM Experimental Set Up

Purpose: *(Fill in depending on purpose of experiment)*

Make the following solutions:

- 1% CH_2O (1.5 mL) -> 40.5 microliters
- 0.03 M $NaBH_3CN$ (1.5 mL) - > 2.83 mg

Labeling On-Tissue by Dimethylation

- Wait for 10 min to allow sample to get through plumbing (Detached Loop)

Mix 1 mL of each of the solutions above and apply using following TM Sprayer method:

  - 0.05 mL/min flow rate
  - 1250 mm/min velocity
  - 24 passes**

- Incubate 2 sections each in:
  - For 1 hour in cell culture oven (37 °C)

Spray with DHB (40 mg/mL) to run on MALDI-Orbitrap

NOTE: Make sure to run a non-labeled brain as a control.

**This will depend on how long it takes to spray all of the solution. We want to apply all 2 mL of this solution mixture. Can stop in the middle of spraying.

Chapter 8

Development of Dimethyl Pyrimidinyl Ornithines (DiPyrO) as Mass Defect-Based Tags for Multiplex Quantitative Proteomics

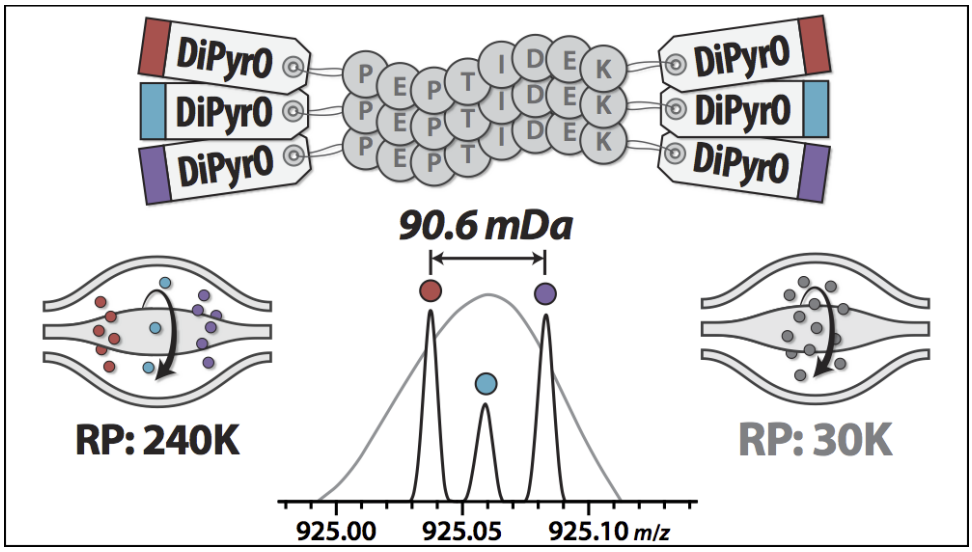

Modified from:

Dustin Frost, **Amanda R. Buchberger**, Lingjun Li. "Development of Dimethyl Pyrimidinyl Ornithines (DiPyrO) as Mass Defect-Based Tags for Quantitative Proteomics." Analytical Chemistry, 2017, 89(20): 10798-10805.

Key Words: Quantitation, Isotopic Labeling, Mass Defect, Proteomics, Mass Spectrometry

Abstract

We have developed a novel amine-reactive mass defect-based chemical tag, dimethyl pyrimidinyl ornithine (DiPyrO), that is compact in size, is suitable for various biological samples, and enables highly multiplexed quantification of peptides at the MS1 level without increasing mass spectral complexity using mass spectrometry (MS). The DiPyrO tag structure incorporates heavy isotopes in a variety of configurations to impart as much as 45.3 milliDalton (mDa) or as little as 5.8 mDa per tag between labeled peptides. Notably, peptides containing lysine are labeled with two tags, doubling the imparted mass defect to up to 90.6 mDa for the duplex tags and effectively reducing the resolving power requirement compared to previously reported mass defect-based quantification approaches. This permits current and previous generation LTQ-Orbitrap platforms to perform confident quantitative analyses of two DiPyrO-labeled samples at 100K resolving power, while triplex and 6-plex quantification are possible at 240K and 480K resolving powers, respectively. In this work, we discuss the design and synthesis of the DiPyrO tag, characterize its effect on labeled proteome analysis by nanoLC-tandem MS, and demonstrate proof-of-principle applications of the duplex and triplex tags for quantitative proteomics using high-resolution MS acquisition on the Orbitrap Elite and Orbitrap Fusion Lumos.

Introduction

Stable-isotope labeling is a core technology for mass spectrometry (MS)-based quantitative proteomics that has seen rapid advances in recent years. Heavy carbon, hydrogen, nitrogen, and oxygen atoms are incorporated onto peptides either metabolically or chemically to impart mass differences that can be detected in mass spectra to differentiate the samples and

allow comparison of ion intensities for relative quantification.[1-12] Typically, a mass difference of 4 Daltons (Da) or greater is ideal in order to minimize overlap between isotopic clusters in MS1 spectra. As the number of quantitative channels increases, so does the spectral complexity, which consequently decreases sampling depth and proteomic coverage. Thus, mass difference approaches, such as stable isotope labeling by amino acids in cell culture (SILAC), dimethyl labeling, and mTRAQ, are typically limited to triplex comparisons, though increased plexing, under special considerations, can be attained with 5-plex SILAC, 5-plex dimethyl labeling, and our custom-designed 5-plex isotopic N,N-dimethyl leucine (iDiLeu). [2-4, 10, 12-15] High levels of multiplexing are possible with isobaric chemical labeling approaches, such as isobaric tags for relative and absolute quantitation (iTRAQ), tandem mass tag (TMT), and our own *N*,*N*-dimethyl leucine (DiLeu) isobaric tags, where labeled peptides are indistinguishable in the MS1 precursor ion scan, in contrast to mass difference, and quantitative information is revealed through reporter ions produced during tandem MS (MS/MS) analysis.[8, 9, 16-20] However, isobaric labeling suffers from ratio distortion due to ubiquitous co-isolation of interfering precursors in complex samples, necessitating MS3-based approaches for accurate reporter ion quantification that reduce both instrument duty cycle and sensitivity with the consequence of fewer identifications and quantified peptides.[21-23] The Orbitrap Fusion tribrid mass spectrometer is equipped with synchronous precursor selection of multiple MS/MS fragment ions for HCD MS3 analysis to significantly increase sensitivity, though proteomic depth is still hindered by the approach.[24, 25]

High-resolution MS platforms have enabled increased multiplexing capacities of the aforementioned strategies through the use of small mDa mass defects. The isobaric 6-plex TMT reagents were increased to 8-plex by exploiting subtle relative mass differences between $^{12}C/^{13}C$ and $^{14}N/^{15}N$ isotopes—by substituting a ^{15}N in place of a ^{14}N atom and a ^{13}C in place of a ^{12}C

atom. The resulting reporter isotopologues differ in mass by 6.3 mDa and can be distinguished at an MSn resolving power (RP) of 30K (at mass-to-charge ratio (*m/z*) 400).[26, 27] The TMT reagents are now offered as a 10-plex set with four mass defect-based isotopologues. Similarly, we were able to triple the multiplexing capacity of our custom isobaric DiLeu reagents from 4-plex to 12-plex with the addition of eight mass defect-based isotopologues.[20] Pseudo-isobaric dimethyl labeling (pIDL) takes advantage of mDa mass differences between isotopes of carbon and hydrogen and high-resolution MS/MS for quantification.[28, 29] Neutron-encoding, or NeuCode, is a term coined by Coon and coworkers for mass defect-based stable isotope labeling for quantification at the MS1 level.[30]

NeuCode SILAC employs isotopologues of lysine, each incorporating up to eight heavy isotopes (^{13}C, ^{2}H, ^{15}N) in unique configurations, to impart mDa mass defect differences between samples via metabolic labeling.[30, 31] Extracted proteins are digested with Lys-C and subjected to MS analysis, where these mass defect signatures, ranging from as little as 5.8 mDa to as much as 36 mDa, are concealed in the MS1 precursor scan at low to moderate resolving powers but are revealed at high resolving power (>200K) to permit quantitative comparison of the differentially labeled peptides. Because the mass difference between multiplexed labeled peptides is so small, all are isolated, fragmented, and analyzed during the same MS/MS scan event, and the resulting spectra are no different from an unlabeled sample at typical resolving powers. Thus, the strategy permits multiplexing without the increased spectral complexity that accompanies traditional SILAC. Since quantification is done at the MS1 level, it does not require MS/MS for quantification, and by extension, it does not suffer from poor quantitative accuracy due to precursor co-isolation like isobaric labeling does. The multiplexing ability of NeuCode scales with MS1 resolution—duplex quantification using 36 mDa lysine isotopologues requires a

resolving power of 240K (at *m/z* 400) for quantification of >95% of a sample's proteome, while triplex and 4-plex quantification using 18 mDa and 12 mDa lysine isotopologues requires resolving powers of 480K and 960K, respectively.[31] These high resolutions require the most sophisticated FT-ICR instruments or Orbitrap platforms employing ultra-high field detectors, and as such, the technology is not yet widely accessible for a majority of researchers. NeuCode metabolic labeling has thus far been demonstrated in cell culture and in mouse tissues.[30-35]

Mass defect-based chemical labeling approaches reported by Coon and coworkers under the NeuCode moniker include duplex quantification via carbamylation and methylamination as well as multiplex quantification via amine-reactive tags.[36-38] The amine-reactive NeuCode tags employ six heavy isotopes (^{13}C and ^{15}N) in differing configurations to create a 4-plex set of tags spanning 37.8 mDa, with each differing in mass by 12.6 mDa. However, the tag consists of three amino acids—acetylated arginine, acetylated lysine, and glycine—and is consequently exceedingly large at 431 Da. Arginine inhibits backbone fragmentation due to charge sequestration, and the tag itself generates many sequence-uninformative product ions, both of which lead to reduced peptide identification rate.[39, 40] While useful for demonstrating the concept of a multiplexed mass defect-based tag for quantitative proteomics, the aforementioned limitations of these amine-reactive tags diminishes their potential for conventional use. A multiplex amine-reactive mass defect-based tag that is small in size and does not undermine identification of labeled peptides is necessary to make the approach a viable one.

We recently demonstrated that our DiLeu isobaric tag can be employed for mass defect-based duplex quantification of peptides and metabolites on an Orbitrap platform, circumventing ratio distortion caused by co-isolation while facilitating chromatographic separation of polar metabolites and improving ionization efficiency.[41] We realized, however, that a purpose-built tag

could make more efficient use of heavy isotopes to achieve a greater maximum mDa mass difference and offer greater multiplexing.

Herein, we describe the design and application of a novel amine-reactive, multiplex mass defect-based tag, DiPyrO, that is not only compact in size but also enhances fragmentation of labeled peptides. The multiplex DiPyrO tags are synthesized in-house in just a few steps using commercially available starting materials. The structure of the tag incorporates six heavy isotopes (^{13}C, ^{2}H, ^{15}N, ^{18}O) in various configurations to impart a mass defect of 45.3 mDa between the lightest and heaviest tag to labeled peptides, and up to 8-plex quantification is possible using isotopologues that differ in mass by a minimum of 5.8 mDa per tag. To demonstrate the viability of the DiPyrO tags, we label yeast protein extract digest samples with duplex and triplex isotopologues and perform proof-of-principle nanoLC-MS quantification experiments on the Orbitrap Elite and Orbitrap Fusion Lumos.

Materials and Methods

Chemicals

Heavy isotopic reagents used for the synthesis of labels were purchased from Isotec (Miamisburg, OH). Yeast protein extract and MS-grade enzymes were purchased from Promega (Madison, WI). ACS grade and Optima LC/MS grade solvents were purchased from Fisher Scientific (Pittsburgh, PA). All other chemicals were purchased from Sigma-Aldrich (St. Louis, MO).

DiPyrO Synthesis

Synthesis of the DiPyrO isotopologues is accomplished using commercially available isotopic reagents. Starting with arginine or heavy isotopic arginine, ^{18}O atoms are introduced by

acid-catalyzed exchange in $H_2{}^{18}O$, if required. The primary amine is dimethylated via Pd/C-catalyzed reaction with formaldehyde or heavy isotopic formaldehyde under H_2 or $^2H_2$ atmosphere, allowing for pairwise incorporation of ^2H and ^{13}C atoms. The guanidinium group is converted to the 4,6-dimethyl pyrimidine by base-catalyzed derivatization with acetylacetone, and the carboxylic acid product is purified by flash column chromatography. Finally, the active DiPyrO triazine ester form is generated by reaction with 4-(4, 6-dimethoxy-1, 3, 5-triazin-2-yl)-4-methylmorpholinium tetra-fluoroborate (DMTMM) and N-methylmorpholine (NMM) in dry DMF.

Yeast Protein Extract Digestion

S. cerevisiae protein extracts were digested by trypsin/Lys C mix or rLys C according to the manufacturer's protocols and desalted using SepPak C18 SPE cartridges (Waters, Milford, MA). Digested peptides were divided into equal aliquots in replicate, dried in vacuo, and dissolved in 60:40 acetonitrile (ACN):0.5M triethylammonium bicarbonate (TEAB) pH 8.5 prior to labeling.

Protein Digest Labeling

DiPyrO labeling was performed by addition of activated label in dry DMF at a label to protein digest ratio of 50:1 (weight (w):w) and incubation with vortexing at ambient temperature for 1 hour. The labeling reaction was quenched by addition of hydroxylamine to a concentration of 0.25%. Labeled peptide samples were combined in known ratios (1:1, 5:1, 10:1, 2:1:2), fractionated by SCX chromatography using SCX SpinTips (Protea Biosciences), and desalted with Omix C18 pipette tips (Agilent Technologies).

NanoLC-MS/MS

Samples were analyzed by nanoLC-MS/MS using either a Waters nanoAcquity UPLC (Milford, MA) coupled to a Thermo Scientific Orbitrap Elite mass spectrometer (San Jose, CA) or a Dionex Ultimate 3000 UPLC coupled to a Thermo Scientific Orbitrap Fusion Lumos mass spectrometer. Labeled peptides were dried in vacuo and dissolved in 3% acetonitrile (CAN), 0.1% formic acid (FA) in water. Samples were loaded onto a 75 µm inner diameter microcapillary column fabricated with an integrated emitter tip and packed with 15 cm of BEH C18 particles (1.7 µm, 130Å, Waters). Mobile phase A was composed of water and 0.1% FA. Mobile phase B was composed of ACN and 0.1% FA. Separation was performed using a gradient elution of 5% to 35% mobile phase B over 120 min at a flow rate of 300 nL/min. On the Orbitrap Elite, FTMS survey scans of peptide precursors from 380-1600 m/z were performed in the Orbitrap mass analyzer at RP 120K or 240K (at 400 m/z) with an AGC target of 5 × 105 and maximum injection time (IT) of 150 ms. The top fifteen precursors were selected for rapid scan CID IT-MS/MS analysis in the LTQ with an isolation width of 2.0 Da, a normalized collision energy (NCE) of 30, an AGC target of 1 × 104, and an IT of 100 ms. Precursors were subject to dynamic exclusion for 20 s with a 10 ppm tolerance. On the Orbitrap Fusion Lumos, FTMS survey scans of peptide precursors from 350-1500 m/z were performed in the Orbitrap at RP 240K or 500K (at 200 m/z) with an AGC target of 1 × 105 and an IT of 100 ms. The top fifteen precursors were selected by quadrupole isolation for rapid scan HCD IT-MS/MS analysis in the LTQ with an isolation width of 0.7 Da, an NCE of 30, an AGC target of 1 × 104, and an IT of 35 ms. Precursors were subject to dynamic exclusion for 20 s with a ±0.05 m/z tolerance.

Data Analysis

Mass spectra were processed using Proteome Discoverer (PD; version 2.1, Thermo Scientific) to identify proteins and peptides. Raw files were searched against the UniProt

Saccharomyces cerevisiae complete database using Sequest HT. Searches were performed with a precursor mass tolerance of 10-25 ppm and a fragment mass tolerance of 0.6 Da. Static modifications consisted of carbamidomethylation of cysteine residues (+57.02146 Da) and either non-isotopic DiPyrO tags (+248.16372 Da) or the appropriate heavy isotopic DiPyrO tags (DPO0041 (+254.15610 Da), DPO2220 (+254.17705 Da), DPO0600 (+254.20138 Da) (four-digit subscript denotes number of incorporated ^{13}C, ^{2}H, ^{15}N, and ^{18}O atoms)) on peptide N-termini and lysine (K) residues. Dynamic modifications consisted of oxidation of methionine residues (+15.995 Da) and acetylation (+42.011 Da) of protein N-termini. Peptide spectral matches (PSMs) were validated based on q-values to 1% FDR using percolator. Quantification of peptides identified by PD was performed using PyQuant.[42] Raw files were converted to mzML format using ProteoWizard msconvert for PyQuant processing with the corresponding MSF files from PD. The label scheme specified duplex and triplex DiPyrO as tags on peptide N-termini and K residues, and quantification was performed with a precursor ppm of 5 or 10 (for triplex or duplex samples, respectively) using the sum of intensities of the first two isotopic peaks in the isotopic cluster. PyQuant script arguments can be found in the Supporting Information.

Results and Discussion

Rationale and Mass Defect Tag Design Considerations

The NeuCode SILAC proteomics studies by Coon and coworkers have demonstrated that mass defect-based isotopic labeling is a viable multiplexed quantitative approach that addresses the drawbacks of both mass difference and isobaric labeling quantification strategies, but there are limitations. First, the minimum resolving power of 240K (at 400 m/z) necessary for duplex

NeuCode SILAC quantification limits its use to researchers with modern Orbitrap platforms. Second, metabolic labeling with heavy isotopic amino acids is restricted to primarily cell culture, as metabolic labeling studies in mammalia (*e.g.,* SILAC mouse) can be cost-prohibitive and time consuming, with further complications of different incorporation rates for different tissues and incomplete incorporation.[43] For studies of most other animal models, notably human tissues and fluids, metabolic labeling is not an option. In contrast, a chemical labeling approach can conveniently be applied to various biological samples, regardless of origin, with high labeling efficiency. Additionally, a chemical tag need not be limited to a single amino acid structure and can be more easily customized to carry a higher density of heavy isotopes in perhaps a wider variety of configurations. The multiplex NeuCode amine-reactive labels reported by Hebert *et al.* demonstrate the potential of such an approach, but due to their complex synthesis, bulky tag size, and production of sequence-uninformative fragment ions and inhibition of backbone fragmentation during MS/MS analysis, they serve only as a proof-of-principle example.[38] We reasoned that an improved amine-reactive mass defect-based chemical tag design could address the deficiencies of previous implementations by offering broad sample compatibility and a more modest resolving power requirement to make the mass defect-based approach more widely accessible.

An ideal mass defect-based tag should afford a large maximum mDa mass difference, yet remain small in size for efficient peptide labeling, and be simple in design to minimize the number of fragments generated during MS/MS analysis. The structure should contain a high density of nitrogen atoms, to impart negative mass defects with ^{15}N, while also providing a straightforward and preferably inexpensive avenue for selective incorporation of ^{13}C, ^{2}H, and ^{18}O to impart positive mass defects and permit the creation of a variety of isotopologues. As a

starting point, we consider an amino acid to be a suitable candidate based on the wide availability of isotopic amino acids as well as the benefit of retaining native fragmentation pathways. Arginine lends itself as a candidate given its four nitrogen atoms, but its polarity, basicity, and hydrophilicity can alter chromatographic retention, increase charge state during ionization, and severely suppress peptide backbone cleavage during fragmentation if used to label peptides.[39, 40, 44] Instead, we consider a dimethyl pyrimidine derivative to attenuate these properties and potentially enhance chromatographic retention, improve electrospray ionization without significant charge augmentation, and enhance tandem mass fragmentation of labeled peptides, as reported previously.[40, 44-52] *N*,*N*-dimethylation of the primary amine allows us to tailor isotopologues both with a pair of ^{13}C isotopes and up to six ^{2}H isotopes to impart substantial positive mass defects, and ^{18}O exchange adds two neutrons at a single isotopic position but with a fairly modest positive mass defect. Combined with the availability of the necessary heavy isotopic starting materials, these synthetic steps enable us to make efficient use of six isotopic positions to create a light tag and a heavy tag that differ in mass by 45.3 mDa.

Given our criteria of a compact tag size, we note that ^{2}H isotopes are key to achieving a sufficient mass defect difference between the lightest and heaviest labels, so we employ them in favor of the alternative of coupling several amino acids to increase the number of ^{15}N isotopes that can be swapped for ^{13}C isotopes. Additionally, they afford the flexibility to more freely tune the mass differences between isotopologues, enabling the creation of several multiplex sets. ^{2}H atoms are often considered a cause for concern due to their effect on chromatographic retention during reversed-phase liquid chromatography (RPLC), but research has indicated that placing ^{2}H atoms around a polar amine, as we do here, decreases their interaction with RPLC stationary phase and minimizes retention time shifts.[53] Our experience with our DiLeu tags supports these

conclusions.[54] By deriving quantification from the entire integrated XIC peak areas for each channel, rather than from a single MS1 scan, slight chromatographic retention time shifts between channels differing in ^{2}H content are inconsequential to quantitative accuracy.[55]

The general structure of the DiPyrO labeling reagent is composed of an N_5(4,6-dimethyl-2-pyrimidinyl)-Nα,Nα-dimethylornithine mass defect tag and an amine-reactive triazine ester group for selective modification of peptide N-termini and lysine side chains (**Figure 1a**). A total of six isotopes are incorporated onto the dimethyl pyrimidinyl ornithine tag structure (notated DPO#^{13}C#^{2}H#^{15}N#^{18}O) in varying configurations (**Figure S1**) to yield unique mass defect-based isotopologues differing in mass by up to 45.28 mDa. Using only commercially available isotopic starting materials, we have formulated duplex, triplex, 4-plex, and 6-plex sets with respective minimum mass defects of 45.28 mDa, 20.95 mDa, 12.64 mDa, and 8.31 mDa between tags, respectively (**Figure 1b**). An 8-plex set with a mass defect of 5.84 mDa is also possible with a custom isotopic starting reagent. The DiPyrO tags are synthesized in-house at high purity and stored dry in the inactive carboxylic acid form until needed, at which point a brief reaction to the triazine ester form is performed immediately prior to a labeling. Peptides are labeled with >99% efficiency within 1 hour, and each incorporated DiPyrO tag adds a moderate mass of 254 Da to the labeled peptide.

Characterization of the DiPyrO Reagent.

In order to characterize the DiPyrO reagent and effect of the tag on peptide analysis, we synthesized a non-isotopic version and verified the structure and synthetic purity by direct infusion MS (**Figure S2**). This tag was used to first optimize activation and labeling reaction times and determine the appropriate label to peptide ratio for high labeling efficiency (Supporting Information). Upon achieving 99% labeling of tryptic and Lys C yeast peptide

samples (**Table S1** & **Figure S3**), normalized collision energy was optimized and labeled peptide fragmentation behavior was evaluated. NanoLC-MS/MS analyses were performed on the Orbitrap Elite, and raw data was processed using Proteome Discoverer and Sequest HT database search.

The optimal collision energy for DiPyrO-labeled peptides was determined by analyzing a labeled yeast tryptic digest using CID fragmentation with NCE values of 24, 27, 30, 33, 36, and 39. The resulting numbers of identified PSMs and median XCorr values were plotted as functions of NCE (**Figure S4**). We observed that an NCE value of 30 yields high numbers of high quality spectra. A similar experiment using HCD fragmentation also found an NCE value of 30 to be optimal.

A particularly attractive benefit of the amine-reactive DiPyrO tag is that peptides with lysine are labeled with two tags, doubling the measured mass difference (**Figure S5**) and reducing the resolving power required for quantification. A pair of formulas described by Coon and coworkers estimate the theoretical rate at which peptides can be successfully quantified at a given Orbitrap resolving power by comparing a peptide's full width at 10% maximum peak height (FWTM) to the m/z difference between labeled peptides.[31] Variables considered in these formulas include Orbitrap resolving power and its reference m/z, the peptide's measured m/z, the peptide's charge, the mass difference between labels, and the number of labels. A peptide is considered resolvable, and thus quantifiable, if its m/z difference is larger than its width at FWTM. Using libraries of ~6,700 unique DiPyrO-labeled yeast tryptic peptides and ~3,500 unique DiPyrO-labeled yeast Lys C peptides identified by data-dependent acquisition on the Orbitrap Elite, we calculated the theoretical resolving powers (at *m/z* 400) necessary to resolve the multiplets of the various multiplex sets of DiPyrO tags given the minimum mass difference

between channels per incorporated tag (**Figure 2**). For tryptic peptide samples, the duplex, triplex, and 4-plex DiPyrO tags can be used at resolving powers of 120K, 240K, and 480K to quantify ≥95% of peptides, and the 6-plex can be used at 480K to quantify 87% of peptides. Quantification using 8-plex DiPyrO would require a future Orbitrap platform or current FT-ICR platform with a resolving power approaching one million in order to quantify 97% of all tryptic peptides. However, if Lys C is used as the enzyme, all peptides will contain C-terminal lysine and will be labeled with two tags, permitting the 6-plex and 8-plex tags to be used at 480K to quantify 96% and 77% of peptides, respectively, which is currently achievable on the Orbitrap Elite with the developer's kit. Compared to the reported resolving powers required for NeuCode SILAC, DiPyrO tags permit greater multiplexing at each resolving power increment for both trypsin or Lys C peptide samples.[31] Notably, the duplex tags permit quantitative analysis at RP 100K, with ~90% of tryptic peptides resolved, putting their use into range of the LTQ Orbitrap and LTQ Orbitrap XL platforms and opening up the approach to a broader cross-section of researchers in the field.

To evaluate the effect of DiPyrO labeling on peptide identification, we compared nanoLC-MS/MS analyses of labeled and unlabeled yeast tryptic digest samples using HCD fragmentation. NCE values of 30 for the labeled sample and 35 for the unlabeled sample were specified while other acquisition parameters were equal. The peptide gas-phase charge state, peptide length, and XCorr value distributions across identified PSMs were plotted as histograms to compare between samples (**Figure 3**). We observe that DiPyrO labeling leads to moderate charge state enhancement—labeled peptides are more evenly distributed between 2+ and 3+ charge states at 42% and 47%, respectively, while unlabeled peptides are largely 2+ (77%), and 4+ charge state is likewise higher for labeled peptides (9%) than for unlabeled (2%). Labeling

also enhances detection and identification of short peptides with 6-8 amino acids (21.6% labeled compared to 12.5% unlabeled). Interestingly, labeling enhances the overall quality of MS/MS spectra, as the distribution of XCorr values spreads considerably further towards higher values—31% of PSMs have an XCorr of 3.0 or greater in the labeled sample compared to 11% in the unlabeled sample, while 14% of labeled PSMs have an XCorr of 4.0 or greater compared to 1% of unlabeled PSMs. This increase in identification confidence indicates that the DiPyrO tag enhances the fragmentation of peptides into sequence-informative product ions. An example HCD MS/MS spectrum of a DiPyrO-labeled yeast tryptic peptide yielding high coverage of b- and y-ions is shown in the Supporting Information (**Figure S6**).

Fragmentation of DiPyrO-labeled peptides yields characteristic fragment ions in the low mass region of HCD MS/MS spectra which are analogous to isobaric tag reporter ions (**Figure S7a**). The non-isotopic DiPyrO tag gives rise to an intense ion at m/z 176.12 and lower intensity ions at m/z 204.11, 221.18, and 249.17. A multiplex set will give rise to several ions in four clusters due to the different isotopic configurations of each tag (**Figure S7b**). While these ions could be used for MS/MS-level quantification in the same manner as isobaric tag reporter ions—particularly those at *m/z* 176.12, 178.11, and 179.11 for the triplex set—they will be subject to the same ratio distortion that arises due to precursor co-isolation. Because these ions exist within the mass range of peptide backbone fragment ions, there is potential for them to be considered during peptide sequence identification. If desired, Proteome Discoverer's 'Non-Fragment Filter' node may be used prior to database search to remove these ions using narrow mass width filters.

Multiplex DiPyrO Quantification

Following characterization of the non-isotopic DiPyrO reagent, we synthesized the triplex isotopologues, DiPyrO0041, DiPyrO2220, and DiPyrO0600, for evaluation. First, we

labeled yeast tryptic digests with the duplex pair (DiPyrO0041 and DiPyrO0600), combined the samples at a ratio of 1:1, and analyzed at MS1 resolving powers of 120K and 240K on the Orbitrap Elite. We inspected the resulting precursor scan spectra to confirm that RP 120K was sufficient for resolving the peptide doublets (**Figure S8**). We also acquired spectra using the dual RP 30K-240K MS1 scan sequence suggested for NeuCode SILAC, in which the 30K scan is used to dictate DDA based on its higher frequency of precursor charge state assignment compared to the high resolving power scan used for quantification.[30] Notably, the 90 mDa mass difference is partially resolved for many peptides in the 30K scan—for 2+ and 3+ charged peptides with two tags, light and heavy peaks are partially resolved at up to m/z ~850 and ~650, respectively (**Figure S9**). This is significant in that it presents two masses for MS/MS acquisition. In order to avoid redundant sampling of such peptides in successive duty cycles, the mass tolerance used for dynamic exclusion should be set to ±0.1 Da or ±0.05 m/z at minimum.

To evaluate quantitative performance, we prepared samples mixed at 1:1, 5:1, and 10:1 ratios (light:heavy; L:H) in duplicate and analyzed them at RP 120K. Raw data was processed with Proteome Discoverer for protein and peptide identification by Sequest HT (PSMs filtered to 1% FDR). Approximately 900 proteins were identified for the combined 1:1 samples, and approximately 1030 proteins were identified for each of the combined 5:1 and 10:1 samples. Unique peptide sequence identifications were comparable as well, yielding approximately 4070, 4370, and 4590 identifications from 15660, 15260, and 14480 PSMs for the 1:1, 5:1, and 10:1 samples, respectively. Identified spectra from the Proteome Discoverer MSF files were then processed with PyQuant for quantification, yielding quantitative ratios for 87%, 78%, and 60% of identified PSMs, corresponding to 94%, 78%, and 71% of proteins, for the 1:1, 5:1, and 10:1 samples, respectively. The resulting L:H median ratios of 0.91, 4.84, and 9.73 (SD = 1.59, 2.00,

and 2.33) for quantified PSMs agree well with the expected ratios, demonstrating reliable quantification across the dynamic range tested (**Figure 4a**). Next, we prepared triplex DiPyrO-labeled samples mixed at 2:1:2 (light:medium:heavy; L:M:H) ratios in duplicate and performed analyses on both the Elite and Fusion Lumos at RP 240K (at *m/z* 400) and 500K (at *m/z* 200, equivalent to ~350K at *m/z* 400), respectively. The Elite yielded 1075 protein identifications from 4600 unique peptide sequences, while the Fusion Lumos yielded nearly 1830 proteins from 7255 unique peptide sequences from the combined samples. Out of 17360 and 24240 identified PSMs on the Elite and Fusion Lumos, 89% and 76% were quantified across all three channels, corresponding to 92% and 87% of proteins, respectively. Quantitative performance of the DiPyrO tags was on par between platforms with L:M, H:M, and L:H median ratios of 2.20, 2.21, and 1.03 (SD = 2.11, 1.89, 1.57) on the Elite and 2.14, 2.07, and 1.05 (SD = 1.66, 1.72, 1.49) on the Fusion Lumos, showing good agreement with the expected ratios (**Figure 4b**).

The triplex DiPyrO-labeled sample was also acquired on the Elite using the dual RP 30K-240K MS1 scan sequence. A representative spectrum, shown in **Figure 5**, confirms that RP 240K was sufficient to resolve the multiplets for all three precursor charge states (4+, 3+, 2+ at m/z 471, 628, and 932, respectively) of a peptide labeled with two DiPyrO tags, ELQDIANPIMSK, that was confidently identified from MS/MS spectra of each charge state precursor.

Following evaluation of the duplex and triplex tags, we synthesized the remaining DiPyrO-OH isotopologues that comprise the 4-plex and 6-plex sets and verified their masses, alongside the triplex set, by direct infusion MS (**Figure S10**). Application of the 4-plex and 6-plex tags is planned for future research efforts.

The DiPyrO tags may be used in a hybrid mode that combines mass difference and mass defect to significantly increase multiplexing at a given resolving power. Isotopologues with two or ten heavy isotopes ('DiPyrO2' and 'DiPyrO10', respectively), which are offset in mass by -4 Da and +4 Da from the current 'DiPyrO6' tags, allow for the creation of additional multiplex sets of tags, which upon combined analysis would produce three isotopic clusters of mass defect multiplets in MS1 spectra. A set comprised of 2-plex DiPyrO2, 3-plex DiPyrO6, and 4-plex DiPyrO10 would permit 9-plex quantification at RP 240K, sufficient for resolving the ~18 mDa minimum mass difference between tags (**Figure S11**). This strategy has also been reported for making 7-plex NeuCode SILAC quantification possible at RP 480K with lysine isotopologues incorporating four, eight, and twelve isotopes. Another hybrid approach could combine triplex SILAC with triplex or 6-plex DiPyrO to achieve 9-plex quantification at RP 240K or 18-plex quantification at RP 480K.

Concluding Remarks

We have presented herein a novel chemical labeling technology, DiPyrO, for highly multiplexed mass defect-based MS1 quantification that aims to address the limitations of current implementations while also making the general approach more accessible through several noteworthy improvements. The reactivity of the compact chemical tags permits complete labeling of various biological samples containing amines, allowing quantification of a broad range of samples, regardless of their origin. Their structure enhances ionization and fragmentation of labeled peptides, leading to more confident sequence identification. The mass defect signatures encoded onto the tags using only six heavy isotopes permit various levels of multiplexing, from duplex to 8-plex, at resolving powers ranging from 100K to ≥1M using an

Orbitrap mass analyzer. The DiPyrO tags permit greater multiplexing than currently available high-resolution MS1-based quantification methods at lower resolving powers—owing to the small tag size and ability to impart up to a 90 mDa mass difference between samples with two tags on lysine-containing peptides—which now enables researchers with previous generation LTQ Orbitrap instruments to adopt the technique for quantitative proteomics, increasing the accessibility of the technology. We have demonstrated accurate and precise quantification using the duplex and triplex DiPyrO tags via proof-of-principle quantitative proteomics experiments on the Orbitrap Elite and Fusion Lumos. Future efforts will endeavor to demonstrate the utility of the 4-plex and 6-plex tags in addition to hybrid approaches that employ mass difference in concert to double or triple multiplexing. We consider the DiPyrO tags to be a valuable new addition to the quantitative proteomics toolkit, and we anticipate that their availability as a viable chemical tag for mass defect-based MS1-level quantification will encourage wider application of the approach.

Acknowledgements

The authors would like to thank Dr. Chris Mitchell for his guidance with the PyQuant software. This research was supported in part by National Institute of Health (NIH) grants R01DK071801, R21AG05537701, S10RR029531, NIH General Medical Sciences NRSA Fellowship 1F31GM119365, a Robert Draper Technology Innovation Fund grant with funding provided by the Wisconsin Alumni Research Foundation (WARF), and funding provided by the Office of the Vice Chancellor for Research and Graduate Education at UW–Madison. L.L. acknowledges an H.I. Romnes Faculty Research Fellowship and a Vilas Distinguished

Achievement Professorship with funding provided by WARF & UW–Madison School of Pharmacy.

References

1. Oda, Y.; Huang, K.; Cross, F. R.; Cowburn, D.; Chait, B. T., *Proceedings of the National Academy of Sciences of the United States of America* **1999,** *96* (12), 6591-6596.

2. Chen, X.; Smith, L. M.; Bradbury, E. M., *Anal Chem* **2000,** *72* (6), 1134-43.

3. Zhu, H. N.; Pan, S. Q.; Gu, S.; Bradbury, E. M.; Chen, X., *Rapid Communications in Mass Spectrometry* **2002,** *16* (22), 2115-2123.

4. Ong, S. E.; Blagoev, B.; Kratchmarova, I.; Kristensen, D. B.; Steen, H.; Pandey, A.; Mann, M., *Molecular & Cellular Proteomics* **2002,** *1* (5), 376-386.

5. Pan, S. Q.; Gu, S.; Bradbury, E. M.; Chen, X., *Analytical Chemistry* **2003,** *75* (6), 1316-1324.

6. Wu, C. C.; MacCoss, M. J.; Howell, K. E.; Matthews, D. E.; Yates, J. R., *Analytical Chemistry* **2004,** *76* (17), 4951-4959.

7. Gygi, S. P.; Rist, B.; Gerber, S. A.; Turecek, F.; Gelb, M. H.; Aebersold, R., *Nature Biotechnology* **1999,** *17* (10), 994-999.

8. Thompson, A.; Schafer, J.; Kuhn, K.; Kienle, S.; Schwarz, J.; Schmidt, G.; Neumann, T.; Johnstone, R.; Mohammed, A. K.; Hamon, C., *Anal Chem* **2003,** *75* (8), 1895-904.

9. Ross, P. L.; Huang, Y. L. N.; Marchese, J. N.; Williamson, B.; Parker, K.; Hattan, S.; Khainovski, N.; Pillai, S.; Dey, S.; Daniels, S.; Purkayastha, S.; Juhasz, P.; Martin, S.; Bartlet-Jones, M.; He, F.; Jacobson, A.; Pappin, D. J., *Molecular & Cellular Proteomics* **2004,** *3* (12), 1154-1169.

10. Hsu, J. L.; Huang, S. Y.; Chow, N. H.; Chen, S. H., *Anal Chem* **2003,** *75* (24), 6843-52.

11. Boersema, P. J.; Raijmakers, R.; Lemeer, S.; Mohammed, S.; Heck, A. J. R., *Nature Protocols* **2009,** *4* (4), 484-494.

12. DeSouza, L. V.; Taylor, A. M.; Li, W.; Minkoff, M. S.; Romaschin, A. D.; Colgan, T. J.; Siu, K. W. M., *Journal of Proteome Research* **2008,** *7* (8), 3525-3534.

13. Molina, H.; Yang, Y.; Ruch, T.; Kim, J. W.; Mortensen, P.; Otto, T.; Nalli, A.; Tang, Q. Q.; Lane, M. D.; Chaerkady, R.; Pandey, A., *Journal of Proteome Research* **2009,** *8* (1), 48-58.

14. Wu, Y.; Wang, F. J.; Liu, Z. Y.; Qin, H. Q.; Song, C. X.; Huang, J. F.; Bian, Y. Y.; Wei, X. L.; Dong, J.; Zou, H. F., *Chemical Communications* **2014,** *50* (14), 1708-1710.

15. Greer, T.; Li, L. J., Isotopic N,N-Dimethyl Leucine (iDiLeu) for Absolute Quantification of Peptides Using a Standard Curve Approach. In *Quantitative Proteomics by Mass Spectrometry, 2nd Edition*, Sechi, S., Ed. Humana Press Inc: Totowa, 2016; Vol. 1410, pp 195-206.

16. Choe, L.; D'Ascenzo, M.; Relkin, N. R.; Pappin, D.; Ross, P.; Williamson, B.; Guertin, S.; Pribil, P.; Lee, K. H., *Proteomics* **2007,** *7* (20), 3651-3660.

17. Dayon, L.; Hainard, A.; Licker, V.; Turck, N.; Kuhn, K.; Hochstrasser, D. F.; Burkhard, P. R.; Sanchez, J. C., *Anal Chem* **2008,** *80* (8), 2921-31.

18. Xiang, F.; Ye, H.; Chen, R. B.; Fu, Q.; Li, L. J., *Analytical Chemistry* **2010,** *82* (7), 2817-2825.

19. Frost, D. C.; Greer, T.; Xiang, F.; Liang, Z. D.; Li, L. J., *Rapid Communications in Mass Spectrometry* **2015,** *29* (12), 1115-1124.

20. Frost, D. C.; Greer, T.; Li, L., *Analytical chemistry* **2015,** *87* (3), 1646-54.

21. Ow, S. Y.; Salim, M.; Noirel, J.; Evans, C.; Rehman, I.; Wright, P. C., *Journal of Proteome Research* **2009,** *8* (11), 5347-5355.

22. Ting, L.; Rad, R.; Gygi, S. P.; Haas, W., *Nature Methods* **2011,** *8* (11), 937-940.

23. McAlister, G. C.; Nusinow, D. P.; Jedrychowski, M. P.; Wuhr, M.; Huttlin, E. L.; Erickson, B. K.; Rad, R.; Haas, W.; Gygi, S. P., *Analytical Chemistry* **2014,** *86* (14), 7150-7158.

24. Erickson, B. K.; Jedrychowski, M. P.; McAlister, G. C.; Everley, R. A.; Kunz, R.; Gygi, S. P., *Analytical Chemistry* **2015,** *87* (2), 1241-1249.

25. Williamson, J. C.; Edwards, A. V. G.; Verano-Braga, T.; Schwammle, V.; Kjeldsen, F.; Jensen, O. N.; Larsen, M. R., *Proteomics* **2016,** *16* (6), 907-914.

26. McAlister, G. C.; Huttlin, E. L.; Haas, W.; Ting, L.; Jedrychowski, M. P.; Rogers, J. C.; Kuhn, K.; Pike, I.; Grothe, R. A.; Blethrow, J. D.; Gygi, S. P., *Analytical Chemistry* **2012,** *84* (17), 7469-7478.

27. Werner, T.; Becher, I.; Sweetman, G.; Doce, C.; Savitski, M. M.; Bantscheff, M., *Analytical Chemistry* **2012,** *84* (16), 7188-7194.

28. Zhou, Y.; Shan, Y. C.; Wu, Q.; Zhang, S.; Zhang, L. H.; Zhang, Y. K., *Analytical Chemistry* **2013,** *85* (22), 10658-10663.

29. Zhang, S.; Chen, L. F.; Shan, Y. C.; Sui, Z. G.; Wu, Q.; Zhang, L. H.; Liang, Z.; Zhang, Y. K., *Analyst* **2016,** *141* (16), 4912-4918.

30. Hebert, A. S.; Merrill, A. E.; Bailey, D. J.; Still, A. J.; Westphall, M. S.; Strieter, E. R.; Pagliarini, D. J.; Coon, J. J., *Nature Methods* **2013,** *10* (4), 332-+.

31. Merrill, A. E.; Hebert, A. S.; MacGilvray, M. E.; Rose, C. M.; Bailey, D. J.; Bradley, J. C.; Wood, W. W.; El Masri, M.; Westphall, M. S.; Gasch, A. P.; Coon, J. J., *Molecular & Cellular Proteomics* **2014,** *13* (9), 2503-2512.

32. Rose, C. M.; Merrill, A. E.; Bailey, D. J.; Hebert, A. S.; Westphall, M. S.; Coon, J. J., *Analytical Chemistry* **2013,** *85* (10), 5129-5137.

33. Richards, A. L.; Vincent, C. E.; Guthals, A.; Rose, C. M.; Westphall, M. S.; Bandeira, N.; Coon, J. J., *Molecular & Cellular Proteomics* **2013,** *12* (12), 3812-3823.

34. Rhoads, T. W.; Rose, C. M.; Bailey, D. J.; Riley, N. M.; Molden, R. C.; Nestler, A. J.; Merrill, A. E.; Smith, L. M.; Hebert, A. S.; Westphall, M. S.; Pagliarini, D. J.; Garcia, B. A.; Coon, J. J., *Analytical Chemistry* **2014,** *86* (5), 2314-2319.

35. Baughman, J. M.; Rose, C. M.; Kolumam, G.; Webster, J. D.; Wilkerson, E. M.; Merrill, A. E.; Rhoads, T. W.; Noubade, R.; Katavolos, P.; Lesch, J.; Stapleton, D. S.; Rabaglia, M. E.; Schueler, K. L.; Asuncion, R.; Domeyer, M.; Zavala-Solorio, J.; Reich, M.; DeVoss, J.; Keller, M. P.; Attie, A. D.; Hebert, A. S.; Westphall, M. S.; Coon, J. J.; Kirkpatrick, D. S.; Dey, A., *Cell Reports* **2016,** *16* (2), 583-595.

36. Ulbrich, A.; Merrill, A. E.; Hebert, A. S.; Westphall, M. S.; Keller, M. P.; Attie, A. D.; Coon, J. J., *Journal of the American Society for Mass Spectrometry* **2014,** *25* (1), 6-9.

37. Ulbrich, A.; Bailey, D. J.; Westphall, M. S.; Coon, J. J., *Analytical Chemistry* **2014,** *86* (9), 4402-4408.

38. Hebert, A. S.; Merrill, A. E.; Stefely, J. A.; Bailey, D. J.; Wenger, C. D.; Westphall, M. S.; Pagliarini, D. J.; Coon, J. J., *Molecular & Cellular Proteomics* **2013,** *12* (11), 3360-3369.

39. Tang, X. J.; Thibault, P.; Boyd, R. K., *Analytical Chemistry* **1993,** *65* (20), 2824-2834.

40. Dikler, S.; Kelly, J. W.; Russell, D. H., *Journal of Mass Spectrometry* **1997,** *32* (12), 1337-1349.

41. Hao, L.; Johnson, J.; Lietz, C. B.; Buchberger, A.; Frost, D.; Kao, W. J.; Li, L. J., *Analytical Chemistry* **2017,** *89* (2), 1138-1146.

42. Mitchell, C. J.; Kim, M. S.; Na, C. H.; Pandey, A., *Molecular & Cellular Proteomics* **2016,** *15* (8), 2829-2838.

43. Kruger, M.; Moser, M.; Ussar, S.; Thievessen, I.; Luber, C. A.; Forner, F.; Schmidt, S.; Zanivan, S.; Fassler, R.; Mann, M., *Cell* **2008,** *134* (2), 353-364.

44. Sullivan, A. G.; Brancia, F. L.; Tyldesley, R.; Bateman, R.; Sidhu, K.; Hubbard, S. J.; Oliver, S. G.; Gaskell, S. J., *International Journal of Mass Spectrometry* **2001,** *210* (1-3), 665-676.

45. Morris, H. R.; Dickinson, R. J.; Williams, D. H., *Biochemical and Biophysical Research Communications* **1973,** *51* (1), 247-255.

46. Kuyama, H.; Sonomura, K.; Shima, K.; Nishimura, O.; Tsunasawa, S., *Rapid Communications in Mass Spectrometry* **2008,** *22* (13), 2063-2072.

47. Foettinger, A.; Leitner, A.; Lindner, W., *Journal of Mass Spectrometry* **2006,** *41* (5), 623-632.

48. Leitner, A.; Lindner, W., *Journal of Mass Spectrometry* **2003,** *38* (8), 891-899.

49. Leitner, A.; Lindner, W., *Analytica Chimica Acta* **2005,** *528* (2), 165-173.

50. Leitner, A.; Foettinger, A.; Lindner, W., *Journal of Mass Spectrometry* **2007,** *42* (7), 950-959.

51. Onofrejova, L.; Leitner, A.; Lindner, W., *Journal of Separation Science* **2008,** *31* (3), 499-506.

52. Dongre, A. R.; Jones, J. L.; Somogyi, A.; Wysocki, V. H., *Journal of the American Chemical Society* **1996,** *118* (35), 8365-8374.

53. Zhang, R.; Sioma, C. S.; Thompson, R. A.; Xiong, L.; Regnier, F. E., *Anal Chem* **2002,** *74* (15), 3662-9.

54. Greer, T.; Lietz, C. B.; Xiang, F.; Li, L. J., *Journal of the American Society for Mass Spectrometry* **2015,** *26* (1), 107-119.

55. Cox, J.; Mann, M., *Nature Biotechnology* **2008,** *26* (12), 1367-1372.

Figures

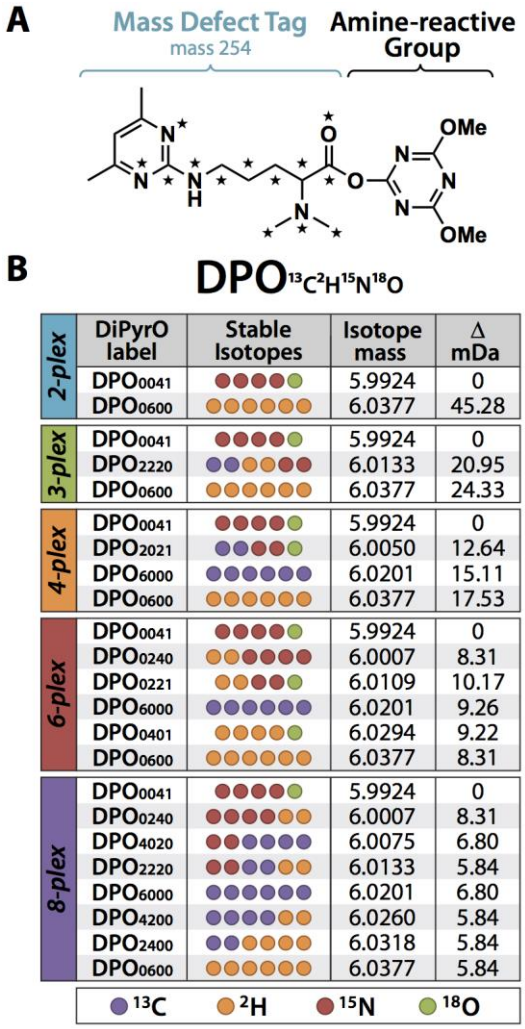

	DiPyrO label	Stable Isotopes	Isotope mass	Δ mDa
2-plex	DPO0041		5.9924	0
	DPO0600		6.0377	45.28
3-plex	DPO0041		5.9924	0
	DPO2220		6.0133	20.95
	DPO0600		6.0377	24.33
4-plex	DPO0041		5.9924	0
	DPO2021		6.0050	12.64
	DPO6000		6.0201	15.11
	DPO0600		6.0377	17.53
6-plex	DPO0041		5.9924	0
	DPO0240		6.0007	8.31
	DPO0221		6.0109	10.17
	DPO6000		6.0201	9.26
	DPO0401		6.0294	9.22
	DPO0600		6.0377	8.31
8-plex	DPO0041		5.9924	0
	DPO0240		6.0007	8.31
	DPO4020		6.0075	6.80
	DPO2220		6.0133	5.84
	DPO6000		6.0201	6.80
	DPO4200		6.0260	5.84
	DPO2400		6.0318	5.84
	DPO0600		6.0377	5.84

Figure 1. DiPyrO general structure and multiplex isotopologues. (a) The DiPyrO labeling reagent consists of a dimethyl pyrimidinyl ornithine mass defect tag and an amine-reactive triazine ester group. (b) A total of six heavy stable isotopes (^{13}C, ^{2}H, ^{15}N, ^{18}O) are incorporated onto the mass defect tag in differing configurations to create 2-plex, 3-plex, 4-plex, 6-plex, and 8-plex sets with minimum mass defects of 45.28 mDa, 20.95 mDa, 12.64 mDa, 8.31

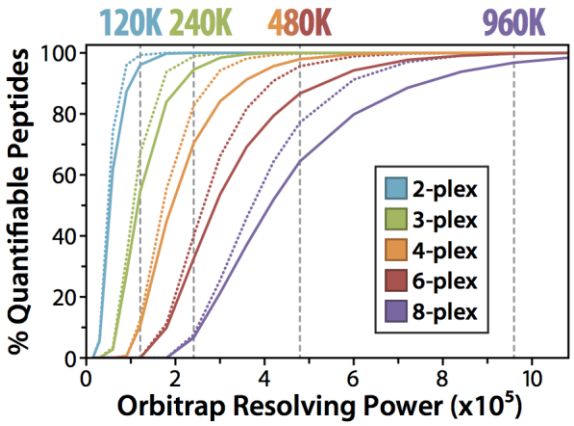

Figure 2. Orbitrap resolving power required to quantify DiPyrO-labeled peptides. Theoretical calculation predicting the percentages of DiPyrO-labeled tryptic peptides (solid lines) and Lys C peptides (dotted lines) that are resolved and quantifiable at full width at 10% maximum peak height for each multiplex set at Orbitrap resolving powers ranging from 15K to 1M.

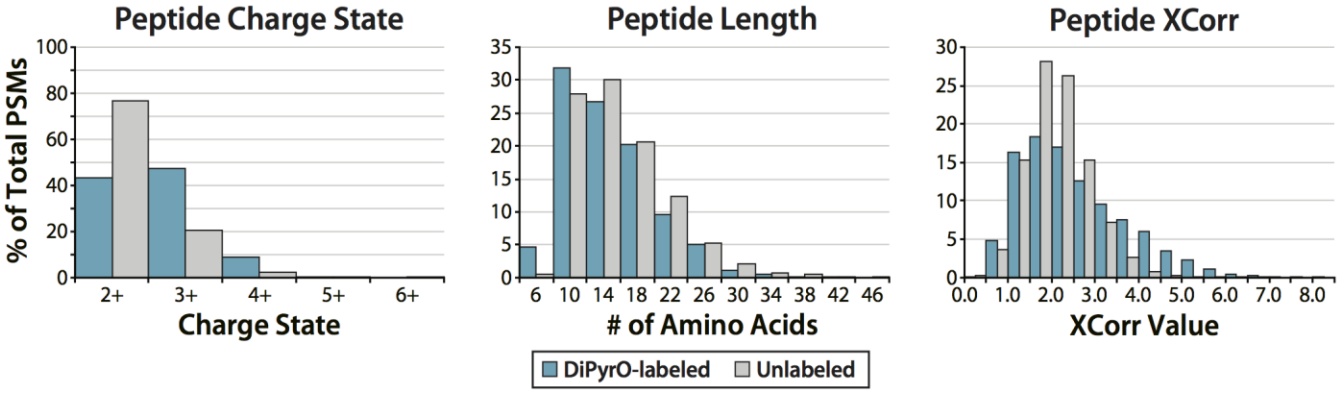

Figure 3. Effect of DiPyrO labeling on peptide identification. DiPyrO-labeled and unlabeled yeast tryptic digest samples were analyzed via nanoLC-MS/MS on the Orbitrap Elite using HCD fragmentation (NCE 30 and 35, respectively). The distribution of peptide charge state, peptide length, and peptide XCorr values of the PSMs from the labeled sample were plotted against those from the unlabeled sample.

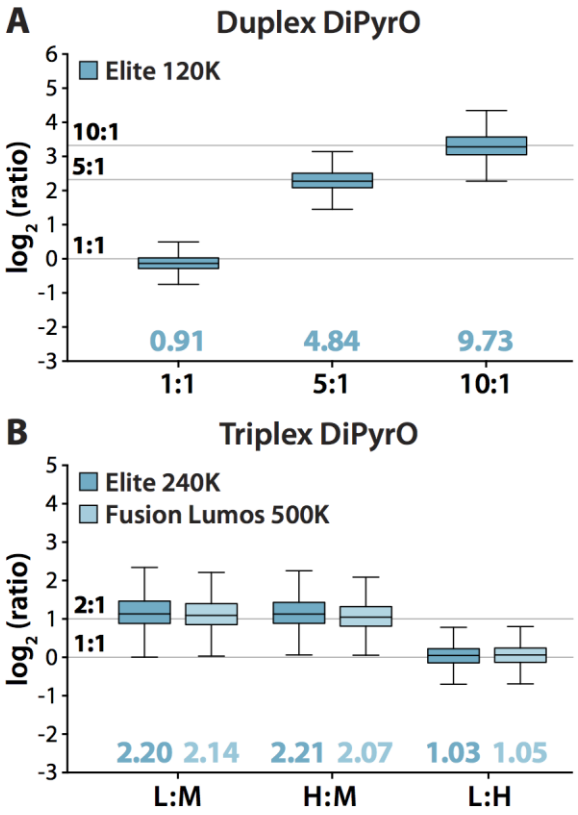

Figure 4. Quantitative performance. Yeast tryptic digest samples were labeled with duplex and triplex DiPyrO tags and analyzed on the Orbitrap Elite and Orbitrap Fusion Lumos. Measured quantitative ratios (box and whiskers) of quantified PSMs are shown for samples mixed at (a) 1:1, 5:1, and 10:1 ratios (Elite analysis, RP 120K) and (b) 2:1:2 ratios (Elite, RP 240K; Fusion Lumos, RP 500K). Box plots demarcate the median (line), the 25th and 75th percentile (interquartile range; box), and 1.5 times the interquartile range (whiskers).

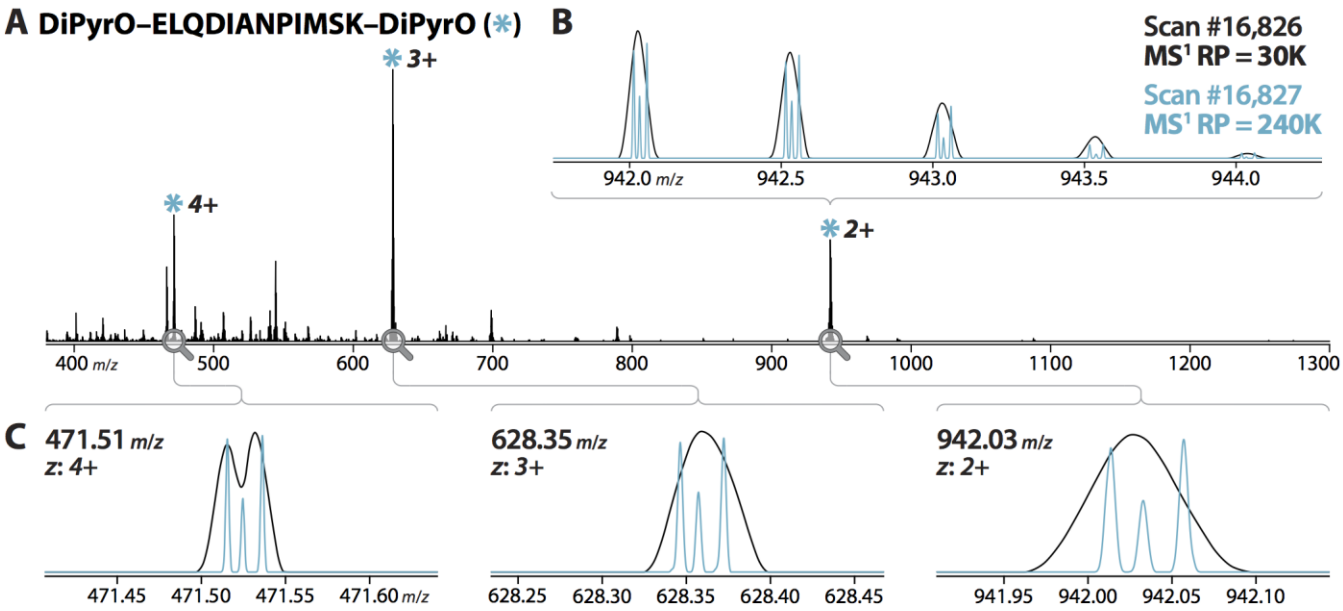

Figure 5. Resolving Triplex DiPyrO Tags for Peptide Quantification. (a) An MS1 survey scan of triplex DiPyrO-labeled yeast tryptic peptides, acquired on the Orbitrap Elite, is shown. Precursor ions of a peptide with charge states of 4+, 3+, and 2+, identified as DiPyrO–ELQDIANPIMSK–DiPyrO in associated MS/MS spectra, are marked (*). (b) MS1 acquisition at RP 240K (blue) reveals quantitative data that is concealed at RP 30K (black). (c) The triplex DiPyrO multiplet is sufficiently resolved at RP 240K (blue) for each charge state, permitting accurate quantification of the peptide.

Supplemental Information

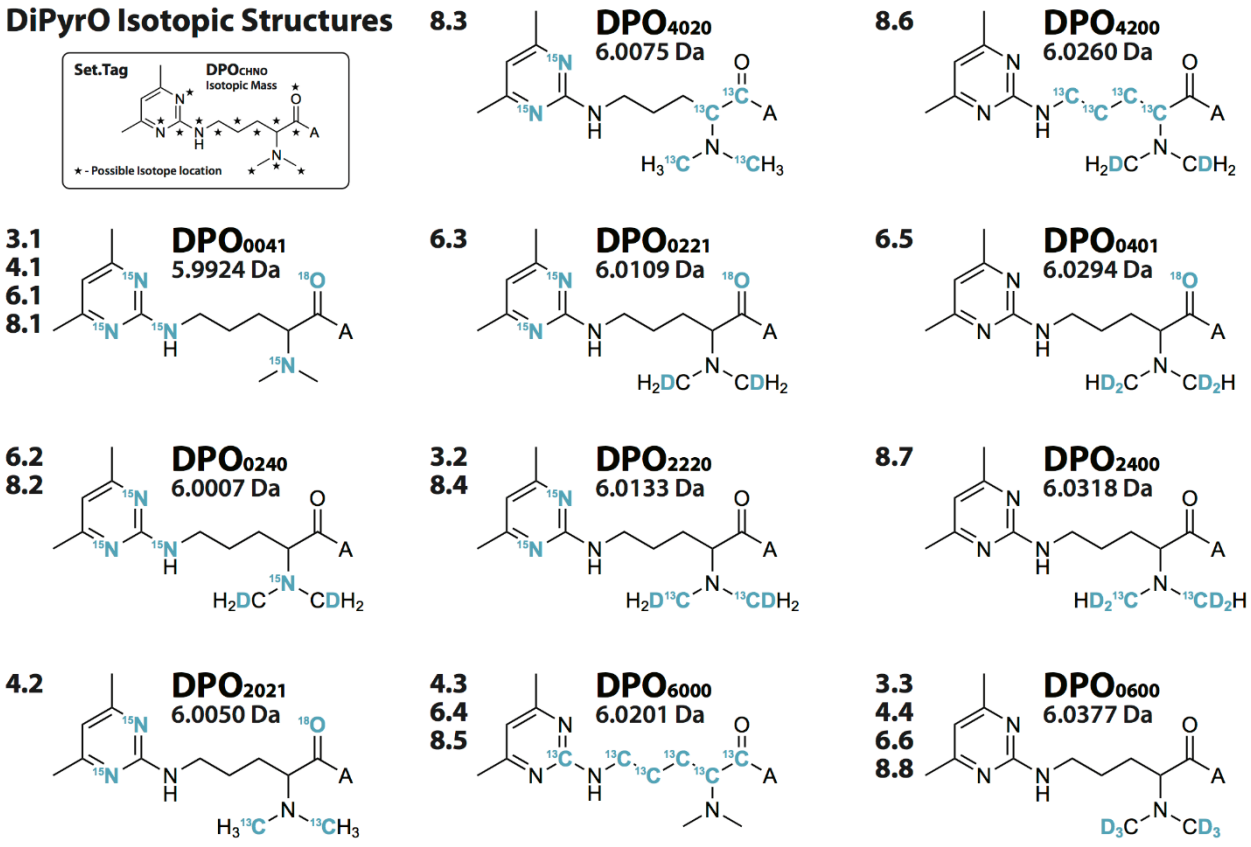

Figure S1. Multiplex DiPyrO isotopic structures. The eleven unique isotopic configurations comprising the duplex, triplex, 4-plex, 6-plex, and 8-plex sets of DiPyrO tags are shown. 'A' represents the amine-reactive moiety (triazine ester). Da: Daltons.

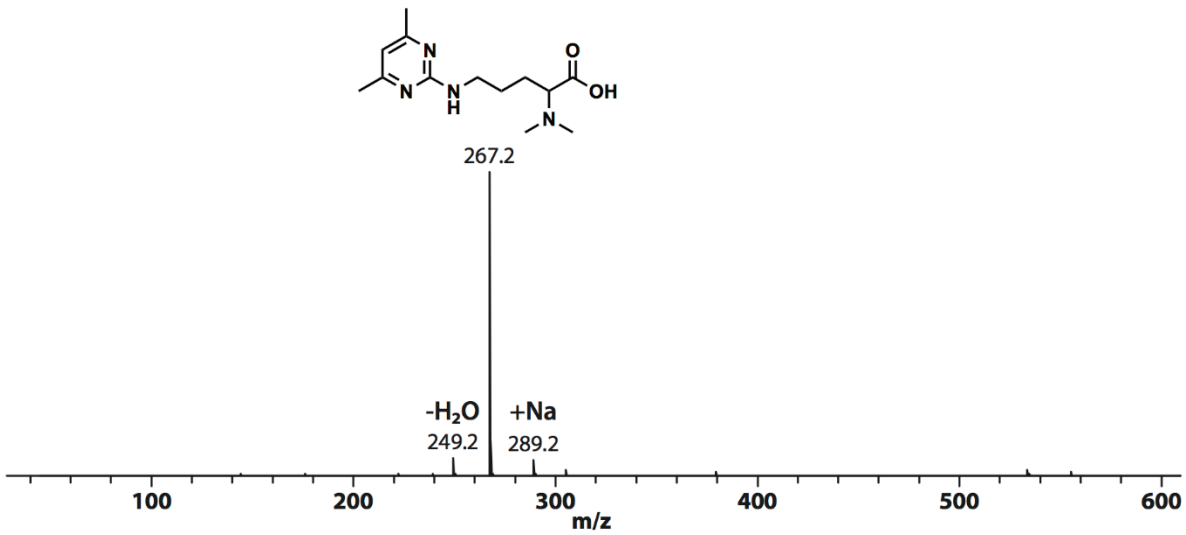

Figure S2. Non-isotopic DiPyrO synthesis – direct infusion MS validation. The DiPyrO carboxylic acid structure was synthesized using non-isotopic starting materials, purified by flash column chromatography, and analyzed by direct infusion MS on a Bruker maXis 4G mass spectrometer. The peak at 267.2 m/z confirms the structure based on its expected nominal mass.

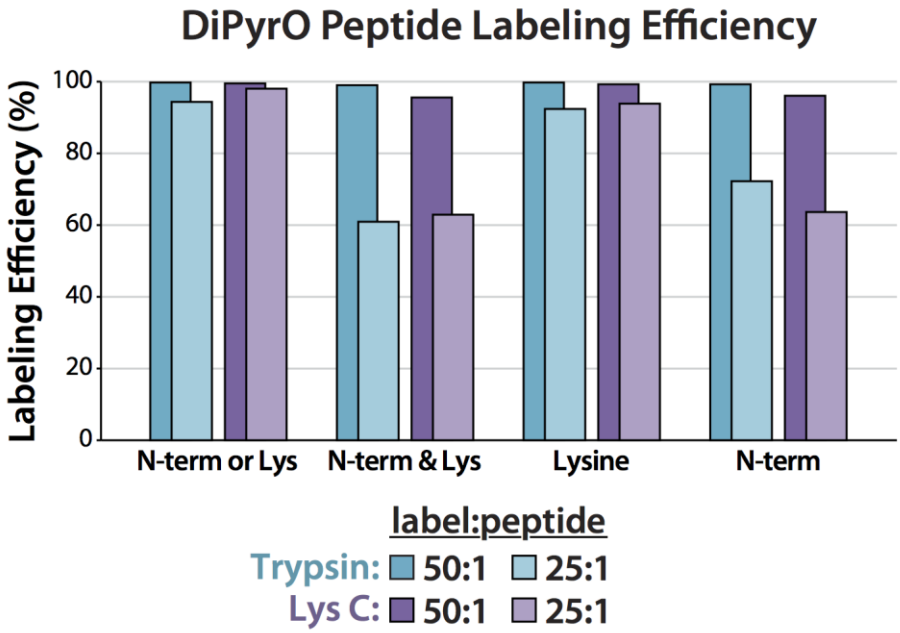

Figure S3. DiPyrO labeling efficiency – trypsin & Lys C yeast digests.

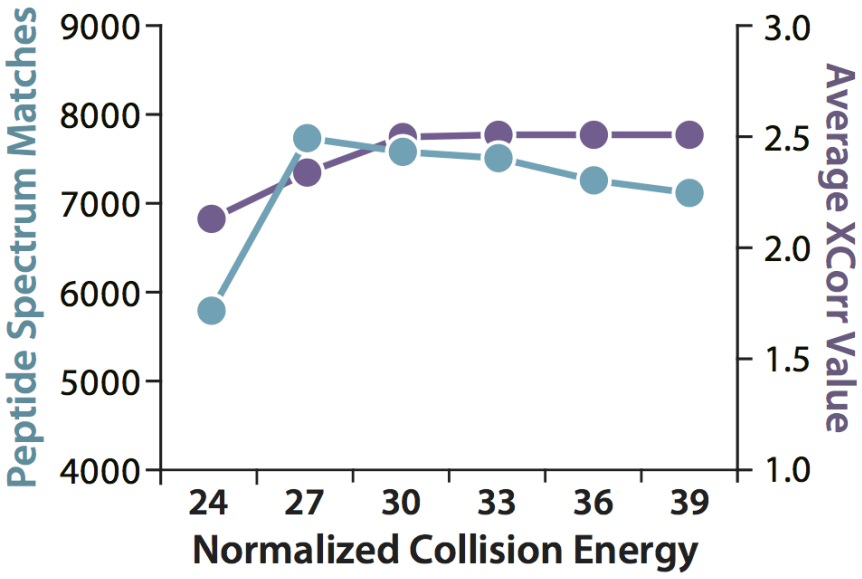

Figure S4. Normalized collision energy optimization. A DiPyrO-labeled yeast tryptic digest sample was analyzed via nanoLC-MS/MS on the Orbitrap Elite using CID fragmentation at NCE values of 24, 27, 30, 33, 36, and 39. The number of identified peptide spectral matches (blue) and median XCorr values (violet) were plotted as functions of NCE. An NCE of 30 was chosen for subsequent experiments based on the greater number of high-quality MS/MS spectra.

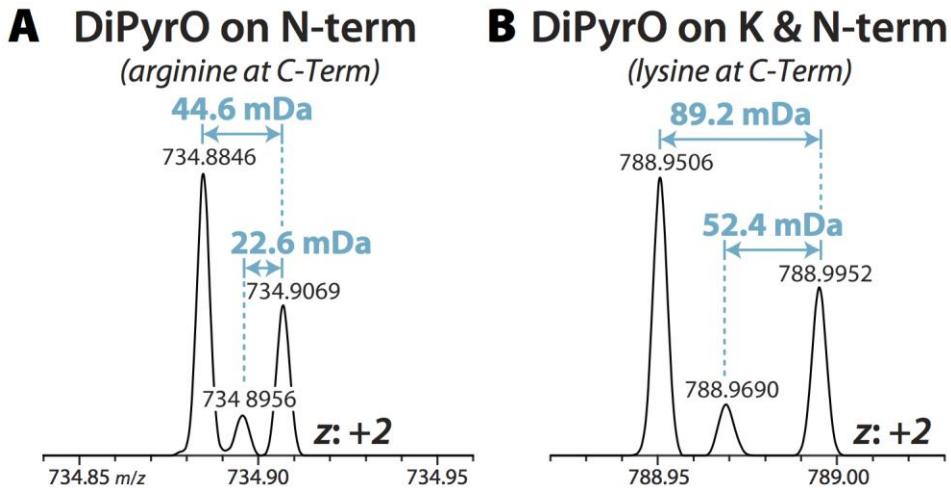

Figure S5. Double mass difference imparted by two DiPyrO tags. Tryptic peptides labeled with triplex DiPyrO tags and acquired on the Orbitrap Elite at RP 240K are shown. Triplex DiPyrO tags impart theoretical mass differences of 21 mDa between light and medium, 24 mDa between medium and heavy, and 45 mDa between light and heavy channels. Measured mass differences between channels can differ from theoretical values due to space-charge effects in the Orbitrap mass analyzer. (a) Peptides containing arginine at the C-termini, derived from digestion with trypsin, are labeled with one DiPyrO tag. (b) Peptides containing lysine at the C-termini, derived from digestion with trypsin or Lys C, are labeled with two DiPyrO tags, doubling the imparted mass difference between labeled peptides and permitting quantification at lower resolving power.

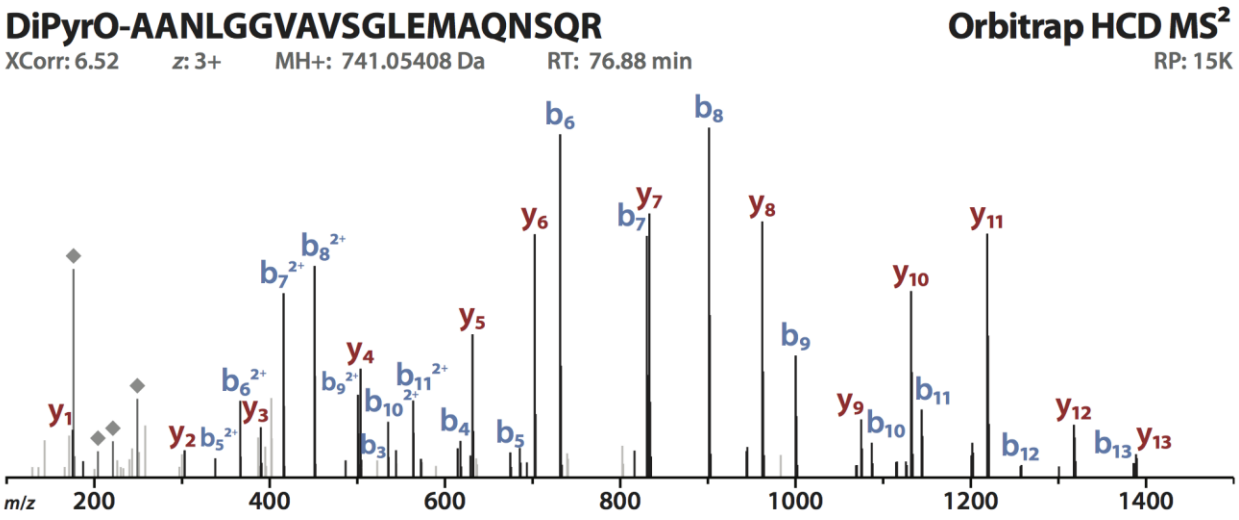

Figure S6. DiPyrO-labeled peptide MS/MS. An MS/MS spectrum of a DiPyrO-labeled yeast tryptic peptide acquired in the Orbitrap following HCD fragmentation is shown. A wealth of b- and y-ions are observed for confident peptide sequence identification. Signature ions in the low mass region produced by fragmentation of the DiPyrO tag are marked by gray diamonds.

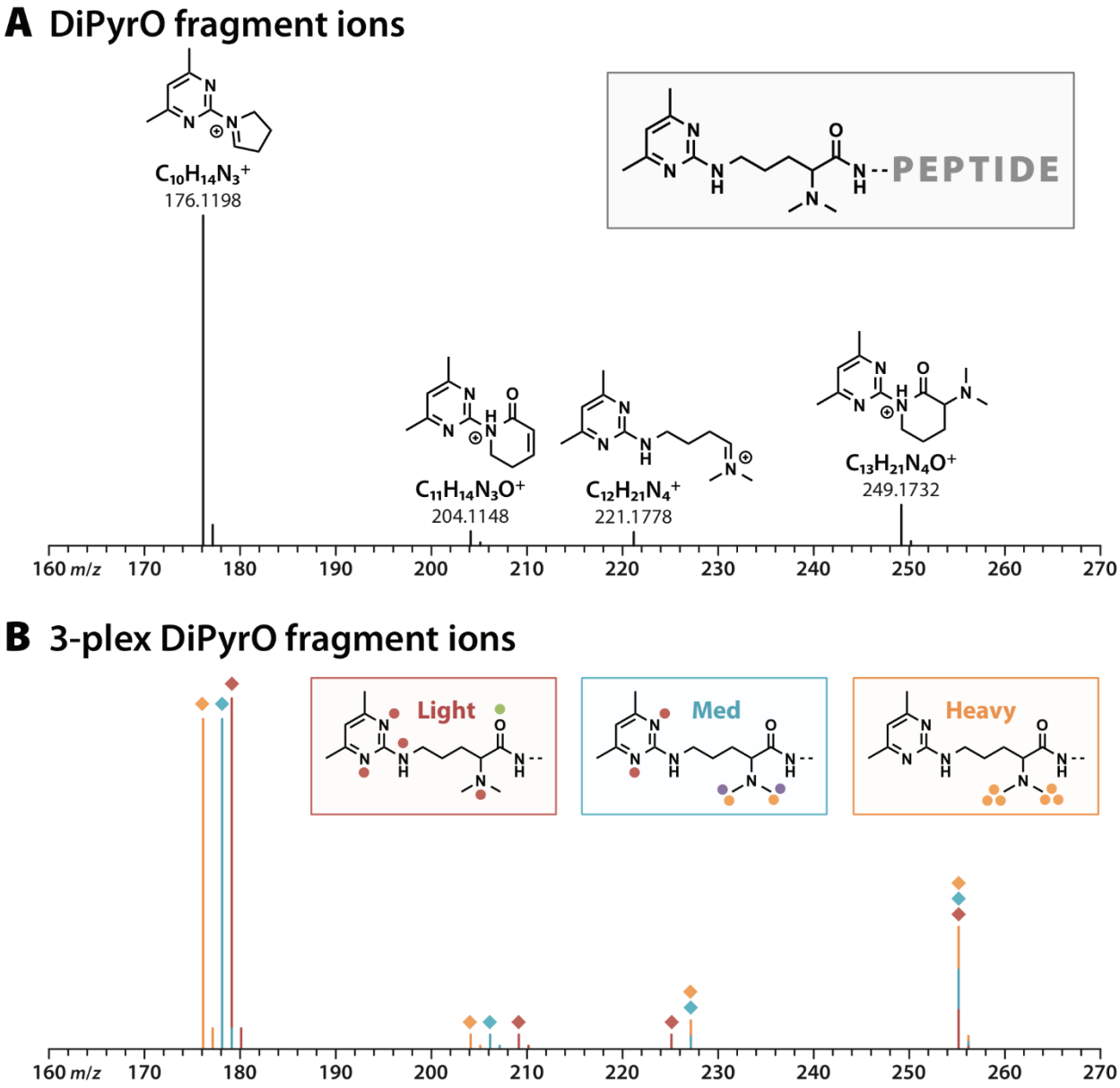

Figure S7. Characteristic DiPyrO fragment ions. (a) Collision-induced dissociation of DiPyrO labeled peptides produces four characteristic fragment ions in the low mass region of MS/MS spectra. Based on the measured masses of the ions, potential gas-phase structures are shown. (b) A theoretical MS/MS spectra illustrates that the 3-plex DiPyrO mass defect isotopologues give rise to additional ions, resulting in four clusters of ions.

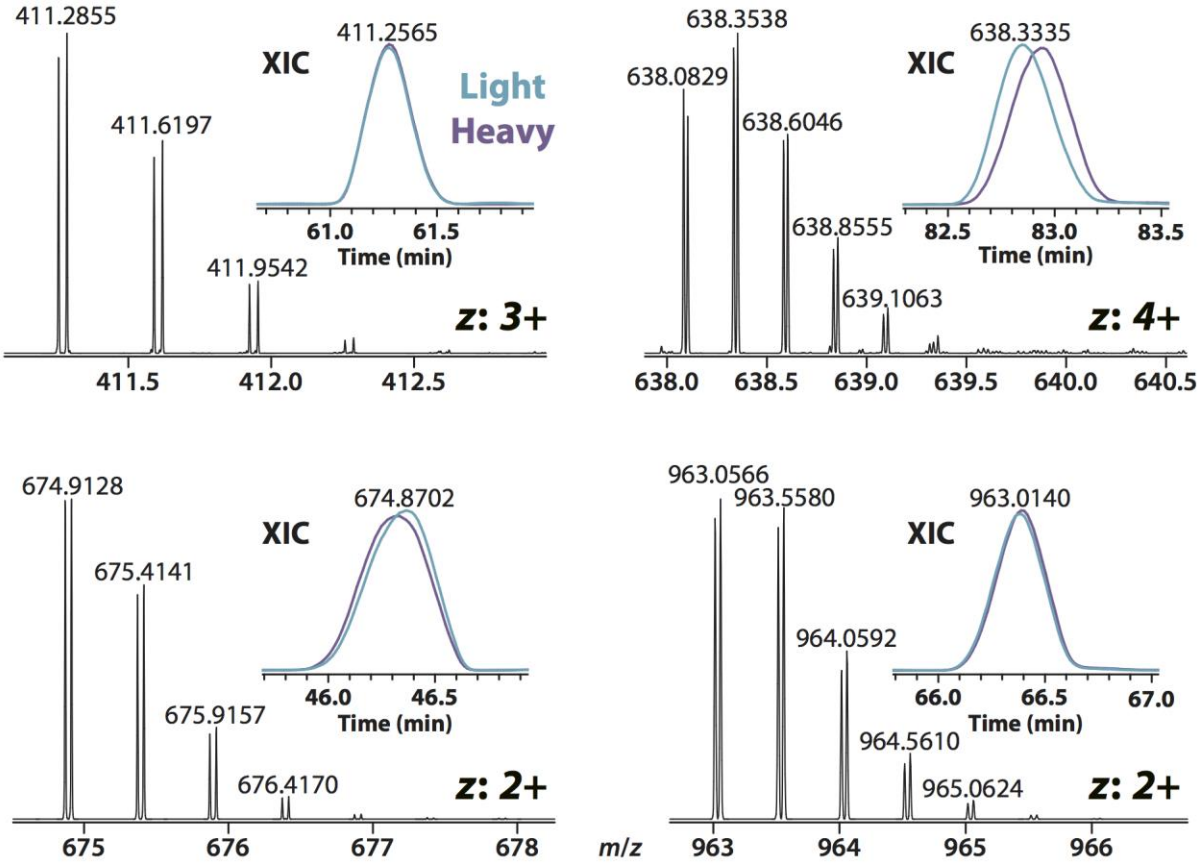

Figure S8. Resolving duplex DiPyrO-labeled peptides at RP 120K. Duplex DiPyrO-labeled peptides, mixed at a 1:1 ratio between light:heavy and acquired at RP 120K on the Orbitrap Elite, are baseline-resolved as doublets in MS1 spectra, suitable for quantification. Slight chromatographic retention time shifts are evident for some peptides due to ^{2}Hs used in the heavy tag.

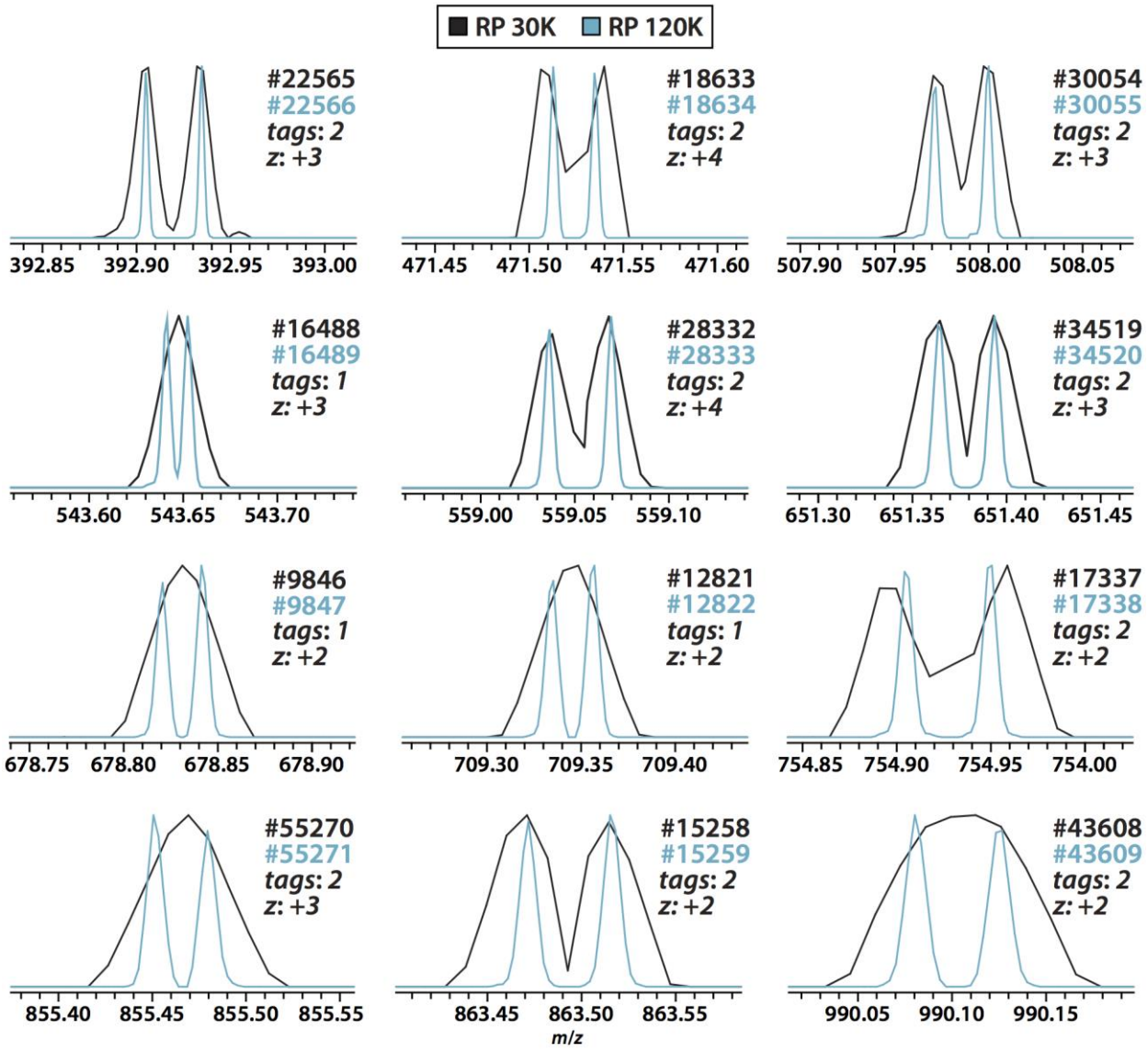

Figure S9. Partially resolved and unresolved duplex DiPyrO-labeled peptides at RP 30K. Duplex DiPyrO-labeled peptides, mixed at a 1:1 ratio between light:heavy and acquired at RP 30K and 120K on the Orbitrap Elite, are partially resolved as doublets at RP 30K in MS1 spectra for certain charge states and in certain mass ranges. This requires consideration of acquisition parameters for DDA and dynamic exclusion in order to avoid redundant sampling of peptides, and data processing parameters should also be tolerant of multiple masses per peptide.

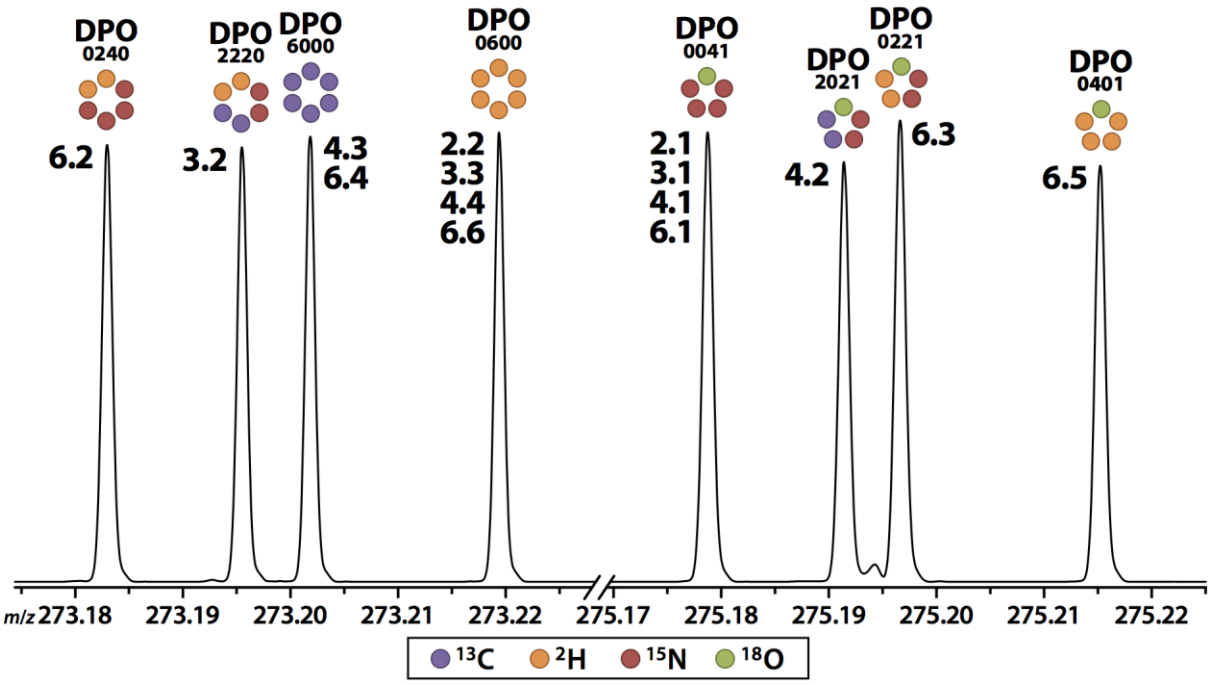

Figure S10. DiPyrO multiplex isotopologues. (A) Each of the eight DiPyrO-OH isotopologues required for the 2-plex, 3-plex, 4-plex, and 6-plex sets were synthesized in-house using commercially available reagents and their exact masses validated by direct infusion MS on the Orbitrap Elite. Prior to activation of the carboxylic acid to the triazine ester, the isotopologues with ^{18}O have two such isotopes, resulting in a nominal mass 2 Da greater than the isotopologues with no ^{18}O isotopes.

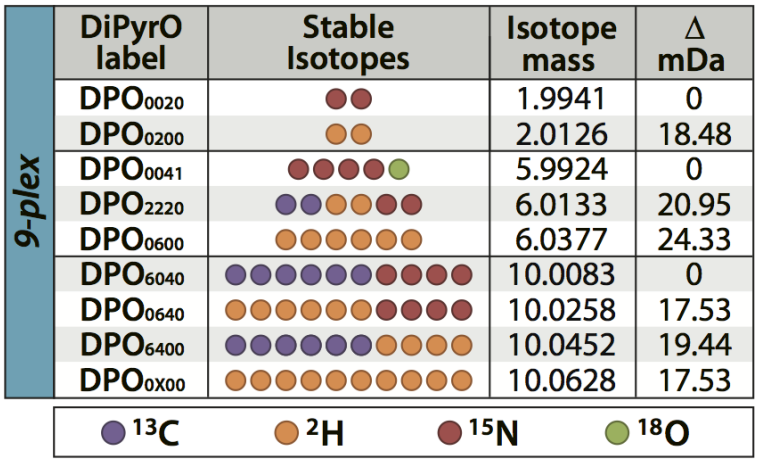

Figure S11. DiPyrO isotopologues for hybrid mass difference approach. DiPyrO isotopologues with two or ten heavy isotopes ('DiPyrO2' and 'DiPyrO10', respectively) allow for the creation of additional multiplex sets of tags with nominal masses of 250 Da and 258 Da that can be used in conjunction with the 254 Da tags ('DiPyrO6') to permit 9-plex quantification at RP 240K across three isotopic clusters that differ in mass by 4 Da.

Table S1. DiPyrO-labeled yeast digest identifications – trypsin & Lys C digests. Yeast peptides generated by digestion with either trypsin or Lys C were labeled for 1 hr with DiPyrO at label:peptide ratios of 50:1 or 25:1 (weight (w)/w), and the samples were analyzed by nanoLC-MS/MS on the Orbitrap Elite. Raw data was searched in Proteome Discoverer 2.1 using Sequest HT with DiPyrO tags specified as dynamic or static modifications on peptide N-termini and K residues. The % labeling efficiency for was calculated by dividing the number of PSMs with the DiPyrO modification by the total number of PSMs or PSMs with K

	Experiment	Proteins	Peptides	PSMS	PSMs w/K	DiPyrO N-term & K	DiPyrO K	DiPyrO N-term	DiPyrO N-term or K
Dynamic DiPyrO Mod	**Trypsin 50:1**	946	3882	8111	5862	5798	5841	8058	8096
	% efficiency					98.9%	99.6%	99.3%	**99.8%**
	Trypsin 25:1	984	5416	10888	7713	4701	7126	7855	10280
	% efficiency					60.9%	92.4%	72.1%	94.4%
	Lys C 50:1	743	2350	4766	4622	4416	4587	4576	4747
	% efficiency					95.5%	99.2%	96.0%	**99.6%**
	Lys C 25:1	749	3885	8194	7591	4765	7126	5211	8037
	% efficiency					62.8%	93.9%	63.6%	98.1%
Static DiPyrO Mod	**Trypsin 50:1**	**965**	**4023**	**8387**	**5971**	**5971**			
	% efficiency					100.0%			
	Trypsin 25:1	887	3520	7381	4589	4589			
	% efficiency					100.0%			
	Lys C 50:1	**768**	**2404**	**4920**	**4752**	**4752**			
	% efficiency					100.0%			
	Lys C 25:1	637	2171	4650	4523	4523			
	% efficiency					100.0%			

Supplemental Methods

Chemicals

All heavy isotopic reagents used for the synthesis of labels were purchased from Isotec (Miamisburg, OH). Mass spec grade trypsin/Lys C mix, rLys C, yeast protein extract, and dithiothreitol (DTT) were purchased from Promega (Madison, WI). ACS grade methanol (MeOH), ACS grade dichloromethane (DCM), ACS grade acetonitrile (ACN), Optima UPLC grade ACN, Optima UPLC grade water, and Optima LC/MS grade formic acid (FA) were purchased from Fisher Scientific (Pittsburgh, PA). Palladium on activated charcoal (Pd/C), hydrogen chloride gas (HCl), deuterium gas ($^2H_2$), L-arginine HCl, formaldehyde (CH2O), Tris-HCl, triethylamine (TEA), acetylacetone, urea, iodoacetamide (IAA), triethylammonium bicarbonate (TEAB), N,N-dimethylformamide (DMF), 4-(4, 6-dimethoxy-1, 3, 5-triazin-2-yl)-4-methylmorpholinium tetrafluoroborate (DMTMM), N-methylmorpholine (NMM), hydroxylamine solution, trifluoroacetic acid (TFA), and dimethyl-sulfoxide (DMSO) were purchased from Sigma-Aldrich (St. Louis, MO).

Yeast Protein Extract Digestion

S. cerevisiae protein extracts (Promega, Madison, WI) were digested by trypsin/Lys C mix (Promega) or rLys C (Promega). Proteins were reduced in a solution of 5 mM DTT (Promega) with 7 M urea in 80 mM ammonium bicarbonate pH 8 at 37 °C for 1 hr followed by alkylation of free thiols by addition of 15 mM IAA and incubation in the dark for 30 min. The alkylation reaction was quenched with 5 mM DTT, and the solution was diluted to 1 M urea with 50 mM Tris-HCl pH 8. Proteins were proteolytically digested by addition of trypsin/Lys C mix at a 1:25 enzyme to protein ratio and incubation at 37 °C for 16 hr. Lys C digests were performed similarly, except that the urea concentration was not diluted prior to addition of protease.

Digestions were quenched with TFA to pH < 3, and peptides were desalted using SepPak C18 SPE cartridges (Waters, Milford, MA).

Data Analysis

Quantification of peptides identified by PD was performed using PyQuant (available at https://chris7.github.io/pyquant/). PyQuant script arguments included the following: --neucode, --overlapping-labels, --precursor-ppm 5 or 10 (for triplex or duplex samples, respectively), --isotopologue-limit 2, --no-rt-guide, --no-contaminant-detection. Overlapping labels is specified for mass defect quantification, declaring that m/z values of the discrete labeled peptides are interleaved within the isotopic envelope. Isotopologue limit determines the number of isotopic peaks within the envelope to consider for quantification, starting with the monoisotopic peak. 'No RT guide' was specified ignores the scan's MS/MS retention time when fitting peak data to the measured extracted ion chromatogram (XIC), and 'no contaminant detection' was specified to disable a routine that could mistake peaks in the multiplets for isotopologues of contaminating species. Resulting data were filtered to require at least 15 isotopic peaks found (per channel) in scans over the peptide's extracted ion chromatogram to reduce distortion of quantification values caused by having too few data points for any channel.

Supplemental Results and Discussion

To optimize the reaction times for activation and labeling, we labeled a yeast tryptic digest and evaluated a number of conditions based on the number of identified proteins & peptides and the number of PSMs containing the DiPyrO label. Activation reactions were carried out for 30 min or 1 hr, and labeling was carried out for 30 min, 1 hr, 2 hr, or 4 hr. Following nanoLC-MS/MS analysis (data not shown), we determined that 30 min activation was sufficient,

whereas 1 hr activation yielded slightly fewer protein and peptide identifications. The 30 min and 1 hr labeling times performed similarly, delivering greater identification rates than 2 hr and 4 hr labeling times.

To assess labeling efficiency, we labeled yeast digests for 1 hr at a 25:1 and 50:1 DiPyrO:peptide ratio by weight and analyzed the samples using a 120 min elution gradient. Raw data was searched with DiPyrO tags specified as dynamic or static modifications on peptide N-termini and K residues. The numbers of identified protein groups, peptides, and PSMs, along with the % efficiency—calculated by dividing the number of PSMs with the DiPyrO modification by the total number of PSMs or PSMs with K—are reported in **Table S1** & **Figure S3**. Overall labeling efficiency is excellent at a 50:1 label to peptide ratio, with over 99% of trypsin and Lys C peptides carrying at least one DiPyrO tag (specified as a dynamic mod on both N-term & K). Approximately 99% of tryptic peptides and 95% of Lys C peptides containing lysine are labeled with two tags. This experiment also highlights the benefit of using trypsin for digestion in a chemical labeling workflow, compared to the requisite Lys C for NeuCode SILAC, as it outperformed Lys C by yielding 25% more protein identifications and nearly 70% more peptide identifications (50:1 ratio).

Multiplex DiPyrO Quantification. In the MS1 spectra of duplex and triplex DiPyrO-labeled yeast protein digest samples acquired on the Orbitrap Elite at RP 120K and 240K, we observed peak coalescence occurring for some peptides with particularly high signal intensities (around 5×10^7 or greater) near the apex of their elution profile, due to space-charge effects in the Orbitrap mass analyzer. The degree of coalescence and ranged from mild, with a reduced mass difference between peak pairs, to complete, with peak pairs converging into a single peak, and the frequency was similar at both resolving power settings. Coalescence affected only the

most abundant isotopic peaks in the isotopic distribution, with those lower in abundance remaining resolved. We found it beneficial to moderate sample loads and reduce the AGC target from 1×10^6 to 5×10^5 in order to control the frequency and extent of coalescence with the consequence of reducing identification rates by some degree. When we acquired similar samples on our Orbitrap Fusion Lumos, which is less susceptible to coalescence due to its higher field Orbitrap mass analyzer, we observed only very slight deviations in the multiplet peaks' measured masses at signal intensities reaching as high as 7×10^7 (AGC target 1×10^5). With particularly high sample concentrations, we were able to induce complete coalescence on the Fusion Lumos, indicating that care must still be taken when calculating sample loads for acquisition.

Chapter 9

Seeing the Big Picture with Small Systems:

Analytical Methods to Understand Stress

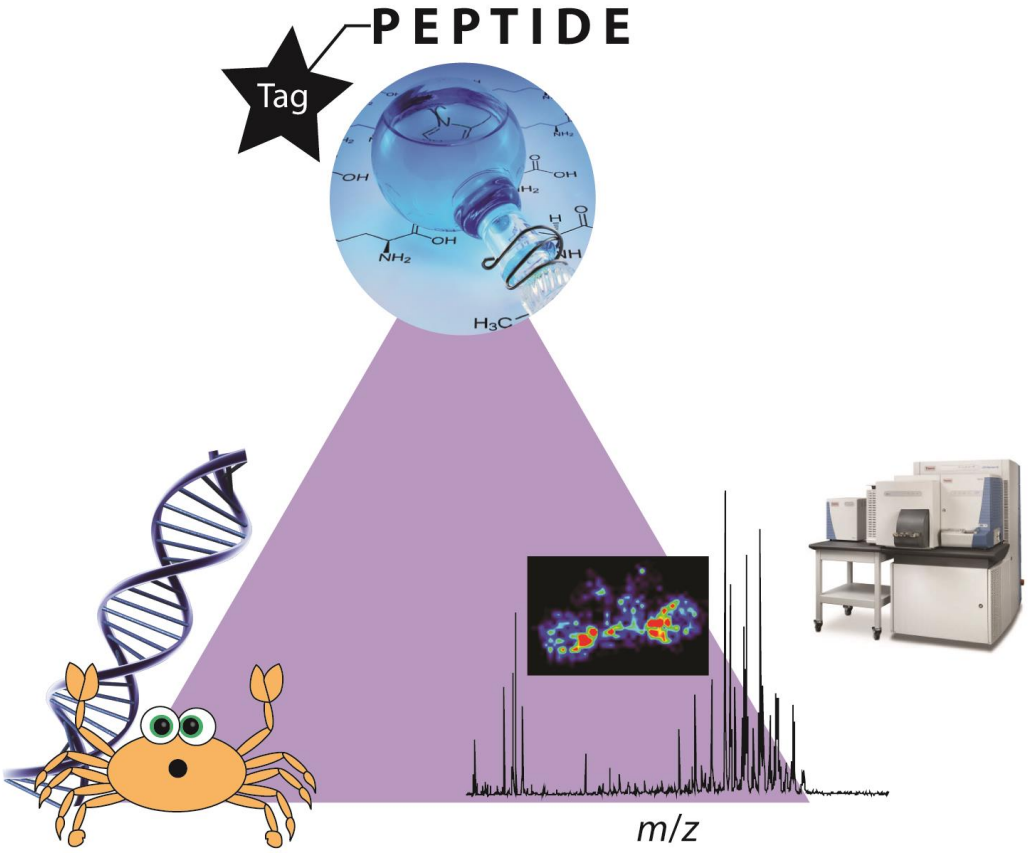

Written in collaboration with the Wisconsin Initiative for Science Literacy to communicate this thesis research to non-specialists.

Key Words: Neuropeptides, Mass Spectrometry, Crustaceans, Hypoxia Stress, Mass Spectrometry Imaging, Labeling

Abstract

In order to understand how humans and animals handle stress, specifically hypoxia, also known as low oxygen levels, my thesis research has focused on utilizing mass spectrometry as an analytical technique to probe the neurological response to this stressor. Instead of humans, we use crustaceans to understand the changes through the whole body due to stress. Our results show changes due to hypoxia stress both quantitatively and how neurological molecules are located in the brain. Theoretically, future studies can apply these results, both medically and environmentally.

Why Stress?

Humans require a state of homeostasis, or the balance of everything in the body.[1] Every day external stimuli challenge our bodies. Even slight changes in homeostasis can be fatal to humans. Some key, recognizable examples of human stress are changes in blood sugar (*e.g.*, hyper- or hypo-glycemia) or body core temperature (*e.g.*, hypothermia or a fever). Our body is amazing; it has developed several different ways to handle stress. For example, when we get an infection, our immune system removes the offending virus or bacteria. Beyond the human body, ecosystems have also evolved to handle stress. During environmental fluctuations, which have increased in frequency due to human activity, stress afflicts aquatic animals. Examples of stimuli include temperature, water saltiness (*i.e.*, salinity), or even water pH changes.[2-5]

During my graduate study, my research has focused on understanding hypoxia, or low oxygen (O_2), stress. Hypoxia stress is well documented in the scientific literature to occur in aquatic estuaries, or areas where freshwater outlets meet saltwater inlets, such as the Maryland coast (*e.g.*, Chesapeake Bay).[6-8] In general, O_2 has a harder time reaching the bottom of these water reservoirs. Human activity amplifies this effect, as chemicals added into the water streams

have caused stratification, or layering. These layers make it even harder for O_2 to reach these lower water levels, creating areas with little to no O_2. Thus, animals that reside on the ocean floor developed mechanisms to either avoid or survive these stressful conditions.

Humans also suffer from hypoxia stress. Even brief periods of hypoxia can cause developmental issues within children, while long term exposure could lead to permanent damage in important regions of our brain.[9-11] In general, lack of O_2 to the organs (hypoxia) or blood (hypoxemia) prevents the cells from using glucose, causing fatigue, cell injury, and eventually death. Medical conditions, including cancer, asthma, pulmonary hypertension, and respiratory distress, tend to be associated with low O_2 levels, although there is limited knowledge about the biological and molecular changes that occur due to episodes of constant O_2 deprivation.[12-14] It is a well-known fact that losing access to O_2 is fatal, and we should investigate these effects (even in short term exposures) more thoroughly. Overall, this research will improve our understanding of the biochemical changes of hypoxia on the nervous system, both in acute and long-term exposure.

Why Neuropeptides?

Within the brain, several players are involved in regulating homeostasis. These range from very small molecules, such as metabolites and neurotransmitters, to things that are 100,000x bigger, such as proteins. The main regulators of the stress response are peptides, which are short chains of amino acids involved in signaling changes in the body. Specifically, neurological peptides (*i.e.*, neuropeptides) allow for this signaling within the brain and the nervous system. Neurons (*i.e.*, cells in the brain) synthesize and secrete these neuropeptides, as depicted in **Figure 1**.[15, 16] Secreted neuropeptides cause a chain reaction of neuron-neuron

signaling prior to affecting the final target tissue. Unlike other neurological molecules (*e.g.*, neurotransmitters), which create an instantaneous, short-term response, neuropeptides have long-lasting effects within the nervous system. Changes due to stress, especially during critical developmental times, can lead to long-term behavior and biological changes. This is also true for aquatic organisms, although they are less well characterized and understood. In general, there is a lack of understanding of the whole-body neurological changes caused by hypoxia exposure.

Why Crustaceans?

Neuropeptides are one of the most complex classes of signaling molecules in the brain. Their sizes range from just a few to several hundred amino acids.[15, 16] Neuropeptide analysis is even more complicated because several other molecules interact with, degrade, or just exist in the sample (*e.g.*, blood, *etc.*). This knowledge gap largely stems from numerous technical difficulties associated with the complete analysis of the highly complex mammalian nervous system. In complex animal models (*e.g.*, rodents), it can be challenging to confidently map the interconnected neurons and analyze the active compounds in the presence of a diverse and highly complex biological matrix. Thus, mammalian systems are much too complicated for us to use in our studies, and working with relatively simple systems is required to get an overall, more comprehensive picture of the changes occurring due to hypoxia stress. The Lingjun Li lab uses crustaceans (*e.g.*, crabs, lobsters, etc.) as model organisms for neuropeptide-based studies.[5, 17] Because crustaceans have a well-characterized and simple nervous system and structure, we can easily find the neuropeptide-rich organs of interest (shown in **Figure 2**), such as the brain.[18] Our lab also developed a very large crustacean neuropeptide database, which we use to identify several key players in environmental stressors, including hypoxia stress.

Hypoxia stress also affects crustaceans.[19-21] Estuaries are home to many crabs, including the blue crab, which has been the main focus of my graduate studies. Interestingly, crustaceans are not only ecologically relevant in terms of hypoxia stress, but they are also good model organisms for translating to higher organisms (*e.g.*, rodents). Because many of the crustacean neuropeptides have similar structures to human neuropeptides, findings using the crustacean model system are transferable to mammals. For example, RFamide-like and tachykinin peptide families are related to human peptides that are involved in how we feel pain.[22-24] These changes in the crustacean model organisms will help us identify similar signaling molecules that may play a role in adaptation to hypoxia in mammals.

Why Mass Spectrometry?

Classically, to study neuropeptides, scientists used techniques with fluorescent molecules that were thought to bind very specifically to a neuropeptide of interest.[25] As you could expect, this means we can only look at one neuropeptide at a time. When trying to look at the changes on a whole-body scale, looking at one at a time can be tedious, time consuming, and inefficient. This situation is made worse by the fact that these fluorescent molecules can actually bind non-specifically, meaning that similar neuropeptides that have distinct functional differences in stress regulation cannot be seen as different.[23] Thus, there is a need for a fast, specific, and sensitive way to look at all the neuropeptides at once.

Mass spectrometry (MS) meets all those requirements. MS is an analytical technique that works by making molecules charged (*e.g.*, become ions) by transferring energy to add or remove hydrogen, allowing them to be measured by an instrument, which is depicted in **Figure 3**. We then use software to graph the "mass-to-charge" (*m/z*) ratio along with a measured intensity onto

a mass spectrum (as shown in **Figure 4**). An *m/z* ratio is just what it sounds like: the mass of a chemical compound divided by the charge that it has. For example, if a molecule is 1000 mass units and is has one charge, then the *m/z* will be ~1000. When we have a specific *m/z* value we are interested in, we can select it to be broken up and measured separately, a process called tandem MS, in order to have its structure rebuilt using computer software.[15] This technique is extremely powerful, as we do not require any prior knowledge of the molecules (*e.g.*, neuropeptides) in order to analyze them. One major method for ionizing neuropeptides is with matrix-assisted laser/desorption ionization (MALDI)-MS. MALDI seems complicated, but, simply, we use a matrix and a laser to charge the neuropeptides. For this method, we usually put a small volume of the crushed and cleaned up brain tissue that has to be mixed with the matrix on a stainless steel plate, where we can estimate and/or quantify how much of a neuropeptide was found in the tissue.[15] While this makes getting a mass spectrum easy, we are unable to get spatial information about the neuropeptides within in the tissue. Both the quantity and the location of a neuropeptide provide important information to understand its function. Instead of crushing up the tissue, we can actually section it into thin slices (~12 μm thick), which can then be covered in matrix for MALDI analysis.[26] On this tissue section, we form a grid. On each grid point, we acquire an individual mass spectrum. The size of the grid and thus number of grid points depends on the spatial resolution, and these squares in the grid can range from 500 μm to 5 μm in length/width. For comparison of the size, blood cells have a diameter of 7-8 μm! For data processing, we can then select the mass of a neuropeptide of interest (*e.g.*, from our crustacean database), and we extract the intensity of that mass from each of the individual mass spectrum (*i.e.*, grid point), forming an image (**Figure 5**).[26] We also generate images for any peak

detected by the MS, meaning scientists can investigate unknown *m/z* values for their roles in environmental stress.[27]

With MS, we have methods we can use to directly compare samples, which is extremely important for our studies since we want to compare a hypoxia-exposed animal to a control animal. To do this, we take advantage of the existence of different, heavy versions of elements. For example, hydrogen, the most common element in the universe, has a heavy version called deuterium. Deuterium and hydrogen differ by one mass unit. This increase in mass makes it heavier in general, but it doesn't change any of its properties. By incorporating a different number of isotopes between two labels, such as adding one hydrogen to one group and one deuterium to the other group and mixing them, we see pairs of peaks in the mass spectrum that are separated by a known distance. In our case, we will be looking for a 2 or 4 *m/z* ratio difference between the peaks when they are singly charged molecules, depending on the number of different conditions we want to compare.[28] **Figure 4** shows an example where 2 samples are differentially labeled (shown in the open and closed hexagons) with 4 *m/z* mass differences in the spectrum. In this case, by comparing the intensity of the light and heavy peak pairs, we can see if neuropeptide levels increase or decrease in a hypoxia-exposed animal compared to a control, which will give us an idea about their function and/or role in hypoxia stress.

Putting it All Together

By combining MS and crustacean neuropeptide analysis, we can provide an overall idea of what is occurring when the crab is exposed to stress, specifically hypoxia. Normal levels range from 8-10 parts per million, which translates to 80-100% maximum O_2 capacity of the water. In order to consistently expose the crabs to hypoxia, we "bubbled" out the O_2 in the water

using nitrogen gas, as depicted in **Figure 6**. Once the level of O_2 reaches the level we are interested in, such as 10% O_2 (*i.e.*, severe hypoxia) compared to 100% O_2 (*i.e.*, normal), we place the crab in the water for a period of time, such as 1 hour, before sacrificing them. In addition to hypoxia-exposed crabs, we also need control crabs, which have a fully aerated tank (80-100% O_2). After sacrificing the crabs, we take out all their neuropeptide-rich organs (see **Figure 2**), isotopically label each sample, and finally analyze by MS (**Figure 7**).

Looking back at **Figure 4**, we can see that hypoxia stress does affect the neuropeptides and their concentrations. In this spectrum, the orcokinin neuropeptide family has been highlighted, and they all appear to be downregulated due to this severe hypoxia (*i.e.*, 10% O_2) stress. This is a trend across many other neuropeptide families not in the spectrum. As stated before, we can translate information from both the RFamides and tachykinin neuropeptide families of crustaceans to mammals, including humans. Several RFamides show changes ranging from 100% increase to 90% decrease. Thus, neuropeptides that are from the same family, meaning they are similar in structure, can have very different functions in the stress response.

Crustaceans are a necessary first step for overall, comprehensive studies, and the next step would be applying these results to more complex organisms, such as mice, for follow up studies. Beyond severe hypoxia (*i.e.*, 10% O_2) for 1 hour, we have also investigated moderate (*i.e.*, 20% O_2) and mild (*i.e.*, 50% O_2) hypoxia for an hour, along with a time course study (*i.e.*, 0 hour, 1 hour, 4 hours, and 8 hours) for severe (*i.e.*, 10% O_2) hypoxia. All of these conditions have shown distinct neuropeptidomic changes due to hypoxic stress.

In order to acquire spatial information of these neuropeptides, we also employed MS imaging, as seen in **Figure 5**. As you can see, some neuropeptides are located all over the tissue (*e.g.*, LNPSNFLRFamide, *m/z* 1106.611), while others are located only around the edges of the

brain (*e.g.*, LPGVNFLRFamide, *m/z* 1061.626). The most interesting neuropeptides are those that either appear or completely disappear after hypoxia stress, as it makes us believe they have a key role in how these animals handle hypoxia stress. It should be noted that when comparing control and hypoxia-exposed animals, no quantitative changes doesn't mean there is no change in the localization of neuropeptides in the tissue. For example, neuropeptides localizing to the outside or the middle can have the same overall concentration, meaning that when we crush up the tissue for labeling (see above), we would not see any change. Also, if we only find the neuropeptide on the outside of the tissue, they could be preparing for release into the crustacean blood (*i.e.*, hemolylmph). Thus, while quantitative information is important, we should consider also looking at the neuropeptide location over time to determine its role in hypoxia stress.

Conclusions and Future Directions

Using the crustacean model organism, we discovered that hypoxia stress can have a significant effect on the expression of several neuropeptides. By gaining further knowledge in basic neurobiology and neurochemistry, society will have a better understanding of the brain and how it changes in medical conditions where hypoxia occurs, including respiratory distress, cancer, asthma, *etc*. While we have found ways to probe these systems, the Lingjun Li lab will explore other areas. Another avenue I have explored is the difference between hypoxia (*i.e.*, low O_2) and hypercapnia (*i.e.*, low O_2 with increased carbon dioxide (CO_2)) stress. Several other graduate students in the lab have been inspired to look at this research from different angles, including sampling crustacean blood (*i.e.*, hemolymph) sampling while the crab is still alive or exploring other similar stressors (*e.g.*, pH).

References

1. Chrousos, G. P.; Gold, P. W., *Jama-Journal of the American Medical Association* **1992,** *267* (9), 1244-1252.

2. Zhang, Y.; Buchberger, A.; Muthuvel, G.; Li, L., *Proteomics* **2015**.

3. Townsend, K.; Spanings-Pierrot, C.; Hartline, D. K.; King, S.; Henry, R. P.; Towle, D. W., *American Zoologist* **2001,** *41* (6), 1608-1609.

4. Puri, S.; Faulkes, Z., *Biology Open* **2015,** *4* (4), 441-U41.

5. Chen, R. B.; Xiao, M. M.; Buchberger, A.; Li, L. J., *Journal of Proteome Research* **2014,** *13* (12), 5767-5776.

6. Diaz, R. J.; Rosenberg, R., *Oceanography and Marine Biology - an Annual Review, Vol 33* **1995,** *33*, 245-303.

7. Bell, G. W.; Eggleston, D. B.; Noga, E. J., *Oecologia* **2010,** *163* (1), 57-68.

8. Bell, G. W.; Eggleston, D. B.; Noga, E. J., *Biological Bulletin* **2009,** *217* (2), 161-172.

9. Bass, J. L.; Corwin, M.; Gozal, D.; Moore, C.; Nishida, H.; Parker, S.; Schonwald, A.; Wilker, R. E.; Stehle, S.; Kinane, T. B., *Pediatrics* **2004,** *114* (3), 805-816.

10. Carlson, J. T.; Hedner, J.; Elam, M.; Ejnell, H.; Sellgren, J.; Wallin, B. G., *Chest* **1993,** *103* (6), 1763-1768.

11. Brown, K. A.; Laferriere, A.; Moss, I. R., *Anesthesiology* **2004,** *100* (4), 806-810.

12. Harris, A. L., *Nature Reviews Cancer* **2002,** *2* (1), 38-47.

13. Cutz, E.; Yeger, H.; Pan, J., *Pediatric and Developmental Pathology* **2007,** *10* (6), 419-435.

14. Kelsen, S. G.; Fleegler, B.; Altose, M. D., *American Review of Respiratory Disease* **1979,** *120* (3), 517-527.

15. Buchberger, A.; Yu, Q.; Li, L., *Annu Rev Anal Chem (Palo Alto Calif)* **2015,** *8* (1), 485-509.

16. Li, L. J.; Sweedler, J. V., Peptides in the Brain: Mass Spectrometry-Based Measurement Approaches and Challenges. In *Annual Review of Analytical Chemistry*, Annual Reviews: Palo Alto, 2008; Vol. 1, pp 451-483.

17. Cape, S. S.; Rehm, K. J.; Ma, M.; Marder, E.; Li, L. J., *Journal of Neurochemistry* **2008,** *105* (3), 690-702.

18. Gutierrez, G. J., *Cancer Borealis* Stomatogastric Nervous System Dissection. Grashow, R. G., Ed. JOVE, 2009.

19. Chung, J. S.; Webster, S. G., *Endocrinology* **2005,** *146* (12), 5545-5551.

20. Gray, J. S.; Wu, R. S. S.; Or, Y. Y., *Marine Ecology Progress Series* **2002,** *238*, 249-279.

21. Tanner, C. A.; Burnett, L. E.; Burnett, K. G., *Comparative Biochemistry and Physiology a-Molecular & Integrative Physiology* **2006,** *144* (2), 218-223.

22. Moss, I. R.; Laferriere, A., *Respiratory Physiology & Neurobiology* **2002,** *131* (1-2), 15-27.

23. Christie, A. E.; Stemmler, E. A.; Dickinson, P. S., *Cell Mol Life Sci* **2010,** *67* (24), 4135-69.

24. Poncet, L.; Denoroy, L.; Dalmaz, Y.; Pequignot, J. M.; Jouvet, M., *Brain Research* **1996,** *733* (1), 64-72.

25. DeLaney, K.; Buchberger, A. R.; Atkinson, L.; Grunder, S.; Mousley, A.; Li, L. J., *Journal of Experimental Biology* **2018,** *221* (3).

26. Buchberger, A. R.; DeLaney, K.; Johnson, J.; Li, L. J., *Analytical Chemistry* **2018,** *90* (1), 240-265.

27. Robichaud, G.; Garrard, K. P.; Barry, J. A.; Muddiman, D. C., *Journal of the American Society for Mass Spectrometry* **2013,** *24* (5), 718-721.

28. Kovanich, D.; Cappadona, S.; Raijmakers, R.; Mohammed, S.; Scholten, A.; Heck, A. J. R., *Analytical and Bioanalytical Chemistry* **2012,** *404* (4), 991-1009.

Figures

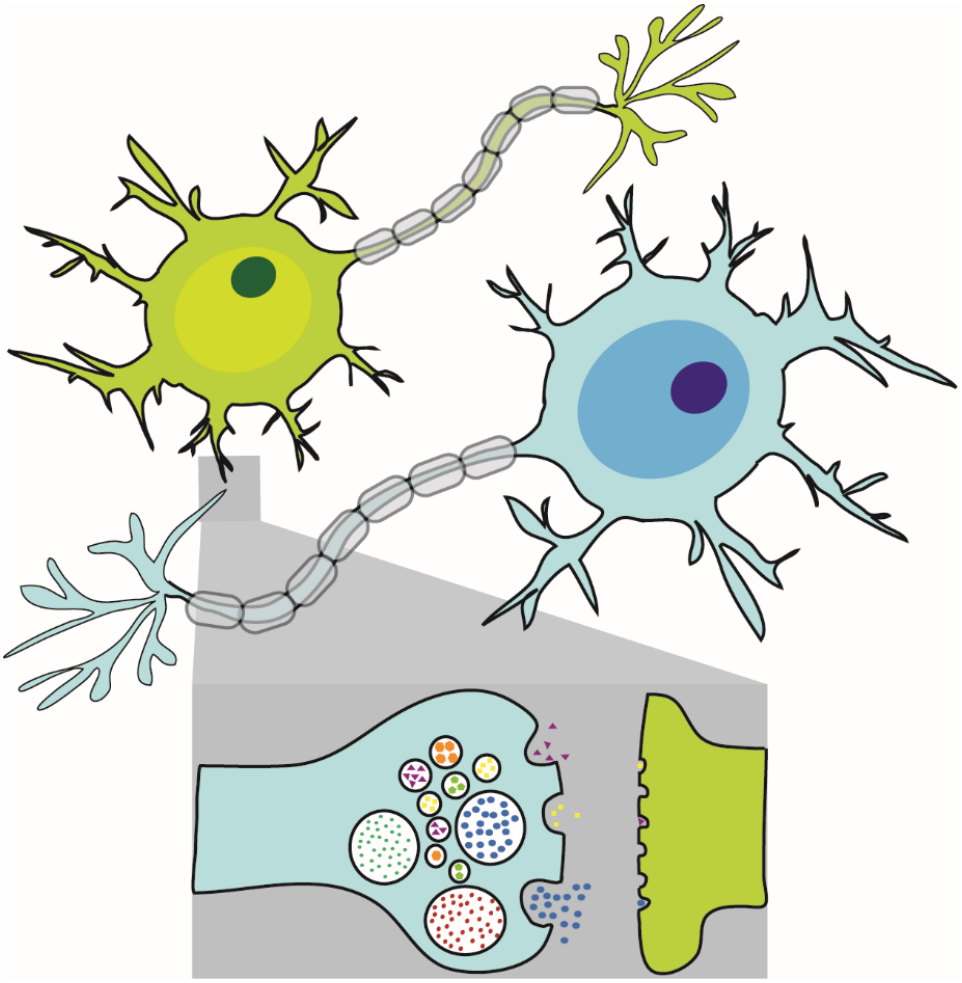

Figure 1. An artistic image of a neuron interacting with another neuron. In the zoomed in region, one can observe several molecules, including neuropeptides, being released.

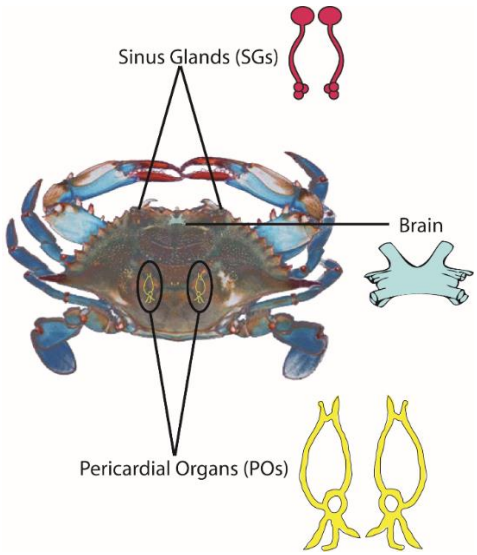

Figure 2. Locations of neuropeptide-rich organs in the crustacean. The sinus glands are located in the eyestalks. The brain is located between the eyestalks above the stomach. The pericardial organs surround the heart in the pericardial ridges.

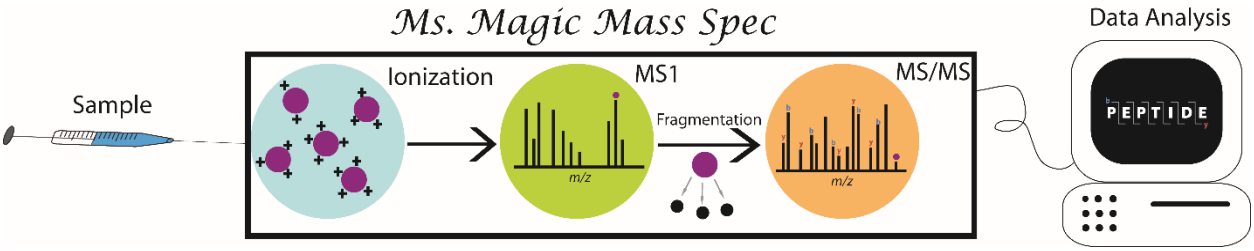

Figure 3. A schematic of a mass spectrometer. After we insert the sample into "Ms. Magic Mass Spec," the molecules become ions (*i.e.*, ionize), meaning they gain a charge. We then visualize the resulting *m/z* values in a mass spectrum (MS1). If an *m/z* value is of interest, the instrument can break it up into smaller pieces by tandem MS (MS/MS). We can then piece the fragments together into the molecule's structure using advanced computer software.

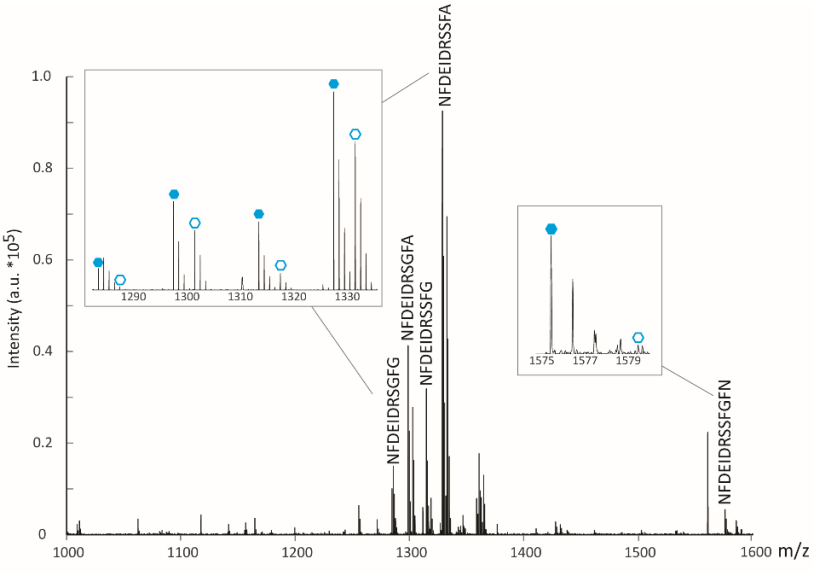

Figure 4. Example MS spectrum, highlighting the heavy and light peak pairs we see when we use duplex labeling. The closed hexagons are the neuropeptides from the control brain sample, while the open hexagons are from the severe hypoxia (*i.e.*, 10% O_2) exposed brain sample.

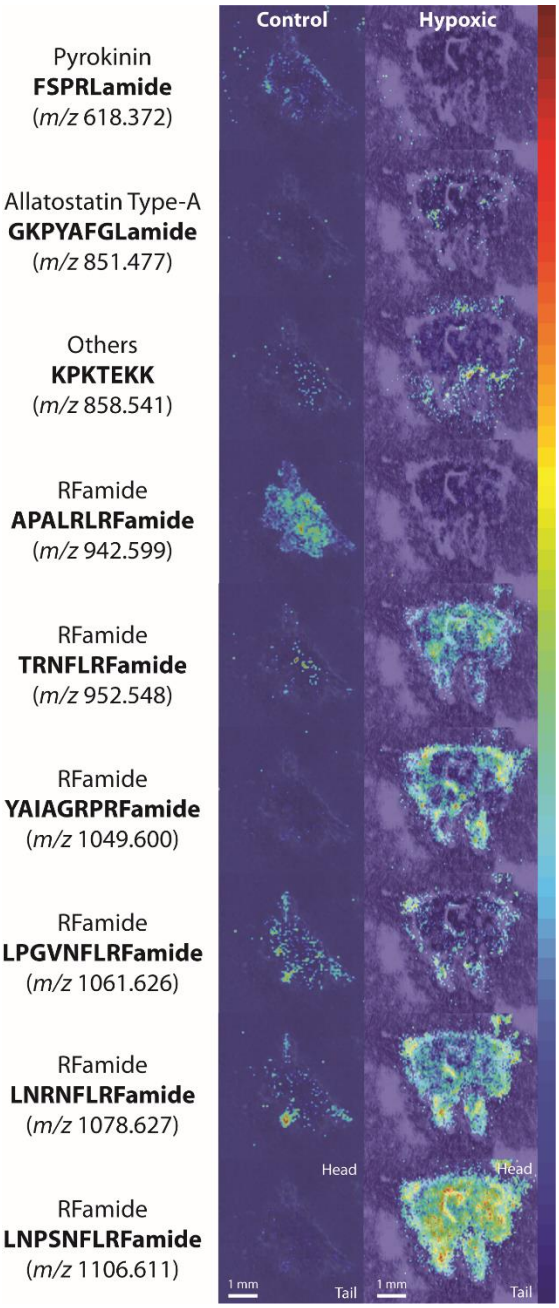

Figure 5. Nine neuropeptide brain distributions found by MS imaging comparing the control (left) and severe hypoxia (*i.e.*, 10% O_2) (right) exposed crab brains. The optical image of the brain is in the background of each of these images. A color bar shows both low (blue) and high (red) intensity.

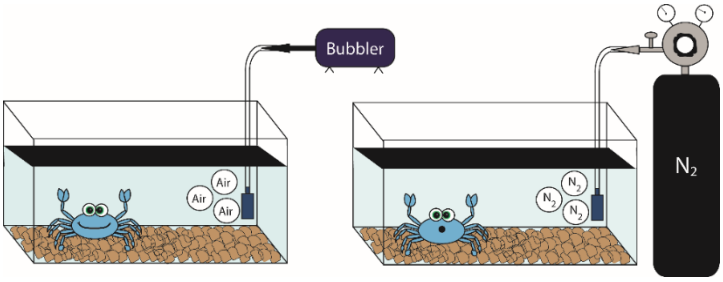

Figure 6. Tank set up for control (left) and hypoxia (right) exposure.

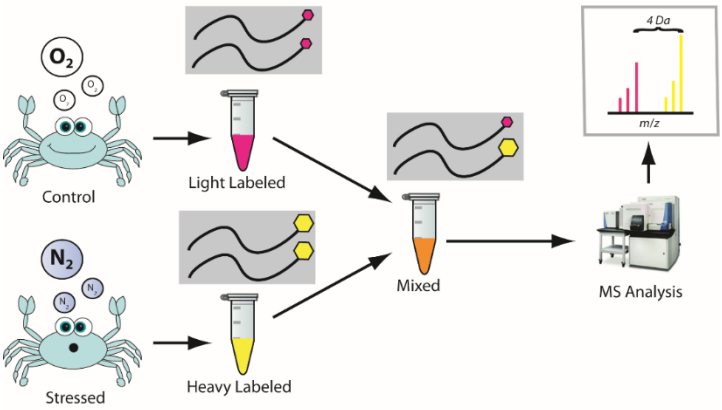

Figure 7. Schematic of the workflow for comparing a control and hypoxia stressed crab by MS. After collecting the tissues of interest, the samples are extracted and differentially labeled using different amounts of stable isotopes. We can then mix and analyze the differentially extracted and labeled peptides by MS, where we see a mass difference between these two samples.

Chapter 10

Conclusions and Future Directions

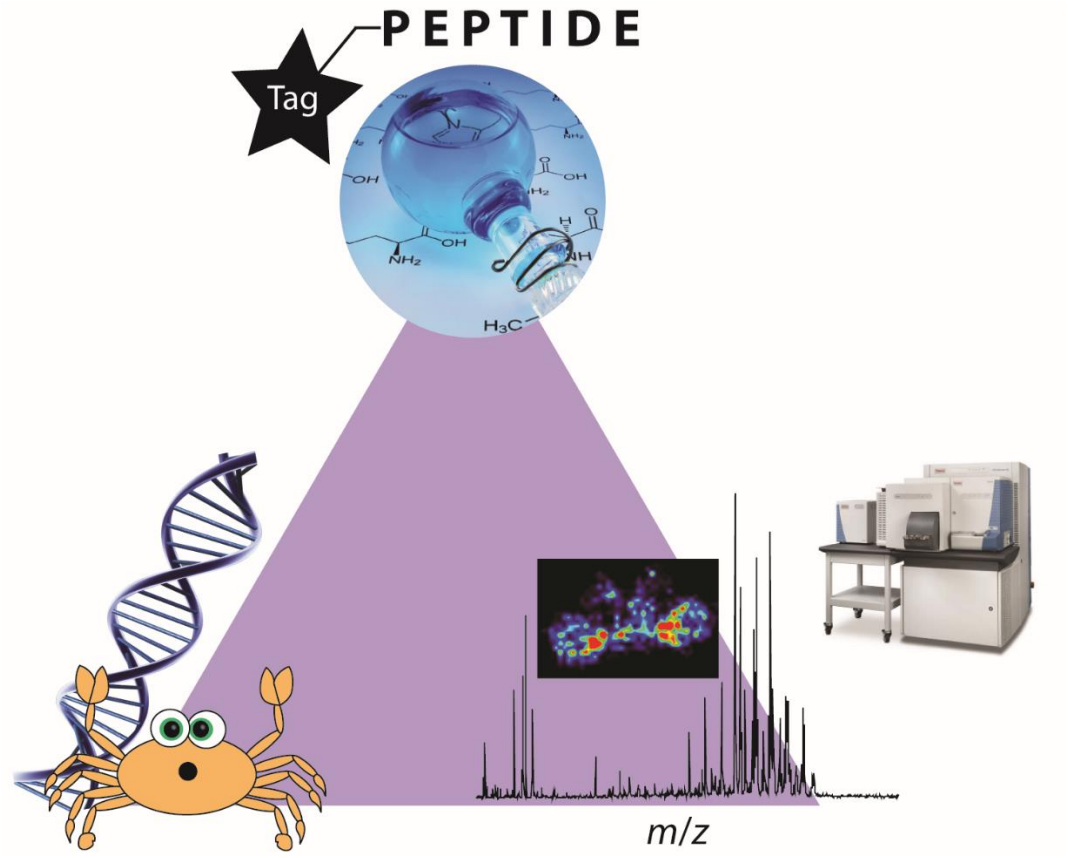

Conclusions

In this dissertation, methods utilizing mass spectrometry (MS) (*i.e.*, electrospray ionization (ESI) and matrix-assisted laser desorption/ionization (MALDI)) and MS imaging were developed to characterize the changes of neuropeptides due to stress in a crustacean model system. In particular, a bridge between translational and basic science research is made evident.

Hypoxia (*i.e.*, low oxygen (O_2) levels) are well-documented in coastal estuaries, where many aquatic species live, and also in human disease (*e.g.*, cancer).[1, 2] In *Chapter 3* we quantified the differences between several neuropeptides in hypoxia stress by using MALDI-MS in three major neuropeptide-rich tissues using 2-plex dimethyl labeling. We were able to infer several neuropeptidomic trends that correlated with hypoxic severity (50%, 20%, and 10% O_2 water saturation) in the blue crab, *Callinectes sapidus*. Neuropeptides that showed distinct trends include crustacean hyperglycemic hormone (CHH) precursor related peptide (CPRP) LSSSNSPSSTLPLG, which showed significant increase in the brain and pericardial organ (PO) regardless of the severity of hypoxia, while others (*e.g.*, orcokinin NFDEIDRSGFGF) had a very unique trend, including a possible "switching point" for survival mechanisms between 20% and 10% O_2 water saturation. This was demonstrated by no change at 50% O_2, a significant increase at 20% O_2, and either a significant decrease or return to baseline for 10% O_2 exposure. However, it would require more experiments to determine exactly at what O_2 level this switch begins along with quantifiable behavioral analysis to confirm our results.

Chapter 4 provided evidence in how crustaceans handled the severe hypoxia (10% O_2 water saturation) over time (0, 1, 4, and 8 hours). This method expanded our quantitation multiplexing from 2- to 4-plex dimethyl labeling along with incorporating both MALDI- and ESI-MS to improve neuropeptidomic coverage. In general, MALDI- and ESI-MS showed

complementary coverage, with 28 and 24 neuropeptides identified, respectively, and only four were overlapping between the two ionization methods. It should be noted that while five different tissue types were analyzed, only 3 (*i.e.,* brain, PO, and sinus gland (SG)) provided peptides that could be evaluated for statistical significance. Ultimately, several distinguishing trends were seen. One neuropeptide (*e.g.,* allatostatin A-type DPYAFGLRHTSFVLYAFGLamide) showed downregulation for 1 hour and 4 hour exposure but returned to a "control" level after 8 hours. Others showed no changes until the longest time point (*i.e.,* 8 hours) (*e.g.,* allatostatin B-type STNWSSLRSAWamide). The most surprising trend showed oscillating changes in the neuropeptide expression, meaning it became up or down regulated only at 1 hour or 8 hours, but not at 4 hours (*e.g.,* Others HL/IGSL/IYRamide). Even with using both MALDI- and ESI-MS, we are still plagued by relatively low number of identifications, limiting our abilities to understand the true global changes due to hypoxia stress overtime. More biological replicates will be investigated to expand our identification and biological understanding.

Medically, hypoxia is interesting, but an analogous stress, hypercapnia (*i.e.,* low O_2 levels with high carbon dioxide (CO_2) levels), is more relevant to human disease and respiratory distress.[3, 4] In *Chapter 5*, we studied the localization differences among neuropeptides in the brain between two different severities of hypoxia (severe and mild) and hypercapnia stress using MALDI-MS imaging. In order to profile more neuropeptides, a wash method of 50:50 ethanol:H_2O for 10 seconds was developed to effectively enrich crustacean neuropeptide numbers (1.15x) and their intensity (5.28x). Using this new method, several neuropeptides were imaged, RFamides in particular, that were shown to have significant differences due to either hypoxia or hypercapnia stress. Interestingly, neuropeptide Y (NPY), which has already been

implicated in hypoxia stress in higher organisms, is homologous to crustacean RFamides.[5-7] The variety of changes seen for different RFamides, including LFDDRLRFamide (mass-to-charge ratio (*m/z*) 1071.562), and their various roles in crustacean nervous system demonstrate the (a) dynamic roles of NPY, (b) validity of studying isoforms in higher organisms, and (c) importance of studying simpler systems to examine a global effect of a stressor.

In *Chapter 6*, we investigated another common environmental stressor for crustacean species: salinity stress.[8, 9] In our study, two different color morphs of the green shore crab showed distinct responses to salinity (*i.e.*, high (60 parts per thousand (ppt)) and low (0 ppt)), with the green color morph showing better tolerance. Even so, multiple neuropeptide families exhibited changes in their relative abundances, including RFamides, RYamides, allatostatins B-type, and orcokinins due to salinity stress, with distinct responses depending on the color morph. The time course study and MALDI-MS imaging also provided dynamic information on how these crustaceans reacted to salinity stress. As we have seen with hypoxia stress, severity, temporal, and localization aspects should be considered, as stress is a dynamic process that is not unidirectional in neuropeptide expression or release.

This thesis has also focused on developing and utilizing different strategies to better quantify neuropeptides and other biomolecules. Beyond 2-plex and 4-plex dimethyl labeling, we can multiplex up to 5-plex with dimethyl labeling (DM) and isotopic N,N-dimethyl leucine (iDiLeu), which has allowed researchers to build in-solution calibration curves to absolutely quantify a molecule of interest in a single MS run.[10] In order to make MS imaging more quantitative, in *Chapter 7*, we took advantage of these 5-plex labeling strategies to build an on-tissue calibration curve on tissue. This required labeling of the biomolecules in the tissue initially with one label, which was the focus of the study. More optimization is required to get consistent,

confident labeling of crustacean brain neuropeptides, which were used for initial method optimization. One neuropeptide (HL/IGSL/IYRamide, *m/z* 844.479) showed >95% labeling when the tissue section was incubated in 50:50 methanol:H_2O, although we were unable to reproduce this result. Throughout the literature, on-tissue derivatization is becoming more common, so promise still exists for both iDiLeu and DM for *in situ* labeling for the absolute quantitation of neuropeptides.

Many of the tags utilized throughout this thesis work have large spacings (2-4 Daltons (Da)) that increase spectral complexity. *Chapter 8* delves into developing, synthesizing, and characterizing a new, MS-compatible quantitative tag entitled dimethyl pyrimidinyl ornithines (DiPyrO).[11] Eight different tag structures incorporating six different heavy isotopic signatures were developed that have mDa mass spacings between each other. At low resolution, the individual, quantifiable peaks are hidden, but, at high resolution, we are able to differentiate the small mass spacings between each tag. Researchers are able to utilize these tags using previous and newer generation LTQ Orbitrap technology with and without double labeling, respectively. Furthermore, beyond quantitation, we demonstrated this new tag's ability to improve fragmentation and thus identification of tryptic peptides from yeast, which makes it a valuable new addition to the quantitative proteomics tool-kit.

Chapter 9 provides a description of a majority of this work for the general public. Overall, this work improved techniques for both qualitative and quantitative profiling of neuropeptides and other biomolecules, which can be applied to answer other challenging questions in analytical chemistry, biochemistry, and pharmaceutical sciences.

Future Directions

Crustaceans survive hypoxia stress with a complex, dynamic response curated by neuropeptides. In order to understand the "switching point" for the blue crab's survival mechanism we observed in *Chapter 3*, more detailed hypoxic severity control and analysis is required, although this is limited by our ability to accurately expose the crab to hypoxia. Due to the constant oxygen exchange between the air and water, it is hard to accurately measure or maintain the true oxygen level in the water. Building a relay system that would constantly monitor and adjust the water tank with either nitrogen (lower oxygen) or oxygen (increase oxygen) would help to control and modulate the hypoxia conditions more precisely.[12, 13] This will also facilitate future studies outlined in *Chapter 4*. Crustaceans are actually regularly exposed to hypoxia for days at a time, so a long term (*e.g.*, 30 days) or a Diel's-cycling hypoxia (*i.e.*, daily periods of hypoxia) study should be considered.[14]

The developed method in *Chapter 5* can be applied to other crustacean based studies (*e.g.*, feeding) or even tissue groups. For example, the PO is known to be difficult to image due to the rapid degradation of neuropeptides in the tissue, with *Chapter 6* showing examples MALDI-MS images of the PO.[8] In order to expand the types of washes and also molecular species that can be washed, formalin fixation is currently being investigated for its power to cross-link neuropeptides and thus "lock them in place" when we wash. This would allow us to utilize both extremes (hydrophobic and hydrophilic solutions) to remove contaminants while keeping the neuropeptides stationary for MALDI-MS imaging. Currently, challenges remain, as neuropeptides may not have the appropriate structure (*i.e.*, several primary amines) for proper cross-linking.

For *Chapters 3* and *4*, complementary hemolymph studies are required to truly understand if the neuropeptides that are downregulated are (a) being released to their target or (b)

degrading. One challenge for this study is the complex nature of hemolymph, which can quench or block the signal of neuropeptides, limiting their analysis by MS. Several methods for concentrating, separating, or enriching crustacean neuropeptides are being developed to improve this analysis.[15-17] This is especially true for live hemolymph sampling (*i.e.*, microdialysis).[15, 18] Also, in general, for *Chapters 3-6*, these stressors should be expanded to different species of crabs in order to understand if we are observing species-specific or general decapod crustacean stress response.

Investigating hypoxia and salinity stress has prompted the investigation of other environmental stressors. Other novel stressors of interest in the Lingjun Li lab are pH (*i.e.*, hypercapnia), copper exposure, and nanoparticles. Another area of interest is neuromodulation due to known addicting behaviors for humans, such as feeding or alcohol.[19] Neuropeptides are thought to be major players in the regulation of addiction (*e.g.*, drugs or food) and the resulting motivating behaviors. Several human neuropeptides involved in stress pathways, such as corticotropin-releasing factor, dynorphin, and NPY, have been implicated in alcohol addiction.[20] Furthermore, several drugs that are rewarding in humans also produce the same effects in crustaceans.[21] Our lab has previously investigated the acute and long term effects of alcohol exposure in the rock crab, *Cancer irroratus*, so expanding this work to other common species, such as the blue crab and Jonah crab, *Cancer borealis*, would be easy to implement. Also, compared to the original study, other neuroendocrine organs, such as the TG and CoG, will be added to the commonly targeted tissues (*i.e.*, brain, PO, and SG). In order to compare several different conditions, utilizing isotopic dimethyl labeling (2- or 4-plex) or even further multiplexing with N, N-dimethyl leucine (DiLeu), which boasts up to 12-plex comparison at the tandem MS level, would be good directions depending on the final goals.[22]

Appendix V discusses another interesting comparison of male versus female crustacean neuropeptide differences. Many of our crustacean studies focus on one gender of a species. For example, the Asian Midway Market (Madison, WI) supplies only female blue crabs, while vendors like The Fresh Lobster Company (Gloucester, MA) sell only male Jonah crabs. For our studies, we were able to get both male and female blue crabs from The LA Crawfish Company (Natchitoches, LA). Using blue crabs, we saw significant differences in neuropeptidomes between the male and female groups. This means that all our stress studies should be either (a) gender specific or (b) consider both genders in the study to ensure accurate results and comparisons. This factor along with consideration of seasons and tissue types for pooling could all affect the outcome of our experiments.[23]

While we have developed methods to accurately quantify peptides (*i.e.,* iDiLeu and dimethyl labeling), it is clear that better methods are required to really profile the depth of dynamic changes due to stress in crustaceans and other model organisms.[8, 10] For example, DiPyrO (*Chapter 8*) could be used for higher multiplexing of crustacean species.[11] Dimethyl labeling also improved fragmentation of peptides, but DiPyrO may provide a slight increase in this effect. DiLeu tagging also provides higher multiplexing but works at the tandem MS level.[22] This means that if a neuropeptide is not selected for fragmentation then it cannot be quantified, making it challenging to implement for crustacean neuropeptides due to their low abundance. Currently, our lab is working towards optimizing the liquid chromatography and instrumental parameters for crustacean neuropeptides labeled with 4-plex DiLeu with the hope of expanding to 12-plex. Another example of quantitative method development appears in *Chapter 7*, where we explore expanding MALDI-MS imaging technology beyond label-free comparison.[24] On-tissue derivatization is becoming more common in the literature, although its application to

quantitation is limited. While this research was unsuccessful as of now, hope still remains with the variety of tagging systems and our abilities to incorporate different isotopes into simple structures. One possibility is that crustacean neuropeptides may be difficult to label due to their low concentration, and targeting other molecular species, such as tryptic peptides or metabolites, may yield more successful outcome.[24]

Finally, in general, peptidomics is a challenging field due to (a) their low concentration and (b) the lack of established data processing workflows and software. Many of the tools utilized in the Lingjun Li Lab (*e.g.,* PEAKS, Proteome Discoverer, MaxQuant) all hold inherent disadvantages for our research due to our relatively low numbers of identifications compared to proteomics. This means we have difficulty applying the same statistical analyses or data integrity filters (*e.g.*, false discovery rate) in order to filter the most important or obvious changes due to stress. Furthermore, the manual processing needed leads to high rates of human error and bias. This is a challenge that will remain in the field until better, more specific bioinformatic tools and sensitive instrumentation are available. Furthermore, the availability of new lasers with high repetition rate and better focused beam (*i.e.,* Bruker RapifleX) have improved the community's ability to image neuropeptides and other molecules,[25] but the fact remains that our computational processing abilities for imaging-based data sets are far behind what is needed due to the (a) massive data set sizes, (b) lack of spatial resolution compared to microscopy images, and (c) lack of online databases to share methods and results across labs.[24] Continued efforts from the Lingjun Li lab and the scientific community will directed toward addressing some of these longstanding challenges.

Overall, this thesis provides a starting point for several studies related to crustacean stress, neuropeptides, and novel quantitation strategies. Beyond application to other model

system and instrumental platforms, this dissertation will assist researches in bioscience, neuropeptidomics, and analytical chemistry, and hopefully inspire the next group of researchers.

References

1. Diaz, R. J.; Rosenberg, R., *Oceanography and Marine Biology - an Annual Review, Vol 33* **1995,** *33*, 245-303.

2. Santana, R.; Lessa, G. C.; Haskins, J.; Wasson, K., *Estuaries and Coasts* **2018,** *41* (1), 99-113.

3. Hardy, K. M.; Burnett, K. G.; Burnett, L. E., *American Journal of Physiology-Regulatory Integrative and Comparative Physiology* **2013,** *305* (11), R1356-R1366.

4. Byrne, M., Impact of Ocean Warming and Ocean Acidification on Marine Invertebrate Life History Stages: Vulnerabilities and Potential for Persistence in a Changing Ocean. In *Oceanography and Marine Biology: an Annual Review, Vol 49*, Gibson, R. N.; Atkinson, R. J. A.; Gordon, J. D. M., Eds. Crc Press-Taylor & Francis Group: Boca Raton, 2011; Vol. 49, pp 1-42.

5. Husson, S. J.; Mertens, I.; Janssen, T.; Lindemans, M.; Schoofs, L., *Prog Neurobiol* **2007,** *82* (1), 33-55.

6. Dockray, G. J., *Exp Physiol* **2004,** *89* (3), 229-35.

7. Coast, G. M.; Schooley, D. A., *Peptides* **2011,** *32* (3), 620-31.

8. Zhang, Y.; Buchberger, A.; Muthuvel, G.; Li, L., *Proteomics* **2015**.

9. Wang, J. H.; Zhang, Y. Z.; Xiang, F.; Zhang, Z. C.; Li, L. J., *Journal of Chromatography A* **2010,** *1217* (26), 4463-4470.

10. Greer, T.; Lietz, C. B.; Xiang, F.; Li, L. J., *Journal of the American Society for Mass Spectrometry* **2015,** *26* (1), 107-119.

11. Frost, D. C.; Buchberger, A. R.; Li, L., *Anal Chem* **2017**.

12. Hassell, K. L.; Coutin, P. C.; Nugegoda, D., *Journal of Experimental Marine Biology and Ecology* **2009,** *371* (2), 147-154.

13. Grecay, P. A.; Stierhoff, K. L., *Journal of Experimental Marine Biology and Ecology* **2002,** *280* (1-2), 53-62.

14. Cheek, A. O., *Journal of Experimental Marine Biology and Ecology* **2011,** *409* (1-2), 13-20.

15. Jiang, S.; Liang, Z. D.; Hao, L.; Li, L. J., *Electrophoresis* **2016,** *37* (7-8), 1031-1038.

16. Schmerberg, C. M.; Li, L. J., *Analytical Chemistry* **2013,** *85* (2), 915-922.

17. Hou, X. W.; Xie, F.; Sweedler, J. V., *Journal of the American Society for Mass Spectrometry* **2012,** *23* (12), 2083-2093.

18. Liang, Z. D.; Schmerberg, C. M.; Li, L. J., *Analyst* **2015,** *140* (11), 3803-3813.

19. Zhang, Y.; DeLaney, K.; Hui, L.; Wang, J.; Sturm, R. M.; Li, L., *J Am Soc Mass Spectrom* **2018**.

20. Skibicka, K. P.; Hansson, C.; Alvarez-Crespo, M.; Friberg, P. A.; Dickson, S. L., *Neuroscience* **2011,** *180*, 129-137.

21. Nathaniel, T. I.; Panksepp, J.; Huber, R., *Behavioural Brain Research* **2009,** *197* (2), 331-338.

22. Frost, D. C.; Li, L. J., High-Throughput Quantitative Proteomics Enabled by Mass Defect-Based 12-Plex DiLeu Isobaric Tags. In *Quantitative Proteomics by Mass Spectrometry, 2nd Edition*, Sechi, S., Ed. Humana Press Inc: Totowa, 2016; Vol. 1410, pp 169-194.

23. Lycett, K. A.; Chung, J. S.; Pitula, J. S., *Plos One* **2018,** *13* (2), 14.

24. Buchberger, A. R.; DeLaney, K.; Johnson, J.; Li, L. J., *Analytical Chemistry* **2018,** *90* (1), 240-265.

25. Potocnik, N. O.; Porta, T.; Becker, M.; Heeren, R. M. A.; Ellis, S. R., *Rapid Communications in Mass Spectrometry* **2015,** *29* (23), 2195-2203.

Appendix I

List of Publications, Presentations, Patents, and Grants

Publications

1. **Amanda R. Buchberger,** Kellen DeLaney, Yang Liu, Kylie Helfenbein, Nhu Vu, Lingjun Li**. "**Mass Spectrometric Profiling of Neuropeptides in *Callinectes sapidus* during Hypoxia Stress**."** In Preparation, 2018.

2. **Amanda R. Buchberger**[¥], Christopher Sauer[¥], Kellen DeLaney, Nhu Vu, Lingjun Li. "A Temporal Study of the Perturbation of Crustacean Neuropeptides Due to Severe Hypoxia Using 4-Plex Reductive Dimethylation." In Preparation, 2018. [¥]Co-first Authors

3. **Amanda R. Buchberger**, Nhu Vu, Jillian Johnson, Lingjun Li. "Improved Sample Preparation for Comparative MALDI-MS Imaging of Neuropeptides in the Crustacean Brain under Hypoxia and Hypercapnia Stress." In Preparation, 2018.

4. Yang Liu, **Amanda R. Buchberger**, Kellen DeLaney, Zihui Li, Lingjun Li. "Multifaceted Mass Spectrometric Investigation of Neuropeptide Changes in the Blue Crab, *Callinectes sapidus*, in Response to Ocean Acidification." In Preparation, 2018.

5. Clara Hu[¥], Kylie Helfenbein[¥], **Amanda R. Buchberger**, Kellen DeLaney, Yang Liu, Lingjun Li. "A Study of Gender Differences in Crustaceans" In Preparation, 2018. [¥]Co-first Authors

6. Xiaofang Zhong, Christopher Lietz, Xudong Shi, **Amanda R. Buchberger**, K. Craig Kent, Lingjun Li. "12-plex Isobaric DiLeu-enabled Quantitative Proteomics and Phosphoproteomics Reveal TGF-B Signaling Stimulates Vascular Smooth Muscle Cells De-differentiation." In Preparation, 2018

7. Ling Hao, Yuerong Zhu, Pingli Wei, Jillian Johnson, **Amanda R. Buchberger**, Dustin Frost, John W. Kao, Lingjun Li. "Metandem: A Software Tool for Mass Spectrometry-based Isobaric Labeling." In Preparation, 2018.

8. **Amanda R. Buchberger**[¥]**,** Jillian Johnson[¥], Lingjun Li. "Quantitative Proteomics for Analyses of Multiple Samples in Parallel with Chemical Perturbation." Invited Book Chapter. *Mass Spectrometry-based Chemical Proteomics*. Submitted, 2017. [¥]Co-first authors

9. Bingming Chen, Feng Yu, Dustin Frost, Xuefei Zhong, **Amanda R. Buchberger**, Jillian Johnson, Meng Xu, Mariam Kim, Diane Puccetti, Carol Diamond, Chrysanthy Ikonomidou, Lingjun Li. "Quantitative Glycomic Analysis by Mass Defect-Based Dimethyl Pyrimidinyl Ornithine (DiPyrO) Tags and High-Resolution Mass Spectrometry." *Analytical Chemistry*. Technical Note. Accepted, 2018.

10. Xiaoyue Jiang, Feng Xiang, Chenxi Jia, **Amanda R. Buchberger**, Anita Metzler, Lingjun Li. "Relative quantitation of neuropeptides at multiple developmental statges of the American lobster using novel N, N-dimethyl leucine isobaric tandem tags." Invited Contribution. *ACS Chemical Neuroscience*. Accepted, 2018.

11. Kellen Delaney, **Amanda R. Buchberger**, Lingjun Li. "Identification, Quantitation, and Imaging of the Crustacean Peptidome." Invited Book Chapter, Springer. *Methods in Molecular Biology*. 2018, 1719: 247-269.

12. Kellen Delaney[¥], **Amanda R. Buchberger**[¥], Lingjun Li. "New techniques, applications and perspectives in neuropeptide research." Invited Contribution. *Journal of Experimental Biology.* 2018, 221:jeb151167. [¥]Co-first authors

13. **Amanda R. Buchberger**, Kellen DeLaney, Jillian Johnson, Lingjun Li. "Mass Spectrometry Imaging: A Review in Emerging Advancements and Future Insights." Invited Contribution. *Analytical Chemistry*. 2018, 90(1): 240-265.

14. Dustin Frost, **Amanda R. Buchberger**, Lingjun Li. "Development of Dimethyl Pyrimidinyl Ornithines (DiPyrO) as Mass Defect-Based Tags for Quantitative Proteomics." *Analytical Chemistry*, 2017, 89(20): 10798-10805.

15. Ling Hao, Jillian Johnson, Christopher Lietz, **Amanda R. Buchberger**, Dustin Frost, John W. Kao, Lingjun Li. "Mass Defect-Based N,N-Dimethyl Leucine (mdDiLeu) Labels for Quantitative Proteomics and Amine Metabolomics of Pancreatic Cancer Cells." *Analytical Chemistry*, 2016, 89(2): 1138-1146.

16. Yuzhuo Zhang[¥], **Amanda R. Buchberger**[¥]**,** Gajan Muthavel, Lingjun Li. "Expression and distribution of neuropeptides in the nervous system of the crab *Carcinus maenas* and their roles in environmental stress." Invited Contribution. *PROTEOMICS*, 2015, 15 (23-24): 3969-79. [¥]Co-first authors

17. **Amanda R. Buchberger**, Qing Yu, Lingjun Li. "Advances in Mass Spectrometric Tools for Probing Neuropeptides." Invited Contribution. *Annual Review of Analytical Chemistry*, 2015, 8: 485-509.

18. Ruibing Chen, Mingming Xiao, **Amanda R. Buchberger**, Lingjun Li. "Quantitative neuropeptidomics study of the effects of temperature change in the crab *Cancer borealis*." *J. Proteome Res.*, 2014, 13 (12): 5767-76.

Presentations

1. **Amanda R. Buchberger**, Lingjun Li. "Improved Sample Preparation for Comparative MALDI-MS Imaging of Neuropeptides in the Crustacean Brain under Hypoxia and Hypercapnia Stress", *ASMS Conference on Mass Spectrometry & Allied Topics,* San Diego, CA, June 2018.

2. **Amanda R. Buchberger**, Lingjun Li. "*In situ* Labeling for the Absolute Quantitation of Crustacean Neuropeptides with Mass Spectrometric Imaging", *ASMS Conference on Mass Spectrometry & Allied Topics,* Indianapolis, IA, June 2017.

3. **Amanda R. Buchberger**, Lingjun Li. "Qualitative and Quantitative Analysis of Crustacean Neuropeptides after Hypoxia Exposure", *ASMS Sanibel Conference,* Clearwater Beach, FL, Jan 2017. Selected for 3 min Oral Intro.

4. **Amanda R. Buchberger**, Lingjun Li. "Development of Dimethyl Pyrimidinyl Ornithines (DiPyrO) as Mass Defect-Based Tags for Quantitative Proteomics", *ASMS Conference on Mass Spectrometry & Allied Topics,* San Antonio, TX, June 2016.

5. **Amanda R. Buchberger**, Lingjun Li. "Mass Spectrometric Investigation of Crustacean Neuropeptides and Their Roles in Environmental Stress", *University of Wisconsin-Madison Department of Chemistry Analytical Division Seminar*. Madison, WI, October 2015. Invited Seminar.

6. **Amanda R. Buchberger**, Lingjun Li. "Multifaceted Mass Spectrometric Profiling of Neuropeptides in *Callinectes sapidus* during Hypoxia", *ASMS Conference on Mass Spectrometry & Allied Topics*, St. Louis, MO, June 2015.

Patents

1. Dustin Frost; **Amanda R. Buchberger**; Lingjun Li. 2015. Mass Defect-Based Multiplex Dimethyl Pyrimidinyl Ornithine (DiPyro) Tags for High-Throughput Quantitative Proteomics and Peptidomics. *P150350WO01US.* Patent Pending.

Grants

1. Multifaceted Mass Spectrometric Investigation of Neuropeptides in *Callinectes sapidus* during Hypoxia
   Funding Agency: NIH/NIGMS
   Type: NRSA F31 Predoctoral Fellowship
   Duration: June 1st, 2016 – May 31st, 2018
   Amount Received: $30,724/year
   Received an impact score of 20 and ranked at 9%.

Appendix II

Crustacean-Focused Methods: An Update

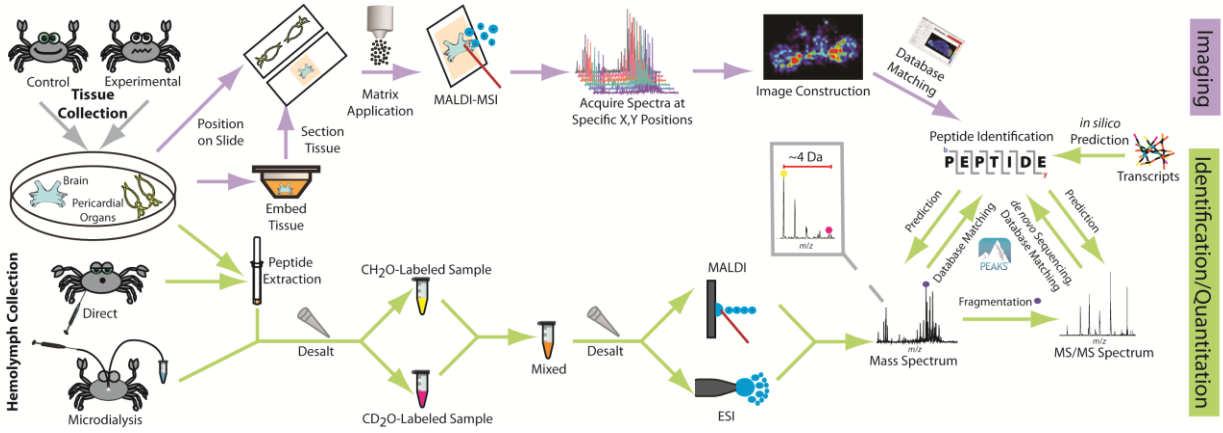

Additional information including on-tissue labeling, tissue section washing, and crustacean cell culture was added.

Modified from:

Kellen DeLaney, **Amanda R. Buchberger**, Lingjun Li. "Identification, Quantitation, and Imaging of the Crustacean Peptidome." Invited Book Chapter. *Methods for Molecular Biology*. 1719, 247-269, 2018. *DOI*: 10.1007/978-1-7537-2_17

Key Words: Crustacean, MALDI Mass Spectrometry Imaging, Microdialysis, Isotopic/Isobaric Labeling, *De novo* Sequencing

Abstract

Crustaceans serve as a useful, simplified model for studying peptides and neuromodulation, as they contain numerous neuropeptide homologs to mammals and enable electrophysiological studies at the single-cell and neural circuit levels. In particular, crustaceans contain well-defined neural networks, including the stomatogastric ganglion, oesophageal ganglion, commissural ganglia, and several neuropeptide-rich organs, such as the brain, pericardial organs, and sinus glands. Due to the lack of a genomic database for crustacean peptides, an important step of crustacean peptidomics involves the discovery and identification of novel peptides and the construction of a database, more recently with the aid of mass spectrometry (MS). Herein, we present a general workflow and detailed methods for MS-based peptidomic analysis of crustacean tissue samples and circulating fluids. In conjunction with profiling, quantitation can also be performed with isotopic or isobaric labeling. Information regarding the localization patterns and changes of peptides can be studied via mass spectrometry imaging. Combining these sample preparation strategies and MS analytical techniques allows for a multi-faceted approach to obtaining a deep knowledge of crustacean peptidergic signaling pathways.

A generic workflow is shown in **Figure 1**.

Materials

Chemicals and Equipment

1. Ultrapure water (H_20), used for all of the solutions listed below
2. Methanol (MeOH)
3. Acetonitrile (ACN)
4. Formic acid (FA)
5. Glacial Acetic Acid (GAA)
6. Acidified MeOHl (90:9:1 MeOH:H_2O:GAA)
7. Isotopic formaldehyde solution (1% volume (v)/v)
8. Borane pyridine solution (30 mM)
9. Ammonium bicarbonate solution (100 mM)
10. Gelatin (100 mg/mL dissolved in H_2O)
11. Matrix-assisted laser desorption/ionization (MALDI) matrix
    a. 2,5-dihydroxybenzoic acid (DHB) dissolved in 50:50 MeOH:H_2O with 0.1% FA (150 mg/mL for spots; 40 mg/mL for imaging)
    b. α-cyano-4-hydroxycinnamic acid (CHCA) dissolved in 50:50 ACN:H_2O with 0.1% FA (10 mg/mL for spots; 5 mg/mL for imaging)
12. Glass manual homogenizer (*e.g.*, Wheaten 1 mL Tissue Grinder, Tenbroeck)
13. Plasic or teflon pestle (*e.g.* Wheaten 1 mL Tissue Grinder, Tapered Pestle)
14. Bath sonicator
15. Centrifuge capable of up to 16,000 g and able to fit microfuge tubes and microfilters (*e.g.*, Eppendorf 5424 R)
16. Vacuum centrifuge/concentrator, such as a SpeedVac
17. 3 kDa or 10 kDa Molecular Weight Cutoff (MWCO) device (*e.g.*, Amicon Ultra)
18. Reversed-phase C18-packed pipette tips (*e.g.*, Omix 100 µL Tips or Millipore P10 ZipTips
19. Sprayer for MALDI imaging (*e.g.*, HTX Technologies TM Sprayer)
20. Crab saline (440 mM NaCl, 11 mM KCl, 26 mM $MgCl_2$, 13 mM $CaCl_2$, 11 mM TRIS, 5 mM maleic acid, adjusted to pH 7.45 with HCl or NaOH. Stored at 4°C)
21. Tweezers
22. Plastic cup (1 inch Height x 1 inch Diameter)
23. Razor blade
24. Syringe pump
25. Syringe
26. Automated sample collector with temperature control
27. Ethanol (EtOH)
28. Sodium hypochlorite
29. Dry box (*e.g.*, desiccator with desiccant) or vacuum desiccator
30. Manual tissue staining system (*e.g.*, Tissue-Tek 12 Well Slide Staining Set)
31. Kim wipe
32. Leibovitz L-15 medium (1x)

33. Antibiotics (*e.g.*, Corning Antibiotic Antimycotic Solution (100x))
34. Sucrose
35. Vacuum Filter with 0.22 μm pore size (*e.g.*, Corning Disposible Vacuum Filtration System, 0.22 μm PES)
36. Vacuum system
37. Tubes (Eppendorf: 0.6, 1.5 and 2 mL; Conical: 15 and 50 mL)
38. Sterilization pouches (various sizes; *e.g.*, 10" by 15")
39. Cell scraper
40. Biosafety cabinet
41. 1X Phosphate buffer saline (PBS) without Ca^{2+} and Mg^{2+}
42. Tissue culture flasks (*e.g.*, 6-well, 12-well, 24-well, T25, and T75 flasks)
43. Typsin-EDTA (0.25%)

Instrumentation and Software

For quantitation and profiling, a Hybrid Quadrupole-Orbitrap Mass Spectrometer (we use Thermo Q-Exactive) with a nano-electrospray ionization (ESI) source can be coupled to a UPLC system (we use Waters nanoAQUITY) for separation of peptides with MS and MS/MS analysis for identification and quantitation. For imaging and complementary profiling, we use a hybrid MALDI- Ion Trap-Orbitrap Mass Spectrometer (Thermo MALDI-LTQ-Orbitrap XL). Other mass spectrometers with a MALDI source and an ESI source may also be used. The associated vendor software Xcalibur and ImageQuest can be used for data analysis and image processing. For MS/MS identification, *de* novo sequencing software can be used, such as PEAKS [1], MaxQuant [2], or PepNovo [3]. Additional image processing can be performed using freely available software, such as MSiReader [4], Image J, and SciLs. In my thesis, I mainly use Java for MALDI-MS data analysis, PEAKS for ESI-MS/MS data analysis, and MSiReader and SCiLs for MALDI-MS imaging data analysis.

Methods

Identification and Quantitation

1.) Sample Collection and Extraction
    a. Tissues
        i. Collection

1. Collect the tissue of interest through dissection [5, 6].
2. Place tissues in a 0.6 mL microfuge tube with 10-50 microliters of acidified MeOH.
3. Store at -80° C until ready to use (*see* **Note 1**).

ii. Extraction

1. Add 100 microliters of acidified MeOH per tissue to a glass manual homogenizer (*see* **Notes 2-5**).
2. Move the tissues to the homogenizer using tweezers. Transfer the storage solution as well.
3. Homogenize the tissue until no large particles are visible. Transfer the liquid to a clean 1.5 mL microfuge tube.
4. Add 100 microliters of acidified MeOH to the homogenizer, breaking up any residual particles. Transfer to same microfuge tube. Repeat once more.
5. Sonicate mixture for 10 minutes.
6. Centrifuge mixture for 20 minutes at >16,000 g.
7. Transfer the supernatant to a new 1.5 mL tube.
8. Rinse the pellet with 100 microliter of acidified MeOH and break it up with a Teflon pestle.
9. Repeat steps 5-7. Discard the pellet.
10. Dry down supernatant in a vacuum centrifuge on medium heat (*see* **Note 6**).

b. Hemolymph

i. Collection

1. Place the crab on ice for 5-10 minutes. Afterwards, place it in a metal dishpan on its back with its tail pointing towards you.
2. Prepare a 25g needle by connecting it to a 1 mL plastic syringe.
3. Place the needle into an exposed leg joint of the crab.
4. Pull up on the syringe to create a vacuum. Hemolymph should come out immediately. If not, wiggle the needle at different angles until the liquid is withdrawn.
5. Add an equal amount of acidified MeOH to the collected hemolymph in a 1.5 or 2 mL microfuge tube (*see* **Note 7**). A protein precipitate will be produced.
6. Store at -80°C till ready to use (*see* **Note 1**).

ii. Extraction

1. Using the Teflon pestle, break up the precipitate in the microfuge tube to produce a homogenous solution.
2. Sonicate tube for 10 minutes.
3. Centrifuge mixture for 20 minutes at >16,000 g.
4. Transfer the supernatant to a new 2 mL microfuge tube.
5. Rinse the pellet with 500 microliters of acidified MeOH and break it up with a Teflon pestle.

6. Repeat steps 2-5. Discard the pellet.
7. Dry down supernatant in vacuum centrifuge on medium heat (*see* **Note 6** *and* **8)**.

iii. Microfiltration

1. Add 200 microliters of 0.1 M NaOH solution to the 3 kDa or 10 kDa MWCO device (*see* **Note 9**). Centrifuge at >14,000 g for 5 minutes.
2. Rinse MWCO device with 500 microliters of 50:50 H_2O:MeOH. Centrifuge for 10 minutes at >14,000 g.
3. Dissolve sample in 500 microliters of 30:70 H_2O:MeOH, vortex, and sonicate for 10 minutes.
4. Add the sample to the MWCO device and run it through the membrane by centrifuging for 30 minutes at >14,000 g. Save the flow-through from this step by placing it in a 1.5 mL microfuge tube (*see* **Note 10**).
5. Rinse the membrane with 100 microliters of 30:70 H_2O:MeOH. Collect the flow-through and add it to the tube from the previous step.
6. Dry down the flow-through in vacuum centrifuge on medium heat.

c. Microdialysis (*see* **Notes 11** *and* **12**)

i. Collection

1. Rinse probe with H_2O and then crab saline using a 3 mL plastic syringe and a syringe pump set to 0.5 microliters per minute.
2. Surgically implant the probe into the animal directly above its heart [7].
3. Allow the animal to recover for 24 to 48 hours (*see* **Note 13**).
4. Collect samples at desired time points. Collection can be done manually with a 0.6 mL centrifuge tube on ice or using an automated sample collector set at 4°C (*see* **Notes 14-16**).
5. Add enough FA to make the total concentration 0.1% (v/v).
6. Store samples at -80°C if they are not being analyzed immediately. However, samples should be used as soon as possible to avoid degradation (*see* **Note 17**).

2.) Desalting

a. Dissolve each sample in 0.1% FA(10 microliters for tissues, 200 microliters for hemolymph) by vortexing and sonicating for 10 minutes. (Microdialysis samples do not need to be redissolved.) If the pH is greater than 3, add small amounts of diluted FA (*e.g.,* 10%) until the pH is below 3.

b. Using the appropriately sized reversed-phase C18 pipette tip and respective volume (*see* **Note 18**) (10 microliter for tissues and microdialysate, 100 microliter for hemolymph), flush the packing material with pure ACN at least 3 times.

c. Flush the packing material with 0.1% FA 3 times.
d. Bind the sample of interest to the packing material by flushing it with dissolved sample at least 15 times.
e. Wash the packing material with 0.1% FA 3 times to wash away salts and other unbound contaminates. Add the first wash to its own tube or to the original sample vial as a precaution in the event that nothing binds to the packing material.
f. Elute the sample into a 0.6 mL tube by flushing 10 microliters of 50:50 ACN:H_2O up and down through the packing material 10 times.
g. Dry down the eluate in a vacuum centrifuge on medium heat.

3.) Quantitative Labeling
a. Dissolve each of the samples (*e.g.,* of stressed and control) in 10 microliters of H_2O by vortexing and then sonicating for 10 minutes.
b. Add in 10 microliters of the isotopic formaldehyde to its designated channel (*see* **Notes 19** *and* **20**).
c. Add in 10 microliters of borane pyridine to each microfuge tube.
d. Place the tubes in a 37°C H_2O bath for 15 minutes to allow complete labeling.
e. Quench the reaction with 10 microliters of ammonium bicarbonate solution.
f. Mix equal amounts of each channel into a 0.6 mL tube. Do this for each set of channels.
g. Dry down mixture in a vacuum centrifuge on medium heat.

4.) Tissue Analysis and Data Acquisition
a. MALDI-MS
i. Matrix Application
1. Dissolve samples in 5 microliters of 0.1% FA for each tissue used by vortexing and sonicating for 10 minutes (*see* **Note 21**).
2. In a separate 0.6 mL tube, mix equal amounts of matrix (*see* **Note 22**) and sample (*see* **Note 23**) solutions, vortexing them to ensure complete mixing.
3. Take 1 microliter out of the tube using a pipette and spot it on the MALDI stainless steel plate. Rub the tip of the pipette along the edges of the spot circle to make sure the whole circle is filled.
4. Allow the matrix to crystalize fully before placing in the instrument.
ii. Analysis on hybrid MALDI- Ion Trap-Orbitrap-MS
1. If necessary, attach a backing plate to the MALDI stainless steel spot plate (MALDI-LTQ-Orbitrap XL requires this), and insert the plate set into the instrument by placing the plate in the correct position and pressing the appropriate button on the vendor's tune page (*e.g.,* the "Insert MALDI sample plate" button on the "MALDI source" window of the instrumental LTQ tune page).

2. Once the plate has inserted, confirm the spot in which you placed your sample and shoot the spot with an appropriate laser energy to obtain a signal intensity (approximately 1E7 for MALDI-LTQ-Orbitrap XL, *see* **Note 24**).
3. Open Thermo Xcalibur Sequence Setup, and create a new sequence (or use alternative vendor's software with regard to its specifications).
4. Fill the sequence, including the title, path (for saving the data), instrumental method (*see* **Note 25**), and spot position (*see* **Note 26**).
5. Start automated or manual acquisition of every spot of the sequence (in Xcalibur: Select each line to be run and press the "Run Sequence" button).

b. ESI-MS (*see* **Notes 27-29**)

i. Sample Prep

1. Dissolve samples (approximately 5 micrograms on average) in 5 microliters of 0.1% FA per tissue used or per 0.25 mL hemolymph by vortexing and then sonicating for 10 minutes.
2. Transfer the volume into a LC vial with a screw top septum (we use Waters vials), making sure to get all the volume to the bottom with no bubbles.

ii. MS analysis (we use Q-Exactive, Thermo)

1. Place the LC vial into the chilled sample compartment of the LC system (we use Waters NanoAquity). Remember the tray number and tray position in which the samples were placed.
2. Make sure the column system has been equilibrated to the starting conditions of the gradient you will be using.
3. On the instrument profile, set up the sequence as described above (*see* **Note 25**).
4. Select each sample in the sequence (*see* **Note 30**) to be run (in Xcalibur: press the "Run Sequence" button).

5.) Data Analysis

a. MALDI-MS

i. Average all the MS spectra collected by left-clicking and dragging across the chromatogram.
ii. Copy the raw data into your vendor's software using the exact masses (Xcalibur: by right-clicking on the spectrum, selecting "Export" and "Clipboard (exact mass))."
iii. Paste data in blank spreadsheet file (we use Excel, Microsoft).
iv. Compare the masses found to the in-house database (unlabeled or labeled) (*see* **Note 31** *and* **32**).

b. ESI-MS

i. Load the data into a *de-novo* sequencing software (we use PEAKS), creating a new project, and loading the raw data into the program (*see* **Note 33**).
ii. Process the samples (using the "PEAKS search" button), indicating any enzyme used, any PTMs expected (*see* **Note 34**), and choosing the in-house database. *De novo* sequencing will be done with the same parameters (*see* **Notes 35)**.
iii. Once the search is complete, quantitative information can be mined (*see* **Note 36**), in PEAKS by using the "Quantification" icon.

Localization by MS Imaging

1.) Sample Preparation
   a. Basics
      i. Small or thin tissue (*e.g.*, PO, STNS, STG as in Fig. 1)
         1. Collect the tissue of interest by means of dissection [6, 8], being mindful of tissue orientation (*see* **Note 37**).
         2. Hold onto tissue with tweezers and briefly submerge it in a microfuge tube of H_2O to desalt (*see* **Note 38**).
         3. Place the clean tissue directly on a glass slide. Use a marker to label the orientation of the tissue (*i.e.* which area is closest to the head, tail, etc.). Stretch the tissue out on the slide to ensure that it is lying flat and easily visible.
         4. Tissue should be analyzed immediately (*see* **Note 39**).
      ii. Large tissue (*e.g.* brain, TG)
         1. Prepare gelatin solution, vortex, and place it in a 37°C H_2O bath until fully dissolved. Keep gelatin warm while not in use.
         2. Pour enough gelatin into a plastic cup to cover the bottom of the cup. Allow the gelatin to solidify at room temperature.
         3. Collect the tissue and desalt as described above for small tissue.
         4. Place the tissue on top of the gelatin layer, making note of the tissue orientation. Fill the cup with warm gelatin. The tissue will float toward the top. Reorient the tissue if necessary to make sure it is centered in the cup.
         5. Immediately place the cup with tissue in dry ice to flash freeze it (*see* **Note 39**).
         6. Store tissue at -80°C until use.
         7. Cross-section tissue using a cryostat.
            a. Remove tissue-embedded gelatin block from plastic cup and trim excess gelatin with a clean razor blade.
            b. Place small droplet of H_2O on cryostat chuck and place tissue block on top. Surround the rest of the block with H_2O, making sure to not get any below the chuck.

c. Keep the block/chuck in the cryostat to allow the H_2O to freeze, attaching the tissue block on the chuck (approximately 15 minutes).
d. Attach the chuck to cryostat and align tissue block so that even slices can be made through tissue.
e. Obtain several 12-16 micron sections from throughout the tissue. Thaw-mount each section to a glass slide by warming the glass slide slightly and placing it directly above section. Section will adhere to slide (*see* **Note 40**).
f. Store slides at -80° C until ready for analysis (*see* **Note 41**).

b. Optional
   i. Washing
      1. If stored in -80° C, place slide in vacuum chamber or dry box until the sample slide is dry (~5-20 minutes).
      2. Use a manual tissue staining system to immerse slide for the desired amount of time into the solvent of interest (*see* **Note 42**).
      3. Place slide in vacuum chamber until the slide is completely dry (*see* **Note 43**).
      4. If not being analyzed immediately, store slides at -80° C until ready for analysis.
   ii. On-Tissue Labeling (*see* **Note 44**)
      1. If stored in -80° C, place slide in vacuum chamber or dry box until the sample slide is dry (~5-20 minutes).
      2. Prepare labeling tag in the appropriate solvent and volume (*see* **Note 45**).
      3. Apply the tag to the section or slide of interest at the desired concentration or density (*see* **Note 45**).
         a. Change configuration of matrix sprayer (we use a TM-Sprayer, all subsequent experimental details refer to that) so that the syringe pump is directly in line with the sprayer (*see* **Note 46**).
         b. Turn on matrix sprayer and solvent syringe pump.
         c. Set nitrogen pressure to 10 PSI.
         d. Open program and set temperature to desired level (*see* **Note 47**).
         e. Set up desired method (see **Note 48**).
         f. Purge sprayer with solvent that tag reagent(s) are dissolved in for 15 minutes (*see* **Note 45**).
         g. Put labeling reagent(s) into a fresh syringe, place that syringe in the syringe pump, and set the desired solvent flow rate.
         h. Wait for the labeling reagent(s) to flow through the tubing (*see* **Note 49**).
         i. Click “Start” on the Sprayer software.
      4. Immediately after application, incubate the sample for a desired amount of time (*see* **Note 50**).
      5. Shut down TM Sprayer.

a. Flush Sprayer with labeling reagent(s) solvents for 15 minutes (*see* **Note 45**).
b. Flush Sprayer with storage solvent (we use 50:50 Meth:H_2O) for 15 minutes.
c. Set the temperature of the sprayer to 30°C. When sprayer has lowered to this temperature, turn off the sprayer, syringe pump, pressurized nitrogen, and software.

6. Change TM Sprayer configuration back to original with loop, changing the filter as needed (*see* **Note 46** *and* **51**).
7. Quench reaction as appropriate (*see* **Note 52**).
8. Analyze as soon as possible.

2.) Image Acquisition (MALDI-MS)

a. Matrix Application via Sprayer (*see* **Note 53**)
   i. Turn on matrix sprayer (we use a TM-Sprayer, all subsequent experimental details refer to that) and solvent syringe pump, setting desired solvent flow rate (*see* **Note 54**).
   ii. Set nitrogen pressure to 10 psi.
   iii. Open program and set temperature to 80°C for DHB (*see* **Notes 22** *and* **55**).
   iv. Set up the desired method (*see* **Note 56**).
   v. Switch the injection loop to "Load" and load matrix using a syringe pump. Switch the injection loop to "Spray" and ensure that matrix is being sprayed. It may take several minutes for matrix to reach the spray nozzle.
   vi. Click "Start" on the Sprayer software (*see* **Note 57** *and* **58**).
   vii. When method has finished, flush the matrix loop with solvent three times and set the temperature of the sprayer to 30°C. When the sprayer temperature has lowered to this temperature, turn off sprayer, syringe pump, pressurized nitrogen, and software.

b. Analysis on MALDI-LTQ-Orbitrap
   i. Insert one or two slides into MALDI imaging plate.
   ii. Place plate face-down in scanner, and scan image of entire plate. Ensure that the white crosses in the corners of the plate are clearly visible in the scanned image; otherwise, the image cannot be aligned to the plate in the instrument.
   iii. Attach the backing plate to the MALDI imaging plate and insert the plate set into the instrument.
   iv. Once the plate has been inserted, click on the "Tissue Imaging" tab of the MALDI Source page and check the box titled "Use tissue imaging feature."
   v. Under "Position File," check "Import Image" and upload the scanned image of the MALDI plate (*see* **Note 59**)
   vi. Enter the appropriate raster size (*see* **Note 60**) and ensure that the size "rectangular" is selected. (Rectangles are the preferred shape for methods.)
   vii. Select "View Plate," and click on the square selection tool. Select the area of the tissue. Close the "View Plate" window and save the position file (*see* **Notes 61-63**).

viii. Click on the "Control" tab and shoot the laser at an area of matrix. Adjust the laser energy as needed in order to obtain sufficient signal (with our instrument on the order of 1E7).
ix. Open the software setup (Thermo Xcalibur Sequence Setup), and create a new sequence as previously described. For the position, copy and paste the directory of the position file for each tissue into its respective row.
x. Select each line to be run and press the "Run Sequence" button.

c. Data Analysis
   i. ImageQuest
      1. Open raw data in ImageQuest.
      2. Click the "New data set" icon and type in the mass of interest and the tolerance window with the "Base Peak" plot type. Under plot type, select the desired normalization, if any (*see* **Note 64**). Click "OK."
      3. To save or export individual images, select the image and click "Copy" in the Edit tab. Paste the image in the desired location (*see* **Note 65**).
   ii. MSiReader (*see* **Note 66**) (12)
      1. Open the raw data in MSiReader using the appropriate open-access format (*see* **Note 67**).
      2. Enter an *m/z* value from ImageQuest that displays a clear distribution in the tissue.
      3. Enter the appropriate parameters for the *m/z* window, normalization (*see* **Note 64**), and color map.
      4. Use the image overlay feature to upload a scanned image of the tissue and align the image to the MS image of the tissue. Set the transparency to around 50% to ensure both optical and MS images are clearly visible.
      5. Generate an image of each neuropeptide signal of interest from a database using "generate an image for each peak in a list" button.
      6. Manually examine images for detected neuropeptides and distinct spatial distributions (*see* **Note 68**).
      7. Search for novel neuropeptides and *m/z* values outside of the database by using the peak finding tool.
   iii. 3D image generation (Image J)
      1. Open grayscale images of consecutive tissue slices with the same *m/z* value (saved from ImageQuest).
      2. Align the images using the functions under "image."
      3. Combine the images into a three-dimensional stack using the "images to stack" button.
      4. View the three-dimensional image by clicking "image," "stacks," and then "3D project." Viewing parameters can be adjusted in the 3D projection window.
   iv. SciLs (*see* **Note 69**)
      1. Convert image files into .imzML format (if using non-Bruker instrument, such as the Thermo MALDI-LTQ-Orbitrap XL) (*see* **Note 67** and **69**).

2. Click “New” to import data. Select the appropriate instrument type. Click “Next.”
3. Add in data files by clicking the red plus sign and selecting files of interest. Select the appropriate “Pixel size (μm)” and “Spectrum representation” (*see* **Note 60** and **70**).
4. Organize data sets by moving their images into a desired order. Click “Next.”
5. In “Mass range settings,” unclick “Auto detect mass axis settings” and select best “axis interpolation mode” for your data in the “Advanced” section. (*see* **Note 71**).
6. Change “Average data point accuracy” to “0.0005 Da.” Click “Next.”
7. Confirm details in the “Import summary.” Click “Import.”
8. Change “Interval Width” to ±5.000 ppm by going into the “File Properties” section in “File.”
9. In “Visualization,” normalize your images appropriately (*see* **Note 64**).
10. Select regions of interest in “Stack View” by clicking “Create new polygonal region.” (*see* **Note 72**)
11. Determine peaks of interest (*see* **Note 73**).
12. Run “Hypothesis Test” or “Find Discriminative m/z Values (ROC)” in the “Tools” section (*see* **Note 74**).
13. Export results by creating a “SciLs Report Table” in “File”.
    a. Select appropriate peak list from drop down menu in “m/z report table” section.
    b. Add tasks run by clicking red plus sign and adding ROC or t-test results (*see* **Note 75**).
    c. Click “Copy table to clipboard” to paste in Excel for further processing.

Other – Crustacean Cell Culture (*see* **Note 76** *and* **77**)

1) Sterile Technique
    a. The UV light must be turned on 30 min prior to operating the biosafety cabinet to sterilize.
    b. Turn off the UV light, turn on the blower and white light, then open sash to appropriate height (marked by red arrows).
    c. Spray gloves, arms, and inside of biosafety cabinet with 70% EtOH and wipe with a Kim wipe.
    d. All items must be sprayed with 70% EtOH before items are placed inside the biosafety cabinet.
2) Making Media (in Sterile Environment)
    a. Supplement L-15 media with L-glutamine (5.13 mL of 200 mM solution into 500 mL of L-15) if not included already.
    b. Mix crab saline and L-15 at 1:1 ratio.
    c. Add in 6.161 grams of sucrose per 50 mL of media to adjust osmolarity to 1,000 mOsm.

   d. Vacuum filter (0.22 micron pore) mixture to sterilize mixture.
   e. Aliquot into 15 or 50 mL conical tubes (labeled) to be stored in fridge. Volume is dependent on tissue culturing needs and the addition of 1% antibiotic (*see* **Note 78** *and* **79**).
   f. Prior to media use, add appropriate volume of the antibiotic solution into the media (*see* **Notes 78-81**).
3) Seeding Cells (Primary Cells from Tissue)
   a. Prepare items required for sterile dissection: sterilized saline (0.22 micron pore vacuum filtered), autoclaved dissection tools (using autoclave bags), 70% EtOH, 10% sodium hypochlorite.
   b. Place crab on ice for 15-30 minutes. Spray down dissection hood with 70% EtOH to clean area.
   c. Clean crab surface with (a) hypochlorite solution then (b) EtOH solution.
   d. Dissect out tissue of interest, taking care to use the sterilized tools and sterile saline in the micro-dissection dish(es).
   e. Transfer sample to Eppendorf tube with media. The amount used will depend on the tissue size (*e.g.*, TG needs ~100 μL).
   f. Gently homogenize the tissue using a plastic or Teflon pestle.
   g. Pipette homogenate into flask. Flask type used depends on tissue (e.g., ½ TG grows well in T25 flask using this method).
   h. Feed cells as required (*see* **Note 82**).
4) Feeding Cells (*see* **Note 82**)
   a. Remove old media by pipetting.
   b. Pipette media volumes into flasks to replace the media in the flask. Cap flask and return cells to incubator (*i.e.*, room temperature biosafety cabinet).
5) Trypsinizing Cells for Harvesting or Re-seeding
   a. Remove old media by pipetting.
   b. Wash cells with PBS 1X (without Ca or Mg^{2+}) (see wash volume; **Note 76**) to remove dead cells and then pipette away wash.
   c. Add trypsin (0.25%) to flask (see trypsin volume; **Note 76**). Incubate for 5 min. Use cell scraper to scrape away cells that are still adhered. Check under microscope and re-scrape as needed.
   d. Neutralize the trypsin with equal volume of media and collect media and cells in a conical tube.
   e. Centrifuge conical tube (typically 15 mL) at 1000 rpm for 5 min with acceleration, but no deceleration.
   f. Return conical tube to biosafety cabinet and pipette media off gently with 1 mL pipette (being very careful to avoid cell pellet at the bottom). Wash pellet with PBS three times if harvesting cells.
   g. Resuspend cell pellet in media (at appropriate concentrations) or just in enough media to re-seed depending on experimental desire.

Notes

1. While storage at -80°C minimizes postmortem degradation, tissues should only be stored for up to six months before use. There are several ways to decrease postmortem degradation for both tissues and hemolymph, which would extend their storage life. For tissues, the use of a Denator heat stabilizer system or boiling of the tissues for heat stabilization has been shown to be effective [9]. For hemolymph, the addition of protease inhibitor cocktail or EDTA can reduce protease activity.
2. Several different extraction solvents have been tested for their ability to extract neuropeptides from tissues, including acidified organic solvents [10]. A method termed "mixing on column" (MOC), where 4 different extraction solvents are incorporated sequentially, has been shown to be extremely effective for mammalian neuropeptides [11], but this technique's usefulness is still being tested for crustacean peptidomics.
3. While a manual homogenizer has been shown to be effective for the small crustacean tissues, an electronic sonicator may be needed to fully break down the tissue walls of large organs. These should be used with the tissues on ice or in a cold room to help with heat dissipation.
4. When deciding how many tissues to pool, it is important to balance biological variance with the amount of tissues required for the study. In most stress-related studies, at least 3 animals' tissues are pooled for each biological replicate.
5. Direct profiling is alternative strategy to extraction. The tissue of interest can be placed on the stainless steel spotting plate, with matrix being spotted directly onto the tissue area of interest. This method has become phased out with the development of new imaging techniques (see "Localization using Imaging" section in this book chapter).

6. Many crustacean peptides vary widely in their molecular masses. For example, crustacean neuropeptides can range from 0.5 to 9 kDa. With many orbitrap-based instruments, it is difficult to analyze the larger peptides without taking a bottom-up approach. This means some sort of digestion prior to analysis may be required to get a full picture of a crustacean peptidome. For crustacean peptides, the digestion is usually done on the initial extract. After reducing all disulfide bonds with dithiothreitol and alkylating with iodoacetamide, an enzyme (*e.g*. trypsin) is added at a 25-50:1 peptide: trypsin ratio. Peptide content can be determined using the bicinchoninic acid assay or a similar assay.
7. Each crab has a limited amount of hemolymph stored in its body. For example, *Callinectus sapidus* has approximately 5 mL. After removal, hemolymph is restored over a period of time. Thus, the amount of hemolymph removed depends on the species of crab and whether it is to survive afterwards. Replacing the volume of removed hemolymph with an equal volume of crab saline can increase the crab's chance at survival.
8. After drying down any hemolymph samples (initially to fully processed), they should be resuspended prior to storage in the -80°C freezer to ensure full dissolution.
9. Depending on the size of the peptides of interest, two versions of MWCO filters are available: 3K or 10K Daltons. 10K is normally used to purify a wide mass range of crustacean peptides (*see* **Note 5**). After digestion, 3K MWCO filters can be used to simplify the sample and allow for a targeted analysis.
10. Many times, the MWCO filters become clogged with proteins that (a) were not fully pelleted in the extraction step or (b) were not dissolved in the H_2O:MeOH mixture that

was added to the extract. In order to lessen the chance of this happening, (a) centrifuge the extract at >16,000 g for 15-20 minutes before putting the supernatant through the filter, (b) separate the extract into two fractions with two MWCO filters, or (c) centrifuge the extract through the filter for a longer period of time (45+ minutes).

11. There are several types of commercial probes that can be used for microdialysis. Alternatively, homemade probes can be implemented at a much lower cost. Whether purchasing or making probes, there are several factors worth considering, including membrane material, the molecular weight cutoff (the expected MWCO is approximately a third of the reported MWCO), area of membrane, and use of polymer coatings [12].
12. The microdialysis technique tends to have low recovery *in vivo*. The recovery can be enhanced through the use of affinity agents [13].
13. It is important to closely monitor the crab while it recovers from surgery, as the majority of post-surgery complications (*i.e.* crab dying, pulling out probe, clogging probe) typically occur within the first twenty-four hours.
14. Collection windows are typically within the range of 30 minutes to 2 hours. This is dependent on the necessary temporal resolution and recovery of sample. Shorter collection durations provide higher resolutions, but yield lower sample volumes. Collection times of several minutes have been shown feasible, often using online microdialysis collection couple to ESI. However, this method also comes with drawbacks [14].
15. The optimum infusion rate for microdialysis is a tradeoff between relative recovery and absolute recovery. Lower flow rates allow for more diffusion of sample through the membrane, but result in less sample volume, while higher flow rates enable the collection

of more sample overall but run the risk of disturbing the crab. We have found the ideal flow rate to be 0.5 microliters per minute.

16. When collecting samples, it is important to account for the dead volume between the tip of the probe and the end of the tubing (and collection needle, if one is being used). The delay from sample diffusing into the probe to reaching the end of the tubing could be an hour or greater, depending on the length of tubing and infusion rate.
17. Microdialysis samples have been shown to degrade rapidly, even within several hours. Therefore, samples should be analyzed as soon as possible after collection. If longer storage time is necessary, there are several methods for improving the lifetime of the samples [14, 15].
18. Many different varieties of separations can be done to increase peptide purity, including strong cation exchange (SCX) and C18 pipette tips (*i.e.,* ZipTips). Success has also been found in increasing peptide coverage in fractionation using C18 pipette tips or an HPLC system [16].
19. Formaldehyde labeling is commonly used to produce 2 or 3 different isotopic forms that differ in mass [17-19], although up to 5 different isotopic forms can be generated with different combinations of heavy and light formaldehyde and reducing agent. Other labeling methods exist, such as isotopic N,N-dimethyl leucine (iDiLeu), which boasts 5-plex labeling capabilities, which allows for relative or absolute quantitation by an in-solution calibration curve [20]. Absolute quantitation of a single peptide can also be done by adding a deuterated-version of the peptide to the original extract of the sample.
20. For crustacean tissues, formaldehyde labeling has been shown to be extremely effective due to its quick and complete labeling of peptides. While MS-based quantitation

strategies are simple, they have limitations, especially when analyzing more than 5 samples or samples with high spectral complexity. On the other hand, MS/MS-based quantitation strategies, such as iTRAQ, TMT, or N,N-dimethyl leucine (DiLeu), allow for higher multiplexing (up to 12 sample comparisons at once have been demonstrated, but up to 18 may be possible) with lower MS spectral complexity [21, 22]. Unfortunately, quantitative depth may suffer because, in order to become quantified, the peptide needs to be selected for MS/MS.

21. Prior to spotting with matrix, an offline separation can be done, for example with capillary electrophoresis or high-pressure liquid chromatography (HPLC). Success has been seen for separating tryptic peptides with both high-pH and strong-cation-exchange chromatography [23, 24].
22. Several matrices work well for crustacean peptide analysis, including DHB and CHCA. While DHB extracts peptides well, CHCA, known for being a "universal matrix," tends to provide a more homogenous layer.
23. Several spotting techniques exist, including the suggested premixing, alternatives are sandwiching, or individual mixing on plate prior to recrystallization.
24. Depending on the instrument, lifetime of the laser, instrumental setup, and the matrix of choice, the laser energy used will need to be optimized for each sample.
25. In order to acquire more confident identifications or perform *de novo* sequencing, tandem MS is necessary. For MALDI instruments, collision-induced dissociation and high-energy collisional dissociation are the main commercially-available options. Unfortunately, MALDI ionization mainly produces singly charged ions, which lead to poor fragmentation. This means that most identifications for MALDI are done through

accurate mass matching. ESI provides much higher-quality fragmentation spectra, meaning that tandem MS can be used for high-confidence identification and discovery of novel peptides. As another fragmentation option, electron transfer dissociation, which is better for post-translational modification analysis, is now being more readily available. Even with high quality tandem MS spectra, *de novo* sequencing of peptides can be challenging. The use of chemical derivatization with a non-isotopic version of formaldehyde (see **Note 19**) has allowed for more complete coverage when *de novo* sequencing putative peptides [19]. Other methods, such as thiol reduction and alkylation have also been used to achieve high-resolution sequencing of larger, disulfide-bonded crustacean peptides [25].

26. Xcalibur software only recognizes plates as having 96 wells, so it will only allow you pick spots that are within that plate size, even if you are using a 384-well plate.
27. Besides classic LC separation, several other complementary options exist. Capillary electrophoresis is compatible offline for both MALDI and ESI analysis for enhanced separation of crustacean neuropeptides [26, 27]. Ion mobility has also been shown to be effective at separating D/L-epimeric crustacean peptides [28].
28. The use of either a commercial or homemade column should be considered. Homemade packing lowers the cost of each column and allows for customization, which may improve peptide separation and thus coverage. However, low uniformity can cause inconsistency between columns in comparison to commercially available columns. Although, these columns can be much more expensive in comparison.
29. For peptides, the reverse-phase C18 column setup uses a gradient of H_2O with 0.1% FA and ACN with 0.1% FA to elute the sample. Depending on the complexity of the sample,

the time of gradient, highest percent ACN added, and instrumental parameters (*e.g.* dynamic exclusion) will need to be adjusted.

30. When beginning any LC-MS experiment, a quality control sample should be run to determine if the instrument is working optimally. Also, blanks should be run between each new sample type to decrease sample overlap.
31. For orbitrap instruments, the standard mass tolerance is ±5 ppm.
32. This can be done manually or with a simple peak-picking program. In the Li Lab, Kellen DeLaney has written a Java-based program to do this. It allows you to adjust ppm error, database, and intensity threshold. She has created programs for unlabeled neuropeptides, duplex-labeled neuropeptides, and also statistical analysis of these labeled neuropeptides between multiple bioreplicates. To use this program, the MALDI spectra must be averaged and exported to a .csv file.
33. Several software packages are capable of performing *de novo* sequencing, database searching, and peak peaking for quantitation besides PEAKS (*e.g.,* Proteome Discoverer).
34. Common post-translational modifications (PTMs) for crustacean neuropeptides include amidation and dehydration. If any labeling is done, it is important to include the tag or modification during the search (*e.g.* dimethylation).
35. PEAKS software package works by first *de novo* sequencing all of the raw data, which will then be matched to the provided database of precursor masses and proposed sequences. It is important to note that, while other databases come from sequenced genomes, the crustacean neuropeptide database has been developed in-house, as there is no genomic database for crustaceans. When looking at peptides with no digestion, PEAKS shows the peptide searched as a “protein” in the program. The “peptides” section

is the individual, full or truncated peptides that match up to the crustacean peptides, which can include cleaved or degraded derivatives. Anything that doesn't match is placed in a "de novo only" tab, which can provide you with possible novel peptide groups. For neuropeptides, these "de novo only" peptides are compared to current family sequences, from which certain sequence themes can be found to identify novel neuropeptides. Programs can that do this include "Pattern Lab for Proteomics" by using "PepExplorer" in the "Filter" tab. Confident identification can then be done by synthesizing standards to confirm MS/MS and LC retention patterns.

36. Both MS and MS/MS-based quantitation can be done, depending on the labeling used in the quantitation step. Label-free quantitation is also possible. It should be noted that in PEAKS, the "dimethylation" modification only assumes the N-terminus and arginines. This should be modified if being used for quantitation, as dimethylation labels all primary amines, including the N-terminus, leucines (K), and arginines (R). Thus, all of these should be included in your dimethylation modification.
37. It may be helpful to label dissection dishes with the orientation of the tissues to avoid uncertainties after the tissue is dissected.
38. Delicate tissue such as the PO can be transferred to the H_2O by either carefully folding the tissue into quarters or by holding the tissue at either end with separate sets of tweezers.
39. To prevent degradation, a Denator heat stabilizer can be implemented immediately after desalting. However, caution must be taken to avoid melting delicate tissue.

40. It is common for slices to fold, tear, or become distorted during the process of thaw mounting. Once the slice is on the slide, thoroughly check it to ensure the integrity of the tissue.
41. For best results, slides should be analyzed as soon as possible. During storage, slides can be wrapped in tin foil to protect them from damage. When removing the slides from the freezer, H_2O will condense on the slides, which can cause diffusion, due to the major temperature change. Place them in a desiccator to minimize this effect.
42. Our optimal method for crustacean neuropeptides has been 50:50 EtOH:H_2O for 10 seconds (see *Chapter 5*).
43. This could range from 5 minutes to 15 minutes depending on the wash used. It is important to make sure the section is dry prior to matrix application to provide homogenous matrix coverage.
44. On-tissue labeling has not been successful. In fact, any case of success has not been reproduced. This method is to working as a reference and/or starting point for all future attempts at performing on-tissue labeling or derivatization.
45. Both DiLeu and dimethyl labeling techniques have been studied for on-tissue labeling. For DiLeu, activation in ACN (instead of DMF) for 45 minutes has been found to be optimal. When working with spots of a neuropeptide standard mixture, 25:1 label:peptide ratio worked the best when the sample was reconstituted in 0.05 M TEAB or NaOH-adjusted pH=8 H_2O prior to the addition of the label. This worked out to ~30% aqueous mixture for labeling. Dimethyl labeling requires no activation prior, and the main solvent of choice has been H_2O. For on-tissue imaging experiments, label:peptide ratio is

estimated by considering the density of peptides (0.00035 mg/mm^2) and the label density based on the parameters of the TM-sprayer using the following equation:

$$Label\ Density\ (\frac{mg}{mm^2})$$

$$= \frac{(Number\ of\ Passes)(Label\ Concentration(\frac{mg}{mL}))(Flow\ Rate\ \left(\frac{mL}{\min}\right))}{(Nozzle\ Velocity\ \left(\frac{mm}{min}\right))(Track\ Spacing\ (mm))}$$

For most DiLeu experiments, 10:1 label:peptide ratio was used to conserve label (see *Chapter 7*). For dimethyl labeling, 1 mL of both the formaldehyde and reductive reagent were mixed and applied.

46. Originally, in order to change the configuration, the line connected to the syringe would need to be removed from the chromatography loop mechanism. The outlet of the chromatography loop mechanism (orange line) is then disconnected from the filter unit, which is located between the chromatography loop area and the sprayer area. The syringe line is then directly connected to the filter unit, thus bypassing the chromatography loop mechanism. This has changed, as the syringe pump (dedicated to spraying enzymes or labels) now has its own filter unit, while the matrix pump system has its own, dedicated bulk solvent pump. In general, though, care should be taken to make sure that there are no leaks, no screws are overtightened, no screws become stripped, *etc*.
47. For labeling reagents, 30°C is the most common temperature used to make sure that a wetter application is used, although diffusion should be considered with a wet application.

48. Desired method will depend on the labeling system, label:peptide ratio, and desired wetness of application.
49. At a flow rate of 0.200 mL/min, in the alternative configuration, it takes 2.5 minutes for the sample to get form the syringe to the sprayer. This will depend on the tubing length though, and should be determined for each individual TM Sprayer set up.
50. Incubation can be done at room temperature, in a hydration chamber (up to 37°C), in a cell incubator (up to 37°C), *etc*. Alternative embedding materials that section well would need to be explored if going beyond that temperature, as gelatin melts at 37°C. A mixture of 2% agarose and 10% gelatin (w/v) has been shown to not melt at 37°C and also sections well.
51. With DiLeu and dimethyl labeling, the filter in the filter unit is changed after every experiment to prevent clogging.
52. This will depend on the labeling reagent and may not need to be done if other compounds beyond matrix are not being applied.
53. There are several methods for applying matrix to a sample, including airbrush, automated sprayer, inkjet printer, sublimation, etc. The method described here utilizes an automated sprayer (*e.g.,* TM-Sprayer) which has been found to be the most reproducible [29].
54. Our TM-Sprayer has recently been upgraded from using a syringe pump to a bulk solvent pump system.
55. The sprayer temperature should be high enough to evaporate the matrix/solvent mixture. For the TM-Sprayer, turn up the temperature slowly until you hear a “puffing” noise. Reduce the temperature by 5°C for the final method.

56. Parameters to consider when choosing a method include the number of times the sprayer passes over and coats the slide, the drying time between coats, the direction the sprayer moves in to coat the slide (*i.e.*, horizontal or vertical), and the system flow rate. Our preferred method includes 12 passes with a 30-second dry time between passes, and the orientation alternating between horizontal and vertical with each pass to provide an even coating at a flow rate of 0.1 mL/min. Methods should be optimized to the peptide group of interest and matrix to minimize diffusion while increasing peptide extraction.
57. The matrix loop only has a finite volume it can hold, and so it may be necessary to reload it with matrix during the course of the method. If this is necessary, wait until the sprayer is done with its current pass, switch the injection loop to "Load," load matrix, and switch the injection loop back to "Spray" before it starts the next pass.
58. After clicking "Start," the system may say the temperature is unstable due to the sensitivity of the system. Since the temperature will never fully stabilize, click "Start Now" to start the method.
59. The MALDI-Orbitrap is also capable of scanning in the whole plate or each individual slide at varying image qualities. Scanning the plate with an external system only takes a few minutes, while scanning one slide at "normal" resolution takes ~25 minutes. For other instruments, images need to be scanned by an external scanner.
60. Raster size determines the spatial resolution (*i.e.*, pixel size) of the tissue being imaged. While small raster sizes provide better image resolution, they can drastically increase the analysis time of the instrument. The MALDI-Orbitrap allows for a raster size of 75 microns without oversampling, but other MALDI instruments boast spatial resolution down to a few microns.

61. After selecting the final area of interest, saving this imaging in the “View Plate” window allows for easier image overlay during data processing.
62. The software tends to shift the selected area unpredictably after closing the window. Therefore, it is recommended to close and reopen the “View Plate” window after a selection has been made to ensure that the area of interest is still within the selection box.
63. It is good practice to include a small amount of area outside of the tissue when selecting the area to be analyzed in order for it to be used as a means to distinguish signal from random noise.
64. Typically, normalization is performed in reference to the total ion current (TIC), in which each mass spectrum is divided by its TIC. This ensures that all spectra have the same integrated area under their curves. Other normalization strategies are emerging [30], but TIC continues to be the most widely used.
65. When comparing multiple images, it is often helpful to set them to the same intensity scale. This can be done by entering the Min and Max Plot Values in the “Scale” tab.
66. MSiReader is a freely-available, open-access software that can be downloaded from http://www.msireader.com/ [4].
67. To convert to imzML in ImageQuest, click File, Export, imzML. Either all peaks or centroids only can be exported.
68. Identifications should be compared to peaks extracted from the full image using the Java search tool (*see* **Note 32**). Peak extraction can be done in ImageQuest by summing the image initially. Then, in the “View” tab, select “View Information”. In the “Spectrum List” tab, unclick “Top 10), which will then generate a through list of peaks that can be

copied and pasted into Excel, saved as a .csv, and searched with a corresponding Java program.

69. SciLs is a commercial statistical analysis tool for MS imaging analysis. Originally only for Bruker instruments, it is now able to work with other open source file formats (*see* **Note 66**).
70. When working with high resolution data, it is best to export in centroid mode prior to uploading into SciLs in order to not crash the program.
71. For the MALDI-LTQ-Orbitrap XL, uploading data in linear mode has been the best for accurate data interpretation.
72. When selecting areas that are of the same conditions, you can color code them to aid in distinguishing groups later.
73. For crustaceans, we can import our database of neuropeptides to aid in investigation. Lists can be imported by going to "File", "Import", and clicking "m/z intervals from CSV or clipboard."
74. For t-tests, no directionality is needed for selecting "Class 1" versus "Class 2." For ROC curves, you can do both directions (*i.e.,* A vs. B and B vs. A) to understand both upregulated and downregulated *m/z* values.
75. When exporting ROC tests, export the "maximum AUC in interval."
76. A variety of flask types were used to culture cells over time, as shown in the table below, along with corresponding volumes of media (approximate), trypsin, and washes to use. The T75 flask was shown to be optimal for culturing 1 TG with the dissociation technique.

Flask Name	Flask Volume	Media Volume	Trypsin Volume	Wash Volume
24-Well	1.9 cm^2	1 mL	0.5 mL	0.5 mL
12-Well	3.8 cm^2	2 mL	1 mL	1 mL
6-Well	9.5 cm^2	5 mL	2mL	2.5 mL
T25	75 cm^2	5 mL	1.5 mL	2.5 mL
T75*	75 cm^2	10 mL	3 mL	5 mL
T150	150 cm^2	20 mL	6 mL	10 mL

77. Since crustaceans are considered biosafety level one (BSL-1), the only PPE required is safety glasses and gloves. Lab coats are required if BSL-2 samples are being worked with.
78. Antibiotic should be 1% of media solution and be added fresh to the media before using it. To reduce freeze-thaw cycles of the antibiotic solution, antibiotic can be pre-aliquoted.
79. Antibiotic is only good for 3 days once thawed (normally stored at -20 °C). Dispose of media accordingly.
80. Media should be used at room temperature for crustacean species.
81. Media is stored at 4°C. Antibiotic is stored at -20°C.
82. Media will become slightly orange when media needs to be replaced. Phenol red is added to the media as an indicator of nutrient consumption. This could be a few day up to a week depending on cell consumption.

R**eferences**

1. Ma, B.; Zhang, K. Z.; Hendrie, C.; Liang, C. Z.; Li, M.; Doherty-Kirby, A.; Lajoie, G., *Rapid Communications in Mass Spectrometry* **2003,** *17* (20), 2337-2342.

2. Cox, J.; Mann, M., *Nature Biotechnology* **2008,** *26* (12), 1367-1372.

3. Frank, A.; Pevzner, P., *Anal Chem* **2005,** *77* (4), 964-73.

4. Bell, G. W.; Eggleston, D. B.; Noga, E. J., *Oecologia* **2010,** *163* (1), 57-68.

5. Bergman, N.; Shevchenko, D.; Bergquist, J., *Analytical and Bioanalytical Chemistry* **2014,** *406* (1), 49-61.

6. Talbi, R.; Klosen, P.; Laran-Chich, M. P.; El Ouezzani, S.; Simonneaux, V., *Journal of Comparative Neurology* **2016,** *524* (18), 3717-3728.

7. Thorpy, M. J., *Current Treatment Options in Neurology* **2015,** *17* (5).

8. Taverna, D.; Norris, J. L.; Caprioli, R. M., *Analytical Chemistry* **2015,** *87* (1), 670-676.

9. Sturm, R. M.; Greer, T.; Woodards, N.; Gemperline, E.; Li, L. J., *Journal of Proteome Research* **2013,** *12* (2), 743-752.

10. Wang, G. R.; Yang, F.; Zhao, W., *Lab on a Chip* **2014,** *14*, 1452-1458.

11. Yin, J.; Mobarec, J. C.; Kolb, P.; Rosenbaum, D. M., *Nature* **2014,** *519*, 247-250.

12. Thorpy, M. J.; Dauvilliers, Y., *Sleep Medicine* **2015,** *16* (1), 9-18.

13. Lietz, C.; Yu, Q.; Li, L., *J Am Soc Mass Spectrom* **2014,** *25* (12), 2009-19.

14. Tierney, A. J.; Kim, T.; Abrams, R., *Microscopy Research and Technique* **2003,** *60* (3), 325-335.

15. Ajdari, A.; Bontoux, N.; Stone, H. A., *Analytical Chemistry* **2006,** *78*, 387-392.

16. Ma, M. M.; Wang, J. H.; Chen, R. B.; Li, L. J., *Journal of Proteome Research* **2009,** *8* (5), 2426-2437.

17. Boersema, P. J.; Aye, T. T.; van Veen, T. A. B.; Heck, A. J. R.; Mohammed, S., *Proteomics* **2008,** *8* (22), 4624-4632.

18. DeKeyser, S. S.; Li, L. J., *Analyst* **2006,** *131* (2), 281-290.

19. Bai, L.; Romanova, E. V.; Sweedler, J. V., *Analytical Chemistry* **2011,** *83* (7), 2794-2800.

20. Behrens, H. L.; Li, L. J., Monitoring Neuropeptides In Vivo via Microdialysis and Mass Spectrometry. In *Peptidomics: Methods and Protocols*, Soloviev, M., Ed. Humana Press Inc: Totowa, 2010; Vol. 615, pp 57-73.

21. Frost, D. C.; Greer, T.; Li, L., *Analytical chemistry* **2015,** *87* (3), 1646-54.

22. McAlister, G. C.; Huttlin, E. L.; Haas, W.; Ting, L.; Jedrychowski, M. P.; Rogers, J. C.; Kuhn, K.; Pike, I.; Grothe, R. A.; Blethrow, J. D.; Gygi, S. P., *Anal Chem* **2012,** *84* (17), 7469-78.

23. Ting, L.; Rad, R.; Gygi, S. P.; Haas, W., *Nature Methods* **2011,** *8* (11), 937-940.

24. Torfs, P.; Nieto, J.; Cerstiaens, A.; Boon, D.; Baggerman, G.; Poulos, C.; Waelkens, E.; Derua, R.; Calderon, J.; De Loof, A.; Schoofs, L., *European Journal of Biochemistry* **2001,** *268* (1), 149-154.

25. Christie, A. E., *Gen Comp Endocrinol* **2014,** *201*, 87-106.

26. Hopkins, P. M., *General and Comparative Endocrinology* **2012,** *175* (3), 357-366.

27. Warkiani, M. E.; Khoo, B. L.; Wu, L.; Tay, A. K. P.; Bhagat, A. A. S.; Han, J.; Lim, C. T., *Nature Protocols* **2016,** *11*, 134-148.

28. Zhang, Z.; Wang, J.; Hui, L.; Li, L., *J. Chromatogr.* **2011,** *1218* (31), 5336-5343.

29. Bergman, P.; Adori, C.; Vas, S.; Kai-Larsen, Y.; Sarkanen, T.; Cederlund, A.; Agerberth, B.; Julkunen, I.; Horvath, B.; Kostyalik, D.; Kalmar, L.; Bagdy, G.; Huutoniemi, A.; Partinen, M.; Hokfelt, T., *Proceedings of the National Academy of Sciences of the United States of America* **2014,** *111* (35), E3735-E3744.

30. Kallback, P.; Shariatgorji, M.; Nilsson, A.; Andren, P. E., *Journal of Proteomics* **2012,** *75* (16), 4941-4951.

Figures

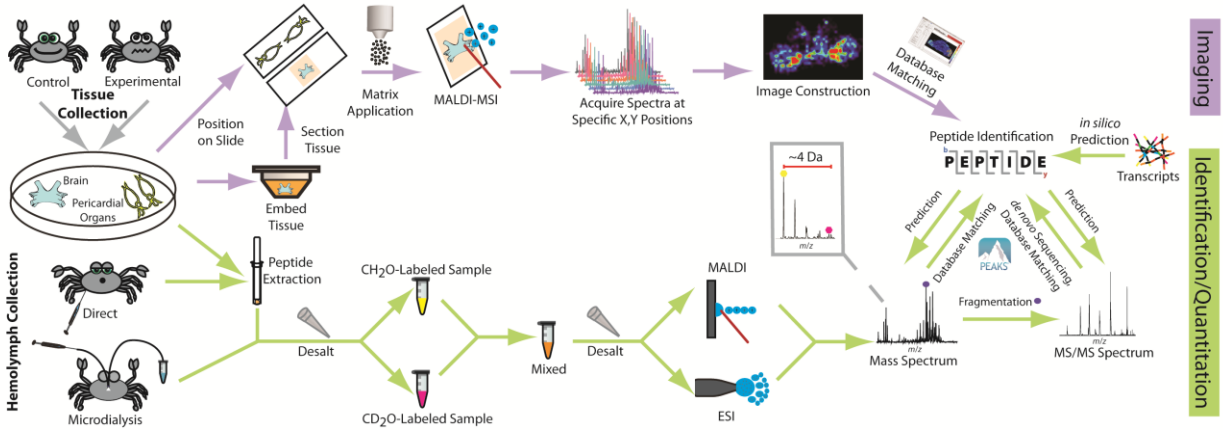

Figure 1. Workflow indicating the steps for sample collection, preparation, and data acquisition and analysis. The workflow contains steps for analysis of tissues, crude hemolymph, and microdialysis samples and describes the processes for both imaging and quantitation. For relative quantitation, duplex formaldehyde labeling is indicated, with CH_2O indicating nonisotopic formaldehyde and C^2H_2O indicating deuterated formaldehyde used.

Appendix III

An Excursion into

Crustacean Cell Culture

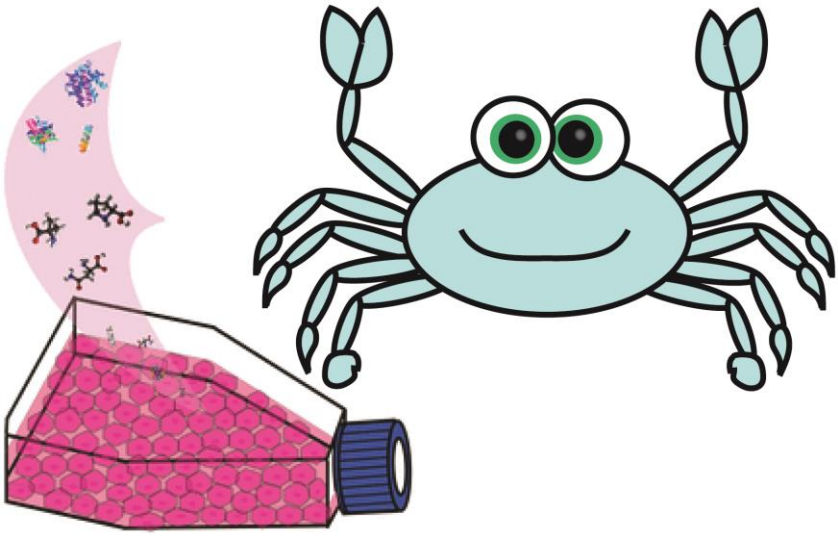

This work was done in collaboration with Jillian Johnson and Nhu Vu. JJ and ARB designed the experiments, while NV assisted in the laboratory work.

Keywords: Cell Culture, *Callinectes sapidus*, Thoracic Ganglion, L-15 Media

Abstract

Invertebrate (*e.g.,* crustacean) cell culture is a relatively unexplored area compared to mammalian cell culture. Furthermore, neuronal cell culture is known to be challenging regardless of the species since mature neurons do not undergo cell division. Using the blue crab, *Callinectes sapidus*, as a model crustacean, known neuronal tissues were cultured to determine the feasibility of crustacean cell culture with neuronal outgrowth being the primary goal. While no neurons appeared to grow, under optimized conditions, the thoracic ganglion proliferated cells that will be characterized by mass spectrometry and staining in the future.

Introduction

Cell culture is a powerful technique that provides researchers endless opportunities for scientific exploration.[1, 2] Already used in biomedical applications, the opportunity for *in vitro* cellular manipulation is powerful for more deep biological understanding of a cell and its function (*i.e.,* when exposed to a drug), especially for basic science research.[3] Furthermore, human tissues are considered precious due to limited availability, and with the ability to immortalize and continue to grow cells from different sources, we can study difficult diseases (*e.g.,* cancer) without requiring as many primary samples/tissues. For humans and other higher order organisms, cell culture provides alternatives to *in vivo* animal experiments while also reducing biological variability for both method development and application.[4]

Currently, mammals are the most utilized source of cells, although invertebrates are considered a promising source for future studies. More than 95% of all species are invertebrates, meaning they are a currently under-tapped resource for basic scientific research.[5, 6] In particular, marine invertebrates, which accounts for 30% of all species, are of interest due to their great

phenotypic differences from mammals, such as shrimp's ability to regenerate without being prone to tumors.[5, 7] Also, invertebrates are known for producing bioactive compounds of interest while also being an economic (*e.g.*, food) interest.[8] Culturing invertebrate cells has been seen in the literature but infrequently (~90 reports through 2004; 47 papers from 2002-2012).[6, 8] No established cell line has been created, and it was only recently that long-term cultures have been achieved without having contamination.[5, 6, 9] Unfortunately, the lack of reports is likely due to researcher's inability to publish negative results. It should also be noted that the cell types chosen for studies are extremely variable, but the most common cell types appear to be hemolymph (*i.e.*, blood) and embryonic cells. On the other hand, it appears that the most challenging cell types to culture are neurons and stem cells, although stem cells are of particular interest due to their potential for continuous replication.[8, 10]

Due to the lack of implemented strategies, the researchers have limited understanding of invertebrate (a) cellular requirements or (b) physiological needs *in vitro*. The two major limiting steps are the media and cell preparation methods.[5, 6, 8, 9, 11] There is no specific media developed for crustacean invertebrate species, which is a clear bottleneck when comparing to insect cell culture. When Grace's Insect Media was published and made available, insect cell culture applications grew exponentially. In the literature, a variety of different media with supplements have been explored, the most popular being Leibovitz's L-15 with various different additives.[7] Beyond media considerations, due to the diversity of invertebrates that can be studied, publications on crustacean cell culture lack consistency on species, tissues, and methods used to study them.[5, 6, 8, 9] This makes comparing different studies very difficult if not impossible.

This study explores developing a method for crustacean neuronal cell culture in order to extend the Lingjun Li lab's abilities to study neuropeptides outside the *in vivo* animal model and

to study adult neurogenesis.[12] By working with a previously unexplored model, the blue crab, *Callinectes sapdius*, we can apply previously published methods for similar decapod crustacean tissues to develop our own techniques.[11, 13-19] Below, our current, optimized methodology and results are described. It is clear from our studies that more optimization is required for crustacean cell culture to be a feasible addition to our neuropeptidomic studies.

Methods

Materials and Chemicals

Methanol (MeOH), glacial acetic acid (GAA), sucrose, ammonium hydroxide (NH_4OH), and all crab saline components (see below) were purchased from Fisher Scientific (Pittsburgh, PA). 2, 5-dihydroxybenzoic acid (DHB) was obtained from Acros Organics (Morris, New Jersey), while formic acid (FA) was purchased through Fluka (Mexico City, Mexico). Liebovitz's L-15 media and L-glutamine solution were acquired from Sigma (St. Louis, MO). 0.25% trypsin-EDTA solution was obtained from Gibco, and Corning provided the phosphate buffer saline (PBS) and antibiotic-antimycotic (100X) solutions. Ethanol (EtOH) utilized in this study was from Pharmco-Aaper (Chicago, IL). All water (H_2O) used in this study was doubly distilled on a Millipore filtration system (Burlington, MA) or HPLC grade, and C18 Ziptips were purchased from Millipore (Burlington, MA). All flasks were from TPP, while all sterile pipettes were Costar brand.

Animals and Tissue Collection

All female and male blue crabs, *Callinectes sapidus*, were purchased through either the Midway Asian Market (Madison, WI) or LA Crawfish Company (Natchitoches, LA). Crabs were allowed to recover from transport for several days in artificial seawater (35 parts per thousand,

12-14 ˚C). Prior to dissection, crabs were anesthetized on ice for 20 minutes. The hood in which dissections occurred was not sterile, but precautions were taken to sterilize the space. For examples, the hood and crustacean were sprayed down with 10% hypochlorite followed by 70% EtOH at the start of the dissection. All dissections were performed in chilled physiological saline (composition: 440 mM NaCl; 11 mM KCl; 13 mM $CaCl_2$; 26 mM $MgCl_2$; 10 mM Trizma acid; pH 7.4 (adjusted with NaOH)). All dissection tools and containers were autoclaved prior to use. If a tissue was being collected for cell culture experiments, the microdissection occurred in sterile saline. The collected tissue was then transferred to media (optimal = 1:1 Leibovitz's L-15 and crab saline with 0.1% antibiotic-antimycotic solution, osmolarity (Osm) = 1,000 mOsm) and transported to a sterile biosafety cabinet for cell culture preparation. The L-15 media can be bought with L-glutamine supplemented or without L-glutamine to be supplemented (2 mM) manually. The initial osmolarity was determined by using an Advanced Instruments Model 325 Single-Sample Osmometer on a sterile 1:1 mix of crustacean saline and L-15 media (640 mOsm). The osmolality was then adjusted by addition of sucrose (30.805 g for 250 mL of 1:1 mix of media) and sterilized again. All solutions were sterilized by vacuum filtration through a 0.22 micron filter in the biosafety cabinet.

Cell Culture

Using a Teflon pestle, the tissue of interest was broken apart gently in 1.5 mL Eppendorf tube and pipetted into the appropriately sized culture flask (*e.g.*, ½ thoracic ganglion in a T25 flask) with supplemental media. Cells were fed as necessary according to the color change of the media. The cells were allowed to culture until 80% confluence was reached before either (a) splitting by 0.25% trypsin-EDTA addition for 5 minutes and then scrapping or (b) collection by the same method. In both cases, the cell pellet was collected by centrifugation at 1000 rpm for 5

minutes (with acceleration, no deceleration). If the cells were collected, the pellet is washed 3 times with PBS prior to storage at -80°C to remove any media components from the cell pellet. It should be noted that the optimal conditions are stated here, but all methods considered will be discussed below.

Sample Preparation

Neuropeptides and metabolites were extracted with acidified MeOH (90:9:1 MeOH:H_2O:GAA) using a probe sonicator (Fisherbrand Model 120 Sonic Dismembrator) at 4°C with the following parameters: 3 pulse sequences, 8 seconds "ON" at 50% amplitude, 15 seconds "OFF." After sonication, the sample was centrifuged at 20,000 rcf (4 ˚C) for 20 minutes, and the supernatant was dried down in a Speedvac (Savant SCV100). Neuropeptides were purified using a C18 Ziptips according to the manufacturer's protocol and dried down using a Speedvac in preparation for analysis. Metabolites, found in the flow through of the ZipTip, were purified using a Waters OASIS PRiME MCX solid phase extraction columns and split into two fractions: MeOH and 5% NH_4OH in MeOH. These samples were not desalted by Ziptips prior to analysis, but all future experiments will include a desalting step. To determine how many cells were needed for analysis compared to a traditional whole tissue preparation, the Pierce Quantitative Colorimetric Peptide Assay was used following the manufacturer's protocol.

Mass Spectrometry (MS) Data Collection

A matrix assisted laser desorption/ionization (MALDI)-LTQ-Orbitrap XL was utilized for initial characterization of the cellular contents. Samples were spotted with 1:1 DHB (150 mg/mL 50:50 MeOH:H_2O with 0.1% FA) and analyzed at 60,000 resolving power in either *m/z* 100-1000 (metabolites) or *m/z* 500-2000 (neuropeptide) mass range. Neuropeptides were identified using an in-house Java program for accurate mass matching to a custom crustacean

database. Metabolites were tentatively identified by accurate mass matching to Metlin online database.

Results and Discussion

Crustacean cell culture is limited in the literature, especially for neurons. This could be due to several factors, including mature neurons not dividing, although there are stem cell-like neurons that exist in defined ganglia, and the lack of defined media.[5, 6, 9, 11, 12] No studies have been performed with the blue crab to our knowledge or for neurons, so this study aims to further our knowledge on this topic.

Five different tissues (*i.e.*, brain, sinus gland (SG), pericardial organ (PO), commissural ganglion (CoG), thoracic ganglion (TG)) were investigated for their ability to culture neurons. From these initial studies, no neurons were observed to grow from any tissue using the standard explant culture method. Thus, the best tissues were chosen based upon the qualitative observation of number of cells grown. The TG and CoG were selected for further studies.

Based upon the literature, several different media have been investigated for crustacean cell culture, and four were selected to test their efficacy for blue crab neuronal tissue. The media chosen are shown in **Table 1** with future alternatives found in the literature in **Table 2**. Several others exist in the literature, such as using L-15 (2X).[5-7, 9, 11, 19] For all media containing hemolymph, the hemolymph was sterilized using a 0.22 micron syringe push filter prior to addition to the media. Blood cells from the hemolymph has been the most frequently used in crustacean cell culture, but our filtering should have removed all cellular species to just provide the nutrients.[8] It should be noted that osmolality was not adjusted until after these studies. Of the

four media types tested, the media 1 (1:1 mix of L-15 and crab saline) produced the largest number of viable cells, and all future studies were done using this media.

In general, several other parameters were found to be optimal for crustacean cell culture. Initially, the explant technique was used to allow outgrowth of cells, but the use of a dissociation method produced better extraction of the tissue's cells of the tissue for initial adherence. This could be due to breaking the complex sheath on many ganglia or other complex interactions that occur between cells. Furthermore, classic trypsinization using a 0.25% trypsin solution was not found to be adequate to release the cells from the flask for collection or splitting. Thus, a scrapping-based method was utilized instead.

A peptide assay was done to determine how many flasks of cells were required to be analogous to one TG tissue. Several flasks of cells were combined for the analysis, and it was determined that about 40 T-25 flasks of cells (<80% confluence) were required. From previous analyses, each TG fills a T-25 flask during the platting phase but does not divide very quickly (*i.e.,* no doubling in 3 week lifetime). This is consistent with what is seen in the literature, where cells stop dividing 24-72 hours after isolation (*i.e.,* cellular quiescence).[10] We are also seeing inefficient adherence, as many cellular species are dying prior to adhering onto the flask. This observation suggests that we would need at least 10 crabs to culture enough cells to be analogous to a single TG.

Visual inspection of all the cell species showed no indication of neuron growth, although some appeared to be morphologically similar (**Figure 1**). **Figure 1a** shows a zoomed out photo of the cellular species observed, with **Figure 1b** highlighting zoomed in photo of a "neuron-like" cell. It should be noted that no known neuropeptides or metabolites/neurotransmitters were identified from cellular extracts using MALDI-MS. Several other cell species were apparent and

will be characterize through liquid chromatography-electrospray ionization MS and stains (**Figure 2**). These species appeared similar to those classified as crustacean glial cells in the literature.[19]

It is clear that the current methodology requires revisions, and other methods, such as growth substrates, different temperatures, pH, dissociation methods (*i.e.*, enzymatic), a crustacean specific PBS, *etc.* should be explored.[8, 9, 19] In fact, analyzing the proteins on the cell surface will be key to understand invertebrate cellular signaling, although, without a sequenced genome, this is even more challenging. Nonetheless, the main bottleneck of growth appears to be the growth medium, as a well-defined medium is not available for crustacean species.[5, 6, 8, 9, 11] In the case of insects, the ability for researchers to utilize insect cell culture exploded when Grace's Insect Media was developed, and this is currently the only media that is invertebrate specific.[8] Unfortunately, invertebrate species biomolecular needs are not well understood, and continued efforts need to be made to fully understand invertebrates and crustacean metabolic requirements. This is a challenge though due to the natural diversity of invertebrates, and the knowledge we have acquired from mammalian cell culture appears to be non-transferable. For example, even though we have an insect specific media, we are unable to use the same media for other invertebrates effectively.[8] Other significant challenges exist due to invertebrate specific contamination and immortalization, but these challenges are outside the current scope of this study.[5]

Concluding Remarks

Invertebrate cell culture is a promising technique for (a) basic science research and (b) animal model alternative, but it is clear that more efforts are needed to address the unique

biomolecular requirements for groups of invertebrates compared to mammals. In general, emphasis should be placed on both characterizing the required growth factors need for proliferation while also considering the physiological demands to allow for prolonged cellular growth and cell division. Furthermore, once we are able to grow cells continually and efficiently, establishing genetically immortalized cell lines will be the next step for continued application of invertebrates in basic science research.

Acknowledgements

We would like to thank Kellen DeLaney for writing the custom Java program for neuropeptide identification. We would also like to thank the Zeeh Station in the University of Wisconsin-Madison School of Pharmacy for use of the Osmometer.

References

1. Carrel, A., *Physiological Reviews* **1924,** *4* (1), 1-20.

2. Huh, D.; Hamilton, G. A.; Ingber, D. E., *Trends in Cell Biology* **2011,** *21* (12), 745-754.

3. Verjans, E. T.; Doijen, J.; Luyten, W.; Landuyt, B.; Schoofs, L., *Journal of Cellular Physiology* **2018,** *233* (4), 2993-3003.

4. Cheluvappa, R.; Scowen, P.; Eri, R., *Pharmacology Research & Perspectives* **2017,** *5* (4), 14.

5. Rinkevich, B., Cell culture form marine invertebrates: obstacles, new approaches, and recent improvements. Journal of Biotechnology, 1999; Vol. 70, pp 133-153.

6. Rinkevich, B., Marine Invertebrate Cell Cultures: New Millennium Trends. Marine Biotechnology, 2005; Vol. 7, pp 429-439.

7. Jayesh, P.; Seena, J.; Singh, I. S. B., *Indian Journal of Virology* **2012,** *23* (2), 244-251.

8. Cai, X. Q.; Zhang, Y., *Journal of Oceanography* **2014,** *70* (5), 405-414.

9. Rinkevich, B., *Cytotechnology* **2013,** *65* (5), 676-676.

10. Rinkevich, B., *Marine Biotechnology* **2011,** *13* (3), 345-354.

11. Toullee, J.-Y., Crustacean primary cell culture: A technical approach. Methods in Cell Science, 1999; Vol. 21, pp 193-198.

12. Schmidt, M., *Chemical Senses* **2007,** *32* (4), 365-384.

13. Shashikumar, A.; Desai, P. V., *Cytotechnology* **2011,** *63* (5), 473-480.

14. Cooke, I.; Graf, R.; Grau, S.; Haylett, B.; Meyers, D.; Ruben, P., *Proceedings of the National Academy of Sciences of the United States of America* **1989,** *86* (1), 402-406.

15. Turrigiano, G. G.; Marder, E., Modulation of Identified Stomatogastric Ganglion Neurons in Primary Cell Culture. Journal of Neurophysiology, 1993; Vol. 69, pp 1993-2002.

16. Keller, R.; Grau, S.; Cooke, I. M., *Cell and Tissue Research* **1995,** *281* (3), 525-532.

17. Turrigiano, G.; LeMasson, G.; Marder, E., Selective Regulation of Current Densities Underlies Spontaneous Changes in the Activity of Cultured Neurons. Society of Neuroscience, 1995; Vol. 15, pp 3640-3652.

18. Saver, M. A.; Wilkens, J. L.; Syed, N. I., *Journal of Neurophysiology* **1999,** *81* (6), 2964-2976.

19. Wajsenzon, I. J. R.; de Carvalho, L. A.; Biancalana, A.; da Silva, W. A. B.; Mermelstein, C. D.; de Araujo, E. G.; Allodi, S., *Cytotechnology* **2016,** *68* (5), 2193-2206.

Figures

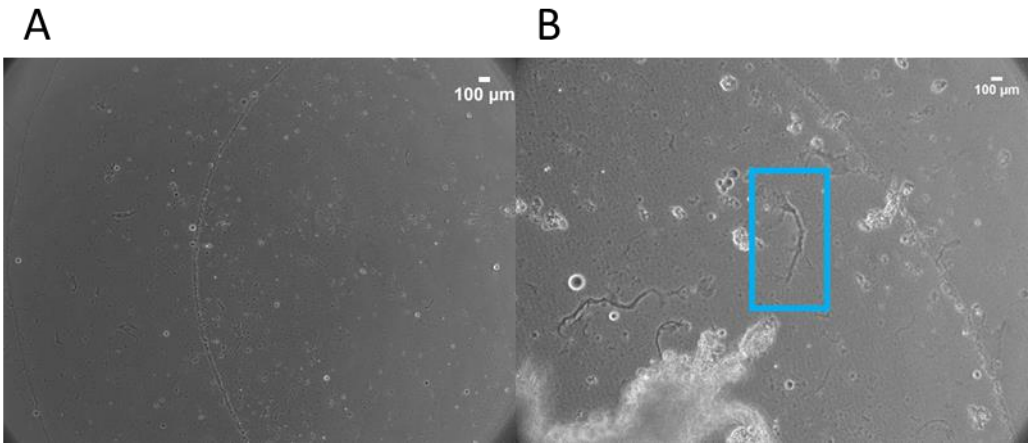

Figure 1. Representative photos of the cellular species seen (a). Highlighted in (b), the area in the blue square resembles a neuron, however further confirmation of neuronal markers is needed for identification.

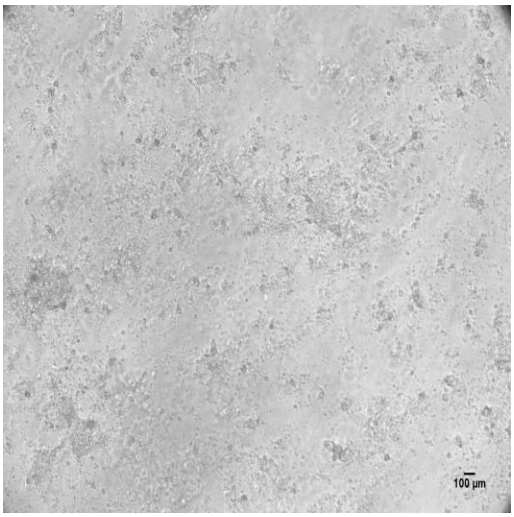

Figure 2. Representative images of non-neuronal cellular species. These resemble glial cells seen in the literature.[19] These cells will be characterized by MS in the future.

Table 1. Four different media combinations explored for crustacean cell culture. Media mixture number "1" was determined to be the best.

	Media Used
1	L-15 + Crab Saline (1:1)
2	L-15 + Crab Saline (1:1) + 10% Fetal Bovine Serum
3	L-15 + Crab Saline (1:1) + 5-10% Hemolymph
4	L-15 + Crab Saline (1:1) + Hemolymph (w/ 0.1 M Sodium Citrate (1:1 Mix with Hemolymph))

Table 2. Four other possible media combinations to consider from the literature.

	Alternatives
1A	L-15 + Crab Saline (1:1) + Corresponding Tissue Extract
2A	L-15 + Crab Saline (1:1) + EGF (10 mg/mL) + Glucose (1 g/L)
3A	Grace's Insect Medium
4A	DMEM-F12 + 10% Fetal Bovine Serum

Appendix III

MALDI Mass Spectrometric Imaging

Analysis of the Rat Uterus

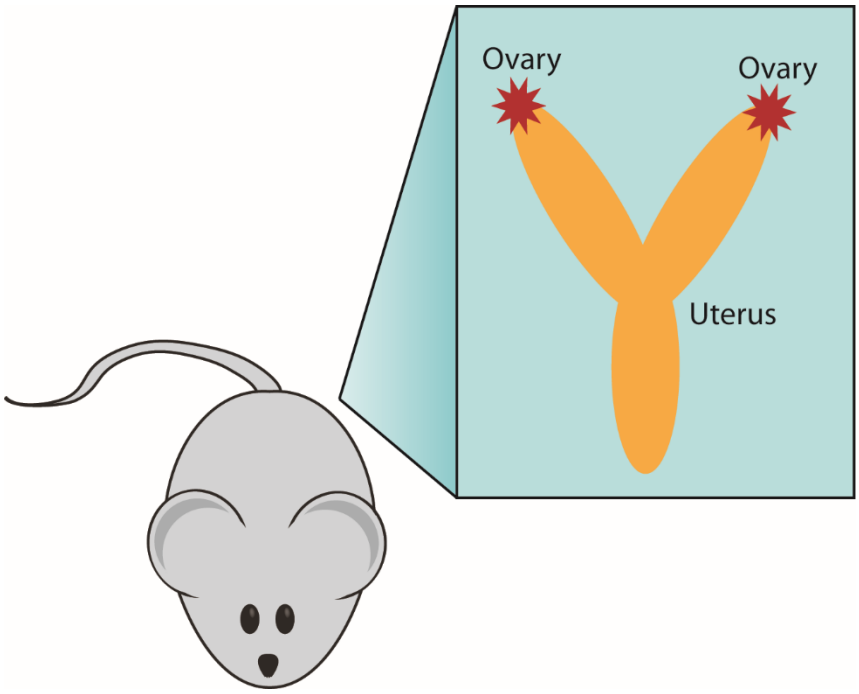

This work was done in collaboration with Megan Spurgeon and Paul Lambert in the McArdle Laboratory for Cancer Research (University of Wisconsin-Madison).

Keywords: Rat Uterus, Cervical Cancer, MALDI-MS imaging, Accurate Mass Matching, Optimal Cutting Temperature

Abstract

Understanding the complex interplay of molecules in cancer is of great interest but also provides a major analytical challenge due to heterogeneity of the tumor microenvironment. Mass spectrometry (MS) imaging allows researchers to map the spatial distribution of molecules of interest without prior knowledge of their structure. Unfortunately, many techniques and materials used in classic medical tissue preparation are incompatible with MS. In this study, control rat uterus sections embedded in optimal cutting temperature compound (OCT), which is traditionally not compatible with MS imaging, were used to investigate which molecular species could be imaged. Various lipids at different *m/z* values were visualized, which can be used to compare control and cancerous tissues in the future.

Introduction

As worldwide major health concern, cancer has received a lot of attention due to the complex signaling mechanisms involved in the disease process.[1-3] Currently, biological imaging techniques focus on either staining of a specific molecular characteristic or specific labeling of a molecule of interest on tissue sections to obtain localization information.[4-6] With genetic profiling, potential signaling molecules of interest can be determined, but this can be difficult if not impossible to obtain a full, global picture of the changes occurring with the variety of post-translational processing steps that occur *in vivo*.[7-9] Overall, there is a limit to the community's ability to discover new factors involved in carcinogenesis, and the development of new techniques is required.

Mass spectrometry (MS) has emerged as a powerful tool for global profiling due to its excellent sensitivity, high speed, and specificity while requiring no prior knowledge.[10, 11] With

the development of MS imaging, the molecular localizations of all ionizable molecular species can be acquired without knowing their structure.[12-15] The first and most common ionization technique used for MS imaging is matrix-assisted laser desorption/ionization (MALDI), which has been extensively used for metabolite, peptide, and protein imaging.[16-18]

Unfortunately, many of the sample preparation strategies used in classical biology are not MS-compatible. For example, in general, an embedding material is used to support the sample prior to sectioning and analysis.[12] These materials range from optimal cutting temperature compound (OCT) to gelatin, the earlier not being compatible for mass spectrometry analysis.[19-21] OCT, a polymer, is known to cause ion suppression and interfere with those molecules that do ionize, although biologist and pathologists still commonly utilize this material.[22]

In this chapter, a rat uterus was used as a method development medium to assess our ability to use MALDI-MS imaging on OCT-embedded tissue sections. Without the use of specialized slides, this research was unable to analyze larger signaling molecules. Furthermore, removal of the OCT was not possible from the tissue section, focusing our imaging range to *m/z* <1000. Several images of metabolites and lipids were acquired with high mass and space resolution, all of which could be potential molecules of interest in the signaling of cancer. Future experiments could include direct comparisons between normal and ovarian cancer tissue samples.

Methods

Materials and Chemicals

Methanol (MeOH) was purchased from Fisher Scientific (Pittsburgh, PA). 2, 5-dihydroxybenzoic acid (DHB) was obtained from Acros Organics (Morris, New Jersey), while

formic acid (FA) was purchased through Fluka (Mexico City, Mexico). Ethanol (EtOH) utilized in this study was from Pharmco-Aaper (Chicago, IL). All water (H_2O) used in this study was doubly distilled on a Millipore filtration system (Burlington, MA) or HPLC grade.

Sample Preparation

All control rat uterus samples were dissected, embedded in OCT, and sectioned at an unknown thickness (~6-20 microns) onto plain glass microscope slides prior to analysis by the Lambert Lab. Serial sections of all samples were stained to help identify and compare differentiation between the epithelial and stromal layers in the cervix. Washes were done with a previously published method using EtOH and H_2O.[21]

Matrix Application

A TM sprayer (HTX Technologies. LLC) was utilized to apply DHB matrix (40 mg/mL in 50:50 MeOH:H_2O with 0.1% FA) onto all tissue sections. For analysis of peptides and proteins, matrix was applied with the following parameters: 0.2 mL/min solvent flow rate, 12 passes, 1250 mm/min velocity, 30 second dry time, 80°C temperature, and 10 PSI gas flow rate. For metabolite analysis, the methodology has been published elsewhere.[23] Briefly, a flow rate of 0.05 mL/min was used as the TM sprayer applied DHB at a velocity of 1250 mm/min at 80°C.

Instrumental Considerations

Three MALDI instruments were used to analyze the tissue sections: (1) Thermo MALDI-LTQ-Orbitrap XL, (2) Bruker MALDI Ultraflextreme (Time of Flight (TOF)/TOF), and (3) Waters MALDI-Synapt G2 (TOF). The instruments were used to analyze metabolites/peptides/lipids (*m/z* 100-4000), peptides/small proteins (*m/z* 4000-7000), and proteins (*m/z* 4000-10,000), respectively. The spatial resolution acquired for all images was 75 micrometers.

Data Processing

Raw data was exported to the .imzML form using Thermo ImageQuest. MSiReader was utilized for all further image processing. The "Peak Finder" program allows for users to differentiate between signal in outside and inside the tissue. Our parameters required that the signal be in at least 50% of the tissue area and less than 10% of the reference (matrix/OCT) region. All identifications were done by accurate mass matching (AMM) to online databases (LIPIDMAPS and Metlin for lipids and metabolites, respectively) within a ±5 parts per million (ppm) mass error.

Results and Discussion

In order to determine which molecule types could ionize efficiently, several instruments and mass analyzers were utilized in conjunction with a MALDI source. As uterus samples were embedded in OCT, a well-known ion suppressor and mass spectrometer contaminant, and were not sectioned on indium tin oxide (ITO) coated slides, both TOF-based instruments were unable to produce adequate signal above the baseline noise with acceptable peak shapes. While OCT can be focused only around the outside of the tissue and not within the tissue (**Figure 1**), OCT contamination on the sectioning blade can then cause OCT contamination in the sample (**Figure 2A**). Thus, the MALDI-Orbitrap was selected at the sole instrumental platform for this analysis.

Initial analysis in the peptide range (*m/z* 500-4000) showed a strong OCT signal outside the tissue **(Figure 1)**, but inside the tissue appeared to be OCT-free. This was not the case in a later analysis **(Figure 2a)**. Depending on the synthesis procedure, OCT can have a polymer signal that ranges from 1000 to 20,000 Daltons due to its polyethylene glycol structure.[24] In our case, this signal spanned from *m/z* 1000-2000, which can limit identifications by ion suppression

or by interfering with true sample peaks.[22] Washing with a previously described method was attempted in order to remove any OCT found on the sample.[21] While the OCT signal was effectively removed, due to the conditions of the washes, many of the other analytes of interested have appeared to have washed off as well (**Figure 2**). This was expected, since this wash method was developed for protein fixation and utilizes high water content in its washes. Since the OCT seems to only contaminate *m/z* 1000 and above, no special processing (*i.e.*, no washing) would be required to analyze the metabolites and small lipids (*m/z* 100-1000) in the uterus tissue section.

Several peaks were visualized on unwashed tissue sections, as shown in **Figure 3 and 4** for the metabolite and peptide/lipids imaging runs respectively, many of which we're able to discern the epithelial and stroma layers (**Figure 5**). From both analysis, several preliminary identifications were made, mainly to several lipid subclasses. The highlighted masses in the distribution analysis (**Figure 3** and **4**) and their possible matching identities are outlined in **Table 1**. It should be noted that many of these were deemed unknown based on our database searches. These unique and interesting masses maybe related to uterine signaling, but without tandem MS (MS/MS) analysis, where fragments are collected from the parent ion in order to determine its original sequence, it will be hard to provide confident identifications. In particular, structural identification from MS/MS can be difficult for metabolites, but peptide identification could rely on *de novo* sequencing. Methods have been developed, including dimethylating the peptide or metabolite, to increase ionization and fragmentation efficiency.[25] Utilizing a spiral step method for better MS/MS spectra collection during imaging, is also another avenue to consider.[26] While most of the masses appear to not be contaminated by OCT embedding media, *m/z* 313.032 on **Figure 3** shows a signal outside the tissue section. Thus, due to the possible contamination and

ion suppression, quantitation between different *m/z* values or even different tissues will be difficult.

Conclusions and Future Directions

While several interesting distributions were found through this analysis, all identifications were made only on AMM. Without targeted confirmation (MS/MS or other biological assays), these can only be considered preliminary identifications. With future replicates, biological samples, and possibly newly developed methodology/instrumentation, these masses and possibly spatial distributions of other interesting molecules could lead to an improved understanding about the cervical carcinogenesis or other samples that have been embedded in OCT by MALDI-MS imaging.

References

1. Zhao, J.; Guan, J. L., *Cancer and Metastasis Reviews* **2009,** *28* (1-2), 35-49.

2. Giampieri, S.; Manning, C.; Hooper, S.; Jones, L.; Hill, C. S.; Sahai, E., *Nature Cell Biology* **2009,** *11* (11), 1287-U49.

3. Uhlen, M.; Fagerberg, L.; Hallstrom, B. M.; Lindskog, C.; Oksvold, P.; Mardinoglu, A.; Sivertsson, A.; Kampf, C.; Sjostedt, E.; Asplund, A.; Olsson, I.; Edlund, K.; Lundberg, E.; Navani, S.; Szigyarto, C. A.; Odeberg, J.; Djureinovic, D.; Takanen, J. O.; Hober, S.; Alm, T.; Edqvist, P. H.; Berling, H.; Tegel, H.; Mulder, J.; Rockberg, J.; Nilsson, P.; Schwenk, J. M.; Hamsten, M.; von Feilitzen, K.; Forsberg, M.; Persson, L.; Johansson, F.; Zwahlen, M.; von Heijne, G.; Nielsen, J.; Ponten, F., *Science* **2015,** *347* (6220), 10.

4. Leung, B. O.; Chou, K. C., *Applied Spectroscopy* **2011,** *65* (9), 967-980.

5. Poobalasingam, T.; Salman, D.; Li, H.; Alcada, J.; Dean, C. H., *Histology and Histopathology* **2017,** *32* (4), 325-337.

6. Feuchtinger, A.; Walch, A.; Dobosz, M., *Histochemistry and Cell Biology* **2016,** *146* (6), 781-806.

7. Khoo, M. L. M.; Carlin, S. M.; Lutherborrow, M. A.; Jayaswal, V.; Ma, D. D. F.; Moore, J. J., *Aging Cell* **2014,** *13* (4), 744-754.

8. Stone, R. A.; Khurana, T. S., *Vision Research* **2010,** *50* (23), 2322-2333.

9. Kazezian, Z.; Gawri, R.; Haglund, L.; Ouellet, J.; Mwale, F.; Tarrant, F.; O'Gaora, P.; Pandit, A.; Alini, M.; Grad, S., *Scientific Reports* **2015,** *5*, 13.

10. Ye, H.; Gemperline, E.; Li, L. J., *Clinica Chimica Acta* **2013,** *420*, 11-22.

11. Hebert, A. S.; Richards, A. L.; Bailey, D. J.; Ulbrich, A.; Coughlin, E. E.; Westphall, M. S.; Coon, J. J., *Molecular & Cellular Proteomics* **2014,** *13* (1), 339-347.

12. Gemperline, E.; Chen, B. M.; Li, L. J., *Bioanalysis* **2014,** *6* (4), 525-540.

13. Buchberger, A.; Yu, Q.; Li, L., *Annu Rev Anal Chem (Palo Alto Calif)* **2015,** *8* (1), 485-509.

14. Lietz, C. B.; Gemperline, E.; Li, L. J., *Advanced Drug Delivery Reviews* **2013,** *65* (8), 1074-1085.

15. Jungmann, J. H.; Heeren, R. M. A., *Journal of Proteomics* **2012,** *75* (16), 5077-5092.

16. Caprioli, R. M.; Farmer, T. B.; Gile, J., *Analytical Chemistry* **1997,** *69* (23), 4751-4760.

17. Dreisewerd, K., *Analytical and Bioanalytical Chemistry* **2014,** *406* (9-10), 2261-2278.

18. Boggio, K. J.; Obasuyi, E.; Sugino, K.; Nelson, S. B.; Agar, N. Y. R.; Agar, J. N., *Expert Review of Proteomics* **2011,** *8* (5), 591-604.

19. Weston, L. A.; Hummon, A. B., *Analyst* **2013,** *138* (21), 6380-6384.

20. Zhang, W.; Sakashita, S.; Taylor, P.; Tsao, M. S.; Moran, M. F., *Methods* **2015,** *81*, 50-55.

21. Chaurand, P.; Rahman, M. A.; Hunt, T.; Mobley, J. A.; Gu, G.; Latham, J. C.; Caprioli, R. M.; Kasper, S., *Molecular & Cellular Proteomics* **2008,** *7* (2), 411-423.

22. Pirman, D. A.; Kiss, A.; Heeren, R. M. A.; Yost, R. A., *Analytical Chemistry* **2013,** *85* (2), 1090-1096.

23. Gemperline, E.; Rawson, S.; Li, L. J., *Analytical Chemistry* **2014,** *86* (20), 10030-10035.

24. Lin-Gibson, S.; Bencherif, S.; Cooper, J. A.; Wetzel, S. J.; Antonucci, J. M.; Vogel, B. M.; Horkay, F.; Washburn, N. R., *Biomacromolecules* **2004,** *5* (4), 1280-1287.

25. Fu, Q.; Li, L. J., *Analytical Chemistry* **2005,** *77* (23), 7783-7795.

26. OuYang, C.; Chen, B.; Li, L., *J Am Soc Mass Spectrom* **2015,** *26* (12), 1992-2001.

27. Spurgeon, M. E.; den Boon, J. A.; Horswill, M.; Barthakur, S.; Forouzan, O.; Rader, J. S.; Beebe, D. J.; Roopra, A.; Ahlquist, P.; Lambert, P. F., *Proceedings of the National Academy of Sciences of the United States of America* **2017,** *114* (43), E9076-E9085.

Figures

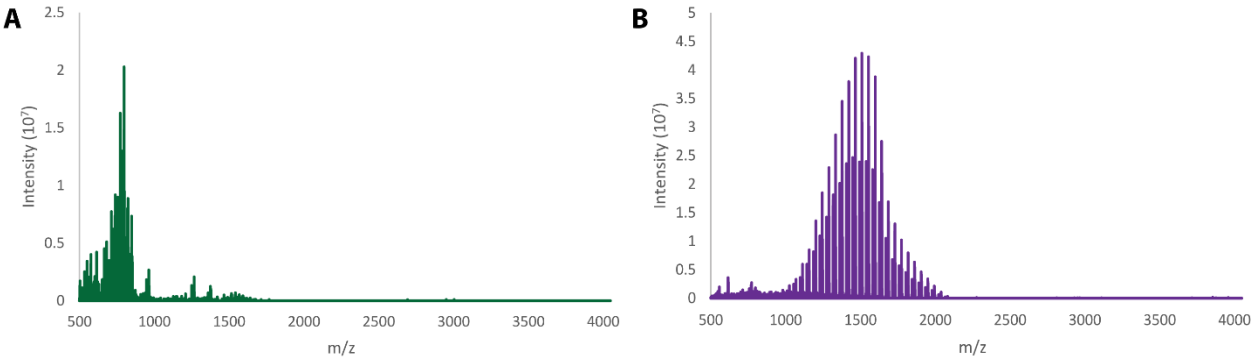

Figure 1. A comparison of the MS spectra from inside the tissue (a) and the outside of the tissue (b). The strong polymer signal outside the tissue is OCT, the embedding material.

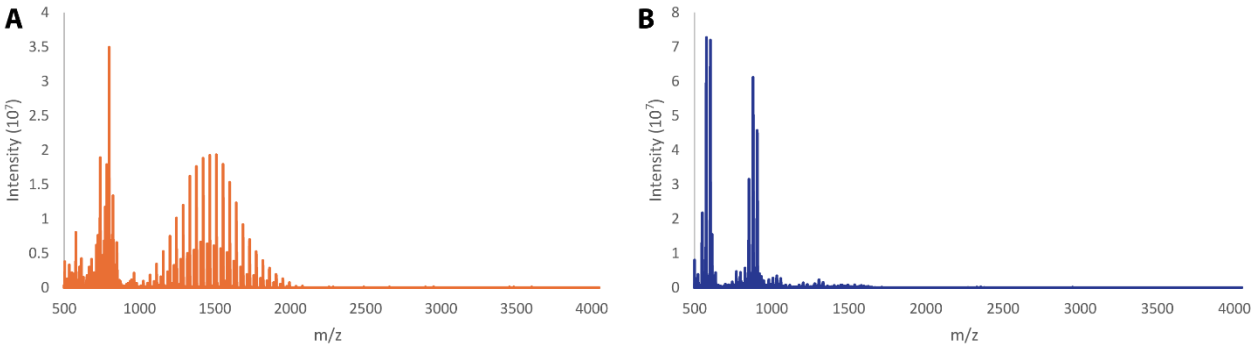

Figure 2. A comparison of MS spectra from inside the tissue before (a) and after (b) washing the tissue. In this case, OCT has contaminated the sample section. Washing the tissue section removed the polymer signal, but the sample has been compromised (*e.g.*, contaminated) otherwise.

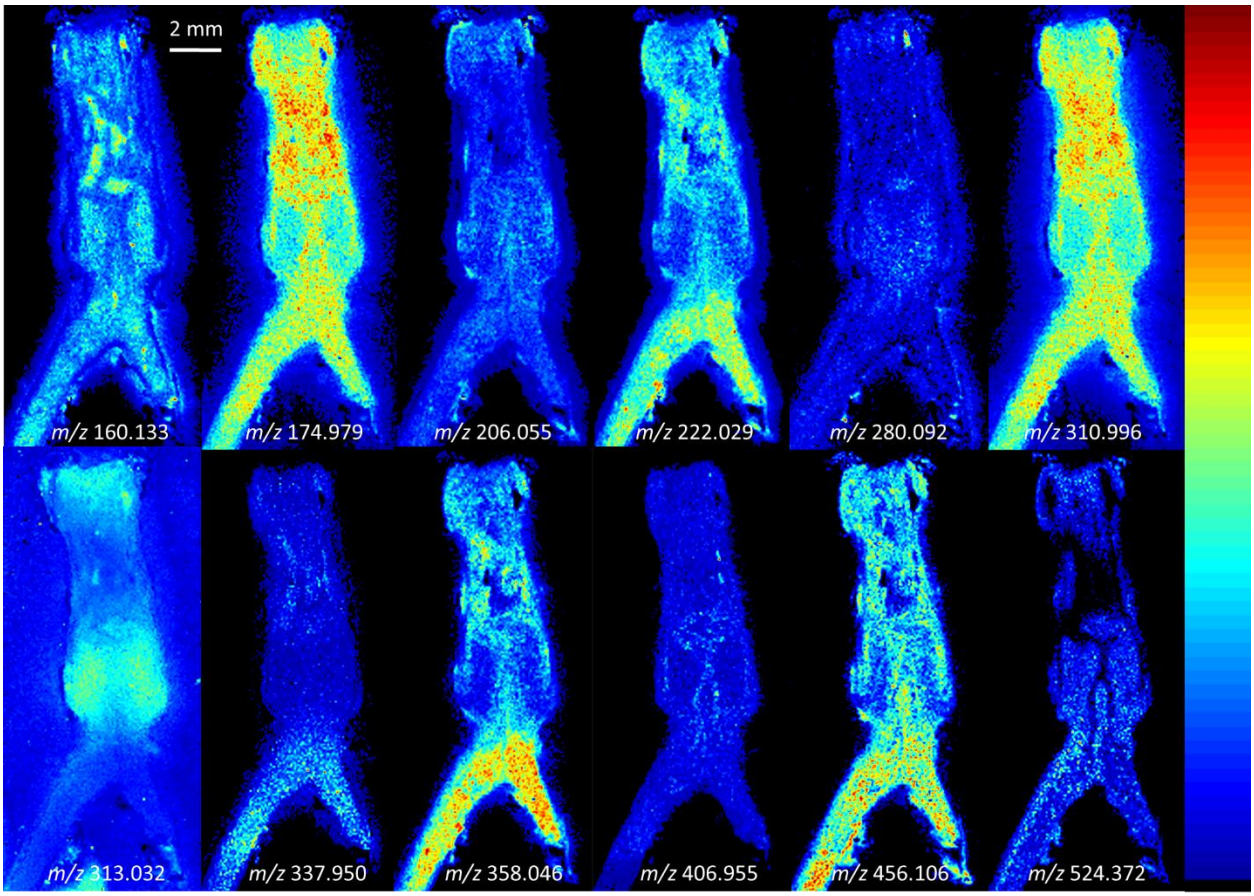

Figure 3. Metabolomic imaging of a section of rat uterus, where the ovaries are attached to the horns (down) away from the vagina (up). Several *m/z* values are highlighted, including those localized in the epithilalal layer (*m/z* 160.133), stromal layer (*m/z* 222.029), within the cervix (*m/z* 313.032), or all over the entire uterus (*m/z* 310.996).

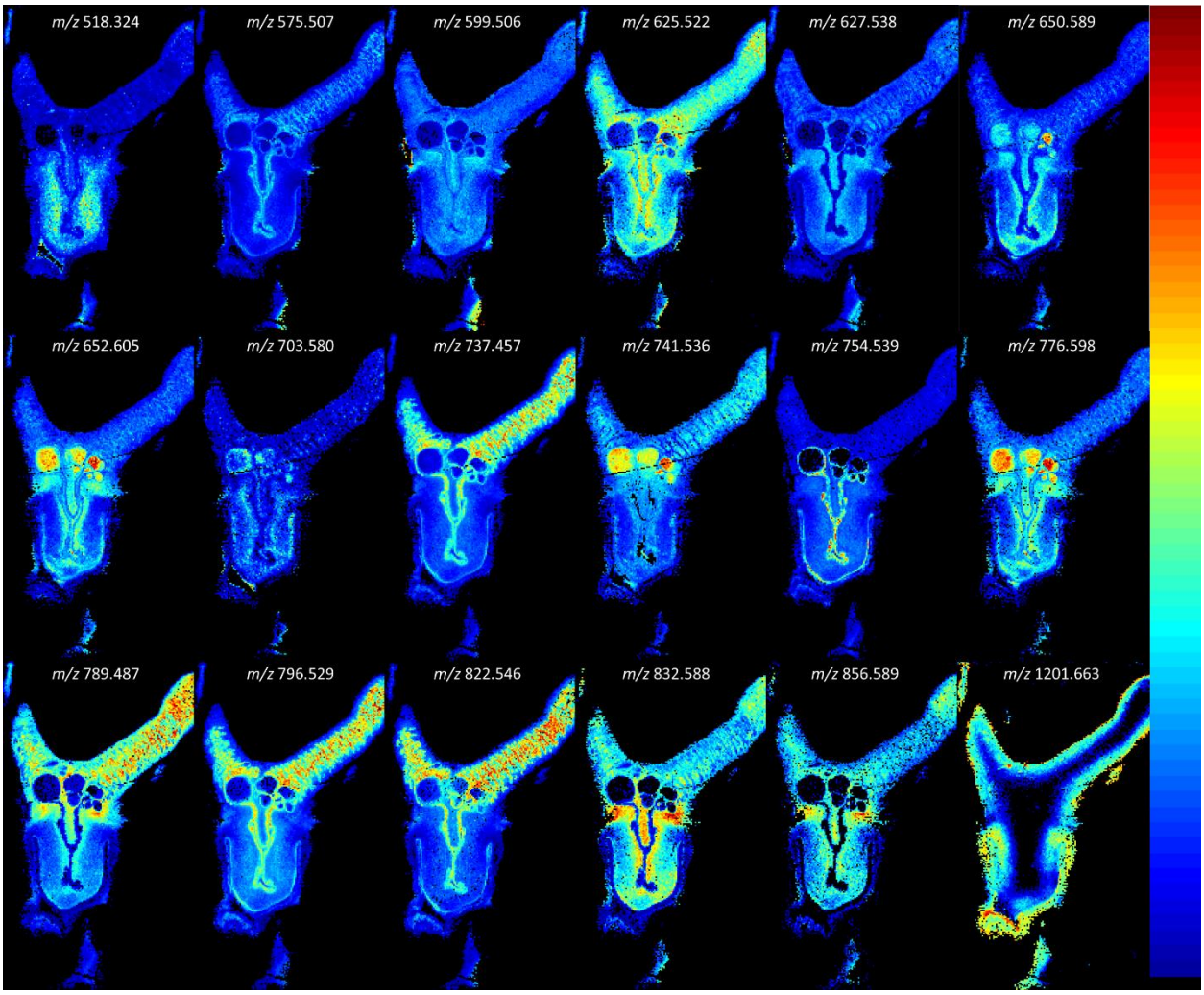

Figure 4. Imaging of a section of rat uterus, where the ovaries are attached the horns (up) away from the vagina (down). Several mass-to-charge values are highlighted, including those localized in the epithelial layer (*m/z* 856.589), stromal layer (*m/z* 754.539), within the cervix (*m/z* 518.324), or all over the entire uterus (*m/z* 625.522).

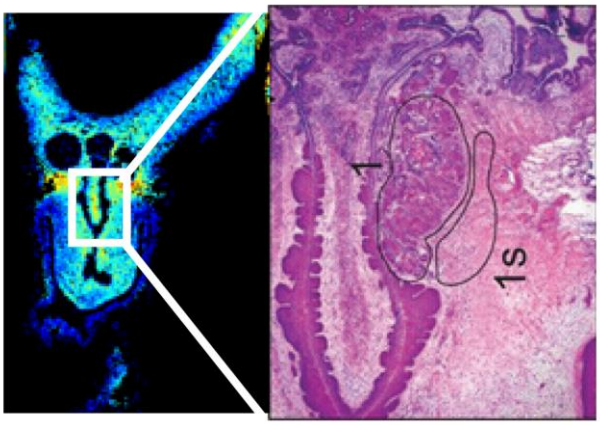

Figure 5. A visualization of the stromal and the epithelial layers in the uterus. “Area 1” is the epithelial layer, while “Area 1s” is the stromal layer. Adapted with permission.[27]

Table 1. Preliminary Identifications for the highlighted MALDI-MS imaging distributions. The ones in red came back with no identifications.

m/z Value	Matched Identity
160.133	DL-2-Aminooctanoic acid
174.979	2-Chloro-4-carboxymethylenebut-2-en-1,4-olide
206.055	Lipoamide
222.029	Unknown
280.092	Unknown
310.996	Unknown
313.032	Several Metabolites
337.95	Unknown
358.046	Unknown
406.955	Unknown
456.106	Unknown
518.324	Various Lipids
524.372	Various Lipds
575.507	Mayolene-19
599.506	3,4-Dihydrospirilloxanthin
625.522	Various Lipids
627.538	Various Lipids
650.589	Unknown
652.605	Unknown
703.58	Various Lipds
737.457	Unknown
741.536	Various Lipds
754.539	Various Lipds
776.598	Various Lipids
789.487	Various Lipids
796.529	Various Lipids
822.546	Various Lipids
832.588	Various Lipids
856.589	Various Lipids
1201.663	Various Lipids

Appendix V

Girls Rule, Boys Drool:

A Study of Gender Differences in Crustaceans

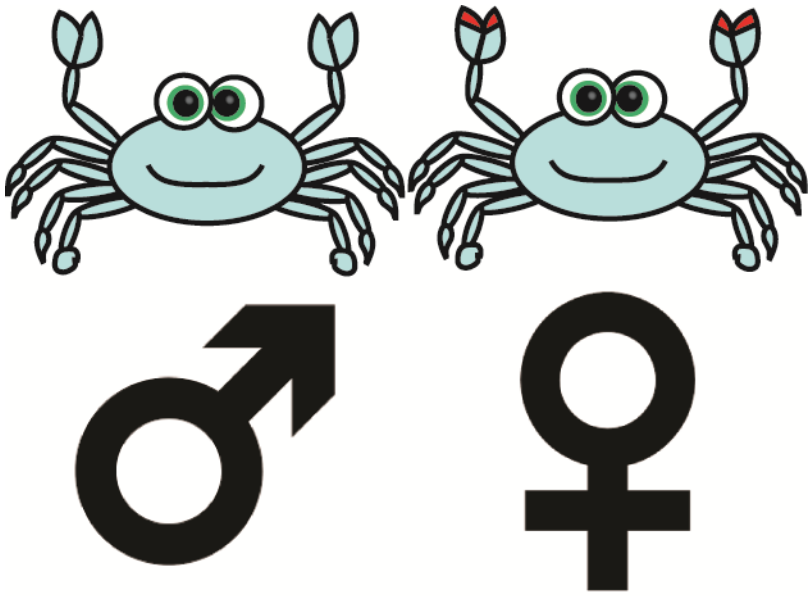

Modified from:

Clara Hu[¥], Kylie Helfenbein[¥], **Amanda R. Buchberger**, Kellen DeLaney, Yang Liu, Lingjun Li. "A Study of Gender Differences in Crustaceans." In Preparation, 2018. [¥]Co-first Authors

Keywords: Mass Spectrometry, Crustacean, Neuropeptides, *Callinectes sapidus*, Female, Male

Abstract

Males and females are well-documented to be socially, physically, and chemically different from each other. These differences manifest in the nervous system, likely due to the natural diversity of biological signaling molecules and their targets. Neuropeptides are known to be key players in the nervous system, drawing from their roles in major physiological processes, including the stress response and feeding. By utilizing both the crustacean model organism and mass spectrometry, various differences were observed between male and female blue crabs in both nervous system tissue and hemolymph. However, it was discovered that, though specific neuropeptide isoforms vary greatly between male and female crabs, the general representation of each family remains largely consistent between the two sexes. Furthermore, it was found that many neuropeptides have statistically significant differences in abundance in male and female crabs, most notably RFamides, which tend to appear in greater abundance in males compared to females. These findings suggest the possibility of sex-specific functions of various neuropeptide isoforms.

Introduction

Male and females have displayed key differences in terms of social behaviors, physical manifestations, and even deeper biological variability.[1-5] Of particular interest is the nervous system, which affects an individual's ability to respond to unfavorable situations and harmful stressors.[6-10] For example, males and females have shown activation in distinct brain regions associated with behaviors and responses to environmental stimuli, with males exhibiting a more active, physical response and females a more emotional, verbal response.[6]

The reason for differences in nervous system activity between males and females is not yet well understood. This lack of knowledge is likely due to the large biological diversity in the nervous system, which includes molecules that range in size from small (*e.g.*, neurotransmitters) to large (*e.g.*, proteins). Neuropeptides, short-chain amino acid sequences with diverse structures, are released from neurons to act as both autocrine and paracrine messengers.[11-13] They also function as long-range circulating hormones when secreted into the circulating fluid (*e.g.*, blood and lymph).[11-13] Due to their important and variable roles in the nervous system, studying these signaling peptides can reveal a more complete picture of male or female differences. In response to environmental changes, sexes have also shown varied detoxification abilities and behaviors, likely due to differences in mechanisms of neurological signaling molecules, such as neuropeptides, which have been previously implicated in the stress response.[14-17] One specific neuro-protein, brain-derived neurotrophic factor (BDNF), has been found in higher levels in varying brain regions of female subjects (*e.g.*, humans and mice) when compared to that of males. In contrast, these levels were not observed to be different in the blood or serum of humans.[9] From studying different components of the nervous system, it is possible to explore the potentially differentiated role of BDNF in males and females in modulating sex-specific activity or expressing activation of sex-specific pathways.

Difficulties in analyzing neuropeptides in mammalian systems stem from the complex biological matrix and less well-characterized networks. In order to characterize nervous system differences on a global scale, several model organisms, including invertebrates, have been utilized.[14, 18-21] For globally profiling neuropeptidomic changes, crustaceans provide a simple, well-characterized, neuropeptide-rich network, which has been utilized to understand several physiological conditions.[15-17, 22, 23] By using crustaceans, we can manipulate external variables to

better understand the role of multiple neuropeptides. In general, there are three major systems of interest for characterizing neuropeptides: the nervous system, the neuroendocrine system, and the circulatory system that transports neuropeptides between the two. Several prominent tissues make up the crustacean nervous system and neuroendocrine system. For example, the pericardial organs (PO) are located near the heart, and neuropeptides released tend to exhibit myotrophic effects directly on the heart tissue.[24] The POs also release neuropeptides into the circulating fluid to travel long-range and exert modulatory effects on tissues in the nervous system (*e.g.*, brain and commissural ganglia (CoG)). In crustaceans, the circulating fluid is comprised of hemolymph, which serves the purpose of both blood and lymph and transports neuropeptides between tissues.[25] Hence, studying both hemolymph and tissues from various parts of the crab can improve the understanding of the secretion of neuropeptides from tissues and their modulatory and hormonal effect on various systems. There have been several previous studies profiling both tissue-based neuropeptides and circulating hormones in crustacean hemolymph, but there has not yet been a comparative study performed on gender differences in neuropeptides present in these model organisms.[15-17, 26, 27] Therefore, combining the data from tissue and hemolymph can provide a deeper neuropeptidomic profiling in order to study the differences in the level of neural responses between male and female crustacean model organisms.

In order to characterize the differences between male and female crustaceans, this study utilizes a duplex reductive dimethylation strategy coupled to matrix-assisted laser/desorption ionization (MALDI) mass spectrometry (MS) to obtain a quantitative global profile of the differences in the blue crab, *Callinectes sapidus*. Interestingly, while males and females possess numerous neuropeptide isoforms that are unique to their sex, the represented families of each remain largely consistent. However, differences in isoforms belonging to families were also

observed, such as the numbers of RFamide and allatostatin A-type (AST-A) neuropeptide isoforms. Quantitatively, 80 neuropeptides detected across 5 neural tissues and the hemolymph were found to be statistically different between male and female crabs. Notably, neuropeptide isoforms belonging to the RFamide family tend to be present in greater abundance in males than females. The use of electrospray ionization (ESI) will be applied in the future to enhance our neuropeptidomic coverage.

Methods

Materials and Chemicals

Methanol (MeOH), glacial acetic acid (GAA), formic acid (FA), sodium hydroxide (NaOH), and all crab saline components (see below) were from Fisher Scientific (Pittsburgh, PA). 10 kDa molecular weight cut-off tubes (MWCO) were purchased from Amicon Utracel (Elgin, IL). Formaldehyde (CH_2O) and borane pyridine complex (~8M BH3) were obtained from Sigma-Aldrich (St. Louis, MO). $^2H_2$-formaldehyde (C^2H_2O) was from Isotech (Miamisburg, OH). 2,5-dihydroxybenzoic acid (DHB) were purchased from MP Biomedicals (Solon, OH). All distilled water (H_2O) was obtained from a Millipore filtration system (Bedford, MA).

Hemolymph Collection and Tissue Dissection

Male and female blue crabs (*Callinectes sapidus*) were obtained from LA Crawfish Company (Natchitoches, LA). All animals were housed in chilled artificial seawater tanks at 12˚C for at least 24 hours prior to use. Each crab was removed from the tank and placed on ice for 10 minutes prior to hemolymph withdrawal. The crab was placed on a metal dissecting pan with ventral side up, and a 25-gauge needle attached to 1 mL syringe (Beckton Dickinson, Franklin Lakes, NJ) was inserted into one of the soft joints. 1 mL of hemolymph was removed.

The crab was then placed on ice for an additional 10 minutes prior to dissection. Five distinct tissue types were isolated during the dissection, including the brain, sinus glands (SG), paired PO, thoracic ganglion (TG) and paired CoG tissue samples, in chilled physiological saline (composition: 440 mM NaCl; 11 mM KCl; 13 mM $CaCl_2$; 26 mM $MgCl_2$; 10 mM Trizma acid; pH 7.4 (adjusted with NaOH)) as previously described.[28, 29]

Hemolymph Extraction and Clean Up

Equal volume of acidified MeOH (90:9:1 MeOH:H_2O:GAA) was added to the hemolymph sample and the mixture was vortexed vigorously. The sample then was sonicated for 5 min to break down large particles followed by centrifugation for 5 min×16,100 g using an Eppendorf 5424R centrifuge (Hauppauge, NY). Supernatant was removed and placed into a new tube. The pellet was homogenized using a Teflon pestle in 0.5 mL acidified MeOH, and the previous steps were repeated two additional times (for a total of 3 extractions). The combined supernatant from each extraction was evaporated in a Savant SC 110 Speedvac (Thermo Electron Corporation, Waltham, MA, USA) at medium heat prior to being resuspended in 0.5 mL 30:70 MeOH:H_2O.

A 10kDa MWCO device prepared by rinsing with 0.2 mL 0.1M NaOH (centrifuged for 4 min×14,000 g) followed by 0.5 mL of 50:50 H_2O:MeOH (centrifuged 8 min×14,000 g). The sample was then loaded into the device (centrifuged for 20 min×16,100 g) followed by rinsing with 0.1 mL of 30:70 MeOH:H_2O (centrifuged 5min×16,100 g). All centrifugation steps were performed at 4˚C. The flow-through was collected from sample and following rinse step, and the combined sample was evaporated by a Speedvac on medium heat. The sample was then dissolved in 150 µL 0.1% FA, vortexed vigorously, and sonicated for 5 min. Samples were then desalted according to manufacturer's recommendations using the Agilent Bond Elute 100 µL C_{18}

OMIX tips (Santa Clara, CA) and dried down in a Speedvac. If storage was required, the sample was resuspended in the solvent needed for the next step of clean up at -80˚C.

Tissue Extraction and Clean Up

Prior to sonication, acidified MeOH (100-150 μL) was added to tissue tube. Neuropeptides were extracted on ice using a Fisher Scientific Sonic Dismembrator (Model 120). Extraction was done in three sets of 8 second pulses (50% amplitude) separated by 15 second pauses. The homogenized extract was then centrifuged at 20,000 g for 15 minutes at 4˚C. The supernatant was then transferred to a new tube to be dried down using a Speedvac. Samples were then desalted according to manufacturer's recommendations using Millipore 10 μL C_{18} ZipTips (Billerica, MA) and dried down. If storage was required, the sample was stored dry at -80˚C.

Isotopic Formaldehyde Labeling

Male and female crab samples were distinguished using duplex isotopic reductive dimethylation as previously published.[30] Briefly, each sample was treated with either 1% CH_2O (light) solution or 1% C^2H_2O (heavy) solution with borane pyridine complex solution (0.03M BH_3). Samples were then incubated at 37˚C for 15 minutes in a warm water bath followed by quenching with ammonium bicarbonate (100 mM). Male and female samples were mixed 1:1 by tissue (or hemolymph) type and dried down in a Speedvac.

Data Collection and Processing

Samples (dissolved in H_2O with 0.1% FA) (n=7) were analyzed on the Thermo MALDI-LTQ-Orbitrap XL after spotting with DHB (150 mg/mL; 50:50 MeOH:H_2O and 0.1% FA) in triplicate at 60,000 mass resolution from *m/z* 500-2000 or 4000. Data from all comparative studies were analyzed using a custom program written in Java for accurate mass matching both light (+28.0313 Da) and heavy (+32.0564 Da) peaks to an in-house crustacean neuropeptide

database. Analysis parameters included an intensity threshold of 100 and mass error of +/-5 ppm. Neuropeptides that were identified in at least two technical replicates and one biological replicate were considered for all qualitative analyses. Quantitative ratios were calculated by dividing the "female" peak intensity by the "male" peak intensity. Only those that were found in at least 2 technical replicates and 3 biological replicates were analyzed for statistical significance, which was done using a student's t-test ($p<0.05$).

Results and Discussion

This study aimed to investigate differences between female and male crabs based on the presence and level of neuropeptides in tissues and circulating fluid (*i.e.,* hemolymph). The data collected indicate the differences in the isoforms, families, and quantitative abundance of various neuropeptide families and individual neuropeptide isoforms.

Differences in the Isoforms of Neuropeptides

In general, each neuropeptide family contains various neuropeptide isoforms. Though neuropeptides from the same family are often pleiotropic, different isoforms are commonly encoded by paralog genes.[31-35] As a result, individual isoforms may have the same or different functions within the nervous and neuroendocrine system. Here, we compared the isoforms detected exclusively in male samples and female samples along with those present in both in hemolymph and five different tissue types (*i.e.,* SG, brain, PO, CoG, and TG) (**Figure 1**). It was observed that female and male *C. sapidus* have several neuropeptide isoforms that are unique to each sex, especially in comparison to those in common between the two groups. In hemolymph, there was a greater overall number of neuropeptides identified in each biological replicate compared to tissue. However, there were fewer neuropeptides detected consistently across

multiple biological replicates, which manifests in the quantitation data discussed later. This is likely due to the circulating nature of neuropeptides in the hemolymph, which introduces a greater variability in neuropeptides present at a given time in a given animal, or interfering protein fragments causing misidentifications. It should be noted that the hemolymph results do reflect the same trend observed in the tissue, where the number of neuropeptides unique to each sex is greater than that shared between the two sexes. The large number of unique isoforms between two samples indicate that different neuropeptide isoforms may participate in providing signals in female and male nervous and neuroendocrine systems. These neuropeptides may also serve functions specific to modulating female and male physiological processes.

Families of Neuropeptides Identified

The large number of unique isoforms indicate that there is substantial diversity of individual neuropeptides between females and males, which indicates the difference between sexes. However, the families each neuropeptide isoform belong to are largely conserved in both tissue and hemolymph. **Figure 2** shows the distribution of families of detected isoforms in all tissue samples analyzed. Most of the families detected are identical between the two sexes, but there are several small differences to be noted. For example, the number of neuropeptides belonging to the AST-A family is greater than that of the RFamide family in females, while the opposite is reflected in male samples. Such trends were also observed in specific tissues, including the PO, SG, brain, and CoG (**Figures S1, S2, S3,** and **S4**, respectively). The TG (**Figure S5**) was the only tissue that did not follow this trend. Another trend is that the numbers of neuropeptides in the kinins, red pigment dispersing hormone (RPCH), and cryptocyanin families are different between female and male, which may be due to the distinct physiological differences in two sexes.

The POs are a prominent neurosecretory release site, so this tissue tends to contain more neuropeptides from a variety of families. Moreover, neuropeptides released from PO are transported directly to the pericardial sinus where hemolymph is collected.[24] Therefore, it is interesting to highlight neuropeptides detected in the PO and to correlate these with those present in the circulating hemolymph. As shown in the pie charts in **Figure S4**, more isoforms of crustacean cardioactive peptide (CCAP) were present in female PO samples, while kinins and pigment dispersing hormone (PDH) are two families where more isoforms were detected in male POs. The differences indicate that more isoforms of CCAP family are needed in female POs to modulate neuroendocrine activities, while these kinins and PDH isoforms may be involved in more male-specific functions. The distribution of families detected in hemolymph (**Figure 4**) from females almost correspond exactly to those in males, except lower amount of kinins, higher amount of cryptocyanin, and the absence of SIFamide. The data indicates that a greater variety in the cryptocyanin family is secreted into the circulating fluid in females than males, and less diversity of neuropeptides and possible proteins are involved in regulating the male neuroendocrine system as circulating hormones. Overall, the families are similar in both tissue and hemolymph samples, which implies that, even though the specific neuropeptide isoforms are different, they may still serve similar functions in female and male *C. sapidus*. It should be noted

Quantitative Differences of Neuropeptides

In addition to the diversity of function based on varying isoforms, the *in vivo* concentration of individual neuropeptides can also affect their modulatory function in the nervous system.[36, 37] Therefore, relative quantitation was performed with reductive dimethylation to compare the abundance of neuropeptides between sexes.[15-17, 22, 30] Those neuropeptides that exhibited statistically significant changes in abundance ($p<0.05$) are shown for each tissue

analyzed (**Figures 4, S6, S7, S8,** and **S9**), as well as hemolymph (**Figure 6**). The numerical results are also available in **Table S1-S6**. Overall, there were many neuropeptides that showed significant differences in abundance between male and female in tissue and hemolymph samples. It is interesting to note that, while six neuropeptide isoforms belonging to the AST-A family were detected at higher levels in the POs of female crabs, three AST-A isoforms (*i.e.*, YSFGLamide, GHYNFGLamide and PRDYAFGLamide) are present in larger amounts in male crabs. Neuropeptides belonging to the RFamide family (*e.g.*, NPSDFLRFamide, AQPSMRLRFamide and YGSDRNFLRFamide) tend to be in greater abundance in males, and the number of neuropeptide isoforms in the same family are also higher in male. This observation suggests that RFamides may be implicated in modulating male-specific functions. Overall, fewer quantifiable neuropeptides were detected in hemolymph samples, which is likely due to the much lower concentrations and greater variability of these circulating peptide hormones. The observed variability of neuropeptides in hemolymph is also possibly attributed to low *in vivo* concentrations and obscured signals due to the presence of interfering artifacts such as lipids and large protein fragments. As a result, fewer neuropeptides are detected consistently across enough biological replicates to enable quantification. Regardless, the quantified neuropeptide trends in the hemolymph are consistent with those observed in the PO. Even though the numbers of neuropeptide isoforms belonging to the RFamide family are similar between male and females, males tend to have a greater relative abundance of RFamide neuropeptides (*e.g.*, NRNFLRFamide and LNQPNFLRFamide), which suggests that they may be involved in male-specific functions in addition to possible other functions. Though the trends in relative abundance of neuropeptide families are similar between PO and hemolymph, the specific neuropeptide isoforms are different. Such differences imply the neuropeptides detected in

hemolymph may originate from other neuroendocrine tissue. Also, not all neuropeptides present in the POs are routinely released into the hemolymph. The neuropeptides detected in the POs may not act as circulating hormones in the nervous system but instead may trigger the release of other neuropeptides. They also may only be released under specific stimuli (*e.g.*, to perform biological processes or respond to environmental changes).[15, 17, 22] One neuropeptide found in hemolymph (*i.e.*, RFamide, GYSKNYLRFamide) has a different trend than the others in the same family, where it has a greater abundance in females than in males. This neuropeptide was also detected in the SGs, though no significant changes were observed (*data not shown*), which indicates that the SG may be secreting this specific neuropeptide into hemolymph. The increased expression of this neuropeptide isoform in females may indicate that it may participate in female-specific functions. Another RFamide neuropeptide (*i.e.*, LNQPNFLRFamide) was found to be significantly increased in female TGs but significantly decreased in female hemolymph. These results may mean that the neuropeptide tends to be secreted from the TG into hemolymph as circulating hormones in males and tends to function more locally in females. Overall, the differences in abundance of neuropeptides between males and females may reflect additional sex-specific functions of various isoforms. Furthermore, comparing the abundance differences in tissue and hemolymph reveals potential long-range and short-range effects.

Conclusions and Future Directions

Overall, this study sought to assess the differences in the neuropeptidome of male and female blue crabs in order to better understand the underlying function of these neuropeptides. It was discovered that, though specific neuropeptide isoforms vary greatly between male and female crabs, the general representation of each family remains largely consistent between the

two sexes. Furthermore, it was found that many neuropeptides have statistically significant differences in abundance in male and female crabs, which indicates the possibility of sex-specific functions of various neuropeptide isoforms. These results may be useful for future studies into the functional roles of neuropeptides in decapod crustacean species, as well as higher-order organisms with neuropeptide homologues. To complement our analysis, identification of known reproductively-related or sex-specific peptide hormones will be mined from this data. Future studies may involve electrophysiology to investigate the specific functions of neuropeptide isoforms with statistically significant changes. Finally, ESI-MS will also be utilized to increase the neuropeptidomic coverage between male and female crustaceans.

Acknowledgements

This work was supported by a National Science Foundation grant (CHE-1710140) and the National Institutes of Health (NIH) through grant 1R01DK071801. A.R.B. acknowledges the NIH General Medical Sciences F31 Fellowship (1F31GM119365) for funding. K.D. acknowledges a predoctoral fellowship supported by the NIH, under Ruth L. Kirschstein National Research Service Award T32HL007936 from the National Heart Lung and Blood Institute to the University of Wisconsin-Madison Cardiovascular Research Center.

References

1. Holland, B.; Rice, W. R., *Evolution* **1998,** *52* (1), 1-7.

2. Ohgaki, H.; Dessen, P.; Jourde, B.; Horstmann, S.; Nishikawa, T.; Di Patre, P. L.; Burkhard, C.; Schuler, D.; Probst-Hensch, N. M.; Maiorka, P. C.; Baeza, N.; Pisani, P.; Yonekawa, Y.; Yasargil, M. G.; Lutolf, U. M.; Kleihues, P., *Cancer Research* **2004,** *64* (19), 6892-6899.

3. Rosen, R.; Brown, C.; Heiman, J.; Leiblum, S.; Meston, C.; Shabsigh, R.; Ferguson, D.; D'Agostino, R., *Journal of Sex & Marital Therapy* **2000,** *26* (2), 191-208.

4. Baron-Cohen, S.; Wheelwright, S.; Skinner, R.; Martin, J.; Clubley, E., *Journal of Autism and Developmental Disorders* **2001,** *31* (1), 5-17.

5. Cypess, A. M.; Lehman, S.; Williams, G.; Tal, I.; Rodman, D.; Goldfine, A. B.; Kuo, F. C.; Palmer, E. L.; Tseng, Y.; Doria, A.; Kolodny, G. M.; Kahn, C. R., *New England Journal of Medicine* **2009,** *360* (15), 1509-1517.

6. Seo, D.; Ahluwalia, A.; Potenza, M. N.; Sinha, R., *Journal of Neuroscience Research* **2017,** *95* (1-2), 115-125.

7. Hommer, R. E.; Seo, D.; Lacadie, C. M.; Chaplin, T. M.; Mayes, L. C.; Sinha, R.; Potenza, M. N., *Human Brain Mapping* **2013,** *34* (10), 2561-2573.

8. Seo, D.; Jia, Z. R.; Lacadie, C. M.; Tsou, K. A.; Bergquist, K.; Sinha, R., *Human Brain Mapping* **2011,** *32* (11), 1998-2013.

9. Chan, C. B.; Ye, K. Q., *Journal of Neuroscience Research* **2017,** *95* (1-2), 328-335.

10. Hogarth, S. J.; Jaehne, E. J.; van den Buuse, M.; Djouma, E., *Behavioural Brain Research* **2018,** *339*, 73-78.

11. Christie, A. E.; Stemmler, E. A.; Dickinson, P. S., *Cell Mol Life Sci* **2010,** *67* (24), 4135-69.

12. Li, L. J.; Sweedler, J. V., Peptides in the Brain: Mass Spectrometry-Based Measurement Approaches and Challenges. In *Annual Review of Analytical Chemistry*, Annual Reviews: Palo Alto, 2008; Vol. 1, pp 451-483.

13. Hokfelt, T.; Broberger, C.; Xu, Z. Q. D.; Sergeyev, V.; Ubink, R.; Diez, M., *Neuropharmacology* **2000,** *39* (8), 1337-1356.

14. McClellan-Green, P.; Romano, J.; Oberdorster, E., *Environmental Research* **2007,** *104* (1), 183-191.

15. Chen, R. B.; Xiao, M. M.; Buchberger, A.; Li, L. J., *Journal of Proteome Research* **2014,** *13* (12), 5767-5776.

16. Wang, J. H.; Zhang, Y. Z.; Xiang, F.; Zhang, Z. C.; Li, L. J., *Journal of Chromatography A* **2010,** *1217* (26), 4463-4470.

17. Zhang, Y.; Buchberger, A.; Muthuvel, G.; Li, L., *Proteomics* **2015**.

18. Bjelobaba, I.; Begovic-Kupresanin, V.; Pekovic, S.; Lavrnja, I., *Journal of Neuroscience Research* **2018,** *96* (6), 1021-1042.

19. Chen, L.; Brown, R. E.; McKenna, J. T.; McCarley, R. W., *Cns & Neurological Disorders-Drug Targets* **2009,** *8* (4), 296-308.

20. Le Bars, D.; Gozariu, M.; Cadden, S. W., *Pharmacological Reviews* **2001,** *53* (4), 597-652.

21. Ma, L.; Zhao, Y. D.; Chen, Y. C.; Cheng, B.; Peng, A. L.; Huang, K., *European Journal of Pharmacology* **2018,** *819*, 169-180.

22. Zhang, Y.; DeLaney, K.; Hui, L.; Wang, J.; Sturm, R. M.; Li, L., *J Am Soc Mass Spectrom* **2018**.

23. Chen, R. B.; Hui, L. M.; Cape, S. S.; Wang, J. H.; Li, L. J., *Acs Chemical Neuroscience* **2010,** *1* (3), 204-214.

24. Hopkins, P. M., *General and Comparative Endocrinology* **2012,** *175* (3), 357-366.

25. McMahon, B. R.; Burnett, L. E., *Physiological Zoology* **1990,** *63* (1), 35-71.

26. Chen, R. B.; Ma, M. M.; Hui, L. M.; Zhang, J.; Li, L. J., *Journal of the American Society for Mass Spectrometry* **2009,** *20* (4), 708-718.

27. Liang, Z. D.; Schmerberg, C. M.; Li, L. J., *Analyst* **2015,** *140* (11), 3803-3813.

28. Gutierrez, G. J., *Cancer Borealis* Stomatogastric Nervous System Dissection. Grashow, R. G., Ed. JOVE, 2009.

29. Gutierrez, G. J.; Grashow, R. G., *J Vis Exp* **2009,** (25).

30. DeLaney, K.; Buchberger, A.; Li, L., *Methods Mol Biol* **2018,** *1719*, 247-269.

31. Veenstra, J. A., *General and Comparative Endocrinology* **2016,** *230*, 153-157.

32. Veenstra, J. A., *Insect Biochemistry and Molecular Biology* **2009,** *39* (3), 161-170.

33. Dircksen, H.; Neupert, S.; Predel, R.; Verleyen, P.; Huybrechts, J.; Strauss, J.; Hauser, F.; Stafflinger, E.; Schneider, M.; Pauwels, K.; Schoofs, L.; Grimmelikhuijzen, C. J. P., *Journal of Proteome Research* **2011,** *10* (10), 4478-4504.

34. Souza-Moreira, L.; Campos-Salinas, J.; Caro, M.; Gonzalez-Rey, E., *Neuroendocrinology* **2011,** *94* (2), 89-100.

35. Elphick, M. R.; Mirabeau, O.; Larhammar, D., *Journal of Experimental Biology* **2018,** *221* (3), 15.

36. Dickinson, P. S.; Kurland, S. C.; Zu, X.; Parker, B. O.; Sreekrishnan, A.; Kwiatkowski, M. A.; Williams, A. H.; Ysasi, A. B.; Christie, A. E., Distinct or shared actions of peptide family isoforms: II. Multiple pyrokinins exert similar effects in the lobster stomatogastric nervous system. Journal of Experimental Biology, 2015; Vol. 218, pp 2905-2917.

37. Dickinson, P. S.; Sreekrishnan, A.; Kwiatkowski, M. A.; Christie, A. E., Distinct or shared actions of peptide family isoforms: I. Peptide-specific actions of pyrokinins in the lobster cardiac neuromuscular system. Journal of Experimental Biology, 2015; Vol. 218, pp 2892-2904.

Figures

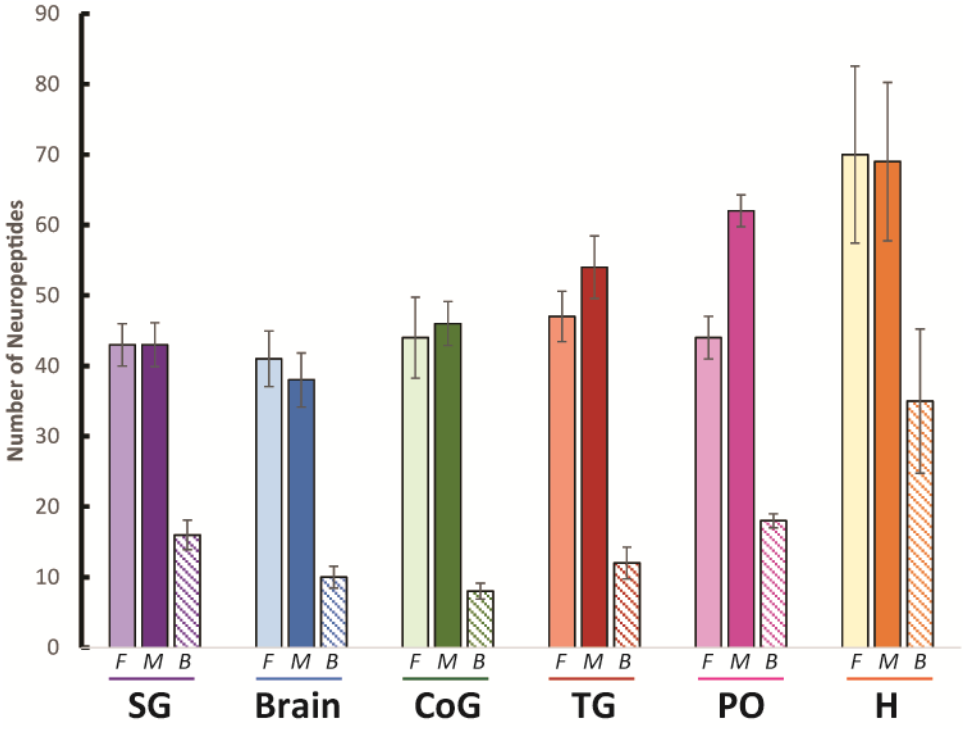

Figure 1. Bar graph showing the average number of neuropeptides identified in tissue and hemolymph samples exclusively found in female (F) and male (M) samples and those detected in both samples (B). The x-axis represents locations of neuropeptides (*i.e.*, specific tissue or hemolymph) and the y-axis indicates the number of neuropeptides identified (n = 7). The error bars represent the standard error of the mean. SG: sinus glands; CoG: commissural ganglion; TG: thoracic ganglion; PO: pericardial organs; H: hemolymph.

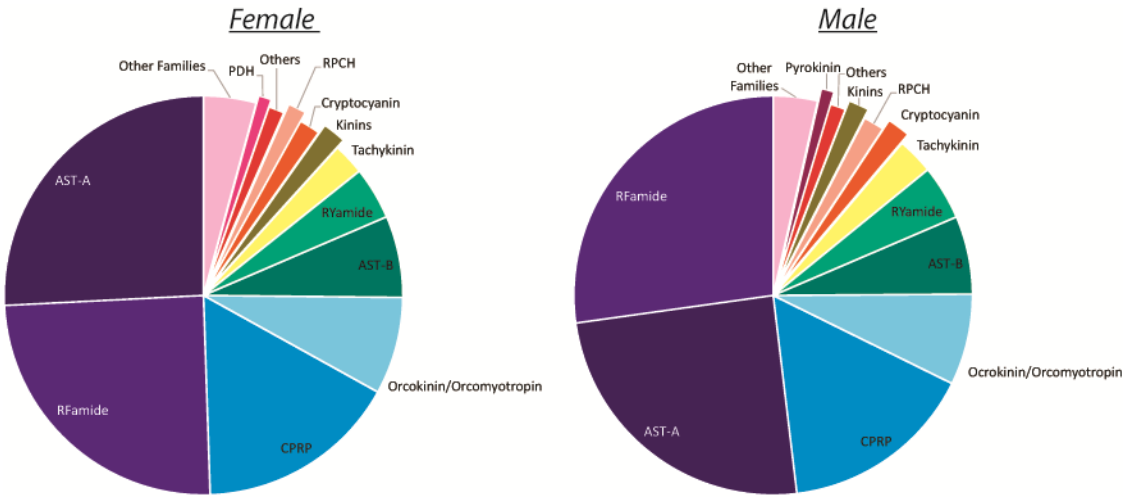

Figure 2. Pie chart depicting the different neuropeptide families identified in female (left) and male (right) blue crabs in at least one biological replicate in all 5 tissues (SG, brain, CoG, PO, or TG). If only one isoform of a family was identified, that family is grouped into the "Other Families" section. AST-A: Allatostatin A-type; CPRP: Crustacean Hyperglycemic Hormone Precursor Related Peptide; AST-B: Allatostatin B-type; RPCH: Red Pigment-Concentrating Hormone; PDH: Pigment Dispersing Hormone.

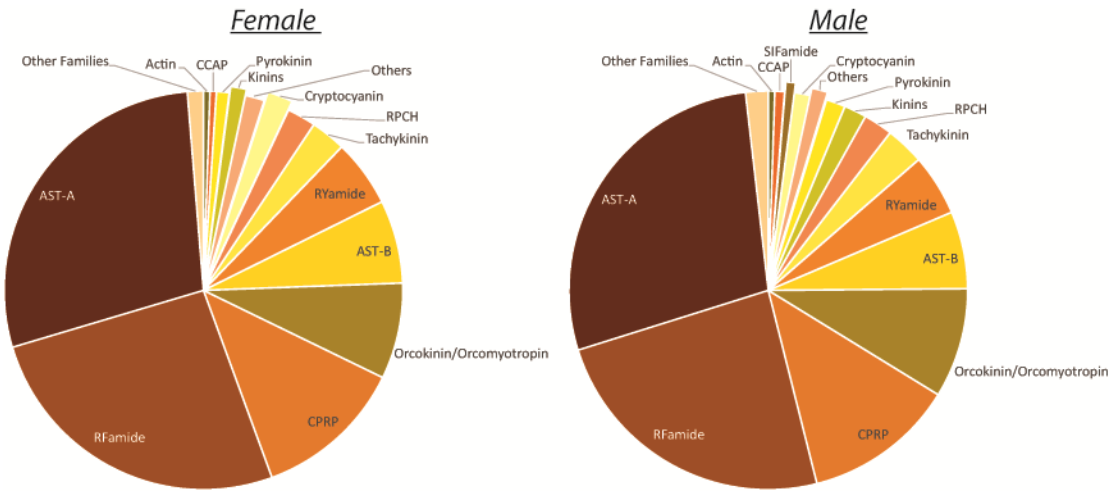

Figure 3 Pie chart depicting the different neuropeptide families identified in female (left) and male (right) blue crabs in at least one biological replicate in hemolymph. If only one isoform of a family was identified, that family is grouped into the "Other Families" section. AST-A: Allatostatin A-type; CPRP: Crustacean Hyperglycemic Hormone Precursor Related Peptide; AST-B: Allatostatin B-type; RPCH: Red Pigment-Concentrating Hormone; CCAP: Crustacean Cardioactive Peptide.

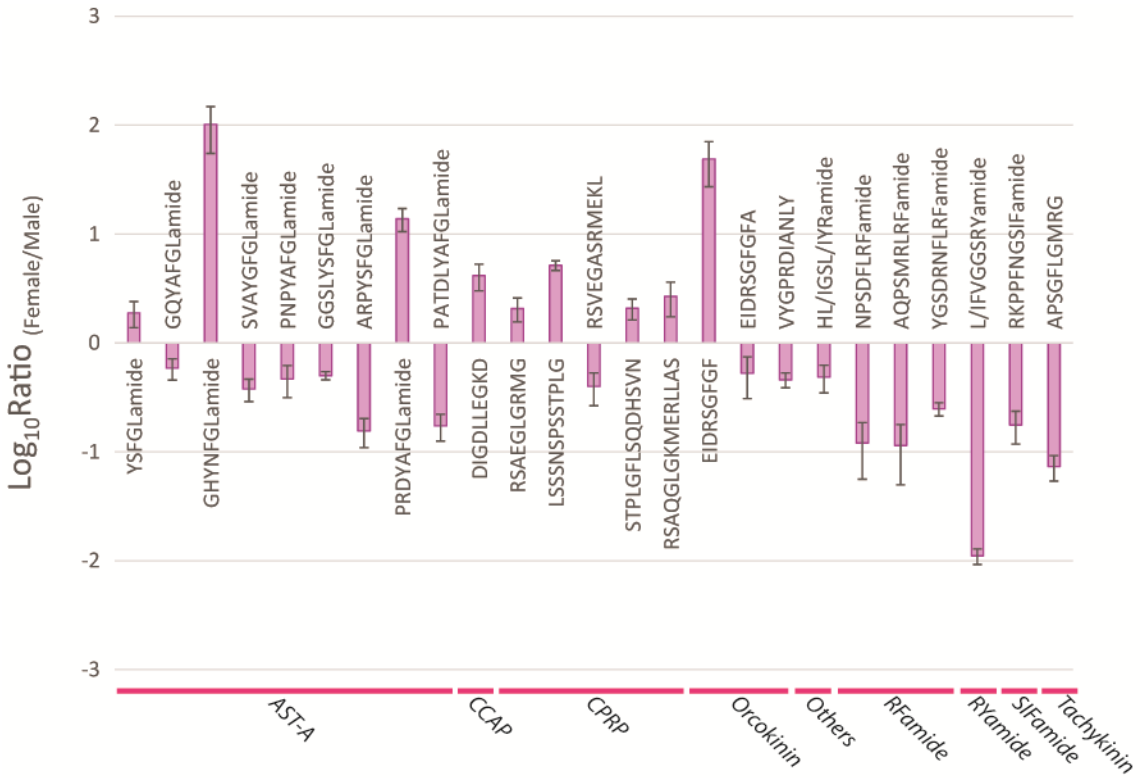

Figure 4. All significantly different neuropeptides identified in at least three biological replicates and their quantitative differences in the POs between male and female blue crabs. The x-axis shows the neuropeptides' sequences, while the y-axis represents the log-base 10 of the ratio. The ratio is calculated by dividing the female intensity by that of the male. A log-base 10 ratio close to 0 indicates no change in neuropeptides for that hypoxia condition compared to the control. AST-A: Allatostatin A-type; CCAP: Crustacean Cardioactive Peptide; CPRP: Crustacean Hyperglycemic Hormone Precursor Related Peptide.

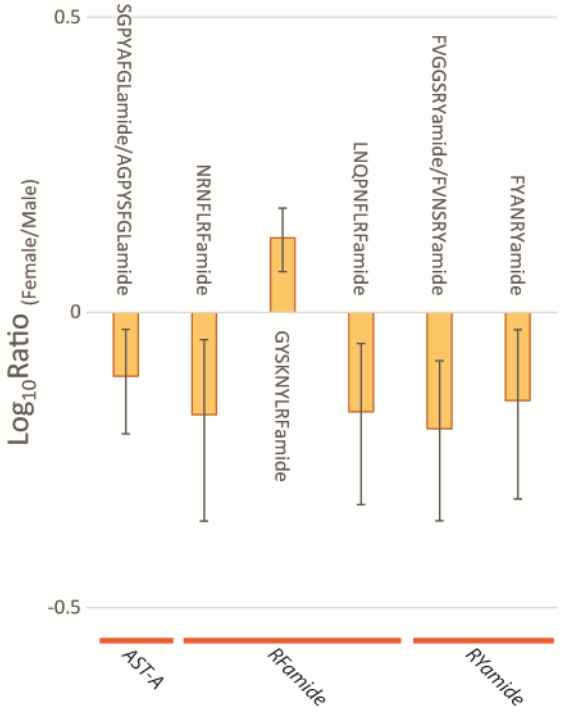

Figure 5. All significantly different neuropeptides identified in at least three biological replicates and their quantitative differences in the POs between male and female blue crabs. The x-axis shows the neuropeptides' sequences, while the y-axis represents the log-base 10 of the ratio. The ratio is calculated by dividing the female intensity by that of the male. A log-base 10 ratio close to 0 indicates no change in neuropeptides for that hypoxia condition compared to the control. AST-A: Allatostatin A-type.

Supplemental Material

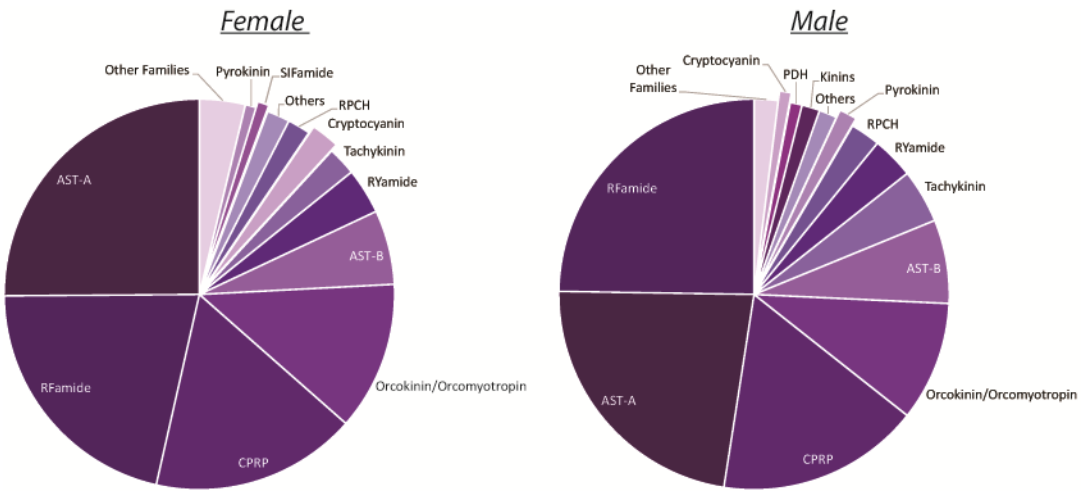

Figure S1. Pie chart depicting the different neuropeptide families identified in female (left) and male (right) blue crabs in at least one biological replicate in the SG. If only one isoform of a family was identified, that family is grouped into the "Other Families" section. AST-A: Allatostatin A-type; CPRP: Crustacean Hyperglycemic Hormone Precursor Related Peptide; AST-B: Allatostatin B-type; RPCH: Red Pigment-Concentrating Hormone; PDH: Pigment Dispersing Hormone.

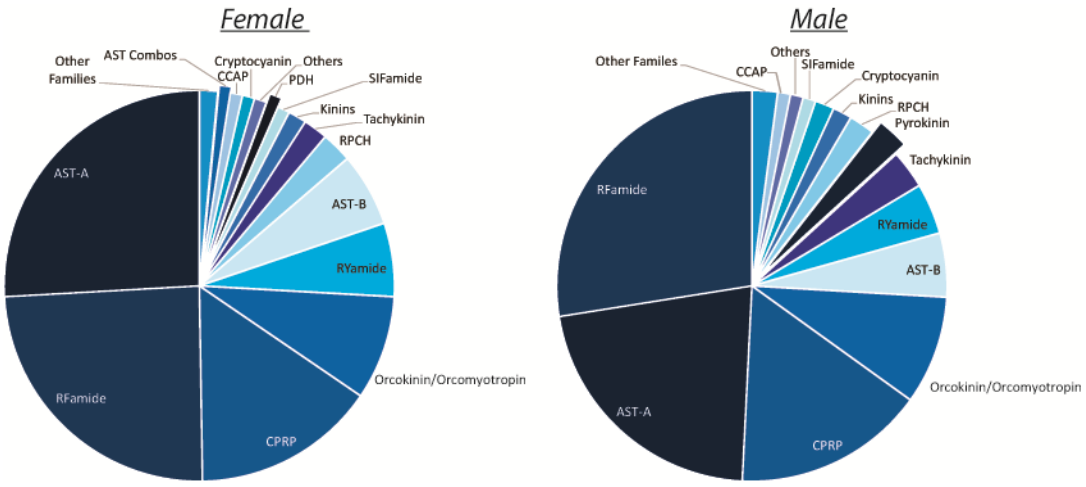

Figure S2. Pie chart depicting the different neuropeptide families identified in female (left) and male (right) blue crabs in at least one biological replicate in the brain. If only one isoform of a family was identified, that family is grouped into the "Other Families" section. AST-A: Allatostatin A-type; CPRP: Crustacean Hyperglycemic Hormone Precursor Related Peptide; AST-B: Allatostatin B-type; RPCH: Red Pigment-Concentrating Hormone; CCAP: Crustacean Cardioactive Peptide; AST: Allatostatin; PDH: Pigment Dispersing Hormone.

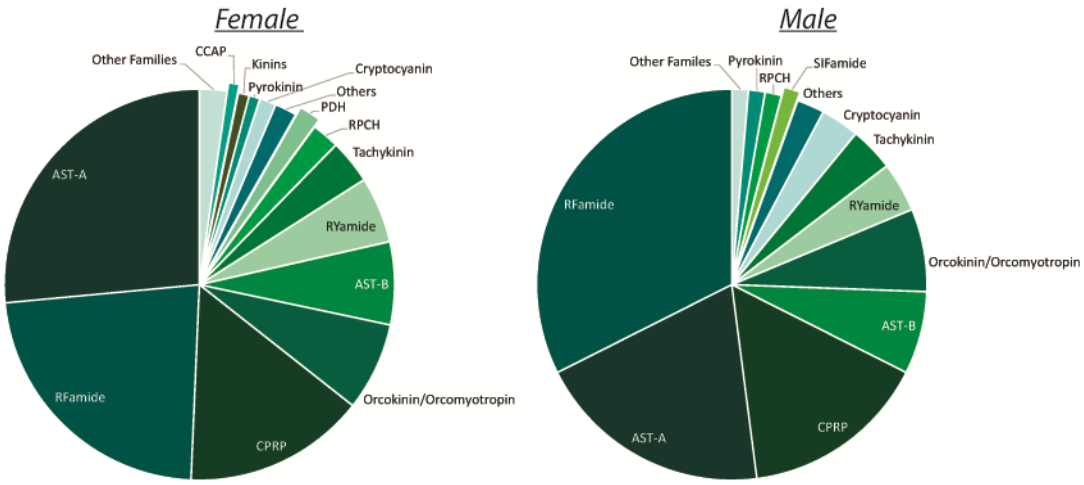

Figure S3. Pie chart depicting the different neuropeptide families identified in female (left) and male (right) blue crabs in at least one biological replicate in the CoG. If only one isoform of a family was identified, that family is grouped into the "Other Families" section. AST-A: Allatostatin A-type; CPRP: Crustacean Hyperglycemic Hormone Precursor Related Peptide; AST-B: Allatostatin B-type; RPCH: Red Pigment-Concentrating Hormone; CCAP: Crustacean Cardioactive Peptide; AST: Allatostatin; PDH: Pigment Dispersing Hormone.

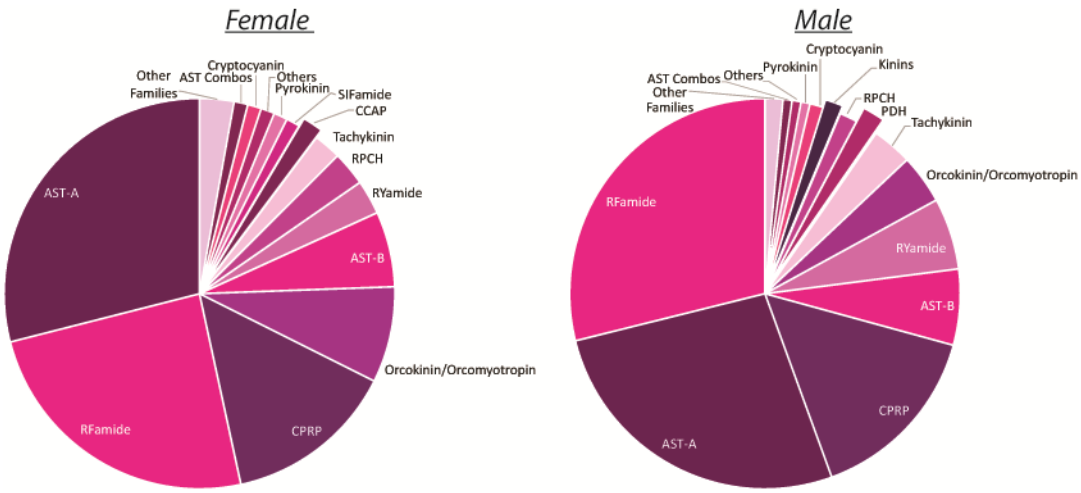

Figure S4 Pie chart depicting the different neuropeptide families identified in female (left) and male (right) blue crabs in at least one biological replicate in PO. If only one isoform of a family was identified, that family is grouped into the "Other Families" section. AST-A: Allatostatin A-type; CPRP: Crustacean Hyperglycemic Hormone Precursor Related Peptide; AST-B: Allatostatin B-type; RPCH: Red Pigment-Concentrating Hormone; CCAP: Crustacean Cardioactive Peptide; AST: Allatostatin; PDH: Pigment Dispersing Hormone.

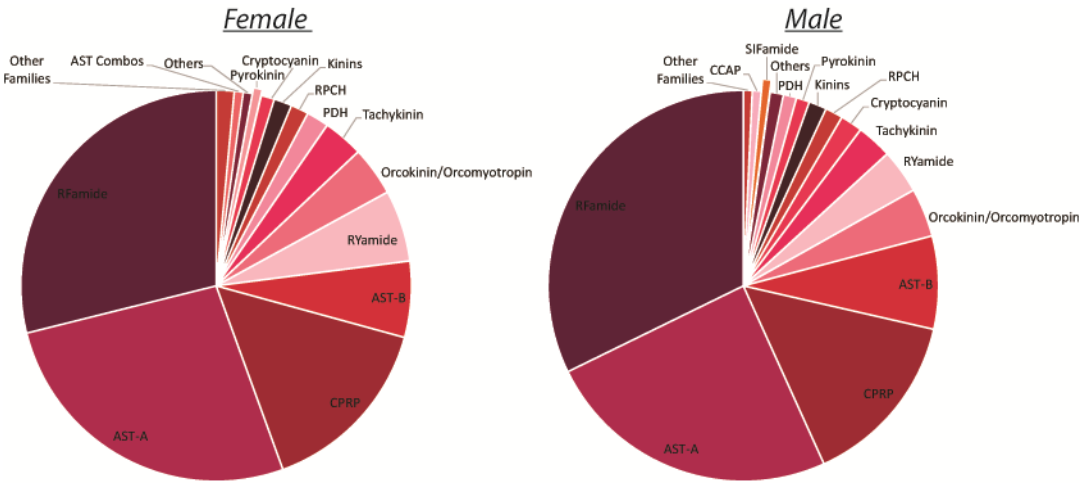

Figure S5. Pie chart depicting the different neuropeptide families identified in female (left) and male (right) blue crabs in at least one biological replicate in the TG. If only one isoform of a family was identified, that family is grouped into the "Other Families" section. AST-A: Allatostatin A-type; CPRP: Crustacean Hyperglycemic Hormone Precursor Related Peptide; AST-B: Allatostatin B-type; RPCH: Red Pigment-Concentrating Hormone; CCAP: Crustacean Cardioactive Peptide; AST: Allatostatin; PDH: Pigment Dispersing Hormone.

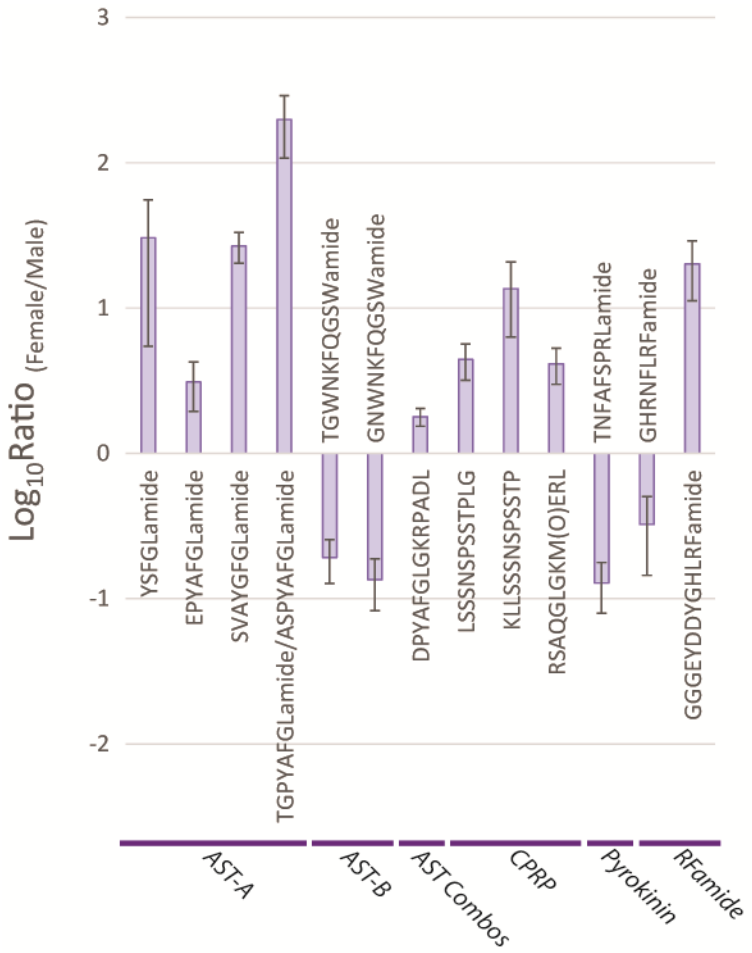

Figure S6. All significantly different neuropeptides identified in at least three biological replicates and their quantitative differences in the SGs between male and female blue crabs. The x-axis shows the neuropeptides' sequences, while the y-axis represents the log-base 10. The ratio is calculated by dividing the female intensity by that of the male. A log-base 10 ratio close to 0 indicates no change in neuropeptides for that hypoxia condition compared to the control. AST-A: Allatostatin A-type; CCAP: Crustacean Cardioactive Peptide; CPRP: Crustacean Hyperglycemic Hormone Precursor Related Peptide.

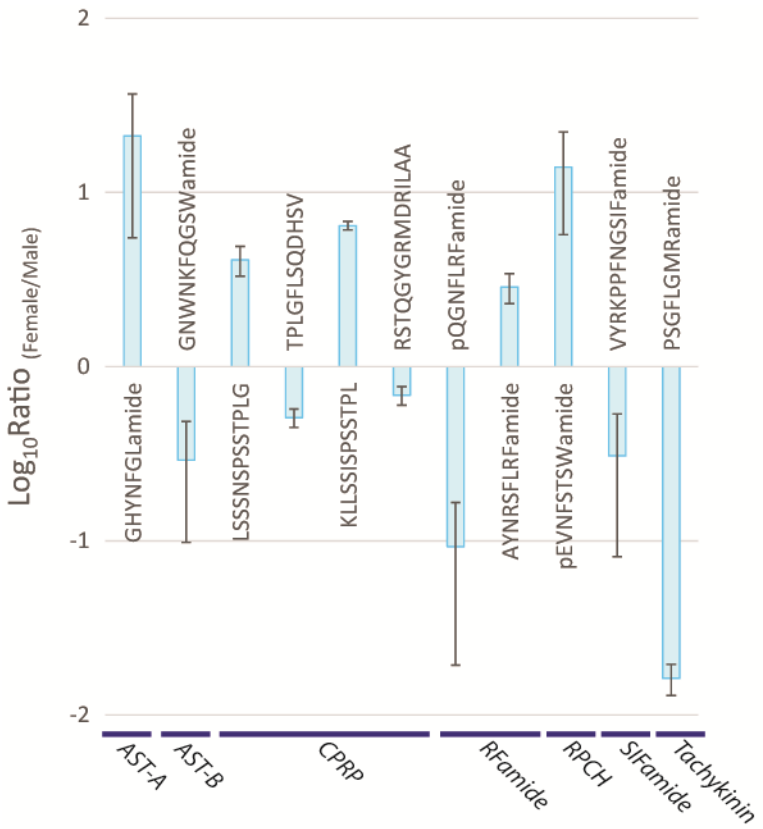

Figure S7. All significantly different neuropeptides identified in at least three biological replicates and their quantitative differences in the brain between male and female blue crabs. The x-axis shows the neuropeptides' sequences, while the y-axis represents the log-base 10 of the ratio. The ratio is calculated by dividing the female intensity by that of the male. A log-base 10 ratio close to 0 indicates no change in neuropeptides for that hypoxia condition compared to the control. AST-A: Allatostatin A-type; CCAP: Crustacean Cardioactive Peptide; CPRP: Crustacean Hyperglycemic Hormone Precursor Related Peptide.

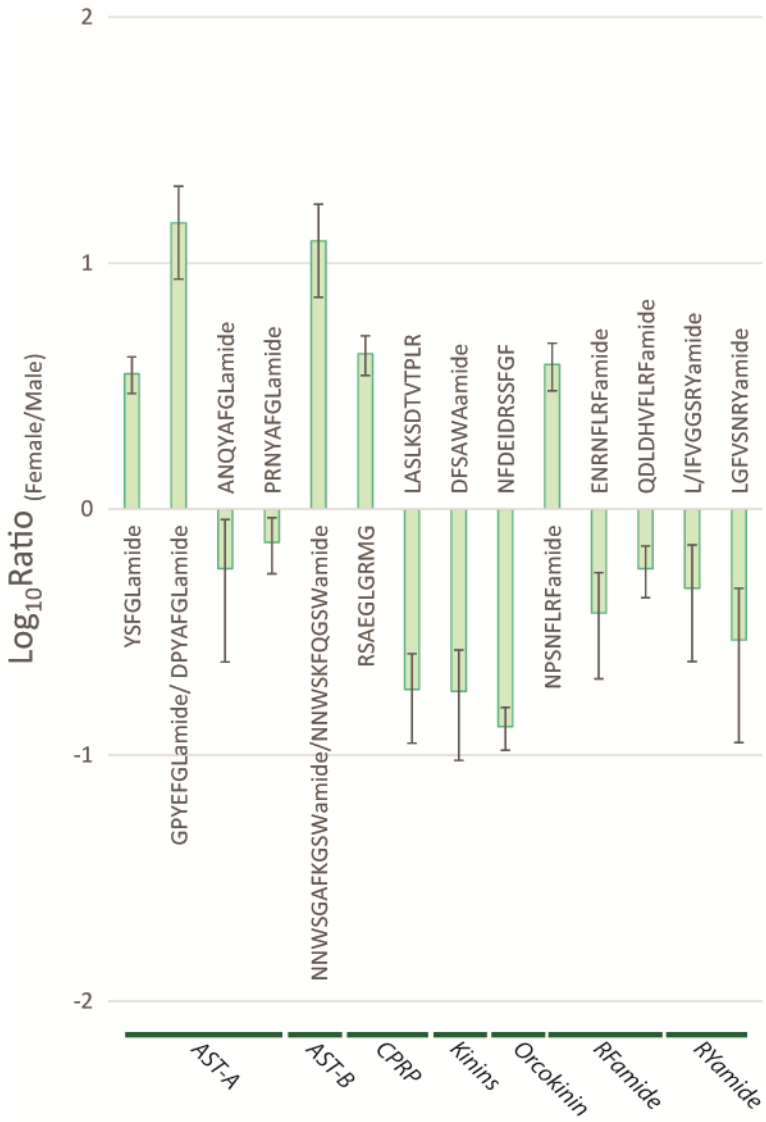

Figure S8. All significantly different neuropeptides identified in at least three biological replicates and their quantitative differences in the CoGs between male and female blue crabs. The x-axis shows the neuropeptides' sequences, while the y-axis represents the log-base 10 of the ratio. The ratio is calculated by dividing the female intensity by that of the male. A log-base 10 ratio close to 0 indicates no change in neuropeptides for that hypoxia condition compared to the control. AST-A: Allatostatin A-type; CCAP: Crustacean Cardioactive Peptide; CPRP: Crustacean Hyperglycemic Hormone Precursor Related Peptide.

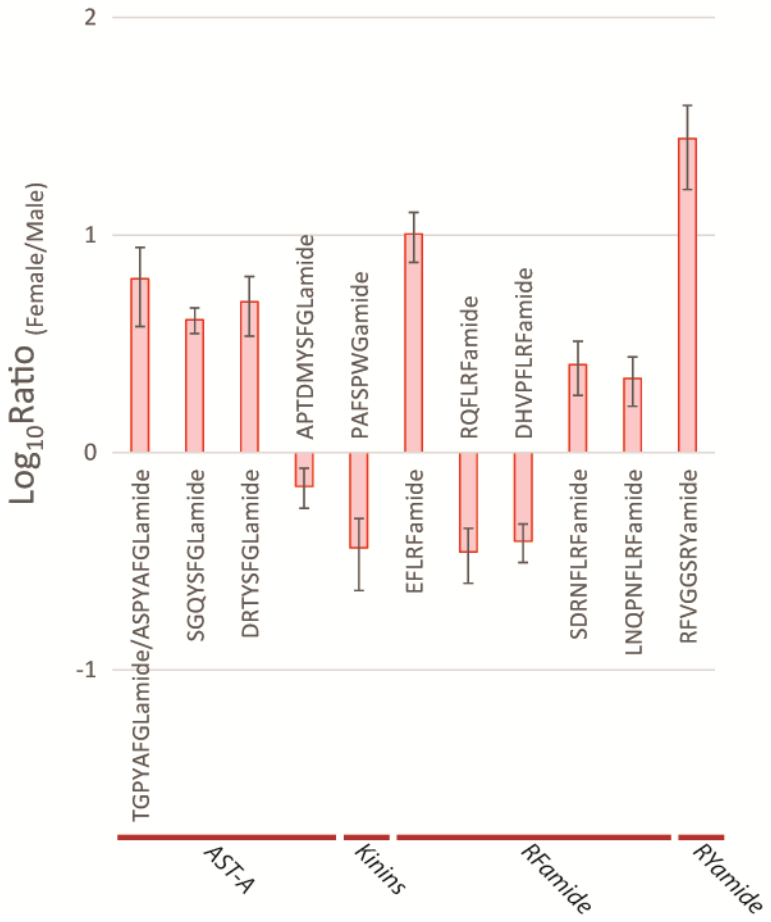

Figure S9. All significantly different neuropeptides identified in at least three biological replicates and their quantitative differences in the TG between male and female blue crabs. The x-axis shows the neuropeptides' sequences, while the y-axis represents the log-base 10 of the ratio. The ratio is calculated by dividing the female intensity by that of the male. A log-base 10 ratio close to 0 indicates no change in neuropeptides for that hypoxia condition compared to the control. AST-A: Allatostatin A-type; CCAP: Crustacean Cardioactive Peptide; CPRP: Crustacean Hyperglycemic Hormone Precursor Related Peptide.

Table S1. All neuropeptides that were found to be significantly different between male and female blue crabs in the SG. The ratio is calculated by dividing the female intensity by that of the male.

Family	Sequence	m/z	Ratio	SEM	p-Value
Allatostatin A-type	YSFGLamide	585.303	30.423	24.976	0.0004
	EPYAFGLamide	795.404	3.099	1.152	0.0226
	SVAYGFGLamide	812.430	26.773	6.381	0.0000
	TGPYAFGLamide/ASPYAFGLamide	824.430	198.438	91.108	0.0000
Allatostatin B-type	TGWNKFQGSWamide	1209.580	0.191	0.064	0.0000
	GNWNKFQGSWamide	1222.575	0.135	0.053	0.0000
Allatostatin Combos	DPYAFGLGKRPADL	1519.790	1.789	0.250	0.0010
CPRP	LSSSNSPSSTPLG	1233.596	4.423	1.238	0.0090
	KLLSSSNSPSSTP	1304.669	13.555	7.215	0.0468
	RSAQGLGKM(O)ERL	1361.732	4.135	1.150	0.0001
Pyrokinin	TNFAFSPRLamide	1051.568	0.128	0.049	0.0001
RFamide	GHRNFLRFamide	1045.580	0.324	0.179	0.0154
	GGGEYDDYGHLRFamide	1484.653	20.105	8.902	0.0007

Table S2. All neuropeptides that were found to be significantly different between male and female blue crabs in the brain. The ratio is calculated by dividing the female intensity by that of the male.

Family	Sequence	*m/z*	Ratio	SEM	p-Value
Allatostatin A-type	GHYNFGLamide	806.394	21.057	15.570	0.0009
Allatostatin B-type	GNWNKFQGSWamide	1222.575	0.291	0.193	0.0145
CPRP	LSSSNSPSSTPLG	1233.596	4.103	0.792	0.0001
	TPLGFLSQDHSV	1300.653	0.509	0.062	0.0009
	KLLSSISPSSTPL	1329.762	6.444	0.359	0.0000
	RSTQGYGRMDRILAA	1694.876	0.684	0.083	0.0102
RFamide	pQGNFLRFamide	863.452	0.093	0.073	0.0005
	AYNRSFLRFamide	1172.632	2.857	0.566	0.0019
RPCH	pEVNFSTSWamide	950.437	13.970	8.248	0.0001
SIFamide	VYRKPPFNGSIFamide	1423.784	0.308	0.226	0.0222
Tachykinin	PSGFLGMRamide	863.456	0.016	0.003	0.0000

Table S3. All neuropeptides that were found to be significantly different between male and female blue crabs in the CoG. The ratio is calculated by dividing the female intensity by that of the male.

Family	Sequence	*m/z*	Ratio	SEM	p-Value
Allatostatin A-type	YSFGLamide	585.303	3.549	0.597	0.0000
	GPYEFGLamide/ DPYAFGLamide	781.388	14.563	5.968	0.0032
	ANQYAFGLamide	882.447	0.573	0.333	0.0271
	PRNYAFGLamide	936.505	0.734	0.188	0.0408
Allatostatin B-type	NNWSGAFKGSWamide/NNWSKFQGSWamide	1252.586	12.308	5.036	0.0002
CPRP	RSAEGLGRMG	1033.521	4.278	0.785	0.0000
	LASLKSDTVTPLR	1400.811	0.185	0.073	0.0007
Kinins	DFSAWAamide	695.315	0.182	0.086	0.0002
Orcokinin	NFDEIDRSSFGF	1433.633	0.131	0.026	0.0000
RFamide	NPSNFLRFamide	993.527	3.871	0.846	0.0002
	ENRNFLRFamide	1094.585	0.378	0.174	0.0144
	QDLDHVFLRFamide	1288.680	0.572	0.136	0.0080
RYamide	L/IFVGGSRYamide	897.494	0.477	0.237	0.0426
	LGFVSNRYamide	954.516	0.294	0.182	0.0126

Table S4. All neuropeptides that were found to be significantly different between male and female blue crabs in the TG. The ratio is calculated by dividing the female intensity by that of the male.

Family	Sequence	m/z	Ratio	SEM	p-value
Allatostatin A-type	TGPYAFGLamide/ASPYAFGLamide	824.430	6.283	2.490	0.0072
	SGQYSFGLamide	857.415	4.071	0.551	0.0001
	DRTYSFGLamide	957.479	4.927	1.506	0.0015
	APTDMYSFGLamide	1100.508	0.699	0.147	0.0481
Kinins	PAFSPWGamide	760.378	0.364	0.133	0.0013
RFamide	EFLRFamide	710.398	10.096	2.615	0.0000
	RQFLRFamide	865.516	0.349	0.099	0.0029
	DHVPFLRFamide	1029.563	0.391	0.079	0.0012
	SDRNFLRFamide	1053.559	2.534	0.706	0.0219
	LNQPNFLRFamide	1147.637	2.189	0.559	0.0072
RYamide	RFVGGSRYamide	940.511	27.789	11.604	0.0000

Table S5. All neuropeptides that were found to be significantly different between male and female blue crabs in the PO. The ratio is calculated by dividing the female intensity by that of the male.

Family	Sequence	*m/z*	Ratio	SEM	p-Value
Allatostatin A-type	YSFGLamide	585.303	1.887	0.510	0.0251
	GQYAFGLamide	754.388	0.585	0.129	0.0191
	GHYNFGLamide	806.394	101.655	46.449	0.0000
	SVAYGFGLamide	812.430	0.377	0.088	0.0004
	PNPYAFGLamide	877.457	0.466	0.152	0.0074
	GGSLYSFGLamide	899.462	0.502	0.044	0.0000
	ARPYSFGLamide	909.494	0.155	0.046	0.0001
	PRDYAFGLamide	937.489	13.833	3.305	0.0000
	PATDLYAFGLamide	1066.557	0.173	0.048	0.0002
CCAP	DIGDLLEGKD	1074.531	4.155	1.147	0.0009
CPRP	RSAEGLGRMG	1033.521	2.071	0.512	0.0041
	LSSSNSPSSTPLG	1233.596	5.151	0.526	0.0000
	RSVEGASRMEKL	1362.716	0.398	0.134	0.0015
	STPLGFLSQDHSVN	1501.728	2.077	0.456	0.0157
	RSAQGLGKMERLLAS	1616.890	2.676	0.940	0.0017
Orcokinin	EIDRSGFGF	1027.484	48.915	21.787	0.0000
	EIDRSGFGFA	1098.521	0.526	0.218	0.0121
	VYGPRDIANLY	1280.663	0.459	0.072	0.0016
Others	HL/IGSL/IYRamide	844.479	0.486	0.140	0.0123
RFamide	NPSDFLRFamide	994.511	0.121	0.065	0.0000
	AQPSMRLRFamide	1104.609	0.114	0.064	0.0003
	YGSDRNFLRFamide	1273.644	0.248	0.035	0.0000
RYamide	L/IFVGGSRYamide	897.494	0.011	0.002	0.0000
SIFamide	RKPPFNGSIFamide	1161.653	0.177	0.059	0.0003
Tachykinin	APSGFLGMRG	992.498	0.073	0.019	0.0000

Table S6. All neuropeptides that were found to be significantly different between male and female blue crabs in the hemolymph. The ratio is calculated by dividing the female intensity by that of the male.

Family	Sequence	m/z	Ratio	SEM	p-Value
Allatostatin A-type	SGPYAFGLamide/AGPYSFGLamide	810.415	0.778	0.156	0.0288
RFamide	NRNFLRFamide	965.543	0.671	0.228	0.0029
	GYSKNYLRFamide	1146.605	1.336	0.164	0.0447
	LNQPNFLRFamide	1147.637	0.678	0.207	0.0029
RYamide	FVGGSRYamide/FVNSRYamide	784.410	0.635	0.192	0.0004
	FYANRYamide	832.410	0.708	0.225	0.0233

Appendix VI

Mass Spectrometry Imaging: A Review of Emerging Advancements and Future Insights

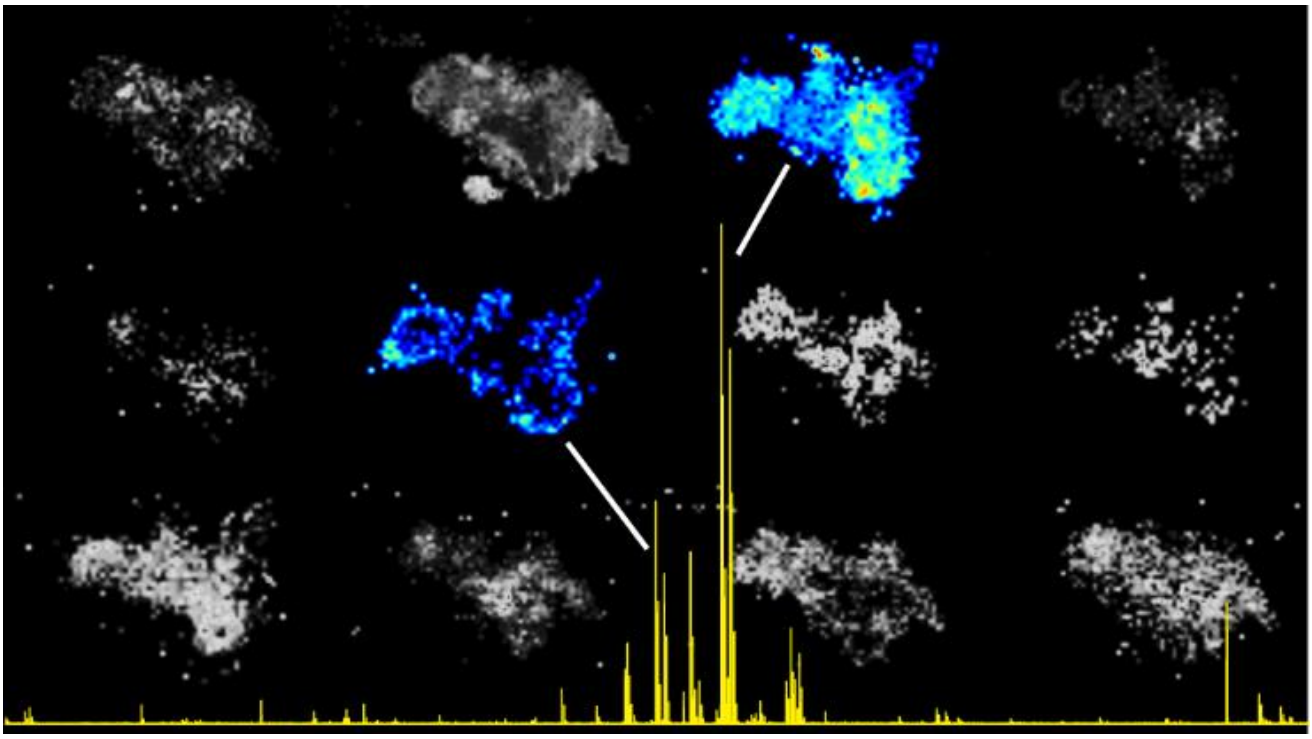

Modified from:

Amanda R. Buchberger, Kellen DeLaney, Jillian Johnson, Lingjun Li. "Mass Spectrometry Imaging: A Review in Emerging Advancements and Future Insights." Invited Contribution. *Analytical Chemistry*. 2018, 90(1), 240-265.

Key Words: Mass Spectrometry Imaging, Sample Preparation, Ionization, Multimodal, Formalin-Fixed Paraffin Embedded

Abstract

Mass spectrometry (MS) imaging is a powerful tool that enables untargeted investigations into the spatial distribution of molecular species in a variety of samples. The combination of information gained from MS and visualization of spatial distributions in thin sample sections makes this a valuable chemical analysis tool for biological characterization. Overall, the aim of this review is to provide an informative resource for those in the MS imaging community who are interested in improving MS imaging data quality and analysis or using MS imaging for novel applications. Particularly, we discuss advances from the last 2 years in sample preparation, instrumentation, quantitation, statistics, and multimodal imaging that have allowed MS imaging to emerge as a powerful technique in various biomedical applications including clinical settings. Also, several novel biological applications are highlighted to demonstrate the potential for the future of the MS imaging field.

Introduction

Mass spectrometry imaging (MS imaging) is a powerful tool that enables untargeted investigations into the spatial distribution of molecular species in a variety of samples. It has the capability to image thousands of molecules, such as metabolites, lipids, peptides, proteins, and glycans, in a single experiment without labeling.[1] The combination of information gained from mass spectrometry (MS) and visualization of spatial distributions in thin sample sections makes this a valuable chemical analysis tool for biological characterization. A summary workflow is depicted in **Figure 1**. After minimal but careful sample preparation, the general setup of an MS imaging experiment involves defining an (x, y) grid over the surface of the sample, with the grid area chosen by the user. The mass spectrometer then ionizes the molecules on the surface of the

sample and collects a mass spectrum at each pixel on the section with the resulting spatial resolution defined by the pixel size. After collecting the spectra, computational software can be used to select an individual mass-to-charge (*m/z*) value, and the intensity of the *m/z* is extracted from each pixel's spectrum. These intensities are then combined into a heat map image depicting the relative distribution of that *m/z* value throughout the sample's surface. In order to determine the identity of a specific *m/z* value, tandem MS (MS/MS) fragmentation can be performed on ions from each pixel, and the fragments can be used to piece together the structure of the unknown molecule. Otherwise, the molecule can be identified based on its intact mass by accurate mass matching to databases of known molecules within a certain mass error range.[2, 3]

With the numerous technological advances in recent years, MS imaging is becoming a more established tool in clinical practice and the pharmaceutical industry.[4-6] Advances include improvements in reproducible sample preparation to ensure reliable interpretation of data and instrumentation that allows for high acquisition speeds and lower spatial resolution, improving throughput and depth of instrumentation. The credibility of MS imaging experiments has further been enhanced by the development of methods for absolute quantitation of detected molecules. To help with large computational endeavors, statistical workflows and machine learning algorithms have been implemented to handle the large imaging data sets being produced with modern day instrumentation. MS imaging can also be combined with other complementary imaging modalities, such as microscopy, Raman spectroscopy, and MRI, to strengthen any biological conclusions. With both hardware and software improvements, 3-dimensional (3D) renderings and even single-cell resolution using MS imaging are emerging as future frontiers. With all the advances in this field, MS imaging is rapidly evolving and requires continuous development to match the current demand.

Overall, the aim of this review is to provide an informative resource for those in the MS imaging community who are interested in improving MS imaging data quality and analysis or using MS imaging for novel applications. Particularly, we discuss advances from the last 2 years in sample preparation, instrumentation, quantitation, statistics, and multimodal imaging that have allowed MS imaging to emerge as a powerful technique in various biomedical applications including clinical settings. Also, several novel biological applications are highlighted to demonstrate the potential for the future of the MS imaging field.

Sample Preparation

The Basics

As with any methodology, one of the most crucial steps for analytical success is proper sample preparation. This is particularly true for MS, as even subtle differences in sample integrity or molecular density can have profound effects on the signal intensity, types of molecules being ionized and detected, or localizations. For example, one of the greatest challenges is ensuring that the spatial mapping of molecules in an MS imaging experiment is consistent with the distribution in *in vivo* conditions. This relies heavily on proper sample preparation strategies. Researchers have even developed a new statistical scoring system to ensure sample preparation quality.[7]

After any necessary dissection or collection, biological tissue samples require a step to halt enzyme activity to reduce degradation and delocalization (*e.g.*, diffusion across the tissue) of the molecules. This is typically done by flash-freezing the sample for MS imaging since many other preparations (*e.g.*, formalin fixation (FF)) are not MS compatible for most molecular species due to being cross-linked (*e.g.*, bound) in the sample, making them unavailable for

ionization. This is not the case though for some lipids, and FF can be used to preserve sample integrity for their analysis.[8] New method developments have made many FF paraffin embedded (FFPE) samples more MS imaging accessible (see discussion below). Prior to sectioning, one unique preparation step is the decellularization (*i.e.*, removal cells from the extracellular matrix scaffold) of the tissues, allowing for the improved signal of extracellular matrix.[9] Next, these samples are thinly sectioned (6-20 μm thickness), thaw-mounted onto appropriate surface (*e.g.*, microscope slides), and placed into a drying system (*e.g.*, desiccator box). In many cases, tissues are fragile and do not section well without support, thus many researchers embed samples prior to sectioning. These embedding materials range from materials such as gelatin,[8, 10] but, as always, MS-compatibility is a concern. Optimal cutting temperature compound (OCT), for example, is popular among histologists but tends to contaminate MS spectra and is thus not recommended. Because of samples flaking or washing off the slide, O'Rourke *et al.* recommend coating the slide in nitrocellulose as a "glue-like" substance to aid the sections in staying on the slides.[11] Here, one major assumption made is that the samples need or even can be sectioned; however, these general steps are not suitable for all samples. For example, researchers have found ways to image analytes in imprinted plant leaves, plant roots, and even agar.[12-14] Others have gone beyond single tissues to whole body imaging, which can have its own unique challenges.[15]

Several different ionization techniques are compatible with MS imaging, and each requires a unique process to preserve the corresponding sample. Matrix-assisted laser desorption/ionization (MALDI) is the most popular ionization technique for MS imaging, especially due to its ability to image a wide range of molecular weights and molecular species (*e.g.*, metabolites and proteins).[16] Its requirement of a matrix for proper ionization and

production of only singly charged ions often limits its applicability to larger proteins. This has prompted the development of laserspray ionization and unique matrices (*e.g.*, 2-nitrophologlucinol (2-NPG)).[17] Of course, no one matrix, application method, or analyte extraction process works for all molecules, so optimization is important and will be discussed later in this review. Other varieties of MALDI MS imaging exist, including scanning microprobe MALDI (SMALDI), infrared-matrix-assisted laser desorption ionization (IR-MALDESI), and surface-assisted laser desorption/ionization (SALDI), although they are not as widely implemented.[15, 18-20] Other techniques worth noting include desorption electrospray ionization (DESI), secondary ion mass spectrometry (SIMS), and more recently easy ambient sonic spray ionization (EASI)[21], which require minimal sample preparation in comparison to MALDI since they do not require the presence of a matrix.[2, 21-25] Unfortunately, each of these is more limited in the molecules they ionize (peptides and metabolites, respectively). In the most general cases, both DESI and SIMS can be performed directly after sectioning, as they depend more on the instrument parameters for proper analyte extraction. Even with all the ionization methods available, researchers are still developing new methodology, such as laser electrospray ionization.[26] Each ionization method has its own advantages and disadvantages, ranging from the molecules that can be analyzed to the spatial resolution achievable, the latter to be discussed further in this review. Finally, after proper preparation and ionization, the instrument itself (*e.g.*, mass analyzer) is important to consider before determining a proper sample handling workflow. For example, the Bruker MALDI-time-of-flight (TOF)-TOF instrument requires ITO coated slides, while the Thermo MALDI-LTQ-Orbitrap XL can analyze samples on plain microscope slides.[9, 27] In general, while selecting the appropriate sample preparation, ionization source, and mass analyzer are important to allow the molecular species of interest to be analyzed, care should

be taken in using instruments with MS/MS abilities or high mass accuracy to allow confident identification of the molecules in question.

Improving the Basics

Applying an Internal Standard

To qualitatively evaluate different tissues or different analytes within a tissue, appropriate normalization and internal standards are expected if semiquantitative comparisons are to be made. These standards could be included as early in the workflow as dosing the animals/cells up to right before the ions enter the instrument.[2, 28, 29] For MALDI, the standards are typically applied prior to matrix application using the same automatic sprayer systems described below.[30-32] Chumbley *et. al.* has done a comprehensive study to determine the proper inclusion of the standard (*e.g.*, with matrix, under the tissue section, or sandwiching the section with matrix), and it was found that depositing the standards followed by matrix to be optimal for MS imaging mapping of spatial distribution of the drug rifampicin.[33] This sample protocol can also be applied to sections used in DESI experiments (applying prior to analysis), or standards can be added directly to the DESI extraction solvent for inclusion in sample analysis.[2]

Matrix Choice and Application (MALDI Only)

For MALDI ionization, a matrix is required to allow proper ionization of the molecules of interest. As the matrix crystallizes, analytes are extracted from the tissue section and cocrystallized. If analytes are not in this crystal structure, it is unlikely that they will be ionized. Thus, the availability of the molecule, the matrix application, and the matrix itself can all have an effect on this process. For the case of some proteins, a fixation wash is necessary to make the molecules available for cocrystallization.[9, 11] The Carnoy's solution (*i.e.*, 6:3:1 ethanol:chloroform:glacial acetic acid) is a common wash used for protein MS imaging.[11] Other

washes, such as ammonium citrate, have also been utilized to analyze low molecular weight species. Besides washing, prespraying with solvents can also aid in the extraction of peptides. The combination of ammonium citrate washes and prespraying with cyclohexane proved to be effective in extracting clozapine from rat brain sections.[34] Vapor chambers have also been found to be effective, specifically trifluoroacetic acid vapors for SIMS imaging of lipids.[23] It should be noted that all of the preparations described here may be applicable for other ionization methodology if appropriate, for example matrix-enhanced nanostructure initiator MS.[35]

Several matrices have found popularity for their "universal analysis" including 2,5-dihydroxybenzoic acid (DHB) and α-cyano-4-hydroxycinnamic acid (CHCA), especially for metabolites and peptides in positive mode. A 1:1 mixture of these matrices is also commonly used.[36] Another matrix, sinapinic acid, has been well vetted for proteins in positive mode. On the other hand, negative mode has been found useful for metabolites, for which 1, 5-diaminonaphthalene (DAN) and 9-aminoacridine (9-AA) are among the most commonly used matrices.[12] Interestingly, the use of water as a "matrix" in MALDESI has been explored recently.[19] Furthermore, nanomaterials have been utilized as an alternative matrix, though oftentimes these situations are considered as a different ionization technique (*e.g.*, SALDI).[20] Matrix has also been used to enhance SIMS signals.[25] It is expected that alternative new matrices possessing similar properties to 2-NPG (*i.e.*, multiply-charged ion production) are likely to be developed and applied to matrix-based or -enhanced MS imaging techniques.

In general, most of the focus for sample preparation has been on the matrix application process. When applying matrix, the best method would provide appropriate analyte extraction, small crystal size, and homogenous application. Unfortunately, no universal method exists. Classically, researchers would spray matrix over the tissue sample using a painter's airbrush.

While this can be reproducible between applications by the same individual, person-to-person variability is high, and there is little adjustability. For example, the "wetness" of the surface of the tissue during application defines the appropriate analyte extraction. An appropriate balance needs to be found, as a too "wet" application can cause molecular diffusion while a too "dry" method may not effectively extract the molecules. "Wet" vs. "dry" methods also have an effect on the crystal size, the wetter methods yielding larger crystal sizes. Substrate (*i.e.,* where the sample is placed) versus its surrounding temperatures have also been thought to affect heterogeneity, but this has been only applied to MALDI spots.[37] Automated sprayers have allowed reproducible application methods across individuals and laboratories, and as such, their popularity has grown in the past few years.[38] Several application notes for different vendors exist, but researchers should take time to optimize their application methods to their specific systems. This will likely increase lab-to-lab reproducibility, but it is expected that similar methodologies will be utilized. To increase clarity, all developed methods and their parameters should be included in publications. Interestingly, alternative ionization methods (SIMS) have been used to characterize the analyte incorporation into spots, and, although difficult to implement, similar imaging-based studies would be interesting.[25] Homogenous application has also been a major focus, and researchers have utilized alternative application methods to improve this facet in the past few years. One example is electrospray deposition, for which units tend to be home-built. This dry application method usually requires an additional "incorporation spray" after the matrix has been applied.[39] Some electrospray devices have allowed for control of the crystal size, which can directly relate to the spatial resolution achievable.[40] Other methods have also benefited from the inclusion of an electric field, decreasing crystal size and thereby increasing spatial resolution.[41] Finally, the "driest" method used is sublimation, which is popular

for its low-cost, small crystal size, and high homogeneity. Commercial and partially-modified apparatuses are highly published.[11, 20, 42] When individuals want to use several matrices on a tissue section or staining, they will tend to wash off the original and apply the new matrix, but this unsurprisingly produces signal loss and diffusion. As an alternative, using a commercial sprayer, Urbanek *et al.* have developed a multigrid MALDI (mMALDI) methodology, where different matrices are "printed" into predefined dots on a grid. By targeting these specific matrix dots during the imaging run, a researcher is able to gather multiple data sets (*e.g.*, metabolites, peptides, and proteins) from a single tissue section without washing.[43] Finally, with all of the variations in equipment and methodology, an emphasis should be placed on sharing automated matrix application methods and cross-lab communication to allow for reproducible results. The use of open-source software and easily fabricated instrumentation is an example of this, although the ease of commercial instrumentation will continually compete with this notion.[44]

Specific Molecular Considerations

On-Tissue Digestion

Molecular imaging of proteins has been of major interest, but high mass resolution analysis of proteins has been out of reach due to the mass range limitations of current mass analyzers (*e.g.*, Orbitraps), especially for MALDI. This has been alleviated for extract analysis by the inclusion of an initial protein digestion step (*i.e.*, bottom- up proteomics), so in some cases trypsin on-tissue digestion protocols have been employed for MS imaging.[9, 30, 45] However, as with every method developed, the steps should be optimized specifically for each tissue type.[30, 46] For example, Heijs *et al.* has shown the appearance of different myelin basic protein fragments over longer trypsin incubation times.[30] With the recent surge of interest in mapping glycans in tissue sections, PNGase F, which cleaves N-glycans, has found application into *in situ* digestion

and sequential enzyme application allowing the imaging of both glycans and protein fragments in a single MS imaging run.[47] Overall, while immunostaining/labeling approaches are very effective, they can be nonspecific due to possible cross-reactivity, and MALDI MS imaging provides an orthogonal yet highly specific cross-validation of the labeling-based strategies. The most challenging part of *in situ* digestion is appropriately identifying the protein fragments. In some cases, on-tissue MS/MS is difficult depending on the instrumentation, and a complementary liquid chromatography coupled with MS/MS experiment may need to be performed.[9, 47] It is worth noting that other ionization techniques (nanoDESI) allow for intact protein imaging up to 15 kDa on Orbitrap systems.[48]

Formalin-Fixed Paraffin Embedded (FFPE) Samples

While there is preference in obtaining freshly excised samples for MS imaging analysis, sometimes that is not possible for hard-to-obtain biological samples, especially rare, human specimens. With the wide availability of FFPE tissues, which are not typically compatible with MS, researchers have been motivated to develop methods to release the analytes of interest to image these tissues.[49] As stated previously, optimization for specific tissue types is important, and Oetjen *et al* has provided a comprehensive, guided study to do this for other researchers.[46] Unfortunately, not all molecular species can be extracted from these tissues, although Pietrowska *et al* reported that lipids can be analyzed by avoiding paraffin embedding after fixing the tissue with formalin.[50] Originally, most studies targeted proteins and peptides in the FFPE tissue sections, mainly using the *in situ* digestion methods described above.[46, 50] More recently, researchers have been able to extract metabolites and glycans.[47, 51] With more standardized protocols, the extensive FFPE samples available will be utilized more readily for MS imaging

workflow, allowing for exciting possibilities to examine many clinical specimens and a flood of new information to help guide researchers in future endeavors.

Chemical Derivatization/On-Tissue Labeling

MS is often touted as a universal technique for all molecular species, but there are several classes of molecules that are difficult to ionize and thus analyzed directly by MS. Most targets thus far have been small molecules, such as metabolites, but the inclusion of derivatizing other molecules, such as peptides and glycans, is expected.[52] The overall goal of derivatizing molecules is to change their physicochemical properties and to aid in ionization for MS analysis. For example, the Girard T (GirT) reagent has been applied successfully to several steroids, including testosterone and triamcinolone acetonide.[31, 53] Other steroids (*e.g.*, tetrahydrocannabinal) have also been targeted using 2-fluoro-1-methylpyridinium *p*-tolunesolfonate as a derivatization agent.[29] N-Glycans (**Figure 2**), fatty acids, and neurotransmitters have all been targets through other, unique on-tissue assays.[28, 42, 52] Compared to the traditional spraying of reagent, which usually produces poor spatial resolutions (>100 μm), electrospray deposition has been successfully utilized to derivatize fatty acids while achieving a high spatial resolution (20 micron).[42]

Developments in Instrumentation

MS imaging often requires specially developed instrumentation in order to address challenges unique to image acquisition, such as spatial resolution or surface homogeneity. Numerous advancements have been made in recent years to improve the quality and reproducibility of generated images. The main distinction between imaging MS and liquid chromatography (LC)-MS experiment is the preservation of a spatial dimension. Thus, most

instrumentation developments have focused on the ionization source, with several exceptions related to ion accumulation. The two main ionization methods for MS imaging are laser-based and secondary ion-based, and most of the progress in recent years has focused on these sources. As such, they will be the focus of discussion of this section.

Laser-Based Ionization

Spatial Resolution

Arguably the most sought-after improvements in MS imaging are related to spatial resolution, which is the area corresponding to each individual mass spectrum in an imaging acquisition. Improving the spatial resolution enables more discrete localization patterns to be observed throughout a tissue, but since improving spatial resolution decreases the area of tissue ionized, there is a trade-off between spatial resolution and sensitivity. The resolution can be changed by adjusting the optics of the ionization source or otherwise changing the instrument's geometry to decrease the laser diameter. Sample preparation can also affect the spatial resolution, which is discussed above. Numerous groups have recently reported drastic instrumental improvements in spatial resolution. Spengler and co-workers reported a lateral spatial resolution of 1.4 μm on an atmospheric pressure MALDI source by adjusting its geometry, allowing for the visualization of subcellular distributions of lipids, metabolites, and peptides.[54] The Lee group achieved a spatial resolution of 5 μm on a vacuum pressure MALDI instrument by using a simple modification to the optical instrument. The system was easily interchangeable between various laser spot sizes, allowing for greater flexibility in the trade-off between sensitivity and resolution based on each individual experiment's needs.[55] Numerous other notable advancements have also been made to improve spatial resolution recently.[56-59]

However, with the rapid developments being reported by researchers across the field, it was found that spatial resolution was being defined differently between groups, instruments, and samples. As this makes it difficult to form a standard of comparison between methods and instruments, developing a universal method for both defining, and measuring spatial resolution is crucial to proper data reporting and comparison of images acquired on different instruments with different sample preparation methods, or with different users. Typically, the limiting factor in spatial resolution is the laser, as the laser spot diameter determines the ablation area. Therefore, efforts have been devoted to characterizing the ablation pattern in imaging experiments, particularly with MALDI-MS imaging, the most widespread imaging technique. It was found that laser ablation patterns follow a Gaussian distribution, with incomplete ionization around the outside of the pixel. Furthermore, there is the ability to "shear" matrix crystals, scattering debris across the sample after laser ablation. This finding led to the assertion that MALDI-MS imaging resolution should be defined as (1) the homogeneity of the matrix crystals once they have been applied and cocrystallized with the analyte and (2) the effective ablation diameter of the laser.[60] The hope is that this new definition will allow for more uniform reporting of spatial resolution between research laboratories on different instruments and with different sample preparation methodologies.

Several research groups have developed methods for measuring the actual spatial resolution achievable by an instrument, which can differ from the reported pixel size of the instrument acquisition parameters due to previously mentioned factors such as crystal size and laser beam profile. A simple way to measure effective spatial resolution of an instrument based on user-defined instrument parameters is with a standardized imaging plate. Caprioli and co-workers developed such a slide that incorporated a pattern of crystal violet using lithography in

order to measure the beam diameter in MALDI-MS imaging experiments by visually inspecting the ablation pattern.[61] Another slide for measuring spatial resolution was developed using a slightly different technique, in which a sample solution can be dragged over the slide's surface, allowing it to be automatically retained in hydrophilic grooves of the slide. The slide can then be imaged on the instrument in order to determine the lower threshold of the instrument's spatial resolution.[62] These strategies can provide a valuable method for testing the spatial resolution when adjusting instrumental parameters or performing quality assurance on images to ensure that proper resolution is being reported.

Matrix-Free Laser-Based Ionization

Though highly beneficial in many regards, MALDI-MS imaging's requirement for a matrix coating is often a major drawback in imaging experiments. Matrix application can be a limitation because it requires an additional step in sample preparation, it suffers from poor homogeneity that can affect spatial resolution, and it results in excessive noise peaks in certain mass ranges of the spectrum due to the interference of matrix ions. As a result, ionization sources are being developed to utilize laser ablation techniques without the requirement of matrix. For example, improvements in the sensitivity and coverage of laser ablation electrospray ionization (LAESI)-MS were made for metabolite analysis.[63] Laser desorption postionization MS, though still in its early stages of development, has been demonstrated to have a promising potential as a complementary tool for *in situ* localization and quantitation. It has the benefit of not requiring matrix application or sample preparation, though currently its resolution and mass accuracy are 500 μm and 300 ppm, respectively, which is not competitive with commercial instruments.[64] However, with further development, it may earn its place as a prominent ionization source. Another method for ionization without the application of matrix is nanophotonic laser desorption

ionization, which ionizes analytes from a highly uniform silicon nanopost array.[65] This method has achieved 40 μm spatial resolution for over 80 molecular species, giving it the potential to be competitive with MALDI upon further exploration.

Throughput

Another frequently cited challenge with MS imaging is the long analysis time typically required, which can range from several hours to several days, depending on the selected area and pixel size. These long analysis times limit the practicality of MS imaging for routine applications, particularly in clinical settings. As a result, developments have been made in order to increase throughput without sacrificing image quality. One notable example involved utilizing a solid state laser with a 5 kHz repetition rate to perform continuous laser raster sampling on a MALDI-TOF/TOF instrument. This method achieved an acquisition rate of up to 50 pixels per second, an 8 to 14-fold improvement over conventional lasers.[66] Throughput becomes even more of a challenge when molecules in the same tissue ionize differently, thus requiring different polarities for acquisition. This is particularly the case with lipid analysis, as lipids are a diverse class with high structural variability. Methods have been developed for imaging in both positive and negative polarity while minimizing analysis time using high speed MALDI-MS imaging technology and precise laser control.[67] The field is moving toward real-time imaging capabilities for immediate spatial analysis for guidance during surgeries. As an example, Fowble *et al* have applied a laser ablation imaging approach in ambient conditions in order to obtain spatial distribution of metabolites with a range of polarities in real time without the use of any matrix or sample pretreatment.[68] Another method couples a picosecond IR laser to an electrospray ionization (ESI) source in order to provide ambient MS imaging without causing thermal damage to tissue. This allows molecules to remain in their native environment until ionization, allowing

better insight into the tissue's condition.[69] The iKnife has also demonstrated real-time capabilities, most recently with real-time analysis of the mucosal lipidome by Takats and co-workers.[70] There have been several other developments in technologies to use MS imaging with surgical procedures in order to guide surgical decision-making using MALDI and nanoDESI MS imaging.[71-73] These developments demonstrate great potential in moving MS imaging technology from laboratories to clinical settings for improved patient treatment.

Another approach for improving throughput is microscope mode MS imaging.[74] Here, ions from a relatively large sample area (typically 100–300 μm in diameter) are desorbed simultaneously. Then the ion optics of the instrument project the ionized substances from this area to a position-sensitive detection system such as Medipix or MicroChannelPlate detectors.[75, 76] These types of detectors allow for registration of a single *m/z* acquired from the whole scanned area at once, while magnifying the image and retaining spatial information. Because in the microscope mode a large area is simultaneously measured, a substantial reduction in analysis time is achieved.

SIMS

Resolution and Mass Accuracy

The other most common method of ionization is SIMS, which has seen notable improvements in instrumentation. In SIMS imaging, spatial resolution is often better than the other MS imaging counterparts, but at the expense of sensitivity. This is largely a consequence of the ion beam, either due to low ionization probability or beam focusing difficulties. An argon gas cluster ion beam is typically used for TOF-SIMS, but, despite its many benefits, it suffers from poor sensitivity and mass accuracy and requires the sacrifice of either spatial or mass resolution. Delayed extraction, a method widely used for MALDI-TOF in which an initial pulse is

implemented on the ions to correct for velocity distributions, is becoming more prominent in TOF-SIMS imaging and has been shown to be successful in maintaining both the high mass resolution and spatial resolution.[77] By implementing external mass calibration, the mass accuracy can also be preserved.[78]

Methods involving delayed extraction have been explored as a means to improve mass resolution, but these methods often make mass calibration difficult, resulting in poor mass accuracy. Other groups have explored alternative primary ion sources, such as a CO_2 cluster ion beam, which possesses many similarities to argon but improved the imaging resolution by more than a factor of 2 due to increased stability of the beam.[79]

Parallel Imaging MS/MS

With the inferior mass spectral resolution of TOF-SIMS compared to other ionization methods, the mass accuracy is usually not high enough to make confident identifications of the detected molecules by mass measurement alone. Therefore, it is usually necessary to acquire MS/MS spectra on ions of interest. However, collecting MS/MS spectra is difficult in imaging experiments because performing sequential MS/MS scans after a full-MS scan causes misalignment between spectra and spatial information. To address this, progress in parallel imaging MS/MS has been implemented, in which MS/MS spectra are collected simultaneously with MS spectra using two mass analyzers. This acquisition method differs from traditional MS/MS acquisitions, in which all ions other than the precursor ion are discarded. As a result, MS and MS/MS images are in perfect alignment with each other, allowing for more precise mapping of molecular distribution.[80, 81] With fully optimized parallel imaging, identification confidence can be drastically improved without sacrificing the integrity of localization information.

Ambient/Low-Vacuum TOF-SIMS

As MS imaging is very commonly used for the analysis of biological tissue, it is highly desirable for analyses to be conducted in near-native environments, such as in the presence of water, in order to get an accurate understanding of the chemical environment. Low-vacuum and ambient MALDI imaging have already been well-explored, but progress has recently been made with SIMS, denoted as Wet-SIMS.[82] Currently, the technique is able to acquire images at 80 Pa in imaging experiments.[83] With further development, this technique could be used to ionize biomolecules in their native environment, allowing for analysis in biologically relevant experimental conditions.

Separation

A significant limitation to MS imaging compared to LC-MS analysis is the lack of separation capabilities, as retaining spatial information typically requires ablating all ions present in a pixel of sample at the same time for a single scan. This often leads to problems such as ion suppression, but techniques that allow postionization separation are being developed to overcome this challenge. To separate analytes from noise or undesired compounds, a simple sample cleanup step was incorporated into MALDI-MS imaging by first introducing laser ablation with vacuum capture to collect the ions. The ions are then eluted by a C18 column (or other packing materials or beads) onto the MALDI target plate, effectively desalting the sample and removing background ions. The method demonstrated an improved signal from the sample and decreased background interference compared to direct MALDI-MS imaging, resulting in higher quality MS/MS data, cleaner spectra, and more confident identification.[84] For separation of analytes, ion mobility has been a popular choice, as it can and has been seamlessly integrated into MALDI-MS imaging workflows, such as demonstrated by Trimpin and co-workers.[85] Enhancements to the sensitivity were recently made by the McLean group using a silver-

sputtered matrix coating.[86] Ion mobility has also been recently demonstrated to be highly effective for coupling with ambient ionization techniques, such as LAESI, LESA, and DESI.[87-89] The results showed an increase in detected molecules and the ability to select specific classes to image and offers the capability of using MS^E fragmentation, in which all ions are fragmented, improving MS/MS coverage.[90] An alternative, pseudoseparation method has also been employed, in which subsequent MS scans covered differing *m/z* windows in order to detect low-intensity ions characteristic of specific ranges, providing the effect of gas-phase fractionation. By implementing a spiral plate motion during imaging, the integrity of spatial information was not lost with this method.[27]

Depth Profiling

Another challenge specific to imaging is achieving uniform ionization over the surface of the sample section, something difficult to accomplish if the tissue is not perfectly flat. While extra care in sample preparation can help alleviate this to an extent in some sample types, often slight variations in the height of the tissue are unavoidable.[91] To remedy this, modifications to instruments have been made that allow for height correction. For example, a novel LAESI source was recently developed that incorporated a confocal distance sensor that both moved the sample to a constant height and recorded the height information to generate a topography map.[92] **Figure 3** shows a schematic of the instrumental setup, both the acquisition workflow and optics, as well as example data indicating the information recorded about both sample height and spatial distributions of specific *m/z* values. Another method combined shear force microscopy with a nano-DESI source to measure and adjust the voltage magnitude to enable a stable feedback signal over surfaces with complex topographies.[93] If a uniform sampling can be ensured over the surface of a tissue, it not only preserves spatial integrity throughout the plane of the sample but

can also allow for three-dimensional (3D) imaging. With 3D imaging, it is imperative that the depth profile of the sample be preserved to ensure accurate record of the tissue profile. Several significant advances have been made in this respect in the area of elemental imaging, such as the development of a femtosecond laser ionization source for multielemental imaging with a 7 μm depth resolution.[94] Submicrometer depth resolution, down to 20 nm, has been demonstrated using extreme ultraviolet laser light, allowing for 3D imaging of bacterial colonies.[95] It is expected that these capabilities will continue to be developed and applied to 3D imaging of more complex systems.

Quantitation

Comparison to LC-ESI-MS/MS: The Past

With the push for multimodal imaging (see below), it is clear that obtaining several pieces of information from a single tissue is imperative. While MS imaging is mainly qualitative, with the appropriate conditions, processing, and software, quantitative information can be extracted, although the degree of accuracy is under close scrutiny. Issues such as tissue heterogeneity, ion suppression, sample topography, *etc*. are all considered significant challenges in this field.[96] Before the development of quantitative MS imaging, the analytes of interest were separately extracted from another tissue section and run on a LC-ESI-based instrument for quantitation. Once the absolute quantity of the analyte of calculated, these values can then be applied to the tissue of interest. This methodology is still in use widely, although it is more commonly utilized for confirmation or a starting point of a quantitative MS imaging study.[42, 97] This concept is similar to Western blot for other LC-MS quantitative results.[33] Quantitative MS imaging is now necessary, as many application-based MS imaging publications focus on the

comparison between two or more sample types. With proper sample preparation, comparisons can be made with the appropriate considerations.

Relative Quantitation

Direct Comparison (with or without Normalization)

As mentioned above, direct comparisons between different tissue sections is commonly done. While these "relative" comparison methods lean toward being "semiquantitative," several techniques and data processing strategies have perpetuated their use. For example, matrix effects and other interfering molecules tend to cause more deviation in the quantitative accuracy, although some researchers have shown that the correlation between MALDI-MS imaging and LC-MS/MS can be quantitative for fatty acids and protein.[42, 98] While these assessments of different molecules in a single tissue are interesting, ion suppression and ionization efficiencies between molecules should always be questioned. The addition of an internal standard can aid in the normalization of the signal.[53] Normalization can also be done with the same molecules within different tissues, and this method still aids in more confident comparisons.[53] The inclusion of a normalization procedure in pre- and post-processing is now an expectation. This strategy is applicable for several other molecular species, including neurotransmitters, nucleotides, lipids, and tryptic peptides.[1, 28, 30] Almost all software available for MS imaging provides the ability to normalize. For example, the use of SciLS software tools allow for normalization to the total ion current (TIC) before further statistical analysis.[36] Using this method, several metabolites were found to be different between the cortex, outer medulla, and inner medulla of the rat kidney between control and furosemide-treated.[36] It should be noted that care should be taken when comparing different regions of a tissue, as their biological matrices can vary slightly.[96] As expected, software is an important component in any imaging-based quantitative strategies, and

Renslow *et al* have further developed tools to nanoSIMS transition from qualitative to quantitative for element incorporation into biofilms.[99]

On-Tissue Labeling – Using Reporter Ions

For LC-MS-based quantitation, two types of techniques are employed. Label-free methods directly compare samples in different runs, which is analogous to the "direct comparison" MS imaging described in the previous section. While label-free quantitation is commonly used in LC-MS and MS imaging applications, instrument variability, instrument limitations, and other factors lead to inconsistent and inaccurate comparisons. In contrast, the incorporation of stable isotopes (*i.e.*, ^{2}H, ^{13}C, ^{15}N, ^{18}O) has allowed for same spectrum relative quantitation, although its application to MS imaging is extremely limited. One example in the literature entitled stable-isotope-label based mass spectrometric imaging (SILMS imaging) utilizes light and heavy chromogens to differentiate between different cancer biomarkers of interest (**Figure 4**).[100] After labeling with a primary and secondary antibody, the addition of the chromogen produces an azo dye that, when ionized by the laser, fragments into distinct, duplex reporter ions. The ratio of these reporter ions to another molecule can then be used to calculate their relative abundance, in this case the estrogen receptor compared to the progesterone receptor.[100] While classically reporter ions can be seen in the MS/MS spectra via isobaric labeling, this same idea has not been implemented in MS imaging experiments, not only due to the poor fragmentation for singly charged ions but likely also due to the incompatibly of the methods for relative quantitation. In comparison, isotopic-based labeling methods can potentially be transitioned to on-tissue MS imaging applications, although the process of derivatizing molecules on-tissue has primarily been used for increasing ionization of different molecules.[28, 42, 52]

Absolute Quantitation

Internal Standard

While relative comparisons are commonplace, absolute quantitation is relatively underdeveloped. While obtaining the true concentration of a molecule is much more difficult, it is also more desirable since it allows for true comparisons between different molecular species without concerns about varying ionization efficiencies. As with LC-MS-based measurements, a straightforward method is to incorporate a deuterated internal standard into the sample. As explained previously, internal standards are now being used extensively to normalize MS imaging data sets, and the inclusion of a very specific standard (*e.g.*, deuterated version of an analyte of interest) facilitates absolute quantitation of that analyte. This has been done primarily for DESI samples, with the standards incorporated into the solvent stream.[2]

Calibration Curve

In general, the creation of a calibration curve is the most confident way to obtain the absolute quantity of an analyte. This has been done with LC-MS in separate and the same runs.[101] Initially, one may think producing an external, separately spotted calibration curve would work for MALDI-MS imaging, but the lack of sample matrix and matrix heterogeneity leads to inaccurate concentrations. Thus, researchers have adopted an on-tissue spotting technique that takes both of these considerations into account. The standards of interest (isotopic or nonisotopic) are spotted/applied on a separate, "control" section.[28, 32, 33] This section is usually a serial section of the one being analyzed, as having the same matrix is important for accurate quantitation.[96] For example, many researchers chose liver tissue for initial optimization or studies, as it is considered extremely homogeneous.[33, 96] Interestingly, in the case of elemental analysis, before spotting on the sample, the sections are washed to remove excess elements (*e.g.*,

sodium).[32] To increase homogeneity of the areas where the standards are placed, researchers have developed methods where the standards are spiked into tissue homogenates themselves. These samples are then placed into a mold, frozen, sectioned, and placed near the imaged section, for which quantitation accuracy is similar, although it was noted that the dried droplet spotting method referenced above is much faster and easier.[96] All of these methods require sophisticated computational tools, and several software packages exist for processing region of interest quantitation.[102, 103] msIQuant is an example software, which has been used to absolutely quantify drugs and neurotransmitters.[103]

Data Analysis

MS imaging data is difficult to process for a number of reasons, including the large size of the data files and the high degree of dimensionality, as acquisitions retain spatial information as well as other information. This is becoming more of a problem with the increase in spatial resolution causing an exponential growth in data file sizes. As such, key software developments have been made to address these challenges and ensure that effective analyses are being done without the loss of valuable information in the process. **Figure 5** presents an overview of a typical workflow including several key data processing steps, all of which will be discussed below.

Visualization

The most important information obtained from an imaging experiment is a visualization of the distribution of various molecules throughout the tissue. As each pixel of an imaging experiment contains an entire mass spectrum, special software is required to handle this specific need in the field. While there have been numerous advancements in this respect, the influx of

progress caused there to be a lack of uniformity, making different software tools incompatible with each other. This means that typically the software could not be applied to large data sets, expensive commercial software would be required, or the software would require the end user to have some degree of programming knowledge to fit the data to the software input. However, recent efforts have been made to design open-source visualization tools that are user-friendly and applicable to multiple instrument platforms[102], particularly in the area of laser ablation-inductively coupled plasma mass spectrometry (LA-ICPMS), which is not as routinely implemented as MALDI-MS imaging or TOF-SIMS.[104-106] MSiReader is a key player in open source visualization, providing both a graphic user interface and MATLAB open source code for users.[102] Additionally, even open source microscopy imaging software like ImageJ have plugins scripts capable of handling MS imaging data sets for visualization.[107] These new tools show promise for making the processing of imaging data more widely accessible and customizable for the MS imaging community.

In addition to improving accessibility, new methods have also been explored for expanding the capabilities of visualization tools. For example, 3D MALDI imaging has been limited by inabilities to reconstruct 3D images, but Patterson and colleagues designed an open-source method for 3D reconstruction using multivariate segmentation.[108] Others have expanded the way data is visualized in a different direction. Instead of using imaging to track a single molecule, they developed a tool to view the localization of biological indices (*e.g.*, energy charge index), mapping the relationship between several specified molecules.[109]

An important note with visualization of data in MS imaging is that it is critical to ensuring that the image shown is an accurate representation of the molecular distribution. It has been found that cropping images to eliminate background can cause the emergence of

distribution patterns not observed in the entire image. As a result, data can become skewed if the analyzed area is too small and does not contain sufficient background area for reference.[110] With MS imaging making an increasing presence in biomedical applications as a diagnostic tool, appropriate representation of visual data is essential.

Preprocessing

Prior to data processing, several steps can be used to ensure accurate and efficient data analysis. These steps include normalization, baseline correction, spectra recalibration, smoothing, and data compression (unsupervised and supervised).[111] Normalization is expected to be incorporated into data analysis, while other steps are frequently omitted. However, these additional steps may be necessary, depending upon chosen statistical analysis and the MS instrumentation used to collect the data, as well as other experimental parameters and conditions. The inclusion of preprocessing steps in the data analysis workflow can also depend upon the specific goals of an individual project. Overall, preprocessing can help to reduce experimental variance within the data set, extract relevant information from large data sets, and draw meaningful conclusions from subsequent statistical analysis.

Normalization is used to remove systematic artifacts that can affect the mass spectra. Sample preparation, matrix application, ion suppression, and differential ionization efficiencies in complex samples can influence the intensity peaks of mass spectra. Some of these random effects in data acquisition can be minimized by proper normalization. Not applying normalization can lead to misleading artifacts and ultimately depict inaccurate ion distributions, statistical analyses, and conclusions about biological significance. There are a few different methods for normalization for MS imaging data sets based on the purpose of the analysis. Normalization to the TIC is the most commonly implemented method.[112] Normalization to the

TIC ensures that all spectra have the same integrated area and is based on the assumption that there is a comparable number of signals in each spectrum.[111, 113] However, in an imaging experiment, it cannot always be assumed that this condition is met since selection of the area is variable run-to-run. TIC normalization can improve the ability to compare expression levels across samples with similar sample types, however is not applicable when comparing very different tissue types.[112] In addition to normalization to the TIC for similar sample types, the TIC normalized data can be further normalized to matrix related peaks for MALDI imaging experiments to correct for uneven matrix coating. This may be necessary depending on how the matrix is applied to the sample. For example, airbrush sprayed matrix applications cannot produce as homogeneous of crystals across the whole tissue as matrix applied with an automated sprayer or automated microspotter.[114] For samples with different tissue types, such as whole body imaging, an externally applied internal standard similar to the compound of interest should ideally be applied before or during matrix application (see above). For this normalization method, each spectrum is normalized to the intensity of the reference molecule for analysis. Normalization to an internal standard reduces the impact of ion suppression that arises from tissue inhomogeneity and improves pixel-to-pixel variability. TIC normalization is not recommended for whole body imaging or for different sample compositions, where internal standard normalization is considered the gold-standard normalization methodology.[115] Other options include normalization to an endogenous molecule that is expected to be consistently expressed throughout the whole tissue, such as a phospholipid headgroup. Additionally, some researchers have calculated tissue extinction coefficients or relative response factors to determine the relative amount of a compound in whole body imaging or different tissue types. This tissue extinction coefficient takes into account ion suppression related to the compound of interest and

the tissue of interest and is then compared to LC-MS/MS data.[116] The tissue extinction coefficients were evaluated for the drugs proponolol and olanzapin on rat whole tissue sections, where kidney, lung, liver, brain, and stomach were chosen as tissues of interest. For both drugs, stomach has the highest extinction coefficient, while the stomach and brain experience the highest variation, likely because of tissue heterogeneity in these organs.[116] The advantage of this method is that no expensive, labeled standards are needed of the compounds of interest, although accuracy of tissue extinction coefficients is still being investigated.

Following normalization, additional preprocessing steps are often taken to ensure accurate interpretation of the data. These include steps typically found in conventional MS workflows (*e.g.,* baseline subtraction and spectral recalibration).[111] Furthermore, to better visualize the data and increase the signal-to-noise ratio, smoothing algorithms are often applied, such as Savitsky Golay Smoothing or Boxcar Smoothing.[49, 117, 118] Smoothing is especially important for imaging data to remove sudden fluctuations between pixels that do not necessarily represent the *in vivo* distributions. These preprocessing steps help to ensure that accurate interpretation of the MS imaging data.

Data Compression

Unsupervised Data Compression

As MS imaging acquisitions tend to create large data files (up to several terabytes per sample), data processing becomes more difficult and requires more strenuous computational methods. To alleviate this problem and make the data files easier to handle and distribute, several compression strategies have been implemented to reduce the size of data while still retaining the important information. Binning mass spectra for each pixel of an imaged tissue and compression based on region of interest (ROI) are the most successful methods, with ROI compression

requiring the least amount of computational power.[119] Autoencoders have also been useful for unsupervised nonlinear dimensionality reduction of imaging data by reducing each pixel one at a time to its core features.[120] Once the size of data has been reduced, it can be more easily processed in subsequent steps of the processing pipeline.

Unsupervised clustering of the data is also used to compress data into features for statistical analysis. Unsupervised analysis can be divided into (1) manual, (2) component, or (3) segmentation analysis. (1) Manual analysis is carried out by selecting *m/z* values unique to the region of interest and generating an image for each *m/z* value. (2) Component analysis requires a statistical or machine learning algorithm to cluster the data. Principal component analysis (PCA) is used to reduce the dimensionality of the data set by converting possibly correlated variables into a set of linearly uncorrelated values, which are called principal components.[121] PCA is an unsupervised statistical method to distinguish principal components that cause the greatest variance in the data. PCA plots the component that causes the greatest variation on the x-axis and the component that causes the second greatest amount of variation on the y axis to induce groupings of related pixels in the data sets.[122] While used as a data compression method, PCA can also be combined with discriminant analysis for statistical analysis of imaging data sets (see statistics section below). PCA can also be used to remove signals which are poorly connected with variability between groups, removing noise. (3) The last method, spatial segmentation, bins together similar spectra into regions of interests and identifies colocalized *m/z* values. Hierarchical clustering, a type spatial segmentation, partitions the image into its constituent regions at hierarchical levels. This only requires knowledge of the similarity between groups of data points and does not take into account spatial position during analysis. Hierarchical clustering is frequently used to rearrange multiple variables to visualize possible groups in the

data.[123] Another segmentation method is k-means clustering. k-Means clusters the number of partitions, n, into k number of clusters, where each cluster is based on the spatial distances between mass spectra. Following k-means clustering, each observation now belongs to the cluster with the nearest mean.[124] Another method, bisecting k-means, is a combination of k-means and hierarchical clustering, although it is computationally more complex. Bisecting k-means is a hierarchical clustering method that uses k-means repeatedly on the parent cluster to determine the best possible split to obtain the next two daughter clusters.[125] All of these methods can be used to compress the data into important features and are chosen based on the goal of the study. Some studies will even use more than one unsupervised data compression method. For example, Mourino-Alvarez *et al.* used both hierarchical clustering and PCA to differentiate proteins in calcified areas and collagen deposits in aortic value tissue. By applying a hierarchical clustering following PCA, they were able to observe several layers that surrounded the calcified deposits that differed in protein expression from other tissue regions.[117]

Supervised Data Compression

Supervised clustering is better suited when a specified set of classes is known and the ultimate goal is to classify new data set into one of those classes. Supervised data compression uses predefined classes or categories, while unsupervised data compression uses similarity between spectra to generate classes to reduce data size.[126] Partial least-squares regression (PLS) is a supervised classification method, where classes of data are annotated with known labels.[127] Partial least-squares regression is similar to PCA, however instead of separating into components based on the maximum variance, it uses a linear regression or classification model to project predicted variables and observable variables to a new space, mathematically speaking. Classification refers to decisions among a typically small and discrete set of choices (tumor vs

normal tissue), while regression refers to an estimation of possibly continuous-valued output variables (diagnosis of the severity of disease). This type of supervised clustering requires a training data set for the classification of groups. Like PCA, PLS can also later be coupled to discriminant analysis for statistical analysis but is described in this section as a supervised data compression method. PLS was used to reduce data into different tumor areas that were histology annotated including stroma, smooth muscle, submucosa, fibrous tissue, tumor, healthy mucosa (tumor adjacent) and healthy mucosa (tumor remote) in colorectal cancer. In this case, PLS was used in combination with discriminant analysis to accurately separate changes in lipids between tumor adjacent and tumor-remote healthy mucosa, supporting the idea that cancer influences the local tissue environment.[128]

Both supervised and unsupervised classification methods reduce data down to the most important *m/z* value distributions. Data compression projects the data to a lower dimension subspace, while maintaining the essence of the data for statistical analysis. With the large degree of dimensionality associated with MS imaging data, especially of biomedical samples, extracting important, relevant features becomes increasingly difficult. Machine learning algorithms for feature detection applied to LC-MS data can be limiting with imaging data, as they do not account for differences in spatial regions of the tissue of interest. A context aware feature mapping machine learning algorithm was recently developed that takes into account the spatial region of features when ranking.[129]

Statistical Analysis

Tests of Significance

Statistical analysis of large imaging data sets is incredibly important for the implementation and utility of MS imaging. Interpreting detected differences between samples

involves statistical hypothesis testing to determine if there is a certain difference that exists between samples or between spatial regions within a sample. The choice of appropriate univariate analysis tests that one *m/z*, identifying to a compound of interest, will depend on the data set. If the data has a Gaussian distribution, a t-test can be used to determine the difference between two samples with ANOVA being used to determine if there is any difference in a group of samples.[46, 130] For MS imaging data sets, t-tests can be performed to compare *m/z* relative intensities between two different regions and ANOVA between three or more regions of interest. For example, peptides and metabolites were evaluated in the cortex region of the brain comparing wild type mice and transgenic mice carrying a missense mutation causing cortical spreading disease, which causes migraines. A t-test was used to evaluate specific changes between the cortex of the wild type mice and the transgenic mice.[131] Unfortunately, a Gaussian distribution of mean intensities cannot be assumed for clinical samples, but mean values may still be used if the central limit theorem is satisfied. If the data has a non-Gaussian distribution, nonparametric tests like the Mann-Whitney U-test can be used as a statistical test of the hypothesis. These tests are useful for finding peaks with an observable change between different regions or experimental conditions.

Discriminant Analysis

Data reduction methods such as PCA or PLS are preprocessing steps to discriminant analysis (DA). These analyses are commonly performed together and abbreviated as PCA-DA or PLS-DA, respectively. DA is a statistical tool to assess the adequacy of a classification system. For any kind of DA, the groups need to be assigned beforehand or in the case of PCA, preprocessed prior to discriminant analysis. DA is particularly useful in determining whether a set of variables is effective in predicting category membership. This is different from an

ANOVA or multiple ANOVA, which is used to predict one or multiple continuous dependent variables by one or more independent categorical variables. DA is used in MS imaging to see how well components separate regions of interest in the data set. For example, PCA-DA was applied to colon spheroids to successfully differentiate the outer, middle, and inner regions of the sample.[132] Additionally, PLS-DA was applied in histology driven data mining of lipid differences between colorectal cancer liver metastasis biopsies, where normal vs tumor were preselected as regions of interest prior to analysis.[133]

Biomarker Tests

Even if statistical differences exist between two conditions for a single *m/z*, this does not necessarily mean that this *m/z* value can act as a biomarker to distinguish the two classes. For univariate biomarker analysis to confirm if a *m/z* can be used as a diagnostic test to distinguish two regions of interests, a receiver operator characteristic (ROC) curve analysis is performed. In ROC analysis, the true positive rate (sensitivity) is plotted in function of the false positive rate (specificity).[134-136] The area under the curve (AUC) in these plots can distinguish whether the *m/z* marker can be used for diagnostics. This is a test of accuracy, where an AUC value between 0.90 and 1 is excellent, 0.80-0.90 is good, 0.70-0.80 is fair, 0.60-0.70 is poor, and 0.50-0.60 is failed test. This test is used to discriminate the ability of a specific marker (*m/z*) to correctly classify groups of interest. MALDI imaging was used to reveal thymosin beta-4 as an independent biomarker in flash frozen colorectal cancer compared with normal tissue using ClinPro Tools software to perform ROC analysis with an AUC of ..80.[137]

However, often in biomarker discovery, one biomarker is not able to correctly classify groups with a high enough AUC for clinical analysis. In this case, multiple biomarkers (multiple *m/z* values) are used for analysis. This is known as multivariate analysis. Here, machine learning

algorithms are used examine multiple biomarkers to search for correlated *m/z* values in the mass spectra that also correlate with the target outcome. This multivariate analysis provides a single ROC curve that is derived from multiple biomarkers. Additionally, an indicator of how much each *m/z* contributes to the score from the resulting algorithm is calculated for each *m/z* value.[138, 139] For regression-based methods such as PLS, the importance of an *m/z* value is a direct result of the model's loading vector. Additionally, colocalization of two individual *m/z* in a tissue can be calculated in a correlation analysis to see how well *m/z* components of the multivariate analysis align based on spatial distributions.[140]

One problem for MS imaging analysis is that salt adducts of the m/z values of interest are identified separately. Therefore, in biomarker analysis, it would be ideal to combine *m/z* values identifying to the same molecular compounds into a single peak for analysis. For instance, *m/z* values can shift based on the presence of a sodium ion, potassium ion, the loss of ammonia, the loss of water, oxidation of methionine, and other common modifications. This can complicate identification and statistical analysis as well as univariate and multivariate biomarker analysis. For MALDI, Alexandrov introduced a method called masses alignment which is used to group masses corresponding to a single peak and then represent them as one *m/z* value.[141] This also reduces the size of the data set, making computation and biological understanding of the data more attainable. It also links *m/z* values that belong to the same biomolecule together for statistical analysis.

Machine Learning Algorithms

Machine learning is starting to play a larger role in developing algorithms to quantify relationships in MS imaging and then using these identified data to make predictions for new data sets. First, the data set is converted from a population of profiles into a "n by m" data

matrix, where “n” is individuals, and “m” is the biomolecules of interest.[142] Following conversion, they can be analyzed using different algorithms that look for correlated structures in the measured data that also correlate with a target outcome. Neuronal networks, support vector machine algorithms, recursive maximum margin criterion, and genetic algorithms are used to build statistical models that use training data to predict the classification of new data sets. This is currently being implemented for automated decision making, modeling, computer aided diagnosis, and can be applied for tumor classification for pathology detection.[143] Specifically, in one example, a PCA support vector machine was used for early detection of ovarian cancer with about 90% accuracy.[144]

Complete Data Analysis Pipelines

Because processing imaging data requires numerous different treatments compared to conventional LC-MS data, software with complete data analysis pipelines are useful for streamlining the entire data analysis process. While there are numerous open source and freely available software packages for processing data, functionality tends to be restricted and there are typically no export options for the data. A widely used software package, MSiReader, has seen rapid developments toward incorporating various aspects of data analysis, including visualization, quantitation, and annotation in a streamlined, easy-to-use platform.[102] A new MS imaging software package, SpectralAnalysis, strives to expand the reach of data processing by incorporating all processing steps from preprocessing to multivariate analysis, within a single package, allowing for the analysis of single experiments as well as large-scale experiments spanning multiple instruments and modalities.[145] Improved data processing pipelines are also being developed in efforts to make full use of the spatial information unique to imaging experiments. One such pipeline, EXIMS, aims to reveal significant molecular distribution

patterns by treating the data set as a collection of intensity images for various *m/z* values. The process incorporates preprocessing, sliding window normalization, denoising and contrast enhancement, spatial distribution-based peak-picking, and clustering of intensity images.[146] *massPix*, a R statistical program, is able to perform multivariate analysis (PCA and clustering) and has integrated lipid feature annotation into the automated pipeline.[147] Another software pipeline is SCiLS, which is available commercially from Bruker. SCiLS software can be used to analyze multiple imaging data sets, performing comparative analysis, colocalization analysis, spatial segmentation, and classification model calculations based on training data sets, and it contains numerous other highly useful features. Additionally, ImageQuest software from ThermoFisher Scientific is frequently used for visualization, normalization, and creation of two- and three-dimensional maps of analyzed tissue, and similar features are offered by High Definition Imaging software by Waters. Following *m/z* mapping to a biological compound, platforms that can handle high-dimensional biology data sets, such as Clustergrammer, a Web-based tool, help to visualize biology changes in heatmap formats that retain the high-dimensionality of the biological data.[148] These pipelines emphasize the importance of special treatment for imaging data compared to LC-MS data.

Repositories

Finally, data storage and sharing of the final results allow for the community to move forward and build upon the ever-growing wealth of knowledge. In order to further drive this, imaging repositories are necessary for allowing researchers access to imaging data for comparison of results and for discovering new answers to biological questions. Previously, such repositories were difficult to implement due to the requirements of large space and computational power, but technological advancements have allowed for the emergence of at least

one such repository, with the promise of more becoming available in the near future.[149] Another currently being developed is METASPACE for bioinformatics for spatial metabolomics, an online engine based on big-data technologies that automatically translates millions of ion images to molecular annotations.[150] The estimated completion time for this project is June 2018.

Multimodal Imaging Systems

While MS imaging is useful for analyzing the spatial distributions of several molecular species, it lacks the molecular depth that other methods provide. The combination of MS imaging with other imaging modalities is sure to evolve into a comprehensive analysis tool to answer biological questions that could otherwise not be answered with a single imaging modality. Multimodal technologies are very commonly implemented in diagnostic imaging techniques,[151] and the concept has been expanded into MS imaging analysis pipelines.[151, 152] Because MS imaging has high chemical specificity but lower spatial resolution compared with other imaging modalities, it is typically combined with modalities that complement these features. For example, MS imaging is combined with imaging modalities that have high spatial resolution or tissue structural information. This is can be done with a single section, from which the complementary data can be powerful and enable greater, more significant discoveries.[153]

Multimodal imaging can be approached by either acquiring images at different times (asynchronous), where the images are fused in data processing step, or by simultaneously acquiring images (synchronous) and merging them during the data acquisition step.[154] Asynchronous post-processing can present some difficulties which arise from the positioning of the same samples between different imaging modality scans at different times, which could cause difficulties in coregistering images for analysis.[155] Coregistration is especially difficult if data

acquisitions are not acquired at the same spatial resolutions, however advances in computational annotation help to improve image analysis.[156] Often, voxels from the lower resolution modality are combined to form the voxel size of the higher spatial resolution.[157] Image coregistration can be achieved by aligning known regions of interest, using calibration points to perform a rigid regression or by selecting a variety of points to perform moving least-squares registration between the images.[158] Additionally, different imaging platforms have distinct sample preparation protocols, which can cause interference for different imaging modalities. For example, flash frozen tissue samples are ideal for MS imaging, although the embedding media that they are frequently stored in, which allow for optimal sectioning and staining, consist of the polymer polyethylene glycol which can cause interfering peaks in the mass spectra. Therefore, it is important that the sample preparation used for other imaging modalities also are compatible for MS imaging. Because of this, not all ideal multimodal systems can be easily combined without changing the sample preparation workflow, depending on the desired analysis. Synchronous imaging is advantageous because consistency is achieved in both time and space, however combining instrumentation to accommodate synchronous acquisitions can require advanced skill and can be very expensive, especially for MS instrumentation. Hybrid systems integrating MS imaging are currently being developed, although it should be noted that some method combinations are not possible due to sample incompatibility. One multimodal instrumentation example integrated a commercial optical microscope, laser microdissection instrument (capable of both bright-field and fluorescent imaging) with an electrospray ionization mass spectrometer capable of submicrometer MS imaging.[56] In general, data analysis becomes even more difficult when integrating quantitative information from multiple existing functional modalities to create composites of three, four, or even five imaging modalities into a single data

analysis pipeline. Multiplexing image modalities presents a “big data” computational challenge, making MS imaging data compression especially important for multimodal system integration. To handle the versatility of multimodal systems, workflow based analysis platforms that integrate existing methods are gaining popularity to handle big data problems for imaging systems.[159] These programs allow separate steps that can be rearranged for customizable workflows and do not require computer programming knowledge. KNIME and Galaxy are commonly used workflows for multimodal imaging analysis.[160, 161] Bouslimani *et al.* created a method to merge microbial 16s rRNA amplicon sequences onto a 3D MS imaging map of the human skin. Computational tools used for this analysis are available as a workflow for KNIME, which can be modified and applied for future use for multimodal analysis.[162] It is also clear though that advances in multimodal technology and instrumentation will allow for synchronous integration to be expanded for multiple imaging modalities, a few of which will be discussed below.

It is safe to predict that this overview of multimodal imaging is only the beginning of imaging combinations that will be possible in the future. Multi-modal systems are rapidly expanding into multiple imaging modalities. Here, selected multimodal systems are highlighted, but other imaging techniques not described here, such as near-infrared microscopy, electron microscopy, coherent antistokes raman spectroscopy, Fourier-transform infrared spectroscopy, *etc.* are also being integrated with MS imaging for multimodal analysis.[163-167] With the largest hurdle in multimodal imaging systems being coregistration and data analysis, there will likely be an increase in the development of integrated systems. Additionally, before mult-modal integrated systems will be used regularly, robust coregistration analysis algorithms need to be incorporated into software platforms to handle complex multimodal data compression and analysis.

Microscopy Multimodality

MS imaging is often combined with microscopy to provide high-resolution morphological and structural information in complement to MS imaging's ability to visualize and identify distributions of specific molecules. For example, Plas *et al.* describes a method for fusing microscopy with MS imaging data to enable prediction of a molecular distribution both at high chemical specificity and at high spatial resolution. This is done postdata acquisition using the microscopy data to sharpen and perform out-of-sample predictions.[168] Here, we focus on using optical light microscopy, including bright-field, fluorescence microscopy, and phase-contrast, to evaluate tissue structure and specific markers. Microscopy is the most common multimodal system currently paired with MS imaging and is very useful for identifying regions of interest for statistical probing or supervised classifications.

Histology

Although tissue sections used for MS imaging can be scanned by the computer during analysis to produce an optical overlay, important structural information on the cellular level is obtained from histological analysis of a sample using light microscopy. In general, light microscopy is used to enlarge details and portions of a tissue section. Samples are stained with a specific dye to highlight tissue structures of interest. Histological overlay is the most common multimodal imaging system combined with MS imaging currently applied in the literature.[71, 169, 170] In the discussion below, the focus will primarily be on mammalian tissue stains, although plants and other organisms can also be studied in this fashion. For example, one study used a nonspecific dye stain of gallotannins and ellagitannins in the root of *Paeonia lactiflora* to overlay the structural histology with MS imaging identification of specific galltonnins and monoterpene glucosides.[171]

The most traditional histological stain is hematoxylin and eosin (H&E) stain, which distinguishes nucleic acids from proteins with blue and red colorings, respectively.[172] This allows the user to visualize the differences between cells and the surrounding extracellular matrix.[173] Other commonly used stains include Masson's trichrome stain used for connective tissue, Alcian Blue for mucins, and periodic acid-Schiff reactions used for staining carbohydrate rich tissue regions.[174] When stained, several key characteristics are analyzed, including, tissue morphology, cell structure, and staining distribution. In a clinical setting, trained pathologists use stained slides to identify different disease states of the tissues to stratify patient specimens and provide diagnostic indices. With the high magnification capabilities of modern microscopes, very fine resolution of spatial features can be achieved, which is complementary to MS imaging's comparatively low spatial resolution. Combining histology with MS asynchronously can allow for the analysis of spatial molecular arrangements without the need for target-specific reagents, which allows, for example, the discovery of diagnostic and prognostic markers of different cancer types.[175, 176] It should be noted that typically a sample should first be analyzed using MS imaging (with a nondestructive ionization method) and then stained, as stained slides increase spectral complexity and histological processes can cause degradation or sample loss if done prior to MS imaging analysis.[177] MS compatible dyes do exist, such as cresyl violet and methylene blue, which can allow histology first, followed by MS imaging analysis; however, tissue degradation and diffusion of molecules are still elements of concern.[178] For destructive ionization mechanisms, a serial section is typically used for histological analysis and is coregistered to its adjacent section. However, with serial sections, artifacts such as physical destruction from cutting and fixations and staining artifacts can cause complex distortion effects, also complicating image registration.[179] Although a serial section may not contain the exact same

molecular structure as the section of interest, most structural features are well conserved section to section. Serial sections are commonly used for asynchronous multimodal imaging.

One interesting example applies the H&E stain serial tissue section to direct analysis of specific tissue regions on the section prepared for MS imaging. Regions of interests, including nontumor, undifferentiated tumor, moderately differentiated tumor, and well differentiated tumor, were selected from the H&E stained sections and only those individual regions of interest of the tumor were analyzed. The differentiation of the cells in the tumor region help the pathologist determine cancer staging, where differentiated cells are most similar to the normal tissue.[180] By imaging only the regions of interest, the user can save significantly on instrument time. This application is particularly useful for high-resolution MS imaging, where data acquisition times can be very long and increased data throughput is needed.

Fluorescence Microscopy

Another microscopy technique uses fluorophore conjugated antibodies to label a molecule of interest, known as immunohistochemistry (IHC). First, a molecule of interest is labeled with a primary antibody. Then, a secondary, fluorescent antibody is added that recognizes the primary antibody. The secondary antibody is conjugated with a fluorophore, which, when excited, will provide a measurable light emission. Because multiple secondary antibodies can bind a single primary antibody, the signal of the protein of interest can be amplified greatly to increase the sensitivity of the assay.[181] Depending on the fluorophore of choice, special emission and excitation filters are needed to visualize the signal using a fluorescent microscope. While less common, the secondary antibody can also be coupled with a colorimetric assay. Using IHC, researchers can confirm spatial distributions seen in MS imaging experiments. For example, Heeren and co-workers looked at the hypoxia marker, Pimonidazole,

in a breast tumor model using MS imaging, for which the distribution was confirmed using a secondary antibody conjugated to a horseradish peroxidase colorimetric assay.[182] Some cells and certain molecules possess intrinsic fluorescence. Examples of proteins or small molecules that naturally fluoresce include NADH, tryptophan, chlorophyll, or green florescence proteins. Becker *et al.* uses the natural fluorescence of stillbenes to discriminate the stillbene region from the rest of the grapevine leaves. This feature was then combined with MS imaging to study metabolite changes in stillbene regions of grapevine leaves after *P. viticola* infection.[183] Alternatively, molecular biology and genetic engineering techniques can label proteins, nucleic acids, lipids, or small molecules with an extrinsic fluorophore. These techniques can be applied in systems ranging from cell culture to human systems. Chughtai *et al.* genetically engineered mice to express tandem dimer tomato red fluorescent protein under control of a hypoxia response element in hypoxic regions of the tumor. They then used MS imaging to compare lipids and proteins in hypoxic and normoxic regions of the tumor.[184] While the examples described above are asynchronous examples of multimodal imaging modalities, many are working on the integration of optical microscopy directly with MS imaging. Some of the limitations of combining fluorescent imaging with MS imaging is that often fluorescence signal requires *in vivo* imaging because of degradation of naturally fluorescent material. For instance, NADPH, a source of autofluorescence, has a half-life on the order of minutes and is sensitive to degradation at high pH conditions. Therefore, fluorescence of NADPH is ideally processed using *in vivo* systems, while commonly-used MS imaging systems process samples *ex vivo*.[185] Logistical sample preparations can also create issues with coregistration because differences in orientation during acquisition can be difficult to correct for during data analysis. However, if the

fluorescent label is stable and can also be ionized in a mass range of interest for MS imaging, registration algorithms are not needed for multimodal analysis.[184]

Although there are many examples where fluorescence has been multiplexed with MS imaging, substantial opportunities for growth still exist in fluorescence and optical microscopy multi-imaging systems for MS imaging. For example, fluorescence technologies including fluorescence lifetime imaging microscopy (FLIM), which measures the amount of time a molecule fluoresces as its primary metabolic readout, or spectral lifetime imaging microscopy (SLIM), which is used to create optical molecular fingerprints based on spectra and lifetime of a fluorescent signal, have never been combined with MS imaging.[186, 187] Additionally, combining MS imaging with multiphoton microscopy, which relies on multiple photons to optically section through a tissue section by acquiring clear images at multiple focal planes at different depths in a tissue, has not been used and could serve as a unique way to connect serial sections for 3D MS imaging.[188]

Allen Brain Atlas Integration: Virtual Multimodality

Although not necessarily another imaging modality, MS imaging of the brain and histology images can be coregistered with the Allen Brain Atlas as a virtual multimodality. The Allen Brain Atlas is a publicly accessible collection of brain anatomy compiled high resolution histology images and genome based on brain regions.[189-191] Brain atlases exist for a variety of species, including mouse, nonhuman primate, and human, and have also been expanded to accommodate different neurological diseases and developmental states. These virtual maps were constructed as a 3D biochemical architecture of the brain, where the anatomy of the brain is paired with genome analysis of each region which averaged between many organisms. For the MS imaging field, MATLAB has been used to conduct automatic alignment of a MS imaging

data set of a mouse or rat brain to the position in the 3D map atlas. **Figure 6** demonstrates how the Allen Brain Atlas can be used to align *m/z* values of interest from MS imaging to a specific region of the brain; in this case, *m/z* 863 is localized in the striatum of the brain. This atlas can also be used for genomic insight for biological interpretation of the data, as the Allen Brain Atlas currently has projects mapping the genetic geography of the brain and cell type in each region and has compiled region-specific electrophysiology studies. The development of automatic alignment and annotation tools has increased the throughput for MS imaging data analysis. It has also enabled MS imaging distributions to be compared in the same coordinate space, although improvement upon these tools will be necessary to handle the increased file sizes.[192, 193] This atlas is a unique example of virtual multimodality that is extremely useful for neuroscience researchers working in the MS imaging field. Additionally, although integrating MS imaging is not currently an advertised focus of the Allen Brain Atlas, the development of MS imaging integrated atlases could be useful for multiomics integration.

Analytical Multimodalities Systems

Multimodal Uses for MS imaging

Different types of MS imaging ionization or biomolecule targets can be multiplexed to analyze compounds simultaneously. Because of the range of ionization mechanisms, MS imaging can actually be multiplexed with itself to provide a more comprehensive analysis of the sample by using different ionization mechanisms to analyze different groups of molecular compounds. An example of this is the combination of DESI and subsequent MALDI analysis to analyze lipid and protein distributions, respectively, on the same section.[194] Another study combined MS imaging ionization techniques to complement the high spatial resolution of TOF-SIMS with the high mass resolution, high mass accuracy, and MS/MS of an AP-MALDI source

coupled to an Orbitrap mass spectrometer to study the distribution of lipids in a colon cancer tissue section. First, TOF-SIMS analyzed the lipid distribution at 1 μm spatial resolution. Then, matrix was applied to the same tissue section and AP-MALDI was used to identify lipids at high mass accuracy and also to perform on-tissue MS/MS.[195] Additionally, the same ionization mechanisms can be used for multimodal systems for analyzing different molecular species. For example, MALDI-MS imaging can be used to analyze both N-glycans and proteins using sequential analysis of the PNGaseF enzyme to release glycans followed by application of trypsin to analyze proteins from the same tissue section using FFPE tissues.[47] This is considered multimodal imaging as two separate enzymatic and matrix applications are necessary for analysis.

Raman Spectroscopy

Raman spectroscopy signal is based on the vibrational structure of the molecules within each sample. Each biological sample consists of multiple molecules that form its complex structure and thus vibrational spectrum, which is known as the molecular fingerprint. Raman can be spatially resolved with microscopy for label-free chemical analysis, known as confocal Raman microscopy (CRM). CRM is a nondestructive technique that has high spatial resolution and allows for 3D analysis, where the samples can be optically sectioned taking different z-stacks of the tissue. CRM, however, can be insensitive without special enhancement and is not capable of molecular identification.[196, 197] MS imaging can thus be combined with CRM to assist with identification of specific components of a molecular fingerprint. Additionally, because Raman is a nondestructive technique, MS imaging can easily be performed post-Raman analysis. Correlated MS imaging and confocal Raman microscopy was used to study the structural and chemical diversity of three-dimensional cell cultures.[157] The necrotic core of the spheroids

experienced greater Raman variability and correlated with the principal component causing the greatest variance in the data.[157] Additionally, CRM was also correlated with C60-SIMS to show consistent distribution of quinolone disruptions between the new analytical techniques, with specific molecular identities determined through MS/MS.[198]

Magnetic Resonance Imaging

Magnetic resonance imaging (MRI) is a medical imaging technique that uses strong magnetic fields and radio waves to generate detailed images of cross sections from tissues of the target sample.[152] MRI enables researchers to obtain a 3D anatomical structure of a sample of interest with significant resolution and gives a precise sample shape. Additionally, MRI is noninvasive, although a contrast material is typically administered to enhance the signal-to-noise ratio for the tissue of interest. MRI complements MS imaging very well because it allows detailed structural information, while MS imaging provides chemical probing of the sample. In one example, MRI and MS imaging were used to study distributions of alkaloids in two structurally distinct regions in maturing areca nuts (seed of *Areca catechu*).[199] Additionally, another study used MS imaging for the detection of the gadoteridol (MRI contrast agent) in human gliomas via DESI-MS imaging following MRI analysis. Detection of a compound by both modalities, as in the example above, is particularly useful for improvements in coregistration between imaging modalities.[200] Overall, MRI, while underutilized with MS imaging in the literature, provides a powerful tool that could be more integrated with other systems, including with the Allen Brain Atlas described above. Scalable Brain Atlases based on MRI data are being developed for nonrigid spatial registration of MS imaging to MRI data.[193] Additionally, new computation pipelines are also being developed to better integrate MRI, 3D MS imaging data, and histology.[201]

Positron Emission Tomography (PET)

Positron emission technology (PET) is commonly used clinically to visualize tumors and tumor metastases in 3D as a noninvasive imaging technique to provide metabolic assessment of a region, for example a cancerous tumor. By administering a radiolabeled metabolite, commonly 18F-fluorodeoxyglucose (FDG), PET monitors the body's uptake of FDG. Tumors tend to have altered, typically increased, metabolism compared to the regions surrounding it.[202] PET can be combined with MS imaging to understand tumor heterogeneity and to show additional metabolic alterations in regions of interest. Biomap software allows for multimodality imaging processing between PET scans and MS imaging data sets. In one study, MALDI-MS imaging was actually used to assist in the development of a new PET radioligand by using MS imaging to image the PET molecule itself as well as the biological receptors for the PET molecule.[203]

Atomic Force Microscopy

Atomic force microscopy (AFM) is able to measure the topography with nanometer spatial resolution by raster scanning the tip of a scanning probe along the (x,y,z) position of a sample. Since tissue sections may not be completely flat, it can be beneficial to collect the surface topography of a tissue section using AFM for MS imaging. This can allow signal intensities to be correlated with surface topography, as uneven surfaces can affect uniform instrument ionization. Using AFM, the morphology of the section is translated into specific quantitative features, such as height, width, area, and volume. AFM and MS imaging can actually be obtained synchronously where the same probe is used without moving the sample from the system as demonstrated by Ovchinnikova *et al.* using proximal probe thermal

desorption/ionization MS.[204] This eliminates the need for postacquisition coregistration, which can be particularly difficult for AFM and MS imaging multimodal systems.

Multimodal imaging systems couple additional structural, biological, morphological, and chemical information with MS imaging analysis. Optimized sample preparation for multimodalities, advances in coregistration, and improvements in computational workflows are required to advance the use of MS imaging integrated multimodal imaging systems.

Biological Applications

It is clear that the increased molecular capabilities of MS imaging have caught the attention of the biological community. The expansion beyond peptides and proteins, MALDI MS imaging, and even fresh tissue sections has broadened the general use of MS imaging in unforeseen directions. In the following sections, several interesting studies will be highlighted, along with specialty applications in the field, all of which have incorporated the advancements described in this review. It should be noted that MS imaging has applicability beyond the biological systems (*e.g.,* imaging of dyes on banknotes), so individuals should not feel limited in the systems where MS imaging can be applied.[167, 205, 206]

Expansion of Molecular Species of Interest

Initially this technique was used to localize proteins and other peptides within a sample, with the first applications toward tissue samples.[130] At first, MALDI was the core technique for imaging, and it is still by far the most popular method for analyzing peptide and protein rich samples.[3, 9, 207] As an example, neuropeptides have been primarily imaged with MALDI, which has been applied to characterizing distribution changes in the pericardial organ of the green crab (red and green morph) after being exposed to salinity stress.[3, 208] In particular, the development

of on-tissue digestion with trypsin has increased protein coverage by allowing not only higher molecular weight species to be analyzed but also by letting other more sensitive, higher resolution instrumental platforms become available for protein analysis.[9, 47] Animal tissues are not the only sample types to have benefitted from this technique, as plant peptides have been imaged to compare those found in seedling and mature *Medicago truncatula.*[209] Alternative ionization techniques beyond MALDI have been applied to better image proteins and peptides. For example, matrix-enhanced SIMS has produced high spatial resolution images of neuropeptides.[210] Furthermore, matrix-free, ambient ionization methods have also found popularity, as both DESI and nanoDESI have just recently been shown that they are capable of imaging global protein distributions.[48, 88] While proteins and peptides maintain their popularity due to their obvious biological roles, it is apparent that many more recent MS imaging studies have focused on mapping the distributions of other molecular species.

The advent of on-tissue digestion with trypsin along with the use of PNGaseF for release of glycans has prompted the analysis of N-glycans with MALDI-MS imaging. As discussed previously, on-tissue digestion sequentially with PNGaseF and trypsin enabled MS imaging analyses of both released N-glycans and tryptic protein fragments on a single tissue.[47] It should be noted though that native glycan imaging has been performed.[211] N-Glycans have been analyzed in variety of samples, including kidney, bone, and cancerous tissues.[38, 212-214] To highlight one example, different bone marrow samples that had either no bone lesions or with various stages of bone lesions were compared, and the glycan $(NeuAc)_2(Hex)_2(HexNAc)_2$ + $(Man)_3(GlcNAc)_2$ was shown to be upregulated in the Stage 1 bone lesion affected marrow.[214] Notably, much of the recent literature has focused on FFPE tissue, which is expected with their increased availability compared to other clinically relevant tissue. In order to assess different N-

glycans, derivatization methods are beginning to emerge, including for sialic acid-containing N-glycans, for which images are shown in **Figure 2**.[52] Beyond derivatization, tissue engineering-based approaches can be used to develop specific probes against different glycan groups to improve ionization and thus detection of these important molecules, though this technique is still in the "proof-of-principle" stage.[215] The methodology for N-glycan imaging is still underdeveloped, and the availability of more derivatization agents, expansion to other ionization sources, and improved sample preparation steps are expected to be developed.

Because of their diagnostic power, lipids are becoming more targeted compounds for MS imaging analysis.[1, 216, 217] For example, folic acid distribution appears to increase in prostate tumor tissue after intravenous administration.[216] Lipids also have the potential to show tumor boundaries, specifically in breast cancer.[217] Because of their diverse structure, several common ionization sources, including MALDI, DESI, SIMS, and IR-MALDESI, have found success in lipid imaging.[1, 18-20, 22, 42, 97, 217-221] Notably, newly developed laser spray ionization (LSI), with its simple sample preparation, is becoming more commonly used for lipids as well.[20, 222] As an example, division of normal and cancerous tissue was easily achieved for a few dozen lipid species, including diglyceride DG (18:1/20:0), which was indicated as a potential biomarker for renal cancer.[222] While tissue sections have obvious popularity in the literature, lipids can be measured in a variety of sources, including fingerprints and plants.[223, 224] Finally, because of their comprehensive distribution, whole body imaging of lipids has been done on the *Anopheles stephensi* mosquito.[15] One caveat of lipid imaging is the difficulty of identification due to lipid diversity, and care should be taken in ensuring proper procedures to confirm their identity, especially if the information is intended to be utilized in the clinic.

Surprisingly, elemental analysis has been done more frequently to distinguish biological samples. By looking at metal species, researchers have the unique advantages of low background noise along with good quantitative dynamic range, unlike most protein or peptide studies.[225] Unfortunately, only select ionization sources are capable of imaging metals, and each method is limited in which metals they can image.[226] Currently, LA-ICPMS and SIMS have been the only methods available to analyze elemental metals.[24, 32, 225, 227-231] With the use of nanoSIMS, mapping at a subcellular resolution (300 nm) has been achieved for copper, phosphorus, iron, and calcium, allowing the discrimination between the cell wall and different vacuoles in a *C. reinhardtii* cell. Notably, this technique can also be useful for drug visualization if metal-based drugs (*e.g.*, cisplatin) are involved by directly analyzing their metal core and not the drug itself.[232] With the recognition that all molecular species can have an effect on human health, metal imaging will likely become more popular in the upcoming years.

By far the most imaged molecular species in the current literature are small molecules. This may come with their broad diversity, as they include TCA cycle components, neurotransmitters, drugs, and even fungicides.[1, 2, 28, 29, 218, 233, 234] Importantly, these diverse small molecule metabolites could be indicative of disease state.[152, 218] Some of the more notable applications include imaging tetrahydrocannabinol (THC) in hair strands (**Figure 7**), determination of antimicrobial metabolites for biocontrol against *F.* oxysporum, and metabolomic distribution analysis of kidney metabolites after rats being treated with furosemide.[29, 36, 235] Because of their structure, metabolites can have poor ionization efficiency, which has prompted the development of many derivatization schemes to increase access to metabolites in samples.[28, 31, 53] Just like lipids, a wide variety of ionization techniques lends well to metabolites, including MALDI, DESI, and LAESI, although, based upon citations alone,

MALDI is by far the most popular.[2, 12, 14, 20, 28, 29, 31, 36, 69, 137, 218, 233-237] This is actually surprising, as most matrices used for MALDI analysis are small organic compounds, meaning they can have their own interfering ions in the metabolite mass range at high concentrations, masking some possible signals of interest. Care should be taken in understanding which peaks come from the matrix, and alternatives, such as deuterated matrices should be sought out if necessary.[238]

Expansion of Sample Sources

It is clear that the expansion of molecular species that can be analyzed by MS imaging has also sparked its application to new and unusual sample sources. Biological samples (*e.g.*, tissue) will likely continue to be utilized for method development and proof-of-principle experiments due to their natural sample complexity and variety.[31, 33, 222, 229, 239] This trend is especially true for clinically inventoried samples, since strategies for analyzing FFPE tissue samples are in high demand.[49, 51, 100, 213] For example, tissue microarrays, which are usually FFPE samples, provide unique opportunities for researchers to perform high-throughput screening of different diseases with little variation in preparation.[51, 211] Beyond FFPE, one unique application of MS imaging on a mammalian tissue sample has been where cannabinoids, such as THC, and other drugs have been imaged with MS and MS/MS on single hair samples, which has promise for integration into toxicology-based screenings (**Figure 7**).[29, 240] Fingerprints have also been targeted for MS imaging analysis.[45, 241]

In addition to mammalian systems, other model organisms, such as crustaceans, grasshoppers, and ants, have also been imaged using MS imaging techniques.[3, 91, 236] Furthermore, the use of plants as an alternative research system is commonplace, so, naturally, researchers have also transitioned to imaging plant-based samples.[234, 242] In the last 2 years, food products, such as onions, cucumbers, and citrus peel extracts, have been analyzed, but it is clear

that theoretically any item can be imaged with the appropriate equipment.[18, 237, 243-245] For example, DESI-MS imaging was utilized to understand the thin-layer chromatography (TLC) separation of the citrus peel extracts directly on the TLC plates (**Figure 8**). Notably, methods have even been developed to image microbial systems, many of which can provide insight into antimicrobial agents or characterization of microbial interactions.[235, 246, 247]

Unique Applications

Clinical Incorporation

With the streamlining of sample preparation, collection, and processing, integration of MS imaging into the clinic is becoming more accepted, which has been highlighted throughout this review. Briefly, MS imaging has shown applicability to determining metal accumulation, discriminating tumor regions, disease diagnosis, and even intraoperative usage[5, 6, 5, 6, 41, 49, 51, 212, 213, 218, 226, 248] MS has already found its way into real-time surgeries with the invention of the iKnife, and it is only a matter of time before MS imaging is utilized in a similar fashion.[70]

3D MS Imaging

The construction of 3D MS-based images has expanded in the past decade with advancements in the throughput of MS instrumentation. 3D analysis incorporates volumetric molecular distribution into the equation. Currently, 3D imaging is commonly done through serial sectioning of a sample, where each section is analyzed in 2D and computational reconstruction of a 3D model based on the distance between section distances is performed.[249-252] For example, Seeley *et al.* utilized a multimodality approach with MRI and MS imaging to rebuild 3D image of a mouse leg with a bone tumor.[249] However, emerging techniques, such as 2.5D (*i.e.*, single section localization within the tissue volume using other imaging modalities), surface, or ablation-based imaging, are also being proposed.[253] Sectioning is not always necessary with

ablation-based methods, such as LA-ICPMS, as "layer-by-layer" of the sample can be analyzed.[254] This idea of "depth profiling" can also be used for samples that cannot be sectioned (*e.g.*, minerals, 3D cell cultures).[94, 95, 254, 255] Limitations exist for 3D imaging though, including throughput, alignment between serial tissue sections, and the computational limits for data size, for which some 3D MS imaging are 200-300 gigabytes.[253, 256] Data compression and/or clustering, supervised or unsupervised, is necessary for each 2D tissue section prior to alignment and reconstruction.[132, 250, 253, 256]

It should be noted that even when sectioned, samples may not lay flat on the slide or they may have density differences along the tissue that could expand or contract during further sample processing. With the slight variations in tissue height, inaccurate quantitative information can be obtained, bringing the significance of any results into question. The advent of topography-integrated MS imaging instrumentation allows for the system to correct based on tissue height.[92, 93] This new modality will surely be incorporated into future instrumentation in the years to come with the goal to obtain more quantitative measures and accurate 3D images from MS imaging data sets.

Single Cell Analysis

While superior in determining vast chemical information, MS imaging is seen as lacking in spatial resolution compared to other imaging techniques. Over the past few years, the achievable spatial resolution of MS imaging, especially for MALDI imaging, has improved greatly.[54, 55] With the development of new instrumentation (see above), a lateral resolution of 5-10 μm is readily achievable with commercial equipment, specifically MALDI, which is within the reaches of assessing individual mammalian cells.[257] While this resolution is technologically impressive, biological heterogeneity is a major concern, and being able to distinguish variation at

the single cell level will only make MS imaging more powerful.[258] For example, with the use of high-resolution ionization (LA-ICP) coupled to cytometry by time-of-flight (*e.g.,* CyTOF, mass cytometry), the cellular subpopulation heterogeneity can be easily highlighted.[259, 260] When reaching these very small pixel sizes, care should be taken that enough material is actually being ionized and thus detected at a significant level. While the development of higher spatial resolution instrumentation, matching optics, and mass analyzers must be implemented as well to move single cell MS imaging forward.

Naturally high spatial resolution instrumentation, such as SIMS, has easily been able to image cells with laser beam focuses of 500 to 30 nm.[255, 261-263] A facet of SIMS, multi-isotope mass spectrometry (MIMS), has been able to reach 50 nm spatial resolution to visualize human adipose tissue and its age-related plasticity loss.[264] Unfortunately, SIMS is unable to ionize most peptides or proteins, although ME-SIMS and the combination of SILAC and TOF-SIMS has allowed for imaging of peptides, lipids, and newly synthesized proteins.[210, 265] In general, though, developments for other ionization sources are a must for these major biomolecules. Comparatively, MALDI is far away from being able to reach comparable spatial resolution levels to SIMS, but in the past few years, researchers have gotten closer to routinely utilizing 5 to 10 μm laser spot sizes (example shown in **Figure 9**).[177, 207, 266] Other ionization techniques that can provide subcellular resolution include LA-ICPMS, single-probe MS, and laser desorption/ionization droplet delivery (LDI-DD).[267-270] Notably, LDI-DD is able to reach 2.4 μm spatial resolution for an ink printed pattern and 3 μm for mouse brain, boasting the importance of developing new ionization techniques for bioanalysis.[270]

Conclusions and Future Directions

The field of MS imaging has expanded drastically in recent years as its utility has been recognized for a wide variety of applications. Because of its ability to analyze thousands of biomolecules without any form of labeling, MS imaging is being increasingly used as an analytical technique both as a complement and replacement to other imaging methods. However, with its rapid expansion, there is an urgent need for improvements in reproducibility at the sample preparation level and for extra care to be taken in ensuring correct interpretation of results. Recent literature has begun to address this, but we are still far from a uniform standard for reproducibility between users, laboratories, and biological samples. The literature also reflects a push toward improved spatial resolution, and this will likely continue to be an area of focus for the foreseeable future. With spatial resolution already approaching submicrometer levels and 3D MS imaging becoming more commonplace, the number of spectra acquired per experiment has increased exponentially, and will only get larger as spatial resolution continues to be improved. As a result, there is a growing need for more sophisticated data analysis tools that can handle the large amounts of data being produced, both in extracting meaningful information and storing data for community access. The incorporation of open-source software has done a remarkable job addressing this challenge, but future efforts need to be made in ensuring ease-of-use for the end user. Ideally, software will be designed in ways that make it possible for various tools from different sources to be incorporated into a single data analysis pipeline, allowing the researcher to customize software for individual imaging experiments. By improving upon sample preparation protocols, instrumental throughput and resolution capabilities, and streamlined data analysis and quantitation, it is anticipated that MS imaging will become routinely utilized in clinical settings.

Acknowledgements

The authors gratefully acknowledge support from the National Institutes of Health (NIH) through grants R56MH110215 and R01 DK071801. A.R.B. acknowledges the NIH General Medical Sciences F31 Fellowship (1F31GM119365) for funding. K.D. acknowledges a predoctoral fellowship supported by the NIH, under Ruth L. Kirschstein National Research Service Award T32 HL 007936 from the National Heart Lung and Blood Institute to the University of Wisconsin-Madison Cardiovascular Research Center. L.L. and J.J. would like to thank the University of Wisconsin Carbone Cancer Center (UWCCC) Pancreas Cancer Task Force for funding support. L.L. acknowledges a Vilas Distinguished Achievement Professorship and Janis Apinis Professorship with funding provided by the Wisconsin Alumni Research Foundation and University of Wisconsin-Madison School of Pharmacy.

Conflict of Interest

The authors declare no conflicts of interest.

References

1. Miyamoto, S.; Hsu, C. C.; Hamm, G.; Darshi, M.; Diamond-Stanic, M.; Decleves, A. E.; Slater, L.; Pennathur, S.; Stauber, J.; Dorrestein, P. C.; Sharma, K., *Ebiomedicine* **2016,** *7*, 121-134.

2. Bergman, H. M.; Lundin, E.; Andersson, M.; Lanekoff, I., *Analyst* **2016,** *141* (12), 3686-3695.

3. Zhang, Y.; Buchberger, A.; Muthuvel, G.; Li, L., *Proteomics* **2015**.

4. Dong, Y. H.; Li, B.; Aharoni, A., *Trends in Plant Science* **2016,** *21* (8), 686-698.

5. St John, E. R.; Rossi, M.; Pruski, P.; Darzi, A.; Takats, Z., *Trac-Trends in Analytical Chemistry* **2016,** *85*, 2-9.

6. Huang, K. T.; Ludy, S.; Calligaris, D.; Dunn, I. F.; Laws, E.; Santagata, S.; Agar, N. Y. R., *Applications of Mass Spectrometry Imaging to Cancer* **2017,** *134*, 257-282.

7. Kooijman, P. C.; Kok, S. J.; Weusten, J.; Honing, M., *Analytica Chimica Acta* **2016,** *919*, 1-10.

8. Carter, C. L.; Jones, J. W.; Farese, A. M.; MacVittie, T. J.; Kane, M. A., *Analytical Chemistry* **2016,** *88* (9), 4788-4794.

9. Gessel, M.; Spraggins, J. M.; Voziyan, P.; Hudson, B. G.; Caprioli, R. M., *Journal of Mass Spectrometry* **2015,** *50* (11), 1288-1293.

10. Gill, E. L.; Yost, R. A.; Vedam-Mai, V.; Garrett, T. J., *Analytical Chemistry* **2017,** *89* (1), 576-580.

11. O'Rourke, M. B.; Raymond, B. B. A.; Djordjevic, S. P.; Padula, M. P., *Rapid Communications in Mass Spectrometry* **2015,** *29* (7), 637-644.

12. Klein, A. T.; Yagnik, G. B.; Hohenstein, J. D.; Ji, Z. Y.; Zi, J. C.; Reichert, M. D.; MacIntosh, G. C.; Yang, B.; Peters, R. J.; Vela, J.; Lee, Y. J., *Analytical Chemistry* **2015,** *87* (10), 5294-5301.

13. Wang, S. J.; Bai, H. R.; Cai, Z. W.; Gao, D.; Jiang, Y. Y.; Liu, J. J.; Liu, H. X., *Electrophoresis* **2016,** *37* (13), 1956-1966.

14. Holzlechner, M.; Reitschmidt, S.; Gruber, S.; Zeilinger, S.; Marchetti-Deschmann, M., *Proteomics* **2016,** *16* (11-12), 1742-1746.

15. Khalil, S. M.; Rompp, A.; Pretzel, J.; Becker, K.; Spengler, B., *Analytical Chemistry* **2015,** *87* (22), 11309-11316.

16. Bai, H. R.; Wang, S. J.; Liu, J. J.; Gao, D.; Jiang, Y. Y.; Liu, H. X.; Cai, Z. W., *Journal of Chromatography B-Analytical Technologies in the Biomedical and Life Sciences* **2016,** *1026*, 263-271.

17. Chen, B.; Lietz, C. B.; Li, L., *Journal of the American Society for Mass Spectrometry* **2014,** *25* (12), 2177-2180.

18. Ekelof, M.; McMurtrie, E. K.; Nazari, M.; Johanningsmeier, S. D.; Muddiman, D. C., *Journal of the American Society for Mass Spectrometry* **2017,** *28* (2), 370-375.

19. Nazari, M.; Muddiman, D. C., *Analyst* **2016,** *141* (2), 595-605.

20. Phan, N. T. N.; Mohammadi, A. S.; Pour, M. D.; Ewing, A. G., *Analytical Chemistry* **2016,** *88* (3), 1734-1741.

21. Alberici, R. M.; Vendramini, P. H.; Eberlin, M. N., *Analytical Methods* **2017,** *9* (34), 5029-5036.

22. Vendramini, P. H.; Gattaz, W. F.; Schmitt, A.; Falkai, P.; Eberlin, M. N.; Martins-de-Souza, D., *Schizophrenia Research* **2016,** *177* (1-3), 67-69.

23. Angerer, T. B.; Pour, M. D.; Malmberg, P.; Fletcher, J. S., *Analytical Chemistry* **2015,** *87* (8), 4305-4313.

24. Vanbellingen, Q. P.; Fu, T. T.; Bich, C.; Amusant, N.; Stien, D.; Della-Negra, S.; Touboul, D.; Brunelle, A., *Journal of Mass Spectrometry* **2016,** *51* (6), 412-423.

25. Korsgen, M.; Pelster, A.; Dreisewerd, K.; Arlinghaus, H. F., *Journal of the American Society for Mass Spectrometry* **2016,** *27* (2), 277-284.

26. Shi, F. J.; Archer, J. J.; Levis, R. J., *Methods* **2016,** *104*, 79-85.

27. OuYang, C.; Chen, B.; Li, L., *Journal of the American Society for Mass Spectrometry* **2015,** *26* (12), 1992-2001.

28. Shariatgorji, M.; Nilsson, A.; Goodwin, R. J. A.; Kallback, P.; Schintu, N.; Zhang, X. Q.; Crossman, A. R.; Bezard, E.; Svenningsson, P.; Andren, P. E., *Neuron* **2014,** *84* (4), 697-707.

29. Beasley, E.; Francese, S.; Bassindale, T., *Analytical Chemistry* **2016,** *88* (20), 10328-10334.

30. Heijs, B.; Tolner, E. A.; Bovee, J. V. M. G.; van den Maagdenberg, A. M. J. M.; McDonnell, L. A., *Journal of Proteome Research* **2015,** *14* (12), 5348-5354.

31. Barre, F. P. Y.; Flinders, B.; Garcia, J. P.; Jansen, I.; Huizing, L. R. S.; Porta, T.; Creemers, L. B.; Heeren, R. M. A.; Cillero-Pastor, B., *Analytical Chemistry* **2016,** *88* (24), 12051-12059.

32. Shariatgorji, M.; Nilsson, A.; Bonta, M.; Gan, J. R.; Marklund, N.; Clausen, F.; Kallback, P.; Loden, H.; Limbeck, A.; Andren, P. E., *Methods* **2016,** *104*, 86-92.

33. Chumbley, C. W.; Reyzer, M. L.; Allen, J. L.; Marriner, G. A.; Via, L. E.; Barry, C. E.; Caprioli, R. M., *Analytical Chemistry* **2016,** *88* (4), 2392-2398.

34. Quiason, C. M.; Shahidi-Latham, S. K., *Journal of the American Society for Mass Spectrometry* **2015,** *26* (6), 967-973.

35. Moening, T. N.; Brown, V. L.; He, L., *Analytical Methods* **2016,** *8* (46), 8234-8240.

36. Jung, J. W.; Lee, M. S.; Choi, H. J.; Jung, S.; Lee, Y. J.; Hwang, G. S.; Kwon, T. H., *American Journal of Physiology-Renal Physiology* **2016,** *310* (11), F1317-F1327.

37. Lai, Y. H.; Cai, Y. H.; Lee, H.; Ou, Y. M.; Hsiao, C. H.; Tsao, C. W.; Chang, H. T.; Wang, Y. S., *Journal of the American Society for Mass Spectrometry* **2016,** *27* (8), 1314-1321.

38. Skraskova, K.; Claude, E.; Jones, E. A.; Towers, M.; Ellis, S. R.; Heeren, R. M. A., *Methods* **2016,** *104*, 69-78.

39. Malys, B. J.; Owens, K. G., *Rapid Communications in Mass Spectrometry* **2017,** *31* (9), 804-812.

40. Li, S. L.; Zhang, Y. Y.; Liu, J. A.; Han, J. J.; Guan, M.; Yang, H.; Lin, Y.; Xiong, S. X.; Zhao, Z. W., *Scientific Reports* **2016,** *6*, 10.

41. Guo, S.; Wang, Y. M.; Zhou, D.; Li, Z. L., *Analytical Chemistry* **2015,** *87* (12), 5860-5865.

42. Wu, Q.; Comi, T. J.; Li, B.; Rubakhin, S. S.; Sweedler, J. V., *Analytical Chemistry* **2016,** *88* (11), 5988-5995.

43. Urbanek, A.; Holzer, S.; Knop, K.; Schubert, U.; von Eggeling, F., *Analytical and Bioanalytical Chemistry* **2016,** *408* (14), 3769-3781.

44. Stoeckli, M.; Staab, D., *Journal of the American Society for Mass Spectrometry* **2015,** *26* (6), 911-914.

45. Kamanna, S.; Henry, J.; Voelcker, N.; Linacre, A.; Kirkbride, K. P., *Rapid Communications in Mass Spectrometry* **2017,** *31* (22), 1927-1937.

46. Oetjen, J.; Lachmund, D.; Palmer, A.; Alexandrov, T.; Becker, M.; Boskamp, T.; Maass, P., *Analytical and Bioanalytical Chemistry* **2016,** *408* (24), 6729-6740.

47. Heijs, B.; Holst, S.; Briaire-de Bruijn, I. H.; van Pelt, G. W.; de Ru, A. H.; van Veelen, P. A.; Drake, R. R.; Mehta, A. S.; Mesker, W. E.; Tollenaar, R. A.; Bovee, J.; Wuhrer, M.; McDonnell, L. A., *Analytical Chemistry* **2016,** *88* (15), 7745-7753.

48. Hsu, C. C.; Chou, P. T.; Zare, R. N., *Analytical Chemistry* **2015,** *87* (22), 11171-11175.

49. Panderi, I.; Yakirevich, E.; Papagerakis, S.; Noble, L.; Lombardo, K.; Pantazatos, D., *Rapid Communications in Mass Spectrometry* **2017,** *31* (2), 160-170.

50. Pietrowska, M.; Gawin, M.; Polanska, J.; Widlak, P., *Proteomics* **2016,** *16* (11-12), 1670-1677.

51. Ly, A.; Buck, A.; Balluff, B.; Sun, N.; Gorzolka, K.; Feuchtinger, A.; Janssen, K. P.; Kuppen, P. J. K.; van de Velde, C. J. H.; Weirich, G.; Erlmeier, F.; Langer, R.; Aubele, M.; Zitzelsberger, H.; McDonnell, L.; Aichler, M.; Walch, A., *Nature Protocols* **2016,** *11* (8), 1428-1443.

52. Holst, S.; Heijs, B.; de Haan, N.; van Zeijl, R. J. M.; Briaire-de Bruijn, I. H.; van Pelt, G. W.; Mehta, A. S.; Angel, P. M.; Mesker, W. E.; Tollenaar, R. A.; Drake, R. R.; Bovee, J.; McDonnell, L. A.; Wuhrer, M., *Analytical Chemistry* **2016,** *88* (11), 5904-5913.

53. Cobice, D. F.; Livingstone, D. E. W.; Mackay, C. L.; Goodwin, R. J. A.; Smith, L. B.; Walker, B. R.; Andrew, R., *Analytical Chemistry* **2016,** *88* (21), 10362-10367.

54. Kompauer, M.; Heiles, S.; Spengler, B., *Nature Methods* **2017,** *14* (1), 90-96.

55. Feenstra, A. D.; Duenas, M. E.; Lee, Y. J., *Journal of the American Society for Mass Spectrometry* **2017,** *28* (3), 434-442.

56. Cahill, J. F.; Kertesz, V.; Van Berkel, G. J., *Analytical Chemistry* **2015,** *87* (21), 11113-11121.

57. Hieta, J. P.; Vaikkinen, A.; Auno, S.; Raikkonen, H.; Haapala, M.; Scotti, G.; Kopra, J.; Piepponen, P.; Kauppila, T. J., *Journal of the American Society for Mass Spectrometry* **2017,** *28* (6), 1060-1065.

58. Li, X. X.; Chen, L. F.; Ouyang, Y. Z.; Feng, F.; Chen, H. W., *Chinese Journal of Analytical Chemistry* **2016,** *44* (1), 25-31.

59. Bajo, K.; Itose, S.; Matsuya, M.; Ishihara, M.; Uchino, K.; Kudo, M.; Sakaguchi, I.; Yurimoto, H., *Surface and Interface Analysis* **2016,** *48* (11), 1190-1193.

60. O'Rourke, M. B.; Raymond, B. B. A.; Padula, M. P., *Journal of the American Society for Mass Spectrometry* **2017,** *28* (5), 895-900.

61. Zubair, F.; Prentice, B. M.; Norris, J. L.; Laibinis, P. E.; Caprioli, R. M., *Analytical Chemistry* **2016,** *88* (14), 7302-7311.

62. Fagerer, S. R.; Rompp, A.; Jefimovs, K.; Bronnimann, R.; Hayenga, G.; Steinhoff, R. F.; Krismer, J.; Pabst, M.; Ibanez, A. J.; Zenobi, R., *Rapid Communications in Mass Spectrometry* **2015,** *29* (11), 1019-1024.

63. Fincher, J. A.; Korte, A. R.; Reschke, B.; Morris, N. J.; Powell, M. J.; Vertes, A., *Analyst* **2017,** *142* (17), 3157-3164.

64. Chen, J. X.; Hu, Y. J.; Lu, Q. A.; Wang, P. C.; Zhan, H. Q., *Analyst* **2017,** *142* (7), 1119-1124.

65. Stopka, S. A.; Rong, C.; Korte, A. R.; Yadavilli, S.; Nazarian, J.; Razunguzwa, T. T.; Morris, N. J.; Vertes, A., *Angewandte Chemie-International Edition* **2016,** *55* (14), 4482-4486.

66. Prentice, B. M.; Chumbley, C. W.; Caprioli, R. M., *Journal of Mass Spectrometry* **2015,** *50* (4), 703-710.

67. Ellis, S. R.; Cappell, J.; Potocnik, N. O.; Balluff, B.; Hamaide, J.; Van der Linden, A.; Heeren, R. M. A., *Analyst* **2016,** *141* (12), 3832-3841.

68. Fowble, K. L.; Teramoto, K.; Cody, R. B.; Edwards, D.; Guarrera, D.; Musah, R. A., *Analytical Chemistry* **2017,** *89* (6), 3421-3429.

69. Zou, J.; Talbot, F.; Tata, A.; Ermini, L.; Franjic, K.; Ventura, M.; Zheng, J. Z.; Ginsberg, H.; Post, M.; Ifa, D. R.; Jaffray, D.; Miller, R. J. D.; Zarrine-Afsar, A., *Analytical Chemistry* **2015,** *87* (24), 12071-12079.

70. Alexander, J.; Gildea, L.; Balog, J.; Speller, A.; McKenzie, J.; Muirhead, L.; Scott, A.; Kontovounisios, C.; Rasheed, S.; Teare, J.; Hoare, J.; Veselkov, K.; Goldin, R.; Tekkis, P.; Darzi, A.; Nicholson, J.; Kinross, J.; Takats, Z., *Surgical Endoscopy and Other Interventional Techniques* **2017,** *31* (3), 1361-1370.

71. Calligaris, D.; Feldman, D. R.; Norton, I.; Brastianos, P. K.; Dunn, I. F.; Santagata, S.; Agar, N. Y. R., *International Journal of Mass Spectrometry* **2015,** *377*, 690-698.

72. Calligaris, D.; Feldman, D. R.; Norton, I.; Olubiyi, O.; Changelian, A. N.; Machaidze, R.; Vestal, M. L.; Laws, E. R.; Dunn, I. F.; Santagata, S.; Agar, N. Y. R., *Proceedings of the National Academy of Sciences of the United States of America* **2015,** *112* (32), 9978-9983.

73. Santagata, S.; Eberlin, L. S.; Norton, I.; Calligaris, D.; Feldman, D. R.; Ide, J. L.; Liu, X. H.; Wiley, J. S.; Vestal, M. L.; Ramkissoon, S. H.; Orringer, D. A.; Gill, K. K.; Dunn, I. F.; Dias-Santagata, D.; Ligon, K. L.; Jolesz, F. A.; Golby, A. J.; Cooks, R. G.; Agar, N. Y. R., *Proceedings of the National Academy of Sciences of the United States of America* **2014,** *111* (30), 11121-11126.

74. Luxembourg, S. L.; Vaezaddeh, A. R.; Amstalden, E. R.; Zimmermann-Ivol, C. G.; Hochstrasser, D. F.; Heeren, R. M. A., *Rapid Communications in Mass Spectrometry* **2006,** *20* (22), 3435-3442.

75. Kiss, A.; Jungmann, J. H.; Smith, D. F.; Heeren, R. M. A., *Review of Scientific Instruments* **2013,** *84* (1), 7.

76. Jungmann, J. H.; MacAleese, L.; Buijs, R.; Giskes, F.; de Snaijer, A.; Visser, J.; Visschers, J.; Vrakking, M. J. J.; Heeren, R. M. A., *Journal of the American Society for Mass Spectrometry* **2010,** *21* (12), 2023-2030.

77. Vanbellingen, Q. P.; Elie, N.; Eller, M. J.; Della-Negra, S.; Touboul, D.; Brunelle, A., *Rapid Communications in Mass Spectrometry* **2015,** *29* (13), 1187-1195.

78. Shon, H. K.; Yoon, S.; Moon, J. H.; Lee, T. G., *Biointerphases* **2016,** *11* (2), 7.

79. Tian, H.; Maciazek, D.; Postawa, Z.; Garrison, B. J.; Winograd, N., *Journal of the American Society for Mass Spectrometry* **2016,** *27* (9), 1476-1482.

80. Fisher, G. L.; Bruinen, A. L.; Potocnik, N. O.; Hammond, J. S.; Bryan, S. R.; Larson, P. E.; Heeren, R. M. A., *Analytical Chemistry* **2016,** *88* (12), 6433-6440.

81. Fisher, G. L.; Hammond, J. S.; Larson, P. E.; Bryan, S. R.; Heeren, R. M. A., *Journal of Vacuum Science & Technology B* **2016,** *34* (3), 4.

82. Seki, T.; Kusakari, M.; Fujii, M.; Aoki, T.; Matsuo, J., *Nuclear Instruments & Methods in Physics Research Section B-Beam Interactions with Materials and Atoms* **2016,** *371*, 189-193.

83. Suzuki, K.; Kusakari, M.; Fujii, M.; Seki, T.; Aoki, T.; Matsuo, J., *Surface and Interface Analysis* **2016,** *48* (11), 1119-1121.

84. Donnarumma, F.; Cao, F.; Murray, K. K., *Journal of the American Society for Mass Spectrometry* **2016,** *27* (1), 108-116.

85. Fischer, J. L.; Lutomski, C. A.; El-Baba, T. J.; Siriwardena-Mahanama, B. N.; Weidner, S. M.; Falkenhagen, J.; Allen, M. J.; Trimpin, S., *Journal of the American Society for Mass Spectrometry* **2015,** *26* (12), 2086-2095.

86. Xu, L. B.; Kliman, M.; Forsythe, J. G.; Korade, Z.; Hmelo, A. B.; Porter, N. A.; McLean, J. A., *Journal of the American Society for Mass Spectrometry* **2015,** *26* (6), 924-933.

87. Griffiths, R. L.; Creese, A. J.; Race, A. M.; Bunch, J.; Cooper, H. J., *Analytical Chemistry* **2016,** *88* (13), 6758-6766.

88. Feider, C. L.; Elizondo, N.; Eberlin, L. S., *Analytical Chemistry* **2016,** *88* (23), 11533-11541.

89. Li, H.; Smith, B. K.; Mark, L.; Nemes, P.; Nazarian, J.; Vertes, A., *International Journal of Mass Spectrometry* **2015,** *377*, 681-689.

90. Lamont, L.; Baumert, M.; Potocnik, N. O.; Allen, M.; Vreeken, R.; Heeren, R. M. A.; Porta, T., *Analytical Chemistry* **2017,** *89* (20), 11143-11150.

91. Gemperline, E.; Horn, H. A.; DeLaney, K.; Currie, C. R.; Li, L. J., *Acs Chemical Biology* **2017,** *12* (8), 1980-1985.

92. Bartels, B.; Kulkarni, P.; Danz, N.; Bocker, S.; Saluz, H. P.; Svatos, A., *Rsc Advances* **2017,** *7* (15), 9045-9050.

93. Nguyen, S. N.; Liyu, A. V.; Chu, R. K.; Anderton, C. R.; Laskin, J., *Analytical Chemistry* **2017,** *89* (2), 1131-1137.

94. He, M. H.; Meng, Y. F.; Yan, S. S.; Hang, W.; Zhou, W. G.; Huang, B. L., *Analytical Chemistry* **2017,** *89* (1), 565-570.

95. Kuznetsov, I.; Filevich, J.; Dong, F.; Woolston, M.; Chao, W. L.; Anderson, E. H.; Bernstein, E. R.; Crick, D. C.; Rocca, J. J.; Menoni, C. S., *Nature Communications* **2015,** *6*, 6.

96. Hansen, H. T.; Janfelt, C., *Analytical Chemistry* **2016,** *88* (23), 11513-11520.

97. Kuchar, L.; Faltyskova, H.; Krasny, L.; Dobrovolny, R.; Hulkova, H.; Ledvinova, J.; Volny, M.; Strohalm, M.; Lemr, K.; Kryspinova, L.; Asfaw, B.; Rybova, J.; Desnick, R. J.; Havlicek, V., *Analytical and Bioanalytical Chemistry* **2015,** *407* (8), 2283-2291.

98. Theron, L.; Centeno, D.; Coudy-Gandilhon, C.; Pujos-Guillot, E.; Astruc, T.; Remond, D.; Barthelemy, J. C.; Roche, F.; Feasson, L.; Hebraud, M.; Bechet, D.; Chambon, C., *Proteomes* **2016,** *4* (4), 16.

99. Renslow, R. S.; Lindemann, S. R.; Cole, J. K.; Zhu, Z. H.; Anderton, C. R., *Biointerphases* **2016,** *11* (2), 9.

100. Wang, H.; DeGnore, J. P.; Kelly, B. D.; True, J.; Garsha, K.; Bieniarz, C., *Journal of Mass Spectrometry* **2015,** *50* (9), 1088-1095.

101. Greer, T.; Lietz, C. B.; Xiang, F.; Li, L. J., *Journal of the American Society for Mass Spectrometry* **2015,** *26* (1), 107-119.

102. Robichaud, G.; Garrard, K. P.; Barry, J. A.; Muddiman, D. C., *Journal of the American Society for Mass Spectrometry* **2013,** *24* (5), 718-721.

103. Kallback, P.; Nilsson, A.; Shariatgorji, M.; Andren, P. E., *Analytical Chemistry* **2016,** *88* (8), 4346-4353.

104. Sforna, M. C.; Lugli, F., *Journal of Analytical Atomic Spectrometry* **2017,** *32* (5), 1035-1043.

105. Lopez-Fernandez, H.; Pessoa, G. D.; Arruda, M. A. Z.; Capelo-Martinez, J. L.; Fdez-Riverola, F.; Glez-Pena, D.; Reboiro-Jato, M., *Journal of Cheminformatics* **2016,** *8*, 10.

106. Uerlings, R.; Matusch, A.; Weiskirchen, R., *International Journal of Mass Spectrometry* **2016,** *395*, 27-35.

107. Gormanns, P.; Reckow, S.; Poczatek, J. C.; Turck, C. W.; Lechene, C., *Plos One* **2012,** *7* (2), 12.

108. Patterson, N. H.; Doonan, R. J.; Daskalopoulou, S. S.; Dufresne, M.; Lenglet, S.; Montecucco, F.; Thomas, A.; Chaurand, P., *Proteomics* **2016,** *16* (11-12), 1642-1651.

109. Hayakawa, E.; Fujimura, Y.; Miura, D., *Bioinformatics* **2016,** *32* (24), 3852-3854.

110. O'Rourke, M. B.; Padula, M. P., *Proteomics Clinical Applications* **2017,** *11* (3-4), 5.

111. Norris, J. L.; Cornett, D. S.; Mobley, J. A.; Andersson, M.; Seeley, E. H.; Chaurand, P.; Caprioli, R. M., *International Journal of Mass Spectrometry* **2007,** *260* (2-3), 212-221.

112. Deininger, S. O.; Cornett, D. S.; Paape, R.; Becker, M.; Pineau, C.; Rauser, S.; Walch, A.; Wolski, E., *Analytical and Bioanalytical Chemistry* **2011,** *401* (1), 167-181.

113. Fonville, J. M.; Carter, C.; Cloarec, O.; Nicholson, J. K.; Lindon, J. C.; Bunch, J.; Holmes, E., *Analytical Chemistry* **2012,** *84* (3), 1310-1319.

114. Gemperline, E.; Rawson, S.; Li, L. J., *Analytical Chemistry* **2014,** *86* (20), 10030-10035.

115. Bokhart, M. T.; Rosen, E.; Thompson, C.; Sykes, C.; Kashuba, A. D. M.; Muddiman, D. C., *Analytical and Bioanalytical Chemistry* **2015,** *407* (8), 2073-2084.

116. Hamm, G.; Bonnel, D.; Legouffe, R.; Pamelard, F.; Delbos, J.-M.; Bouzom, F.; Stauber, J., *Journal of Proteomics* **2012,** *75* (16), 4952-4961.

117. Mourino-Alvarez, L.; Iloro, I.; de la Cuesta, F.; Azkargorta, M.; Sastre-Oliva, T.; Escobes, I.; Lopez-Almodovar, L. F.; Sanchez, P. L.; Urreta, H.; Fernandez-Aviles, F.; Pinto, A.; Padial, L. R.; Akerstrom, F.; Elortza, F.; Barderas, M. G., *Scientific Reports* **2016,** *6*, 12.

118. Jones, E. A.; Deininger, S. O.; Hogendoorn, P. C. W.; Deelder, A. M.; McDonnell, L. A., *Journal of Proteomics* **2012,** *75* (16), 4962-4989.

119. Bedia, C.; Tauler, R.; Jaumot, J., *Journal of Chemometrics* **2016,** *30* (10), 575-588.

120. Thomas, S. A.; Race, A. M.; Steven, R. T.; Gilmore, I. S.; Bunch, J.; Ieee, *Proceedings of 2016 Ieee Symposium Series on Computational Intelligence (Ssci)* **2016**, 7.

121. Bro, R.; Smilde, A. K., *Analytical Methods* **2014,** *6* (9), 2812-2831.

122. Jones, E. A.; van Remoortere, A.; van Zeijl, R. J. M.; Hogendoorn, P. C. W.; Bovee, J.; Deelder, A. M.; McDonnell, L. A., *Plos One* **2011,** *6* (9), 14.

123. Deininger, S. O.; Ebert, M. P.; Futterer, A.; Gerhard, M.; Rocken, C., *Journal of Proteome Research* **2008,** *7* (12), 5230-5236.

124. Sarkari, S.; Kaddi, C. D.; Bennett, R. V.; Fernandez, F. M.; Wang, M. D.; Ieee In *Comparison of Clustering Pipelines for the Analysis of Mass Spectrometry Imaging Data*, 36th Annual International Conference of the IEEE-Engineering-in-Medicine-and-Biology-Society (EMBC), Chicago, IL, Aug 26-30; Ieee: Chicago, IL, 2014; pp 4771-4774.

125. Trede, D.; Schiffler, S.; Becker, M.; Wirtz, S.; Steinhorst, K.; Strehlow, J.; Aichler, M.; Kobarg, J. H.; Oetjen, J.; Dyatloy, A.; Heldmann, S.; Walch, A.; Thiele, H.; Maass, P.; Alexandrov, T., *Analytical Chemistry* **2012,** *84* (14), 6079-6087.

126. Jirasko, R.; Holcapek, M.; Khalikova, M.; Vrana, D.; Student, V.; Prouzova, Z.; Melichar, B., *Journal of the American Society for Mass Spectrometry* **2017,** *28* (8), 1562-1574.

127. Ilin, Y.; Kraft, M. L., *Current Opinion in Biotechnology* **2015,** *31*, 108-116.

128. Mirnezami, R.; Spagou, K.; Vorkas, P. A.; Lewis, M. R.; Kinross, J.; Want, E.; Shion, H.; Goldin, R. D.; Darzi, A.; Takats, Z.; Holmes, E.; Cloarec, O.; Nicholson, J. K., *Molecular Oncology* **2014,** *8* (1), 39-49.

129. Minhas, F. U. A.; Asif, A.; Arif, M., *Computers in Biology and Medicine* **2016,** *79*, 68-79.

130. Marczyk, M.; Drazek, G.; Pietrowska, M.; Widlak, P.; Polanska, J.; Polanski, A., *International Conference on Computational Science, Iccs 2015 Computational Science at the Gates of Nature* **2015,** *51*, 693-702.

131. Carreira, R. J.; Shyti, R.; Balluff, B.; Abdelmoula, W. M.; van Heiningen, S. H.; van Zeijl, R. J.; Dijkstra, J.; Ferrari, M. D.; Tolner, E. A.; McDonnell, L. A.; van den Maagdenberg, A., *Journal of the American Society for Mass Spectrometry* **2015,** *26* (6), 853-861.

132. Weaver, E. M.; Hummon, A. B.; Keithley, R. B., *Analytical Methods* **2015,** *7* (17), 7208-7219.

133. Thomas, A.; Patterson, N. H.; Marcinkiewicz, M. M.; Lazaris, A.; Metrakos, P.; Chaurand, P., *Analytical Chemistry* **2013,** *85* (5), 2860-2866.

134. Grund, B.; Sabin, C., *Current Opinion in Hiv and Aids* **2010,** *5* (6), 473-479.

135. Metz, C. E., *Radiol Phys Technol* **2008,** *1* (1), 2-12.

136. Scheipers, U.; Perrey, C.; Siebers, S.; Hansen, C.; Ermert, H., *Ultrasonic Imaging* **2005,** *27* (3), 181-198.

137. Gemoll, T.; Strohkamp, S.; Schillo, K.; Thorns, C.; Habermann, J. K., *Oncotarget* **2015,** *6* (41), 43869-43880.

138. Shultz, E. K., *Clinical Chemistry* **1995,** *41* (8), 1248-1255.

139. Wang, M. C.; Li, S. S., *Lifetime Data Analysis* **2013,** *19* (2), 257-277.

140. McDonnell, L. A.; van Remoortere, A.; van Zeijl, R. J. M.; Deelder, A. M., *Journal of Proteome Research* **2008,** *7* (8), 3619-3627.

141. Alexandrov, T., *Bmc Bioinformatics* **2012,** *13*, 13.

142. Galli, M.; Zoppis, I.; Smith, A.; Magni, F.; Mauri, G., *Expert Review of Proteomics* **2016,** *13* (7), 685-696.

143. Kourou, K.; Exarchos, T. P.; Exarchos, K. P.; Karamouzis, M. V.; Fotiadis, D. I., *Computational and Structural Biotechnology Journal* **2015,** *13*, 8-17.

144. Wu, J.; Ji, Y. J.; Zhao, L.; Ji, M. Y.; Ye, Z.; Li, S. Y., *Computational and Mathematical Methods in Medicine* **2016**, 6.

145. Race, A. M.; Palmer, A. D.; Dexter, A.; Steven, R. T.; Styles, I. B.; Bunch, J., *Analytical Chemistry* **2016,** *88* (19), 9451-9458.

146. Wijetunge, C. D.; Saeed, I.; Boughton, B. A.; Spraggins, J. M.; Caprioli, R. M.; Bacic, A.; Roessner, U.; Halgamuge, S. K., *Bioinformatics* **2015,** *31* (19), 3198-3206.

147. Bond, N. J.; Koulman, A.; Griffin, J. L.; Hall, Z., *Metabolomics* **2017,** *13* (11), 5.

148. Fernandez, N. F.; Gundersen, G. W.; Rahman, A.; Grimes, M. L.; Rikova, K.; Hornbeck, P.; Ma'ayan, A., *Scientific Data* **2017,** *4*, 12.

149. Rompp, A.; Wang, R.; Albar, J. P.; Urbani, A.; Hermjakob, H.; Spengler, B.; Vizcano, J. A., *Analytical and Bioanalytical Chemistry* **2015,** *407* (8), 2027-2033.

150. Alexandrov, T. METASPACE. (accessed Sept 17th).

151. Cherry, S. R., *Seminars in Nuclear Medicine* **2009,** *39* (5), 348-353.

152. Ho, Y. N.; Shu, L. J.; Yang, Y. L., *Wiley Interdisciplinary Reviews-Systems Biology and Medicine* **2017,** *9* (5), 32.

153. Vogler, N.; Heuke, S.; Bocklitz, T. W.; Schmitt, M.; Popp, J., Multimodal Imaging Spectroscopy of Tissue. In *Annual Review of Analytical Chemistry, Vol 8*, Cooks, R. G.; Pemberton, J. E., Eds. Annual Reviews: Palo Alto, 2015; Vol. 8, pp 359-387.

154. Marti-Bonmati, L.; Sopena, R.; Bartumeus, P.; Sopena, P., *Contrast Media & Molecular Imaging* **2010,** *5* (4), 180-189.

155. Meyer, C.; Ma, B.; Kunju, L. P.; Davenport, M.; Piert, M., *European Journal of Nuclear Medicine and Molecular Imaging* **2013,** *40*, S72-S78.

156. Eliceiri, K. W.; Berthold, M. R.; Goldberg, I. G.; Ibanez, L.; Manjunath, B. S.; Martone, M. E.; Murphy, R. F.; Peng, H. C.; Plant, A. L.; Roysam, B.; Stuurmann, N.; Swedlow, J. R.; Tomancak, P.; Carpenter, A. E., *Nature Methods* **2012,** *9* (7), 697-710.

157. Ahlf, D. R.; Masyuko, R. N.; Hummon, A. B.; Bohn, P. W., *Analyst* **2014,** *139* (18), 4578-4585.

158. Huhdanpaa, H.; Hwang, D. H.; Gasparian, G. G.; Booker, M. T.; Cen, Y.; Lerner, A.; Boyko, O. B.; Go, J. L.; Kim, P. E.; Rajamohan, A.; Law, M.; Shiroishi, M. S., *Journal of Digital Imaging* **2014,** *27* (3), 369-379.

159. Wollmann, T.; Erfle, H.; Eils, R.; Rohr, K.; Gunkel, M., *Journal of Biotechnology* **2017,** *261*, 70-75.

160. Afgan, E.; Baker, D.; Coraor, N.; Chapman, B.; Nekrutenko, A.; Taylor, J., *Bmc Bioinformatics* **2010,** *11*, 6.

161. Berthold, M. R.; Cebron, N.; Dill, F.; Gabriel, T. R.; Kotter, T.; Meinl, T.; Ohl, P.; Sieb, C.; Thiel, K.; Wiswedel, B., *Data Analysis, Machine Learning and Applications* **2008**, 319-326.

162. Bouslimani, A.; Porto, C.; Rath, C. M.; Wang, M. X.; Guo, Y. R.; Gonzalez, A.; Berg-Lyon, D.; Ackermann, G.; Christensen, G. J. M.; Nakatsuji, T.; Zhang, L. J.; Borkowski, A. W.; Meehan, M. J.; Dorrestein, K.; Gallo, R. L.; Bandeira, N.; Knight, R.; Alexandrov, T.; Dorrestein, P. C., *Proceedings of the National Academy of Sciences of the United States of America* **2015,** *112* (17), E2120-E2129.

163. Vollnhals, F.; Audinot, J. N.; Wirtz, T.; Mercier-Bonin, M.; Fourquaux, I.; Schroeppel, B.; Kraushaar, U.; Lev-Ram, V.; Ellisman, M. H.; Eswara, S., *Analytical Chemistry* **2017,** *89* (20), 10702-10710.

164. Aoyagi, S.; Abe, K.; Yamagishi, T.; Iwai, H.; Yamaguchi, S.; Sunohara, T., *Analytical and Bioanalytical Chemistry* **2017,** *409* (27), 6387-6396.

165. Balbekova, A.; Bonta, M.; Torok, S.; Ofner, J.; Dome, B.; Limbeck, A.; Lendl, B., *Analytical Methods* **2017,** *9* (37), 5464-5471.

166. Marty, F.; Rago, G.; Smith, D. F.; Gao, X. L.; Eijkel, G. B.; MacAleese, L.; Bonn, M.; Brunner, E.; Basler, K.; Heeren, R. M. A., *Analytical Chemistry* **2017,** *89* (18), 9664-9670.

167. Silva, L. M. A.; Alves, E. G.; Simpson, A. J.; Monteiro, M. R.; Cabral, E. C.; Ifa, D. R.; Venancio, T., *Talanta* **2017,** *173*, 22-27.

168. Van de Plas, R.; Yang, J. H.; Spraggins, J.; Caprioli, R. M., *Nature Methods* **2015,** *12* (4), 366-U138.

169. Taverna, D.; Pollins, A. C.; Sindona, G.; Caprioli, R. M.; Nanney, L. B., *Journal of Proteome Research* **2015,** *14* (2), 986-996.

170. Rauser, S.; Marquardt, C.; Balluff, B.; Deininger, S. O.; Albers, C.; Belau, E.; Hartmer, R.; Suckau, D.; Specht, K.; Ebert, M. P.; Schmitt, M.; Aubele, M.; Hofler, H.; Walch, A., *Journal of Proteome Research* **2010,** *9* (4), 1854-1863.

171. Li, B.; Bhandari, D. R.; Rompp, A.; Spengler, B., *Scientific Reports* **2016,** *6*, 12.

172. Eberlin, L. S.; Tibshirani, R. J.; Zhang, J. L.; Longacre, T. A.; Berry, G. J.; Bingham, D. B.; Norton, J. A.; Zare, R. N.; Poultsides, G. A., *Proceedings of the National Academy of Sciences of the United States of America* **2014,** *111* (7), 2436-2441.

173. Fischer, A. H.; Jacobson, K. A.; Rose, J.; Zeller, R., *CSH Protoc* **2008,** *2008*, pdb.prot4986.

174. Lewin, K., *Journal of Anatomy* **1969,** *105*, 171-&.

175. Sans, M.; Gharpure, K.; Tibshirani, R.; Zhang, J. L.; Liang, L.; Liu, J. S.; Young, J. H.; Dood, R. L.; Sood, A. K.; Eberlin, L. S., *Cancer Research* **2017,** *77* (11), 2903-2913.

176. Hinsch, A.; Buchholz, M.; Odinga, S.; Borkowski, C.; Koop, C.; Izbicki, J. R.; Wurlitzer, M.; Krech, T.; Wilczak, W.; Steurer, S.; Jacobsen, F.; Burandt, E. C.; Stahl, P.; Simon, R.; Sauter, G.; Schluter, H., *Journal of Mass Spectrometry* **2017,** *52* (3), 165-173.

177. Deutskens, F.; Yang, J. H.; Caprioli, R. M., *Journal of Mass Spectrometry* **2011,** *46* (6), 568-571.

178. Chaurand, P.; Schwartz, S. A.; Billheimer, D.; Xu, B. G. J.; Crecelius, A.; Caprioli, R. M., *Analytical Chemistry* **2004,** *76* (4), 1145-1155.

179. Wang, C. W.; Ka, S. M.; Chen, A., *Scientific Reports* **2014,** *4*, 12.

180. Heijs, B.; Abdelmoula, W. M.; Lou, S.; Briaire-de Bruijn, I. H.; Dijkstra, J.; Bovee, J.; McDonnell, L. A., *Analytical Chemistry* **2015,** *87* (24), 11978-11983.

181. Levenson, R. M.; Borowsky, A. D.; Angelo, M., *Laboratory Investigation* **2015,** *95* (4), 397-405.

182. Mascini, N. E.; Cheng, M. L.; Jiang, L.; Rizwan, A.; Podmore, H.; Bhandari, D. R.; Rompp, A.; Glunde, K.; Heeren, R. M. A., *Analytical Chemistry* **2016,** *88* (6), 3107-3114.

183. Becker, L.; Bellow, S.; Carre, V.; Latouche, G.; Poutaraud, A.; Merdinoglu, D.; Brown, S. C.; Cerovic, Z. G.; Chaimbault, P., *Analytical Chemistry* **2017,** *89* (13), 7099-7106.

184. Chughtai, K.; Jiang, L.; Post, H.; Winnard, P. T.; Greenwood, T. R.; Raman, V.; Bhujwalla, Z. M.; Heeren, R. M. A.; Glunde, K., *Journal of the American Society for Mass Spectrometry* **2013,** *24* (5), 711-717.

185. Wu, J. T.; Wu, L. H.; Knight, J. A., *Clinical Chemistry* **1986,** *32* (2), 314-319.

186. Walsh, A. J.; Skala, M. C., *Biomedical Optics Express* **2015,** *6* (2), 559-573.

187. Provenzano, P. P.; Rueden, C. T.; Trier, S. M.; Yan, L.; Ponik, S. M.; Inman, D. R.; Keely, P. J.; Eliceiri, K. W., *Journal of Biomedical Optics* **2008,** *13* (3), 11.

188. Provenzano, P. P.; Eliceiri, K. W.; Keely, P. J., *Clinical & Experimental Metastasis* **2009,** *26* (4), 357-370.

189. Lein, E. S.; Hawrylycz, M. J.; Ao, N.; Ayres, M.; Bensinger, A.; Bernard, A.; Boe, A. F.; Boguski, M. S.; Brockway, K. S.; Byrnes, E. J.; Chen, L.; Chen, T. M.; Chin, M. C.; Chong, J.; Crook, B. E.; Czaplinska, A.; Dang, C. N.; Datta, S.; Dee, N. R.; Desaki, A. L.; Desta, T.; Diep, E.; Dolbeare, T. A.; Donelan, M. J.; Dong, H. W.; Dougherty, J. G.; Duncan, B. J.; Ebbert, A. J.; Eichele, G.; Estin, L. K.; Faber, C.; Facer, B. A.; Fields, R.; Fischer, S. R.; Fliss, T. P.; Frensley, C.; Gates, S. N.; Glattfelder, K. J.; Halverson, K. R.; Hart, M. R.; Hohmann, J. G.; Howell, M. P.; Jeung, D. P.; Johnson, R. A.; Karr, P. T.; Kawal, R.; Kidney, J. M.; Knapik, R. H.; Kuan, C. L.; Lake, J. H.; Laramee, A. R.; Larsen, K. D.; Lau, C.; Lemon, T. A.; Liang, A. J.; Liu, Y.; Luong, L. T.; Michaels, J.; Morgan, J. J.; Morgan, R. J.; Mortrud, M. T.; Mosqueda, N. F.; Ng, L. L.; Ng, R.; Orta, G. J.; Overly, C. C.; Pak, T. H.; Parry, S. E.; Pathak, S. D.; Pearson, O. C.; Puchalski, R. B.; Riley, Z. L.; Rockett, H. R.; Rowland, S. A.; Royall, J. J.; Ruiz, M. J.; Sarno, N. R.; Schaffnit, K.; Shapovalova, N. V.; Sivisay, T.; Slaughterbeck, C. R.; Smith, S. C.; Smith, K. A.; Smith, B. I.; Sodt, A. J.; Stewart, N. N.; Stumpf, K. R.; Sunkin, S. M.; Sutram, M.; Tam, A.; Teemer, C. D.; Thaller, C.; Thompson, C. L.; Varnam, L. R.; Visel, A.; Whitlock, R. M.; Wohnoutka, P. E.; Wolkey, C. K.; Wong, V. Y.; Wood, M.; Yaylaoglu, M. B.; Young, R. C.; Youngstrom, B. L.; Yuan, X. F.; Zhang, B.; Zwingman, T. A.; Jones, A. R., *Nature* **2007,** *445* (7124), 168-176.

190. Jones, A. R.; Overly, C. C.; Sunkin, S. M., *Nature Reviews Neuroscience* **2009,** *10* (11), 821-U78.

191. Hawrylycz, M. J.; Lein, E. S.; Guillozet-Bongaarts, A. L.; Shen, E. H.; Ng, L.; Miller, J. A.; van de Lagemaat, L. N.; Smith, K. A.; Ebbert, A.; Riley, Z. L.; Abajian, C.; Beckmann, C. F.; Bernard, A.; Bertagnolli, D.; Boe, A. F.; Cartagena, P. M.; Chakravarty, M. M.; Chapin, M.; Chong, J.; Dalley, R. A.; Daly, B. D.; Dang, C.; Datta, S.; Dee, N.; Dolbeare, T. A.; Faber, V.; Feng, D.; Fowler, D. R.; Goldy, J.; Gregor, B. W.; Haradon, Z.; Haynor, D. R.; Hohmann, J. G.; Horvath, S.; Howard, R. E.; Jeromin, A.; Jochim, J. M.; Kinnunen, M.; Lau, C.; Lazarz, E. T.; Lee, C.; Lemon, T. A.; Li, L.; Li, Y.; Morris, J. A.; Overly, C. C.; Parker, P. D.; Parry, S. E.; Reding, M.; Royall, J. J.; Schulkin, J.; Sequeira, P. A.; Slaughterbeck, C. R.; Smith, S. C.; Sodt, A. J.; Sunkin, S. M.; Swanson, B. E.; Vawter, M. P.; Williams, D.; Wohnoutka, P.; Zielke, H. R.; Geschwind, D. H.; Hof, P. R.; Smith, S. M.; Koch, C.; Grant, S. G. N.; Jones, A. R., *Nature* **2012,** *489* (7416), 391-399.

192. Abdelmoula, W. M.; Carreira, R. J.; Shyti, R.; Balluff, B.; van Zeijl, R. J. M.; Tolner, E. A.; Lelieveldt, B. F. P.; van den Maagdenberg, A.; McDonnell, L. A.; Dijkstra, J., *Analytical Chemistry* **2014,** *86* (8), 3947-3954.

193. Verbeeck, N.; Spraggins, J. M.; Murphy, M. J. M.; Wang, H. D.; Deutch, A. Y.; Caprioli, R. M.; Van de Plas, R., *Biochimica Et Biophysica Acta-Proteins and Proteomics* **2017,** *1865* (7), 967-977.

194. Eberlin, L. S.; Liu, X. H.; Ferreira, C. R.; Santagata, S.; Agar, N. Y. R.; Cooks, R. G., *Analytical Chemistry* **2011,** *83* (22), 8366-8371.

195. Desbenoit, N.; Walch, A.; Spengler, B.; Brunelle, A.; Rompp, A., *Rapid Communications in Mass Spectrometry* **2018,** *32* (2), 159-166.

196. Li, Z.; Chu, L. Q.; Sweedler, J. V.; Bohn, P. W., *Analytical Chemistry* **2010,** *82* (7), 2608-2611.

197. Butler, H. J.; Ashton, L.; Bird, B.; Cinque, G.; Curtis, K.; Dorney, J.; Esmonde-White, K.; Fullwood, N. J.; Gardner, B.; Martin-Hirsch, P. L.; Walsh, M. J.; McAinsh, M. R.; Stone, N.; Martin, F. L., *Nature Protocols* **2016,** *11* (4), 664-687.

198. Lanni, E. J.; Masyuko, R. N.; Driscoll, C. M.; Aerts, J. T.; Shrout, J. D.; Bohn, P. W.; Sweedler, J. V., *Analytical Chemistry* **2014,** *86* (18), 9139-9145.

199. Srimany, A.; George, C.; Naik, H. R.; Pinto, D. G.; Chandrakumar, N.; Pradeep, T., *Phytochemistry* **2016,** *125*, 35-42.

200. Tata, A.; Zheng, J. Z.; Ginsberg, H. J.; Jaffray, D. A.; Ifa, D. R.; Zarrine-Afsar, A., *Analytical Chemistry* **2015,** *87* (15), 7683-7689.

201. Oetjen, J.; Aichler, M.; Trede, D.; Strehlow, J.; Berger, J.; Heldmann, S.; Becker, M.; Gottschalk, M.; Kobarg, J. H.; Wirtz, S.; Schiffler, S.; Thiele, H.; Walch, A.; Maass, P.; Alexandrov, T., *Journal of Proteomics* **2013,** *90*, 52-60.

202. Zhu, A. Z.; Lee, D.; Shim, H., *Seminars in Oncology* **2011,** *38* (1), 55-69.

203. Goodwin, R. J. A.; Mackay, C. L.; Nilsson, A.; Harrison, D. J.; Farde, L.; Andren, P. E.; Iverson, S. L., *Analytical Chemistry* **2011,** *83* (24), 9694-9701.

204. Ovchinnikova, O. S.; Kjoller, K.; Hurst, G. B.; Pelletier, D. A.; Van Berkel, G. J., *Analytical Chemistry* **2014,** *86* (2), 1083-1090.

205. Correa, D. N.; Zacca, J. J.; Rocha, W. F. D.; Borges, R.; de Souza, W.; Augusti, R.; Eberlin, M. N.; Vendramini, P. H., *Forensic Science International* **2016,** *260*, 22-26.

206. Karki, V.; Singh, M., *International Journal of Mass Spectrometry* **2017,** *421*, 51-60.

207. Silva, D. B.; Aschenbrenner, A. K.; Lopes, N. P.; Spring, O., *Molecules* **2017,** *22* (5), 11.

208. Buchberger, A.; Yu, Q.; Li, L., *Annu Rev Anal Chem (Palo Alto Calif)* **2015,** *8* (1), 485-509.

209. Gemperline, E.; Keller, C.; Jayaraman, D.; Maeda, J.; Sussman, M. R.; Ane, J. M.; Li, L. J., *Journal of Proteome Research* **2016,** *15* (12), 4403-4411.

210. Potocnik, N. O.; Fisher, G. L.; Prop, A.; Heeren, R. M. A., *Analytical Chemistry* **2017,** *89* (16), 8223-8227.

211. Kunzke, T.; Balluff, B.; Feuchtinger, A.; Buck, A.; Langer, R.; Luber, B.; Lordick, F.; Zitzelsberger, H.; Aichler, M.; Walch, A., *Oncotarget* **2017,** *8* (40), 68012-68025.

212. Powers, T. W.; Holst, S.; Wuhrer, M.; Mehta, A. S.; Drake, R. R., *Biomolecules* **2015,** *5* (4), 2554-2572.

213. Everest-Dass, A. V.; Briggs, M. T.; Kaur, G.; Oehler, M. K.; Hoffmann, P.; Packer, N. H., *Molecular & Cellular Proteomics* **2016,** *15* (9), 3003-3016.

214. Briggs, M. T.; Kuliwaba, J. S.; Muratovic, D.; Everest-Dass, A. V.; Packer, N. H.; Findlay, D. M.; Hoffmann, P., *Proteomics* **2016,** *16* (11-12), 1736-1741.

215. He, Z. Y.; Chen, Q. S.; Chen, F. M.; Zhang, J.; Li, H. F.; Lin, J. M., *Chemical Science* **2016,** *7* (8), 5448-5452.

216. Lu, Q.; Hu, Y. J.; Chen, J. X.; Jin, S., *Analytical Chemistry* **2017,** *89* (16), 8238-8243.

217. Tata, A.; Gribble, A.; Ventura, M.; Ganguly, M.; Bluemke, E.; Ginsberg, H. J.; Jaffray, D. A.; Ifa, D. R.; Vitkin, A.; Zarrine-Afsar, A., *Chemical Science* **2016,** *7* (3), 2162-2169.

218. Banerjee, S.; Zare, R. N.; Tibshirani, R. J.; Kunder, C. A.; Nolley, R.; Fan, R.; Brooks, J. D.; Sonn, G. A., *Proceedings of the National Academy of Sciences of the United States of America* **2017,** *114* (13), 3334-3339.

219. Phan, N. T. N.; Munem, M.; Ewing, A. G.; Fletcher, J. S., *Analytical and Bioanalytical Chemistry* **2017,** *409* (16), 3923-3932.

220. Cai, L. S.; Sheng, L. F.; Xia, M. C.; Li, Z. P.; Zhang, S. C.; Zhang, X. R.; Chen, H. Y., *Journal of the American Society for Mass Spectrometry* **2017,** *28* (3), 399-408.

221. Tian, H.; Sparvero, L. J.; Amoscato, A. A.; Bloom, A.; Bayir, H.; Kagan, V. E.; Winograd, N., *Analytical Chemistry* **2017,** *89* (8), 4611-4619.

222. Niziol, J.; Ossolinski, K.; Ossolinski, T.; Ossolinska, A.; Bonifay, V.; Sekula, J.; Dobrowolski, Z.; Sunner, J.; Beech, I.; Ruman, T., *Analytical Chemistry* **2016,** *88* (14), 7365-7371.

223. Gustafsson, O. J. R.; Guinan, T. M.; Rudd, D.; Kobus, H.; Benkendorff, K.; Voelcker, N. H., *Rapid Communications in Mass Spectrometry* **2017,** *31* (12), 991-1000.

224. Duenas, M. E.; Klein, A. T.; Alexander, L. E.; Yandeau-Nelson, M. D.; Nikolau, B. J.; Lee, Y. J., *Plant Journal* **2017,** *89* (4), 825-838.

225. Pluhacek, T.; Petrik, M.; Luptakova, D.; Benada, O.; Palyzova, A.; Lemr, K.; Havlicek, V., *Proteomics* **2016,** *16* (11-12), 1785-1792.

226. Susnea, I.; Weiskirchen, R., *Mass Spectrometry Reviews* **2016,** *35* (6), 666-686.

227. Niedzwiecki, M. M.; Austin, C.; Remark, R.; Merad, M.; Gnjatic, S.; Estrada-Gutierrez, G.; Espejel-Nunez, A.; Borboa-Olivares, H.; Guzman-Huerta, M.; Wright, R. J.; Wright, R. O.; Arora, M., *Metallomics* **2016,** *8* (4), 444-452.

228. Bishop, D. P.; Clases, D.; Fryer, F.; Williams, E.; Wilkins, S.; Hare, D. J.; Cole, N.; Karst, U.; Doble, P. A., *Journal of Analytical Atomic Spectrometry* **2016,** *31* (1), 197-202.

229. Bussweiler, Y.; Borovinskaya, O.; Tanner, M., *Spectroscopy* **2017,** *32* (5), 14-20.

230. Bonta, M.; Hegedus, B.; Limbeck, A., *Analytica Chimica Acta* **2016,** *908*, 54-62.

231. Penen, F.; Malherbe, J.; Isaure, M. P.; Dobritzsch, D.; Bertalan, I.; Gontier, E.; Le Coustumer, P.; Schaumloffel, D., *Journal of Trace Elements in Medicine and Biology* **2016,** *37*, 62-68.

232. Lee, R. F. S.; Theiner, S.; Meibom, A.; Koellensperger, G.; Keppler, B. K.; Dyson, P. J., *Metallomics* **2017,** *9* (4), 365-381.

233. Feenstra, A. D.; Hansen, R. L.; Lee, Y. J., *Analyst* **2015,** *140* (21), 7293-7304.

234. Annangudi, S. P.; Myung, K.; Adame, C. A.; Gilbert, J. R., *Environmental Science & Technology* **2015,** *49* (9), 5579-5583.

235. Araujo, F. D. D.; Araujo, W. L.; Eberlin, M. N., *Journal of the American Society for Mass Spectrometry* **2017,** *28* (5), 901-907.

236. Crecelius, A. C.; Michalzik, B.; Potthast, K.; Meyer, S.; Schubert, U. S., *Analytical and Bioanalytical Chemistry* **2017,** *409* (15), 3807-3820.

237. Bagatela, B. S.; Lopes, A. P.; Cabral, E. C.; Perazzo, F. F.; Ifa, D. R., *Rapid Communications in Mass Spectrometry* **2015,** *29* (16), 1530-1534.

238. Shariatgorji, M.; Nilsson, A.; Goodwin, R. J. A.; Svenningsson, P.; Schintu, N.; Banka, Z.; Kladni, L.; Hasko, T.; Szabo, A.; Andren, P. E., *Analytical Chemistry* **2012,** *84* (16), 7152-7157.

239. de Macedo, C. S.; Anderson, D. M.; Schey, K. L., *Talanta* **2017,** *174*, 325-335.

240. Flinders, B.; Beasley, E.; Verlaan, R. M.; Cuypers, E.; Francese, S.; Bassindale, T.; Clench, M. R.; Heeren, R. M. A., *Journal of the American Society for Mass Spectrometry* **2017,** *28* (11), 2462-2468.

241. Becue, A., *Analytical Methods* **2016,** *8* (45), 7983-8003.

242. Takahashi, K.; Kozuka, T.; Anegawa, A.; Nagatani, A.; Mimura, T., *Plant and Cell Physiology* **2015,** *56* (7), 1329-1338.

243. Sekula, J.; Niziol, J.; Misiorek, M.; Dec, P.; Wrona, A.; Arendowski, A.; Ruman, T., *Analytica Chimica Acta* **2015,** *895*, 45-53.

244. Yoshimura, Y.; Goto-Inoue, N.; Moriyama, T.; Zaima, N., *Food Chemistry* **2016,** *210*, 200-211.

245. Li, B.; Dunham, S. J. B.; Dong, Y. H.; Yoon, S.; Zeng, M. M.; Sweedler, J. V., *Trends in Food Science & Technology* **2016,** *47*, 50-63.

246. Stasulli, N. M.; Shank, E. A., *Fems Microbiology Reviews* **2016,** *40* (6), 807-813.

247. Hoffmann, T.; Dorrestein, P. C., *Journal of the American Society for Mass Spectrometry* **2015,** *26* (11), 1959-1962.

248. Taverna, D.; Norris, J. L.; Caprioli, R. M., *Analytical Chemistry* **2015,** *87* (1), 670-676.

249. Seeley, E. H.; Wilson, K. J.; Yankeelov, T. E.; Johnson, R. W.; Gore, J. C.; Caprioli, R. M.; Matrisian, L. M.; Sterling, J. A., *Bone* **2014,** *61*, 208-216.

250. Inglese, P.; McKenzie, J. S.; Mroz, A.; Kinross, J.; Veselkov, K.; Holmes, E.; Takats, Z.; Nicholson, J. K.; Glen, R. C., *Chemical Science* **2017,** *8* (5), 3500-3511.

251. Liu, X.; Hummon, A. B., *Analytical Chemistry* **2015,** *87* (19), 9508-9519.

252. **!!! INVALID CITATION !!!**

253. Palmer, A. D.; Alexandrov, T., *Analytical Chemistry* **2015,** *87* (8), 4055-4062.

254. Chirinos, J. R.; Oropeza, D. D.; Gonzalez, J. J.; Hou, H. M.; Morey, M.; Zorba, V.; Russo, R. E., *Journal of Analytical Atomic Spectrometry* **2014,** *29* (7), 1292-1298.

255. Vanbellingen, Q. P.; Castellanos, A.; Rodriguez-Silva, M.; Paudel, I.; Chambers, J. W.; Fernandez-Lima, F. A., *Journal of the American Society for Mass Spectrometry* **2016,** *27* (12), 2033-2040.

256. Thiele, H.; Heldmann, S.; Trede, D.; Strehlow, J.; Wirtz, S.; Dreher, W.; Berger, J.; Oetjen, J.; Kobarg, J. H.; Fischer, B.; Maass, P., *Biochimica Et Biophysica Acta-Proteins and Proteomics* **2014,** *1844* (1), 117-137.

257. Potocnik, N. O.; Porta, T.; Becker, M.; Heeren, R. M. A.; Ellis, S. R., *Rapid Communications in Mass Spectrometry* **2015,** *29* (23), 2195-2203.

258. Gough, A.; Stern, A. M.; Maier, J.; Lezon, T.; Shun, T. Y.; Chennubhotla, C.; Schurdak, M. E.; Haney, S. A.; Taylor, D. L., *Slas Discovery* **2017,** *22* (3), 213-237.

259. Newell, E. W.; Sigal, N.; Bendall, S. C.; Nolan, G. P.; Davis, M. M., *Immunity* **2012,** *36* (1), 142-152.

260. Giesen, C.; Wang, H. A. O.; Schapiro, D.; Zivanovic, N.; Jacobs, A.; Hattendorf, B.; Schuffler, P. J.; Grolimund, D.; Buhmann, J. M.; Brandt, S.; Varga, Z.; Wild, P. J.; Gunther, D.; Bodenmiller, B., *Nature Methods* **2014,** *11* (4), 417-+.

261. Bloom, A. N.; Tian, H.; Schoen, C.; Winograd, N., *Analytical and Bioanalytical Chemistry* **2017,** *409* (12), 3067-3076.

262. Wu, K.; Jia, F. F.; Zheng, W.; Luo, Q.; Zhao, Y.; Wang, F. Y., *Journal of Biological Inorganic Chemistry* **2017,** *22* (5), 653-661.

263. Tian, H.; Six, D. A.; Krucker, T.; Leeds, J. A.; Winograd, N., *Analytical Chemistry* **2017,** *89* (9), 5050-5057.

264. Guillermier, C.; Fazeli, P. K.; Kim, S.; Lun, M.; Zuflacht, J. P.; Milian, J.; Lee, H.; Francois-Saint-Cyr, H.; Horreard, F.; Larson, D.; Rosen, E. D.; Lee, R. T.; Lechene, C. P.; Steinhauser, M. L., *Jci Insight* **2017,** *2* (5), 11.

265. Sheng, L. F.; Cai, L. S.; Wang, J.; Li, Z. P.; Mo, Y. X.; Zhang, S. C.; Xu, J. J.; Zhang, X. R.; Chen, H. Y., *International Journal of Mass Spectrometry* **2017,** *421*, 238-244.

266. Korte, A. R.; Yandeau-Nelson, M. D.; Nikolau, B. J.; Lee, Y. J., *Analytical and Bioanalytical Chemistry* **2015,** *407* (8), 2301-2309.

267. Mueller, L.; Herrmann, A. J.; Techritz, S.; Panne, U.; Jakubowski, N., *Analytical and Bioanalytical Chemistry* **2017,** *409* (14), 3667-3676.

268. Herrmann, A. J.; Techritz, S.; Jakubowski, N.; Haase, A.; Luch, A.; Panne, U.; Mueller, L., *Analyst* **2017,** *142* (10), 1703-1710.

269. Rao, W.; Pan, N.; Yang, Z. B., *Jove-Journal of Visualized Experiments* **2016,** (112), 9.

270. Lee, J. K.; Jansson, E. T.; Nam, H. G.; Zare, R. N., *Analytical Chemistry* **2016,** *88* (10), 5453-5461.

Figures

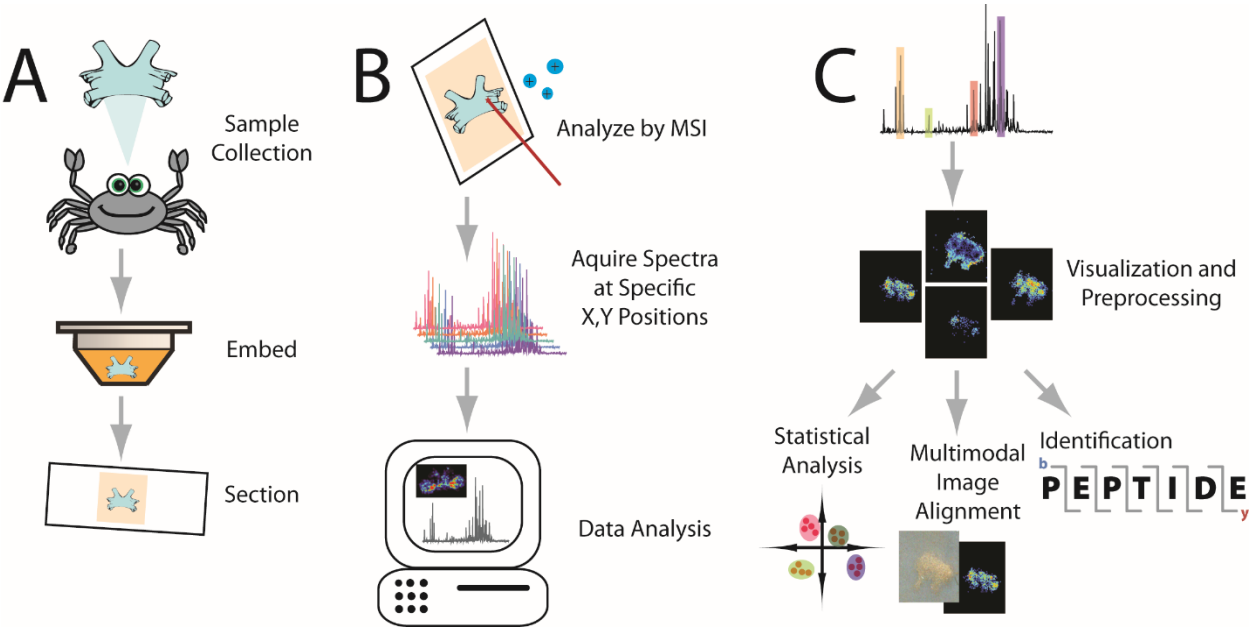

Figure 1. Visual workflow for the MS imaging analysis. A crustacean's brain is used as an example tissue for this workflow. (A) Sample preparation. After collection from the animal, the sample is embedded in a supporting medium for sectioning onto slides. Other sample processing, such as applications of enzymes, matrix, or derivatization agents, may be done depending on the molecular species of interest or the instrument being used. (B) Sample analysis. After acquiring a spectrum at each (x, y) grid point on the tissue, sophisticated software tools are used to process and visualize the data. A laser is used to ionize molecules in the figure above, although several nonlaser based methods are also used. (C) Data processing. After preprocessing the data (*e.g.*, baseline correction), the distribution of selected molecules can be visualized. From there, identification of the *m/z* values, statistical analysis between different images, or image coregistration with other image modalities can occur.

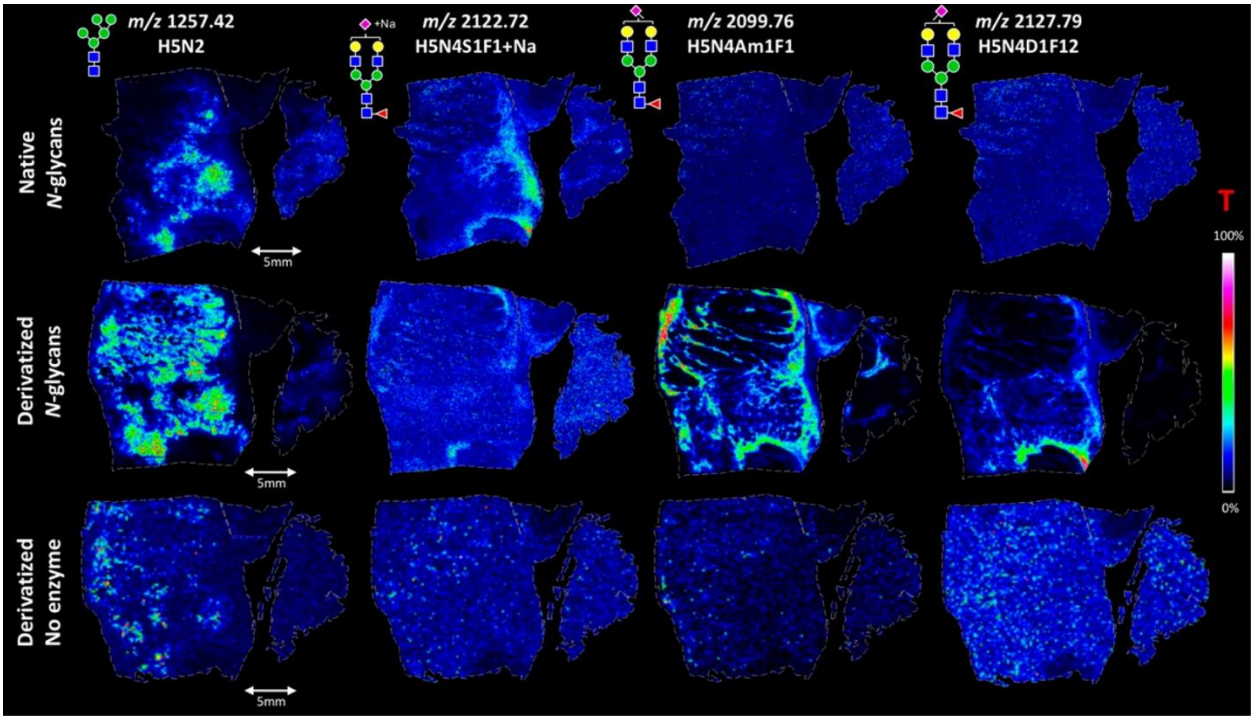

Figure 2. MS imaging comparison of digestion and derivatization of N-glycans in FFPE colon carcinoma sections. Different section preparations are shown in each row, while each column is a different N-glycan. Native N-glycans (*e.g.*, digested) are shown in the first row. The second row shows the digested, derivatized samples. This *in situ* derivatization specifically targeted sialic acids by dimethylation and subsequent amidation. Finally, the last row shows a negative control sample where derivatization was performed but no digestion was done. Without a digestion step, N-glycans should not be available for analysis. On the basis of the results, it is clear that the derivatized, digested N-glycan (middle row) method produces the best extraction and ionization of N-glycans with sialic acids. Green circle: mannose; yellow circle: galactose, blue square: N-acetylglucosamine, yellow square: N-acetylgalactosamine, white square: N-acetylhexosamine, red triangle: fucose, purple diamond: N-acetylneuraminic acids, T: total ion current normalization. Adapted with permission.[52]

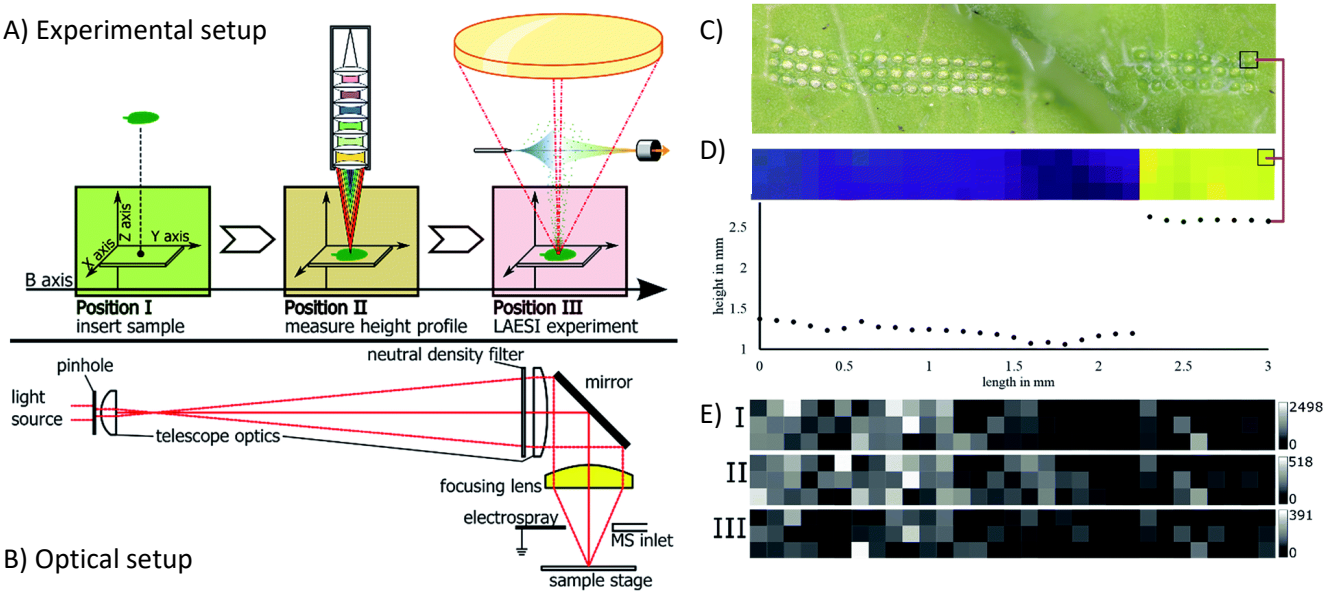

Figure 3. Overall setup and demonstration of capabilities of a LAESI source for samples with uneven surfaces. (a) Workflow representation of experimental setup related to the LAESI source, including sample insertion, measurement of height profile, and LAESI experiment for MS acquisition. (b) Schematic of the telescope optics implemented to focus the laser. (c) Optical image of *R. sativus* leaf after LAESI experiment, showing the laser ablation pattern. Note the even distance between ablation spots throughout sample despite uneven surface. (d) Topographical height profile of leaf surface along the ablation pattern, showing the change in height across the sample. The red line indicates identical positions on the sample surface. (e) MS imaging intensity maps of *m/z* values 418.051, 434.024, and 447.054, showing differences in spatial resolution. These *m/z* distributions were acquired in the same experiment as the topographical profile. Adapted with permission.[92]

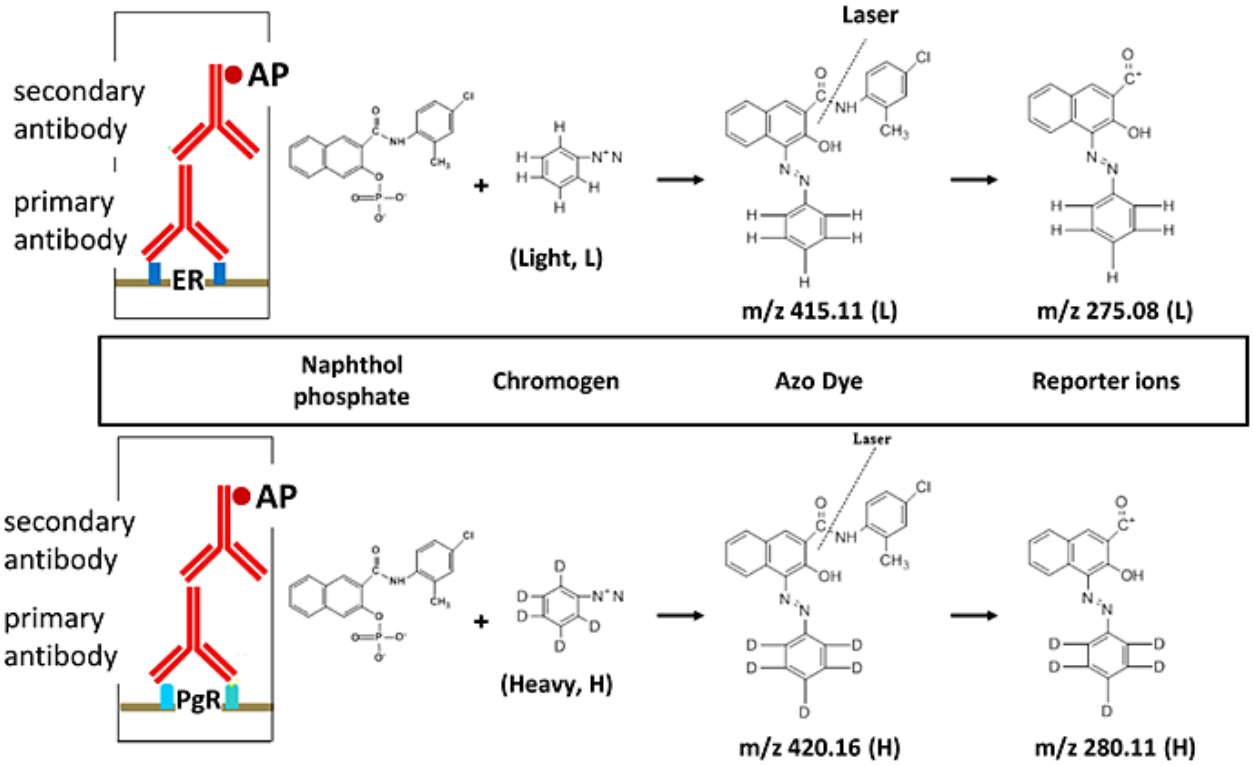

Figure 4. Schematic of the general working principle of SILMS imaging. After incubating the section with a primary antibody for the biomarker of interest, in this case PgR and ER, a secondary antibody is applied that is conjugated with alkaline phosphatase (AP). AP cleaves naphthol from naphthol phosphate. The naphthol mixes with the heavy or light chromagen to form an azo dye precipitate on the tissue. The incubation of the two antibodies can be done on the same tissue with proper washing. In the instrument, the azo dye absorbs energy from the laser, creating fragments including characteristic reporter ions. The heavy and light reporter ions are separated by 5 Da in the MS spectrum. Adapted with permission.[100]

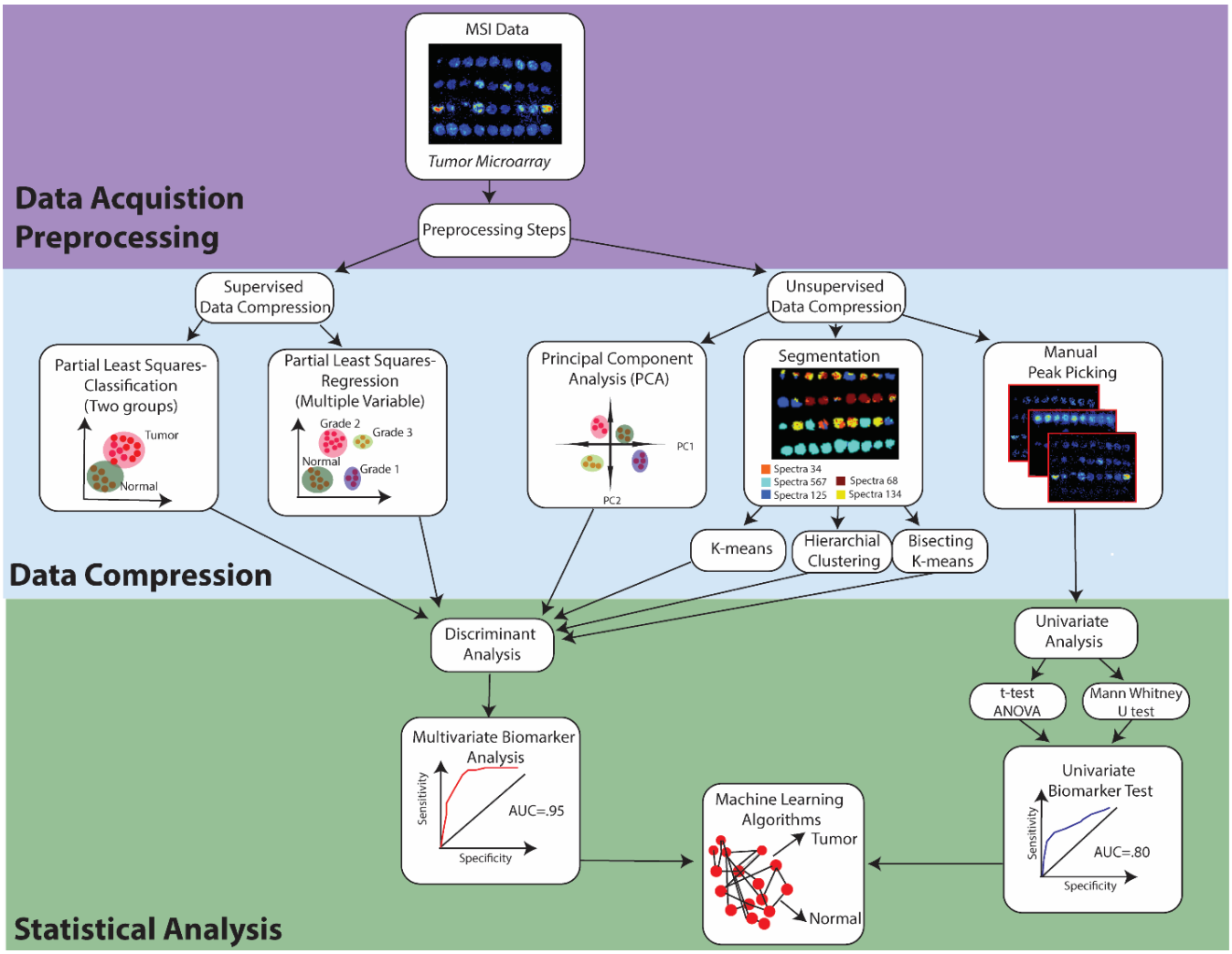

Figure 5. Workflow for data processing and data analysis for MS imaging data. After data acquisition, MS imaging data are subjected to preprocessing including normalization, baseline compression, smoothing, and spectral recalibration. Next, data are compressed to reduce computational load for statistical analysis. This includes supervised data compression, where the groups are defined. If two groups are used, it is known as classification, or if more than two groups are used, linear regression is used for analysis. Data can also be compressed without preclassifying the data through unsupervised data compression. Here, we describe three main methods: principal component analysis, segmentation, and manual peak picking. Unsupervised data compression includes k-means, hierarchical clustering, and bisecting k-means. Following

compression of multiple variables, discriminant analysis is used to evaluate how well the chosen classification system separates groups of data. Manual peak picking helps pull out a few *m/z* peaks of interest. Univariate analysis can be done using either a t-test or ANOVA (Gaussian distribution) or Mann-Whitney U test (non-Gaussian distribution) to test for significance between groups of data. If the user is interested in biomarker discovery, a specific *m/z* or group of *m/z* values can be used to conduct a biomarker analysis, where an AUC value closer to 1 indicates a perfect predictive biomarker. Following biomarker analysis, machine learning algorithms can then be used to predict the classification of new data sets into the existing data classifications.

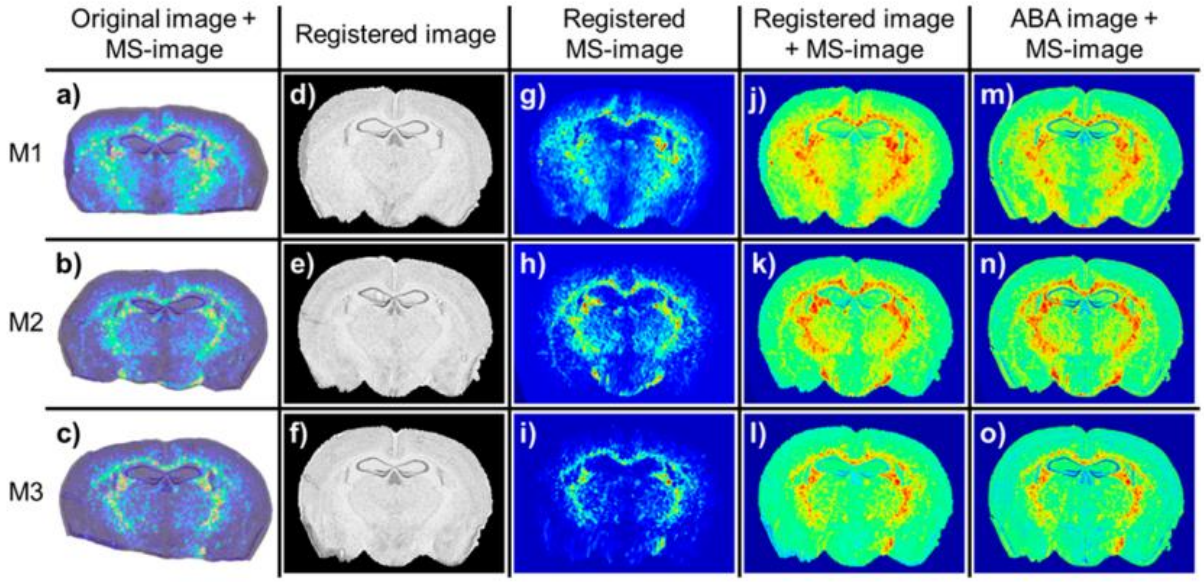

Figure 6. MS imaging acquired on a mouse brain is registered to corresponding histology and then to the Allen Brain Atlas (ABA) to understand where *m/z* values colocalize with anatomical brain regions. Shown here are three coronal sections from three different mouse brains (M1, M2, and M3) and their respective MS imaging images. (a, b, and c) Distribution of *m/z* 863 before preprocessing and registration. (d, e, and f) Samples after preprocessing and registration to histology. (g, h, and i) Distribution of *m/z* 863 after registration to histology, where histology image is removed. (j, k, and l) Registered images and registered MS imaging images are superimposed to display the visual distribution of ion *m/z* 863. (m, n, and o) Registered images with the MS imaging distribution are then registered again with the ABA. On the basis of the alignment, it appears that *m/z* 863 is expressed mainly in the striatum of the brain for these brain sections. Adapted with permission.[192]

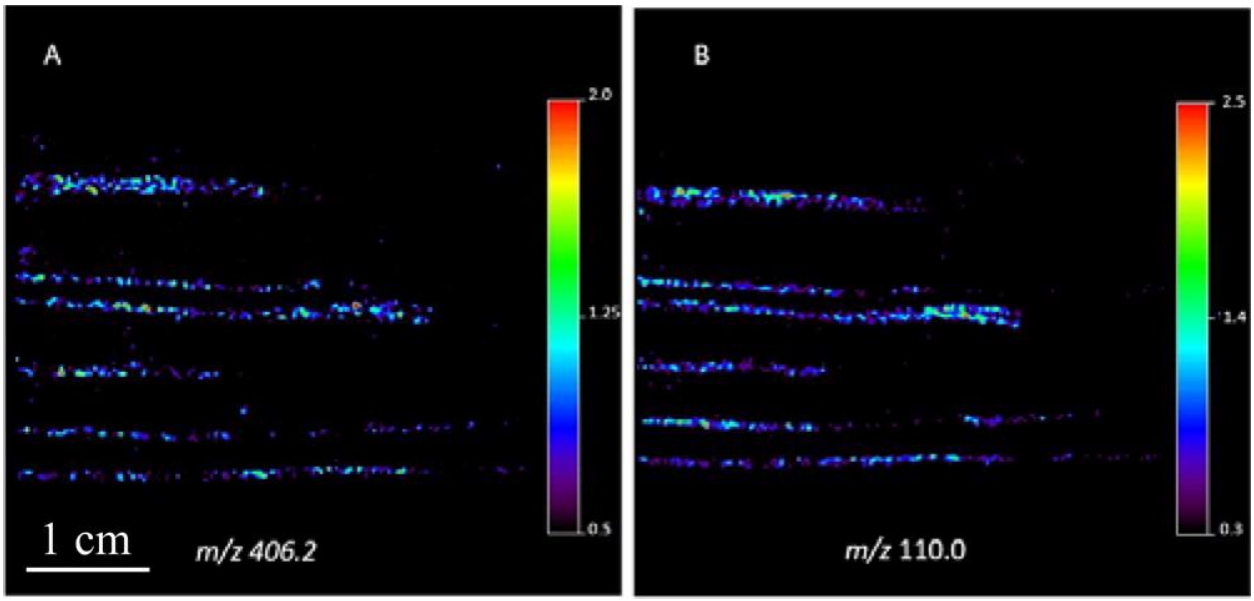

Figure 7. MALDI-MS imaging MS/MS was utilized to confidently identify THC drugs in single hair samples. (A) Parent ion images (*m/z* 406.2). (B) Characteristic fragment ion (*m/z* 110.0). The distributions match each other for all hair samples, indicating they belong to the same ion. Adapted with permission.[29]

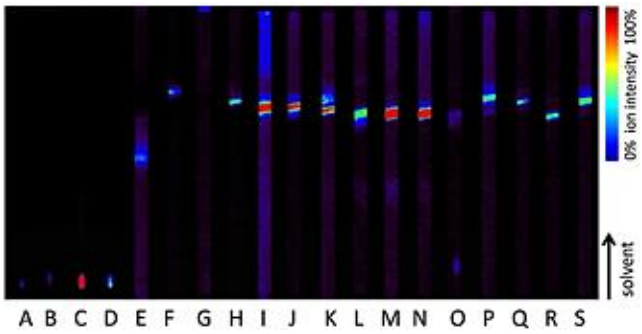

Figure 8. Extracted ion images from a positive ion mode DESI-MS imaged high-performance TLC plate, showing the separation of a variety of metabolic compounds. A: *m*/*z* 138; B: *m*/*z* 152; C: *m*/*z* 166; D: *m*/*z* 168; E: *m*/*z* 261; F: *m*/*z* 303; G: *m*/*z* 373; H: *m*/*z* 403; I: *m*/*z* 433; J: *m*/*z* 463; K: *m*/*z* 579; L: *m*/*z* 581; M: *m*/*z* 609; N: *m*/*z* 611; O: *m*/*z* 625; P: *m*/*z* 667; Q: *m*/*z* 725; R: *m*/*z* 741; S: *m*/*z* 755. Adapted with permission.[237]

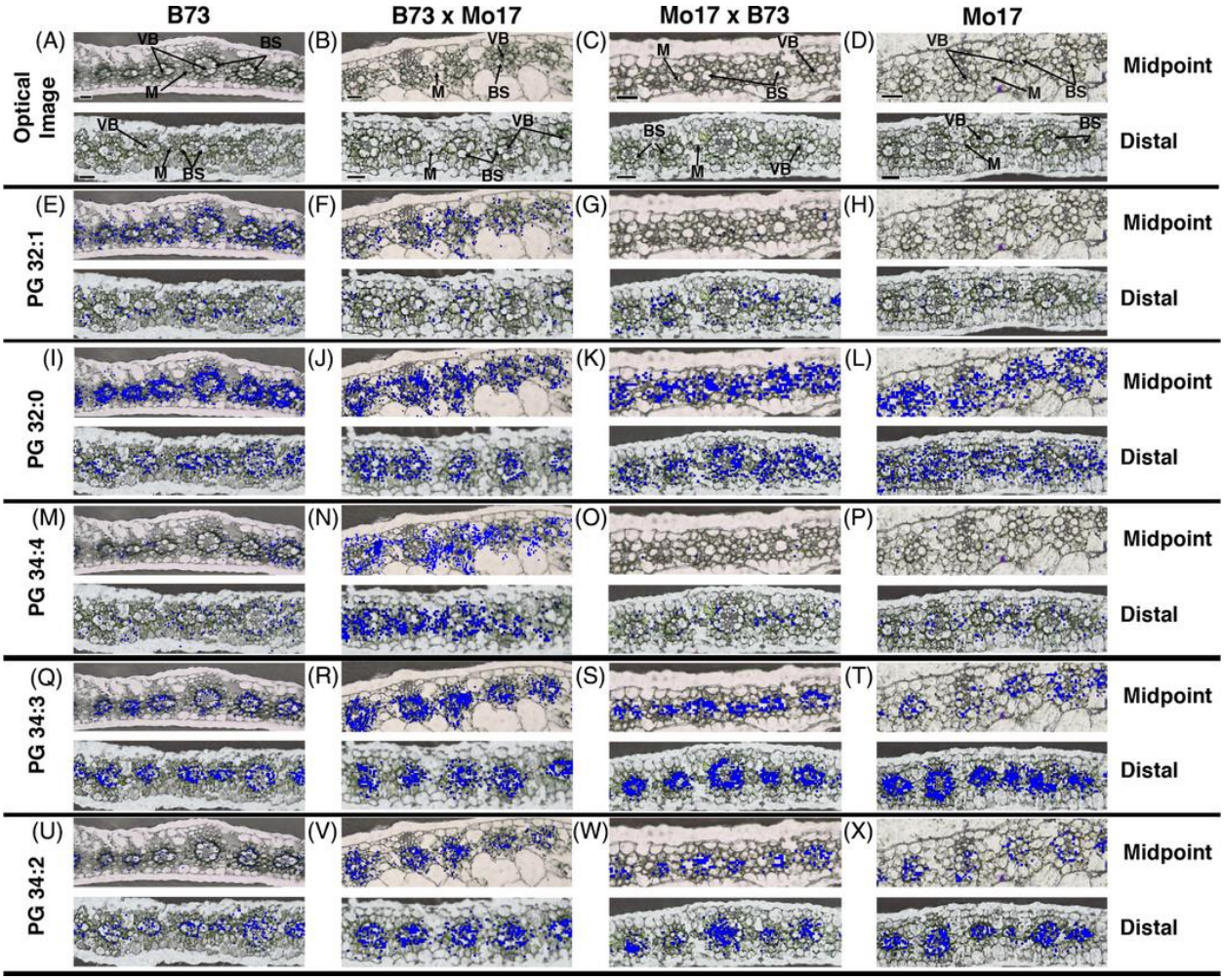

Figure 9. Demonstration of 5μm, subcellular resolution MALDI-MS images for several lipid species (rows) overlaid on their optical image across four different genotypes of maize leaves (columns) at the midpoint and distal regions. The scale bar for the images is 50 μm for all images, and it is noted that the Mo17 and Mo17 x B73 have slightly larger scale bars. Adapted with permission.[224]

Appendix VII

New Techniques, Applications, and Perspectives in Neuropeptide Research

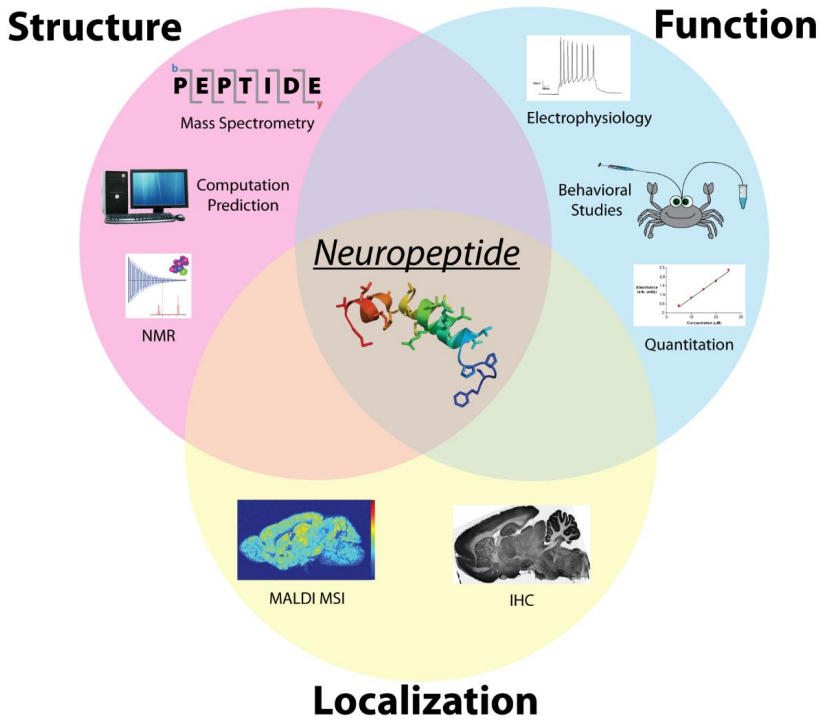

Modified from:

Kellen Delaney[¥], **Amanda R. Buchberger**[¥], Lingjun Li. "New techniques, applications and perspectives in neuropeptide research." Invited Contribution. *Journal of Experimental Biology*. 2018, 221:jeb151167. [¥]Co-first authors

Key Words: Neuropeptides; Mass Spectrometry; Peptide-gated Ion Channel; FaNaC/HyNaC; Immunochemistry; Electrophysiology

Abstract

Neuropeptides are one of the most diverse classes of signaling molecules and have attracted great interest over the years owing to their roles in regulation of a wide range of physiological processes. However, there are unique challenges associated with neuropeptide studies stemming from the highly variable molecular sizes of the peptides, low *in vivo* concentrations, high degree of structural diversity, and large number of isoforms. As a result, much effort has been focused on developing new techniques for studying neuropeptides, as well as novel applications directed towards learning more about these endogenous peptides. The areas of importance for neuropeptide studies include structure, localization within tissues, interaction with their receptors, including ion channels, and physiological function. Here we discuss these aspects and the associated techniques, focusing on technologies that have demonstrated potential in advancing the field in recent years. Most identification and structural information has been gained by mass spectrometry, either alone or with confirmations from other techniques, such as nuclear magnetic resonance spectroscopy and other spectroscopic tools. While mass spectrometry and bioinformatic tools have proven to be the most powerful for large-scale analyses, they still rely heavily on complementary methods for confirmation. Localization within tissues, for example, can be probed by mass spectrometry imaging, immunohistochemistry, and radioimmunoassays. Functional information has been gained primarily from behavioral studies coupled with tissue-specific assays, electrophysiology, mass spectrometry, and optogenetic tools. Concerning the receptors for neuropeptides, the discovery of ion channels that are directly gated by neuropeptides opens up the possibility of developing a new generation of tools for neuroscience, which could be used to monitor neuropeptide release or to specifically change the

membrane potential of neurons. It is expected that future neuropeptide research will involve the integration of complementary bioanalytical technologies and functional assays.

Introduction

Neuropeptides are a class of endogenous peptides that act as long-lasting neurotransmitters in the nervous system and other target organs. By signaling via synapses or volume transmission via diffusion, as well as via long-range signaling as circulating hormones, neuropeptides and their receptors play an important role in several key processes. When a neuron releases neuropeptides, the binding of the neuropeptide to its receptor on a receiving cell causes conformational changes within the receptor that, depending on the type of receptor, either open ion channels or activate coupled G proteins that can cause a series of downstream effects within the cell .[1] As neuropeptides are a highly diverse class of signaling molecules in the brain and other peripheral organs, their structures, functions, and localization are of great interest and relevance.[2] The extent of their implied roles in normal biological processes has been a point of focus in studies over the years.[3, 4] Abnormalities in their expression can contribute to various neurological diseases by altering the function of specific neurons, and so understanding the mechanisms of neuropeptide signaling can help researchers to better understand these diseases and develop more focused and effective treatments.[5] Furthermore, neuropeptides have been implicated in the regulation of normal biological functions, such as feeding regulation and the adaptation to external factors, such as temperature fluctuation and internal stress factors, including depression, anxiety, and post-traumatic stress disorder.[6-10] As a result, understanding the specific role individual neuropeptides play in response to interactions with the environment and in the execution of biological functions can provide a greater understanding of the

underlying mechanisms at the cellular and systemic level. Investigations of the relationship between neuropeptides and their receptors are useful for the development of drug molecules for treating diseases or for otherwise manipulating interactions between peptidergic neurons, such as the treatment of specific symptoms (*e.g.*, chemotherapy-induced emesis).[11]

While neuropeptides are interesting biomolecules that have important roles in regulating a wide range of physiological processes, they have numerous characteristics that make them challenging to study. Because neuropeptides can be used as modulators for signaling locally between neurons as well as functioning as hormones that can travel a long distance to target sites, the *in vivo* concentrations can vary dramatically. Furthermore, low concentrations of neuropeptides can have profound effects – these signaling molecules are typically present at low endogenous concentrations, up to 1000-fold or lower than classical neurotransmitters and other metabolites.[12] This challenge is exacerbated by the lack of a digesting enzyme for a typical neuropeptide analysis workflow as these molecules are products of proteolytic processing and post-translational modifications (PTMs) that occur inside cells or during transportation. As such, there is only one opportunity for detecting each peptide, unlike in 'bottom-up' proteomic studies, where a single unique tryptic fragment is sufficient to detect a protein.[13] This necessitates the development of highly sensitive detection methods in order to avoid large sample requirements. Additionally, sample processing methods need to be fast because, as with other signaling molecules, neuropeptides are prone to rapid degradation to prevent concentration increases with sequential release. Thus, it is often difficult to identify peptides as endogenous and not simply the product of a degraded larger protein, further complicating analysis.[14] Additionally, there is a large amount of variability between different neuropeptides, either owing to possession of different sequences but with the same mass or because of them having numerous PTMs.[15] Even

when the structure has been identified, there are still complications. Neuropeptides can have the same structure but different functions or have different functions depending on the cell-type and nearby receptors.[16] Furthermore, as many isoforms exist for various neuropeptide families, localization of specific neuropeptides can be challenging owing to difficulties assigning mass spectral peaks to specific peptides.[17]

Despite these difficulties, much progress has been made over the years to characterize neuropeptides, including gaining information about their structure, function, and localization within cells and the whole neuroendocrine system. Here we focus on reviewing recent advancements made in developing techniques and applications to study neuropeptides and their receptors, while pausing to offer insights into the direction in which the field is moving. The areas described include structural elucidation of neuropeptides, methods for their localization, and their functional assessment, as depicted in **Figure 1** and summarized in **Table 1**, all of which are required to understand neuropeptide biology comprehensively. We also present a case study on the characterization of peptide-gated ion channels and how they might be modified into new tools for neuroscience. While space constraints mean that we do not intend to provide a comprehensive account of all recent publications, we nevertheless provide notable highlights of some key developments made within the past few years.

Elucidation of Neuropeptide Structures

Perhaps the most important information gained about neuropeptides relates to their structures (*e.g.*, amino acid sequence, PTMs, folding pattern, binding sites, etc.), as these provide insights into their function and biological mechanisms. However, gaining this information can be challenging and cumbersome. While it has been almost a century since the first neuropeptide,

substance P, was discovered and nearly 50 years since the sequence of that peptide was determined, technology has since developed impressively, and there are now records of almost 6000 neuropeptide sequences across all species.[18-20]

Early work in structural elucidation relied on Edman degradation, a technique developed by Pehr Edman, in which peptides are reacted with phenyl isothiocyanate at the N-terminus and analyzed one amino acid at a time as each residue is removed.[21] Successful sequencing using Edman degradation relies on the peptide being present in high concentrations (>1 picomolar) and at high purity. While Edman degradation is a classic method that allowed for the sequencing of many neuropeptides early on, it is less widely used, as other, more high-throughput, methods have emerged in recent years. The technique is still used in some applications, although mostly coupled with mass spectrometry (MS). For example, it has been successfully used to sequence a novel neuropeptide, Y-HS, in leeches, to discover a novel arrangement of cysteine residues in a neuropeptide from a worm-hunting snail, and to determine the sequence of human and mouse urocortin 2, a member of the corticotropin-releasing factor neuropeptide family.[22-24] Although Edman degradation has proven to be a useful addition to other techniques in these applications, the method has largely been replaced with higher-throughput and more-sensitive methods such as MS in the past decade.

Currently, MS serves as the method of choice for sequencing and determining the PTMs of neuropeptides.[12, 15, 25, 26] MS has proven to be useful for detecting small amounts of peptides in complex biological samples, making it a high-throughput and versatile technique ideal for the study of endogenous neuropeptides. This advancement has enabled the emergence of ‘neuropeptidomics’, studying the entire neuropeptide complement as a whole either by comparing spectra to a database of known neuropeptides or *de novo* sequencing to discover new

neuropeptides.[27] **Figure 2** shows how MS spectra can be used to assign sequences by matching fragment ion masses to amino acids based on cleavage patterns and comparing the *de novo* sequences to those predicted based on genomic data.

Numerous studies have been performed using a variety of specific MS techniques. These techniques and their results have been comprehensively reviewed elsewhere, but noteworthy strides have been made recently, such as developments in analyzing neuropeptides rich in disulfide bonds, which in the past has been a particularly laborious task.[12, 28] A new method has recently been developed for identifying disulfide bonds by alkylating peptides and then performing targeted fragmentation on disulfide-bonded peptides.[29] Another method has integrated MS and nuclear magnetic resonance (NMR) techniques for rapid identification and characterization of disulfide bonds using only 4 ng of a peptide sample. The method involved studying the mass differences between folded and unfolded neuropeptides. As disulfide bond formation results in a mass difference of about ~2 Da due to the loss of two hydrogen atoms, and these disulfide bonds are not present in unfolded peptides, the mass differences can be used to assess the number of disulfide bonds present in a folded peptide. The presence of disulfide bonds can then be confirmed with NMR.[30] Another challenge with neuropeptidomics is that neuropeptides degrade substantially over time. A new, high-throughput framework for neuropeptide identification has recently been developed for fast, high-throughput analysis, minimizing neuropeptide degradation. With this method, researchers were able to successfully identify thousands of neuropeptides and post-translational modifications (Secher et al., 2016). Additionally, neuropeptide sequence coverage has been shown to improve when coupling several techniques of fragmentation (*e.g.*, high-energy collisional dissociation and electron-transfer

dissociation), especially when utilizing dual fragmentation with electron-transfer high-energy collisional dissociation (EThcD).[31-35]

Advances have also been made in the characterization of novel neuropeptides from model organisms, expanding our knowledge of existing neuropeptides. By combining matrix-assisted laser desorption/ionization (MALDI) and electrospray ionization (ESI) MS to characterize the carpenter ant neuropeptidome, 39 neuropeptides were identified.[36] The beetle neuropeptidome has also been expanded within the past year, with novel neuropeptides from the adipokinetic hormone family sequenced with ESI-MS and tandem MS. These were confirmed by co-eluting each naturally existing neuropeptide with its synthetic neuropeptide by means of liquid chromatography (LC).[37, 38] One other noteworthy group of organisms seeing significant growth in knowledge of its neuropeptidome has been members of the subphylum crustacea. Multidimensional MS techniques have been successfully implemented in both defining neuropeptidomes, such as that of the spiny lobster, and discovering numerous novel neuropeptides.[39-41] As a complementary separation technique, ion mobility spectrometry (IMS) is currently experiencing rapid growth, and its use in conjunction with MS has allowed for a more comprehensive study of peptide structure.[42] Recently, ion mobility spectrometry (IMS) has been used for conformational studies investigating the role of the penultimate proline residue and D-amino acid containing peptide epimers, and it is expected that more structural knowledge will come from IMS in future studies.[43-45]

The capabilities of MS for discovery and characterization of neuropeptides have been greatly assisted by the development of computational methods for predicting neuropeptides from precursor proteins and gene sequences. The area of *in silico* prediction has seen substantial growth in the past few years, with neuropeptidomes being predicted for a wide variety of

organisms and novel neuropeptides being targeted for more focused analyses.[46] Coupling these informatics approaches to other methods of analysis, particularly MS, has allowed for an expanded coverage of neuropeptidomes, which is important for species without a fully sequenced genome, especially when one transcript can produce several neuropeptides.[46, 47] For example, the crab *Cancer borealis* peptidome was doubled by mining its neural transcriptome.[48] As a complementary technique, researchers have also made use of *in silico* prediction methods to characterize neuropeptide receptors, which gives insight into both structural and functional properties by assessing similarities to previously characterized receptors.[49] Computational efforts have further been directed toward compiling databases of known neuropeptides to provide comprehensive coverage and compare neuropeptides detected in different species. The most recent of these, NeuroPep, contains almost 6000 entries.[20] Resampling approaches are being developed to improve database matching, allowing for better identifications in terms of both quality and quantity.[50]

By combining information about structure gained from MS with other powerful analytical tools, researchers have been able to gain better insight into the overall structural composition of neuropeptides. Various types of NMR techniques have been implemented for studying neuropeptides, which are particularly valuable for characterizing folding patterns. **Figure 3** shows an example of how several complementary NMR experiments can be combined to assess the structural conformation of a neuropeptide, as was done to determine the conformational patterns of the hormone pheromonotropin that controls larval sex pheromone production.[51] Several recent advances have been made in understanding the secondary structure of neuropeptides. As an example, a precursor protein existing in marine snail venom was investigated by using solution NMR structural determination and was found to have a disulfide-

directed β-hairpin fold, which initiates folding in other disulfide-containing areas of the peptide.[52] Some neuropeptides have been found to lack secondary structure, as in the case of an RFamide neuropeptide discovered in cone snail venom.[53] As structural characteristics are important for the interaction between neuropeptides and their receptors, many recent advances have used NMR to characterize these relationships, such as determining which conformations are important for biological activity, as has been investigated for various analogs of an allatostatin neuropeptide, as well as determining which part of the receptor neuropeptides were bound to, as has been accomplished with solid-state NMR for neuropeptide Y and its receptor.[54, 55] The relationship with receptor sites has been extended to assess the structure of agonists and antagonists bound to neuropeptide receptors and study their respective conformations, for example of dynorphin bound to the human κ-opioid receptor.[56] These characterizations of neuropeptide and neuropeptide–receptor conformations should enable future advances in developing drugs to mimic or block neuropeptide binding.

Other spectroscopic methods have also been useful in the characterization of neuropeptides. Infrared (IR) spectroscopy has successfully been used to provide a quantitative estimate of secondary-structural elements. When analyzed by IR spectroscopy, peptides demonstrate characteristic peaks for different folding patterns, including α-helices, β-sheets, and turns, as has been characterized in human neuropeptide peptide YY.[57] Circular dichroism (CD) spectra have also shown utility in the rapid determination of secondary structure, and have provided evidence for the existence of α-helices in tachykinin-related peptides and β-sheets in melanocyte-stimulating hormone (MSH) peptides that increase with increasing charge state.[58] X-ray crystallography benefits from providing sub-angstrom resolution of key structural sites. The binding structures of neuropeptides with their receptors have been well characterized with X-ray

crystallography, including studies of the receptor for neuropeptide S and human OX_2 receptor.[59, 60] Information from crystallography can provide useful details about neuropeptide structure that might lead to insights about function.

Methods for Neuropeptide Localization

Neuropeptide localization in species and/or tissue(s) enables mapping in neuronal subtypes relative to structural components of the cell, tissue, or whole organism, which can then be used to inform the function of a target neuropeptide and to direct functional biology experiments.[61] Overall, the rapid increase in 'omics'-derived neuropeptide sequence data has revolutionized our approach to the localization of neuropeptides and their signaling pathway components and facilitated our ability to construct species- and neuropeptide-specific 'connectomes'.[62, 63] The application of localization techniques across species, tissue-, and cell-types is fundamental to understanding the complexity of neuropeptidergic signaling and has trans-disciplinary importance; indeed these techniques have been applied to cell cultures (2D, 3D, or single cells) and entire organisms (whole and sections).[64-69] Neuropeptide localization in thick tissues, such as whole organisms or invertebrate brain tissue, can be achieved by using 3D mapping and ion density reconstruction of individual tissue sections to produce 3D representations of neuropeptide distributions.[70] The advances in the tools and techniques described here have facilitated exploration of neurocircuitry landscapes such that knowledge about neuropeptide localization and expression is accumulating rapidly.

Visualization or detection of neuropeptides at the cellular, tissue, whole organism, or bio-fluid levels has been enabled by the application of radioimmunoassays (RIAs), immunohistochemistry (IHC), immunocytochemistry (ICC), and immunoelectron microscopy to

the extent that these techniques have provided most of our former and current knowledge on the localization of neuropeptides.[71] Compared with traditional histology-based approaches, these techniques enable enhanced specificity and sensitivity through the use of antibodies – for example for the detection of the specific psychostimulant neuropeptide CART (cocaine- and amphetamine-regulated transcript peptide).[72] Antibodies can theoretically also be raised against virtually any peptide, however, many invertebrate neuropeptide genes encode more than one biologically active peptide that show high structural similarity to each other, leading to antibody cross-reactivity.[73-75] Generation of N-terminally directed antisera, which can readily distinguish between peptides with highly similar C-terminal motifs, can help overcome cross reactivity issues.[76] Another limiting factor is the number of peptides (and peptide signaling pathway components) that can be co-localized at the same time through traditional IHC and ICC approaches, which is in contrast to what is seen with MS-based peptidomics tools (see below) that enable the complete neuropeptide profile of the animal, tissue, organ or even a single cell to be deduced at any given time readily enabling the identification of multiple co-localization events.

In situ hybridization (ISH) methods facilitate target-specific expression mapping of neuropeptide-encoding genes at the whole animal, tissue and single-cell level by determining the RNA localization. This involves hybridization of a single-stranded RNA oligoprobe and the complementary native mRNA sequence in the tissue or cell. The field of ISH and fluorescence ISH (FISH) has advanced significantly to enable the high-sensitivity detection of multi-target RNAs simultaneously in multiple species coupled with automated data collection and analysis systems.[77] There are several different approaches for detection of hybridized probes, including non-radioactive and radioisotope strategies. Regardless of the approach, careful consideration

should be given to transcript abundance, where the detection of low-level or single-copy transcripts [*e.g.*, of G-protien-coupled receptors (GPCRs)] can benefit from the use of target, signal or probe amplification techniques.[78] Whilst one caveat of ISH is that the information it provides on RNA localization gives no definite indication of translated peptide distribution, it can relate valuable spatio-temporal information to gene activity when used in conjunction with ICC and IHC.[79]

Reporter gene constructs encode proteins that function as site specific gene expression markers when fused to the regulatory regions (promoters) of a gene of interest. They offer an alternative detection method to ISH that is useful for transcript detection in living cells and organisms. The method requires the promoter region of the neuropeptide gene and coding region of the reporter gene to be fused and inserted into the organism of choice for use as a reporter of gene expression. It is important that the reporter gene [which often encodes green fluorescent protein (GFP)] is non-native, assayed easily (*e.g.*, by visual detection), and does not affect the normal physiology of the organism under study. The use of promoter::reporter gene constructs as localization tools is popular in model organisms such as the fruit fly *Drosophila melanogaster* and the nematode *Caenorhabditis elegans*, where transgenesis is readily achievable.[80-82] A cautionary note should be given to the reliance on transcriptional reporters however, as they do not always provide complete and reliable gene expression data in comparison to translational reporters that include important intron and 3' untranslated region (UTR) regulatory elements.[83]

Techniques for localization of the complete neuropeptidome of an organism have seen progress with the use of MS since its recent development as a molecular imaging tool.[84-86] Because no prior knowledge of the molecules is needed for analysis, theoretically hundreds or thousands of molecules can be imaged in one sample run. Among the various ionization sources

available, MALDI has been the most prominent in imaging peptides and neuropeptides, although success of detecting or identifying the neuropeptides is dictated by sample preparation and the detector coupled to the MALDI source.[87, 88] Time-of-flight based instruments have a niche in analyzing larger neuropeptides with a fast speed, but the low resolution and sensitivity have motivated the development of alternative ionization techniques for larger neuropeptides, including matrix-assisted ionization in vacuum and laserspray ionization, which can be accomplished with commercial MALDI sources.[89-91] For example, Chen et al. was able to ionize an 18.7 kDa protein on a commercial MALDI-LTQ-Orbitrap XL, which is usually limited to molecules smaller than 4 kDa. It should be noted that some of the matrices required are more compatible with long imaging runs than others. Moving forward, refinements have recently been made recently in the optimization of sample preparation methods for MS imaging. For example, when sectioning tissue, only certain embedding materials with MS.[92, 93] Optimal cutting temperature embedding material is commonly used for the classical histology staining, but due to its polymer structure, it tends to suppress and mask the analyte signal, especially in the mass range of most neuropeptides. Another major problem is that, prior to any histology analysis, samples tend to be passed through the fixation process to help maintain tissue structure and deactivate any degradation processes, which limits neuropeptide MS analysis.[94, 95] Tissue fixation requires many washes, which may remove neuropeptides, and possibly a crosslinking step, which will make neuropeptides unavailable for extraction by the matrix and thus ionization. To complicate the situation further, the choice and application of the matrix is extremely important for the proper extraction of neuropeptides, and extensive effort has been devoted to developing better, more effective methods.[96, 97] For example, by utilizing electrospray deposition of the matrix α-cyano-4-hydroxycinnamic acid, researchers have imaged the FMRFamide

neuropeptide family from a snail at a 5 μm spatial resolution, allowing confirmation of the localization found via IHC analysis.[98] For more details, readers may consult recent reviews for MS imaging and its application to neuropeptides.[28, 84, 99, 100]

In general, the reliance of mass matching for compound identification in MS imaging poses limitations in identification confidence. Owing to the low abundance of neuropeptides, performing tandem MS during imaging is often challenging. Therefore, accurate mass matching is the easiest way to identify a putative neuropeptide. The incorporation of high-quality tandem MS in a hybrid linear ion-trap–orbitrap instrument has provided improved *in situ* neuropeptide identification.[101-103] The development of a spiral step method (**Figure 4**), instead of the standard raster step, has allowed for further enhancement of chemical information by improving the depth of profiling and producing higher-quality images on Orbitrap-based instruments.[104] Another technique, IMS, has the potential to be used before detection and to remove interfering molecules and thus increase the image quality.[105] Overall, the unparalleled chemical information and multiplexing capacity offered by MS imaging technology provides an attractive tool for high-throughput mapping the localization of neuropeptides, although the inherent limitations of laser beam size and matrix crystal size of the MSI technique prevent it from having the same spatial resolution offered by IHC/ICC approaches. Further technology development is needed to improve these aspects and sensitivity to allow MS imaging to become a central tool for neuropeptide localization in the nervous system.

Recent advances in bioimaging and microscopy tools in parallel with upgrades in computer processing and digital storage capabilities have significantly enhanced the ability to capture and describe the neuroanatomy of invertebrates. Traditionally, light microscopy has been used in invertebrate neuroscience research to map the coarse architecture of the nervous system,

with electron microscopy being employed for fine ultrastructural analysis.[106] More recently, confocal and multiphoton microscopy have facilitated the generation of high-resolution 2D and 3D images of both thicker whole-mount and live specimens.[107] Laser microdissection tools provide an alternative to labor-intensive antibody-based experiments by enabling the post-capture profiling of neuropeptides (*e.g.*, via RNAseq) in specific neurons or in tissues embedded in heterogeneous samples.[108] Advances in image-analysis software programs make the comparative quantitation of neuropeptides in the nervous system more streamlined, and facilitate the integration of optical imaging technologies into the functional genomics 'toolbox'.[109, 110] Additionally, integrating multimodal imaging studies through MALDI-MS imaging and microscopy-based imaging could provide enhanced spatial and chemical information for neuropeptide localization.

Web-based databanks for curating neuropeptide data in invertebrates are a much-needed resource that will greatly facilitate invertebrate neuropeptide research and enable inter and cross-phyla comparative analyses, in addition to providing a 'go to' repository for researchers. These types of resources are currently available for a number of invertebrate phyla and provide a range of data-types in user-friendly formats; the database NeuroPep collates pan-phylum data and enables comparisons of neuropeptide structure, expression, and function.[20, 111] Furthermore, the availability of species-specific anatomical maps of the nervous system is essential for the precise and comparable morphological description of peptidergic neurons in invertebrates. These data are currently available for only a few invertebrate species, including key model organisms (for example, *C. elegans*: Wormatlas; *Drosophila melanogaster*: Neurokernal, Virtual Fly Brain; zebrafish: Z-brain; and *Macrostomum lignano*) – however, they are all at different stages of completion and vary in terms of their resolution, presentation, and data source.[112-118] These data

are extremely valuable to our understanding of invertebrate nervous system structure and function and will inform functional biology. Efforts to generate similar maps for other species of interest are under way, but significant attention and support should be directed to the curation and maintenance of these resources, as there are many online databases that are no longer active owing to the termination of funding.[119]

Assessing the Function of Neuropeptides

While the identification of neuropeptides is important, understanding their role in the nervous system is key to finding further applications. Understanding function is extremely difficult, as neuropeptides can have completely different functions within different tissues. Furthermore, even slightly different neuropeptide isoforms from the same family can have drastically different effects. Interestingly, even with the development of new, technologically advanced alternatives, older, well-vetted methods are still present in the literature either as a method of analysis or to confirm the observed results.[120, 121] Function can be explored at many levels, ranging from the macro (*e.g.,* behavioral) to the molecular scale (*e.g.,* signaling pathways). Localization can also aid elucidation of neuropeptide function, as the tissue(s) a peptide is localized in may provide key clues about its role in the organism.[122] A variety of functional biology tools and techniques can be employed to determine the function of a neuropeptide, including those applied in either *in vivo* or *in vitro* settings. Two major approaches for functional analysis will be discussed below: altering the neuropeptide content and measuring neuropeptide levels.

Altering Neuropeptide Content

The most commonly performed and observed *in vivo* studies involve assessing behavioral and/or physical changes arising from the introduction of a neuropeptide into an organism or by using reverse genetics (RNA interference) to down-regulate a specific neuropeptide (*e.g.*, using siRNAs).[123, 124] These approaches can provide a range of information from a general understanding of the physiological function of a neuropeptide to judging whether neuropeptides are therapeutically active.[125, 126] Neuropeptides, their antagonists, and siRNAs can be delivered to an organism in several different ways, including by injection, incubation in media, and even microdialysis.[6, 127-130] siRNA, RNA molecules that interfere with an expression of a gene, may require more sophisticated methods of delivery (*e.g.*, transfection) or can also be injected for the induction of gene-silencing and thus knockdown of the neuropeptide.[131, 132] Beyond introducing a neuropeptide or a neuropeptide antagonist, neuropeptide production can be altered at the genetic level in organisms, such as mice, through the production of knockout or transgenic animals, or through genome editing approaches (*e.g.*, CRISPR/Cas systems).[133-135] CRISPR/Cas has gained a lot of popularity for its speed, ease of use and efficiency compared to other methods used to knockout genes or create transgenic animals.[136] It should be noted that this technology is new and can be expensive to implement on a large scale. Furthermore, its application is not possible in non-model organisms. In all the cases described above, careful planning is required to determine the most appropriate and applicable technique to alter neuropeptide levels in an organism.

After alteration of the neuropeptide content, several behavioral observations or tests can be performed to assess change. Examples of behavior tests for animals (*e.g.*, Wistar rats) are open-field-based or maze-based tests, and these tests are applicable to numerous species, including invertebrates such as planarians and *C. elegans*.[137-140] While these tests are easily

performed and are normally the starting-point for functional studies, behavioral studies are based on observations, meaning that data misinterpretation or choice of test to monitor changes can produce misleading data.[141] Thus, care should be taken on choosing the most appropriate tests, methods, or animal models to assess behavioral changes attributable to application of neuropeptides.

As neurons transmit signals through electrical currents, another facet of function to consider is electrophysiology. By selective or global activation, researchers are able to understand synaptic mechanisms by which neurons communicate and modulate their electrical activities (**Figure 5**).[142] These readings can be performed in a few ways depending on the goal of the study, including intracellular versus extracellular electrophysiological recording, whole-cell versus whole-network, or *in vitro* versus *in vivo*.[142-149] In terms of neurological studies, *in vitro* whole-cell recordings are the most common, although *in vivo* live-animal recordings, which are inherently more difficult, are becoming more refined.[150] Crustacean model systems have been used heavily for electrophysiological studies.[151-153] For example, the effects of neuromodulators on the same neuronal circuit was explored for the Jonah crab gastric mill motor pattern, which was interestingly explained by using a mathematical model.[154] In general, to better understand neuronal modulation at the single-neuron and network level, crustaceans provide an excellent model to derive detailed knowledge about synaptic mechanism and neuronal connection owing to their possession of a much simplified system compared with the mammalian system.[155] Interestingly, the coupling of electrophysiological probes for simultaneous monitoring of other chemicals has been incorporated recently. This could include selective applications (*e.g.*, oxygen, glucose, *etc.*) or could be more global, such as microdialysis, which would allow for direct dosing of neuropeptides.[147, 156] Notably, some researchers believe that electrophysiology, while

never replaceable, might be overshadowed or combined with other optical imaging techniques that allow localization of the neurological signals.[150] One can postulate that combining the temporal resolution of classical electrophysiology and spatial resolution of optical imaging could lead to significant discoveries in neuroscience.

Measuring Neuropeptide Levels

Physiological changes related to neuropeptide actions are most commonly studied *in vivo* by performing quantitative analyses on the whole organism. It should be noted that this can be the first step in many cases to understanding the function of a peptide, as it might not be known that a neuropeptide is involved in a process until it is administered or a condition is applied (*e.g.*, a change in environment).[126] After the organism has been exposed to the neuropeptide or changed condition, it can be sacrificed and the tissues of interest collected for quantitative comparison.[157] Alternatively, the tissue can be removed from the animal and incubated before analysis.[158] Classically, this has been performed for individual proteins using western blotting, which is still widely reported in the current literature.[121, 123] Owing to the typically small size of neuropeptides, western blotting is normally used to assess other, related protein changes or expression of neuropeptide receptors.[123, 159] Other complementary examples of a targeted technique are enzyme-linked immunosorbent assay (ELISA) and use of radioactively labeled ligand and a γ-counter.[120, 127, 160] While these methods are excellent if one has a target of interest, a non-biased global view of the dynamic changes of all the neuropeptides is often needed to understand fully the role of neuropeptides and their possible function at the system level.

With the advancement of technology, MS is becoming a useful addition to functional studies as it is able to reveal changes in neuropeptide levels that might correlate with function. This technique is especially attractive for analysis of organisms without a sequenced genome, as

no prior knowledge of the molecule, such as the metabolite, protein, or peptide, is needed. To highlight some key areas of success, crustacean neuropeptide research has benefited from MS, allowing researchers to quantify several neuropeptide changes arising from stress caused by changes in salinity or temperature.[8, 161] Microdialysis of neuropeptides has also been coupled to MS, and several reviews highlight considerations for coupling these two techniques.[85, 100] Multiplexed quantitation beyond duplex has been implemented in proteomics.[162-164] In this technique, by using different combinations of stable isotopes (*i.e.*, ^{13}C, ^{15}N, ^{2}H, and ^{18}O), samples are differentially labeled prior to being mixed and analyzed together in the MS. It is expected that multiplexing will be applied more commonly in neuropeptide analysis of multiple samples.[165, 166] Although the use of MS is attractive, the depth at which it can profile depends upon many instrument characteristics, such as analysis time, resolution, and mass range. Using an analyte target list can increase neuropeptidomic coverage, although sensitivity and interfering species can introduce difficulties. Owing to the natural complexity of biological samples, the coupling of separations to MS has not only improved detection but also enabled accurate quantitation. This coupling includes capillary electrophoresis (CE), LC, or IMS before MS detection.[28, 105, 167] By reductive dimethylation of comparative samples before CE separation, it has been shown that neuropeptides can be separated and quantified accurately, allowing for more-in-depth profiling.[168, 169] Furthermore, new instrument methods, such as analysis at the MS3 level, have helped facilitate accurate quantitation.[170] It should be noted that, from these data, individual peptides can be selected for further analysis and validation by the above, targeted, methods. Finally, MS data are inherently more complicated, and the use and development of appropriate software to predict, identify or quantify is challenging, but necessary, for neuropeptidomics to continue progressing.[3, 171, 172]

Upon understanding the peptide changes, gene analysis can be conducted to help provide information on the global impact on the plasticity of the system. Although the specific neuropeptide, its propeptide, and its pre-propeptide cannot be differentiated from each other at the mRNA level, global gene analysis is most easily achieved by measuring the mRNA changes using a quantitative real-tine PCR (qPCR).[158, 173] This approach differs from Western blotting and ELISAs, the latter of which measures the translated peptide but does not require antibodies. By using qPCR, it has been shown that dosing of amphetamine not only affects rat food intake but also affects hypothalamic mRNA levels of neuropeptide Y.[141] While more mRNA usually means enhanced gene expression, protein levels do not always correlate with the mRNA data, and the use of an orthogonal method (see above) should be performed to verify any conclusions. This is true for all of the methods above as all of them have complementary advantages and disadvantages.

The Use of Modified Peptide-Gated Channels as a Tool to Study Neuroscience

The effect of a neuropeptide ultimately is determined by its receptor. While GPCRs mediate slow and more modulatory neurotransmission by changing the membrane potential, ion channel receptors by contrast mediate fast and transient neurotransmission, rapidly depolarizing or hyperpolarizing the postsynaptic membrane. It has been common knowledge for decades that neuropeptides mainly bind to and activate mainly GPCRs, rather than ion channel receptors. There are now a few exceptions to this rule: ion channels directly activated by neuropeptides have been cloned and functionally characterized from different snails (molluscs) and the freshwater polyp *Hydra* (Cnidaria), unambiguously demonstrating the existence of ion channel receptors for neuropeptides in different animal phyla (**Figure 6**). Moreover, genomic data have

revealed the presence of related channels in other phyla and electrophysiological data suggest the existence of a peptide-gated Cl^--channel in the nematode *Ascaris suum*.[174-176] Thus, we speculate that the distribution of peptide-gated channels is at present vastly underestimated and that they might mediate some of the physiological functions of neuropeptides in several animals; maybe even in humans, although this is at present thought to be unlikely. Here, we will briefly describe the discovery of the known peptide-gated channels, introduce their properties and then focus on how they might be developed into tools for neuroscience.

The first observations of a peptide-gated ion channel were made by Cottrell and co-workers, who showed that the cerebral C2 neuron of the snail *Helix aspersa* is rapidly excited by the neuropeptide FMRFamide.[177, 178] Peptides related to FMRFamide, RFamide neuropeptides, are found in many animals. The excitation was fast and also observed in outside-out patches containing 5´-O-(2-thiophosphate), which blocks G-protein-coupled responses, in the patch pipette.[178] These results strongly suggested that FMRFamide directly activated ion channels in these neurons. The currents were Na^+-selective and sensitive to the diuretic amiloride.[178] These biophysical and pharmacological properties are reminiscent of the epithelial Na^+ channel (ENaC) from vertebrates, and, in 1995, by means of homology to ENaC, the FMRFamide-gated Na^+ channel (FaNaC) was cloned from *H. aspersa* – the first peptide-gated channel.[179] A single FaNaC subunit is sufficient to produce functional channels with properties similar to the native channel in C2 neurons: they are Na^+ selective and sensitive to amiloride (EC_{50} = 0.6 µM; **Table 2**).[179] Although it was reported that FaNaC is a tetramer, there is now compelling evidence from crystallization of closely related acid-sensing ion channels (ASICs), as well as from single-molecule imaging, that channels of the degenerin (DEG)/ENaC gene family have a trimeric stoichiometry (**Figure 6a**).[180-183] In addition, species orthologs of FaNaC have been cloned from

three other molluscs, including *Aplysia*, but so far no additional subunits have been cloned.[184-186] Thus, although it cannot be ruled out formally that the native channel contains other subunits, it is likely that FaNaC functions as a homotrimer. **Table 2** provides an overview of the properties of known peptide-gated channels.

In 2007, by means of homology to ENaC and FaNaC, four related subunits were cloned from the freshwater polyp *Hydra*, which belongs to the ancient phylum Cnidaria.[187] It was found that two of them, when co-expressed in a heterologous expression system, formed an ion channel that was directly activated by two neuropeptides, which had been previously isolated from the *Hydra* nervous system using a RIA.[187, 188] Like FaNaC, the channel also conducts Na^+ and therefore was named the Hydra Na^+ channel (HyNaC). These two neuropeptides, Hydra-RFamides I and II, share a C-terminal RFamide group with FMRFamide, the ligand of FaNaC. HyNaC is not the species ortholog of FaNaC, however, as it is more closely related to mammalian ASICs than to FaNaC or ENaC, it is likely that peptide-gated channels are ancient and evolved before the cnidarian–bilaterian split.[187] Three years after the identification of these neuropeptides, another HyNaC subunit was cloned that assembles with the two previously cloned subunits, suggesting that the native channel is a heterotrimer containing three different subunits.[189] In contrast to FaNaC, HyNaC is an unselective cation channel with a high Ca^{2+} permeability (**Table 2**).[189] Soon after, all 12 DEG/ENaCs of *Hydra* were cloned, and it was shown that *Hydra* likely contains at least six different functional HyNaCs.[190] All are heterotrimers consisting of three different subunits activated by Hydra-RFamides I and II, and all are unselective cation channels (**Table 1**).[190] It is not clear why *Hydra* evolved such a variety of peptide-gated channels with similar properties, but differential targeting and differential ligand-affinity are two possibilities.

ISH revealed that two of the six HyNaCs are most likely expressed in epitheliomuscular cells at the oral side of the tentacle base, two at the aboral side and two in the foot region.[190] Application of amiloride or diminazene, two inhibitors of HyNaCs (Table 1), delayed the feeding reaction of living *Hydra*, which is characterized by a bending of the tentacles.[189, 190] Collectively, these results suggest that the *Hydra* RFamide peptides are released at neuromuscular junctions and that HyNaCs contribute to fast neuromuscular transmission.[191]

Usually, ligand-gated ion channels desensitize in the continued presence of the ligand. This feature, together with rapid re-uptake or hydrolysis of small-molecule transmitters, makes transmission with ligand-gated channels transient. HyNaCs, by contrast, could also mediate longer-lasting depolarization of the postsynaptic membrane – they do not desensitize (**Figure 6b**), and there is no known rapid re-uptake mechanism for their ligand.[192] In combination with their high Ca^{2+} permeability, these features could endow HyNaC-expressing cells with an efficient entry path for extracellular Ca^{2+}, which could be important for muscle contraction.[191]

DEG/ENaCs with high levels of sequence similarity to either FaNaC or HyNaCs are present in several genomes, for example in that of *Nematostella vectensis*, a cnidarian that belongs to the subphylum anthozoa that is not closely related to Hydrozoans, and in that of the placozoan *Trichoplax adhaerens*.[191] As *T. adhaerens* does not contain a nervous system, the presence of putative peptide-gated channels in this organism suggests that the channel-peptide ligand system predated the emergence of nervous systems and might have a role for example in paracrine signalling. Molecular cloning and functional analysis of these channels will improve our understanding of the physiological function of peptide-gated channels.

In addition to their importance in understanding neurotransmission in different organisms, peptide-gated ion channels might also be modified into interesting tools for

neuroscience. For example, FaNaC has been used as a reporter of neuropeptide-release and that achieves high temporal resolution.[193] FMRFa has been used to tag a neuropeptide prohormone, and FaNaC has acted as a reporter to monitor release of FMRFa and thereby also of the tagged neuropeptide.[193]

In another example, it has been shown that heterologous expression of FaNaC in mammalian hippocampal neurons provides a means to depolarize the neurons and induce bursts of action potentials upon focal application of FMRFa.[194] FaNaC has a somato-dendritic localization and is absent from axons.[194] As FMRFa is not present in the mammalian nervous system, and endogenous RFamides apparently do not activate FaNaC, it is in principle possible to activate specific subsets of neurons selectively in intact nervous tissue.[194] Transgenic expression of FaNaC under the control of specific promoters would enable driving of its expression only in specific subsets of neurons in living animals. Moreover, the possibility to 'cage' FMRFa chemically with a photolabile protecting group allows its release within milliseconds upon exposure to both single- and two-photon light sources to rapidly excite cells expressing FaNaC.[195] As HyNaCs are obligate heteromers, their heterologous expression in neurons is more difficult, but would allow expression of a foreign ion channel with high Ca^{2+} permeability. The cloning of further peptide-gated channels, such as the Cl^- channel from *A. suum*, will further increase the toolbox of peptide-gated channels.

A better understanding of the molecular binding site of peptide ligands on their ion channel receptors could also allow the future design of small molecules that gate the channels independently of peptides. This might allow peptide-gated channels to be employed, much like some GPCRs, as 'designer' receptors exclusively activated by designer drugs (DREADDs).[196]

The identification of the peptide-binding site might also allow the covalent attachment of FMRFa (or other peptides) close to its binding site via a photoisomerizable molecule (a 'photoswitch') such that light would move the peptide in and out of its binding site to open and close the channel (**Figure 6c**).[197, 198] Azobenzenes have been successfully used as such photoswitches, as they undergo fast trans-to-cis isomerization, much like retinal, upon illumination with near-UV light.[197] They can be coupled via maleimides to single cysteine residues engineered into the primary sequence of a channel. High-resolution structures are not only useful for the identification of the peptide-binding site but also a pre-requisite for the identification of suitable attachment sites of peptide ligands close to the binding site. As chicken ASIC1, a close homolog of HyNaCs, has been crystallized, appropriate homology models of the HyNaC structure, and perhaps also of the FaNaC structure, are feasible could feasibly be constructed.[181] Such photo-sensitive channels would allow experimenters to control the membrane potential of a neuron by light instead of a peptide ligand. Examples that such a synthetic optogenetics approach (Berlin & Isacoff, 2017) is feasible have been provided, among others, for ionotropic glutamate and $GABA_A$ receptors.[197, 199, 200] Clearly, peptide-gated ion channels have great potential to serve as useful tools for neuroscience.

Concluding Remarks

It is clear that neuropeptide research has benefited tremendously from the substantial advancements of technology for neuropeptide structural elucidation, localization mapping, and functional understanding, although any single technique itself still does not provide us with all the answers we seek. A particularly promising technique is MS imaging with tandem MS but sensitivity issues might be limiting when single-cell resolution is needed. In general, the

development the MS-based neuropeptidomics technique has proven to be the most influential technique for analyzing neuropeptides in a high-throughput and global manner, but other, often classical, methods provide validation and confirmation of all results generated by MS. Owing to its non-bias and global analysis, MS will likely be a central tool for all future neuropeptide studies, especially with the continued development of new methodology and technology. Furthermore, another area that has proven to be extremely influential has been computational prediction and processing. Without sophisticated bioinformatics tools, not only would the identification of novel neuropeptides be slow, but MS datasets, which are naturally large and complex, would be extremely difficult to process and interpret. At the moment, the pace of investigating the neuropeptidome will continue to be set by the development of both of these areas, although new techniques that are complementary or capable of providing structure, function, and localization information are welcome additions to the study of neuropeptides. In addition, peptide-gated ion channels might be modified into promising new tools for neuroscience. Finally, the integration of multiple bioanalytical techniques and molecular neuropharmacological tools will drive the field of neuropeptide research towards new frontiers.

References

1. van den Pol, A. N., *Neuron* **2012,** *76* (1), 98-115.

2. Hughes, J.; Woodruff, G. N., *Arzneimittelforschung* **1992,** *42* (2a), 250-5.

3. Hook, V.; Bandeira, N., *J Am Soc Mass Spectrom* **2015,** *26* (12), 1970-80.

4. Zhang, X.; Petruzziello, F.; Rainer, G., *EuPA* **2014,** *3*, 273–279.

5. Beal, M. F.; Department of Neurology, M. G. H. a. H. M. S., Boston MA; Neurology Research 4, M. G. H., Fruit St, Boston MA 02114; Martin, J. B., *Annals of Neurology* **2016,** *20* (5), 547-565.

6. Chen, J. T.; Reiher, W.; Hermann-Luibl, C.; Sellami, A.; Cognigni, P.; Kondo, S.; Helfrich-Forster, C.; Veenstra, J. A.; Wegener, C., *Plos Genetics* **2016,** *12* (9), 33.

7. Gomes, I.; Aryal, D. K.; Wardman, J. H.; Gupta, A.; Gagnidze, K.; Rodriguiz, R. M.; Kumar, S.; Wetsel, W. C.; Pintar, J. E.; Fricker, L. D.; Devi, L. A., *Proc Natl Acad Sci U S A* **2013,** *110* (40), 16211-6.

8. Chen, R. B.; Xiao, M. M.; Buchberger, A.; Li, L. J., *Journal of Proteome Research* **2014,** *13* (12), 5767-5776.

9. Kormos, V.; Gaszner, B., *Neuropeptides* **2013,** *47* (6), 401–419.

10. Reichmann, F.; Holzer, P., *Neuropeptides* **2016,** *55*, 99-109.

11. Hokfelt, T.; Bartfai, T.; Bloom, F., *Lancet Neurol* **2003,** *2* (8), 463-472.

12. Romanova, E. V.; Sweedler, J. V., *Trends in Pharmacological Sciences* **2015,** *36* (9), 579-586.

13. Fricker, L. D.; Lim, J. Y.; Pan, H.; Che, F. Y., *Mass Spectrometry Reviews* **2006,** *25* (2), 327-344.

14. Schrader, M.; Schulz-Knappe, P.; Fricker, L. D., *EuPA Open Proteomics* **2014,** *3*, 171-182.

15. Li, L. J.; Sweedler, J. V., Peptides in the Brain: Mass Spectrometry-Based Measurement Approaches and Challenges. In *Annual Review of Analytical Chemistry*, Annual Reviews: Palo Alto, 2008; Vol. 1, pp 451-483.

16. Morimoto, R.; Satoh, F.; Murakami, O.; Totsune, K.; Saruta, M.; Suzuki, T.; Sasano, H.; Ito, S.; Takahashi, K., *Nutrition* **2008,** *24* (9), 878-884.

17. Hanrieder, J.; Ljungdahl, A.; Andersson, M., *Journal of visualized experiments : JoVE* **2012,** (60).

18. von Euler, U. S.; Gaddum, J. H., *The Journal of Physiology* **1931,** *72* (1), 74-87.

19. Chang, M. M.; Leeman, S. E.; Niall, H. D., *Nature* **1971,** *232* (29), 86-87.

20. Wang, Y.; Wang, M.; Yin, S.; Jang, R.; Wang, J.; Xue, Z.; Xu, T., *Database (Oxford)* **2015,** *2015*, bav038.

21. Edman, P., *Acta 	 Chemica 	 Scandinavica* **1950,** *4*, 283-293.

22. Liu, W. H.; Chen, Y.; Bai, X. W.; Yao, H. M.; Zhang, X. G.; Yan, X. W.; Lai, R., *Chinese Journal of Natural Medicines* **2016,** *14* (9), 677-682.

23. Aguilar, M. B.; Zugasti-Cruz, A.; Falcon, A.; Batista, C. V. F.; Olivera, B. M.; de la Cotera, E. P. H., *Peptides* **2013,** *41*, 38-44.

24. Vaughan, J. M.; Donaldson, C. J.; Fischer, W. H.; Perrin, M. H.; Rivier, J. E.; Sawchenko, P. E.; Vale, W. W., *Endocrinology* **2013,** *154* (4), 1553-64.

25. Gilsh, G. L.; Vachet, R. W., *Nature Reviews Drug Discovery* **2003,** *2* (2), 140-150.

26. Potocnik, N. O.; Fisher, G. L.; Prop, A.; Heeren, R. M. A., *Analytical Chemistry* **2017,** *89* (16), 8223-8227.

27. Steen, H.; Mann, M., *Nature Reviews Molecular Cell Biology* **2004,** *5* (9), 699-711.

28. Buchberger, A.; Yu, Q.; Li, L., *Annu Rev Anal Chem (Palo Alto Calif)* **2015,** *8* (1), 485-509.

29. Yu, X.; Khani, A.; Ye, X.; Petruzziello, F.; Gao, H.; Zhang, X.; Rainer, G., *Analytical Chemistry* **2015,** *87* (23), 11646-11651.

30. Anand, P.; Grigoryan, A.; Bhuiyan, M. H.; Ueberheide, B.; Russell, V.; Quinonez, J.; Moy, P.; Chait, B. T.; Poget, S. F.; Holford, M., *PLOS ONE* **2016,** *9* (4), e94122.

31. Frese, C. K.; Boender, A. J.; Mohammed, S.; Heck, A. J. R.; Adan, R. A. H.; Altelaar, A. F. M., *Analytical Chemistry* **2013,** *85* (9), 4594-4604.

32. Schmidlin, T.; Boender, A. J.; Frese, C. K.; Heck, A. J.; Adan, R. A.; Altelaar, A. F., *Anal Chem* **2015,** *87* (19), 9966-73.

33. Shen, Y.; Tolić, N.; Xie, F.; Zhao, R.; Purvine, S. O.; Schepmoes, A. A.; Ronald, J. M.; Anderson, G. A.; Smith, R. D., *J Proteome Res* **2011,** *10* (9), 3929-43.

34. Frese, C. K.; Altelaar, A. F.; van den Toorn, H.; Nolting, D.; Griep-Raming, J.; Heck, A. J.; Mohammed, S., *Anal Chem* **2012,** *84* (22), 9668-73.

35. Yu, Q.; Wang, B.; Chen, Z.; Urabe, G.; Glover, M. S.; Shi, X.; Guo, L. W.; Kent, K. C.; Li, L., *J Am Soc Mass Spectrom* **2017,** *In press*.

36. Schmitt, F.; Vanselow, J. T.; Schlosser, A.; Kahnt, J.; Rossler, W.; Wegener, C., *J Proteome Res* **2015,** *14* (3), 1504-14.

37. Gade, G.; Simek, P.; Marco, H. G., *Amino Acids* **2015,** *47* (11), 2323-33.

38. Gade, G.; Simek, P.; Marco, H. G., *Amino Acids* **2016,** *48* (12), 2785-2798.

39. Ye, H.; Wang, J.; Zhang, Z.; Jia, C.; Schmerberg, C.; Catherman, A. D.; Thomas, P. M.; Kelleher, N. L.; Li, L., *Journal of Proteome Research* **2015,** *14* (11), 4776-4791.

40. Hui, L. M.; D'Andrea, B. T.; Jia, C. X.; Liang, Z. D.; Christie, A. E.; Li, L. J., *General and Comparative Endocrinology* **2013,** *184*, 22-34.

41. Jia, C. X.; Lietz, C. B.; Ye, H.; Hui, L. M.; Yu, Q.; Yoo, S.; Li, L. J., *Journal of Proteomics* **2013,** *91*, 1-12.

42. Kanu, A. B.; Dwivedi, P.; Tam, M.; Matz, L.; Hill, H. H., *Journal of Mass Spectrometry* **2008,** *43* (1), 1-22.

43. Jia, C. X.; Lietz, C. B.; Yu, Q.; Li, L. J., *Analytical Chemistry* **2014,** *86* (6), 2972-2981.

44. Pang, X.; Jia, C.; Chen, Z.; Li, L., *J Am Soc Mass Spectrom* **2017,** *28* (1), 110-118.

45. Glover, M. S.; Bellinger, E. P.; Radivojac, P.; Clemmer, D. E., *Analytical Chemistry* **2015,** *87* (16), 8466-8472.

46. Christie, A. E., *Gen Comp Endocrinol* **2014,** *201*, 87-106.

47. Wong, Y. H.; Yu, L.; Zhang, G.; He, L. S.; Qian, P. Y., *PLoS One* **2016,** *11* (8), e0160271.

48. Christie, A. E.; Pascual, M. G., *Gen Comp Endocrinol* **2016,** *237*, 53-67.

49. Bigot, L.; Beets, I.; Dubos, M.-P.; Boundry, P.; Schoofs, L.; Favrel, P., *Journal of Experimental Biology* **2014,** *217*, 2974-2982.

50. Akhtar, M. N.; Southey, B. R.; Andren, P. E.; Sweedler, J. V.; Rodriguez-Zas, S. L., *Journal of Bioinformatics and Computational Biology* **2014,** *12* (5), 15.

51. Bhattacharya, D.; Mishra, N.; Coutinho, E. C.; Srivastava, S.; Pissurlenkar, R. R.; Shaikh, M., *Pharmaceutica Analytica Acta* **2015,** *6* (5), 359.

52. Robinson, S. D.; Chhabra, S.; Belgi, A.; Chittoor, B.; Safavi-Hemami, H.; Robinson, A. J.; Papenfuss, A. T.; Purcell, A. W.; Norton, R. S., *Structure* **2016,** *24* (2), 293-299.

53. Robinson, S. D.; Safavi-Hemami, H.; Raghuraman, S.; Imperial, J. S.; Papenfuss, A. T.; Teichert, R. W.; Purcell, A. W.; Olivera, B. M.; Norton, R. S., *J Proteomics* **2015,** *114*, 38-47.

54. Xie, Y.; Zhang, L.; Wu, X. Q.; Zhang, C. L.; Yang, X. L.; Tobe, S. S., *Peptides* **2015,** *68*, 214-8.

55. Kaiser, A.; Muller, P.; Zellmann, T.; Scheidt, H. A.; Thomas, L.; Bosse, M.; Meier, R.; Meiler, J.; Huster, D.; Beck-Sickinger, A. G.; Schmidt, P., *Angew Chem Int Ed Engl* **2015,** *54* (25), 7446-9.

56. O'Connor, C.; White, K. L.; Doncescu, N.; Didenko, T.; Roth, B. L.; Czaplicki, G.; Stevens, R. C.; Wuthrich, K.; Milon, A., *Proc Natl Acad Sci U S A* **2015,** *112* (38), 11852-7.

57. Hegefeld, W. A.; Kuczera, K.; Jas, G. S., *Biopolymers* **2011,** *95* (7), 487-502.

58. Schneider, S. C.; Brown, T. C.; Gonzalez, J. D.; Levonyak, N. S.; Rush, L. A.; Cremeens, M. E., *Journal of Molecular Structure* **2016,** *1106*, 108-113.

59. Hassler, C.; Zhang, Y.; Gilmour, B.; Graf, T.; Fennell, T.; Snyder, R.; Deschamps, J. R.; Reinscheid, R. K.; Garau, C.; Runyon, S. P., *ACS Chemical Neuroscience* **2014,** *5* (8), 731-744.

60. Yin, J.; Mobarec, J. C.; Kolb, P.; Rosenbaum, D. M., *Nature* **2014,** *519*, 247-250.

61. Hoelters, L.; O'Grady, J. F.; Webster, S. G.; Wilcockson, D. C., *General and Comparative Endocrinology* **2016,** *237*, 43-52.

62. Elphick, M. R.; Mirabeau, O., *Frontiers in Endocrinology* **2014,** *5*.

63. Shahidi, R.; Williams, E. A.; Conzelmann, M.; Asadulina, A.; Veraszto, C.; Jasek, S.; Bezares-Calderon, L. A.; Jekely, G., *Elife* **2015,** *4*.

64. De Haes, W.; Van Sinay, E.; Detienne, G.; Temmerman, L.; Schoofs, L.; Boonen, K., *Biochimica Et Biophysica Acta-Proteins and Proteomics* **2015,** *1854* (7), 812-826.

65. Wheatcraft, D. R. A.; Liu, X.; Hummon, A. B., *Jove-Journal of Visualized Experiments* **2014,** (94), 7.

66. Janson, E. T.; Comi, T. J.; Rubakhin, S. S.; Sweedler, J. V., *Acs Chemical Biology* **2016,** *11* (9), 2588-2595.

67. Zimmerman, T. A.; Rubakhin, S. S.; Sweedler, J. V., *Journal of the American Society for Mass Spectrometry* **2011,** *22* (5), 828-836.

68. Condro, M. C.; Matynia, A.; Foster, N. N.; Ago, Y.; Rajbhandari, A. K.; Van, C.; Jayaram, B.; Parikh, S.; Diep, A. L.; Nguyen, E.; May, V.; Dong, H. W.; Waschek, J. A., *Journal of Comparative Neurology* **2016,** *524* (18), 3827-3848.

69. Khatib-Shahidi, S.; Andersson, M.; Herman, J. L.; Gillespie, T. A.; Caprioli, R. M., *Analytical Chemistry* **2006,** *78* (18), 6448-6456.

70. Chen, R. B.; Hui, L. M.; Sturm, R. M.; Li, L. J., *Journal of the American Society for Mass Spectrometry* **2009,** *20* (6), 1068-1077.

71. Yalow, R. S.; Berson, S. A., *J Clin Invest* **1960,** *39* (7), 1157-75.

72. Singh, O.; Kumar, S.; Singh, U.; Kumar, V.; Lechan, R. M.; Singru, P. S., *Journal of Comparative Neurology* **2016,** *524* (15), 3014-3041.

73. Husson, S. J.; Lindemans, M.; Janssen, T.; Schoofs, L., *Trends Parasitol* **2009,** *25* (4), 171-81.

74. McVeigh, P.; Mair, G. R.; Atkinson, L.; Ladurner, P.; Zamanian, M.; Novozhilova, E.; Marks, N. J.; Day, T. A.; Maule, A. G., *Int J Parasitol* **2009,** *39* (11), 1243-52.

75. Rowe, M. L.; Elphick, M. R., *Gen Comp Endocrinol* **2012,** *179* (3), 331-44.

76. Atkinson, L. E.; Miskelly, I. R.; Moffett, C. L.; McCoy, C. J.; Maule, A. G.; Marks, N. J.; Mousley, A., *International Journal for Parasitology* **2016,** *46* (11), 723-736.

77. Levsky, J. M.; Singer, R. H., *J Cell Sci* **2003,** *116* (Pt 14), 2833-8.

78. Qian, X.; Lloyd, R. V., *Diagn Mol Pathol* **2003,** *12* (1), 1-13.

79. Atkinson, L. E.; Miskelly, I. R.; Moffett, C. L.; McCoy, C. J.; Maule, A. G.; Marks, N. J.; Mousley, A., Unraveling flp-11/flp-32 dichotomy in nematodes. In *Int J Parasitol*, 2016; Vol. 46, pp 723-36.

80. Clynen, E.; Liu, F.; Husson, S. J.; Landuyt, B.; Hayakawa, E.; Baggerman, G.; Wets, G.; Schoofs, L., Bioinformatic Approaches to the Identification of Novel Neuropeptide Precursors. In *Peptidomics: Methods and Protocols*, Soloviev, M., Ed. Humana Press Inc: Totowa, 2010; Vol. 615, pp 357-374.

81. Husson, S. J.; Mertens, I.; Janssen, T.; Lindemans, M.; Schoofs, L., *Prog Neurobiol* **2007,** *82* (1), 33-55.

82. Kim, K.; Li, C., *J Comp Neurol* **2004,** *475* (4), 540-50.

83. Turek, M.; Besseling, J.; Spies, J. P.; Konig, S.; Bringmann, H., *Elife* **2016,** *5*.

84. Caprioli, R. M.; Farmer, T. B.; Gile, J., *Analytical Chemistry* **1997,** *69* (23), 4751-4760.

85. OuYang, C. Z.; Liang, Z. D.; Li, L. J., *Biochimica Et Biophysica Acta-Proteins and Proteomics* **2015,** *1854* (7), 798-811.

86. Ye, H.; Greer, T.; Li, L. J., *Journal of Proteomics* **2012,** *75* (16), 5014-5026.

87. Ye, H.; Hui, L. M.; Kellersberger, K.; Li, L. J., *Journal of the American Society for Mass Spectrometry* **2013,** *24* (1), 134-147.

88. Boggio, K. J.; Obasuyi, E.; Sugino, K.; Nelson, S. B.; Agar, N. Y. R.; Agar, J. N., *Expert Review of Proteomics* **2011,** *8* (5), 591-604.

89. Chen, B. M.; Lietz, C. B.; OuYang, C. Z.; Zhong, X. F.; Xu, M.; Li, L. J., *Analytica Chimica Acta* **2016,** *916*, 52-59.

90. McEwen, C. N.; Larsen, B. S.; Trimpin, S., *Analytical Chemistry* **2010,** *82* (12), 4998-5001.

91. Trimpin, S.; Inutan, E. D., *Journal of the American Society for Mass Spectrometry* **2013,** *24* (5), 722-732.

92. Niehoff, A. C.; Kettling, H.; Pirkl, A.; Chiang, Y. N.; Dreisewerd, K.; Yew, J. Y., *Analytical Chemistry* **2014,** *86* (22), 11086-11092.

93. Strohalm, M.; Strohalm, J.; Kaftan, F.; Krasny, L.; Volny, M.; Novak, P.; Ulbrich, K.; Havlicek, V., *Analytical Chemistry* **2011,** *83* (13), 5458-5462.

94. Casadonte, R.; Caprioli, R. M., *Nature Protocols* **2011,** *6* (11), 1695-1709.

95. Chaurand, P.; Latham, J. C.; Lane, K. B.; Mobley, J. A.; Polosukhin, V. V.; Wirth, P. S.; Nanney, L. B.; Caprioli, R. M., *Journal of Proteome Research* **2008,** *7* (8), 3543-3555.

96. Gemperline, E.; Rawson, S.; Li, L. J., *Analytical Chemistry* **2014,** *86* (20), 10030-10035.

97. Guenther, S.; Rompp, A.; Kummer, W.; Spengler, B., *International Journal of Mass Spectrometry* **2011,** *305* (2-3), 228-237.

98. Mark, L.; Maasz, G.; Pirger, Z., *Acta Biologica Hungarica* **2012,** *63*, 113-122.

99. Caprioli, R. M., *Journal of the American Society for Mass Spectrometry* **2015,** *26* (6), 850-852.

100. Schmerberg, C. M.; Li, L. J., *Protein and Peptide Letters* **2013,** *20* (6), 681-694.

101. Chen, R. B.; Jiang, X. Y.; Conaway, M. C. P.; Mohtashemi, I.; Hui, L. M.; Viner, R.; Li, L. J., *Journal of Proteome Research* **2010,** *9* (2), 818-832.

102. Rompp, A.; Guenther, S.; Schober, Y.; Schulz, O.; Takats, Z.; Kummer, W.; Spengler, B., *Angew Chem Int Ed Engl* **2010,** *49* (22), 3834-8.

103. Verhaert, P.; Pinkse, M. W. H.; Strupat, K.; Conaway, M. C. P., Imaging of Similar Mass Neuropeptides in Neuronal Tissue by Enhanced Resolution MALDI MS with an Ion Trap - Orbitrap (TM) Hybrid Instrument. In *Mass Spectrometry Imaging: Principles and Protocols*, Rubakhin, S. S.; Sweedler, J. V., Eds. Humana Press Inc: Totowa, 2010; Vol. 656, pp 433-449.

104. OuYang, C.; Chen, B.; Li, L., *Journal of the American Society for Mass Spectrometry* **2015,** *26* (12), 1992-2001.

105. Sturm, R. M.; Lietz, C. B.; Li, L. J., *Rapid Communications in Mass Spectrometry* **2014,** *28* (9), 1051-1060.

106. Schmidt-Rhaesa, A.; Harzsch, S.; Purschke, G., Structure and Evolution of Invertebrate Nervous Systems. In *The Quarterly Review of Biology*, Oxford University Press: 2016; Vol. 92, pp 102-103.

107. Bixel, G. M.; Fretham, S. J.; Aschner, M., *Curr Protoc Toxicol* **2015,** *64*, 11.19.1-11.

108. Fricker, L. D., *Cell Chemical Biology* **2012,** *19* (8), 931-932.

109. Atkinson, L. E.; Stevenson, M.; McCoy, C. J.; Marks, N. J.; Fleming, C.; Zamanian, M.; Day, T. A.; Kimber, M. J.; Maule, A. G.; Mousley, A., *Plos Pathogens* **2013,** *9* (2).

110. Robichaud, G.; Garrard, K. P.; Barry, J. A.; Muddiman, D. C., *Journal of the American Society for Mass Spectrometry* **2013,** *24* (5), 718-721.

111. Yeoh, J. G. C.; Pandit, A. A.; Zandawala, M.; Nässel, D. R.; Davies, S. A.; Dow, J. A. T., *Insect Biochem Mol Biol* **2017,** *86*, 9-19.

112. Menzel, R., *Front Syst Neurosci* **2012,** *6*, 24.

113. Altun, Z. F.; Herndon, L. A.; Wolkow, C. A.; Crocker, C.; Lints, R.; Hall, D. H., WormAtlas. 2002.

114. Armstrong, J. D.; Kaiser, K.; Muller, A.; Fischbach, K. F.; Merchant, N.; Strausfeld, N. J., Flybrain, an on-line atlas and database of the Drosophila nervous system. In *Neuron*, United States, 1995; Vol. 15, pp 17-20.

115. Chiang, A. S.; Lin, C. Y.; Chuang, C. C.; Chang, H. M.; Hsieh, C. H.; Yeh, C. W.; Shih, C. T.; Wu, J. J.; Wang, G. T.; Chen, Y. C.; Wu, C. C.; Chen, G. Y.; Ching, Y. T.; Lee, P. C.; Lin, H. H.; Hsu, H. W.; Huang, Y. A.; Chen, J. Y.; Chiang, H. J.; Lu, C. F.; Ni, R. F.; Yeh, C. Y.; Hwang, J. K., *Curr Biol* **2011,** *21* (1), 1-11.

116. Givon, L. E.; Lazar, A. A., *Plos One* **2016,** *11* (1).

117. Randlett, O.; Wee, C. L.; Naumann, E. A.; Nnaemeka, O.; Schoppik, D.; Fitzgerald, J. E.; Portugues, R.; Lacoste, A. M. B.; Riegler, C.; Engert, F.; Schier, A. F., *Nature Methods* **2015,** *12* (11), 1039-1046.

118. Morris, J.; Cardona, A.; De Miguel-Bonet Mdel, M.; Hartenstein, V., *Dev Genes Evol* **2007,** *217* (8), 569-84.

119. Katz, P. S.; Calin-Jageman, R.; Dhawan, A.; Frederick, C.; Guo, S.; Dissanayaka, R.; Hiremath, N.; Ma, W.; Shen, X.; Wang, H. C.; Yang, H.; Prasad, S.; Sunderraman, R.; Zhu, Y., *Front Syst Neurosci* **2010,** *4*, 9.

120. Bilgic, A.; Toker, A.; Uysal, S., *Psychiatry and Clinical Neurosciences* **2016,** *70* (10), 442-447.

121. Liu, H. J.; Yan, H.; Yan, J.; Li, H.; Chen, L.; Han, L. R.; Yang, X. F., *Plos One* **2016,** *11* (10), 18.

122. Bruzzone, F.; Lectez, B.; Tollemer, H.; Leprince, J.; Dujardin, C.; Rachidi, W.; Chatenet, D.; Baroncini, M.; Beauvillain, J. C.; Vallarino, M.; Vaudry, H.; Chartrel, N., *Journal of Neurochemistry* **2006,** *99* (2), 616-627.

123. Bayerl, D. S.; Honig, J. N.; Bosch, O. J., *Behavioural Brain Research* **2016,** *305*, 18-22.

124. Lin, Y. T.; Liu, T. Y.; Yang, C. Y.; Yu, Y. L.; Chen, T. C.; Day, Y. J.; Chang, C. C.; Huan, G. J.; Chen, J. C., *Psychoneuroendocrinology* **2016,** *71*, 73-85.

125. Wickstrom, H. R.; Berner, J.; Holgert, H.; Hokfelt, T.; Lagercrantz, H., *Respiratory Physiology & Neurobiology* **2004,** *140* (1), 19-31.

126. Zhang, M. D.; Barde, S.; Yang, T.; Lei, B. L.; Eriksson, L. I.; Mathew, J. P.; Andreska, T.; Akassoglou, K.; Harkany, T.; Hokfelt, T. G. M.; Terrando, N., *Proceedings of the National Academy of Sciences of the United States of America* **2016,** *113* (43), E6686-E6695.

127. Javadian, N.; Rahimi, N.; Javadi-Paydar, M.; Doustimotlagh, A. H.; Dehpour, A. R., *Epilepsy Research* **2016,** *126*, 134-140.

128. Narvaez, M.; Borroto-Escuela, D. O.; Millon, C.; Gago, B.; Flores-Burgess, A.; Santin, L.; Fuxe, K.; Narvaez, J. A.; Diaz-Cabiale, Z., *Brain Structure & Function* **2016,** *221* (8), 4129-4139.

129. Kasica, N.; Podlasz, P.; Sundvik, M.; Tamas, A.; Reglodi, D.; Kaleczyc, J., *Neurotoxicity Research* **2016,** *30* (4), 633-647.

130. Torregrossa, M. M.; Kalivas, P. W., *Pharmacology Biochemistry and Behavior* **2008,** *90* (2), 261-272.

131. Flores-Burgess, A.; Millon, C.; Gago, B.; Narvaez, M.; Borroto-Escuela, D. O.; Mengod, G.; Narvaez, J. A.; Fuxe, K.; Santin, L.; Diaz-Cabiale, Z., *Neuropharmacology* **2017,** *118*, 233-241.

132. Yang, Y.; Liu, L.; Luo, H.; Li, Y.; Li, H.; Xu, Z. D., *Mol Neurobiol* **2017,** *54* (6), 4421-4431.

133. Hay, E. A.; Knowles, C.; Kolb, A.; MacKenzie, A., *Neuropeptides* **2017,** *64*, 19-25.

134. Shao, L. W.; Niu, R.; Liu, Y., *Cell Research* **2016,** *26* (11), 1182-1196.

135. Van Sinay, E.; Mirabeau, O.; Depuydt, G.; Van Hiel, M. B.; Peymen, K.; Watteyne, J.; Zels, S.; Schoofs, L.; Beets, I., *Proceedings of the National Academy of Sciences of the United States of America* **2017,** *114* (20), E4065-E4074.

136. Hay, E. A.; Khalaf, A. R.; Marini, P.; Brown, A.; Heath, K.; Sheppard, D.; MacKenzie, A., *Neuropeptides* **2017,** *64*, 101-107.

137. Bahaaddini, M.; Khatamsaz, S.; Esmaeili-Mahani, S.; Abbasnejad, M.; Raoof, M., *Neuroreport* **2016,** *27* (15), 1107-1113.

138. Chrousos, G. P.; Gold, P. W., *Jama-Journal of the American Medical Association* **1992,** *267* (9), 1244-1252.

139. Hagstrom, D.; Cochet-Escartin, O.; Collins, E. M. S., *Regeneration* **2016,** *3*, 65-77.

140. Qin, J.; Wheeler, A. R., *Lab on a Chip* **2006,** *7*, 186-192.

141. Chu, S. C.; Yu, C. H.; Chen, P. N.; Hsieh, Y. S.; Kuo, D. Y., *Psychoneuroendocrinology* **2016,** *71*, 1-11.

142. Kuksis, M.; Ferguson, A. V., *Journal of Neuroendocrinology* **2014,** *26* (4), 237-246.

143. Matthews, R. T.; Lee, W. L., *Neuroscience* **1991,** *42* (2), 451-462.

144. Beenhakker, M. P.; Blitz, D. M.; Nusbaum, M. P., *Journal of Neurophysiology* **2004,** *91* (1), 78-91.

145. Qiu, J.; Nestor, C. C.; Zhang, C. G.; Padilla, S. L.; Palmiter, R. D.; Kelly, M. J.; Ronnekleiv, O. K., *Elife* **2016,** *5*, 24.

146. Zhao, Y.; Singh, C.; Prober, D. A.; Wayne, N. L., *Endocrinology* **2016,** *157* (10), 4012-4020.

147. Li, C. Y.; Limnuson, K.; Wu, Z. Z.; Amin, A.; Narayan, A.; Golanov, E. V.; Ahn, C. H.; Hartings, J. A.; Narayan, R. K., *Biosensors & Bioelectronics* **2016,** *77*, 62-68.

148. Marder, E.; Bucher, D., *Annu Rev Physiol* **2007,** *69*, 291-316.

149. Nusbaum, M. P.; Blitz, D. M.; Marder, E., *Nat Rev Neurosci* **2017,** *18* (7), 389-403.

150. Scanziani, M.; Hausser, M., *Nature* **2009,** *461* (7266), 930-939.

151. Daur, N.; Nadim, F.; Bucher, D., *Current Opinion in Neurobiology* **2016,** *41*, 1-7.

152. Dickinson, P. S.; Qu, X.; Stanhope, M. E., *Current Opinion in Neurobiology* **2016,** *41*, 149-157.

153. Otopalik, A. G.; Goeritz, M. L.; Sutton, A. C.; Brookings, T.; Guerini, C.; Marder, E., *Elife* **2017,** *6*, 32.

154. Kintos, N.; Nusbaum, M. P.; Nadim, F., *Journal of Computational Neuroscience* **2016,** *40* (2), 113-135.

155. Marder, E.; Gutierrez, G. J.; Nusbaum, M. P., *Developmental Neurobiology* **2017,** *77* (5), 597-609.

156. Szabo, T. M.; Chen, R. B.; Goeritz, M. L.; Maloney, R. T.; Tang, L. S.; Li, L. J.; Marder, E., *Journal of Comparative Neurology* **2011,** *519* (13), 2658-2676.

157. Abels, M.; Riva, M.; Bennet, H.; Ahlqvist, E.; Dyachok, O.; Nagaraj, V.; Shcherbina, L.; Fred, R. G.; Poon, W.; Sorhede-Winzell, M.; Fadista, J.; Lindqvist, A.; Kask, L.; Sathanoori, R.; Dekker-Nitert, M.; Kuhar, M. J.; Ahren, B.; Wollheim, C. B.; Hansson, O.; Tengholm, A.; Fex, M.; Renstrom, E.; Groop, L.; Lyssenko, V.; Wierup, N., *Diabetologia* **2016,** *59* (9), 1928-1937.

158. Peng, W.; Cao, M. X.; Chen, J.; Li, Y. M.; Wang, Y. P.; Zhu, Z. Y.; Hu, W., *General and Comparative Endocrinology* **2016,** *235*, 18-28.

159. Liu, S.; Jin, D.; Wu, J. Q.; Xu, Z. Y.; Fu, S.; Mei, G.; Zou, Z. L.; Ma, S. H., *Neuropeptides* **2016,** *56*, 105-113.

160. Dhuria, S. V.; Fine, J. M.; Bingham, D.; Svitak, A. L.; Burns, R. B.; Baillargeon, A. M.; Panter, S. S.; Kazi, A. N.; William, H. F.; Hanson, L. R., *Neuroscience Letters* **2016,** *627*, 155-159.

161. Zhang, Y.; Buchberger, A.; Muthuvel, G.; Li, L., *Proteomics* **2015**.

162. Frost, D. C.; Greer, T.; Li, L., *Anal Chem* **2015,** *87* (3), 1646-54.

163. Wang, J. H.; Zhang, Y. Z.; Xiang, F.; Zhang, Z. C.; Li, L. J., *Journal of Chromatography A* **2010,** *1217* (26), 4463-4470.

164. Xiang, F.; Ye, H.; Chen, R. B.; Fu, Q.; Li, L. J., *Analytical Chemistry* **2010,** *82* (7), 2817-2825.

165. Bark, S. J.; Lu, W. Y. D.; Hook, V., *Analytical Biochemistry* **2009,** *389* (1), 18-26.

166. Che, F. Y.; Fricker, L. D., *Journal of Mass Spectrometry* **2005,** *40* (2), 238-249.

167. Zhong, X. F.; Zhang, Z. C.; Jiang, S.; Li, L. J., *Electrophoresis* **2014,** *35* (9), 1214-1225.

168. Warkiani, M. E.; Khoo, B. L.; Wu, L.; Tay, A. K. P.; Bhagat, A. A. S.; Han, J.; Lim, C. T., *Nature Protocols* **2016,** *11*, 134-148.

169. Zhang, Z. C.; Ye, H.; Wang, J. H.; Hui, L. M.; Li, L. J., *Analytical Chemistry* **2012,** *84* (18), 7684-7691.

170. Ting, L.; Rad, R.; Gygi, S. P.; Haas, W., *Nature Methods* **2011,** *8* (11), 937-940.

171. Falth, M.; Skold, K.; Norrman, M.; Svensson, M.; Fenyo, D.; Andren, P. E., *Molecular & Cellular Proteomics* **2006,** *5* (6), 998-1005.

172. Ma, B.; Zhang, K. Z.; Hendrie, C.; Liang, C. Z.; Li, M.; Doherty-Kirby, A.; Lajoie, G., *Rapid Communications in Mass Spectrometry* **2003,** *17* (20), 2337-2342.

173. Caers, J.; Peymen, K.; Van Hiel, M. B.; Van Rompay, L.; Van Den Abbeele, J.; Schoofs, L.; Beets, I., *General and Comparative Endocrinology* **2016,** *235*, 142-149.

174. Holden-Dye, L.; Brownlee, D. J.; Walker, R. J., *Br J Pharmacol* **1997,** *120* (3), 379-86.

175. Purcell, J.; Robertson, A. P.; Thompson, D. P.; Martin, R. J., *Parasitology* **2002,** *124* (Pt 6), 649-56.

176. Purcell, J.; Robertson, A. P.; Thompson, D. P.; Martin, R. J., *Eur J Pharmacol* **2002,** *456* (1-3), 11-7.

177. Cottrell, G. A.; Green, K. A.; Davies, N. W., *Pflugers Arch* **1990,** *416* (5), 612-4.

178. Green, K. A.; Falconer, S. W.; Cottrell, G. A., *Pflugers Arch* **1994,** *428* (3-4), 232-40.

179. Lingueglia, E.; Champigny, G.; Lazdunski, M.; Barbry, P., *Nature* **1995,** *378* (6558), 730-3.

180. Coscoy, S.; Lingueglia, E.; Lazdunski, M.; Barbry, P., *J Biol Chem* **1998,** *273* (14), 8317-22.

181. Jasti, J.; Furukawa, H.; Gonzales, E. B.; Gouaux, E., *Nature* **2007,** *449* (7160), 316-23.

182. Bartoi, T.; Augustinowski, K.; Polleichtner, G.; Grunder, S.; Ulbrich, M. H., *Proceedings of the National Academy of Sciences of the United States of America* **2014,** *111* (22), 8281-8286.

183. Chen, Q.; de Lecea, L.; Hu, Z.; Gao, D., *Medicinal Research Reviews* **2015,** *35* (1), 152-197.

184. Furukawa, Y.; Miyawaki, Y.; Abe, G., *Pflugers Arch* **2006,** *451* (5), 646-56.

185. Jeziorski, M. C.; Green, K. A.; Sommerville, J.; Cottrell, G. A., *J Physiol* **2000,** *526 Pt 1*, 13-25.

186. Perry, S. J.; Straub, V. A.; Schofield, M. G.; Burke, J. F.; Benjamin, P. R., *J Neurosci* **2001,** *21* (15), 5559-67.

187. Golubovic, A.; Kuhn, A.; Williamson, M.; Kalbacher, H.; Holstein, T. W.; Grimmelikhuijzen, C. J.; Gründer, S., *J Biol Chem* **2007,** *282* (48), 35098-103.

188. Moosler, A.; Rinehart, K. L.; Grimmelikhuijzen, C. J., *Biochem Biophys Res Commun* **1996,** *229* (2), 596-602.

189. Dürrnagel, S.; Kuhn, A.; Tsiairis, C. D.; Williamson, M.; Kalbacher, H.; Grimmelikhuijzen, C. J.; Holstein, T. W.; Gründer, S., *J Biol Chem* **2010,** *285* (16), 11958-65.

190. Assmann, M.; Kuhn, A.; Durrnagel, S.; Holstein, T. W.; Grunder, S., *Bmc Biology* **2014,** *12*, 14.

191. Gründer, S.; Assmann, M., *J Exp Biol* **2015,** *218* (Pt 4), 551-561.

192. Dürrnagel, S.; Falkenburger, B. H.; Gründer, S., *J Gen Physiol* **2012,** *140* (4), 391-402.

193. Whim, M. D.; Moss, G. W., *Neuron* **2001,** *30* (1), 37-50.

194. Schanuel, S. M.; Bell, K. A.; Henderson, S. C.; McQuiston, A. R., *Neuroscience* **2008,** *155* (2), 374-86.

195. Janett, E.; Bernardinelli, Y.; Muller, D.; Bochet, C. G., *Bioconjug Chem* **2015,** *26* (12), 2408-18.

196. Roth, B. L., *Neuron* **2016,** *89* (4), 683-94.

197. Berlin, S.; Isacoff, E. Y., *Embo Reports* **2017,** *18* (5), 677-692.

198. Kramer, R. H.; Fortin, D. L.; Trauner, D., *Curr Opin Neurobiol* **2009,** *19* (5), 544-52.

199. Lin, W. C.; Tsai, M. C.; Davenport, C. M.; Smith, C. M.; Veit, J.; Wilson, N. M.; Adesnik, H.; Kramer, R. H., *Neuron* **2015,** *88* (5), 879-91.

200. Volgraf, M.; Gorostiza, P.; Numano, R.; Kramer, R. H.; Isacoff, E. Y.; Trauner, D., *Nat Chem Biol* **2006,** *2* (1), 47-52.

Figures

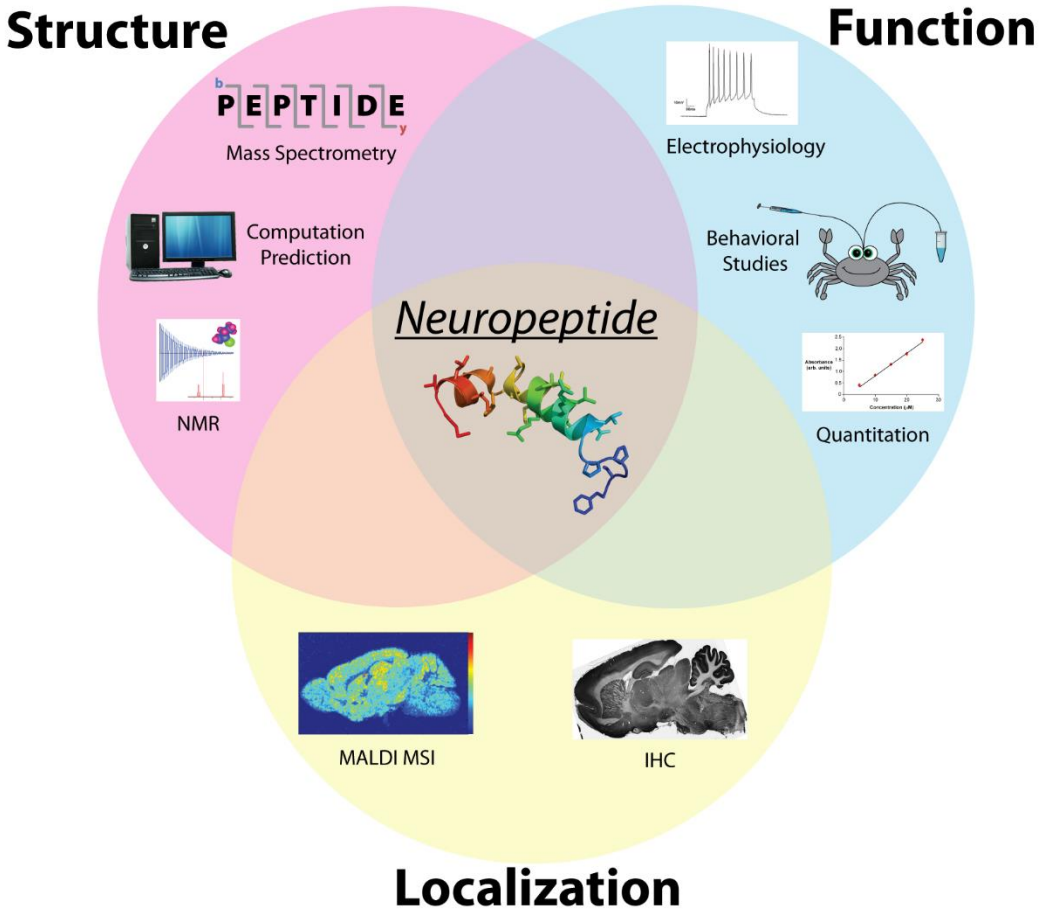

Figure 1. A general depiction of the importance of structure, function, and localization to provide key information about a neuropeptide. Several methods for each area of the Venn diagram are highlighted. For structure tools, mass spectrometry, computational prediction, and nuclear magnetic resonance (NMR) are shown. MALDI-MSI and immunohistochemistry (IHC) are the examples depicted for tools to provide localization. For understanding functionality, quantitation, behavioral studies, and electrophysiology are core techniques.

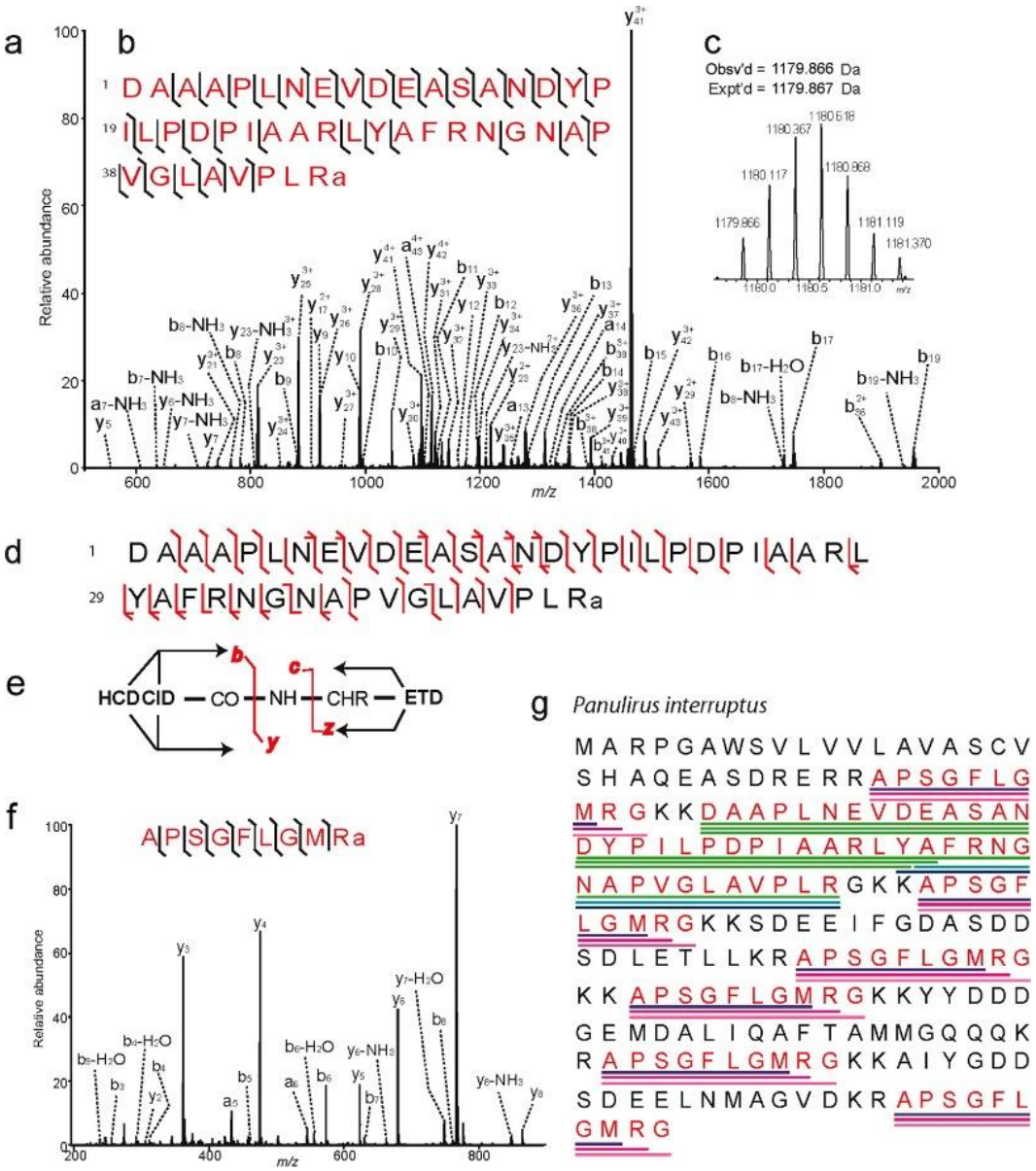

Figure 2. Depiction of *de novo* sequencing of peptides by using MS. (a) High-resolution tandem mass spectrum with sequence-specific fragment ions annotated. (b) Sequence assignment based on fragmentations, in which mass differences between adjacent fragment ion peaks are matched to amino acids. (c) Enlarged, high-resolution spectrum showing mass accuracy and isotopic distribution (necessary for measurements of differences between molecules with the same nominal mass). (d) Display of the sequence coverage. Each tick mark indicates the cleavage of the peptide yielding a fragment that has been detected in the MS spectrum. The more fragments

that are detected, the greater the sequence coverage is. (e) Representation of the different types of ions produced in tandem MS depending on fragmentation method used and bond cleavage sites. The cleavage sites are indicative of typical fragmentation patterns characteristic of the two common types of fragmentation methods. The b and y ions are produced during HCD and CID fragmentation, and c and z ions are produced during ETD fragmentation. (f) Tandem mass spectrum of another peptide (from Jonah crab *Cancer borealis* tachykinin-related peptide) with fragments indicated. (g) Comparison between peptides detected with MS (different colored lines indicate different detected peptides) and those predicted based on the precursor cDNA sequence of the spiny lobster *Panulirus interruptus* (highlighted in red). Adapted with permission.[39] CID, collision-induced dissociation; ETD, electron transfer dissociation; HCD, higher-energy collisional dissociation.

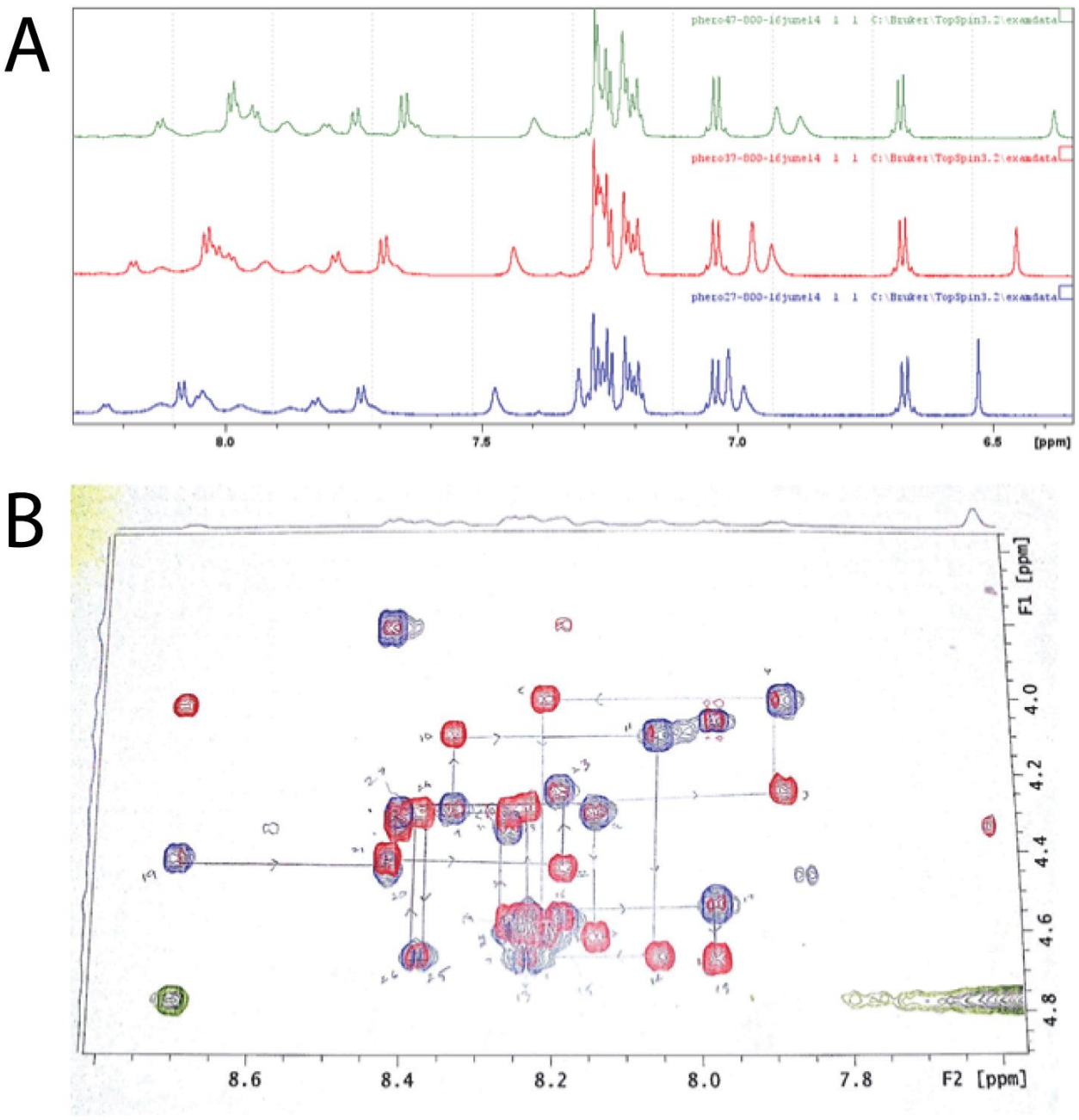

Figure 3. Nuclear magnetic resonance (NMR) spectra of the a peptide standard of the neuropeptide pheromonotropin, originally discovered in an extract from the head of *P. separuta* (armyworm) larvae. (a) One-dimensional [^{1}H] NMR spectra collected at different temperatures, showing differences in chemical shift of NH protons in the peptide. The dependence of chemical shift on temperature is indicative of the degree of hydrogen bonding. Values below 3.00 ppb

(chemical shift) per unit Kelvin indicate the presence of strong hydrogen bonds. As can be seen, the values for this peptide fall above that threshold, revealing that the protons are freely exposed to the solvent in this conformation. (b) Two-dimensional NMR spectra [total correlated spectroscopy (TOCSY)] in blue, and rotating-frame Overhauser spectroscopy (ROESY) in red], showing a sequential assignment walk. The TOCSY spectrum provided information on NH-αH cross peaks, while the ROESY spectrum's cross peaks represent NH_i-$\alpha H_{(i-1)}$ Adapted with permission.[51]

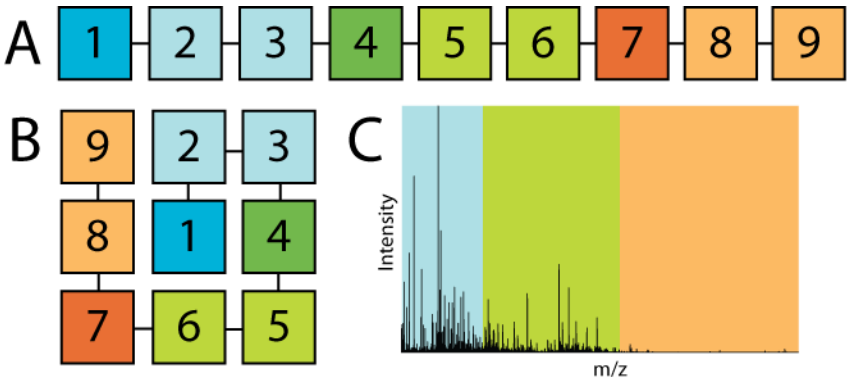

Figure 4. In order to achieve better profiling depth during MS imaging of neuropeptides, a spiral step method has been developed. Instead of the classical raster step (a), a spiral square (b) is set up. In the example spiral, the square is broken into 9 individual steps. The first square is an MS scan (dark blue), while the two following squares (light blue) are tandem MS scans. This repeats three times until all 9 steps in the spiral are completed. Each square is a raster step of 50 µm, with the whole spiral being 150 µm. This system can be customized to balance MS and tandem MS scans. For example, step one could be an MS scan, while squares 2-9 could be tandem MS scans if the user desires. Furthermore, this method can be targeted or used with data dependent acquisition (DDA). For DDA experiments, the highest intensity peaks are chosen for tandem MS analysis. Since neuropeptides tend to be in low abundance compared to lipids and have a wide mass range, we can segregate the spiral step method into multiple mass ranges (*e.g.*, three) to improve sampling of neuropeptides (c).[104]

Figure 5. A graphical representation of whole-cell patch clamp electrophysiology readings. In this image, subfornical organ neurons from rat brains are being exposed to 10 nM nesfatin-1, an anorexigenic neuropeptide, at the time frame indicated by the line under the graph. When exposed, neurons can either become slightly depolarized, which is associated with an increase in firing frequency (a) or slightly hyperpolarized, which is associated with a decrease in firing frequency (b). Adapted with permission.[142]

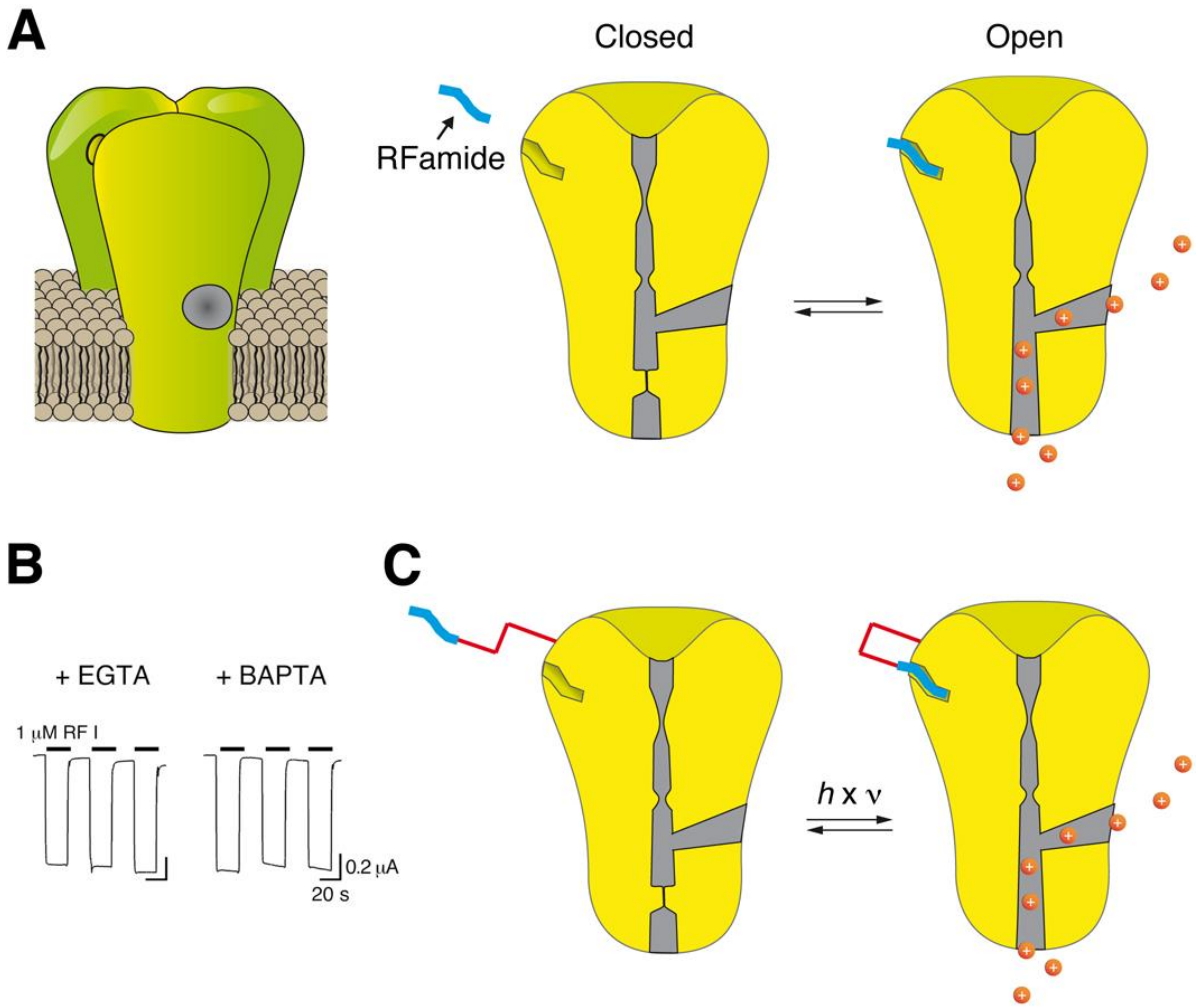

Figure 6. Properties of peptide-gated HyNaCs. (A) Left, cartoon illustrating the three-dimensional structure of a channel. The ligand binding site is unknown and is drawn here at the interface of two subunits for illustration. Right, HyNaCs can be either open or closed. The equilibrium between these two conformations is shifted by binding of a RFamide peptide (blue) to the extracellular domain. (B) HyNaCs can be repeatedly activated by their ligand, Hydra-RFamide I (RF I), and do not desensitize. The inward current is carried by Na^+ and Ca^{2+} (orange circles). Used with permission.[192] (C) Cartoon illustrating how a peptide covalently linked to the channel could be moved into and out of its binding site by application of light via a photoisomerizable linker (a "light-switch", red).

Table 1. A summary of notable techniques commonly used to provide information about the three major areas of neuropeptide research: structure, localization, and function. Each technique described has the potential to provide deep insight into neuropeptide biology, and often provide complementary information to other techniques. Several key references are indicated for each that demonstrate current trends in the field.

Area of interest	Technique	Description	Key references
Structure	Mass spectrometry	Determines sequences, PTMs and structural information	Secher et al., 2016; Gade et al., 2016; Glover et al., 2015
	In silico prediction	Predicts sequences and structure from precursor protein and gene sequences	Christie, 2014; Wong et al., 2016; Bigot et al., 2014
	NMR	Gives information into conformations and folding patterns	Robinson et al., 2016; Xie et al., 2015; Kaiser et al., 2015
	Spectroscopy	Uses characteristic peaks to identify folding patterns	Hegefeld et al., 2011; Schneider et al., 2016
	X-ray crystallography	Characterizes key structural sites with high spatial resolution	Hassler et al., 2014; Yin et al., 2014
Localization	Immuno assays	Enables localization for virtually any peptide using antibodies	Singh et al., 2016; Husson et al., 2009; Rowe and Elphick, 2012
	In situ hybridization	Target-specific expression mapping of neuropeptide-encoding genes	Levsky and Singer, 2003; Qian and Lloyd, 2003; Atkinson et al., 2016
	Promotor::reporter gene constructs	Enables transcript detection in living cells and organisms	Kim and Li, 2004; Clynen et al., 2010; Turek et al., 2016
	MSI	Capable of imaging entire neuropeptidomes without prior knowledge	Chen et al., 2016a; Mark et al., 2012; OuYang et al., 2015a
	Bio imaging and microscopy	Maps the architecture of the nervous system	Schmidt-Rhaesa et al., 2016; Fricker, 2012; Bixel et al., 2015
Function	Behavioral studies	Common first step to obtaining a general understanding of function to judging potential for disease treatment	Zhang et al., 2016; Kasica et al., 2016; Flores-Burgess et al., 2017
	Electrophysiology	Provides understanding of synaptic mechanisms	Kuksis and Ferguson, 2014; Li et al., 2016; Otopalik et al., 2017
	Quantitative analyses (western blotting, ELISA, MS, etc.)	Implies functions by measuring changes in neuropeptide levels due to specific behaviors or conditions	Liu et al., 2016a; Schmerberg and Li, 2013b; Bilgic et al., 2016

Table 2. Properties of peptide-gated ion channels.

Channel	Gene family	Stoichiometry	Ligand	Ligand affinity	Kinetics	Ion selectivity	Pharmacology
FaNaC	DEG/ENaC	Homo-trimer	FMRF-NH_2	2–70 µmol l^{-1}[a,b]	Partially desensitizing (τ ~1 min)[c]	Na^+-selective P_{Na}/P_K>10[a]	EC_{50}(amil)=0.6 µmol l^{-1}[a]
HyNaCs	DEG/ENaC	Hetero-trimer[e,f]	pQWLGGRF-NH_2 pQWFNGRF-NH_2	0.04–>30 µmol l^{-1}[e,f]	Non-desensitizing[f,g]	Cation-unselective P_{Na}/P_K=3[g] P_{Ca}/P_{Na}=4[g]	EC_{50}(amil)=100 µmol l^{-1}[e] EC_{50}(dimi)=0.05–5 µmol l^{-1}[f]
Ascaris suum channel	Unknown	Unknown	KPNFLRF-NH_2 (or similar)	0.001–0.1 µmol l^{-1}[h,i]	Non-desensitizing[h,i]	Cl^--selective[h,i]	

Amil, amiloride; dimi, diminazene.
[a]Linguelia et al., 1995, [b]Jeziorski et al., 2000, [c]Kodani and Furukawa, 2010, [d]Golubovic et al., 2007, [e]Dürrnagel et al., 2010, [f]Assmann et al., 2014, [g]Dürrnagel et al., 2012, [h]Holden-Dye et al., 1997, [i]Purcell et al., 2002a.

Appendix VIII

Quantitative Proteomics for Analyses of Multiple Samples in Parallel with Chemical Perturbation

Modified from:

Amanda R. Buchberger[¥]**,** Jillian Johnson[¥], Lingjun Li. "Quantitative Proteomics for Analyses of Multiple Samples in Parallel with Chemical Perturbation." Invited Book Chapter. *Mass Spectrometry-based Chemical Proteomics*. Submitted, 2017. [¥]Co-first authors

Keywords: Mass Spectrometry, Chemical Tagging, Multiplexing, Chemical Perturbation

Abstract

Due to their pivotal role in all biological processes, quantitative proteomics is vital for biomarker discovery for studying different disease conditions and other universal, biological research questions. In this book chapter, we review label-free quantitation, metabolic labeling, and chemical stable isotope labeling strategies for quantitative proteomics and discuss strategies for selecting the appropriate labeling approach for the intended proteomic analysis. Additionally, we provide a detailed methods section for an economical and efficient dimethylated alanine (DiAla) and dimethylated valine (DiVal) isobaric labeling strategy developed in our lab.

Introduction

Due to their pivotal role in all biological processes, quantitative proteomics is vital for biomarker discovery for studying different disease conditions and other universal, biological research questions.[1] To study the proteome of an organism, advanced technology, such as mass spectrometry (MS), has been utilized heavily.[2-11] MS has the unique advantage that thousands of proteins can be analyzed simultaneously, which is useful for both profiling and targeted molecule analysis. In particular, protein-based biomarker discovery is an exciting focus for proteomics, as clinical specimens, such as urine, tissues, and blood can be utilized for the discovery of molecular signatures that enable diagnosis, prognosis, or therapeutic prediction. There are two main methods for analyzing proteins: top-down and bottom-up proteomics. In top down proteomics, intact proteins or large protein fragments are ionized, although protein folding and other technical difficulties has limited its regular use for quantitation.[12] In comparison, bottom-up proteomics uses peptides from enzymatic digestion of proteins for analysis, which will be the focus in this review. Bottom-up proteomics typically has higher sensitivity, and peptides can be

easily separated using liquid chromatography (LC) to decrease sample complexity, allowing larger proteome coverage. LC separation can be performed either offline or online, and its common to even couple several dimensions of separations to analyze low abundance proteins.[3, 13] After injection into the instrument, quantitation can occur at the MS1 level. For identification, a mass-to-charge ratio (*m/z*) value (*i.e.,* a theoretical peptide) can be selected for tandem MS (*i.e.,* MS/MS), although quantitation can also occur after fragmentation. Quantitative proteomics typically relies on MS to quantitate peptides, while MS/MS is typically required for identification of peptides. The MS/MS data is searched against peptide databases, which computationally maps the peptides back to its original protein counterpart. Because protein expression is dynamic, quantitative proteomics encompasses more than sampling and identifying proteins in a sample and can also be used for understanding global protein kinetics and molecular mechanisms of biological processes.

While biomarker studies rely heavily on quantitative proteomics, these experiments could be very time consuming and instrument intensive depending on the number of samples. This also greatly depends on the quantitation strategy being chosen (*e.g.,* absolute vs. relative quantitation). In this book chapter, we review label-free quantitation, metabolic labeling, and chemical stable isotope labeling strategies for quantitative proteomics and discuss strategies for selecting the appropriate labeling approach for the intended proteomic analysis. Additionally, we provide a detailed methods section for an economical and efficient dimethylated alanine (DiAla) and dimethylated valine (DiVal) isobaric labeling strategy developed in our lab.

Relative and Absolute Label-free Quantitation Strategies

In general, label-free quantitation determines the relative amount of proteins in two or more biological samples, where each biological sample is analyzed independently in a separate mass spectrometry run. Beyond sample extraction and clean up, the sample can be directly analyzed with minimal sample loss, allowing for high proteome coverage. Samples are then compared to each other following their individual mass spectrometry analysis. Due to the run-to-run variation where slight differences can be misinterpreted, label-free quantitation is ideal for measuring large fold protein changes.[14]

Two different techniques are regularly used for relative comparison: extracted ion chromatogram (XIC) comparison or spectral counting. By looking at the LC chromatogram and extracting the "area under the curve," for which should directly correlate to concentration, XIC comparison allows for more accurate quantitation than directly comparing spectral intensities.[14, 15] This has been utilized recently to study both glycoproteins and endogenous peptides from the cerebrospinal fluid (CSF) of Alzheimer's disease patients to assess for biomarkers.[16] It should be noted that variations between runs can be so large that intensity-based quantitation without standards is generally not considered as reliable quantitation. For accurate quantitation, sensitive computer algorithms are required for peak alignment and sample comparison.[17-20] To compare, spectral counting physically counts the number of MS/MS spectra that are generated for a peptide and uses that as a quantitative measure.[14, 21] The thought is that the proteins/peptides in a sample that are higher in abundance will be selected for tandem MS more frequently. Between the two methods, spectral counting has been shown to offer a higher dynamic range for quantitation and better reproducibility. Spectral counting also does not require special computational algorithms beyond simple normalization. Mandel-Kolbach *et al.* has shown its feasibility by studying the urine proteins of former urinary stone patients.[22] Absolute

quantitation, or the determination of the actual concentration of a protein in a sample, can be in done in label-free analysis, but is less accepted and thus not done as often. Some methods include absolute protein expression (APEX) and exponentially modified protein abundance index (emPAI).[14, 23] If the goal is to quantify a target protein in a small number of samples, the use of an internal standard is a viable option as well, although stable isotopes likely incorporated (see below).

The advantage to label-free proteomics analysis is that the number of biological conditions that can be analyzed is not limited by the availability of isotopic or isobaric tags for an experiment, making it possible to analyze any number of samples. This is particularly attractive when there are many conditions, disease states, or biological systems that need to be analyzed and/or compared for an experiment. Overall, label-free quantitation has the significant disadvantage of requiring the most instrumental time compared to all other techniques discussed here. Highly sophisticated software is often required, which can make label-free analysis expensive for commercial bioinformatics tools. Additionally, variations from different mass spectrometry runs can cause fluctuations and errors in the data, making it harder to distinguish instrumental noise from biological significance unless large changes are shown.[14] Thus, more biological replicates are needed to minimize technical variability between samples. These disadvantages have really inspired other researchers to develop techniques for further multiplexing by utilizing stable isotopes, which will be discussed in the next sections. For more details on label-free quantitation, several reviews exist in the literature.[14, 19, 24]

Stable Isotope-Based Quantitative Proteomics

Relative Quantitation

In order to increase multiplexing, researchers have adopted the use of stable isotopes (*e.g.*, ^{18}O, ^{13}C, ^{15}N, and ^{2}H) into all facets of the sample preparation workflow. This means that stable isotopes can be incorporated before sample collection (*e.g.,* metabolic labeling), after extraction (*e.g.,* isobaric and isotopic labeling), or right before injection into the mass spectrometer (*e.g.,* AQUA).

Metabolic labeling requires an *in vivo* biological system for peptide labeling, where isotopes are incorporated into their energy sources for protein synthesis. This type of labeling was first reported by Oda *et al.* by incorporating heavy nitrogen into yeast's only nitrogen source ammonium persulfate in the yeast cell culture medium to generate labeled proteins.[25] The approach was expanded by Mann's group into mammalian cell culture system, with the invention of stable isotope labeled by amino acids (SILAC).[26] Instead of heavy nitrogen, ^{13}C lysine and arginine were incorporated into the culture media and incorporated into the cellular proteins. This guarantees that when the sample is enzymatically digested by trypsin after protein extraction that every protein fragment will have a heavy isotope incorporated. Thus, heavy and light labeled samples from two different biological conditions can be paired (*e.g.*, mixed) for analysis in the same run and distinguished by a mass difference of Daltons (Da) at the MS1 level. Since some cells are able to convert arginine into proline, accounting for the possibility of heavy prolines is recommended.[27] Typically, it takes about 5+ passages to obtain >90% incorporation in cells lines, which can take a significant amount of culturing time without 100% efficiency achieved.[26] Luckily, because labeling occurs at the protein synthesis stage, there is very little room for sample processing errors and therefore little quantitation bias. This metabolic method, unlike label-free quantitation, is very sensitive to small changes in protein levels or post-translational modifications between biological conditions, and it shows popularity in the

literature.[8, 9, 28] This technique has been applied to higher organisms, such as mice and plants, although the incorporation of the heavy isotopes varies greatly depending of which tissue of interest.[5, 6, 29] By utilizing a SILAC labeled mouse, researchers were able to study kindling-3 and its role in red blood cell function.[5] Researchers have been creative to devise new ways to utilize SILAC, such as a super-SILAC where a standard is SILAC labeled and mixed with several different biological systems.[30]

Compared to others, multiplexing for SILAC-based techniques has been limited to duplex or triplex due to the bioavailability of amino acids for incorporating isotope.[31] Researchers developed a new methodology based on the idea of mass defect, or that the neutron-binding energies of stable isotopes are different from each other.[32, 33] Thus, only when examined with high resolution, a small mass difference (mDa) can be discerned when comparing two different molecular isotopes (*e.g.*, heavy nitrogen vs. deuterium). By switching different isotopes, smaller (mDa) spacings can be achieved, allowing for higher multiplexing without an increase in spectral complexity. Termed "neutron-encoding" (NeuCode) by Coon and coworkers, NeuCode SILAC has expanded multiplexing for metabolic labeling up to 18-plex.[34, 35] The literature has shown its use for only 4- or 3-plex analysis.[36, 37] Evidently, NeuCode-based systems require the most advanced technology for their use, which means that the market of researchers that can use NeuCode SILAC could be limited.

Compared to metabolic labeling, isotopic chemical labeling is commonly used for samples that cannot be metabolically labeled, including biological fluids and tissues samples.[2, 10, 11, 38, 39] Instead of labeling prior to the start of protein collection, the extracted, digested proteins are chemically or enzymatically labeled with a combination of isotopes, commonly with the addition of a presynthesized tag.[32, 40-42] Just like in the metabolic labeling, the samples are then

mixed analyzed in a single mass spectrometry run, although relative comparisons can be done at the MS1 or MS/MS level, both of which will be discussed.

One chemical isotopic labeling strategy (*i.e.*, mass difference) relies on mass differences at the MS1 level, just like metabolic labeling. ^{18}O enzymatic labeling is one of the simplest methods available and still used regularly.[7, 39, 43] Incubation with ^{18}O water causes an exchange of any oxygen on the C-terminus with heavy isotopes. Biological systems, such as proteins in neurons, can be analyzed as doublets in the MS1 spectra.[39] While back exchange can occur, rapid analysis can help. Another commonly used isotopic labeling technique uses formaldehyde coupled with a reducing agent (*e.g.*, sodium cyanoborohydride or borane pyridine complex) to label amines with isotopically enriched methyl groups.[44, 45] Primary amines, which all digested peptides have at the N-terminus, are all easily labeled with two methyl groups. For the duplex or triplex version, a mass difference of 4 Da is seen between labeled samples, whereas the 4- and 5-plex have spacings of 2 Da in the spectrum if two methyl groups are added.[46, 47] This type of labeling has been useful in our lab for crustacean peptidomic studies, but it is also very popular in other groups.[45, 48-51] In general, this method is easy to use, fast, requires little to no clean up, and is relatively cheap compared with other labeling techniques.

In terms of chemical labeling, the synthesis and/or purchasing of tags is also common for further multiplexing as it allows the addition of more isotopes into analysis. At the MS1 level, isotopic-coded affinity tag (ICAT) is a commercially available tag.[41] Its major limitation is that it requires a free thiol from a cysteine for reaction, limiting its use to cysteine rich systems, such as aging human or mouse eyes, or targeted protein analysis.[41, 52] Isotope-coded protein labeling (ICPL), on the other hand, targets lysine residues (*i.e.*, primary amines), although this technique was developed for triplex intact protein analysis.[53] Another commercial option is “mass

differential tags for relative and absolute quantitation" (mTRAQ) provides options up to triplex comparison with either 4 or 8 Da spacings between labels by targeting amine-containing peptides.[54] mTRAQ can also be used for absolute quantitation using an internal standard, which will be discussed further below.[42]

MS1 level quantitation techniques have also been developed to reduce the sample complexity and multiplexing by utilizing mass defect.[55] By linking several amino acids together so that several isotopes can be incorporated, Coon and coworkers developed a NeuCode chemical tag as a proof-of-principle system, although the large tag size and structure makes it impractical for large-scale protein analysis.[56] To compare and expand on this work, our lab has developed a new amine-reactive tag entitled dimethyl pyrimidinyl ornithine (DiPyrO).[57] Going up to 8-plex analysis, this tag boasts the mass differences between tags that can be analyzed by lower end mass spectrometers, unlike most of the NeuCode-based labeling systems.[34, 35, 56] This would require the proteome samples being digested by LysC, which means primary amines will be at both N- and C-terminus, allowing for double labeling to occur. This idea could be applied to all amine-reactive tags, although DiPyrO's unique mass differences make it particularly useful. Mass defect N, N-dimethyl leucine (mdDiLeu) has also provided a low cost, duplex method for accurate quantitation at the MS1 level.[58] It has even been applied to studying the proteomic and metabolomics in pancreatic cancer cells.[58] In many cases, these mass defect-based tags also increase proteome coverage compared to its counterparts. This is due to the fact that at lower resolution, these multiplets look like one peak, and they will be sampled as such for MS/MS. With higher mass differences, different peaks that may correspond to the same peptide can both be sampled.[59] Then, lower abundance peaks may be missed due to the instrument's duty cycle.

To avoid double sampling, protein quantitation can also be done at the MS/MS level. Also known as isobaric labeling, labeled peptides from different samples will co-elute and ionize together, appearing to having the same mass in the MS1 spectra. Then, when the mass of interest is selected for fragmentation, characteristic reporter ions are generated, usually in the low mass range, which can be compared for relative abundance with their intensity and then mapped back to the corresponding biological sample. With a simpler MS1 spectra, better proteomic coverage can be achieved, although a peptide is not able to be quantified unless selected for fragmentation. These tags can suffer from reporter ion ratio distortion caused by co-isolation of inferring, isobaric ions, although the use of MS3 or Multinotch MS3 can alleviate this.[60, 61] All of the tags developed have similar structures that include a reporter group, a balance group, and a reactive group [40, 41]. Reactive group dictates what functional group of a molecule is targeted, although amines are the most common with the use of triazine and N-hydroxysuccinamide esters.[32, 40] The reporter group is produced during MS/MS and enables relative quantitation. Finally, the balance group is the group that allows for the differentially labeled samples to be the same mass at the MS1 level. Isotopes are incorporated on both the reporter and balance group, although careful considerations should be made when determining their positions.

Several commercial tags exist with various amounts of multiplexing. “Isobaric tags for relative and absolute quantitation” (iTRAQ) and tandem mass tags (TMT) are the most prominent in the literature.[2, 10, 32, 62, 63] iTRAQ varies from 4- to 8-plex depending on the experimental needs of the researcher.[63] Unfortunately, these tags can only target the amines in the peptide. TMT, on the other hand, has variations that can label amines, cysteines, and carbonyl groups, although only the amine-specific tags can multiplex beyond 6-plex.[32, 62] Amine-

reactive TMT packages vary from 2- to 11-plex. Unfortunately, both iTRAQ and TMT can be quite expensive, running from hundreds to a few thousand dollars per experiment.

In order to fill a void in the research community, our lab has been heavily involved in developing new isobaric tags for MS analysis that are more cost effective (*i.e.*, <$10 per experiment).[40, 64-66] Back in 2010, we published our first set of tags entitled N, N-dimethyl leucine (DiLeu), which was originally developed as a 4-plex system.[40] Recently, this has been used to quantitatively study the proteome of men affected by lower urinary tract symptoms (LUTS).[11] By dimethylating the amino acid leucine, we were able to incorporate isotopes easily, cheaply, and quickly into the starting reagents. Thus, unlike most tags, these can be synthesized easily in a researcher's lab with high purity. Over the years, we have expanded DiLeu's multiplexing to 8- and 12-plex, by using either an extended balance group or mass defect technology, respectively.[64, 67] A detailed book chapter exist for the synthesis and use of the 12-plex version of DiLeu.[68] While MS1 is shown to be more accurate, mdDiLeu, as discussed above, can also be used for MS/MS-based quantitation if lower resolution is required (**Figure 1**).[58] In fact, the duplex tag set is actually two of the tags from the 12-plex set, so the protocol references above can also be utilized for mdDiLeu.[58, 64] This is due to the small (20.5 mDa) spacings between DiLeu 115a and 118d, which is not visible until the development and implementation of higher resolution instrumentation such as the Orbitrap. It should be noted that the modest size of DiLeu is a benefit, as it does not produce interfering fragmentation species that can impede peptide and/or protein identification. Our lab has also chosen to delve into other amino acids beyond leucine, such as alanine and valine.[65] Even DiPyrO, which is discussed above, is a modified and dimethylated form of arginine.[57] N, N-dimethyl alanine (DiAla) and N, N-dimethyl valine (DiVal) have both been synthesized, although only DiAla was shown to be

effective of 100% labeling of tryptic peptides.[65] The methodology behind synthesis and labeling of both tags are described in a later section. In combination, the 4-plex of both DiLeu and DiAla were used to study the proteomics of the TGF-beta/Smad3 signaling pathway, as these tags provide complementary proteomic coverage.[65] It should be noted that the same extended balance group and mass defect strategy used for DiLeu can be applied to DiAla to increase multiplexing, although DiLeu produces better MS/MS spectra for protein identification over DiAla.[65]

When it comes to incorporating stable isotopes, increasing spectral complexity is a concern, especially when the difference between the conditions is only a few Da. Obviously, mass defect has been utilized to alleviate this, but the need for advanced technology limits its widespread use.[55] Furthermore, isotopic interference also can be a concern even with mass defect, although several researchers have developed methods to correct for this isotopic post-data collection [64]. Furthermore, the isotope or tag addition can cause elution differences. For example, the "deuterium effect" is well documented in the literature.[69, 70] Advanced computational algorithms should be utilized whenever possible to provide accurate quantitation.[71-73] Finally, when comparing all these different types of tags, each focuses on different functional groups within a protein sequence (*e.g.*, free amines and cysteine). While this can reduce the sample complexity, it will also limit the protein sequence coverage and quantitative capacity. Thus, when choosing the appropriate quantitation strategy, the structure of the targets should be considered carefully.

Absolute Quantitation

Relative quantitation is very important first step for determining biomarkers in diseases. Especially by using LC-MS, hundreds of proteins can be screened for a possible target protein. After validation with a more targeted assay, such as Western blot, absolute quantitation of the

possible biomarker is the next step.[65] Classically, the two accepted methods for absolute quantitation that apply to mass spectrometry are the use of an internal standard or building a calibration curve.

One of the more popular techniques for absolute quantitation is the use of a heavy peptide standard, where the heavy peptide is spiked into a protein digest. The mixture can then be analyzed at the MS1 level by XIC comparison or by constructing a calibration curve by selected reaction monitoring (SRM) or multiple reaction monitoring (MRM), also known as the absolute quantitation (AQUA) strategy.[74, 75] Bozzacco *et al.* has utilized this strategy for studying peptides present on MHC II molecules in the mouse spleen.[76] It should be noted that SRM only selects for one ion, while MRM selects for two (*i.e.*, both the peptide signal and the spiked heavy standard) and compares selected ions in the MS/MS spectra to absolutely quantify the ion of interest. It should be noted that MRM experiments are typically performed with triple quadrupole instruments due to their selectivity and sensitivity.[77] In general, AQUA grade peptides can be costly, and it is suggested that researchers work with low quality, crude peptide during the method developmental phase. The idea of using a standard peptide can also be applied without the need for expensive heavy isotope-encoded peptides. By utilizing any of the variety of tags above (*e.g.*, mTRAQ and mdDiLeu), one channel is labeled with the standard of interest, and the sample of interest is labeled with another channel.[78, 79] Simply, a duplex labeling strategy is appropriate if only one sample needs to be quantitated. Expanding this thought, since several of these labeling systems have multiple channels, several samples can be absolutely quantitated in a single run. While popular, this technique can be inaccurate since only one point is used as a reference for quantitation.

In comparison, calibration curves tend to be a more accurate method for absolute quantitation due to the use of multiple points. The same strategy can be used above in this case, although the standard peptide (heavy or normal) is utilized as more of a normalization factor than a quantitative marker. In this case, using the duplex labeling strategy outlined in the above paragraph as an example, a ratio is calculated for each standard concentration infused into the mass spectrometer (heavy/light). Then, after building the calibration curve, instead of labeling the concentration of interest using the light channel, the sample of interest is labeled. After infusion of this new mixture, the ratio is then fit to the calibration curve previously generated. Instead of labeling, a heavy version of the peptide can also be used.[80] This is very common, but the generation of the calibration curve from different runs is less than ideal and leads to inaccuracy. Care should also be taken when creating the calibration curve, as the standards should be placed in a matrix similar to that of the sample of interest. Our lab has developed a new strategy entitled isotopic *N, N*-dimethyl leucine (iDiLeu), which is a MS1-based quantitative tag derivative from our amine-reactive DiLeu family.[66] As a 5-plex labeling strategy, one channel will be labeled with the sample of interest. Then, the four other channels are labeled with varying concentrations of the standard of interest. Once the sample and these labeled standards are mixed, an XIC-based calibration curve will then be generated in a single MS run.[66] A detailed protocol for its synthesis and use is described elsewhere.[81] This same strategy has also been performed at the MS/MS level using TMT to study proteins in human CSF post-mortem.[82] While the main purpose of these tags is absolute quantitation, iDiLeu can also be used for relative comparison, without the concern of co-isolation and co-fragmentation like DiLeu enabled isobaric quantitation. iDiLeu can also be easily and cheaply synthesized in lab, and a detailed protocol for their synthesis is available elsewhere.

Conclusions and Future Directions

Quantitative proteomics is a field that is booming with new technology due to the need for knowledge about chemical perturbation on a global scale. Label-free will always be an option, but the majority of advancements have been on the incorporation of stable isotopes. While commercial options exist for all the labeling strategies above, our lab has created low cost options that can make these techniques more available and accessible to researchers, and a decision tree for choosing an appropriate dimethylated amino acid system is shown in **Figure 2**. While this review has focused on their use for quantitative proteomics, all the tag systems described can be applied to other biologically-relevant molecular species. For example, amine-containing metabolites are an easy target for any of the amine-reactive tags described and theoretically improve their separation, as shown with DiLeu and mdDiLeu.[58, 83] Post-translational modifications can also be a focus, such as phospho- or glyco-proteins.[16, 84] Furthermore, the continued use of these tags also can span into different separations beyond LC, such as CE and ion mobility.[83, 85] Continued developments in technology will only inspire new tag development and increase multiplexing, possibly making label-free obsolete.

Methodology

Materials

a. Alanines: L-alanine (Cambridge Isotope Laboratories Inc. (Tewksbury, MA)) and L-alanine-1-^{13}C, ^{15}N (Cambridge Isotope Laboratories Inc.)
b. Valines: L-valine (Cambridge Isotope Laboratories Inc.) and L-valine-1-^{13}C, ^{15}N (Cambridge Isotope Laboratories Inc.)
c. Isotopic waters: 97% $H_2{}^{18}O$ (Cambridge Isotope Laboratories Inc.) and D_2O (ISOTEC, Miamisburg, OH)
d. Hydrogen Chloride (HCl) gas (Sigma Aldrich, St. Louis, MO)
e. MP-Carbonate (Biotage, Charlotte, NC)
f. Isotopic formaldehydes: 37% CH_2O (Sigma Aldrich) and 20% C^2H_2O (ISOTEC)

g. Isotopic sodium cyanoborohydrides: $NaBH_3CN$ (Sigma-Aldrich) and $NaBD_3CN$ (Sigma-Aldrich)
h. Büchi RE 111 Rotovapor (Flawil, Switzerland)
i. Ninhydrin (Sigma-Aldrich)
j. Flash Chromatography Column (Ace Glass, Vineland, NJ)
k. Silica gel, 40-63 μm particle size (Silicycle (Quebec City, Quebec, Canada))
l. ACS grade dicholormethane (DCM, Fisher Scientific)
m. ACS grade methanol (MeOH, Fisher Scientific)
n. Anhydrous dimethylformamide (DMF, Sigma Aldrich)
o. 4-(4-6-Dimethoxy-1,3,5-triazin-2-yl)-4-methyl-morpholinium tetrafluoroborate (DMTMM, Sigma-Aldrich)
p. 1 M triethylammonium bicarbonate buffer (TEAB, Sigma-Aldrich)
q. N-Methylmorpholine (NMM, TCI America (Tokyo, Japan))
r. 50% aq. Solution hydroxylamine (Alfa Aesar (Ward Hill, MA))
s. Savant SC 110 SpeedVac (Thermo Scientific)
t. Strong cation exchange (SCX) spintips and buffers (Protea Biosciences (Morgantown, WV))
u. C_{18} OMIX tips (Agilent Technologies (Santa Clara, California))
v. Optima grade formic acid (FA, Fisher Scientific)
w. Optima grade water (Fisher Scientific)
x. Optima grade acetonitrile (ACN, Fisher Scientific)
y. *e.g.* NanoAcquity UPLC system (Waters) (see *Note 27*)
z. Q-Exactive Orbitrap (Thermo Scientific) (see *Note 28*)
aa. Proteome Discoverer 1.4 (Thermo Scientific) (see *Note 29*)

Methods

1.) Tag Synthesis (See *Note 1*)
    a. ^{18}O Exchange
        i. Dissolve alanine or valine isotopic variant into HCl (g) acidified $H_2{}^{18}O$ over heat (see *Note 2-4*)
        ii. Stir at 65°C overnight (see *Note 5*).
        iii. Evaporate HCl using Rotavapor and MeOH washes (see *Note 6*).
        iv. Scavenger remaining acid using MP-carbonate beads by shaking for 3+ hours (see *Note 7 and 8*).
        v. Dry down reaction using Rotovapor.
    b. Dimethylation

Depending on the end goal, the appropriate isotopic version of the amino acids and other starting reagents are outlined in **Figure 3**.

        i. Suspend alanine or valine isotopic variant in H_2O or D_2O with a 2.5x molar excess of $NaBH_3CN$ or $NaBD_3CN$ (see *Note 9*).
        ii. Stir the reaction vial in a hood on an ice water bath.
        iii. Add 2.5x molar excess CH_2O or C^2H_2O to the vial and allow to stir till the reaction is complete (see *Note 10* and *11*).
        iv. Dry down reaction using Rotovapor.
        v. Purify label using a flash column (DCM/Meth) (see *Notes 12, 13, and 14).*

2.) Multiplexed Labeling (see *Notes 15, 16,* and *17*)

a. Tag Activation
    i. Dissolve each 1 mg tag aliquot in anhydrous DMF with a 0.7x molar ratio of DMTMM and NMM (see *Note 18*).
    ii. Vortex solution at room temperature for 60 minutes (see *Note 19*).
    iii. Spin down excess, unactivated label (see *Note 20*).
b. Labeling
    i. Resuspend peptide sample of interest in 0.5 M TEAB.
    ii. Add 10x (w/w) excess of activated label supernatant to the sample (see *Note 21*).
    iii. Add DMF till the organic: aqueous ratio is ~70%.
    iv. Vortex the mixture at room temperature for 2 hours (see *Note 22*).
    v. Quench the reaction to a final concentration of 0.25% (v/v) hydroxylamine.
    vi. Combine peptide channels of interest 1:1 ratios of all channels.
    vii. Dry down samples for further processing in Speedvac.
c. Sample Clean Up
    i. Remove tag reagent byproducts by performing clean up using the SCX spin tips, following the manufacturer's outlined protocol (see *Note 23*).
    ii. Dry down sample in Speedvac.
    iii. Desalt labeled peptides with C18 OMIX tips (see *Note 24*).
    iv. Dry down sample in Speedvac.

3.) Instrumental and Data Analysis

Each set of tags (4-plex DiLeu, 12-plex DiLeu, 4-plex DiAla, 5-plex iDiLeu, and 2-plex mdDiLeu) has unique instrument parameters required. Major instrument considerations will be included below, but other considerations (*e.g.*, LC gradients) should be made for the specific sample and/or consulted from the publications.

a. Dissolved mixed samples in Optima grade 0.1% FA (v/v) (Solvent A).
b. Perform a reversed-phase separation using a home-packed column (15-16 cm) in line with a commercial liquid chromatography system connected to a mass spectrometer (see *Note 25*).
c. Identify and quantify proteins using appropriate software (see *Note 26*).

Notes

1. This chapter will focus on the synthesis of DiVal and DiAla, as detailed chapters already exist for 12-plex (which includes mdDiLeu and the original 4-plex) and isotopic DiLeu [68, 81]. In general, similar synthesis techniques are utilized; the major difference is the starting reagents required.

2. In this case, the optimal ratio of acidified ^{18}O water to amino acid (μL/mg) is ~5:1.

3. Since the system is under heat, the use of a vented vial (*e.g.*, with a pre-cut septum) is recommended.
4. The amino acid will not fully dissolve in the water until the appropriate heat level is reached. A heat gun can be used to gently help this process.
5. Depending on the amino acid, the time required varies from 4 hours to 24 hours to complete ^{18}O exchange on all available oxygen. The exchange of only one oxygen is necessary if doing quantitation at the MS/MS level, as the second oxygen fragments off and does not affect the reporter ion. But, if you are doing MS1-based quantitation, longer ^{18}O exchange times are recommended.
6. A "sharp" smell will come from the sample if acid is present. Washes are recommended to be done till this smell disappears.
7. The optimal ratio of MP-carbonate beads to acidified ^{18}O water (mg/μL) is ~2:1.
8. After proper deacidification, an obvious precipitate should have formed in the mixture. This is the basic form of the amino acid. If a precipitate has not formed, the mixture can be shaken longer or more beads can be added to the system to improve odds of precipitation.
9. The addition of formaldehyde causes the production of heat in the system. The use of vented vial (*e.g.*, pre-cut septum) is recommended.
10. During the demethylation process, a precipitate may form.
11. Depending on the amino acid and purity of the reagents, this reaction may take between 30 minutes to 3 hours. It can be checked with a ninhydrin stain to determine if the reaction is complete. If the reaction is complete, the spot should appear white (*i.e.*, no free amines present).

12. The following conditions were used for fractionate the DiVal and DiAla tags (in mL) with a ~2.5 cm diameter flash column:

DCM	MeOH
150	0
360	40
160	40
140	60
120	80

Fractions should be collected on the 140/60 (DCM/MeOH) elution [65].

13. A $KMnO_4$ stain should be used to determine which fractions of the flash column contain the most sample. All chosen fractions can then be dried down and aliquoted for future use (see *Note 14*).
14. For convenience, each inactivated tag is placed into tubes in one mg aliquots.
15. Depending on the needs of your experiments, a variety of tag options exist. **Figure 2** shows a decision tree for choosing the best tags to answer your biological question from those that have been developed with dimethylated amino acids from our group, and all tag structures are shown in **Figure 4**. All the labels highlighted follow a similar activation protocol.
16. DiVal was found to not label completely and was discarded as a future labeling strategy for peptidomic applications [65].

17. While this chapter focuses on its applications to proteomics (*e.g.*, tryptic peptides), these tags are capable of labeling any molecule with a primary amine, including endogenous peptides [66] or amine-containing metabolites [83].
18. The tags are not fully activated in order to consume all added DMTMM, which can cause unwanted side reactions.
19. Optimal activation time varies depending on the tag system and molecule of interest.
20. It is best to use the activated label immediately, as over time it will break down due to water production.
21. Depending on the molecule of interest and labeling times, the optimal ratio of label-to-peptide can range from 5x to 25x.
22. Optimal labeling time varies depending on the tag system and molecule of interest.
23. The manufacturer provides two protocols. Simple samples can use the supplied "elution" solution, but more complex samples have the option of being fractionated with the spintips. Furthermore, if they spintips do not provide adequate separation or binding capacity, a HPLC system can be utilized instead for proper SCX clean up.
24. If the binding capacity of the OMIX tips is not enough, a Water SepPak system can be used as an alternative desalting method.
25. Due to the resolution requirements of each tag system, the appropriate mass spectrometer should be chosen with care. For example, the 4-plex reagents (*i.e.*, DiLeu, DiVal, and DiAla) can be visualized at a 15K resolution at the MS/MS level, but the 12-plex DiLeu requires 60K [64, 65]. Another example can be seen with iDiLeu and mdDiLeu, which need 140K and 240K, respectively, at the MS1 level [58, 66]. In general, most of these tag systems require an Orbitrap system.

26. While most can be easily identified and quantified with commercial software, mdDiLeu requires a software package designed for high resolution mass spectrometry, such as MaxQuant.

Acknowledgements

This work was supported in part by the National Institutes of Health (NIH) grants R01 DK071801, S10RR029531, P41GM108538, and the University of Wisconsin-Madison, Office of the Vice Chancellor for Research and Graduate Education with funding from the Wisconsin Alumni Research Foundation. L.L. acknowledges a Vilas Distinguished Achievement Professorship and Janis Apinis Professorship with funding provided by the Wisconsin Alumni Research Foundation and University of Wisconsin-Madison School of Pharmacy. A.R.B. would like to thank the NIH for a General Medical Sciences NRSA Fellowship (1F31GM119365-01).

Conflicts of Interest

The authors have declared no conflict of interest.

References

1. Aebersold, R.; Mann, M., *Nature* **2003,** *422* (6928), 198-207.

2. Plubell, D. L.; Wilmarth, P. A.; Zhao, Y. Q.; Fenton, A. M.; Minnier, J.; Reddy, A. P.; Klimek, J.; Yang, X.; David, L. L.; Pamir, N., *Molecular & Cellular Proteomics* **2017,** *16* (5), 873-890.

3. Reinders, J.; Zahedi, R. P.; Pfanner, N.; Meisinger, C.; Sickmann, A., *Journal of Proteome Research* **2006,** *5* (7), 1543-1554.

4. Johansson, C.; Samskog, J.; Sundstrom, L.; Wadensten, H.; Bjorkesten, L.; Flensburg, J., *Proteomics* **2006,** *6* (16), 4475-4485.

5. Kruger, M.; Moser, M.; Ussar, S.; Thievessen, I.; Luber, C. A.; Forner, F.; Schmidt, S.; Zanivan, S.; Fassler, R.; Mann, M., *Cell* **2008,** *134* (2), 353-364.

6. Lewandowska, D.; ten Have, S.; Hodge, K.; Tillemans, V.; Lamond, A. I.; Brown, J. W. S., *Plos One* **2013,** *8* (8), 8.

7. Zhang, W. L.; Long, J.; Zhang, C.; Cai, N. X.; Liu, Z. H.; Wang, Y.; Wang, X. C.; Chen, P.; Liang, S. P., *Journal of Mass Spectrometry* **2014,** *49* (5), 400-408.

8. Wang, M. C.; Tian, F.; Ying, W. T.; Qian, X. H., *Scientific Reports* **2017,** *7*, 17.

9. Zhang, C. H.; Zhai, Z. C.; Tang, M.; Cheng, Z. Y.; Li, T. T.; Wang, H. Y.; Zhu, W. G., *Proteomics* **2017,** *17* (13-14), 12.

10. Lin, J. P.; Wu, Y. S.; Han, B.; Chen, Y.; Wang, L. Q.; Li, X. L.; Liu, M. J.; Huang, J. C., *Theriogenology* **2017,** *101*, 99-108.

11. Greer, T.; Hao, L.; Nechyporenko, A.; Lee, S.; Vezina, C. M.; Ricke, W. A.; Marker, P. C.; Bjorling, D. E.; Bushman, W.; Li, L. J., *Plos One* **2015,** *10* (8), 20.

12. Angel, T. E.; Aryal, U. K.; Hengel, S. M.; Baker, E. S.; Kelly, R. T.; Robinson, E. W.; Smith, R. D., *Chemical Society Reviews* **2012,** *41* (10), 3912-3928.

13. Dong, Q.; Yan, X. J.; Liang, Y. X.; Stein, S. E., *Journal of Proteome Research* **2016,** *15* (5), 1472-1486.

14. Neilson, K. A.; Ali, N. A.; Muralidharan, S.; Mirzaei, M.; Mariani, M.; Assadourian, G.; Lee, A.; van Sluyter, S. C.; Haynes, P. A., *Proteomics* **2011,** *11* (4), 535-553.

15. Chelius, D.; Bondarenko, P. V., *Journal of Proteome Research* **2002,** *1* (4), 317-323.

16. Wang, J. X.; Cunningham, R.; Zetterberg, H.; Asthana, S.; Carlsson, C.; Okonkwo, O.; Li, L. J., *Proteomics Clinical Applications* **2016,** *10* (12), 1225-1241.

17. Kultima, K.; Nilsson, A.; Scholz, B.; Rossbach, U. L.; Falth, M.; Andren, P. E., *Molecular & Cellular Proteomics* **2009,** *8* (10), 2285-2295.

18. Schilling, B.; Rardin, M. J.; MacLean, B. X.; Zawadzka, A. M.; Frewen, B. E.; Cusack, M. P.; Sorensen, D. J.; Bereman, M. S.; Jing, E. X.; Wu, C. C.; Verdin, E.; Kahn, C. R.; MacCoss, M. J.; Gibson, B. W., *Molecular & Cellular Proteomics* **2012,** *11* (5), 202-214.

19. Nahnsen, S.; Bielow, C.; Reinert, K.; Kohlbacher, O., *Molecular & Cellular Proteomics* **2013,** *12* (3), 549-556.

20. Tsou, C. C.; Tsai, C. F.; Tsui, Y. H.; Sudhir, P. R.; Wang, Y. T.; Chen, Y. J.; Chen, J. Y.; Sung, T. Y.; Hsu, W. L., *Molecular & Cellular Proteomics* **2010,** *9* (1), 131-144.

21. Liu, H. B.; Sadygov, R. G.; Yates, J. R., *Analytical Chemistry* **2004,** *76* (14), 4193-4201.

22. Kolbach-Mandel, A. M.; Mandel, N. S.; Hoffmann, B. R.; Kleinman, J. G.; Wesson, J. A., *Urolithiasis* **2017,** *45* (4), 337-346.

23. Shinoda, K.; Tomita, M.; Ishihama, Y., *Bioinformatics* **2010,** *26* (4), 576-577.

24. Megger, D. A.; Bracht, T.; Meyer, H. E.; Sitek, B., *Biochimica Et Biophysica Acta-Proteins and Proteomics* **2013,** *1834* (8), 1581-1590.

25. Oda, Y.; Huang, K.; Cross, F. R.; Cowburn, D.; Chait, B. T., *Proceedings of the National Academy of Sciences of the United States of America* **1999,** *96* (12), 6591-6596.

26. Ong, S. E.; Blagoev, B.; Kratchmarova, I.; Kristensen, D. B.; Steen, H.; Pandey, A.; Mann, M., *Molecular & Cellular Proteomics* **2002,** *1* (5), 376-386.

27. Bendall, S. C.; Hughes, C.; Stewart, M. H.; Doble, B.; Bhatia, M.; Lajoie, G. A., *Molecular & Cellular Proteomics* **2008,** *7* (9), 1587-1597.

28. Hummon, A.; LaBonia, G. J., *Molecular & Cellular Proteomics* **2017,** *16* (8), S13-S13.

29. Zanivan, S.; Krueger, M.; Mann, M., In Vivo Quantitative Proteomics: The SILAC Mouse. In *Integrin and Cell Adhesion Molecules: Methods and Protocols*, Shimaoka, M., Ed. Humana Press Inc: Totowa, 2011; Vol. 757, pp 435-450.

30. Geiger, T.; Cox, J.; Ostasiewicz, P.; Wisniewski, J. R.; Mann, M., *Nature Methods* **2010,** *7* (5), 383-U64.

31. Mann, M., *Nature Reviews Molecular Cell Biology* **2006,** *7* (12), 952-958.

32. McAlister, G. C.; Huttlin, E. L.; Haas, W.; Ting, L.; Jedrychowski, M. P.; Rogers, J. C.; Kuhn, K.; Pike, I.; Grothe, R. A.; Blethrow, J. D.; Gygi, S. P., *Analytical Chemistry* **2012,** *84* (17), 7469-7478.

33. Zhou, Y.; Shan, Y. C.; Wu, Q.; Zhang, S.; Zhang, L. H.; Zhang, Y. K., *Analytical Chemistry* **2013,** *85* (22), 10658-10663.

34. Merrill, A. E.; Hebert, A. S.; MacGilvray, M. E.; Rose, C. M.; Bailey, D. J.; Bradley, J. C.; Wood, W. W.; El Masri, M.; Westphall, M. S.; Gasch, A. P.; Coon, J. J., *Molecular & Cellular Proteomics* **2014,** *13* (9), 2503-2512.

35. Rhoads, T. W.; Rose, C. M.; Bailey, D. J.; Riley, N. M.; Molden, R. C.; Nestler, A. J.; Merrill, A. E.; Smith, L. M.; Hebert, A. S.; Westphall, M. S.; Pagliarini, D. J.; Garcia, B. A.; Coon, J. J., *Analytical Chemistry* **2014,** *86* (5), 2314-2319.

36. Rhoads, T. W.; Prasad, A.; Kwiecien, N. W.; Merrill, A. E.; Zawack, K.; Westphall, M. S.; Schroeder, F. C.; Kimble, J.; Coon, J. J., *Molecular & Cellular Proteomics* **2015,** *14* (11), 2922-2935.

37. Baughman, J. M.; Rose, C. M.; Kolumam, G.; Webster, J. D.; Wilkerson, E. M.; Merrill, A. E.; Rhoads, T. W.; Noubade, R.; Katavolos, P.; Lesch, J.; Stapleton, D. S.; Rabaglia, M. E.; Schueler, K. L.; Asuncion, R.; Domeyer, M.; Zavala-Solorio, J.; Reich, M.; DeVoss, J.; Keller, M. P.; Attie, A. D.; Hebert, A. S.; Westphall, M. S.; Coon, J. J.; Kirkpatrick, D. S.; Dey, A., *Cell Reports* **2016,** *16* (2), 583-595.

38. Choe, L.; D'Ascenzo, M.; Relkin, N. R.; Pappin, D.; Ross, P.; Williamson, B.; Guertin, S.; Pribil, P.; Lee, K. H., *Proteomics* **2007,** *7* (20), 3651-3660.

39. Hashimoto, M.; Bogdanovic, N.; Nakagawa, H.; Volkmann, I.; Aoki, M.; Winblad, B.; Sakai, J.; Tjernberg, L. O., *Journal of Cellular and Molecular Medicine* **2012,** *16* (8), 1686-1700.

40. Xiang, F.; Ye, H.; Chen, R. B.; Fu, Q.; Li, L. J., *Analytical Chemistry* **2010,** *82* (7), 2817-2825.

41. Gygi, S. P.; Rist, B.; Gerber, S. A.; Turecek, F.; Gelb, M. H.; Aebersold, R., *Nature Biotechnology* **1999,** *17* (10), 994-999.

42. Kang, U. B.; Yeom, J.; Kim, H.; Lee, C., *Journal of Proteome Research* **2010,** *9* (7), 3750-3758.

43. Hicks, W. A.; Halligan, B. D.; Slyper, R. Y.; Twigger, S. N.; Greene, A. S.; Olivier, M., *Journal of the American Society for Mass Spectrometry* **2005,** *16* (6), 916-925.

44. Kovanich, D.; Cappadona, S.; Raijmakers, R.; Mohammed, S.; Scholten, A.; Heck, A. J. R., *Analytical and Bioanalytical Chemistry* **2012,** *404* (4), 991-1009.

45. Chen, R. B.; Xiao, M. M.; Buchberger, A.; Li, L. J., *Journal of Proteome Research* **2014,** *13* (12), 5767-5776.

46. Boersema, P. J.; Aye, T. T.; van Veen, T. A. B.; Heck, A. J. R.; Mohammed, S., *Proteomics* **2008,** *8* (22), 4624-4632.

47. Wu, Y.; Wang, F. J.; Liu, Z. Y.; Qin, H. Q.; Song, C. X.; Huang, J. F.; Bian, Y. Y.; Wei, X. L.; Dong, J.; Zou, H. F., *Chemical Communications* **2014,** *50* (14), 1708-1710.

48. Zhang, Y.; Buchberger, A.; Muthuvel, G.; Li, L., *Proteomics* **2015**.

49. Valdes, A.; Garcia-Canas, V.; Artemenko, K. A.; Simo, C.; Bergquist, J.; Cifuentes, A., *Molecular & Cellular Proteomics* **2017,** *16* (1), 8-22.

50. Li, X.; Dai, J. G.; Tang, Y. J.; Li, L. L.; Jin, G., *Marine Drugs* **2017,** *15* (1), 25.

51. Yu, C. L.; Brooks, S.; Li, Y.; Subramanian, M.; Summers, R.; Pope, M., Rapid Proteomics to Prospect and Validate Novel Bacterial Metabolism Induced by Environmental Burden. In *Proteomics in Biology, Pt B*, Shukla, A. K., Ed. Elsevier Academic Press Inc: San Diego, 2017; Vol. 586, pp 379-411.

52. Wang, B. L.; Hom, G.; Zhou, S.; Guo, M. F.; Li, B. B.; Yang, J.; Monnier, V. M.; Fan, X. J., *Aging Cell* **2017,** *16* (2), 244-261.

53. Schmidt, A.; Kellermann, J.; Lottspeich, F., *Proteomics* **2005,** *5* (1), 4-15.

54. Prochazkova, I.; Lenco, J.; Fucikova, A.; Dresler, J.; Capkova, L.; Hrstka, R.; Nenutil, R.; Bouchal, P., *Biochimica Et Biophysica Acta-Proteins and Proteomics* **2017,** *1865* (5), 488-498.

55. Sleno, L., *Journal of Mass Spectrometry* **2012,** *47* (2), 226-236.

56. Hebert, A. S.; Merrill, A. E.; Stefely, J. A.; Bailey, D. J.; Wenger, C. D.; Westphall, M. S.; Pagliarini, D. J.; Coon, J. J., *Molecular & Cellular Proteomics* **2013,** *12* (11), 3360-3369.

57. Frost, D. C.; Buchberger, A. R.; Li, L., *Anal Chem* **2017**.

58. Hao, L.; Johnson, J.; Lietz, C. B.; Buchberger, A.; Frost, D.; Kao, W. J.; Li, L. J., *Analytical Chemistry* **2017,** *89* (2), 1138-1146.

59. Mertins, P.; Udeshi, N. D.; Clauser, K. R.; Mani, D. R.; Patel, J.; Ong, S. E.; Jaffe, J. D.; Carr, S. A., *Molecular & Cellular Proteomics* **2012,** *11* (6), 12.

60. Ting, L.; Rad, R.; Gygi, S. P.; Haas, W., *Nature Methods* **2011,** *8* (11), 937-940.

61. McAlister, G. C.; Nusinow, D. P.; Jedrychowski, M. P.; Wuhr, M.; Huttlin, E. L.; Erickson, B. K.; Rad, R.; Haas, W.; Gygi, S. P., *Analytical Chemistry* **2014,** *86* (14), 7150-7158.

62. Shakir, S.; Vinh, J.; Chiappetta, G., *Analytical and Bioanalytical Chemistry* **2017,** *409* (15), 3821-3830.

63. Wiese, S.; Reidegeld, K. A.; Meyer, H. E.; Warscheid, B., *Proteomics* **2007,** *7* (3), 340-350.

64. Frost, D. C.; Greer, T.; Li, L., *Analytical chemistry* **2015,** *87* (3), 1646-54.

65. Yu, Q.; Shi, X. D.; Greer, T.; Lietz, C. B.; Kent, K. C.; Li, L. J., *Journal of Proteome Research* **2016,** *15* (9), 3420-3431.

66. Greer, T.; Lietz, C. B.; Xiang, F.; Li, L. J., *Journal of the American Society for Mass Spectrometry* **2015,** *26* (1), 107-119.

67. Frost, D. C.; Greer, T.; Xiang, F.; Liang, Z. D.; Li, L. J., *Rapid Communications in Mass Spectrometry* **2015,** *29* (12), 1115-1124.

68. Frost, D. C.; Li, L. J., High-Throughput Quantitative Proteomics Enabled by Mass Defect-Based 12-Plex DiLeu Isobaric Tags. In *Quantitative Proteomics by Mass Spectrometry, 2nd Edition*, Sechi, S., Ed. Humana Press Inc: Totowa, 2016; Vol. 1410, pp 169-194.

69. Turowski, M.; Yamakawa, N.; Meller, J.; Kimata, K.; Ikegami, T.; Hosoya, K.; Tanaka, N.; Thornton, E. R., *Journal of the American Chemical Society* **2003,** *125* (45), 13836-13849.

70. Wade, D., *Chemico-Biological Interactions* **1999,** *117* (3), 191-217.

71. Cox, J.; Mann, M., *Nature Biotechnology* **2008,** *26* (12), 1367-1372.

72. Tyanova, S.; Temu, T.; Cox, J., *Nature Protocols* **2016,** *11* (12), 2301-2319.

73. Mitchell, C. J.; Kim, M. S.; Na, C. H.; Pandey, A., *Molecular & Cellular Proteomics* **2016,** *15* (8), 2829-2838.

74. Gerber, S. A.; Rush, J.; Stemman, O.; Kirschner, M. W.; Gygi, S. P., *Proceedings of the National Academy of Sciences of the United States of America* **2003,** *100* (12), 6940-6945.

75. Brun, V.; Masselon, C.; Garin, J.; Dupuis, A., *Journal of Proteomics* **2009,** *72* (5), 740-749.

76. Bozzacco, L.; Yu, H. Q.; Zebroski, H. A.; Dengjel, J.; Deng, H. T.; Mojsov, S.; Steinman, R. M., *Journal of Proteome Research* **2011,** *10* (11), 5016-5030.

77. Picotti, P.; Aebersold, R., *Nature Methods* **2012,** *9* (6), 555-566.

78. DeSouza, L. V.; Taylor, A. M.; Li, W.; Minkoff, M. S.; Romaschin, A. D.; Colgan, T. J.; Siu, K. W. M., *Journal of Proteome Research* **2008,** *7* (8), 3525-3534.

79. DeSouza, L. V.; Krakovska, O.; Darfler, M. M.; Krizman, D. B.; Romaschin, A. D.; Colgan, T. J.; Siu, K. W. M., *Proteomics* **2010,** *10* (17), 3108-3116.

80. Xu, X.; Roman, J. M.; Issaq, H. J.; Keefer, L. K.; Veenstra, T. D.; Zieger, R. G., *Analytical Chemistry* **2007,** *79* (20), 7813-7821.

81. Greer, T.; Li, L. J., Isotopic N,N-Dimethyl Leucine (iDiLeu) for Absolute Quantification of Peptides Using a Standard Curve Approach. In *Quantitative Proteomics by Mass Spectrometry, 2nd Edition*, Sechi, S., Ed. Humana Press Inc: Totowa, 2016; Vol. 1410, pp 195-206.

82. Dayon, L.; Turck, N.; Kienle, S.; Schulz-Knappe, P.; Hochstrasser, D. F.; Scherl, A.; Sanchez, J. C., *Analytical Chemistry* **2010,** *82* (3), 848-858.

83. Hao, L.; Zhong, X. F.; Greer, T.; Ye, H.; Li, L. J., *Analyst* **2015,** *140* (2), 467-475.

84. Yu, Q.; Shi, X. D.; Feng, Y.; Kent, K. C.; Li, L. J., *Analytica Chimica Acta* **2017,** *968*, 40-49.

85. Sturm, R. M.; Lietz, C. B.; Li, L. J., *Rapid Communications in Mass Spectrometry* **2014,** *28* (9), 1051-1060.

Figures

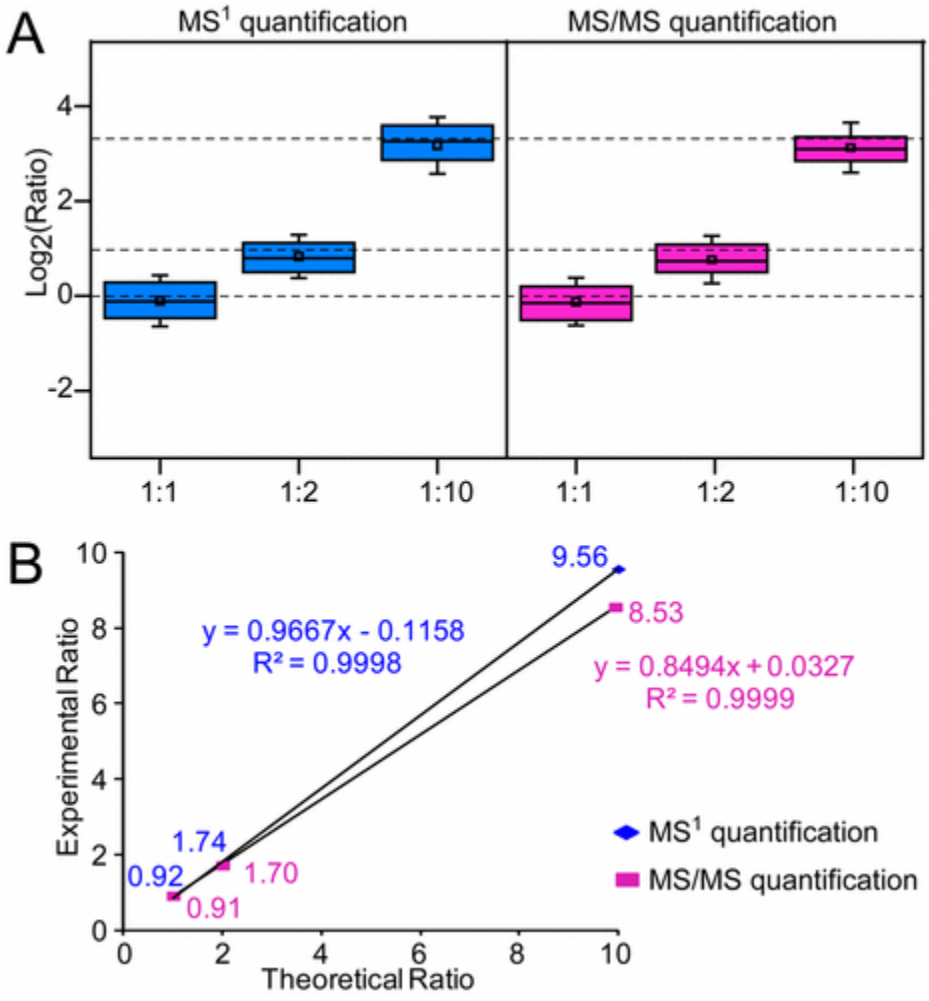

Figure 1. Comparison of MS1 and MS/MS based quantitation with duplex mdDiLeu. Reprinted with permission from [58].

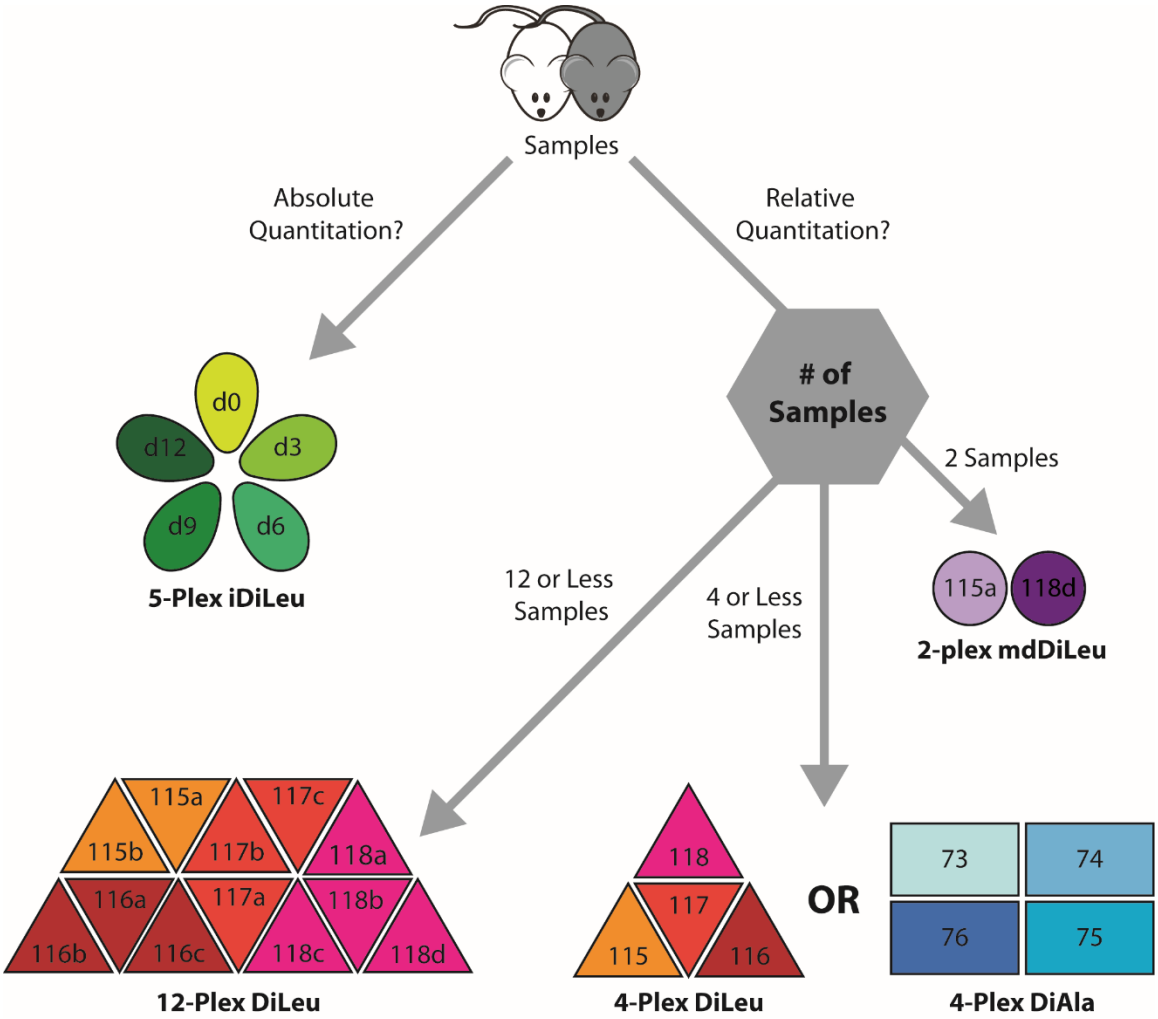

Figure 2. Decision tree for picking the appropriate tag system for a researcher's biological question. iDiLeu can also be used for relative quantitation at the MS1 level, especially if MS/MS sampling depth is a concern. If more than 12 samples need to be compared, label-free quantitation should be considered.

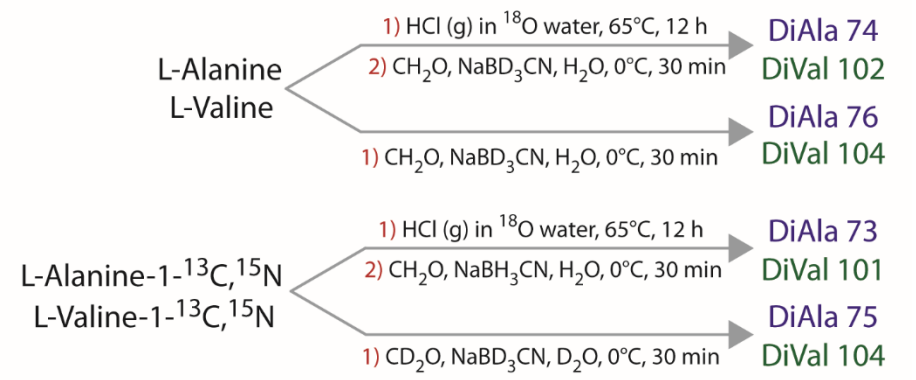

Figure 3. Synthesis strategies for the 4-plex DiAla and DiVal tags.

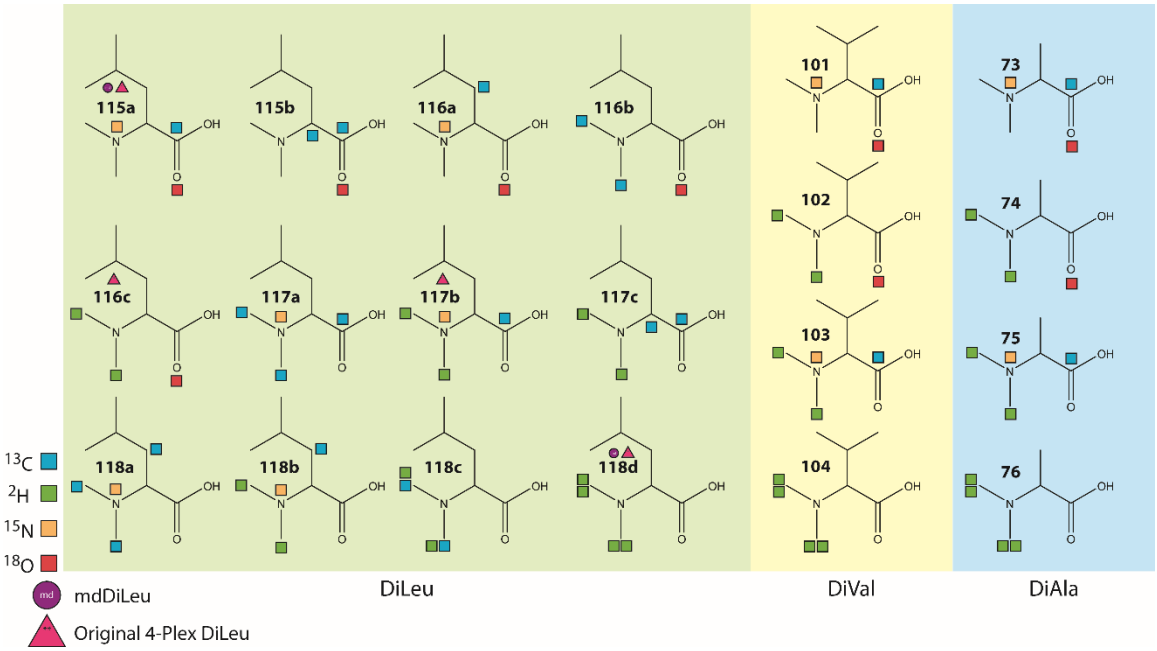

Figure 4. Tag isotopic structures for all chemical tags discussed, including DiLeu, DiVal and DiAla. Tags specific to the original 4-plex DiLeu and mdDiLeu are noted.